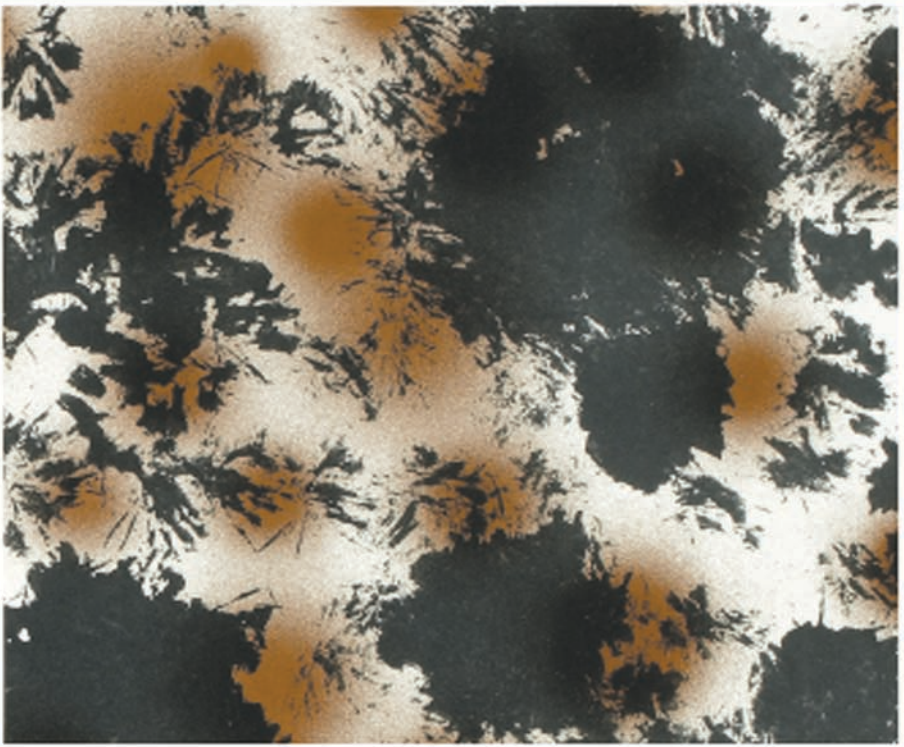


L
I
Q
U
I
D



ATOMIZATION

**L. BAYVEL
Z. ORZECHOWSKI**

COMBUSTION
AN INTERNATIONAL SERIES

LIQUID ATOMIZATION

Combustion: An International Series

Norman Chigier, Editor

Bayvel and Orzechowski, Liquid Atomization

Chigier, Combustion Measurements

Kuznetsov and Sabel'nikov, Turbulence and Combustion

Lefebvre, Atomization and Sprays

Forthcoming titles

Chigier, Stevenson, and Hirleman, Flow Velocity and Particle Size Measurement

Libby, Introduction to Turbulence

LIQUID ATOMIZATION

L. Bayvel

King's College

University of London

Z. Orzechowski

Technical University of Łódź



Taylor & Francis

Publishers since 1798

USA	Publishing Office:	Taylor & Francis 1101 Vermont Avenue, N. W., Suite 200 Washington, DC 20005-3521 Tel: (202) 289-2174 Fax: (202) 289-3665
	Distribution Center:	Taylor & Francis 1900 Frost Road, Suite 101 Bristol, PA 19007-1598 Tel: (215) 785-5800 Fax: (215) 785-5515
UK		Taylor & Francis, Ltd. 4 John St. London WC1N 2ET Tel: 071 405 2237 Fax: 071 831 2035

LIQUID ATOMIZATION

Copyright © 1993 Taylor & Francis. All rights reserved. Printed in the United States of America. Except as permitted under the United States Copyright Act of 1976, no part of this publication may be reproduced or distributed in any form or by any means, or stored in a database or retrieval system, without the prior written permission of the publisher.

1 2 3 4 5 6 7 8 9 0 B R B R 9 8 7 6 5 4 3

This book was set in Times Roman by Technical Typesetting, Inc. The editors were Mary Prescott and Ellen K. Grover; the production supervisor was Peggy M. Rote. Cover design by Michelle Fleitz. Printing and binding by Braun-Brumfield, Inc.

A CIP catalog record for this book is available from the British Library. © The paper in this publication meets the requirements of the ANSI Standard Z39.48-1984 (Permanence of Paper)

Library of Congress Cataloging-in-Publication Data

Liquid atomization / L. Bayvel, Z. Orzechowski.

p.cm.

1. Spraying. 2. Atomization. I. Bayvel, L. II. Orzechowski, Z.

TP156.S6L57 1993

660'.2945—dc20

93-8528

CIP

ISBN 0-89116-959-8

ISSN 1040-2756

CONTENTS

Preface	vii
Nomenclature	xi
1 Introductory Concepts	1
1-1 Various Methods of Liquid Atomization	1
1-2 Areas of Application of Atomized Liquids	7
1-3 Liquids Used for Atomization Processes	22
References	35
2 Theoretical Basis of the Process of Atomization	37
2-1 Theory of Disintegration of Jets, Sheets, and Drops	37
2-2 Stability and Disintegration of Liquid Jets and Sheets	41
2-3 Dimensionless Criteria of the Atomization Process	63
2-4 Disintegration and Coalescence	69
2-5 Drop Ballistics	84
2-6 Uniform Drops	109
References	119
3 Parameters of Atomized Liquid	123
3-1 Flow Rate of Atomized Liquid	123
3-2 Macrostructure of Atomized Liquid	131
3-3 Microstructure of Atomized Liquid	143
References	158

4 Types of Atomizers	159
4-1 Jet Atomizers	160
4-2 Swirl Atomizers	172
4-3 Jet-Swirl Atomizers	189
4-4 Pneumatic (Twin-Fluid) Atomizers	194
4-5 Rotary Atomizers	208
4-6 Miscellaneous Atomizers	220
4-7 Material, Technological, and Maintenance Problems	230
References	235
5 Design of Atomizers	237
5-1 Design of Jet Atomizers	237
5-2 Design of a Swirl Atomizer	252
5-3 Design of Jet-Swirl Atomizers	273
5-4 Design of Pneumatic Atomizers	280
5-5 Design of Rotary Atomizers	289
References	301
6 Experimental Results	303
6-1 Jet Atomizers	303
6-2 Swirl Atomizers	322
6-3 Pneumatic Atomizers	351
6-4 Rotary Atomizers	368
References	381
7 Experimental Techniques and Measuring Devices	385
7-1 Scope of Investigation of Atomizers	385
7-2 Measurement of the Flow Rate of the Atomized Liquid	387
7-3 Measurement of Macrostructure of the Atomized Liquid	396
7-4 Drop Sizing Methods Based on Drop Sampling	405
7-5 Optical Drop Sizing Methods	416
7-6 Analysis of Drop Size Distribution Data to Obtain the "Best" Fit to Standard Distributions and Distribution Parameters	437
References	445
Author Index	451
Subject Index	457

PREFACE

The atomization of liquids is a process of great practical importance. It finds implementation in many branches of industry: mechanical, chemical, aerospace, and civil engineering; material science and technology; transportation; metallurgy; food; pharmaceuticals; forestry; environmental protection; medicine; agriculture; meteorology and others. Liquid atomization and spray systems are used in spray combustion in furnaces, gas turbines, engines and rockets, spray drying and cooling, air conditioning, industrial cleaning, crop spraying, powdered metallurgy, spray painting and coating, fire protection, humidification, inhalation therapy, food preservation and cleaning, water treatment and many other areas.

Fuels and water are the most commonly atomized liquids. Liquid fuels are still the basic sources of energy worldwide. Water is generally used in cooling and cleaning processes. Water solutions, oil solutions, and water-oil solutions are used as crop protections (fungicides, herbicides, and others). An increasing number of non-Newtonian fluids, such as various solutions, emulsions, suspensions, and liquid metals, is coming into use. For combustion, various mixtures are being used: fuels which are a mixture of fuel oil and water; solid-liquid fuels, in the form of pulverized coal suspensions in fuel oil; and coal slurries, in the form of pulverized coal suspensions in water. Properties of atomized liquids differ. Of all its properties, a liquid's viscosity has the greatest influence on the atomization process.

The design of atomizers used for liquid atomization depends on the application of the atomized liquid, liquid properties, and operating conditions. In the case of high flow rate of a liquid, rotary atomizers are used most frequently. If

very fine atomization is required, then the atomizers with a low flow rate and high energy consumption, or a special type of energy consumption, are used. Examples of these would be diesel atomizers (with a pressure on the order of tens of megapascals) or ultrasonic atomizers (energy of vibrations). Atomization of very viscous liquids, emulsions, and suspensions is realized by means of pneumatic and pneumatic-rotary atomizers. When there is a need for a uniform distribution of liquid in a jet, jet-rotary and pneumatic atomizers are used.

Researchers, engineers, and specialists working in the above mentioned areas of activity must have basic knowledge of the physical processes of atomization; the types of atomizers and their design; and spray characteristics and measurement techniques. They then can choose the type of atomizer most suitable to solve their particular problem and design this atomizer.

The purpose of this book is to familiarize the readers with the physical processes of liquid atomization, main types of atomizers and their design, measurements of spray characteristics, experimental investigations of atomizers, and application of atomizers. The book consists of seven chapters. Chapter 1 concerns methods of liquid atomization; atomizer classification and applications; and basic properties of liquids and their influence on atomization conditions. Chapter 2 concerns the theory of liquid disintegration and the processes of jet, sheet and drop formation; processes of drops disintegration, especially of secondary drop disintegration due to aerodynamic forces; ballistics of single drops and drop jets; and different methods of liquid disintegration related to the monodisperse disintegration. Chapter 3 concerns atomization characteristics; flow rate; and macrostructure and microstructure of atomized liquids. Chapter 4 covers the main types of atomizers; various modifications of these atomizers; and atomizer technology and operation. Chapter 5 is about the design of different types of atomizers. Chapter 6 concerns experimental investigations of atomizers and the results. Chapter 7 is about measurements of various spray characteristics, with special emphasis on non-intrusive optical methods.

This book could be used as a textbook supplementing various courses in mechanical, chemical, fuel, aeronautical, civil and agricultural engineering. It includes many numerical problems which could be used for student tutorials.

One of the main features of this book is that the experience of West and East is blended and equally represented. The book covers results obtained by Western researchers, such as N. Chigier, J. S. Chin, E. J. Crosby, N. Dombrowski, P. Eisenklam, M. M. Elkotb, E. Giffen, H. Hiroyasu, R. D. Ingebo, A. J. Kelly, T. Kurabayashi, A. H. Lefebvre, K. Masters, S. Matsumoto, A. Muraszew, N. Nagai, S. Nukiyama, N. K. Rizk, T. Sakai, G. T. Sato, H. C. Simmons, J. Swithenbank, Y. Takashima, Y. Tanasawa, R. W. Tate, A. Yule and S. Zanelli, as well as Russian and East European researchers, including V. G. Bazarov, V. A. Borodin, Yu. F. Dityakin, V. S. Galustov, L. A. Klyachko, L. V. Kulagin, A. S. Lyshevskii, Z. Orzechowski, D. G. Pazhi, B. V. Raushenbakh, L. Vitman, M. S. Volynskii, V. V. Voronin, and V. I. Yagodkin.

The book includes descriptions of extensive and important work done in the fields of liquid atomization, spray systems and drop characterization by scientists

and engineers in the former USSR and Eastern Europe during the last forty years. Much of this information is not known in the West. In some cases, the terminology common to the Russian and East European literature is used in the book to facilitate the approach to appropriate references.

The authors sincerely hope that this book will be useful for various specialists and students dealing with problems of liquid atomization.



Taylor & Francis
Taylor & Francis Group
<http://taylorandfrancis.com>

NOMENCLATURE

Latin Letters

- a* velocity of sound
a_u coefficient of free turbulence
A area
b gas/liquid mass ratio
B_o Bond number $\left(B_o = \frac{\rho_L d^2}{\sigma} \right)$
C_D drag coefficient
d diameter of a jet
D drop diameter
D_m mass median drop diameter
D_M modal diameter; value of *D* corresponding to peak of the drop size number distribution curve
D₀ initial drop diameter
D_s swirl chamber diameter
D_{0.1} drop diameter such that 10% of total liquid volume is in drops of smaller diameter
D_{0.9} drop diameter such that 90% of total liquid volume is in drops of smaller diameter
D₁₀ length mean diameter
D₂₀ surface area mean diameter
D₃₀ volume mean diameter

D_{32}	volume/surface area mean diameter (Sauter mean diameter, SMD)
E	energy
E	power
f	frequency
F	force
FN	flow number ($\text{FN} = Q / \sqrt{P}$)
g	acceleration due to gravity
G	mass flow rate
H	hydraulic head
i	number of tangential inlet orifices
k	wave number ($k = 2\pi/\lambda$)
K	geometric constant of swirl atomizer
l	nozzle length
L	characteristic linear dimension
L_c	length of compact jet
L_p	Laplace number ($L_p = \rho_L \sigma_L / \mu_L^2$)
m	mass
M	criterion number ($M = \rho_G / \rho_L$)
Ma	Mach number ($\text{Ma} = V_G / a$)
n	number of droplets
N	criterion number ($N = \mu_G / \mu_L$)
P	pressure
ΔP	pressure drop
P_0	ambient pressure
q	spray density
Q	volumetric flow rate
r	radius
r_r	aircore radius
R	atomizer radius of feed entry
Re	Reynolds number ($\text{Re} = VL / \nu$)
t	time
T	absolute temperature
u	axial velocity
v	tangential velocity
V_D	drop velocity
V_W	flow rate per pulse, (mm^3/pulse)
w	radial velocity
We	Weber number ($\text{We} = \rho V^2 L / \sigma$)
X	characteristic diameter in Rosin-Rammler equation
Z	Ohnesorge number ($Z = \mu / \sqrt{\rho \sigma L}$)

Greek letters

α	spray cone angle
δ	Rosin-Rammler drop size distribution parameter

λ	wavelength
μ	dynamic viscosity
ν	kinematic viscosity
ρ	density
σ	surface tension
ω	angular velocity

Subscripts

a	axial
A	area
G	gas
L	liquid



Taylor & Francis

Taylor & Francis Group

<http://taylorandfrancis.com>

INTRODUCTORY CONCEPTS

1-1 VARIOUS METHODS OF LIQUID ATOMIZATION

A device used for liquid atomization (i.e., disintegration of liquid into drops) is most frequently called an atomizer. An atomizer can be an independent device or part of a bigger device such as a diesel injector, furnace burner, spray gun, spray drier, or sprinkle chamber. Atomizers can be used either as individual devices or in groups.

Atomized liquid can be generated in other ways than by using an atomizer. For example, in the carburetor of a carburetor engine or in the low-pressure section of a steam turbine, very small droplets form because of evaporation or condensation. These methods of drop formation will not be discussed in this book.

The *classification of atomizers* [21] can be based on various principles. A classification that takes into account the type of energy used for atomization seems preferable (Fig. 1-1). As can be seen, the sources of energy are very diverse.

The energy most commonly used is that of the liquid itself. The pressure drop is converted in an atomizer into kinetic energy, which leads to atomization of the liquid. This is the principle of operation of *pressure atomizers* (hydrodynamic) with a simple discharge (jet) or swirl discharge. It is also the rationale for dividing this group of atomizers into three types: jet atomizers, swirl atomizers, and jet-swirl atomizers. Pressure atomizers are more economical than other atomizers when power demand is considered. They are used mostly because of

2 LIQUID ATOMIZATION

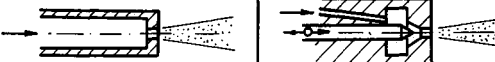
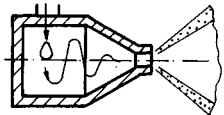
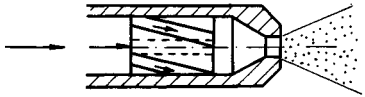
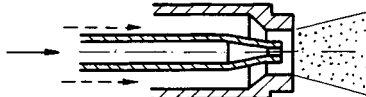
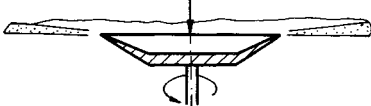
Liquid energy	Jet atomizers continuous intermittent	
		
	Swirl atomizers 	
Jet-swirl atomizers 		
Gas energy	Pneumatic atomizers 	
Mechanical energy	Rotary atomizers 	
Vibration energy, electric energy, etc.	Various atomizers: acoustic , ultrasonic, electrostatic, etc.	

Figure 1-1 Classification of atomizers.

their simplicity, but they are not suitable for atomization of very viscous liquids and their atomization quality decreases with increasing flow rate.

Jet atomizers are divided into two types: continuous (open) atomizers and intermittent (closed) atomizers. Continuous atomizers are the simplest of all atomizers; intermittent atomizers are the most complex in design and technol-

ogy. These characteristics result from the different types of operation (continuous or intermittent). Continuous atomizers are used in rocket engines, for spray painting, and so forth, and intermittent atomizers are used in diesel engines.

A jet atomizer produces a jet that disintegrates at some distance from the atomizer (Fig. 1-2). The process of disintegration and final effect depend on the type of the liquid, discharge orifice diameter, velocity of discharge, and ambient conditions. For a given atomizer the jet disintegration can be speeded up by increasing the discharge velocity (increasing the injection pressure). To this end,

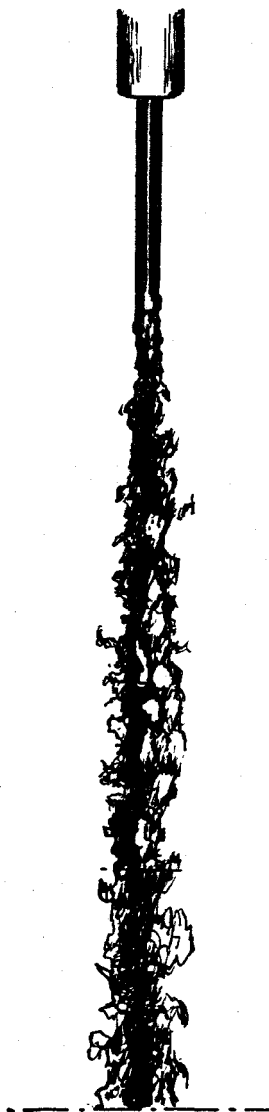


Figure 1-2 A liquid jet discharging from a jet atomizer.

4 LIQUID ATOMIZATION

high injection pressures are used; in the case of intermittent atomizers the injection pressures reach tens of megapascals.

Jet disintegration can be speeded up by the development of a flat jet in fan spray atomizers. Such a jet, or in fact a flat film, disintegrates into drops much more easily than a cylindrical jet of the same flow rate. Another way to speed up the disintegration of a cylindrical jet is to have it collide with a solid object (impact atomization). Jet atomizers with two colliding liquid jets are also used to speed up disintegration.

The name *swirl atomizer* originates from the swirling of the liquid inside the atomizer. These atomizers are divided into several types, each of which generally ensures good disintegration for moderate and even for small pressure drops (small injection pressures). Because of this and their relatively simple design, swirl atomizers are the most widely used of all types of atomizers. Examples of their application include gas turbines, steam attemperators, and air conditioners.

The operation of swirl atomizers is based on the principle that the liquid swirling in the swirl chamber leaves it not as a compact jet but as a conical sheet. The disintegration of the sheet into drops proceeds differently depending on the discharge velocity. For small velocities the sheet disintegration is due to perforation, for higher velocities it is due to wave phenomena, and for very high velocities it is due to aerodynamic action of an ambient gas (Fig. 1-3). In practice, the term liquid atomization is understood to mean the latter case of sheet disintegration.

Jet-swirl atomizers have the combined features of jet and swirl atomizers. This results in a new type of atomizer, in which the distribution of the jet density in the cross section perpendicular to the jet axis can be arbitrarily adjusted according to need. Therefore, one can also obtain a uniform distribution—an advantage in all of these applications, in which one needs the most efficient heat and mass exchange between the drops and the environment. Because of the nature of the combination of two different types of atomizers, part of the fluid flows as an unswirled axial jet and part as a swirled annular jet. The mass and momentum exchange between these jets determines the distribution of the liquid in the transverse cross section and the atomization quality.

Pneumatic atomizers (gas-assist atomizers) use the energy of a gas, usually air or steam. Gas having high kinetic energy ensures good disintegration of jets or sheets of the liquid. Pneumatic atomizers find application in various fields, but are especially useful in the atomization of very viscous fuel oils using steam. Pneumatic atomizers are most complex as far as the flow is concerned, because there is an interaction between two phases, liquid and gas. This interaction can have a parallel, crossing, or swirled direction and the liquid and gas can occur as jets or sheets. In the case of parallel interaction, waves develop on the interaction surface and cause the disintegration of the liquid into drops. In a crossing interaction the liquid disintegrates because of the dynamic action of the gas. In a concurrent or backward swirl interaction, both wave and dynamic phenomena occur [8] (Fig. 1-4). The interaction between jets of liquid and gas in a pneumatic atomizer can take place inside or outside the atomizer.

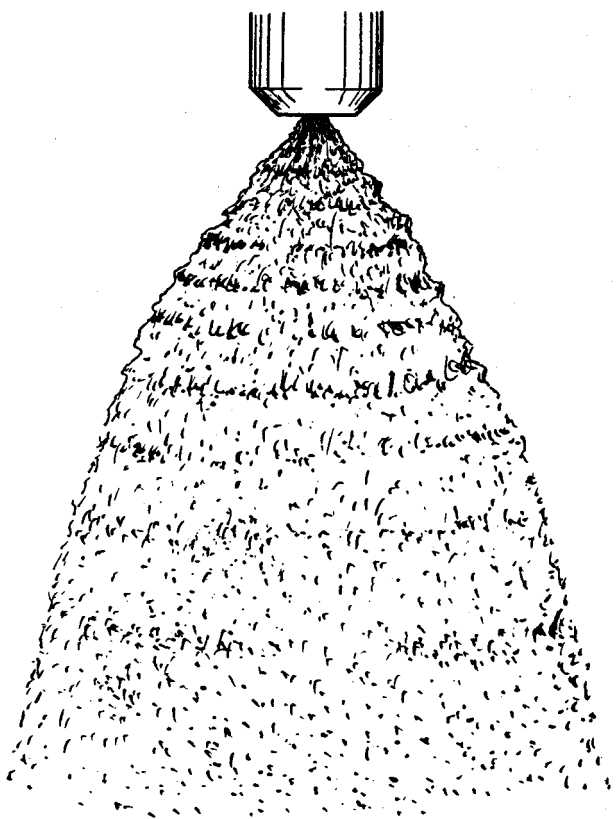


Figure 1-3 Liquid atomization using a swirl atomizer.

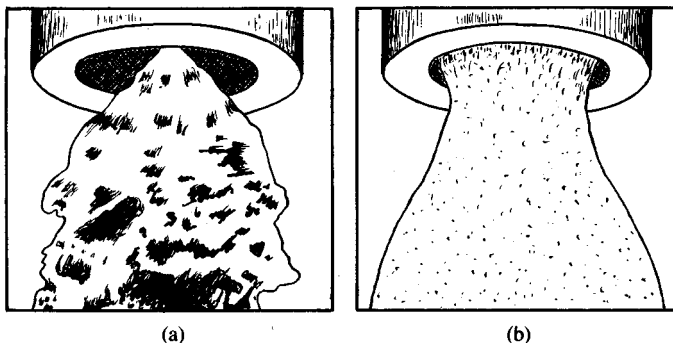


Figure 1-4 Sheet disintegration in an atomizer with whirl flow. (a) Without air flow; (b) with air flow.

6 LIQUID ATOMIZATION

Rotary atomizers are most commonly driven by an electric motor and rotate around their own vertical or horizontal axis. The energy of the atomizer is transmitted to the liquid, which causes the liquid to leave the atomizer with high kinetic energy and disintegrate. Under certain conditions this type of atomizer can ensure good atomization and even generate homogeneous drops. Rotary atomizers are used mainly for atomization of solutions, for instance, in drying (Fig. 1-5), because the atomizer can be fed with a liquid at low pressure [15].

Rotary atomizers are generally divided into disk and wheel atomizers. The latter have many design types. The principle of operation of rotary atomizers is based on the centrifugal forces acting on the liquid. The liquid supplied in the vicinity of the axis of rotation spreads on the atomizer's surface and then, on the perimeter, is ejected with high speed into the environment. This requires a high rotation speed, which is the main disadvantage of rotary atomizers. Efforts in design are directed toward efficient energy transfer from the atomizer to the liquid, for instance, by using vaned wheels.

The atomizers that are referred to as "various" in Fig. 1-1 have diverse principles of operation. They are finding increasing technical applications.

In practical design, some atomizers represent the combination of two or even three types of atomizers. For example, rotary atomizers in boiler burners use additional air energy; that is, they are pneumatic-rotary atomizers.

The energy E supplied to the atomizer is given by

$$E = E_A + E_K + E_L \quad (1-1)$$

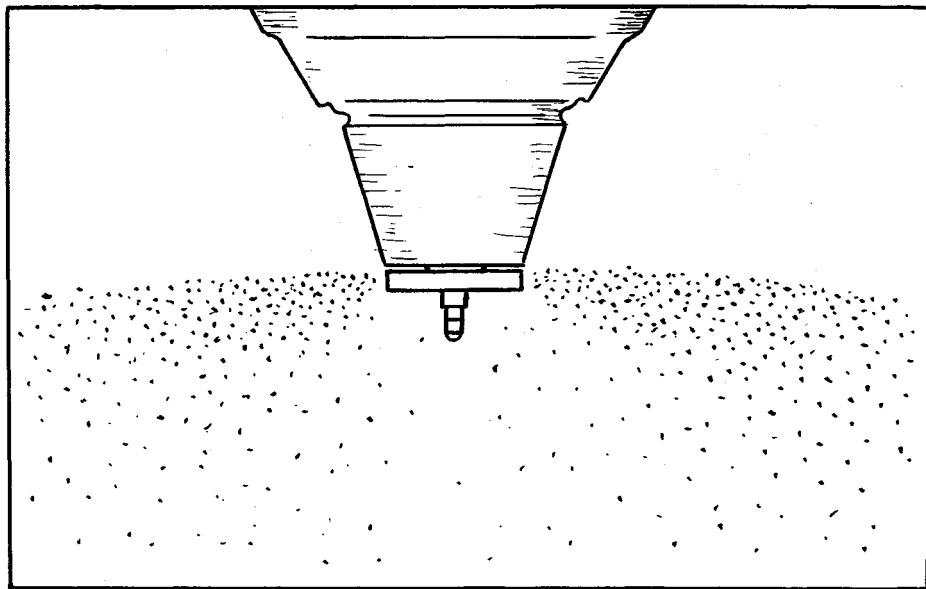


Figure 1-5 Liquid atomization using a rotary atomizer.

Table 1-1 Power demand for the disintegration of 1 kg of liquid

Type of atomizer	Power, W/kg
Jet atomizers	2–4
Swirl atomizers	2–4
Pneumatic atomizers	50–60
Rotary atomizers	15

where E_A = energy of atomization (surface energy), i.e., energy used to overcome the resistance of surface tension forces during disintegration of liquid into drops

E_K = kinetic energy, i.e., energy used to set the liquid in translational and rotational motion

E_L = energy loss, i.e., energy used to overcome frictional forces in the atomizer

In [22] the energy balance in the process of atomization is presented in detail. The *efficiency of atomization* is given by

$$\eta = \frac{E_A}{E} \quad (1-2)$$

The efficiency η is defined as the ratio of the energy E_A used for the development of a new liquid surface (surface of drops) to the total energy used in this process. For all traditionally used atomizers the efficiency is very small, namely $\eta < 0.1\%$.

The efficiency of atomization depends mainly on the type of atomizer, drop diameter, and physical properties of the liquid. Improvement of atomization is related to energy demand; i.e., increased energy demand corresponds to a decrease of the efficiency of atomization. Pressure atomizers have an efficiency $\eta = 0.05\text{--}0.07\%$ for generating drops with a diameter of $100 \mu\text{m}$ and several thousandths of a percent for generating drops with a diameter of $50 \mu\text{m}$. For other types of atomizers the efficiency of atomization is even lower.

Table 1-1 shows the approximate energy demand for atomization of 1 kg of liquid. Pressure atomizers (jet, swirl) are most efficient in this respect.

1-2 AREAS OF APPLICATION OF ATOMIZED LIQUIDS

Liquid atomization became popular over 100 years ago and was associated with crude oil refining. At present, it is used in all branches of industry.

1-2.1 Power Engineering

Power engineering—in the broad meaning of the term, including big conventional and nuclear power plants as well as small power- and heat-generating units—is the largest area of application of devices using atomized liquid. These devices are used in processes such as combustion, steam attemperation, and ash removal.

Combustion. Combustion as a basic energy process is realized by means of burners of various types, such as liquid fuel burners. One of the basic elements of such a burner is a fuel atomizer (Fig. 1-6). Usually the burner is equipped with a device to control the amounts of fuel and air designated for combustion and with an ignition system.

The burners can be of various sizes, ranging from very large ones in power boilers to very small ones in small heating units. Boilers in power units of intermediate power (order of 50 MW) using fuel oil have 16 to 18 burners with an oil flow rate of 1.1–1.8 t/h in each burner. High-power units have even bigger burners; for instance, Sulzer's 300-MW unit has 20 burners with an oil flow rate of 3.5 t/h in each burner. Because the new power units being built are bigger and it is necessary to facilitate the mechanization and automation of the fuel supply, there is a tendency toward limiting the number of burners. However, this leads to increased burner dimensions, which is not advisable because it causes an increase of drop sizes. For this reason a fuel flow rate of 0.6–0.8 t/h per burner is considered the limiting value, while there are already existing burners with a flow rate of 12 t/h [20]. This is related to the problem of fuel pressure drop. Most commonly, pressure drops in the range 1.2–3.0 MPa are used, but in the case of heavy oil fuels additional means have to be used to facilitate atomization.

Small boilers and heating units have burners with a very small fuel flow rate, of order 5 kg/h. Such burners are structurally integrated with the combustion chamber and are used in vehicles with internal combustion engines, civil

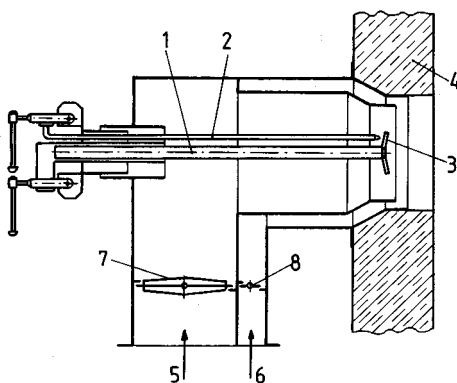


Figure 1-6 Boiler burner with a swirl atomizer.
 1, Main atomizer; 2, ignition atomizer; 3, disk stabilizer; 4, boiler body; 5, primary air; 6, secondary air; 7, 8, throttles.

engineering, and public utilities. The widely used aggregate burners brought to the heated object represent a variation of these types of burners. In central heating systems the fuel oil consumption in these smallest burners is only 2 kg/h. The disadvantage is that their discharge orifice, which in this case has a diameter of order 0.5 mm, tends to clog. The burners are equipped mainly with swirl atomizers; however, ultrasonic atomizers are also frequently used [5].

Burners for oil-water emulsions are distinct among various types of burners. The emulsion basically consists of fuel oil with about 25% added water. Faster and more complete combustion is achieved, which ensures lower emission of fly ash and nitric oxide into the atmosphere [21].

It turns out that for a water content of 13–20% in fuel oil one can increase the efficiency of combustion by over 5% and simultaneously decrease the temperature of combustion products by 20–30 K and reduce the amounts released into the atmosphere. Combustion of oil-water emulsions can result in fuel savings of 15–20%. Suitable emulsifiers are required.

The liquid fuel economy in the 1970s led to an increase of interest in solid-liquid fuels, which are suspensions of coal dust in fuel oil. After the energy crisis, interest in these fuels decreased worldwide; however, extensive research is still being conducted on the combustion of these fuels [2, 17, 18]. In the case of boilers using oils, there are additional problems such as erosion of heating surfaces, dust removal from combustion products, and slag disposal. The most difficult problem is the development of a pump resistant to erosion by oil-water emulsions.

Attemperation of steam. The goal of steam attemperation in boilers is to control the temperature of superheated steam. In the reduction-attemperation plants, it serves the purpose of process steam generation. Attemperation involves direct injection of water into the flowing steam. The amount of injected water in large boiler superheaters is tens of t/h. The main problem is the quality of atomization of such large amounts of water. This purpose is best served by pneumatic atomizers (steam-water), which utilize the easily accessible steam. The temperature of superheated steam is controlled by changing the amount of atomized water. With decreasing amounts of water the quality of atomization decreases, but in the case of pneumatic atomizers one can avoid this, and even improve the quality of atomization, as long as the amount of steam supplied to the atomizer does not decrease [1].

Water cooling. Water used in condensers of steam turbines and heat exchangers, for example, in oil exchangers, is cooled in cooling towers. The towers contain a large number of atomizers, which in most cases are jet-impact or swirl atomizers of simple design. With these atomizers, however, it is not possible to obtain a uniform distribution of the drop jet, which is necessary for proper heat exchange between the drops and the cooling air. An improved drop distribution can be achieved by using regular jet atomizers with a circular or square cross section or by using swirl-jet atomizers. In the first case, however, a decrease of

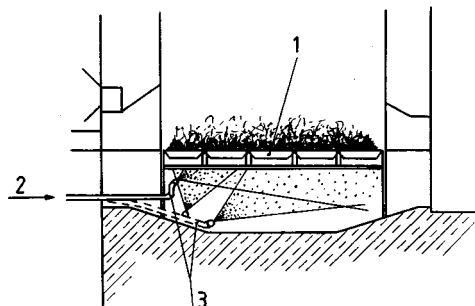


Figure 1-7 Cooling of a fire grate using water spray. 1, Fire grate; 2, water supply; 3, atomizer.

atomization quality can be expected; whereas in the second case, due to the complex design of the atomizers, the price can be expected to be higher.

Cleaning of boiler pipe screens. Pipe screens in boilers using coal dust are covered constantly with soot or fluid ash. It is necessary to conduct in-service removal of these contaminants. Special atomizers (water nozzles) serve this purpose, and their effectiveness is higher the longer the compact (nonatomized) portion of the jet.

Water treatment. In the process of water treatment in the power industry, water decarbonization and water deaeration play an important part. The objective of these processes is to separate from water the active and corrosive gases (mainly CO_2). Water is atomized under a pressure of 0.2–0.3 MPa. In recent years special atomizers have become more popular [9].

Improvement of the composition of combustion products. Water injection or steam supply to a residual fuel oil furnace reduces the concentration of NO_x 4 to 4.5 times in combustion products, while mixing water and residual fuel oil (up to 15% water) lowers this concentration by only 20–30%.

Other applications. Several other applications of atomized liquids in the power industry are as follows:

- Cooling of fire grate with atomized water (Fig. 1-7), which also improves the air supply for combustion
- Water atomization in dust separators
- Fly ash and slag water spraying during reloading
- Air humidification to intensify the cooling of heated surfaces

1-2.2 Mechanical Engineering

Oil mist lubrication. Lubrication of machine parts with oil mist is one of the most modern methods of lubrication. The application of this method in the

metal industry began in the 1950s. The method is based on feeding the lubrication points with a suspension of oil drops in compressed air. It is used to lubricate machines such as grinders and other high-speed machines, metal rolling mills, belt and chain conveyors, vibrators, etc.

Oil mist lubrication is used when there is a need for a continuous supply of small quantities of oil to numerous lubricating points. Lubricating points can be at a long distance, even more than 100 m, from the oil mist generator. The mist is usually generated with pneumatic atomizers; however, there have been attempts to use atomizers that provide more uniform and finer atomization. This is because 90 to 95% of atomized oil drops have diameters larger than $5 \mu\text{m}$ and desirable oil mist should have smaller drop diameters, $2 \mu\text{m}$ for instance, for which the oil precipitation in supply conduits is only around 3%. These data refer to the optimal flow velocity of oil mist of around 3.4 m/s. The oil mist should be supplied to the lubricating points at a concentration of $2.2\text{--}2.5 \text{ g/m}^3$ and not less than 1.0 g/m^3 [4, 27].

Liquid metal atomization. Gas atomization of liquid metal is widely used for the production of pure metal powders with diameters of $1\text{--}5000 \mu\text{m}$. The powders obtained in such a manner are used for the production of sintered machine parts, materials for hard soldering and spraying, chemicals, paints, explosives, etc. Liquid lead and tin (melting points 327°C and 232°C , respectively) are atomized by the collision with jets of compressed nitrogen [25] (Fig. 1-8). Liquid zinc (melting point 419°C) can be atomized without using a neutral atmosphere, i.e., by using an air jet. Jet velocities close to sonic velocity have been used [26].

Besides liquid metals, liquid slag has been atomized for use in cement production. The slag is atomized with a cup rotary atomizer, and after cooling the granulated product has dimensions of 1–2 mm. Such dry granulation of slag has the advantage over wet slag cooling that it avoids the heat losses needed for drying [24].

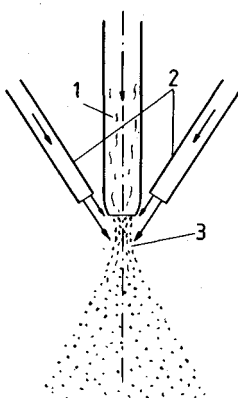


Figure 1-8 Liquid metal atomization. 1, Liquid metal; 2, atomizing gas; 3, region of atomization.

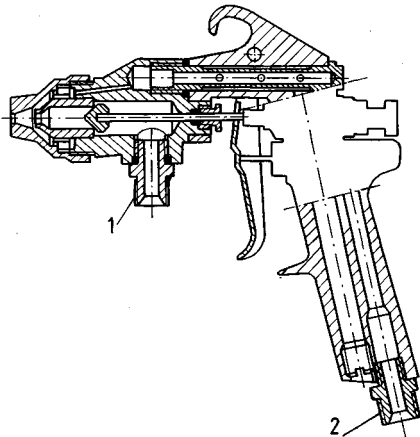


Figure 1-9 Pneumatic spray gun. 1, Paint supply;
2, compressed gas supply.

Spray coating. In mechanical engineering, jet, swirl, and pneumatic atomizers are widely used for spray paint coating. This is done in an automated way in special spray chambers, for example, in car production, or manually by using spray guns [22] (Fig. 1-9). Spray coating applications include:

- Deposition of anticorrosion coatings (especially important in places where accessibility is difficult)
- Coating with plastics, resins, or adhesives
- Coating of paper tape
- Fabric dyeing
- Paint coating furniture, food cans, bottles, etc.
- Ceramic and stoneware glazing

Washing and cleaning. Metal parts are washed using a jet of atomized liquid in order to degrease and neutralize the surfaces, preparing them for subsequent physical or chemical processes. Complete devices, machines, and vehicles are also washed. Scale and other contaminants are removed, especially from surfaces where accessibility is difficult, like the interiors of tanks or cisterns (Fig. 1-10). In these cases combined jet atomizers, providing a spherical atomizing head, are used.

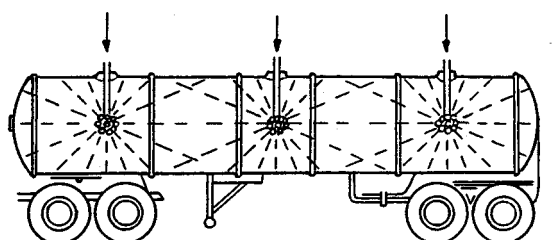


Figure 1-10 Cleaning the inside of a tank using atomizers.

Cooling. Manufacture of castings and metallurgic products (plates, profiles) requires intensive water cooling of the products themselves, as well as production machines (mills, etc.). Jet and pneumatic atomizers are used for this purpose. The jet atomizers should develop a strong jet that can rip the steam cushion that develops on the surface being cooled. The pneumatic atomizers do not have to satisfy this requirement because the small drops they develop collect the heat by evaporation, which decreases the water demand by 30–40% [11].

1-2.3 Transport

In combustion chambers of piston engines, ramjet engines, and rocket engines the fuel is atomized by various types of atomizers. Intermittent atomizers are used in piston engines and continuous atomizers in other types of engines.

Piston engines. Diesel engines (compression-ignition engines) represent a vast field of application for atomizers. Very good atomization is required, especially in the case of direct injection into the combustion chamber (Fig. 1-11) to minimize the ignition delay. This requires very high injection pressures, of the order of tens of megapascals. The fuel charge, ignition advance angle, injection rate, and enrichment of fuel charge must also be adjusted to the engine regime. This is done by using central electronic control. The single charge of injected fuel is small, of order of tens of cubic millimeters. Under these conditions the diameters of the discharge orifices are much smaller than in the case of continuous atomizers, but bigger than a certain minimum value (0.2 mm).

Attempts have been made to improve the combustion process in diesel engines by minimizing the ignition delay and by smoothing the process of pressure buildup in the cylinder [32]. These attempts are based on either dual fueling, where a portion of fuel charge is supplied to the suction line, or

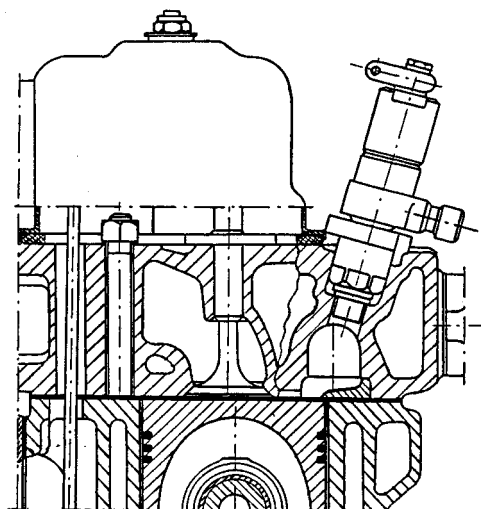


Figure 1-11 Part of a piston engine with direct injection.

two-phase injection, where the principal charge is preceded by a precharge representing 5–15% of the total charge.

Spark-ignition engines. These can be not only of carburetor type but also of injection type. In the latter case the injection of light fuel is applied in four-stroke engines as well as in two-stroke engines. In four-stroke engines the operation of the injector can be continuous or intermittent. Among the most popular systems used in four-stroke engines are the Texaco system, which is based on injection of fuel in the direction of the spark plug at the end of the compression stroke, and the Ford PROCO system, which is based on fuel injection into a deep chamber in the piston at an early stage of compression. In two-stroke engines, direct injection into the cylinder during the compression should be used. Because low injection pressures are desired (0.5–2.5 MPa), for which the drop sizes are significantly larger than in diesel engines, one often selects injection into the suction conduit in order to increase the path of drop evaporation.

Flow engines. The group of flow engines, which are used mainly in aircraft, includes gas turbines (jet turbine engines), pulse jet engines, and ramjet engines. Most popular are the gas turbines (jet turbine engines), which are used in aircraft as well as for other purposes. Figure 1-12 shows one of the typical cylindrical combustion chambers with the most commonly encountered cocurrent injection. Gas turbines have, in principle, several cylindrical chambers or one annular chamber. The atomizers in gas turbines are similar to those in burners, but they are made with higher precision, especially for aircraft. The small volumes of combustion chambers require good fuel atomization, i.e., drop diameters of 50–200 μm .

Rocket engines. We consider rocket engines using liquid propellants (liquid fuel and liquid oxidizer). There are several atomizers in small engines, several hundred in medium-sized engines, and several thousand in big engines; for example, the rocket engine of the first stage of the carrier rocket Saturn 5 had 2600 atomizers for the oxidizer discharge of 2000 kg/s and 3700 atomizers for the fuel discharge of 1000 kg/s. The atomizers are most commonly the regular orifices made in the head of the combustion chamber [21] (Fig. 1-13).

Airfield service. Fog brooding over the runways causes large financial losses for airline companies. Despite many long-term efforts, a rational (i.e., effective and

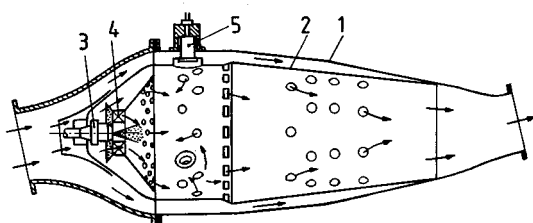


Figure 1-12 Combustion chamber of a gas turbine. 1, Housing; 2, flame tube; 3, atomizer; 4, primary air swirl vane; 5, ignition atomizer.

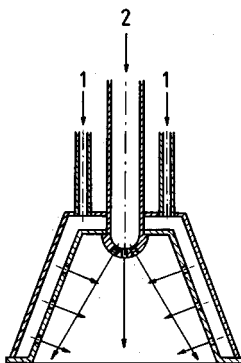


Figure 1-13 Scheme of the combustion chamber head of a rocket engine operating on liquid propellant. 1, Fuel; 2, oxidizer.

cheap) method of fog removal could not be developed. A promising method was based on the generation of curtains of falling drops of water (Fig. 1-14). The circulation created on both sides of the curtain, together with the wind, causes the fog to move. The water in the closed cycle is sprayed to a high altitude, often higher than 50 m. Fog drop diameters are typically of order $10 \mu\text{m}$, whereas the diameters of sprayed water are 0.3 to 1.0 mm. The velocity of falling drops is therefore two or three orders of magnitude higher than the velocity of fog drops, which leads to their collision and coalescence [12].

In civil aviation, jet atomizers are used to remove layers of ice, frost, and snow. These atomizers generate a compact jet of a water solution of a liquid whose freezing point is adjusted to the ambient temperature.

The addition of polymer solutions of low concentration to propellants is used in aviation to prevent fuels from igniting during emergency landings. The additive, called antimisting (AM), changes the morphology of fuel jets emerging from the damaged tanks and prevents the development of a disintegrated fuel mixture, which results in the generation of a compact fuel jet [6].

1-2-4 Agriculture and Forest Industry

The spraying of fields, forests, orchards, and greenhouse cultivations constitutes a vast branch of application of atomizers (Fig. 1-15). The spraying has as an objective plant protection and the fertilization and watering of the soil [7]. Chemical crop protection products (pesticides) are highly toxic compounds.

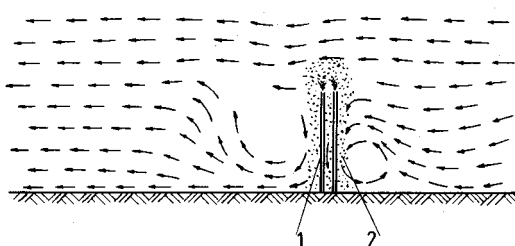


Figure 1-14 Schematic of air circulation caused by a curtain of falling drops during mist removal at an airport. 1, Pipeline with an atomizer; 2, falling drops.

16 LIQUID ATOMIZATION

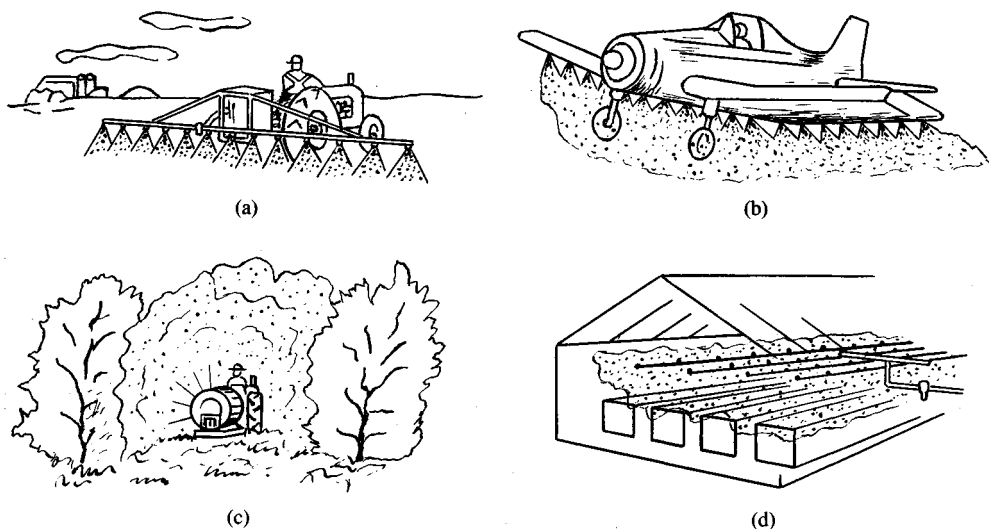


Figure 1-15 Agricultural treatment. (a) Field spraying; (b) field and forest spraying; (c) orchard spraying; (d) greenhouse humidification.

They are used in the form of water solutions or oily liquids. The latter have higher efficiency because they spread better on the leaf surface.

The term *spraying* encompasses both profuse wetting of the plants with a low-grade jet of liquid with coarse drops (conventional spraying) and spreading of concentrated liquid disintegrated into very small drops (modern spraying). Depending on the type of spraying, the following mean drop diameters are used:

Less than 60 μm , aerosols in closed spaces

60 to 160 μm , pest and pathogen control

160 to 260 μm , weed control

Besides this classification, there is the following practical classification based on the amount of liquid used for 1 hectare of the crop being protected:

Large-volume spraying (conventional), 300 to 600 L/ha or more

Medium-volume spraying with the limitation on water usage, approximately 100 L/ha

Small-volume spraying, 10 to 50 L/ha

Ultrasmall-volume spraying, less than 10 L/ha

The drop sizes and liquid quantity per hectare are related to the leaf surface covered by the drops. The degree of coverage is determined for each protective treatment, and the number of drops per square centimeter should be less than 100; 25 drops/cm² is often satisfactory.

The major difficulty during spraying is high nonuniformity of drop sizes. Very small drops evaporate quickly and drift easily because of wind outside the spraying area, whereas big drops bounce and roll down on the plant.

These problems require the application of various atomization techniques and methods of liquid deposition on protected plants. The techniques must be adjusted to the type of treatment and to weather conditions; for example, spraying from an aircraft can be effective only for wind velocities lower than 4 to 5 m/s.

Because of the very diverse requirements, all types of atomizers are used in practice. In recent years, efforts have focused on manufacturing atomizers with limited water consumption. For this purpose, low-pressure fan atomizers with a flat jet of drops are employed for wide usage. These types of atomizers, however, are susceptible to clogging while spraying suspensions, so other approaches have been sought. For ground spraying, the most promising are rotary atomizers that generate drops in a limited arc (120° to 140°) of their perimeters.

Atomizers are one part of the equipment used for plant protection. This equipment is divided into spraying machines and aerosol generators.

Spraying machines, depending on the principle of operation, are divided into those with jet atomizers (fan atomizers) and those with rotary atomizers. In both cases, an additional jet of air can be used; for velocities of 30 to 40 m/s the air jet helps in drop transport, and for velocities higher than 80 m/s it plays the main role in liquid atomization. In the latter case a pneumatic atomizer is created. Depending on the type of drive, the machines are divided into hand-operated, motor-operated (engine drive, electric drive), horse-driven, tractor-driven (field, orchard, greenhouse), and aviation (aircraft, helicopter) atomizers. Depending on the mode of relocation, the spraying machines are divided into hand operated, transportable, mobile, self-propelled, etc.

Aerosol generators produce drops with diameters less than $60 \mu\text{m}$ and are divided into thermal generators (condensation) and dispersive generators. Thermal generators operate on the principle of liquid evaporation in hot gases and steam condensation in the atmosphere. Dispersive generators are based on the principle of mechanical atomization of the liquid by using pneumatic atomizers or pulse jets.

Aircraft are used for operations over forests without any limitations regarding tree height and over fields and meadows with obstacles not higher than 3 m; helicopters are used mainly for operations in orchards. The flight altitude over the crops is 2 to 5 m and over the treetops from 5 to 10 m. The aircraft velocity ranges from 100 to 140 m/s; the velocity of helicopters is 20 to 100 m/s. Aircraft are used for spraying areas 25 to 60 m wide, and helicopters for areas 25 to 25 m wide, whereas the width for ground spraying machines is 8 to 10 m.

1-2.5 Chemical Engineering

Chemical engineering is a field in which liquid atomization is often used. Atomization can provide a very large liquid surface, which is necessary for all

18 LIQUID ATOMIZATION

contact processes. Various atomizers adjusted to the properties of the liquid, mainly its viscosity, are used. More and more, non-Newtonian liquids are in the picture, among them various solutions, emulsions and suspensions, and even gelatins. Atomization of these liquids is difficult for obvious reasons.

Atomization of liquids is used in chemical engineering in such processes as spray-drying, dust granulation, distillation, liquid absorption and desorption, injection crystallization, and gas elution (rinsing). The specifics of the first two processes will be characterized briefly.

Spray-drying. In spray-drying, liquid substances are sprayed into an area of flowing air in order to remove the moisture [15]. There are four stages of drying (Fig. 1-16):

1. Atomization
2. Drop-air contact
3. Evaporation
4. Product recovery and cleaning of the outlet air

The moisture evaporates rapidly because of the large surface of drops; for example, 1 m³ of liquid creates 2×10^{12} uniform drops of diameter 100 μm with a total surface area of 60,000 m².

Spray-drying has the following advantages:

It is the only rational method for producing powdered substances.

Any substance that can be pumped in its liquid form, such as suspensions, slimes, and pastes, can be dried.

Single industrial systems can be built with a capacity ranging from several kilograms per hour to 100 t/h of dried products.

It is a continuous, simple process that is easy to automate.

The disadvantages of spray-drying are:

Large installation costs and dimensions of the installation per unit of dried product which are bigger than for driers of other types,

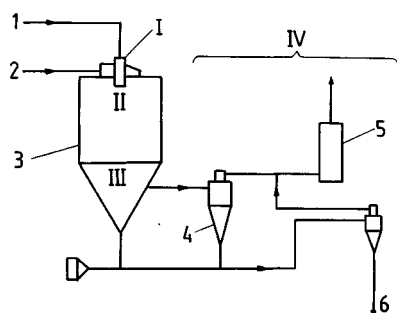


Figure 1-16 Open cycle of cocurrent spray drying. 1, Supply of liquid substance; 2, air supply; 3, drying chamber; 4, cyclone; 5, scrubber; 6, final product.

Relatively low thermal efficiency for inlet air temperatures reaching 350°C (often encountered in practical use), which stems from difficulties in utilizing the low-temperature outlet heat.

Dust granulation. Dust granulation in wet methods of agglomeration is based on supplying atomized binding liquid to the dust. This results in a population of granulation nuclei that have similar saturation and equalized granulometric composition. For liquid atomization, pressure and pneumatic atomizers are used; the latter give better results because the atomization quality can be changed while keeping the discharge constant.

The quality of atomization selected depends on the properties of dust and the desired granulometric composition of the product. During an evaluation of talc granulation and dust granulation in an iron foundry, it was found that granulation does not proceed until the drop diameter reaches 200 to 300 μm [3].

1-2.6 Environmental Protection

One of the most important problems of environmental protection is air pollution control. The main sources of pollution are fuel combustion, industrial activity, and fires. The best method for gas cleaning is gas scrubbing using atomizers.

Gas scrubbing. Devices for wet gas cleaning are often called scrubbers [30]. The process of dust extraction is based mainly on the deposition of dust particles on water drops in spray extractors (Fig. 1-17). Particle deposition proceeds relatively easily when the relative velocity of the particles moving along with the gas and drops is high and when the drops are small. Small drops, however, accelerate easily and quickly achieve the velocity of the gas, and independently of this they can evaporate. For these reasons the drop size should be 50 to 100 times larger than the size of the dust particles.

Other wet dust collectors include centrifugal collectors, mechanical collectors, collectors with stationary and moving fillings, and venturi scrubbers. Centrifugal collectors (cyclones) with sprinkled walls demonstrate the improvement of operation for additional supplies of dusted gas. Mechanical dust collectors are a diverse group of devices in which dust extraction is a result of rotation of plates, cylinders, etc. while atomized water is supplied to their interiors. Collectors with a stationary filling (e.g., in the form of Raschig's rings) are used to remove gas pollutants and operate mainly with the liquid atomized in the countercurrent direction. Collectors with a moving filling, so called fluidal scrubbers, operate on the principle of three-phase fluidization. Venturi scrubbers are a vast group of devices that operate well and have various means of water atomization.

Pollution propagation protection. Industrial activity involves many point sources of pollution that can be easily separated from the environment by using an atomized liquid. This also applies to public utilities, chemical processing plants,

20 LIQUID ATOMIZATION

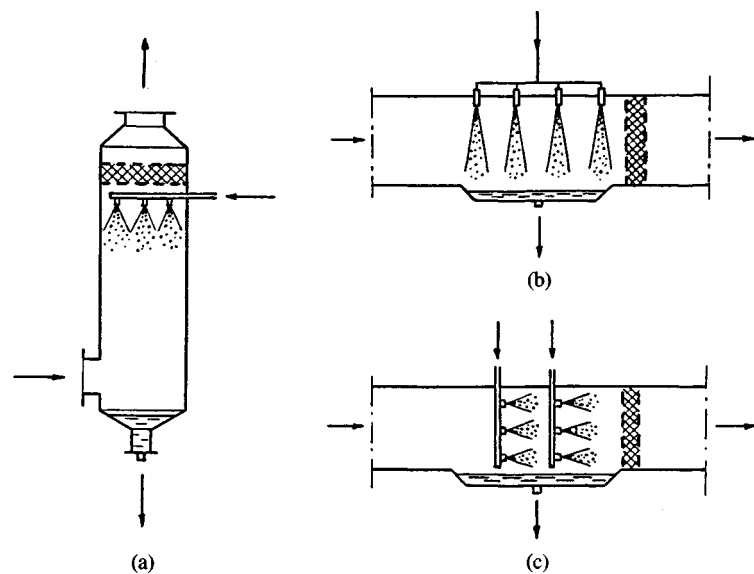


Figure 1-17 Spraying installation. (a) Countercurrent flow; (b) cross flow; (c) cocurrent flow.

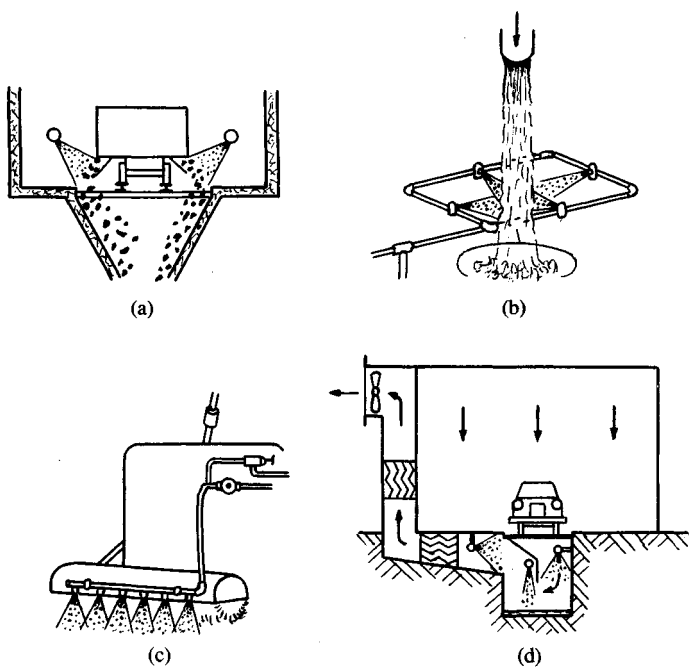


Figure 1-18 Protection against contamination. (a) Coal unloading; (b) pouring of the dust forming materials; (c) sweeping; (d) paint mist development.

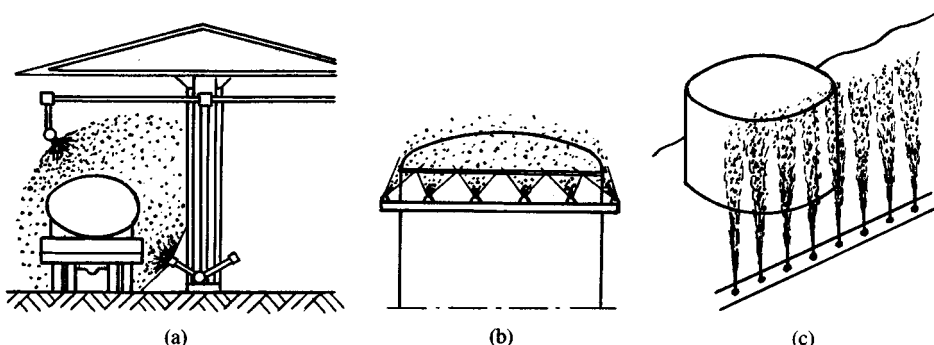


Figure 1-19 Fire protection. (a) Fuel transportation; (b) tank sprinkling; (c) water curtains.

lacquerers, and so forth. Schematic examples of protection against the propagation of pollution of this type are shown in Fig. 1-18.

Fire protection. In fire protection, systems of water nozzles located in places of potential fire hazards are most important (Fig. 1-19). Fire protection systems are used to protect property as well as the environment. Water nozzles should have a large discharge capability and large angles of spraying, which enables coverage of the whole protected area with a drop jet.

1-2.7 Various Applications

Atomized liquid is used in many other applications, which will be discussed briefly.

Air conditioning. The preparation of air for air-conditioning purposes includes its humidification, which takes place in a spraying chamber. The basic elements of the spraying chamber are water nozzles located in such a way as to ensure the best contact between the water and the flowing air. Simple swirl nozzles operating at a low water pressure (0.2 to 0.35 MPa) are used predominantly and provide drops with diameters of the order of hundreds of micrometers. Better atomization is not required because after the humidification the drops do not evaporate completely but fall into the bottom of the chamber.

Air conditioning is particularly important in the metallurgy, the textile industry, the electronics industry, and public utilities. Direct humidification of rooms is often achieved in the textile industry by using humidifiers with rotary atomizers. For direct humidification, very good atomization of a water mist type should be used so that the mist drops evaporate completely in a short time [21].

Health protection. Liquid atomization is used in the pharmaceutical industry in such processes as granulating powdered matter during the fabrication of tablets,

pills, and capsules; coating them with polymer solutions; and generating very fine emulsions of nonmixable liquids. The atomized liquids are also used directly in therapeutics as showers or in the form of aerosols (inhalations, administration of antibiotics, etc.) [19, 20]. Atomization of various disinfectant substances plays an important role in health protection.

Water treatment. Water treatment is done in closed aerators and is based on water atomization. This leads to the aeration of water, i.e., to the extraction of detrimental impurities. In the most simple cases the water treatment is performed in open or semiopen installations (e.g., showers or filter beds).

Food industry. Atomization of liquids is used to conserve food products; clean installations in breweries, sugar factories, distilleries, etc.; spray and coat food products (bakery products, candies, and others); and humidify cheese storage areas.

Other applications. The remaining applications are the following:

- Spatter humidification of loose materials during transport for explosion protection
- Water spraying for explosion protection in mines
- Humidification and painting of textiles
- Painting and spray plastering in the building industry
- Spraying of impregnating substances for wood conservation
- Water spraying for decorative purposes (fountains, showers)

1-3 LIQUIDS USED FOR ATOMIZATION PROCESSES

1-3.1 Types of Liquids

Among the atomized liquids fuels and water are predominant, but in principle almost all liquids with very diverse properties are atomized. The type of liquid strongly affects the processes of drop development.

Liquid fuels. Liquid fuels originate mainly from petroleum processing and are mixtures of three basic hydrocarbon groups (paraffins, naphthenes, aromatics). From the crude oil one obtains 40% petrol, 5% kerosene, 20% diesel oil, 25% heating oil, and 10% other products (lubricating oil, asphalt, and others).

Liquid fuels are still the major source of energy worldwide (Table 1-2). The highest demand is for diesel oil, and the demand for petrol is slightly increasing.

In industrial boilers, particularly in heating boilers, liquid fuels are mostly used. In power boilers liquid fuels have an auxiliary role with respect to coal fuels.

Table 1-2 Application of liquid fuels

Source of energy	Fuel
Burners	
Industrial boiler, heating boilers	Diesel oil, heating oil
Power boilers	Heating oil
Piston engines	
Diesel engines	Diesel oil, synthetic oil, hydrogenated oil
Spark ignition engines	Petrol, petrol-benzol, petrol-alcohol
Jet engines	
Aircraft engines (turbine engines, pulsejet engines, ramjet engines)	Kerosene (mainly paraffin), multifraction fuel
Other (ship engines, stationary engines)	Diesel oil, heating oil
Rocket engines	
Rocket engines using liquid fuels	Hydrocarbon fuels, alcohols and ethers, nitrogen compounds, amines, boranes, etc.

High-speed diesel engines use lighter fuel oils, and other diesel engines use other fuel oils including the heavy oils. These fuels should have short ignition delay (high cetane number).

In ramjet engines, according to the generally accepted opinion, a very large assortment of liquid fuels can be burned. These fuels do not have to satisfy particular requirements; only the aircraft fuels must have specific physical properties (freezing point, volatility, etc.).

In rocket engines burning liquid propellants, the liquid fuel and oxidizers are atomized. The liquid propellants for rocket engines are highly diverse in their chemical and physical properties.

In order to conserve liquid fuel and improve combustion conditions to reduce the emission of detrimental substances in combustion products, various emulsions and mixtures are being used. The advantages of using some of them in the power industry have been discussed in Sec. 1-2.1.

Water-in-oil emulsions, i.e., fuels based on heavy hydrocarbons, are liquids in which water (20–30%) is the dispersed phase. Every drop of the residual fuel oil and soft asphalts contains water particles, which are the source of a microexplosion of drops due to the different boiling points of water and oil. The exploded drops evaporate faster, which reduces the degree of oil thermal destruction and enables fuel and oxygen to intermix better. In effect, the conditions of combustion improve.

Solid-liquid fuels, also called coal-in-oil mixtures (COMs), are coal-oil fuels (oil-dust fuels) in which residual fuel oil is the liquid fuel. Those fuels have the following advantages:

Lower costs than liquid fuels

Utilization of low-grade coals

Increased emissivity because of the presence of solid particles

Utilization of coal with a high sulfur content, because the mixing yields fuels with an overall sulfur level lower than allowable standards

There are also some difficulties, including that of atomizing a suspension. Good intermixing of the suspension is required; otherwise the outlet orifice of the atomizer clogs very easily. It has been shown [33] that for a mass fraction of coal dust of approximately 30%, the diameter of the dust particles should not be larger than $150 \mu\text{m}$ and the atomization pressure not lower than 0.5 to 0.6 MPa. For a mass fraction of coal dust higher than 55% difficulties with ignition and stable combustion appear.

Coal-water slurries (CWSs) of fluid consistency can also be atomized and burned in the power industry [2]. Research on atomization of such slurries by using a pneumatic atomizer and by using compressed air with a maximum pressure of 1 MPa and mass fractions of air to fuel in the range 7–15% [18] has been conducted for several years.

Fuels with metal additives are used to raise the calorific value of the fuel. The powdered metals, such as magnesium or aluminum, must be in the form of a very fine powder (less than $1 \mu\text{m}$) to avoid sedimentation. Otherwise colloidal solutions form, which in the general case are the non-Newtonian liquids, and their viscosity increases 10^2 to 10^3 times [21].

Water. After fuels, the liquid that is most commonly atomized is water. In many cases the water requires not only good purification but also specific physical and chemical treatment. This refers to attemperation of overheated steam in boilers, and direct humidification of rooms, among other uses. There are also cases in which coarse purification is sufficient because it takes place in closed systems in gas scrubbing, spray cooling, and so forth.

Liquid pesticides. This vast group consists of liquid compounds used for spraying, watering, and seed disinfection. They occur in the form of water solutions, oil solutions, and water-oil solutions. The pesticides can be divided according to purpose as follows:

Pesticides, agents for pest control
Bactericides, agents for bacteria control
Fungicides, agents for fungus control
Herbicides, agents for weed control

The liquid agents have various concentrations, which affect their properties during spraying.

Non-Newtonian liquids. In most cases the liquid atomized in various processes in chemical engineering is nonhomogeneous, i.e., a mixture of liquids, chemical solutions, colloidal solutions, suspensions, and emulsions. These non-Newtonian

Table 1-3 Densities of various fuels (temperature 15 to 20°C, atmospheric pressure)

Type of fuel	Petrol	Kerosene	Diesel oil	Heating oil processed from		
				Petroleum	Shale	Coal
Density kgm ⁻³	680–776	790–830	830–880	918–990	980–1015	1200

liquids have very diverse rheological properties, i.e., properties manifested during flow.

1-3.2 Basic Properties of Liquids

Of all the properties of a liquid only three—density, viscosity, and surface tension—have an influence on the atomization process.

Liquid density. The density of a homogeneous liquid is defined as the ratio of the mass m to the volume V_m of the liquid under certain conditions (temperature, pressure):

$$\rho = \frac{m}{V_m} \quad (1-3)$$

The density ρ (kg/m³) is a unique characteristic of every liquid. This does not apply to hydrocarbon fuels, however, because their manufacture involves various raw materials and technological processes and also diverse additives to improve their service properties. Table 1-3 shows the density-range of various fuels.

As the temperature increases by $\Delta T = T_2 - T_1$, the density decreases from ρ_1 to ρ_2 .

$$\rho_2 = \frac{\rho_1}{1 + \alpha \Delta T} \quad (1-4)$$

where α is the coefficient of volumetric expansion; one should use the mean value of α in the temperature range ΔT because the coefficient α increases slightly as temperature increases. The values of α for some liquids are presented in Table 1-4.

The influence of pressure on the density of a liquid can be neglected because of the very small compressibility of liquids.

Table 1-4 Coefficients of volumetric expansion α for some liquids (20°C)

Type of liquid	Water	Alcohol	Glycerine	Kerosene	Petroleum
$\alpha \times 10^4 \text{ K}^{-1}$	2.1	11.0	4.7	10.4	9.2 to 10.0

In the fuel systems of diesel engines, in which pressures of the order of tens of MPa are present, one must take into consideration the change in density of the injected fuel charge due to pressure change. For a pressure increase of ΔP , the liquid density increases from ρ_1 to ρ_2

$$\rho_2 = \frac{\rho_1}{1 - \beta \Delta P} \quad (1-5)$$

where $\beta = 1/E$ = coefficient of compressibility (MPa^{-1})

E = modulus of elasticity of the liquid (MPa)

For a given liquid, β depends on the pressure and temperature. Figure 1-20 shows the dependence of β on the pressure for several fuels. As can be seen, β is smaller for fuels of higher density and decreases as the pressure decreases. The character of the change of β is not the same for different fuels, which indicates that Hooke's law does not apply to fuels. For fuels with a high density ($\rho > 0.84 \text{ kg/m}^3$) the change in β is small. For calculations for a diesel oil use $\beta = 0.625 \times 10^{-3} \text{ MPa}^{-1}$, i.e., $E = 1600 \text{ MPa}$, which is marked on Fig. 1-20 with a dashed line.

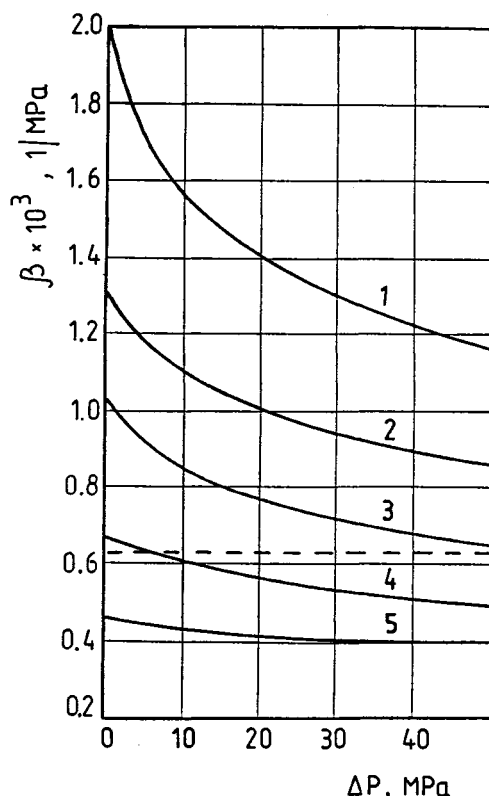


Figure 1-20 Compressibility coefficient β for fuels as a function of pressure increase ΔP (temperature 20°C). 1, Petrol; 2, kerosene; 3, 4, diesel fuels; 5, heating oil from coal [21].

The coefficient β increases (modulus E decreases) as the temperature increases. The relationship between modulus E and pressure P and temperature for fuels can be expressed by an empirical equation [21]:

$$E = E_0 + 93.75P - 0.0625P^2 \quad (1-6)$$

where E_0 = modulus of elasticity of the fuel for the atmospheric pressure and given temperature (MPa^{-1})

P = pressure of the fuel (MPa)

Equation (1-6) gives a relative error of approximately 5% and is convenient for numerical calculations.

If the liquid constitutes a two-phase mixture, in which the continuous phase is a liquid of density ρ_1 and the dispersed phase is in the form of liquid or a solid of density ρ_2 , then the density of the mixture, ρ , is given by [22]

$$\rho = (1 - c_v)\rho_1 + c_v\rho_2 = \epsilon\rho_1 + (1 - \epsilon)\rho_2 \quad (1-7)$$

or

$$\frac{1}{\rho} = \frac{1 - c_m}{\rho_1} + \frac{c_m}{\rho_2} \quad (1-8)$$

where c_v, c_m = volumetric and mass fractions of the dispersed phase

$\epsilon = 1 - c_v$ = porosity

Equation (1.7) expresses the additive law of the density of the components and Eq. (1.8) the additive law of the specific volumes of the components (the specific volume is the reciprocal of the density).

Liquid viscosity. Liquid viscosity is a complex subject. The viscosity of a *homogeneous liquid* depends on the properties of the liquid only in the range of laminar flow; in the range of turbulent flow it depends on the motion of the liquid. For laminar flow *Newton's formula* holds, which says that the shear stress τ is proportional to the increase of the velocity in the direction normal to the flow direction (velocity gradient), dV/dy :

$$\tau = \mu \frac{dV}{dy} \quad (1-9)$$

where μ is the *dynamic viscosity*. Liquids that satisfy this condition are called *Newtonian liquids*. The *kinematic viscosity* ν , which combines two properties of the liquid, viscosity and density, is often used:

$$\nu = \frac{\mu}{\rho} \quad (1-10)$$

The standard unit of dynamic viscosity is $\text{Pa} \cdot \text{s}$ ($\text{kgm}^{-1}\text{s}^{-1}$), and of kinematic viscosity m^2s^{-1} .

Viscosity decreases as temperature increases. There are many formulas that describe the influence of temperature on the viscosity for various liquids. Their suitability, however, is low, and therefore information about the viscosity of

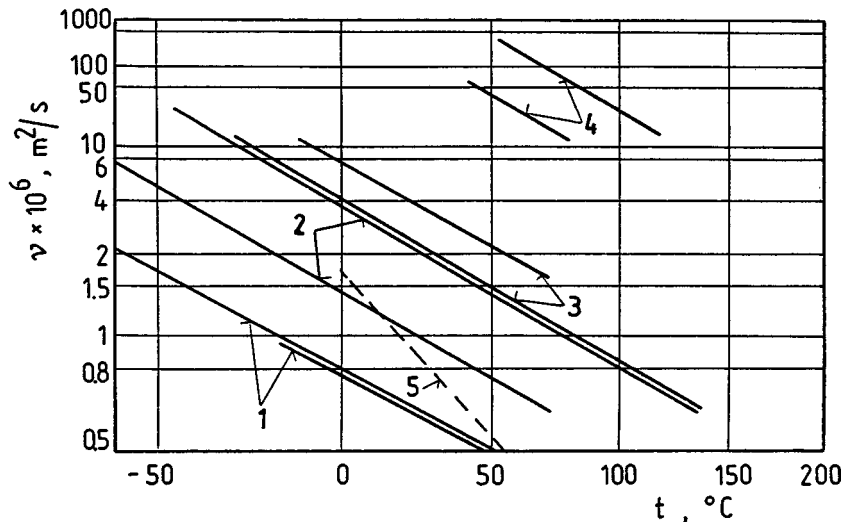


Figure 1-21 Dependence of the viscosity of water and fuels on temperature. 1, Petrol; 2, kerosene; 3, diesel fuel; 4, heating oil; 5, water [21].

liquids is derived from experimental data. Figure 1-21 shows the relationship between kinematic density and temperature for hydro-carbon fuels and water. In the logarithmic coordinate system the character of the viscosity is linear and the lines representing fuels have almost the same slope. In this case, one has to know only the viscosity of the fuel for one temperature in order to obtain the viscosity for different temperatures on the straight line passing through this point.

With some exceptions, an increase in pressure, causes an increase in liquid viscosity. The effect of pressure is very small and must be considered only in the case of fuel injection in diesel engines.

Nonhomogeneous liquids with a low concentration of the dispersed phase are treated as Newtonian liquids. For higher concentrations, all mixtures (emulsions, suspensions, etc.) have the characteristics of non-Newtonian liquids. It is not possible to calculate the viscosity from the viscosities of the mixture's components because the additive law does not apply to the viscosity of a mixture. There are some rheological models that can be used for three basic non-Newtonian liquids: rheo-stable liquids, rheo-unstable liquids, and viscoelastic liquids [13].

For the most frequently occurring rheo-stable liquids, of which the Newtonian liquid is a special case, the *apparent viscosity* μ' is expressed in the same way as the dynamic (absolute) viscosity μ in Eq. (1-9):

$$\mu' = \frac{\tau}{\dot{\gamma}} \neq \text{const} \quad (1-11)$$

where $\dot{\gamma}$ denotes the velocity gradient (shear velocity), $\dot{\gamma} = dV/dy$. The apparent viscosity μ' is not a proportionality coefficient as viscosity μ is. Hence, the flow curve $\tau = f(\dot{\gamma})$ is not a straight line passing through the origin of the τ - $\dot{\gamma}$ coordinate system, as it is in the case of Newtonian liquids.

Viscosity data for nonhomogeneous liquids are obtained experimentally. Figure 1-22 shows the viscosity of an emulsion of heating oil (continuous phase) with water (dispersed phase) [21]. The mass fraction of water in the emulsion is 10 to 60%, and the size of water drops is 5–10 μm to 50 μm , respectively. The water viscosity in the given temperature range was 0.556×10^{-6} to 0.328×10^{-6} m^2/s (on the scale of the figure it is a horizontal line). As seen, the viscosity of the emulsion is significantly higher than the viscosities of the individual component, increases—instead of decreasing—with an increase in the fraction of a component with low viscosity (water), and decreases as the temperature increases. It must be emphasized that the results depend strongly on the state of

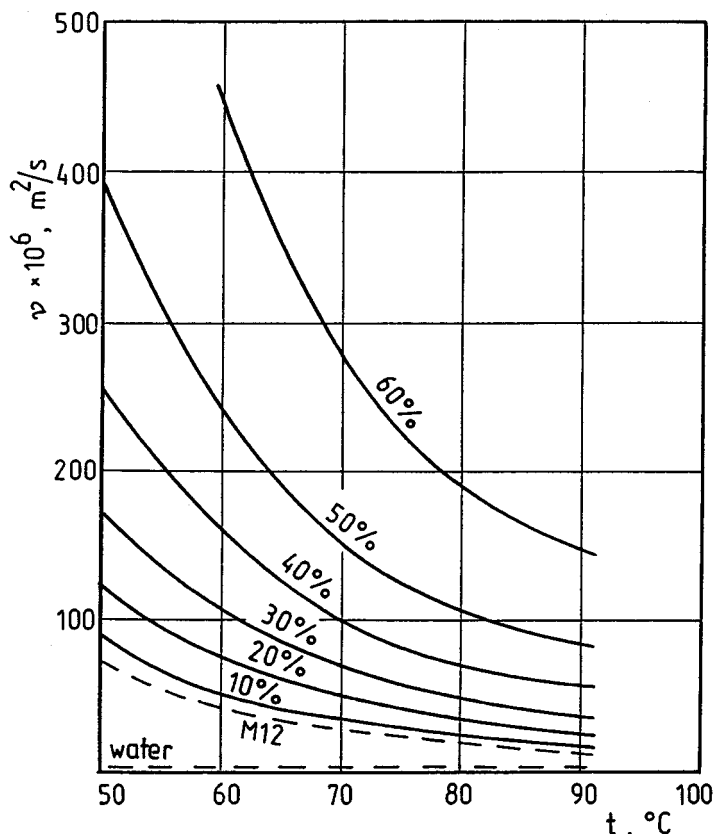


Figure 1-22 Viscosity of a heating oil-water emulsion (M-12); oil density (temperature 0°C) $\rho = 936.4 \text{ kg/m}^3$ [21].

the dispersion, i.e., on the dimension of the dispersed phase and the degree of intermixing.

Some empirical equations can be used to calculate the viscosity of emulsions, but they give very divergent results. Most useful is the equation [22]

$$\mu_e = \mu \exp(kc_v) \quad (1-12)$$

where μ = dynamic viscosity of the emulsion and continuous phase, respectively

k = constant,

c_v = volumetric fraction of the dispersed phase in the emulsion

The results derived from Eq. (1-12) for $k = 3.5\text{--}3.6$ are most consistent with the experimental data in Fig. 1-22; for the water-in-oil emulsion $k < 5$ [21].

For non-Newtonian mixtures of the water-solid phase type and for high velocity gradients one can also use Eq. (1-12). The constant k can be determined from the properties of the particles of the solid phase. Values of k are higher for small particles than for big ones, because small particles coagulate and the forces of interaction increase the viscosity. For a suspension of particles in water one can use Thomas's equation [21].

$$k = 2.5 + \frac{14}{\sqrt{d}} \varphi \quad (1-13)$$

where d = particle diameter (μm)

φ = shape factor, i.e., the ratio of the particle surface to the surface of a sphere with the same volume (for spherical particles $\varphi = 1$)

The viscosity of the solid-liquid fuels mentioned in Sec. 1-3.1 depends mainly on the grain sizes and on the fraction of coal in residual oil. For mass fractions of the dust higher than 40%, the density of the fuel increases 15 to 30 times in proportion to the viscosity of residual oil [31].

Surface tension. The surface tension σ (J/m^2) on the interface between the solid and gaseous phases is equal

$$\sigma = \frac{dE_A}{dA} \quad (1-14)$$

where dE_A (J) is the surface energy, i.e., the energy used to increase the liquid surface by dA . This definition is synonymous with the definition of the surface tension σ (N/m) as a force F acting on a unit length of the free surface of the liquid, where the force is tangential to the surface and simultaneously perpendicular to the segment l .

$$\sigma = \frac{F}{l} \quad (1-15)$$

Every system tends to achieve such a state, which corresponds to the minimum free energy. Because the minimum surface energy corresponds to the

spherical shape of the liquid, the disintegrated liquid forms spheroidal drops. Inside the drop the excess pressure ΔP is higher the lower the radius R of the drop. For a spherical drop,

$$dE_A = 4\pi R^2 \Delta P dR$$

$$A = 4\pi R^2$$

$$dA = 8\pi R dR$$

Therefore from Eq. (1-14)

$$\sigma = \frac{\Delta PR}{2} \quad (1-16)$$

For water with the surface tension $\sigma = 73 \times 10^{-3}$ N/m, the excess pressure inside a drop of diameter $D = 50 \mu\text{m}$ is given by

$$\Delta P = \frac{2\sigma}{R} = \frac{4\sigma}{D} = \frac{4 \times 73 \times 10^{-3}}{5 \times 10^{-5}} = 5840 \text{ Pa}$$

The surface tension decreases as the temperature of the liquid increases, which facilitates the disintegration and evaporation of drops. The dependence of σ on the temperature for various fuels is shown in Fig. 1-23.

In the case of mixtures, the problem of surface tension is very complex. In general, the surface tension depends on the type of mixture and the concentrations of its components. Measurements show that higher concentrations of chemical agents in water used for plant spraying significantly reduce the surface tension, even over 50% in comparison with pure water. This is typical for surfactants. For example, a fraction of 0.04 g/L of Rokafenol N8 reduced the surface tension of water from 72.9×10^{-3} to 32.7×10^{-3} N/m, approximately by 55% [16].

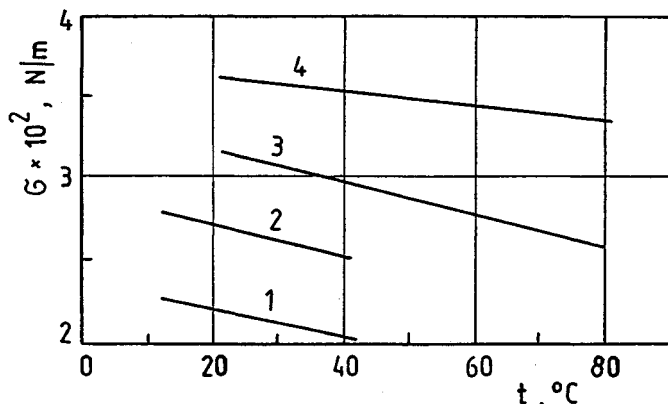


Figure 1-23 Surface tension σ for fuels as a function of temperature. 1, Petrol; 2, kerosene; 3, diesel fuel; 4, heating oil from coal.

1-3.3 Influence of Liquid Properties on Atomization Conditions

As mentioned, atomization conditions depend on the following properties of the liquid: density, viscosity, and surface tension. However, the influence of these properties is distinct only when the atomization proceeds with small velocities or in a vacuum. Under normal atomization conditions the ambient medium has a significant influence (see Sec. 2-2).

For the liquids generally used, the influence of the three liquid properties on the drop size can be estimated as follows:

Liquids with higher density have higher kinetic energy and consequently smaller drops develop.

Liquids with higher viscosity generate larger drops.

Liquids with higher surface tension disintegrate into drops with larger diameters.

These generalizations require more elaborate discussion.

The influence of liquid density on atomization conditions is least distinct, because atomized liquids do not show large density differences. For liquids with significantly different densities this influence is noticeable. Figure 1-24 depicts the operation of a fan atomizer, which generates a flat sheet suitable for observation. As can be seen, mercury, which has very high density and very high surface tension, behaves in a completely different way than liquid sodium and petroleum gel, which have significantly lower density. Liquid sodium, which has a high surface tension, disintegrates right after it leaves the atomizer, whereas petroleum gel, which has a low surface tension and very high viscosity, disintegrates relatively easily but creates durable threads of liquid. The analysis of the influence of density on atomization conditions is hindered by the fact that the other properties of the evaluated liquids are not comparable.

The influence of liquid viscosity on atomization conditions is clearly seen in Fig. 1-25, because the liquids have different viscosities. A jet atomizer was used for this investigation, and the atomization took place under the same conditions. As can be seen, the jet of petrol was atomized but the jet of lubricating oil did not disintegrate at all. Therefore, for low viscosities the influence of viscosity on

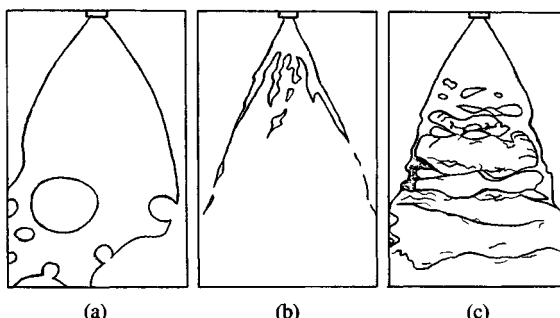


Figure 1-24 Influence of the type of liquid on sheet disintegration. (a) Mercury; (b) liquid sodium; (c) petroleum gel [21].

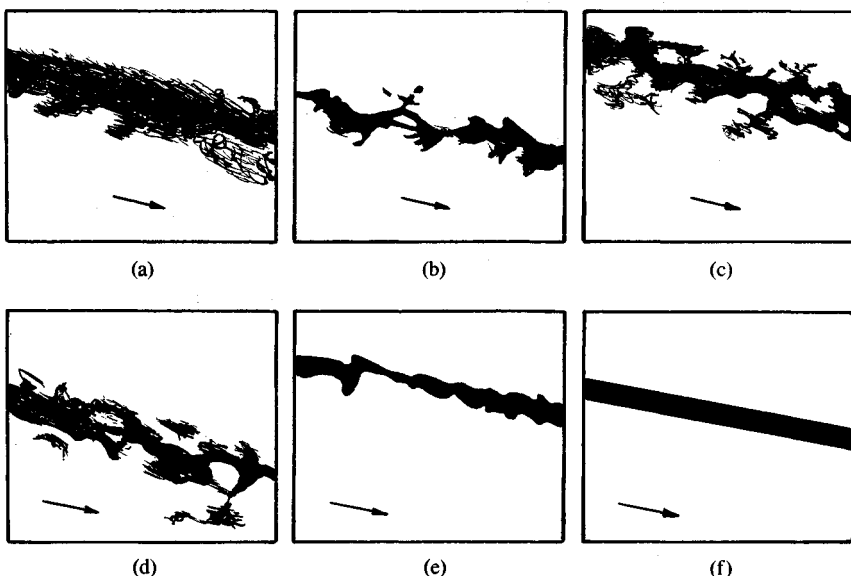


Figure 1-25 Disintegration of jets of various liquids. (a) Petrol; (b) water; (c) ethanol; (d) light diesel fuel; (e) heavy diesel fuel; (f) lube oil. Diameter of the discharge orifice, 0.5 mm; liquid pressure, 10.3 MPa; ambient pressure, 0.1 MPa; distance from nozzle, 127 mm [10].

atomization conditions is insignificant, but for higher viscosities it starts to increase rapidly.

High viscosity hinders atomization and requires that special means be employed. Table 1-5 shows experimental data on the allowable maximal viscosity of fuels used in various installations. Comparison of the data in Table 1-5 and Fig. 1-21 indicates that for correct atomization the fuel must be preheated, sometimes even to the high temperatures of 90 to 130°C. However, this is not always successful, and a heavy fuel is defined as one whose viscosity cannot be decreased lower than 40×10^{-6} m²/s by preheating [21].

Table 1-5 Maximum kinematic viscosities of liquids that enable proper atomization

Installation	Type of atomizer	Maximum viscosity, 10^{-6} m ² /s
Boiler burners	Swirl	12–25
	Pneumatic	115
Piston traction engines	Jet	3.5–23
Gas turbines		
Stationary	Swirl	10–25
Aircraft	Swirl	10–15

The results of an investigation of the improvement of atomization by fuel preheating have been presented in [14]. For very viscous diesel oils the following relationship was obtained:

$$\frac{D_1}{D_2} = \left(\frac{\nu_1}{\nu_2} \right)^n \quad (1-17)$$

where D_1 = mean drop diameter corresponding to the kinematic viscosity of the preheated fuel, ν_1

D_2 = known mean drop diameter corresponding to the kinematic viscosity of the fuel, ν_2

$n = 1.444$ to 1.54 is an exponent whose mean value is 1.5

Another way to overcome the difficulties caused by high liquid viscosity is to use the kinetic energy of the gas in pneumatic atomizers. During the atomization of a very viscous liquid (malt syrup) with dynamic viscosity $2 \text{ Pa} \cdot \text{s}$ (approximate kinematic viscosity $1300 \times 10^{-6} \text{ m}^2/\text{s}$)—one order of magnitude higher than the values in Table 1-5—drop diameters lower than $100 \mu\text{m}$ were obtained for a ratio of mass discharges of the air and the liquid of $G_G/G_L = 1.0$ [28].

The influence of surface tension on atomization conditions has not been explored much. Consideration of slow disintegration of the liquid into drops leads to the conclusion that low surface tension should facilitate this disintegration. The data on this subject, for actual atomization conditions, are divergent or even contradictory. For example, the relationship between the drop diameter D and the surface tension σ during the atomization of water is expressed as $D \sim \sigma^{0.1}$ according to one set of data and $D \sim \sigma^{-0.11}$ for another set of data [16]. On the basis of their own research, the same authors [16] demonstrated that even doubling the surface tension (while keeping the density and viscosity of the liquid constant) does not have any influence on the size spectrum of the drops for discharge velocities of several hundreds of meters per second or more.

However, surface tension has a distinct influence on the degree of covering of crops being sprayed. Chemical agents with low surface tension have a small angle of contact, which causes them to spread better on the plant surface (they create larger traces of drops) and therefore produce a higher degree of coating of the sprayed surfaces. The lower the surface tension of the liquid, the higher the retention of the drops on the leaf surface.

Finally, it is worth discussing briefly the influence of polymer additives on atomization conditions. The atomization of aircraft fuels, toluene, and water with the addition of 12 polymers, including polyisobutylene, polyethylene oxide, and polyacrylamide, at mass concentrations of 50 to 3000 ppm has been investigated [6]. However, the mechanism of functioning of the polymer additives is not sufficiently understood; it is certain that increasing the concentration causes the small drops to decay and leads to the formation of large drops, which are distorted into the form of one or many thin, long fibers.

Figure 1-26 shows the pneumatic atomization of fuel with added polymer. The pure fuel is atomized into completely invisible drops (with diameters less

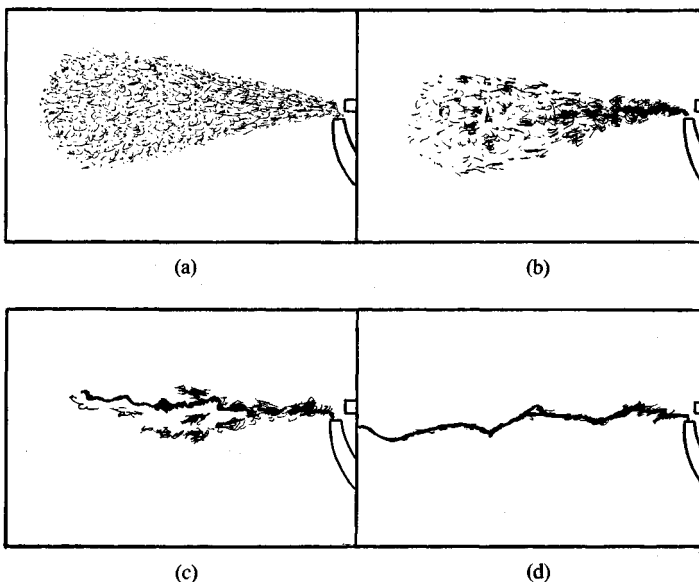


Figure 1-26 Change of the structure of the Jet—A fuel type sprayed at $0.33 \text{ cm}^3/\text{s}$ by an air jet with a velocity of 67 m/s for various concentrations of Oppanol B 200 polymer. (a) No polymer. (b) 50 ppm. (c) 1000 ppm. (d) 3000 ppm.

than $50 \mu\text{m}$), whereas after the addition of polymer the liquid discharges in the form of a compact jet. As mentioned in Sec. 1-2.3, this fact is utilized to reduce the ignitability of fuels during emergency landings in aviation.

REFERENCES

1. Adamovich, K., Orzechowski, Z. Design of a pneumatic atomizer for steam cooling. *Teploenergetika*, No. 1, 1978 (in Russian).
2. Andreussi, P., Tognetti, L., Graziado, M., Morelli, F. Preliminary investigation on CWS-air flow within a twin fluid atomizer. Proceedings of the Two Day Meeting on Sprays and Their Applications, Milan, Italy, 1986.
3. Antkowiak, W., Heim, A. An evaluation of spraying characteristics of a pneumatic nozzle applied for wetting of granulated dust. *Chem. Process Eng.*, Vol. 8, No. 1, 1987 (in Polish).
4. Bednarek, K. Methodology of evaluation of the influence of selected parameters of oil mist on oil film development on active face of a tooth in a gear. Ph.D. thesis, Academy of Mining and Metallurgy, Crakow, Poland, 1980 (in Polish).
5. Berger, H. L. Characterization of a class of widely applicable ultrasonic nozzles. *Proc. ICCLASS-85*, London, IA/2/1-13, 1985.
6. Chao, K. K., Child, C. A., Grens, E. A. II, Williams, M. C. Antimisting action of polymeric additives in jet fuels. *AICHE J.*, Vol. 30, No. 1, 1984.
7. Courshee, R. J. Droplet size and biological efficiency of pesticides. *Proc. ICCLASS-85*, London, IP/2/1-15, 1985.

36 LIQUID ATOMIZATION

8. Eisenklam P. Atomization of liquid fuel for combustion. *J. Inst. Fuel*, Vol. 34, No. 243, April 1961.
9. Galustov, V. S., Fedder, I. E. A model of processes of water treatment in straight-through sprayers. *Teploenergetika*, No. 5, 1986 (in Russian).
10. Giffen, E., Muraszew, A. *The Atomization of Liquid Fuels*. Chapman & Hall, London, 1953.
11. Kasperski, K., Biasi, L. The application of an air/mist cooling to continuous castings. Proceedings of the Two Day Meeting on Sprays and Their Applications, Milan, Italy, 1986.
12. Keller, V. W., Anderson, B. J., Burns, R. A., Lala, G. G., Meyer, M. B. Large volume water sprays for dispersing warm fogs, Proceedings of the ICLASS-85, London, 1985, LP/VIIC/4/1-10.
13. Kemblowski, Z. *Rheometry of Non-Newtonian Fluids*. WNT, Warsaw, 1973 (in Polish).
14. Kutovoi, V. A. *Fuel Injection in Diesel Engines*. Mashinostroenie, Moscow, 1981 (in Russian).
15. Masters, K. *Spray Drying Handbook*. George Godwin, London, 1985.
16. Melaniuk, M., Orzechowski, Z. The influence of surface tension on liquid atomization. *Eng. Trans.*, Vol. 26, No. 1, pp. 41-50, 1978.
17. Meyer, P. L., Chigier, N. Characterization of the atomization process in coal-water slurry sprays. *Proc. ICLASS-85*, London, IV (b)/1/1-23, 1985.
18. De Michele, G., Graziadio, M., Morelli, F., Tognotti, L. Atomization of some commercial coal-water slurries. Proceedings of the Two Day Meeting on Sprays and Their Applications. Milan, Italy, 1986.
19. Moren, F., Hathaway, D. Characterization of particle size from pressurized aerosols intended for oral inhalation. *Proc. ICLASS-85*, London, IIIB/1/1-6, 1985.
20. Newman, S. P., Pellow, P. G. D., Clay, M. M., Clarke, S. W. Output, droplet size and administration time of hypertonic saline aerosol from four brands of jet nebuliser. *Proc. ICLASS-85*, London, IIIB/3/1-10, 1985.
21. Orzechowski, Z. *Liquid Atomization*. WNT, Warsaw, 1976 (in Polish).
22. Orzechowski, Z. *Two-Phase Flow*. PWN, Warsaw, 1990 (in Polish).
23. Petela, R. Exergetic analysis of atomization process of liquid. *Fuel*, Vol. 63, March, 1984.
24. Roylance, T. F., Pickering, S. J., Hay, N., Thomas, G. H. A rotary cup air blast atomizer for molten slag—an investigation of particle size and spray trajectory. *Proc. ICLASS-85*, London, LP/VB/2/1-16, 1985.
25. See, J. B., Johnston, G. H. Interactions between nitrogen jets and liquid lead and tin streams. *Powder Technol.*, Vol. 21, pp. 119-133, 1978.
26. Smith, N. P., Norris, J. O. W., Hemsley, D. J., Yeoman, M. L. Measurement of the size and velocity of liquid metal drops during atomization. *Proc. ICLASS-85*, London, LP/IVB(b)/1/1-9, 1985.
27. Szydlo, Z. Investigation of the influence of stream velocity of oil mist on precipitation of oil drops in conduits with a circular cross section. Ph.D. thesis, Academy of Mining and Metallurgy, Krakow, 1984 (in Polish).
28. Tanno, S., Miura, T., Ohtani, S. Atomization of high viscosity liquid by pneumatic nozzle. *Proc. ICLASS-85*, London, LP/VB/6/1-8, 1985.
29. Tumanovskii, A. G., Tul'skii, V. F. The influence of water injection on the formation of the nitrogen oxides behind the combustion chamber with a successive air supply into the combustion zone. *Teploenergetika*, No. 6, 1982 (in Russian).
30. Warych, J. *Gas Scrubbing*. WNT, Warsaw, 1979 (in Polish).
31. Wilk, R., Zajdel, A. Investigation of the application of oil-dust mixtures for firing a boiler OP-215 type. Scientific Transactions of Silesian Polytechnic, Power Engineering, Gliwice, Poland, No. 94, 1986 (in Polish).
32. Zablocki, M. Injection and combustion of fuel in diesel engines. Transportation and Communication Publications, Warsaw, 1976 (in Polish).
33. Zajdel, A. Investigation of dust-liquid fuel. Ph.D. thesis, Silesian Polytechnic, Gliwice, Poland, 1979 (in Polish).

THEORETICAL BASIS OF THE PROCESS OF ATOMIZATION

2-1 THEORY OF DISINTEGRATION OF JETS, SHEETS, AND DROPS

The process of atomization is one in which liquid is disintegrated into drops by the acting forces. It proceeds more easily if the liquid is present in a form that is more susceptible to disintegration. The most susceptible forms are thin jets or sheets of liquid, because they have the highest surface energy and thus the greatest instability. It follows that atomizers must first develop jets or sheets of liquid.

The literature on the *theory of liquid disintegration* is fairly extensive, but it deals with low-velocity discharge of liquid from atomizers, which is not very important in practice. Up to now there is no theory for disintegration at a high velocity of liquid discharge; therefore an answer does not exist to the fundamental question—what spectrum of drop diameters can be obtained under given conditions? This is due to the highly complex flow phenomena occurring during disintegration as well as due to the vast diversity of atomizers.

Some phenomena, however, are common and crucial for the process of atomization. These phenomena are the development of waves on a liquid surface, the increase in their amplitude, and the loss of stability. Waves form on the surfaces of the jets and sheets of liquid as well as on the surfaces of drops moving in the gaseous medium. The disintegration of the liquid is caused by

these waves, whose amplitudes grow rapidly. Such a process can easily be observed for low velocities of liquid motion.

The theoretical work that has been reported is based mainly on investigating instability by means of the *method of small disturbances*. This method, which is widely applied in fluid mechanics, is based on analysis of the superposition of the arbitrary small vibrations and the main fluid motion. These vibrations, which have various frequencies, are of internal or external origin.

The *internal causes* stem from disturbances in the atomizer itself and originate from liquid swirling, liquid expansion due to pressure drop, vibration of the atomizer (especially vibrations of intermittent atomizers due to the motion of the needle), disturbances of the liquid motion on the edges of the inlet and outlet orifices and on any type of rough surfaces, and so forth. The *external causes* result from interaction with the surrounding media, that is, from the reaction of aerodynamic forces, which depend on the relative velocity of the liquid and the ambient gas, the density of the gas, and the dimensions of liquid leaving the nozzle. The problem can be solved by inserting the values of velocities and pressure switch infinitesimal increments into differential equations of hydrodynamics. After linearization and integration, one obtains a system of equations that can be used to evaluate the frequencies for which there is an especially large increase in the amplitude of the vibrations that leads to disintegration of the liquid into drops. The first solution to this problem was given by Rayleigh as early as 1878–1879. He considered the vibrations and breakup of a cylindrical jet of nonviscous liquid in a vacuum, including only the forces of surface tension. The results obtained can be confirmed experimentally for low velocities of discharge from orifices (laminar flow). In his later work, Rayleigh took into consideration the viscosity of the liquid and demonstrated its influence on the disturbance growth rate. The method of small disturbances was also employed by Rayleigh to analyze the stability and breakup of a stationary drop of an ideal liquid in a vacuum.

Rayleigh's theory was extended by C. Weber, who in addition considered the effect of aerodynamic forces acting on the liquid jet. A. S. Lyshevskii [29] and Yu F. Dityakin, L. A. Klyachko, V. I. Yagodkin and V. A. Borodin [10] investigated the effect of the velocity and density of the ambient gas and the viscosity of the liquid on the stability and breakup of a cylindrical liquid jet.

Such considerations regarding the disintegration of jets are valid when the disturbances are small (15% for example) compared to the jet radius. However, the amplitude of disturbances during disintegration is of the same order as the jet radius. The problem is therefore difficult and requires solving nonlinear equations or implementing other methods.

The disintegration of a liquid jet caused by axisymmetric waves has been investigated theoretically and experimentally [46]. Nonlinear equations were employed in order to calculate the volume of the large drops and satellite droplets. Good agreement between the theoretical and experimental results was obtained, except that satellites developed in all experiments, whereas according to the theory they should not develop for wave numbers $k > 0.7$.

Other work [36] was devoted to evaluating the nonlinear stage of development of instability of a viscous liquid jet in conditions that allow the effect of surrounding media to be neglected; the results were in agreement with experimental data. The nonlinear aspects of jet disintegration were also investigated by D. P. Wang, Juen Man Chuen, P. Lafrance, K. C. Chaudhary and L. G. Redekopp [15]. Among other work, Sato and Saito [48] has to be mentioned.

The problem of the development and interaction of nonlinear, two-dimensional disturbances in a swirling thin liquid jet has been explored [15]. Attention was directed to evaluating the nonhomogeneous jet disintegration taking into account the effect of an assisting air jet and the effect of swirling. The solution was derived by using the Galerkin method.

The stability and disintegration of a sheet of nonviscous liquid has been investigated by J. York, H. Stubbs and M. Tek [38]. The problem of the disintegration of liquid sheets has also been considered by other authors, among them Borodin et al. [10], who dealt with the stability and disintegration of a cylindrical sheet of ideal liquid in a motionless environment.

The works cited contributed to recognition of the mechanisms of disintegration of liquids into drops. They refer, however, to small discharge velocities from the atomizer and therefore are of little practical importance. Under real conditions, for high discharge velocities, the disintegration is due to waves whose wavelengths are significantly shorter than those for low discharge velocities.

Another direction of theoretical research on liquid disintegration is based on the assumption that the disintegration proceeds in the vicinity of the outlet orifice and is due only to the turbulent pulsations that develop in the atomizer. For high turbulence, liquid disintegration can also proceed through the separation of single drops or groups of drops, liquid threads, etc. from the surface of the liquid.

Another view is that the liquid disintegration is due to cavitation. For high discharge velocities, the pressure of the liquid drops to the value of the vapor pressure, causing rapid evaporation of the liquid. This refers particularly to liquids with high volatility or those preheated to a high temperature. Experiments that could confirm this theory are, however, difficult to conduct.

As seen, theoretical description of the disintegration of jets and sheets is difficult even for the simplest methods of atomization. For more complex methods of atomization, with rotary atomizers and particularly pneumatic atomizers, the degree of difficulty is even higher. In pneumatic atomizers, due to the flow of the gas, waves develop on the surface of the liquid, gradually grow, and cause separation of the drops. The waves are of a capillary character because the disintegration does not depend on the spatial position of the surface of the liquid-gas separation. The theory of this disintegration is presented in [37].

The theories of the disintegration of a liquid into drops basically concern Newtonian liquids. In the case of the non-Newtonian liquids, experimental research dominates. Of the theoretical work on this subject, [24] is noteworthy.

Atomization often proceeds under unsteady conditions. Such conditions occur in combustion chambers with a high thermal load, where the turbulent

pulsations of pressure can reach up to 5% of the pressure in the chamber. The forced or free pulsations in the frequency range from tens to several thousands of hertz cause very significant changes of the atomization quality. There are few works on this subject, and the most significant among them are those by Bazarov [4].

The theory of atomization is not limited to the disintegration of jets and sheets into drops but also comprises the disintegration of drops into smaller droplets—so-called secondary drop disintegration—which proceed in the flow of the gas. Attempts have been made to determine the diameter of a stable drop, which is derived from the critical Weber number We^* , by evaluating the equilibrium condition of the surface tension and the aerodynamic force acting on the drop. It is difficult to derive the proper solution because the severe deformations of the drop make it impossible to determine the drop drag coefficient.

The majority of works on secondary drop disintegration refer to the method of small disturbances. The critical Weber number We^* was calculated under the assumption that drop deformation is symmetrical with respect to the flow direction and the distribution of normal and shear stresses does not change during the deformation. Lyshevskii [29] assumed a simplified pressure distribution in the gas flow around the drop; other authors have investigated various forms of disturbances on the drop surface. The linearization of the equations made it possible to establish that the drop spreads in the transverse direction and assumes the shape of a spheroid [54].

It is difficult to calculate We^* by the method of small disturbances because the undisturbed motion of the drop and gas is transient. The transient motion of the drop has been calculated by solving Navier-Stokes equations by the method of small parameters [21]. Voronin [55], applying the method of small disturbances, obtained equations describing the drop dynamics in a jet of noncompressible gas and as a result determined the stability criteria, time of drop collapse, and critical value $We^* = 10.4$.

Spalding [50] and other authors point out the feasibility of applying numerical fluid mechanics to the process of fluid atomization. At present, too many phenomena are not suitable for computer simulation; however, there are some phenomena that satisfy this requirement. Among them are the flow phenomena occurring inside pressure atomizers (diesel engines), swirl atomizers, and rotary atomizers and phenomena occurring on a small scale, such as two-drop or drop-wall collisions.

Taking into consideration the complexity of processes of liquid atomization, it is hard to expect that there will be significant progress in the development of the theory of atomization in the near future. Consequently, dimensionless analysis should still be used. This analysis yields many formulas expressing the relationship between various nondimensional criteria characterizing the properties of the atomizer, the liquid, and the conditions of atomization. Formulas for calculating mean drop diameters are the most important ones.

2-2 STABILITY AND DISINTEGRATION OF LIQUID JETS AND SHEETS

2-2.1 Stability and Disintegration of Liquid Jets

The character of liquid jet disintegration depends on the velocity of discharge from the nozzle (Fig. 2-1). Generally speaking, there are three characteristic forms of disintegration, caused by axisymmetric waves, asymmetric waves, and aerodynamic forces. These forms of disintegration apply to velocities of order 1, 10, and 100 m/s, respectively, and therefore to increasing influence of aerodynamic forces.

In disintegration of a liquid jet caused by axisymmetric waves (Fig. 2-1a), incidental internal perturbations cause narrow bands to develop in the jet. In narrow bands the pressure of the liquid, P_1 , is larger than in wider bands, which stems from the condition of equilibrium for pressure forces and surface tension forces:

$$d_1 l P_1 = 2l\sigma$$

$$d_2 l P_2 = 2l\sigma$$

hence:

$$P_1 = \frac{d_1}{d_2} P_2 \quad (2-1)$$

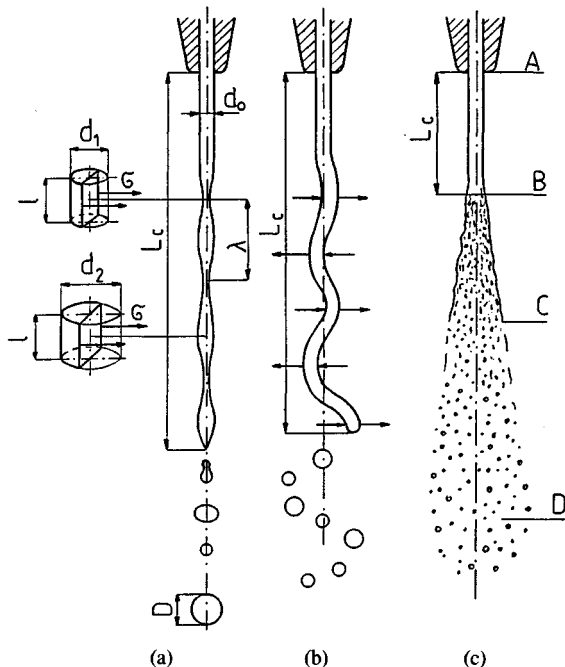


Figure 2-1 Disintegration of a cylindrical jet of liquid caused by (a) axisymmetric waves; (b) asymmetric waves; (c) aerodynamic forces.

or $P_1 > P_2$, since $d_1 < d_2$. The liquid is forced from the narrow bands to wider bands, leading to the development of drops. In this case the drops develop because of surface tension only. The volume of a drop of diameter D is equal to the volume of a jet segment of diameter d_0 and length λ .

$$\frac{\pi D^3}{6} = \frac{\pi d_0^2}{4} \lambda$$

The surface energy is a product of the surface tension and the surface area. The lower the surface energy (or the smaller the surface area), the more stable the system, which means that for a drop and for a jet segment we can write

$$\pi D^2 \sigma \leq \pi d_0 \lambda \sigma$$

From the foregoing equations,

$$D \geq 1.5d_0 \quad (2-2)$$

As mentioned in Sec. 2-1, the problem of disintegration of such a jet in a vacuum originally was solved by Raleigh, who obtained

$$D \geq 1.436d_0 \quad (2-3)$$

From Rayleigh's solution, it follows that the jet is unstable for disturbances whose wavelength is greater than the perimeter of the jet. The amplitudes of waves of length $\lambda_{\text{opt}} = 4.508d_0$ grow most rapidly. Using this wavelength in the calculations yields $D \approx 1.9d_0$.

The relationship derived by Rayleigh was extended by C. Weber, who obtained for a viscous liquid

$$\frac{D}{d_0} = 1.436 \left(1 + 3 \frac{\text{We}_L^{0.5}}{\text{Re}} \right)^{1/6} \quad (2-4)$$

where We_L is the Weber number

$$\text{We}_L = \frac{\rho_L V_L^2 d_0}{\sigma} \quad (2-5)$$

and Re the Reynolds number

$$\text{Re} = \frac{\rho_L V_L d_0}{\mu_L} \quad (2-6)$$

where V_L , ρ_L , and μ_L denote the velocity, density, and viscosity of the liquid, respectively. The expression $\text{We}_L^{0.5}/\text{Re}$ is known as the Ohnesorge number Z :

$$Z = \frac{\text{We}_L^{0.5}}{\text{Re}} = \frac{\mu_L}{(\rho_L \sigma d_0)^{0.5}} \quad (2-7)$$

For a nonviscous fluid, i.e., for $\mu_L = 0$, Eq. (2-4) assumes the form of Eq. (2-3). In reality, the drops have various diameters because they develop from segments of the jet with different constrictions. The influence of liquid viscosity is manifested by vibration dumping, which causes delay or lack of jet disintegration. An example of lack of disintegration is the behavior of jets of very viscous

liquids in the production of artificial fibers, mineral wool, glass wool, and so forth.

When the discharge velocity increases, the jet is acted upon by aerodynamic forces that cause distortions of its axis (Fig. 2-1b). These distortions increase constantly because of pressure forces caused by the environment, e.g., air acting on the jet. The directions of action of these forces are consistent with the directions of the arrows in Fig. 2-1b, since the air moving along the jet accelerates in the vicinity of convexities and decelerates in the vicinity of concavities in the jet. As a result, negative pressure develops in the convexities and overpressure develops in the concavities under the influence of *asymmetric waves*, and the jet disintegrates into smaller drops than are produced by axisymmetric waves. During the intensive action of the *aerodynamic forces* the jet disintegrates into relatively small drops; i.e., actual atomization takes place. It is not an immediate process, as seen in Fig. 2-1c, and one can distinguish three zones:

AB—compact jet zone

BC—disintegration zone

CD—drop zone

In the compact zone, vibrations develop. The length of the compact jet, L_c , decreases as the discharge velocity increases, but it never vanishes. The jet disintegration in zone BC proceeds because of waves with small lengths compared to the jet diameter. Such waves and crests of waves can be recorded by using high-speed photography. For very high velocities the liquid disintegrates almost immediately into small jets and consequently into drops before waves can develop.

The aerodynamic force also depends on the density of the ambient air, i.e., on the air pressure. Figure 2-2 depicts the action of ambient air of different

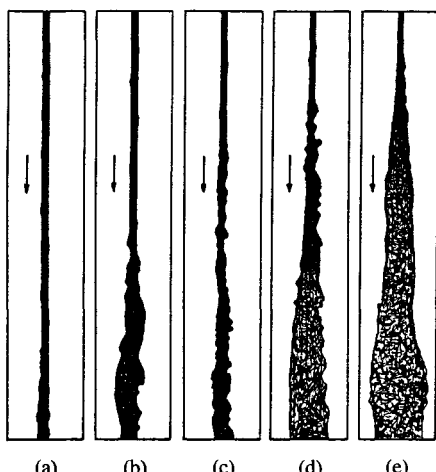


Figure 2-2 Effect of ambient air pressure on fuel jet disintegration: (a) 0.0013 MPa; (b) 0.1 MPa; (c) 0.44 MPa; (d) 0.78 MPa; (e) 1.45 MPa. Outlet orifice diameter, 0.5 mm; fuel pressure drop, 1.75 MPa; fuel viscosity, 130×10^{-4} Pa · s.

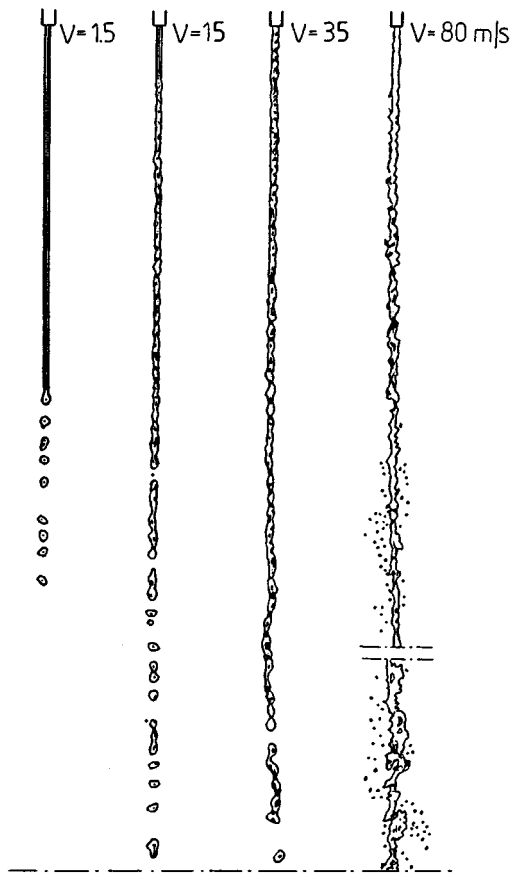


Figure 2-3 Structure of a water jet for various velocities of discharge; ratio of the length to the orifice diameter $l/d_0 = 60$.

pressures. Under conditions approaching a vacuum, aerodynamic forces are virtually nonexistent. For atmospheric pressure (0.1 MPa), the aerodynamic forces are big enough to lead to surface disturbances and eventually to jet disintegration. As the air pressure continues to increase the aerodynamic forces increase significantly, accelerating and intensifying the jet disintegration [18].

Four jet structures during the discharge of water from a long orifice (Fig. 2-3) have been distinguished [31]. The first, called the capillary structure or Rayleigh structure, occurs for small discharge velocities and its characteristic feature is the presence of axisymmetric waves. With increasing velocity the effect of aerodynamic forces begins to appear, and two other structures are distinguished which differ in that the length L_c of the compact jet is greater for the third structure. The fourth structure is typical of proper jet atomization into small drops.

As mentioned in Sec. 2-1, almost all considerations of jet disintegration are based on the method of small disturbances. In this method the disturbance parameters are added to the parameters of liquid flow. In the equations obtained, terms containing the products of the disturbances and their derivatives

are neglected. The field of small disturbances obtained in such a manner corresponds to the particular field of the linearized differential equations containing the term $e^{i\omega t}$, which is a function of time and the complex frequency of vibrations. The equation is solved with boundary conditions and the final solution is analyzed. Stability is evaluated by checking the sign of the real solution of this equation; a negative sign means amplitude increasing in time and loss of stability.

The general solutions of the linearized equations lead to an infinite number of particular solutions, which require further analysis. The procedure is of little practical value, and it is more useful to evaluate one of the particular solutions. One can then determine the conditions of the loss of jet stability and the influence of various parameters on the development of the disturbances. The following considerations refer to phenomena at the interface of the jet [29]. The two-dimensional coordinate system x, y will be used with the origin located at the outlet cross section of an atomizer (Fig. 2-4).

A jet of a viscous liquid with a wavy surface and infinite length is moving with velocity V in a stationary, incompressible, and viscous gas. The Navier-Stokes equations, neglecting the mass forces and the flow continuity equation, have the following form:

$$\begin{aligned}\frac{\partial u}{\partial t} + u \frac{\partial u}{\partial x} + v \frac{\partial u}{\partial y} &= -\frac{1}{\rho_j} \frac{\partial P_j}{\partial x} + \nu_j \left(\frac{\partial^2 u}{\partial x^2} + \frac{\partial^2 u}{\partial y^2} \right) \\ \frac{\partial v}{\partial t} + u \frac{\partial v}{\partial x} + v \frac{\partial v}{\partial y} &= -\frac{1}{\rho_j} \frac{\partial P_j}{\partial y} + \nu_j \left(\frac{\partial^2 v}{\partial x^2} + \frac{\partial^2 v}{\partial y^2} \right)\end{aligned}\quad (2-8)$$

$$\frac{\partial u}{\partial x} + \frac{\partial v}{\partial y} = 0 \quad (2-9)$$

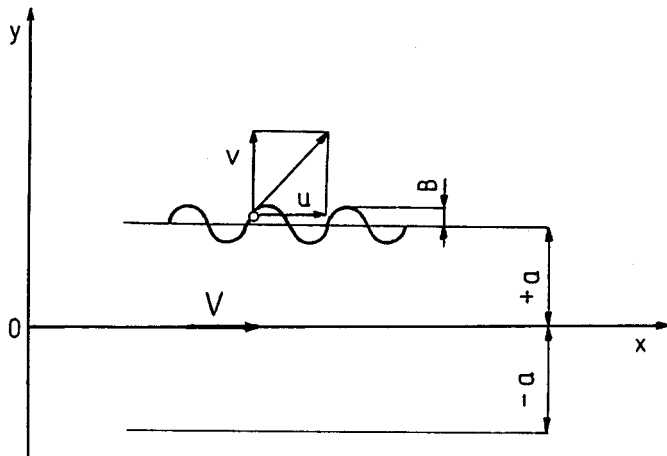


Figure 2-4 Scheme of the surface profile of a liquid jet.

where u, v = liquid velocity components on the jet boundary

j = index of the fluid type ($j = 1$ for the jet, $j = 2$ for the environment)

In Eqs. (2-8) and (2-9) for the liquid ($j = 1$) one should substitute:

$$u = V + u_1, \quad v = v_1, \quad P = P_0 + P_1$$

where v = liquid velocity

u_1, v_1, P_1 = parameters of the disturbances

P_0 = liquid pressure before superposition of the disturbances

After neglecting higher-order terms,

$$\left. \begin{aligned} \frac{\partial u_1}{\partial t} + V \frac{\partial u_1}{\partial x} &= -\frac{1}{\rho_1} \frac{\partial P_1}{\partial x} + \nu_1 \left(\frac{\partial^2 u_1}{\partial x^2} + \frac{\partial^2 u_1}{\partial y^2} \right) \\ \frac{\partial v_1}{\partial t} + V \frac{\partial v_1}{\partial y} &= -\frac{1}{\rho_1} \frac{\partial P_1}{\partial y} + \nu_1 \left(\frac{\partial^2 v_1}{\partial x^2} + \frac{\partial^2 v_1}{\partial y^2} \right) \end{aligned} \right\} \quad (2-10)$$

$$\frac{\partial u_1}{\partial x} + \frac{\partial v_1}{\partial y} = 0 \quad (2-11)$$

Differential equations (2-10) and (2-11) describe the development of disturbances on the surface of the liquid jet.

The parameters of the disturbed motion are periodic functions of the x coordinate and time t . The solution of Eqs. (2-10) and (2-11) has the following form:

$$u_1 = \{ik[A_1 \cosh(ky) + A_2 \sinh(ky)] + \gamma_1[B_1 \cosh(\gamma_1 y) + B_2 \sinh(\gamma_1 y)]\} \exp i(kx - \omega t) \quad (2-12)$$

$$v_1 = \{k[A_1 \sinh(ky) + A_2 \cosh(ky)] - ik[B_1 \sinh(\gamma_1 y) + B_2 \cosh(\gamma_1 y)]\} \exp i(kx - \omega t) \quad (2-13)$$

$$P_1 = \rho_1[A_1 \cosh(ky) + A_2 \sinh(ky)]i(\omega - kV) \exp i(kx - \omega t) + \text{const} \quad (2-14)$$

where $k = 2\pi/\lambda$ = wave number

λ = wavelength of the disturbance

ω = frequency of vibrations

A_1, A_2, B_1, B_2 = constants

and

$$\gamma_1^2 = k^2 - \frac{i(\omega - kV)}{\nu_1}$$

For the ambient environment ($j = 2$), Eqs. (2-10) and (2-11) have a similar form and describe the development of disturbances in this medium.

$$u_2 = [ik(C_1 e^{ky} + C_2 e^{-ky}) + \gamma_2(D_1 e^{\gamma_2 y} - D_2 e^{-\gamma_2 y})] \exp i(kx - \omega t) \quad (2-15)$$

$$v_2 = [k(C_1 e^{ky} - C_2 e^{-ky}) - ik(D_1 e^{\gamma_2 y} + D_2 e^{-\gamma_2 y})] \exp i(kx - \omega t) \quad (2-16)$$

$$P_2 = \rho_2(C_1 e^{ky} + C_2 e^{-ky})i\omega \exp i(kx - \omega t) + \text{const} \quad (2-17)$$

where C_1 , C_2 , D_1 , and D_2 are constants and

$$\gamma_2^2 = k^2 - \frac{i\omega}{\nu_2}$$

The pressure P_σ in the fluid caused by the surface tension σ is given by

$$P_\sigma = \sigma \left(\frac{1}{r_1} + \frac{1}{r_{II}} \right) \quad (2-18)$$

Equation (2-18) reduces to (1-16) if the main radii of curvature at a given point in the liquid are equal, i.e., $r_1 = r_{II} = R$. For the two-dimensional case considered, one radius is infinite, i.e., $1/r_{II} = 0$, and the other for small disturbances is given approximately by

$$\frac{1}{r_1} \approx \frac{\partial^2 b}{\partial x^2}$$

The distance b —the deflection of the liquid surface from the state of equilibrium—is a periodic function of x and t :

$$b = B \exp i(kx - \omega t) \quad (2-19)$$

where B is the amplitude (Fig. 2-4). After these substitutions Eq. (2-18) assumes the form

$$P_\sigma = \sigma k^2 B \exp i(kx - \omega t) \quad (2-20)$$

The problem is now reduced to the determination of all constants A_1 , A_2 , B_1 , B_2 , C_1 , C_2 , D_1 , D_2 , and amplitude B from the boundary conditions, and because of the small value of the distance b and the boundary conditions it can refer to the undisturbed surface. The boundary conditions are as follows:

1. At infinity the disturbances decay; i.e., for $y = +\infty$, $C_1 = D_1 = 0$ and for $y = -\infty$, $C_2 = D_2 = 0$.
2. The velocity of motion of the jet surface (boundary) must be equal to the transverse velocity component for $y = \pm a$ (Fig. 2-4); therefore the jet we obtain

$$\frac{\partial b}{\partial t} + V \frac{\partial b}{\partial x} = v_1 \quad (2-21)$$

and for the stationary environment

$$\frac{\partial b}{\partial t} = v_2 \quad (2-22)$$

For the following analysis we consider only one side of the jet ($y = +a$); therefore $A_1 = B_1 = 0$. From Eqs. (2-21) and (2-22),

$$B = -\frac{k[A_2 \cosh(ka) - iB_2 \cosh(\gamma_1 a)]}{i(\omega - kV)} \quad (2-23)$$

$$i\frac{B_2}{A_2} \cosh(\gamma_1 a) - \frac{C_2}{A_2} \frac{\alpha_1}{\alpha_2} e^{-ka} - i\frac{D_2}{A_2} \frac{\alpha_1}{\alpha_2} e^{-\gamma_2 a} = \cosh(ka) \quad (2-24)$$

where

$$\frac{\alpha_1}{\alpha_2} = \frac{i(\omega - kV)}{i\omega}$$

3. For $y = \pm a$ the requirement of lack of slip between the liquid and ambient medium must be satisfied; i.e., $u_1 = u_2$. For $y = +a$,

$$\begin{aligned} i\frac{B_2}{A_2} \gamma_1 \sinh(\gamma_1 a) + \frac{C_2}{A_2} k e^{-ka} + i\frac{D_2}{A_2} \gamma_2 e^{-\gamma_2 a} \\ = k \sinh(ka) \end{aligned} \quad (2-25)$$

4. For $y = \pm a$ the continuity of shear stresses must be preserved:

$$\mu_1 \left(\frac{\partial u_1}{\partial y} + \frac{\partial v_1}{\partial x} \right) = \mu_2 \left(\frac{\partial u_2}{\partial y} + \frac{\partial v_2}{\partial x} \right) \quad (2-26)$$

After substitution of velocity derivatives,

$$\begin{aligned} i\frac{B_2}{A_2} (\gamma_1^2 + k^2) \cosh(\gamma_1 a) - \frac{C_2}{A_2} 2k^2 \frac{\mu_2}{\mu_1} e^{-ka} \\ - i\frac{D_2}{A_2} (\gamma_2^2 + k^2) \frac{\mu_2}{\mu_1} e^{-\gamma_2 a} = 2k^2 \cosh(ka) \end{aligned} \quad (2-27)$$

5. The pressure difference for the liquid and ambient medium at $y = \pm a$ is balanced by the pressure P_σ :

$$P_1 - P_2 = P_\sigma \quad (2-28)$$

where pressures P_1 and P_2 are given by

$$\begin{aligned} P_1 = \{ \rho_1 i(\omega - kV) A_2 \sinh(ka) + 2\mu_1 [k^2 A_2 \sinh(ka) - ik\gamma_1 B_2 \sinh(\gamma_1 a)] \} \\ \cdot \exp i(kx - \omega t) + \text{const} \end{aligned} \quad (2-29)$$

$$\begin{aligned} P_2 = [-\rho_2 i\omega C_2 e^{-ka} + 2\mu_2 (k^2 C_2 e^{-ka} + ik\gamma_2 D_2 e^{-\gamma_2 a})] \\ \cdot \exp i(kx - \omega t) + \text{const} \end{aligned} \quad (2-30)$$

Substituting P_1, P_2, σ into Eq. (2-28), substituting B from the Eq. (2-23), and assuming $\text{const} = 0$, we obtain an equation expressing the relationship between the frequency of vibrations and the parameters describing the character of vibrations

$$\begin{aligned} & \rho_1 [i(\omega - k\omega)]^2 \sinh(ka) - 2 \left\{ \mu_1 \left[k^2 \sinh(ka) - i \frac{B_2}{A_2} k \gamma_1 \sinh(\gamma_1 a) \right] \right. \\ & \quad \left. - \mu_2 \left(\frac{C_2}{A_2} k^2 e^{-ka} + i \frac{D_2}{A_2} \gamma_2 k e^{-\gamma_2 a} \right) \right\} i(\omega - kV) \\ & \quad - \frac{C_2}{A_2} \rho_2 e^{-ka} i \omega i(\omega - kV) \\ & = -\sigma k^3 \left[\cosh(ka) - i \frac{B_2}{A_2} \cosh(\gamma_1 a) \right] \end{aligned} \quad (2-31)$$

The values

$$i \frac{B_2}{A_2}, \quad \frac{C_2}{A_2}, \quad i \frac{D_2}{A_2}$$

should be determined from the boundary conditions (2-24), (2-25), (2-27).

Equation (2-31) is the basis of the analysis of jet disintegration. However, it is too complex to be used in its general form. In most cases the atomization conditions are such that one can neglect the viscosity of the liquid and the environment, e.g., the atomization of water in air or the atomization of fuels in engines. Equation (2-31) after transformations assumes the form

$$\begin{aligned} & \left[\tgh(ka) + \frac{\rho_2}{\rho_1} \right] (i\omega)^2 - 2k \left[\frac{\mu_1 k}{\rho_1} \tgh(ka) + \frac{\mu_2 k}{\rho_1} + iV \tgh(ka) \right] i\omega \\ & + \frac{\sigma k^3}{\rho_1} - k^2 V^2 \tgh(ka) + \frac{2\mu_1 k^3}{\rho_1} iV \tgh(ka) = 0 \end{aligned} \quad (2-32)$$

This equation can be written in the dimensionless form

$$H(i\omega_1)^2 + 2(K + iL)i\omega_1 + R + iS = 0 \quad (2-33)$$

where

$$H = 1 + M \operatorname{ctgh} \epsilon, \quad K = \sqrt{\frac{2}{Lp}} \epsilon^2 (1 + N \operatorname{ctgh} \epsilon)$$

$$L = \frac{1}{\sqrt{2}} \epsilon \sqrt{We}, \quad R = \epsilon^2 (\epsilon \operatorname{ctgh} \epsilon - \frac{1}{2} We)$$

$$S = 2\epsilon^3 \sqrt{\frac{We}{Lp}}, \quad \epsilon = ka, \quad i = \omega_1 = i\omega \sqrt{\frac{\rho_1 a^3}{\sigma}}$$

and

$$\text{We} = \frac{\rho_1 V^2 2a}{\sigma}, \quad \frac{1}{L_p} = \frac{\mu_1^2}{\rho_1 \sigma 2a}, \quad M = \frac{\rho_2}{\rho_1}, \quad N = \frac{\mu_2}{\mu_1} \quad (2-34)$$

Equation (2-33) is a quadratic equation with respect to the vibration frequency $i\omega$. The solution of this equation must be analyzed. Its imaginary part determines the character of the motion's stability. The positive sign of the real part denotes the vibrational decay, and the negative sign denotes the increase in amplitude that leads to loss of stability and disintegration into drops. The real part of the solution of Eq. (2-33), representing the increase in amplitude, has the following form:

$$i\omega_1 = \frac{1}{1 + M \operatorname{ctgh} \epsilon} \left\{ \epsilon^2 \sqrt{\frac{2}{L_p}} (1 + N \operatorname{ctgh} \epsilon) - \sqrt{\frac{1}{2} \epsilon^2 \left\{ \frac{2\epsilon^2}{L_p} (1 + N \operatorname{ctgh} \epsilon)^2 - \operatorname{ctgh} \epsilon \left[\epsilon(1 + M \operatorname{ctgh} \epsilon) - \frac{M \text{We}}{2} \right] \right\}} \right\} \\ \cdot \left\{ \sqrt{1 + \sqrt{1 + \left\{ \frac{2\epsilon\sqrt{\text{We}/L_p} (N - M) \operatorname{ctgh} \epsilon}{(2\epsilon^2/L_p)(1 + \operatorname{ctgh} \epsilon)^2 - \operatorname{ctgh} \epsilon[\epsilon(1 + M \operatorname{ctgh} \epsilon) - M \text{We}/2]} \right\}^2}} \right\} \quad (2-35)$$

In the case of atomization of a liquid in a gaseous medium, terms M and N are very small. For the small wavelengths considered here ($\lambda < 2a$) the dimensionless wave number is $\epsilon > 3$. For these conditions Eq. (2-35) assumes the simplified form

$$\omega_1 = \epsilon^2 \sqrt{\frac{2}{L_p}} - \sqrt{\epsilon^2 \left(\frac{2\epsilon^2}{L_p} - \epsilon + \frac{M \text{We}}{2} \right)} \quad (2-36)$$

Now Eqs. (2-35) and (2-36) will be analyzed to demonstrate the influence of the individual dimensionless criteria on the optimal value of the wave number ϵ_{opt} and the corresponding maximal vibration frequency $\omega_{1\text{max}}$. The dimensionless criteria characterizing the atomization process are represented by Eq. (2-34), namely

We—Weber number

Lp—Laplace number

M—ratio of gas and liquid densities

N—ratio of gas and liquid viscosities

Figure 2-5 shows the graph of $\omega_1 = f(\epsilon)$ for various values of $1/L_p$ and constant values We, M, N [29]. This graph was prepared on the basis of Eq. (2-35), but Eq. (2-36) also has satisfactory accuracy. The dashed line determines

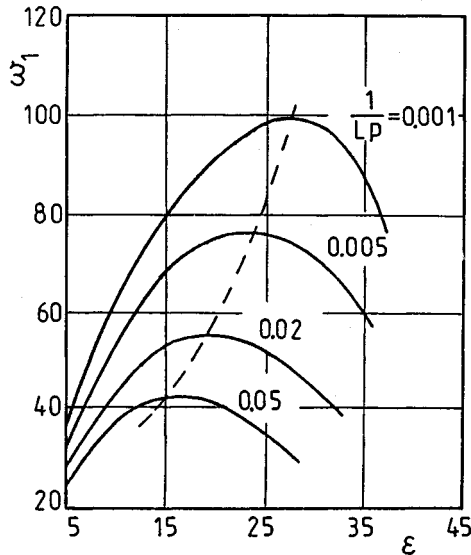


Figure 2-5 Function $\omega_1 = f(\epsilon)$; $We = 1 \cdot 10^5$, $M = 0,001$, $N = 0,005$.

the corresponding values $\omega_{1\max}$ and ϵ_{opt} . By preparing many such graphs, one obtains the dimensionless equations

$$\omega_{1\max} = \text{const } Lp^{0.308}, \quad \epsilon_{opt} = \text{const } Lp^{0.22}$$

The other dimensionless equations can be obtained in a similar manner. From these equations it appears that the N criterion can be neglected for $N < 0.1$, which is almost always the case in practice. On the basis of many diagrams, generalized relationships were determined (Fig. 2-6) that have the form

$$\omega_{1\max} = -0.0536(M We)^{1.21} Lp^{0.308} \quad (2-37)$$

$$\epsilon_{opt} = 0.173(M We)^{0.8} Lp^{0.22} \quad (2-38)$$

Equation (2-38) will be used for calculating the length of the compact jet; from Eq. (2-38),

$$\frac{\bar{D}}{d_0} = K(We M)^{-0.266} Lp^{-0.0733} \quad (2-39)$$

which allows the average diameter of the drop, \bar{D} , to be determined. This equation applies to disturbances with very short wavelengths. The short wavelength disturbances are accompanied by propagation of long-wavelength disturbances, which leads to the development of large drops. The coefficient $K = 3.01$ obtained in [29] for continuous jet atomizers can have different values depending on the design of the atomizer, the method of averaging of drop diameters, etc.

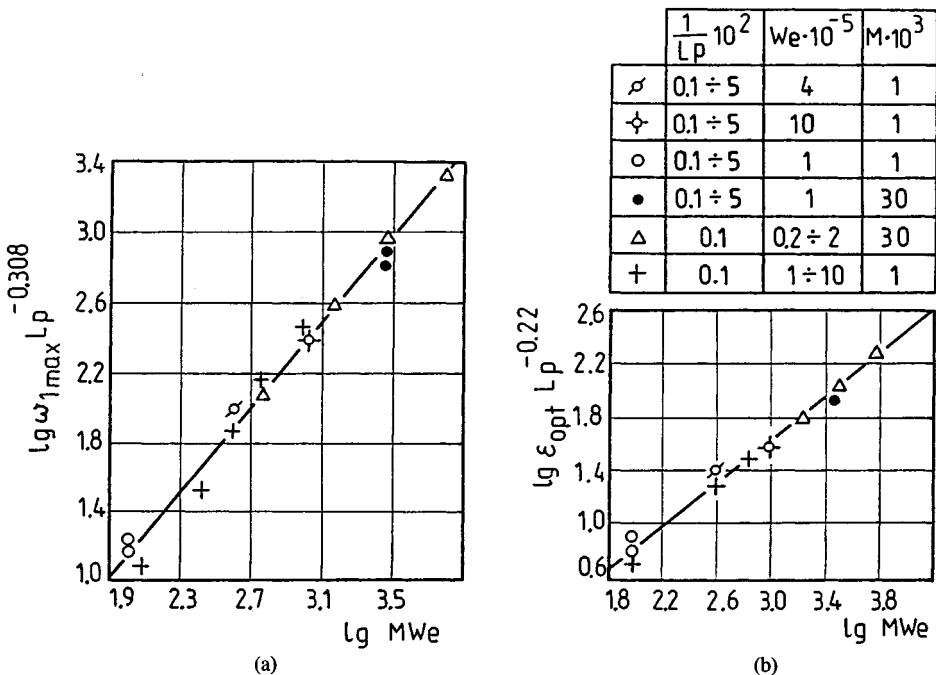


Figure 2-6 Generalized diagrams of parameters: (a) $W_{1\max}$, (b) ϵ_{opt} . In both cases $N = 0.005$.

The length of compact jet, L_c , leaving the atomizer is an important parameter, and knowledge of this length is of major practical importance. In most cases, particularly in piston engines, the minimal length is desired for obvious reasons. In some cases, as in firefighting or in-service cleaning of the water-wall tubes in boilers, a long compact jet of water discharged with high velocity that can reach long distances is needed.

The length L_c depends mostly on the jet velocity, geometry of the outlet orifice, character of the jet, physical properties of the fluid, and ambient medium. These parameters are interrelated, and therefore most data on length L_c were obtained experimentally and only some for laminar flow were derived analytically. The general dependence of L_c on the fluid discharge velocity from an orifice is shown in Fig. 2-7.

Extensive information regarding L_c for a free liquid discharge from various orifices is contained in [22]. For the jet, which disintegrates because of axisymmetric waves, L_c is derived from the *Weber equation*

$$\frac{L_c}{d_0} = \ln \frac{R}{\delta} \sqrt{We} \quad (2-40)$$

The parameter $\ln(R/\delta)$ is determined experimentally and depends on the

character of the jet: for a laminar jet $\ln(R/\delta) \approx 24$; for a turbulent jet $\ln(R/\delta) \approx 4$.

Laminar streams are very sensitive to any internal disturbances, which can reduce L_c by 50% or more. The influence of the discharge orifice length on the disintegration of a laminar jet in air and in liquids that do not mix with the jet has been investigated [25]. The longer the orifice l , the longer is the compact jet L_c . This length approaches a constant value for every orifice diameter d_0 when the ratio $1/d_0$ exceeds a critical value. The critical value tends to decrease as the liquid viscosity increases. The practical value of this research is insignificant because of the low velocities of the liquid.

Numerical methods were used to derive a universal equation for the length L_c of a laminar compact jet in air [30]. This equation is in agreement with the experimental data, particularly for the jets discharging from orifices with sharp edges; however, it is too complex for practical purposes.

The influence of coaxial air flow on the disintegration of a liquid jet discharging from a capillary has been investigated [35]. It was found that the wavelength of the axisymmetric disturbances on the liquid surface and the length of the compact jet decrease during the air flow. The wavelength depends on the liquid velocity in the motionless air. Such coaxial flow of liquid and air jets is an example of a most simple pneumatic atomizer. However, no changes of drop diameters during the liquid jet disintegration have been found.

The average length \bar{L}_c of a compact jet for coaxial flow of air is given by [35]

$$\frac{\bar{L}_c}{d_0} = 9.28 \exp(-0.05V_G)(We^{0.5})^{0.063\sqrt{V_G} + 0.72}$$

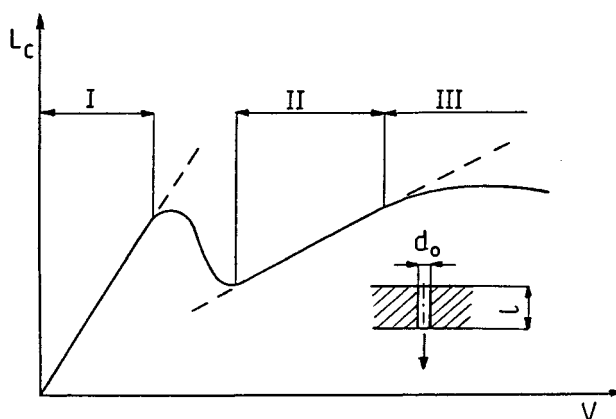


Figure 2-7 Dependence of the length of a compact jet on the discharge velocity V ; I, laminar jet region; II, turbulent jet region; III, environment-jet interaction region.

where V_G = air velocity,

$$We = \frac{\rho_L V_L^2 d_0}{\sigma} = \text{Weber number}$$

ρ_L = liquid density

V_L = liquid velocity in outlet orifice

This equation was derived for an orifice diameter $d_0 = 2.09$ mm; for smaller diameters the power of the Weber number was increased.

Turbulent jets do not show any effect of internal disturbances and the length and geometry of the orifice on the length L_c . Turbulence is completely developed for sharp inlet edges for $l/d_0 > 5$ and $Re > 3000$ and for conical edges for $l/d_0 > 15$ and $Re > 4000$. For completely developed turbulence during axisymmetric jet disintegration it was found that [22]

$$\frac{L_c}{d_0} = 11.5 We^{0.31} \quad (2-41)$$

Results of the investigation for a typical jet atomizer during discharge of a diesel oil are shown in Fig. 2-8 [29]. As in Fig. 2-7, it is seen that in the range of small velocities the length L_c of the compact jet increases linearly. The end of the linear relationship is marked with dashed line I. As the velocity increases further, L_c increases slightly up to dashed line II and then decreases significantly. Line II corresponds to the transition from disintegration caused by axisymmetric waves to disintegration caused by asymmetric waves.

The influence of the geometry of the outlet orifice on the relative length L_c/d_0 of the compact jet for discharge of water is shown in Fig. 2-9. The curves refer to the various relative lengths of the orifices l/d_0 ; curves 1, 2, and 3 refer

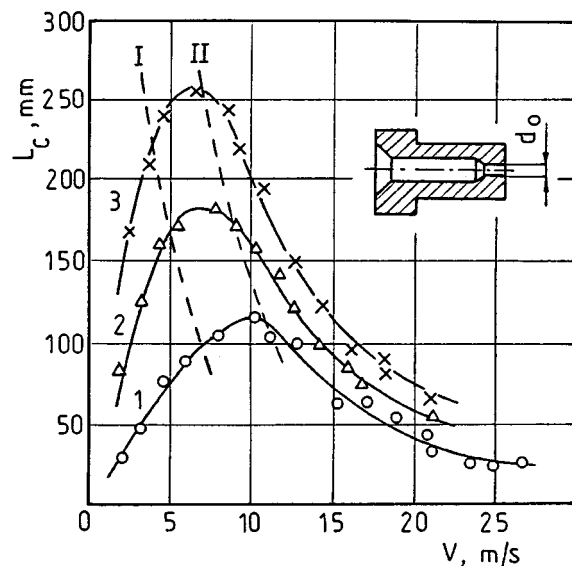


Figure 2-8 Length of a compact jet, L_c , as a function of discharge velocity V ; 1, $d_0 = 0.38$ mm; 2, $d_0 = 0.7$ mm; 3, $d_0 = 1.04$ mm.

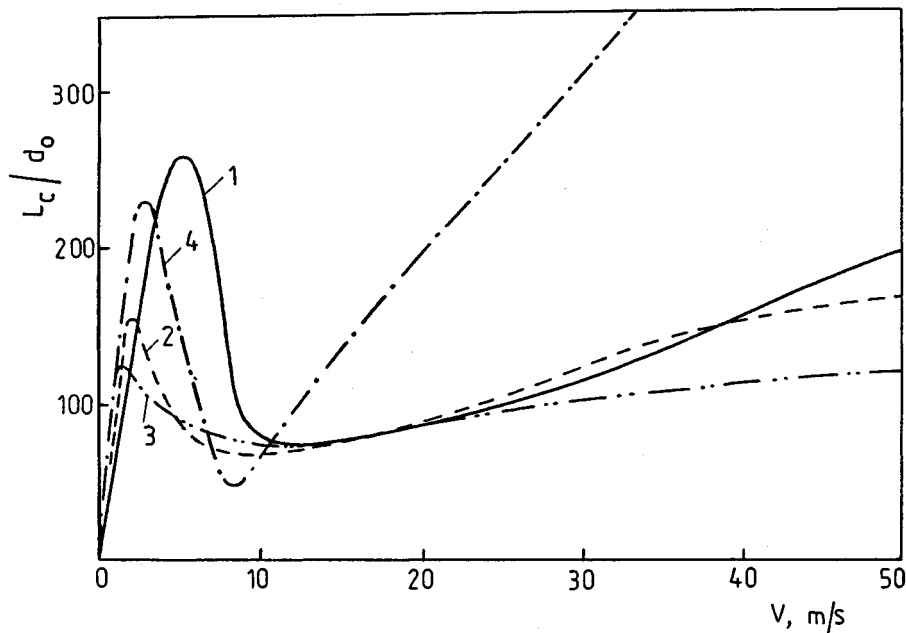


Figure 2-9 Dependence of the relative length L_c/d_0 of a compact jet on the velocity V of discharge from orifices with different relative length l/d_0 ; 1, $l/d_0 = 60$; 2, $l/d_0 = 30$; 3 and 4, $l/d_0 = 4$.

to an orifice with a sharp inlet edge and curve 4 refers to a conical inlet [31]. The character of the curves is similar to that in Fig. 2-7.

Returning to Eq. (2-37), it should be mentioned that a dimensionless equation was derived from it [29]:

$$\frac{L_c}{d_0} = C \text{We}^{-0.71} \text{Lp}^{-0.308} M^{-1.21} \quad (2-42)$$

where $d_0 = 2a$ (see Fig. 2-4), $C = 442$ is a constant for continuous jet atomizers, and $C = 372$ is a constant for intermittent jet atomizers.

2-2.2 Stability and Disintegration of Liquid Sheets

The disintegration of a sheet, like that of a jet, depends mainly on the liquid discharge velocity. Common to both of these processes is loss of jet stability, since the sheet disintegrates initially into jets and subsequently into drops. Three characteristic modes of sheet disintegration can be distinguished, depending on the velocity of discharge from a rotary atomizer (Fig. 2-10).

In Fig. 2-10a, discharge with a velocity of several meters per second is shown. As the distance from the atomizer increases, the thickness of the sheet decreases and perforations develop in sufficiently thin areas. The perforations

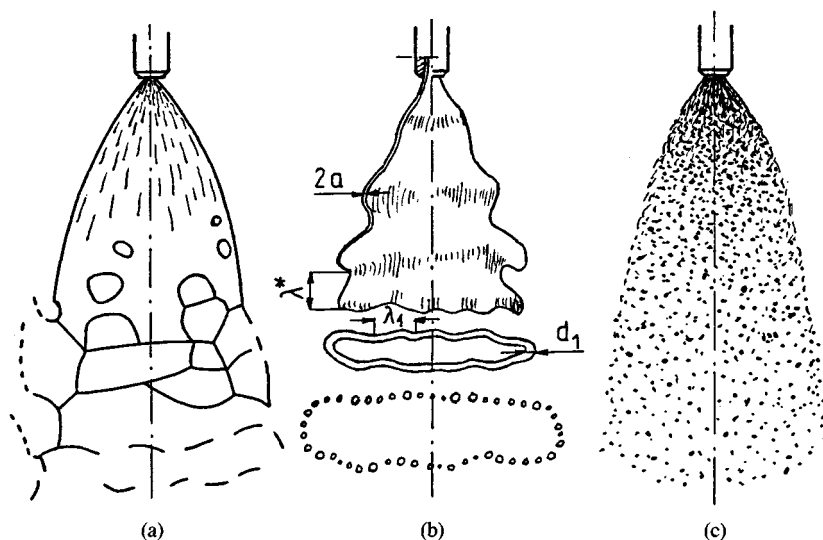


Figure 2-10 Drop development in a swirl atomizer: (a) sheet disintegration due to perforation; (b) sheet disintegration due to wave phenomena; (c) liquid atomization.

are particularly visible during discharge in a vacuum. The perforations grow and create a net of narrow jets, which after loss of stability disintegrate into drops.

For higher discharge velocities the sheet experiences wave disturbances (Fig. 2-10b). Annular waves and circumferential waves appear. The annular waves have a longitudinal direction with respect to the discharge and are the primary cause of sheet disintegration into annuli. The annuli, having the shape of jets in cross section, subsequently disintegrate into drops.

For very high discharge velocities (approximately 100 m/s) proper liquid disintegration takes place (Fig. 2-10c). Under these conditions short-length waves develop. The amplitudes of the waves increase and, due to the loss of stability, the liquid separates from the apexes of the waves before the sheet would disintegrate into annuli. For very high velocities the ambient medium causes such strong disturbances that the sheet disintegrates into drops before the waves develop.

Sheets of liquid develop in all types of atomizers except jet atomizers, although in the latter they can develop under specific conditions. Examples are the fan atomizers and atomizers that produce a fan spray by the collision of impinging jets. Figure 2-11 shows the process of collision of two impinging jets of a liquid [38]. During the collision of jets that move with a velocity of several meters per second, the sheet develops and symmetrical waves are generated on it (see the sheet cross section in Fig. 2-11a). Drops separate from only some places on the sheet perimeter. During the collision of jets moving with a velocity of approximately 20 m/s, asymmetric waves develop on the sheet and lead to

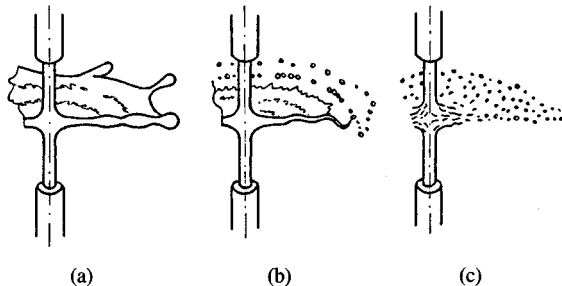


Figure 2-11 Disintegration of a sheet generated by the collision of two jets: (a) symmetric jets; (b) asymmetric jets; (c) liquid atomization.

disintegration of the sheet into annuli. The annuli disintegrate into drops due to the circumferential waves. Figure 2-11c shows the liquid disintegration for very high velocities of impinging jets, when the sheet disintegrates before the waves develop.

The analysis of liquid sheet disintegration will now be presented [38]. Disturbances on one side of the flat surface of the sheet will be considered (Fig. 2-12), but extension to disturbances on both sides would not change the final solution. The following assumptions were made:

- Both fluids (the liquid and ambient gas) are nonviscous and noncompressive.
- The amplitudes of initial disturbances are small compared to the wavelengths.
- The liquid is stationary with respect to the coordinate system.
- Gas flows with constant velocity V in the x axis direction, where in general V is a relative velocity of the liquid and gas.
- The sheet has infinite length.
- The sheet thickness is limited by the coordinates $y = +a$ and $y = -a$.

During the relative motion along the sheet, a gas causes a pressure distribution that increases the amplitude of the disturbances (see Sec. 2-2.1). The

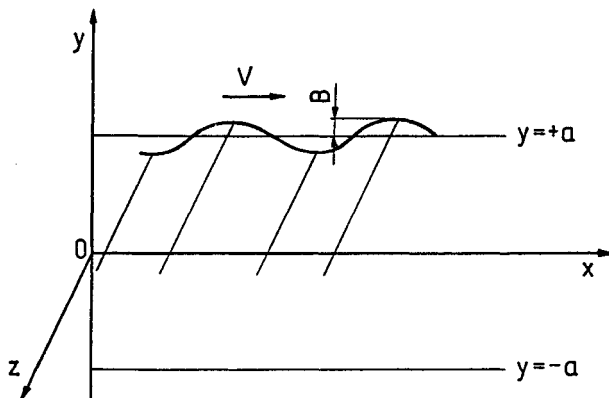


Figure 2-12 Scheme of the disturbed surface of a liquid sheet.

difference between the liquid pressure P_1 and the ambient pressure P_2 , as in Eq. (2-28), is balanced by the pressure P_σ , which originates from the liquid surface tension:

$$P_1 - P_2 = -\sigma \frac{\partial^2 b}{\partial x^2} \quad (2-43)$$

where b is the displacement of the liquid surface from the equilibrium position. The solution of this equation corresponds to the maximum instability. The equation of the disturbed surface has the form

$$y = a + B \cos(nt + kx) \quad (2-44)$$

where n = time coefficient; $k = \frac{2\pi}{i}$ = wave number;

B = amplitude, which for loss of stability goes to infinity for time t

Pressures P_1 and P_2 will be determined from the velocity fields. The assumptions allow the application of equations for potential motion. The equation of continuity for a liquid has the form

$$\frac{\partial^2 \Phi_1}{\partial x^2} + \frac{\partial^2 \Phi_1}{\partial y^2} = 0 \quad (2-45)$$

From the boundary conditions and the definition of the velocity potential Φ it follows (Fig. 2-12) that for $y \approx +a$

$$\frac{\partial \Phi_1}{\partial y} = \frac{dy}{dt} = \frac{\partial b}{\partial t} + V \frac{\partial b}{\partial x} \quad (2-46)$$

and for $y \approx -a$

$$\frac{\partial \Phi_1}{\partial y} = 0 \quad (2-47)$$

because according to the assumptions the normal velocity component for the liquid, dy/dt , exists only for the upper surface.

The solution of Eq. (2-45) has the form

$$\Phi_1 = [C \cosh(ky) + D \sinh(ky)][E \cos(nt + kx) + F \sin(nt + kx)] \quad (2-48)$$

Constants C, D, E, F can be derived from Eqs. (2-44) and (2-46) to (2-48), yielding

$$\Phi_1 = \frac{1}{2k} \left[\frac{\cosh(ky)}{\sinh(ka)} + \frac{\sinh(ky)}{\cosh(ka)} \right] \cdot [\dot{B} \cos(nt + kx) - Bn \sin(nt + kx)] \quad (2-49)$$

where $\dot{B} = dB/dt$.

Similarly, for the ambient gas

$$\frac{\partial^2 \Phi_2}{\partial x^2} + \frac{\partial^2 \Phi_2}{\partial y^2} = 0 \quad (2-50)$$

$$\frac{\partial \Phi_2}{\partial y} = \frac{dy}{dt} = \frac{\partial b}{\partial t} + V \frac{\partial b}{\partial x} \quad d\ln y \approx a \quad (2-51)$$

$$\Phi_2 = Vx \quad \text{for } y = \infty, \quad (2-52)$$

$$\Phi_2 = e^{-ky} [K \cos(nt + kx) + L \sin(nt + kx)] + Vx \quad (2-53)$$

$$\Phi_2 = \frac{e^{-ky}}{ke^{-ka}} [B(n + kV) \sin(nt + kx) - \dot{B} \cos(nt + kx)] + Vx \quad (2-54)$$

Constants K and L were calculated from Eqs. (2-44), (2-51), and (2-53). The pressures of both fluids on the plane of their separation are derived from Lamb's equation

$$P_j = C_j - \rho_j \left[\frac{\partial \Phi_j}{\partial t} + \frac{1}{2} \left(\frac{\partial \Phi_j}{\partial x} \right)^2 + \frac{1}{2} \left(\frac{\partial \Phi_j}{\partial y} \right)^2 \right] \quad (2-55)$$

where $j = 1$ refers to the liquid and $j = 2$ to the gas. Differentiating Eqs. (2-48) and (2-49), substituting into Eq. (2-55), and neglecting the squares of terms B and \dot{B} , we obtain for the liquid and gas correspondingly

$$P_1 = C_1 + \rho_1 \left[\frac{-\alpha}{2k} (\ddot{B} - n^2 B) \cos(nt + kx) + \frac{n\alpha \dot{B}}{k} \sin(nt + kx) \right] \quad (2-56)$$

$$P_2 = C_2 - \frac{1}{2} \rho_2 V^2 - \rho_2 \left\{ \frac{1}{k} [B(n + kV)^2 - \dot{B}] \cos(ht + kx) + \frac{2\dot{B}}{k} (n + kV) \sin(nt + kx) \right\} \quad (2-57)$$

where $\alpha = \tgh(ka) + ctgh(ka)$ and $\ddot{B} = d^2 B / dt^2$.

Constants C_1 and C_2 can be calculated as follows. From Eq. (2-43), for a flat surface (i.e., in the absence of disturbances), $P_1 = P_2$; therefore the terms in brackets in Eqs. (2-56) and (2-57) are equal to zero and we obtain

$$C_1 = C_2 - \frac{1}{2} \rho_2 V^2$$

Equation (2-44) after differentiation assumes the form

$$\frac{\partial^2 b}{\partial x^2} = -k^2 B \cos(nt + kx) \quad (2-58)$$

Substituting Eq. (2-56) to (2-58) to the initial equation (2-43) yields

$$\left\{ \rho_1 \frac{\alpha}{2k} (n^2 B - \ddot{B}) + \frac{\rho_2}{k} [B(n + kV)^2 - \ddot{B}] - \sigma k^2 B \right\} \cos(nt + kx) + \left[\rho_1 \frac{\alpha}{k} n \dot{B} + 2\rho_2 \frac{\dot{B}}{k} (n + kV) \right] \sin(nt + kx) = 0 \quad (2-59)$$

Equation (2-59) is satisfied when the terms in front of sines and cosines are equal to zero; hence

$$\frac{\ddot{B}}{B} = n^2 + \frac{4MkV}{\alpha + 2M} n + \frac{2Mk^2 V^2}{\alpha + 2M} - \frac{2\sigma k^3}{\rho_1(\alpha + 2M)} \quad (2-60)$$

$$\dot{B} \left(n + \frac{2MkV}{\alpha + 2M} \right) = 0 \quad (2-61)$$

where $M = \rho_2/\rho_1$.

In order to determine the stability conditions the system of Eqs. (2-60) and (2-61) has to be solved. Two solutions are obtained, from which four cases follow; one refers to waves with constant amplitude and the others refer to waves with amplitudes that are functions of time ($\dot{B} \neq 0$). For $\dot{B} \neq 0$, from Eq. (2.61),

$$n = -\frac{2MkV}{\alpha + 2M} \quad (2-62)$$

and, after substituting to Eq. (2-60),

$$\frac{\ddot{B}}{B} = \frac{2\alpha M k^2 V^2}{(\alpha + 2M)^2} - \frac{2\sigma k^3}{\rho_1(\alpha + 2M)} \quad (2-63)$$

The left-hand side of Eq. (2-63) expresses the relative acceleration of wave amplitude; the right-hand side represents the aerodynamic and surface tension forces. Of three cases that need to be considered, the most important is the case of positive acceleration of the amplitude, i.e., $\ddot{B}/B > 0$. From Eq. (2-63), it follows that this acceleration occurs when

$$V > \sqrt{\frac{\sigma k(\alpha + 2M)}{\alpha M \rho_1}} \quad (2-64)$$

or

$$\lambda > \frac{2\pi\sigma(\alpha + 2M)}{\alpha M \rho_1 V^2} \quad (2-65)$$

The condition $\ddot{B}/B > 0$ can be expressed as $\ddot{B}/B = \beta^2$, i.e.,

$$\ddot{B} - \beta^2 B = 0$$

The solution of this equation has an exponential form

$$B = Ke^{\beta t} + Le^{-\beta t} \quad (2-66)$$

where K and L are constants. The power of the amplitude increase β is determined by Eq. (2-63), which can be written in dimensionless form as

$$\frac{\beta a}{V} = \frac{2\pi}{m} \left[\frac{2\alpha M}{(\alpha + 2M)^2} - \frac{4\pi\sigma}{amV^2\rho_1(\alpha + 2M)} \right]^{1/2} \quad (2-67)$$

where $m = \lambda/a$. In Eq. (2-67) two dimensionless terms are present, the velocity of amplitude growth

$$S = \frac{\beta a}{V}$$

and the Weber number

$$We_1 = \frac{\rho_1 V^2 a}{\sigma}$$

Eventually one obtains

$$S = \frac{2\pi}{m} \left[\frac{2\alpha M}{(\alpha + 2M)^2} - \frac{4\pi}{We_1 m (\alpha + 2M)} \right]^{1/2} \quad (2-68)$$

Figure 2-13 shows Eq. (2-68) as a function of m for various values of the Weber number We_1 during the atomization of water in air which corresponds to the ratio $M = \rho_2/\rho_1 \approx 0.00112$. The velocity of amplitude growth S has a

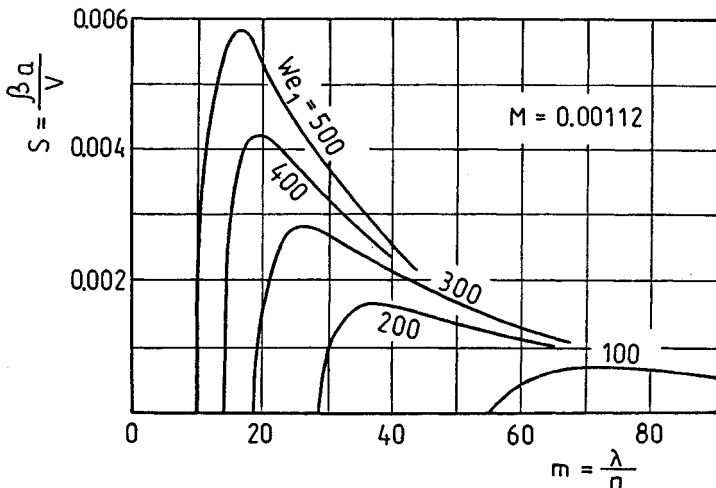


Figure 2-13 Influence of Weber number We_1 on the amplitude growth rate S .

maximum that is more distinct and shifted to the left (toward shorter waves) the higher the Weber number We_1 . There is a lower limit of m beneath which the sheet is stable, which means that short waves do not cause disintegration of thick sheets unless there is a sufficient increase of We_1 . During intense disintegration of sheets into small drops, values of We_1 are significantly higher than those shown in Fig. 2-13.

This analysis of sheet stability explains explicitly why atomizers convert efficiently only a small fraction of energy supplied to them. The disturbances with small wavelengths needed to develop small drops can become unstable only when the relative liquid velocity is high. In order to create high velocities (high Weber numbers), high energy is required.

With this analysis one can estimate the approximate dimensions of drops. According to the model presented in Fig. 2-10b, the sheet disintegrates primarily into annuli, which disintegrate into drops. It was assumed that the annulus of a sheet with thickness $2a$ and width λ^* is transformed by surface tension into an annulus with a circular cross section. The diameter of the annulus cross section, d_1 , is derived from the approximate value

$$\frac{\pi d_1^2}{4} \approx 2a\lambda^*$$

The disintegration of an annulus into drops proceeds, according to Rayleigh's theory for wavelength $\lambda_1 \approx 4.5d_1$. The drop diameter can be determined from the condition that the volumes of a sphere with diameter D and the volume of a cylinder with diameter d_1 and length λ_1 are equal.

$$\frac{\pi D^3}{6} = \frac{\pi d_1^2}{4} \lambda_1$$

These equations yield the drop diameter

$$D = 2.12\sqrt{2a\lambda^*} \quad (2-69)$$

The wavelength λ^* corresponding to the maximum velocity of amplitude growth is incorporated in the Weber number defined as follows:

$$We^* = \frac{\rho_2 V^2 \lambda^*}{\sigma} \quad (2-70)$$

One can introduce another form of the Weber number

$$We_2 = \frac{\rho_2 V^2 a}{\sigma} \quad (2-71)$$

where the relationship between We_1 and We_2 is $We_2 = M We_1$. In Fig. 2-13 a corresponding value We_2 can be assigned to each value of We_1 . By determining the wavelength $\lambda = \lambda^*$ corresponding to the maximum velocity of amplitude growth for a given Weber number We_2 , one can find the relationship between We_1 and We_2 . This relationship for various values M is shown in Fig. 2-14.

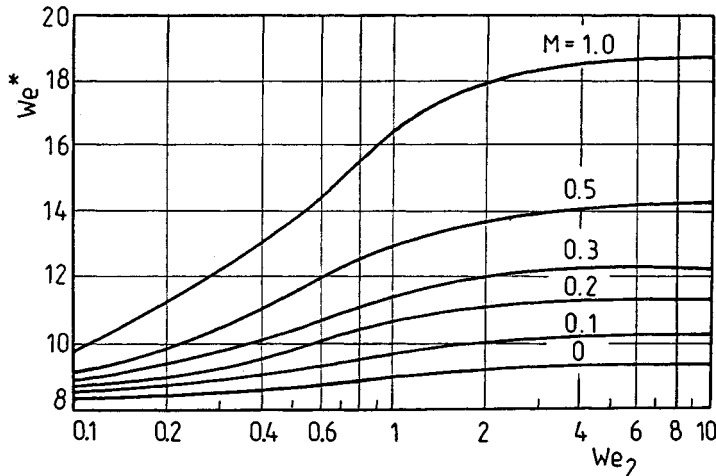


Figure 2-14 Effect of the sheet thickness included in Weber number We_2 on the wavelength λ^* included in We^* .

Example 2-1 Determine the diameter of drops that develop during the disintegration of a water sheet of thickness $2a = 20 \mu\text{m} = 20 \times 10^{-6} \text{ m}$ in air. For the calculations assume the following values: $\rho_1 = 1000 \text{ kg/m}^3$, water density; $\rho_2 = 1.12 \text{ kg/m}^3$, air density; $\sigma = 74 \times 10^{-3} \text{ N/m}$, water surface tension; $V = 19.1 \text{ m/s}$, relative velocity of water and air.

SOLUTION Substituting the data into Eq. (2-71) yields

$$We_2 = \frac{\rho_2 V^2 a}{\sigma} = \frac{(1.12)(19.1^2)(10 \times 10^{-6})}{74 \times 10^{-3}} = 0.055$$

For $We_2 = 0.055$ and $M \approx 0.001$ the value $We_2 \approx 8.2$ can be extrapolated from Fig. 2-14. Substituting λ^* from Eq. (2-70) into Eq. (2-69), we obtain

$$\begin{aligned} D &= \frac{2.12}{V} \sqrt{\frac{2a We^* \sigma}{\rho_2}} = \frac{2.12}{19.1} \sqrt{\frac{(20 \times 10^{-6})(8.2)(74 \times 10^{-3})}{1.12}} \\ &= 0.000364 \text{ m} = 364 \mu\text{m} \end{aligned}$$

The diameter D determined in this way corresponds in principle to the maximum drop diameter and is in agreement with experimental data. In reality, drops with a wide diameter spread develop.

2-3 DIMENSIONLESS CRITERIA OF THE ATOMIZATION PROCESS

The foregoing theoretical considerations lead to the utilization of some dimensionless criteria. Establishing dimensionless criteria is, as is well known, the

subject of *dimensional analysis*. It is worth checking whether the dimensional analysis leads to the same results as the preceding considerations based on the phenomenon of stability loss. The results of dimensional analysis depend on the proper selection of physical parameters (parameters of a given physical process). The atomization process is characterized first of all by the *average drop diameter* \bar{D} . The following parameters affect \bar{D} :

- L —characteristic linear dimension of an atomizer, e.g., diameter of outlet orifice
- V —initial relative velocity of liquid and ambient gas
- σ —surface tension
- ρ_L, ρ_G —liquid density and gas density, respectively
- μ_L, μ_G —dynamic viscosity of liquid and ambient gas, respectively

The number of selected parameters is eight. It should be pointed out that the atomizer was characterized by only one parameter, L , whereas a real atomization process depends on the designs and technology of the atomizer. The parameter dimensions contain $m = 3$ units, i.e., m, kg, s. The quantities L , V , and ρ_G were assumed to be basic parameters because they are dimensionally independent and they contain the aforementioned three units. Dimensionally independent parameters are those whose dimension cannot be expressed as an arbitrary combination of the dimensions of other parameters; for example, the diameter cannot be expressed by using mass or time. The first theorem of dimensional analysis states, that the dimension of any parameter can be expressed in the form of the product of powers of dimensions of basic parameters, i.e., length, mass, and time (m, kg, s). The second theorem of dimensional analysis or the Buckingham theorem (Π theorem) allows one to describe any relationship by means of an equation containing $(n - m)$ dimensionless criteria. In this case $n - m = 8 - 3 = 5$; hence the equation assumes the form

$$f(K_1, K_2, K_3, K_4, K_5) = 0 \quad (2-72)$$

where

$$\left. \begin{aligned} K_1 &= \bar{D} L^{a_1} V^{b_1} \rho_G^{c_1} \\ K_2 &= \sigma L^{a_2} V^{b_2} \rho_G^{c_2} \\ K_3 &= \mu_L L^{a_3} V^{b_3} \rho_G^{c_3} \\ K_4 &= \mu_G L^{a_4} V^{b_4} \rho_G^{c_4} \\ K_5 &= \rho_L L^{a_5} V^{b_5} \rho_G^{c_5} \end{aligned} \right\} \quad (2-73)$$

The condition that criteria K are dimensionless requires that the right-hand sides of Eqs. (2-73) are also dimensionless. From this condition the powers can be determined. For the first Eq. (2-73) we obtain:

Linear dimension (meter) m:

$$0 = 1 + a_1 + b_1 + c_1$$

Mass (kilogram) kg:

$$0 = c_1$$

Time (second) s

$$0 = -b_1$$

Therefore,

$$a_1 = -1, \quad b_1 = 0, \quad c_1 = 0$$

and

$$K_1 = \bar{D}L^{-1} = \frac{\bar{D}}{L}$$

Similar analysis for the rest of Eq. (2.73) gives the complete set of criteria:

$$\begin{aligned} K_1 &= \frac{\bar{D}}{L} \\ K_2 &= \frac{\sigma}{\rho_G V^2 L} \\ K_3 &= \frac{\mu_L}{\rho_G V L} \\ K_4 &= \frac{\mu_G}{\rho_G V L} \\ K_5 &= \frac{\rho_L}{\rho_G} \end{aligned}$$

Criterion K_3 can be replaced by K'_3 :

$$K'_3 = \frac{K_3^2}{K_2 K_5} = \frac{\mu_L^2}{\rho_L \sigma L} \quad (2-74)$$

and criterion K_4 by K'_4 :

$$K'_4 = \frac{K_3}{K_4} = \frac{\mu_L}{\mu_G} \quad (2-75)$$

After substitutions, we obtain a new form of Eq. (2-72):

$$\frac{\bar{D}}{L} = f\left(\frac{\rho_G V^2 L}{\sigma}, \frac{\rho_L \sigma L}{\mu_L^2}, \frac{\rho_G}{\rho_L}, \frac{\mu_G}{\mu_L}\right) \quad (2-76)$$

or

$$\frac{\bar{D}}{L} = f(\text{We}, \text{Lp}, M, N) \quad (2-77)$$

As expected, the set of criteria (characteristic numbers) obtained is the same as that derived from the considerations of loss of stability, i.e., as in Eq. (2-34). We should point out the physical meaning of these characteristic numbers.

The *Weber number* We

$$We = We_2 = We_G = \frac{\rho_G V^2 L}{\sigma} \quad (2-78)$$

as in Eq. (2-71), it expresses the ratio of dynamic forces of an ambient gas to the surface tension. The Weber number defines the effect of external factors on the drop development. Generally speaking, the velocity V is the relative velocity of the liquid and gas, but during injection into a stationary environment it is simply the liquid discharge velocity. There is also the Weber number We_L [Eq. (2-5)], involving the liquid density ρ_L instead of the density of gas ρ_G . Therefore, $We_L = M We_G$.

The *Laplace number* Lp

$$Lp = \frac{\rho_L \sigma L}{\mu_L^2} \quad (2-79)$$

expresses the ratio of surface tension forces to liquid viscosity forces. For some liquids, such as hydrocarbonic fuels, the density and surface tension change insignificantly, and in these cases the Laplace number represents simply the effect of the liquid viscosity on the atomization process.

The *characteristic number* M

$$M = \frac{\rho_G}{\rho_L} \quad (2-80)$$

denotes the ratio of the density of ambient gas to the density of atomized liquid, and the *characteristic number* N

$$N = \frac{\mu_G}{\mu_L} \quad (2-81)$$

denotes the ratio of the dynamic viscosity of ambient gas to the dynamic viscosity of atomized liquid. The following relationship holds between the numbers We, Lp, M, and Re:

$$Re = \sqrt{\frac{We Lp}{M}} \quad (2-82)$$

where the *Reynolds number* has the form

$$Re = \frac{\rho_L V L}{\mu_L} = \frac{V L}{\nu_L} \quad (2-83)$$

Equation (2-77) is determined for various types of atomizers in an experimental way. The set of characteristic numbers is more correct than other sets encoun-

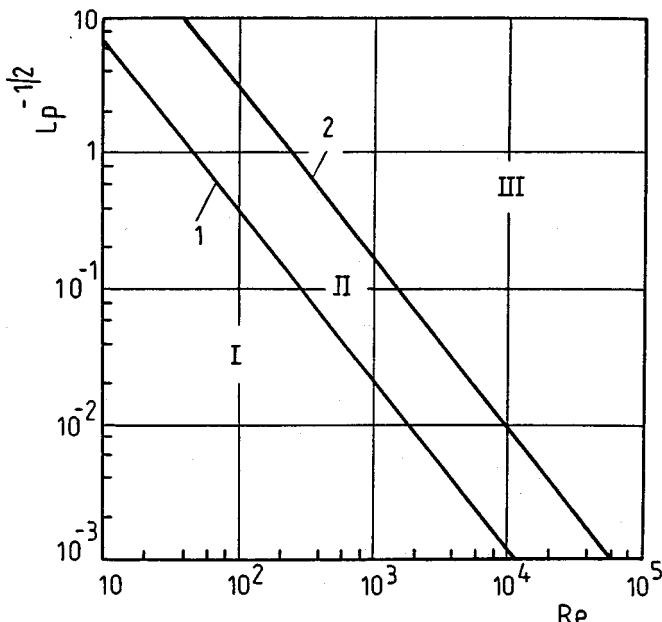


Figure 2-15 Regions of liquid jet disintegration; I, disintegration due to axisymmetric waves; II, disintegration due to asymmetric waves; III, disintegration due to aerodynamic forces; 1, Eq. (2-84); 2, Eq. (2-85).

tered in the literature because of the unique character of these numbers. The discharge velocity appears only in the Weber criterion We . The properties of the liquid are characterized by the Laplace criterion L_p . The properties of the ambient medium are contained in the two remaining criteria, M and N . The dimensionless set of characteristic numbers was used in order to generalize the results of the investigation aimed at determining conditions for various types of disintegration of liquid jets and sheets. This investigation consisted of visual observation or photographic registration of these states when one type of disintegration was transformed into another. Thereafter, some results regarding jet atomizers will be presented.

The results for liquid jet disintegration obtained by Ohnesorge are shown in Fig. 2-15 [11]. The numbers L_p and Re are derived from Eqs. (2-79) and (2-83), respectively, and the linear dimension L denotes the diameter d_o of the outlet orifice. The characteristic number L_p does not depend on the disturbances and constitutes an invariant parameter for a given outlet orifice. Lines 1 and 2 separate the areas that correspond to the three forms of disintegration described earlier (see Fig. 2-1). Line 1 satisfies the equation

$$We_L = \frac{1.74 \times 10^4}{Re^{1/2}} \quad (2-84)$$

and line 2 satisfies the equation

$$\text{We}_L = \frac{9.4 \times 10^5}{\text{Re}^{1/2}} \quad (2-85)$$

where the Weber number follows from Eq. (2-5).

The disintegration of a jet caused by aerodynamic forces, or liquid atomization, requires that the discharge velocity have a certain value, which can be determined from Eq. (2-85):

$$V \geq 2.45 \times 10^2 \frac{\sigma^{0.4} \mu_L^{0.2}}{d_o^{0.6} \rho_L^{0.6}} \quad (2-86)$$

Numerous experiments have shown that the velocity calculated in this way is not always correct, since line 2 can shift parallel to its initial position. For strong disturbances and for small disturbances the opposite takes place.

Lyshevskii [29] analyzed the results of jet disintegration using a different approach. From his own experiments and those of many other authors, he determined that the limiting discharge velocity V_{lim} , the velocity corresponding to the transition to the disintegration form, can be expressed as

$$V_{\text{lim}} = f(d_o, \sigma, \mu_L, \rho_L, \rho_G) \quad (2-87)$$

The viscosity of ambient gas μ_G was neglected because it affects the length of the compact jet, L_c , but has a very small effect on V_{lim} .

Using dimensional analysis, the following characteristic equation was derived from Eq. (2-87):

$$\text{We}_{\text{lim}} = f(\text{Lp}, M) \quad (2-88)$$

where

$$\text{We}_{\text{lim}} = \frac{\rho_L V_{\text{lim}}^2 d_o}{\sigma}, \quad \text{Lp} = \frac{\rho_L \sigma d_o}{\mu_L^2}, \quad M = \frac{\rho_G}{\rho_L}$$

equation (2-88) can be expressed as follows:

$$(\text{We}_{\text{lim}})_i = K_i \text{Lp}^{m_i} M^{n_i} \quad (2-89)$$

where K , n , and m are constants obtained from experiments for individual limiting cases in Fig. 2-8, $i = \text{I, II, III}$ = limiting cases.

The first limiting case ($i = \text{I}$) refers to the end of linear relationship $L_c = f(V)$ that corresponds to line I in Fig. 2-16. The constants are $K_1 = 10$, $m_1 = 0.455$, $n_1 = -1.08$, and Eq. (2-89) assumes the form

$$(\text{We}_{\text{lim}})_\text{I} = 10 \text{Lp}^{-0.455} M^{-1.08} \quad (2-90)$$

The second limiting case ($i = \text{II}$) refers to the transition from the disintegration caused by axisymmetric waves to the disintegration caused by asymmetric waves, which corresponds to line II. Equation (2-89) in this case has the form

$$(\text{We}_{\text{lim}})_\text{II} = 16.6 \text{Lp}^{-0.302} M^{-1.05} \quad (2-91)$$

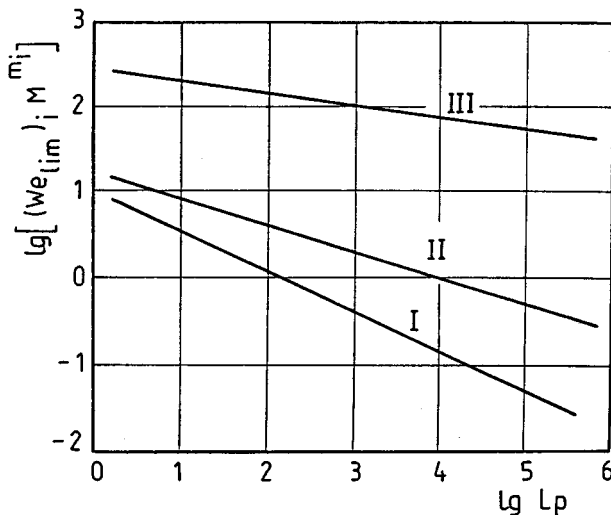


Figure 2-16 Limiting lines corresponding to Eqs. (2-90)–(2-92).

The third limiting case ($i = \text{III}$) refers to the transition from the disintegration caused by asymmetric waves to the disintegration caused by aerodynamic forces, i.e., to liquid atomization, which corresponds to line III. This line is not present in Fig. 2-8. Equation (2-89) assumes the form

$$(We_{\text{lim}})_{\text{III}} = 266Lp^{-0.133}M^{-0.8} \quad (2-92)$$

Lines I, II, III in Fig. 2-16 were extrapolated on the basis of numerous experiments with various liquids, and the most difficult task was determining line III. The experiments were conducted using simple jet atomizers without internal components that would cause additional disturbances. For jet atomizers of other designs, separate research must be conducted to determine the constants in the foregoing equations.

2-4 DISINTEGRATION AND COALESCENCE

Drops moving in the ambient gas are always subjected to vibrations and deformations, and the liquid inside the drops circulates. It does not, however, affect the disintegration of the drop unless the aerodynamic forces of the ambient gas are sufficiently high.

Moving drops can collide with each other. Drop linking follows, but under certain conditions the linking is not permanent and leads to secondary disintegration of drops.

2-4.1 Secondary Disintegration of Drops

Secondary drop disintegration occurs because of aerodynamic forces, when the drops enter an area where the dynamic pressure of the gas ($\rho_G V^2/2$) is

increased. The dynamic pressure increases as the gas density ρ_G increases, but in the first place it increases as the relative velocity V of the gas and the drop increases. Because of the gas flow around the drop, a pressure distribution develops on its surface and leads to deformation of the drop. In the case of a low-viscosity liquid the only force acting against the deformation of the drop is the surface tension force. In the case of a high-viscosity liquid there are additional shear stress forces.

Secondary disintegration of drops can also be due to collision of the drops with a solid or liquid surface. It must be emphasized however, that such a collision does not always lead to drop disintegration. This fact has found an application in one of the methods of drop diameter measurement, i.e., the method of drop collection (Chapter 7).

As mentioned, two main forces act on a drop: aerodynamic and surface tension forces. When the first is higher than the second, the drop deforms and disintegrates. The equilibrium condition for the forces is as follows:

$$C_D = \frac{\pi D^2}{4} \frac{\rho_G V^2}{2} = \pi D \sigma \quad (2-93)$$

and we obtain

$$\text{We}^* = \frac{\rho_G V^2 D}{\sigma} = \frac{8}{C_D} \quad (2-94)$$

where C_D is a *drag coefficient* and We^* is a *critical Weber number*.

The critical Weber number We^* represents the criterion for deformations that lead to secondary disintegration of a drop. From Eq. (2-94) we can determine the critical drop diameter, that is, *the maximum drop diameter* $D = D_{\max}$ that can exist under given conditions, since all drops bigger than D_{\max} should disintegrate:

$$D_{\max} = \frac{\sigma \text{We}^*}{\rho_G V^2} \quad (2-95)$$

Table 2-1 contains the results of calculations of diameter D_{\max} for various fuels (taking their viscosity into consideration) and for various relative velocities. As seen, the drop diameters D_{\max} for conventional fuels are approximately the same for a given relative velocity.

We can also introduce a minimum drop diameter D_{\min} , for which drops do not disintegrate even for the gas flow with the greatest velocity. Drops with diameters $D < D_{\min}$ drift easily with gas, excluding the possibility of their disintegration. Of course, in the drop size spectrum drops smaller than D_{\min} can exist, since such drops can develop in the normal process of atomization. The problem of minimal drops is poorly explored because of the difficulties in measurement.

Secondary disintegration of drops proceeds when $\text{We} \geq \text{We}^*$. The higher the Weber number, the smaller the sizes of secondary drops. There is a great

Table 2-1 Maximum drop diameters D_{\max}

Quantity	Units	Diesel oil			
		Light	Medium	Heavy	Kerosene
Density	kg/m^3	850	850	894	800
Dynamic viscosity	$10^4 \text{ Pa} \cdot \text{s}$	59.5	82.5	134	16.3
Surface tension	$10^3 \text{ N}/\text{m}$	24	21	20	26
Maximum diameter D_{\max}					
$V_G = 340 \text{ m/s}$	μm	3.6	3.7	4.2	2.9
$V_G = 170 \text{ m/s}$		12	12	13	11
$V_G = 86 \text{ m/s}$		42	40	43	40
$V_G = 43 \text{ m/s}$		157	152	146	155

deal of experimental data regarding the critical Weber number We^* , but the data are not consistent. It was established that secondary disintegration occurs in a range whose lower limit is We_1^* and upper limit We_2^* . For $We = We_1^*$ 10 to 20% drops disintegrate, and for $We = We_2^*$ the remaining drops disintegrate that should do so under the given conditions. For example Borodin et al. derived $We_1^* = 10.7$ and $We_2^* = 14.0$, M. S. Volynskii $We_1^* = 10.0$ and $We_2^* = 14.0$, and Bukhman $We_1^* = 2.6$ and $We_2^* = 3.6$ [38]. Eisenklam obtained for a liquid with very low viscosity $We^* = 13$ and for injection of drops into a stationary gas $We^* = 22$ [13].

In the past it was thought that the main sources of discrepancy in the results were the error of measuring the relative velocity and neglect of the influence of liquid viscosity. More recently, it has been determined that secondary disintegration also depends on other factors and can assume different forms. The secondary disintegration of drops has a complex character and, despite the large amount of experimental work, it has not yet been sufficiently explored. It was established that in the range of Weber numbers $We^* = 6$ to 50 three types of disintegration can exist. The differences between them stem from the complex interaction between the gas flow and the drop:

1. During gas flow around a drop a nonuniform pressure distribution (shown in Fig. 2-32) develops on the drop surface; this distribution is the main cause of drop deformation.
2. Because of the gas flow, a boundary layer develops on the surface of the drop.
3. The drop accelerates because of the gas acting on its front surface, which causes Taylor instabilities to develop on the surface.

We have no precise systematics of secondary drop disintegration. In general, there are two kinds of drop disintegration, which subsequently are divided into several types (modes) of disintegration. All types of disintegration start from the flattening of the drop; i.e., the drop assumes the shape of a “liquid disk”.

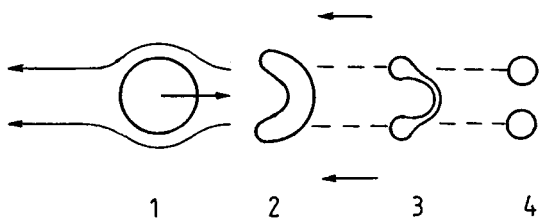


Figure 2-17 Simple drop division; 1–4, consecutive stages of disintegration.

The first kind of disintegration includes the following types:

1. *Simple drop division.* The drop disintegrates into almost identical secondary drops, whose number in general does not exceed four (Fig. 2-17).
2. *"Parachute"-type disintegration (bag mechanism) and some variations.* The drop flattens (assumes the shape of an oblate ellipsoid of rotation) and is blown out in the direction of flowing gas in the form of a parachute. Afterwards, the parachute canopy and rim disintegration, respectively, into small and large drops (Fig. 2-18).
3. *Chaotic disintegration (chaotic mechanism).* Several parachutes develop on one drop and during disintegration produce small drops and liquid threads of various shapes (closed and open).

The second kind of disintegration includes the following types:

1. *Shear mechanism.* The surface layer of liquid is torn off from the rim of the oblate drop and rapidly transforms into a cloud of small drops; the rest of the drop disintegrates into several parts after reaching critical deformation.
2. *Burst disintegration.* The drop disintegration proceeds so rapidly in the whole volume that the "shearing" is almost unnoticeable.

Attempts have been made to determine theoretically the conditions of drop disintegration. An analysis of linear stability was carried out in which the disintegration was treated in terms of local appearance of Taylor disturbances on the drop surface [19]. The results indicate that in the range $5 < \text{We} < 60$ a

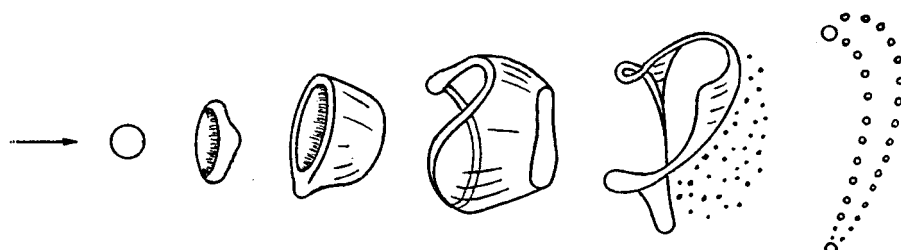


Figure 2-18 Parachute-type drop disintegration.

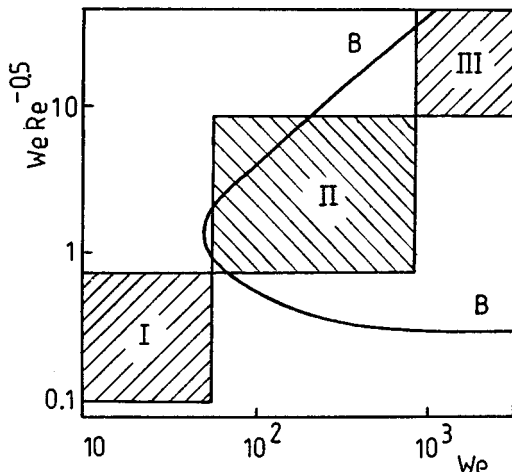


Figure 2-19 Empirical regimes of drop disintegration.

drop is subjected to disturbances whose wavelengths λ are comparable to the transverse dimension of the deformed drop, D_d . When the condition $\lambda/2 < D_d$ is satisfied, which corresponds to $We > We^* \approx 5$, disintegration proceeds easily. It was established that the parameter $We Re^{-0.5}$ plays an important role in the assessment of disintegration type; for calculating the numbers We and Re one should use the velocity of the gas and the initial drop diameter. The large number of experiments was systematized. Figure 2-19 shows areas I, II, and III referring to various types of drop disintegration and the region A encircled by the line B-B. In areas I and II the Taylor disturbances play an important role, leading to disintegrations of the parachute and "claviform" types, as shown in Fig. 2-20. The action of the disturbance in the form $\lambda/2 \approx D_d$ initially leads to bending of the oblate drop (Fig. 2-20a) and then to its stretching and development of the liquid film in the shape of a parachute. When the form of the wave is as shown in Fig. 2-20b, a "bag" develops with a central thread of liquid directed toward oncoming gas, creating a claviform that corresponds to $We > 30$. For $We > 60$ there are many disturbances acting on the oblate drop; superimposed on them are periodic disturbances acting on the rim of the drop, which lead to the drop's chaotic disintegration.

The lower part of curve B-B in Fig. 2-19 corresponds to the condition $We Re^{-0.5} > 0.3$, where periodic disturbances appear on the drop surface. It is in agreement with experiments, which show the shearing off of the surface layer of the liquid from the drop. Obviously, in this mechanism only disturbances with adequately short wavelengths can participate. As the term $We Re^{-0.5}$ increases, the shearing off of the surface layer occurs on the larger surface, which leads to burst disintegration (area III in Fig. 2-19).

On the basis of data from numerous experimental publications, a diagram similar to the one in Fig. 2-19 was constructed [8]. It was, however, limited to relatively small ranges of We and $We Re^{-0.5}$. The diagram confirms the results

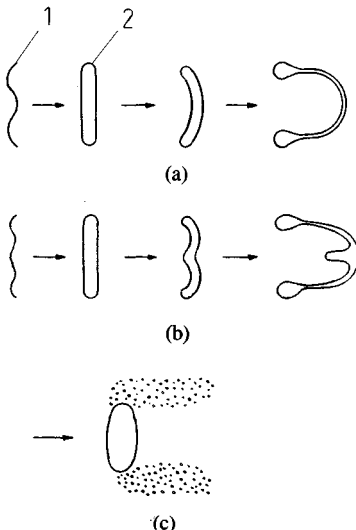


Figure 2-20 Scheme of drop disintegration; (a) parachute type; (b) claviform type; (c) tearing off of the liquid layer; 1, waveform; 2, oblate drop with diameter D_d .

presented in Fig. 2-19, but because of significant discrepancies between data obtained by different authors a more precise systematization of these data is not feasible.

The critical Weber number We^* is not the only criterion, because the following factors also affect secondary drop disintegration:

The type of the load acting on the drop

Liquid viscosity (Laplace number)

The duration of contact between gas and water (time of disintegration)

Drop diameter

The influence of these factors is discussed in the following.

The type of load acting on the drop depends on whether the drop is acted on by decreasing or increasing relative velocity of the gas and the drop. If the drop is rapidly injected into a gas flowing with a constant velocity, or if it is subjected to a shock wave, it is subjected to load and deformation of a dynamic character; because of the motion of the gas drop velocity increases and the relative velocity decreases. The relative velocity decreases rather fast or even drops to zero (drop drifting), and the deformations that do not cause secondary disintegration decay with the decrease in relative velocity. However, if the drop is introduced into a gas that accelerates in the confusor, it is subjected to load and deformation of a static character; the drop does not keep up with the gas and therefore the relative velocity increases.

During decreasing relative velocity the drop is subjected to various types of disintegration. One of them, disintegration of the parachute type, is shown schematically in Fig. 2-18. The shell (sheet) of the parachute disintegrates into a

large number of small drops, and the rim disintegrates into a smaller number of large drops. Figure 2-21 shows both of these groups of drops, small drops with a diameter $D = 0.1D_0$ and larger ones with $D = (0.2 \text{ to } 0.3)D_0$, where D_0 denotes the initial drop diameter. Although the quantitative fraction $\Delta\bar{n}_i$ (%) of small drops is much higher than that of larger drops, the mass of the latter constitutes approximately 70% of the initial drop mass.

Figure 2-22 shows the real process drop disintegration. This disintegration is of the claviform type [26].

Secondary disintegration of drops behind shock waves was investigated for various liquids in the wide range of Mach numbers $Ma = 1.1$ to 5, Reynolds numbers $Re = 10$ to 10^4 , and Weber numbers $We_G = 10$ to 600 [16]. The aforementioned types of disintegration were observed, and, depending on the type of liquid, drop dimensions, and values of Ma , Re , and We_G , significant discrepancies were found, especially regarding the drop spectrum. Therefore it is difficult to establish the critical values of the Weber numbers, which vary from several to tens depending on the type of disintegration.

For increasing relative velocity, the critical Weber number is $We^* = 20$ to 30 [9]. There are two types of deformation [28]: for liquids with high viscosity ($L_p > 200$) the drop disintegration proceeds as we have just described, in the case of liquids with low viscosity the oblate drop is blown out not in the form of a parachute but in the form of a "hat," which is directed with its convex side toward the oncoming gas (Fig. 2-23).

Such a form of the drop is explained as follows: after reaching the critical stage of deformation in the confusor, the drop is in dynamic equilibrium with the gas flow, but during a further increase of the dynamic pressure the drop tends to assume a form that compensates for this increase, i.e., the form that ensures the lowest drag coefficient. In the case of a viscous liquid, such compensation is hindered by the forces of internal friction.

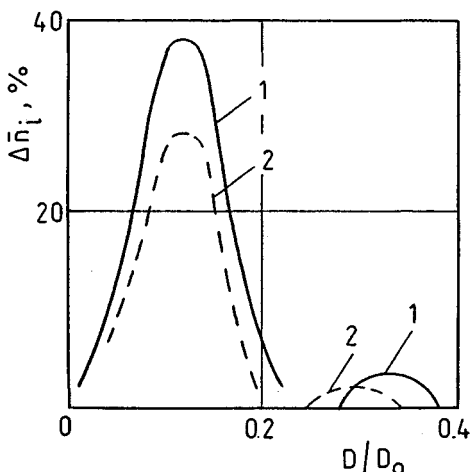


Figure 2-21 Spectrum of secondary drops; 1, $D_0 = 0.5 \text{ mm}$; 2, $D_0 = 0.9 \text{ mm}$.

76 LIQUID ATOMIZATION

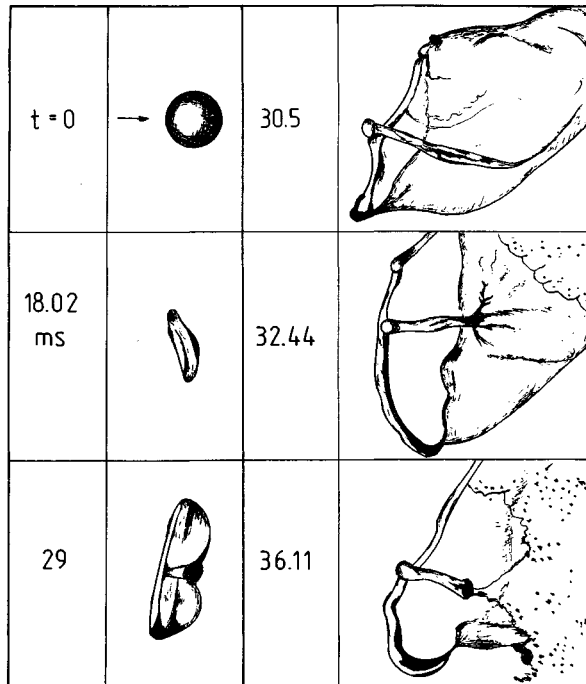


Figure 2-22 Stages of deformation and disintegration of a drop; $D_0 = 5.7$ mm; $V_G = 13.5$ m/s; $We = 18$.

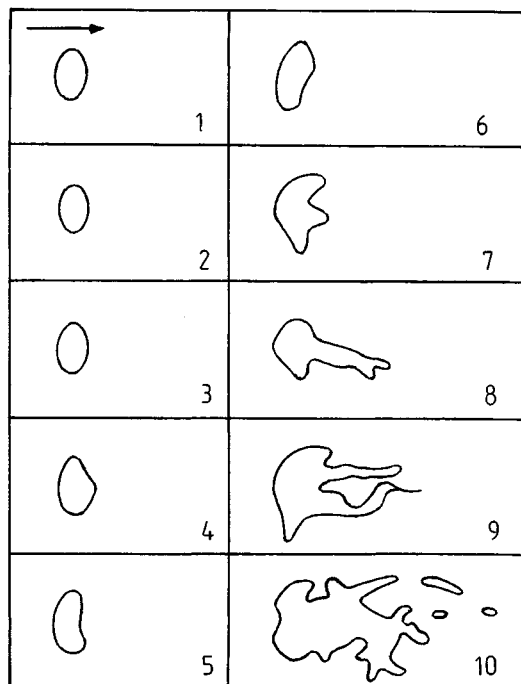


Figure 2-23 Stages of the deformation of a drop of diameter $D_0 = 0.32$ mm in a Venturi tube. Time between the consecutive frames is $0.13 \mu s$. Direction of motion of the gas and the drop is shown in frame 1.

When the gas velocity significantly exceeds the critical conditions, drop disintegration proceeds through tearing off of the liquid surface layer from the drop, as shown schematically in Fig. 2-20c. In a certain phase of deformation, perforation occurs and the drop disintegrates. During the action of strong pulses of pressure and velocity, burst disintegration of the drop into small droplets can occur. This disintegration is caused by the Rayleigh-Lamb-Taylor instability. The development of the instability on the windward (front) side of the drop is related to its acceleration, which is derived from the *Bond number*

$$Bo = \frac{a \rho_L d^2}{\sigma} > Bo^* \quad (2-96)$$

where a = drop acceleration

$$Bo^* \approx 5 \times 10^3 = \text{critical Bond number}$$

$$Bo = 1.5 C_D We \quad (2-97)$$

$$C_D = \text{drop drag coefficient}$$

The increasing relative velocity is traditionally obtained in a confusor. Smooth acceleration of the gas can also be achieved in an expansion wave generated in the shock tube. This latter approach has the advantages in that it does not require large quantities of gas and it allows synchronization of the beginning of interaction between the gas and the drop. Disintegration by the shear mechanism has been investigated [9], as shown schematically in Fig. 2-20c. This type of disintegration occurred for $We Re^{-0.5} > 10$ to 20. The critical Weber numbers were $We^* = 40$ to 60, depending on the rate of velocity increase (pressure drop) in the expansion wave.

The influence of viscosity on the critical Weber number We^* is shown in Fig. 2-24 [28] for both decreasing and increasing relative velocities of the gas and the drop. The Laplace number is defined by Eq. (2-79), in which the linear

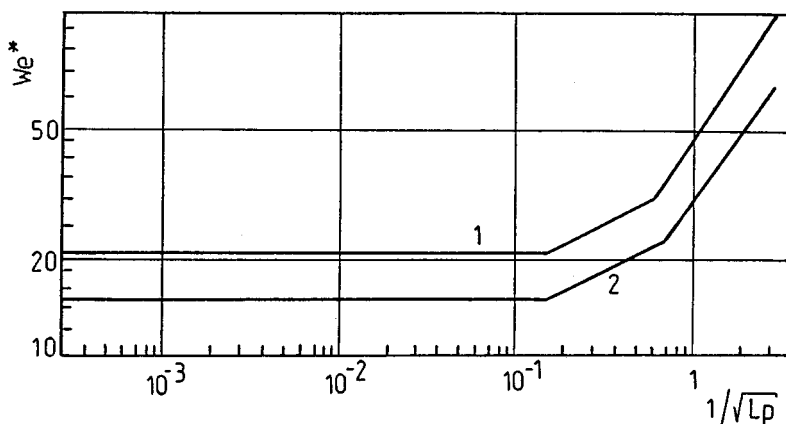


Figure 2-24 Influence of viscosity on the critical Weber number We^* : 1, increasing relative velocity; 2, decreasing relative velocity.

dimension L is represented by the initial drop diameter $D = D_0$. The values Re^* for both curves differ by approximately 40%. The curves can be divided into three parts. The first part ($1/\sqrt{Lp} < 0.12$) indicates absence of the viscosity effect, since the shear stresses in the liquid are very small compared to the forces of surface tension. The second part ($0.12 < 1/\sqrt{Lp} < 0.7$) indicates an increasing effect of viscosity, and in this case for the increasing relative velocity we have

$$\text{We}^* = 36.5 Lp^{-0.14} \quad (2-98)$$

The third part of the curves ($1/\sqrt{Lp} > 0.7$) indicates a significant effect of the viscosity, and for the increasing relative velocity the following equation holds:

$$\text{We}^* = 43 Lp^{-0.4} \quad (2-99)$$

The influence of the duration of contact between a drop and gas on We^* is characterized by the fact that for increasing contact time, We^* decreases. The drop disintegration then assumes the character of a quasistable process, since the decreasing intensity of the growth of aerodynamic forces leads to decreasing deformation rate tensor. The time of drop disintegration can be calculated approximately from empirical equations. It was established [26] that the best agreement with experimental data was obtained with the Engel equation

$$t = 2.8 \frac{D}{V} \sqrt{\frac{\rho_L}{\rho_G}} \quad (2-100)$$

where t = time of disintegration (ms)

D = drop diameter (mm)

V = relative velocity of drop and gas (m/s)

During the contact between the gas and the drop, an important role is played by the durations of such processes as drop deformation, drop acceleration, boundary layer formation on the drop, and increase of the amplitude of disturbances on the drop surface. If the durations of these processes are different, the drop disintegration is controlled by the process with the shortest duration. Information on this subject can be found in [8, 16].

The effect of drop diameter on We^* is poorly explored. Experiments have shown that small drops, particularly of viscous liquids, are more resistant to secondary disintegration, which corresponds to higher We^* values. This is illustrated by Fig. 2-25.

It is worth discussing briefly the secondary disintegration of drops of a nonhomogeneous liquid [42, 58]. If the drop contains one grain (for simplicity a spherical grain was assumed), then the liquid is blown off the grain surface and drop disintegration can proceed in the manner shown in Fig. 2-26. In stage IV the thickness of the liquid layer is maximum ($\delta = \delta_{\max}$) for given conditions, and the liquid is not blown off the grain farther for a given relative velocity V . The aerodynamic force is balanced by the forces of surface tension, so by analogy

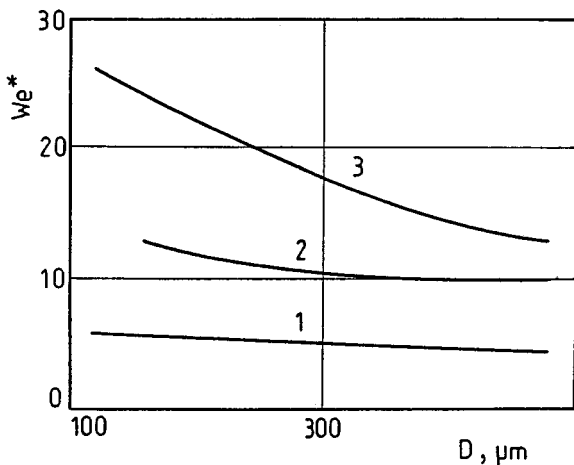


Figure 2-25 Dependence of the critical Weber number We^* on the drop diameter D ; 1, $\mu_L = 1 \times 10^{-3}$ Pa·s; 2, $\mu_L = 4.8 \times 10^{-3}$ Pa·s; 3, $\mu_L = 97 \times 10^{-3}$ Pa·s.

with Eq. (2-93) we can write

$$C_D \left(\frac{\pi D^2}{4} - \frac{\pi d^2}{4} \right) \frac{\rho_G V^2}{2} = \pi D \sigma \quad (2-101)$$

where D is drop diameter and d is grain diameter. Introducing the liquid thickness δ ,

$$\delta = \frac{D}{2} - \frac{d}{2}$$

we obtain the maximum thickness δ_{\max} of the liquid layer:

$$\delta_{\max} = \frac{d}{2} \left[\frac{\sigma We^*}{2d\rho_G V^2} + 1 + \sqrt{\left(\frac{\sigma We^*}{2d\rho_G V^2} \right)^2 + 1} \right] \quad (2-102)$$

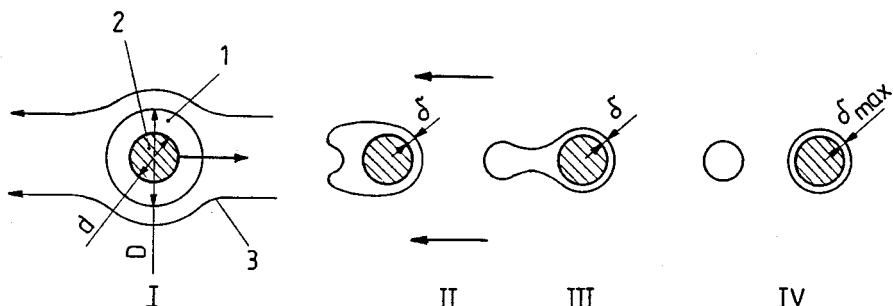


Figure 2-26 Consecutive stages of the secondary disintegration of a drop containing a solid particle; 1, drop; 2, grain; 3, gas streamline.

From Eq. (2-102) it follows that for grain diameter d approaching zero, the thickness δ_{\max} approaches the limit

$$\lim_{d \rightarrow 0} \delta_{\max} = \frac{\sigma We^*}{2 \rho_G V^2}$$

which, according to Eq. (2-95), corresponds to half of the maximum diameter D_{\max} of the drop in given conditions, i.e.,

$$(\delta_{\max})_{d=0} = \frac{D_{\max}}{2} \quad (2-103)$$

From Eq. (2-102) it also follows that the maximum thickness of the liquid layer decreases as the relative velocity increases ($\delta_{\max} \rightarrow 0$ where $V \rightarrow \infty$) and as the gas velocity increases; however, it increases as the surface tension increases.

When the drop contains more than one grain, several stages of secondary disintegration can be distinguished (Fig. 2-27). It should be assumed that in the equilibrium state between the aerodynamic force and surface tension each grain is embedded in a liquid layer of thickness δ_{\max} .

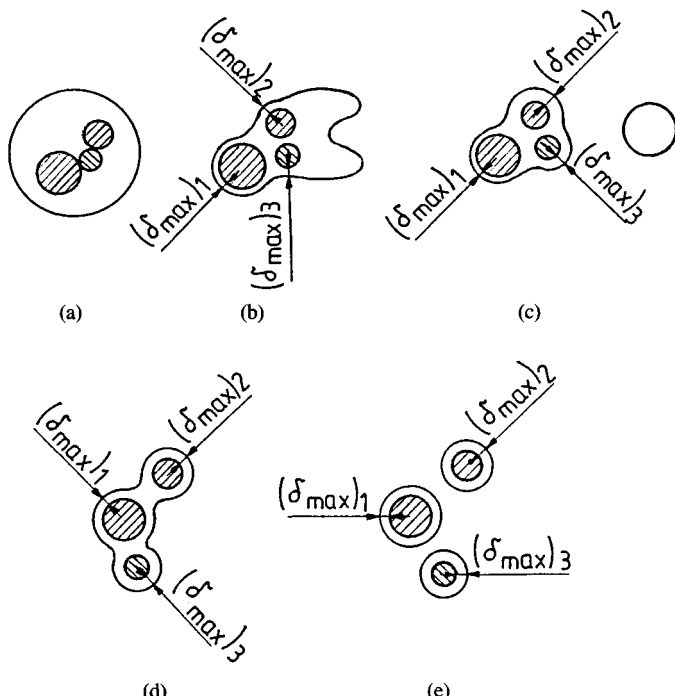


Figure 2-27 Model of the disintegration of a drop containing three grains; (a–e) consecutive stages of disintegration.

Example 2-2 Determine the air velocity V_G in a boiler burner in which secondary disintegration of the fuel drops occurs at $We^* = 14$. The burner of the cocurrent type contains a rotary atomizer, which generates the drop jet with a disintegration angle of 90° (45° with respect to the direction of air flow). Additional data: the velocity of the drops discharging from the atomizer $V_L^1 = 80$ m/s, drop diameter $D = 1$ mm, fuel surface tension at temperature $115^\circ = \sigma = 20 \times 10^{-3}$ N/m, air density at temperature 300°C is $\rho_G = 0.61$ kg/m³.

SOLUTION The minimum relative velocity (critical velocity) of the air, which is able to cause the secondary disintegration of drops, follows from Eq. (2-95):

$$V = V_{\min} = \sqrt{\frac{\sigma We^*}{\rho_G D}} = \sqrt{\frac{(20 \times 10^{-3})(14)}{(0.61)(1 \times 10^{-3})}} \approx 21 \text{ m/s}$$

The axial velocity of drops equals

$$V_L = V_L' \cos 45^\circ = 80 \times 0.7 = 56 \text{ m/s}$$

Therefore the air velocity equals

$$V_G = V_L + V_{\min} = 56 + 21 = 77 \text{ m/s}$$

It is a high velocity, which requires that a blower with a compression of 4000 Pa (400 mm H₂O) and high power consumption be used.

2-4.2 Collision of Drops

Collision of drops with each other or with other solids can lead to disintegration or coalescence of the drops. Collision of drops after they leave the atomizer is unlikely, since the drops move on their trajectories and do not come in contact with each other. However, larger drops move faster than smaller ones and can catch up and collide with the latter.

Various atomizing devices, such as climatic chambers, scrubbers, and agricultural sprayers, have a large number of atomizers operating simultaneously, and their drop jets can cross each other in an intended or unintended way. It turns out that such collisions of drop jets do not change the drop spectrum significantly, since the range of Weber numbers in this case is only $We = 0.5$ to 10 [41]. It should also be taken into consideration that the collision of drops can cause their coalescence as well as disintegration.

An extensive evaluation was carried out [3] regarding the collision of drops of a water-glycerol mixture with density $\rho_L = 1230$ kg/m³, viscosity $\mu_L = 15 \times 10^{-2}$ to 50×10^{-2} Pa · s, and surface tension $\sigma = 67 \times 10^{-3}$ N/m at the conditions $R_2/R_1 = 1$ to 2.5, $Re = 10$ to 25, $We = 80$ to 500, $\Omega = 0$ to 20, where the drop radii R_1 and R_2 were in the range 0.2 to 0.4 mm, the Reynolds number

$$Re = \frac{\rho_L |\mathbf{V}_1 - \mathbf{V}_2| 2R_1}{\mu_L}$$

the Weber number

$$We = \frac{\rho_L |\mathbf{V}_1 - \mathbf{V}_2|^2 2R_1}{\sigma}$$

and the parameter

$$\Omega = \frac{|\mathbf{M}|}{\sqrt{\rho_L \sigma} R_0^{7/2}}$$

An angular momentum \mathbf{M} arises for nonaxial drop collision. A system of two drops has an angular momentum with the pole located at the center of masses of the drops:

$$\mathbf{M} = (\mathbf{R}_1 \times \mathbf{V}_1)m_1 + (\mathbf{R}_2 \times \mathbf{V}_2)m_2 = m_2$$

Here m_1 and m_2 are the masses of the colliding drops, \mathbf{V}_1 and \mathbf{V}_2 are the velocity vectors of the drops, the relative velocities of collision were 3 to 8 m/s, and the radius

$$R_0 = (R_1^3 - R_2^3)^{1/3}$$

Figure 2-28 shows film frames for three cases of drop linking. In the first case (Fig. 2-28a), i.e., for $\Omega < \Omega_{1*} \approx 3.4 \pm 0.5$, the rotating drop assumes a form similar to an ellipsoid. In the second case (Fig. 2-28b), for $\Omega > \Omega_{2*}$, the drop assumes the shape of an ellipsoid and rotates around its shorter axis without any

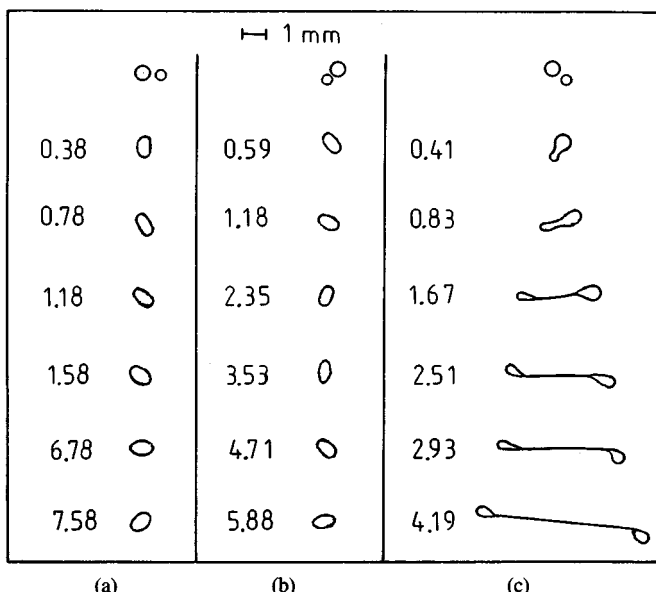


Figure 2-28 Frames of a film illustrating drop coalescence; numbers denote the time from the collision in milliseconds.

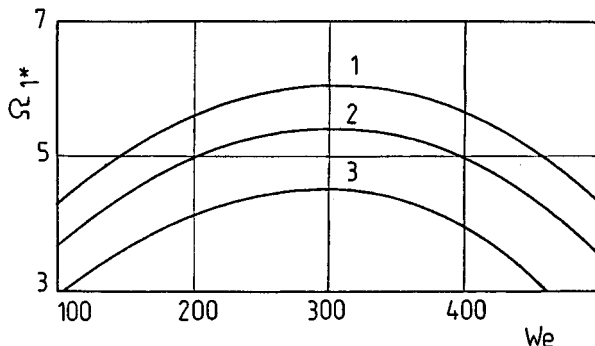


Figure 2-29 Function $\Omega_{1*} = f(We, R_2/R_1)$; 1, $R_2/R_1 = 1.1$; 2, $R_2/R_1 = 1.4$; 3, $R_2/R_1 = 2.05$.

significant change of shape. As the parameter Ω increases, the ellipsoid elongates. In the third case (Fig. 2-28c), for $\Omega > \Omega_{1*} \approx 6 \pm 0.9$, only drop linking that eventually led to their disintegration was observed. As a result of disintegration, two drops were obtained with dimensions comparable to those of the initial drops, or three to four drops (satellites) developed after the thin thread linking the drops disintegrated.

The border separating drop linking from drop disintegration is shown in Fig. 2-29. For $\Omega > \Omega_{1*}$ secondary disintegration occurs, and for $\Omega < \Omega_{1*}$ drop coalescence occurs.

A different approach to drop collision is presented in [40]. The five characteristic cases of collision of drops with various diameters in the stationary gas are as follows (Fig. 2-30):

1. Range $0.35 \leq We \leq 0.75$. Because of the small relative velocities of colliding drops, the small drop rebounds from the big one.
2. Range $1 \leq We \leq 7.5$. Drop coalescence occurs; however, the large drop deforms and when a certain aerodynamic interaction occurs it may disintegrate.

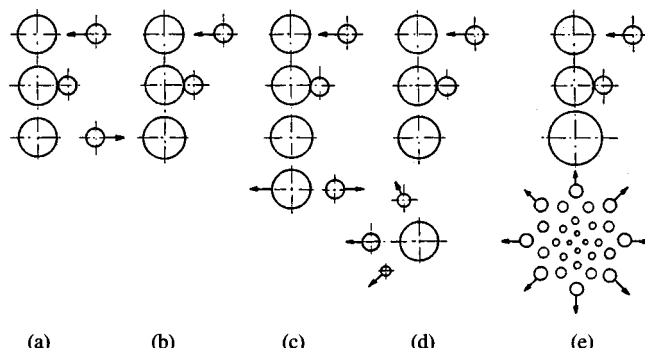


Figure 2-30 Schematic diagram of the result of drop collision as a function of Weber number.

3. Range $7.5 < \text{We} < 20$. Momentary drop coalescence occurs and the final disintegration is into drops with dimensions similar to those of the drops before the collision.
4. Range $\text{We} > 25$. Puncture of the large drop occurs, and small drops may develop as well.
5. Range $\text{We} > 50$. An explosive breakup of the large drop into a large number of small drops occurs.

An example of the collision of drops with solid bodies is the collision with wire nets. Wire nets of mesh size $a = 1.2 \times 1.2$ to 10×10 mm and wire diameter $d = 0.4$ to 1.2 mm were used [34]: The wire nets were placed 250 to 2000 mm behind the atomizer. An optimum ratio $a/d = 5$ was found, since for larger ratios the probability of collision between the drop and the mesh decreases, and for smaller ratios the flow capacity of the mesh worsens and the mesh acts as a generator of large drops.

This approach was implemented for coagulation of drops of various chemical compounds during aerial agricultural spraying [51]. Atomizers were also used with wire screens, and as an effect of screening the median drop diameter increased approximately 1.7-fold and small drop sizes decreased more than 3-fold [45]. Drop coagulation in agricultural spraying, especially in spraying from an aircraft, is often used to accelerate the drop fall (reduction of drop drifting caused by the wind).

The research described in [34] established that the collision of drops and the mesh improves the atomization by 20 to 24%. An equation was derived that can be used to calculate the ratio of mean diameter for the disintegrated drops D_2 and initial drops D_1 with an error lower than 5%:

$$\frac{D_2}{D_1} = 4.36 \text{We}^{-0.2} \left(\frac{a}{d} \right)^{-0.49} e^{0.1(a/d)} \quad (2-104)$$

while

$$\text{We} = \frac{\rho_L V_D^2 D_1}{\sigma}$$

where ρ_L = liquid density

V_D = velocity of drop at the moment of collision with the mesh.

2-5 DROP BALLISTICS

Drop disintegration can be an indirect or direct process. In the first case the jet of drops is subjected to further transformations, which takes place, for instance, during combustion. In the second case the jet of drops is utilized directly, as in paint spraying. In both cases the atomized liquid can be used appropriately only when it moves in an intentional way. This requires, of course, that the drop trajectory be known, in particular the trajectory of the whole jet of drops.

The problem of drop ballistics is a complex one and difficult to define in an analytical as well as an experimental way. The difficulty stems from the following reasons:

1. The motion of drops occurs in a field of different changing forces.
2. The motion of a single drop and the motion of the jet of drops are described by different laws.
3. The jet of drops contains drops of various diameters, and their motion is different from that of drops with the mean diameter (all calculations are done for drops with the mean diameter).
4. Drops deform and their size changes (secondary disintegration, evaporation) as they move, which is especially noticeable for certain distances from the atomizer (greater than 0.5 to 1.0 m).
5. Solid particles can deposit on the drop surface, changing its mass.
6. The motion on drops is in general unsteady.

2-5.1 The Motion of Individual Drops

Drop falling is the simplest case of motion. It often occurs in air or in other media. It occurs in spray drying, combustion, and agricultural spraying.

Spray drying is used, among other things, to produce spherical granules in the pharmaceutical industry. Medication, dissolved or dispersed in various easily melting materials (fat, sugar), is sprayed upward, and during the rise and fall it cools down and solidifies; the cooling air can be supplied from below. An extensive theoretical analysis of the rise and fall of drops has been conducted [33]. The objective was to determine the height of a spray drying column, and the results obtained were confirmed experimentally.

In fuel combustion in boiler burners, the air velocity can be adjusted to the velocity of the falling drops in such a way that the drops do not fall but are suspended in air, which makes the combustion easier. Such conditions are satisfied, for instance, for drops with a diameter of 2 to 3 mm for an air velocity 10 to 15 m/s [38].

Knowledge of the process of the drop fall is most useful in the case of agricultural spraying. Such spraying poses a serious threat of pollution due to improper spread of pesticides. The velocity of drop fall is determined by using the equation of free fall, which will be discussed later. Chemical drifting caused by the motion of the aircraft and wind results in a change of the drop trajectories.

The drops most susceptible to a change of trajectory and therefore more desirable are small drops with diameter $D > 150 \mu\text{m}$; for herbicides these diameters are even larger ($D = 300$ to $500 \mu\text{m}$). The increase in drop diameter leads to an increase in the fall velocity and therefore reduces the drop drifting.

During the motion of an aircraft a significant role is played by the free vortex flowing off the lifting surface. For most agricultural aircraft the typical air velocities in the vortex are approximately 2 m/s [45], so the motion of drops

with diameter $D < 500 \mu\text{m}$ will be disturbed by the vortex because this fall velocity is also approximately 2 m/s. The motion of a helicopter generates a propeller race, which is a vortex moving toward the ground with velocity 12 to 20 m/s. The drops move along with the vortex, which causes the axial and circumferential components of velocity to be large. When the circumferential component of velocity is large, some of the drops can escape beyond the crop region.

There have been attempts at a theoretical approach to this difficult problem of drop fall during agricultural spraying. Goering et al. [20] explored three approaches: regression models, diffusion models, and trajectory models. The regression models use experimental observations relating the dependent variables to required independent variables. Such models do not explore the physical phenomena occurring during drop fall and can be applied only to cases of fall to which the collected observations refer. The diffusion models are based on the similarity of drop spreading in the atmosphere to molecular diffusion. Their accuracy depends on the accuracy of determining the average wind velocity and the motion or vortices. The trajectory models are based on Newton's second law. The components of acceleration are derived from the components of the forces acting on the individual drops. The accelerations are integrated to determine the components of velocity and displacement of drops as a function of time. In trajectory models the data obtained in wind tunnels for small turbulence are used.

The drift distance L due to the wind action during agricultural treatment can be approximately derived from the equation

$$L = H \frac{V_G}{V_\infty}$$

where H = altitude

V_G = wind velocity

V_∞ = drop fall velocity

All calculations of drop fall require that the fall velocity be known. The drops fall initially in an accelerated motion, but the distance traveled in this way is only a small fraction of the whole distance of fall. When the weight of the drop G (decreased by the buoyancy of the drop) is balanced by the aerodynamic drag F , i.e., when

$$G = F \quad (2-105)$$

the drop assumes the uniform motion. The weight of a drop with a spherical shape (decreased by the buoyancy of the drop) is equal to

$$G = \frac{\pi D^3}{6} g (\rho_L - \rho_G) \quad (2-106)$$

and the *aerodynamic drag* is equal to

$$F = C_D \frac{\pi D^2}{4} \frac{\rho_G V_\infty^2}{2} \quad (2-107)$$

where C_D is the aerodynamic drag coefficient.

The velocity of drop fall V_∞ is a characteristic parameter in the theory of drop fall. The index ∞ denotes that the fall proceeds in an unlimited medium. This is the drop free fall in the gravitational field. The free character of fall is ensured when the fall proceeds uniformly in a motionless gas with a concentration of drops so small that there is no interaction between them. When the ambient gas moves upward, the velocity V_∞ is the relative velocity between the drop and gas.

From these equations we obtain the velocity of drop fall:

$$V_\infty = \sqrt{\frac{4 g (\rho_L - \rho_G) D}{3 \rho_G C_D}} \quad (2-108)$$

Since $\rho_L \gg \rho_G$, Eq. (2-108) assumes the form

$$V_\infty = \sqrt{\frac{4 g \rho_L D}{3 \rho_G C_D}} \quad (2-109)$$

To determine the velocity V_∞ it is necessary to know the value of the aerodynamic drag coefficient C_D . For the case of the free fall of spherical particles (not drops) this problem has been solved completely. The coefficient C_D is then a function of Reynolds number Re_∞ :

$$Re_\infty = \frac{V_\infty D}{\nu_G} = \frac{\rho_G V_\infty D}{\mu_G} \quad (2-110)$$

The coefficient C_D for spherical particles was established experimentally in the wide range of Reynolds numbers Re_∞ (Fig. 2-31). Curve 1 has a complicated shape. It can be divided into three ranges, which correspond to different types of motion:

- I—laminar range, $1 \times 10^{-4} < Re_\infty < 0.4$
- II—transient range, $0.4 < Re_\infty < 1 \times 10^3$
- III—turbulent range, $1 \times 10^3 < Re_\infty < 2 \times 10^5$

The laminar range starts with the Reynolds number $Re_\infty \approx 1 \times 10^{-4}$, since for smaller values the influence of Brownian motion on the fall is manifest. The border between the laminar and transient ranges corresponds to the point of tangency of curve 1 and line 2. Often this border broadens even up to $Re_\infty = 2$, which does not cause significant errors and simplifies the calculations.

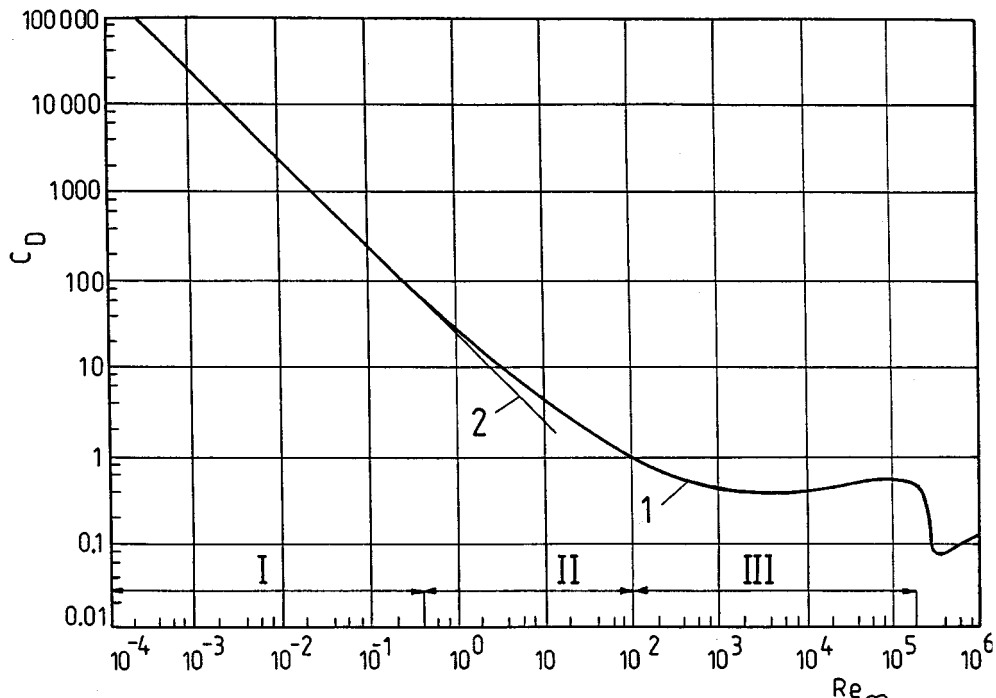


Figure 2-31 Drag coefficient $C_D = f(\text{Re}_\infty)$; 1, experimental curve; 2, straight line according to Eq. (2-111).

To analyze the character of curve $C_D = f(\text{Re}_\infty)$, we must evaluate the conditions of the flow around a sphere. The sphere is acted on by aerodynamic drag, which is the sum of the frictional resistance and pressure resistance. The frictional resistance is a resultant of the tangential forces, and the pressure resistance is a resultant of pressure forces acting on the surface of the sphere.

The pressure distribution on the sphere's surface is shown in Fig. 2-32. At point 0, called the *stagnation point*, deceleration of the flow occurs; the maximum overpressure in Fig. 2-32 corresponds to this point. The velocity of flow increases from point 0 to point 1 while the pressure decreases; i.e., a negative pressure gradient exists. The lowest static pressure (the maximum negative pressure) is at point 1.

From point 1 the flow velocity decreases and the pressure increases; i.e., positive pressure gradient exists. The positive pressure gradient, as is well known, causes separation of the boundary layer. If the boundary layer formed at the sphere surface is of a laminar character its separation begins at point 2.

If the laminar boundary layer changes into a turbulent boundary layer, its separation will start on the right side after point 2, which will cause a decrease of the vortex region behind the sphere. This is represented in Fig. 2-31 by a jump in the curve, which corresponds to the transition from a laminar to a

turbulent boundary layer, which occurs at the critical Reynolds number $\text{Re}_\infty = \text{Re} \approx 3 \times 10^5$. The coefficient C_D decreases three- to fivefold in this case. This phenomenon is called the *resistance crisis*, but it does not affect drop fall because it occurs in the range of smaller Reynolds numbers.

The names of the regions I, II, III are conventional and do not have anything in common with the character of the boundary layer, since in all of these regions the boundary layer is laminar. These names are, however, legitimate, which will be proved. The coefficient of drop resistance will be discussed further; for current considerations, however, the resistance coefficient for spherical particles will be used.

In the laminar region, I, line 2 is part of curve 1 (Fig. 2-31) and satisfies the equation

$$C_D = \frac{24}{\text{Re}_\infty} \quad (2-111)$$

Substituting Eq. (2-11) into Eq. (2-107) and taking Eq. (2-110) into consideration, we obtain

$$F = 3\pi\mu_G DV_\infty \quad (2-112)$$

This is the *Stokes equation*, which indicates that the resistance F is proportional to the dynamic viscosity of the gas, sphere diameter, and velocity of fall and does not depend on the gas density, which is typical of laminar flows. Equation (2-112) is commonly used in the theory of motion of small rigid spheres. This equation is also applied to the motion of drops.

In the *transient range, II*, various equations are applied to approximate curve 1 in this range of Reynolds numbers Re_∞ . One of these, which is particularly useful in the range $2 < \text{Re}_\infty < 500$, is the *Allen equation*

$$C_D = \frac{18.5}{\text{Re}_\infty^{0.6}} \quad (2-113)$$

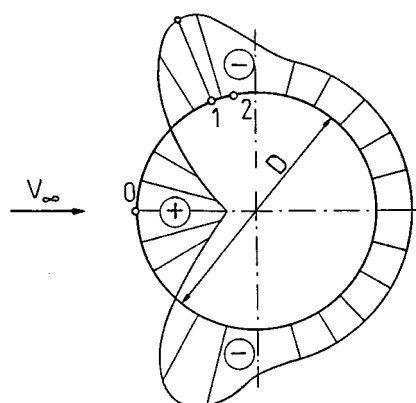


Figure 2-32 Pressure distribution on the surface of a sphere.

Substituting Eq. (2-113) into Eq. (2-107) and including Eq. (2-110), we obtain

$$F = 2.3\pi\rho_G^{0.4}\mu_G^{0.6}D^{1.4}V_\infty^{1.4} \quad (2-114)$$

In the *turbulent range, III*, a constant C_D value is assumed:

$$C_D \approx 0.44 \quad (2-115)$$

which is justified by the character of curve 1 in this range of Reynolds numbers Re_∞ .

Substituting Eq. (2-115) into Eq. (2-107), we obtain

$$F = 0.44 \frac{\pi D^2}{4} \frac{\rho_G V_\infty^2}{2} \quad (2-116)$$

This is the *Newton equation*, which indicates that the resistance is proportional to the square of diameter, the square of sphere velocity, and the gas velocity and does not depend on the gas viscosity, which is typical for turbulent flows.

Having defined C_D in the individual regions, we can establish the equations for the *fall velocity* V . For the *laminar region*, after substituting C_D from Eq. (2-111) into (2-108) and accounting for Eq. (2-110), we obtain

$$\dot{V}_\infty = \frac{g(\rho_L - \rho_G)D^2}{18\mu_G} \quad (2-117)$$

As seen, the velocity of laminar fall is proportional to the square of the sphere diameter.

For *turbulent flow*, after substituting C_D from Eq. (2-115) into Eq. (2-108), we obtain

$$V_\infty = 1.74 \sqrt{\frac{g(\rho_L - \rho_G)D}{\rho_G}} \quad (2-118)$$

As seen, the velocity of turbulent fall is proportional to the square root of the sphere diameter. It is worth determining the diameters of spheres whose fall motion is turbulent. Assign the limiting value $Re_\infty = 1 \times 10^3$, we obtain from Eqs. (2-118) and (2-110)

$$D \geq 69 \sqrt[3]{\frac{\mu_G^2}{g(\rho_L - \rho_G)\rho_G}} \quad (2-119)$$

From this equation it follows that in the case of drops falling in the air, $D \geq 2$ mm. Such large drops, of course, deform during the fall.

Summarizing the problem of the fall of spherical particles in a stationary gas, we can draw a *curve of the fall velocity* (Fig. 2-33) that defines the relation of fall velocity V_∞ to particle diameter D . In the laminar range the velocity curve according to Eq. (2-117) is a parabola, curve 1, with a vertical axis of symmetry, and in the turbulent range according to Eq. (2-118) it is a parabola, curve 3, with

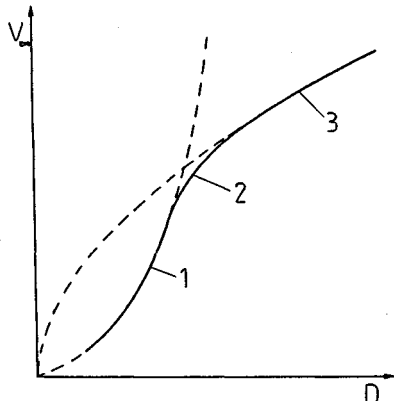


Figure 2-33 Fall velocity; 1, laminar region; 2, transient region; 3, turbulent region.

a horizontal axis of symmetry. In the transient range the intermediate line 2 occurs. The drop drag coefficient C_D should be lower than the drag coefficient of a spherical particle with the same volume. This is because the drop surface is flexible, since circulation develops inside the drop, whereas the surface of the particle is rigid. This causes the velocity gradient on the drop surface to decrease, which causes the force of resistance also to decrease. Hadamard and Rybczynski independently derived the equations for the free falling velocity V_∞ and aerodynamic drag F for the drop in the laminar range, i.e. in the range of small drops subjected to deformations [39].

$$V_\infty = V'_\infty \frac{3\mu_G + 3\mu_L}{2\mu_G + 2\mu_L} = V'_\infty \frac{1 + \mu_G/\mu_L}{1 + \frac{2}{3}(\mu_G/\mu_L)} \quad (2-120)$$

$$F = F' \frac{2\mu_G + 3\mu_L}{3\mu_G + 3\mu_L} = F' \frac{1 + \frac{2}{3}(\mu_G/\mu_L)}{1 + \mu_G/\mu_L} \quad (2-121)$$

where V'_∞ = velocity of fall of a spherical particle from Eq. (2-117)

F' = aerodynamic resistance for a spherical particle from Eq. (2-112)

μ_G, μ_L = dynamic viscosities for ambient gas and liquid (drops), respectively
In the case of rigid particles, whose viscosity is $\mu_L = \infty$, it follows from Eqs. (2-120) and (2.121) that $V_\infty = V'_\infty$ and $F = F'$; i.e., the equations for drops assume the form of equations for particles.

Experimental research shows that the character of curves 1, 2, and 3 representing the resistance coefficient $C_D = f(\text{Re})$ for drops is different from the curve for spherical particles, 4 which is shown in Fig. 2-34. The curves for drops display characteristic features. For a certain value of Re the resistance coefficient C_D increases rapidly, which takes place sooner the lower the surface tension σ is. The increase of C_D results from the drop deformation and lasts until the drop disintegrates. In the range of small Reynolds number, i.e., for small drops, the curves representing C_D fall beneath curve 4, which indicates the effect of liquid circulation inside the drop. There can be different cases, however, as depicted by curve 3.

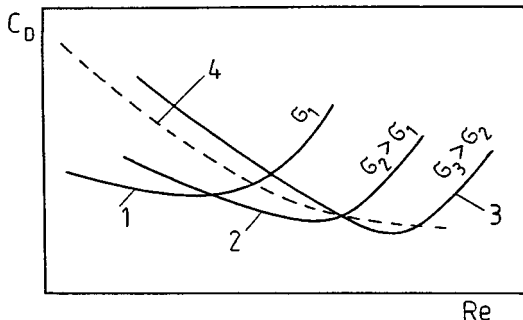


Figure 2-34 Comparison of the drag coefficient for drops with different surface tension (curves 1, 2, and 3) and for a spherical particle (curve 4).

Figure 2-35 shows the results of investigation of the drop drag coefficient as a function of Weber number, which allows assessment of the influence of drop deformation [39]. The relative drag coefficient was used:

$$\bar{C}_D = \frac{C_D}{C'_D} \quad (2-122)$$

where C'_D denotes the drag coefficient of a spherical particle with the same volume as the drop. The Weber number is equal to

$$We = \frac{\rho_G V_D^2 D}{\sigma} \quad (2-123)$$

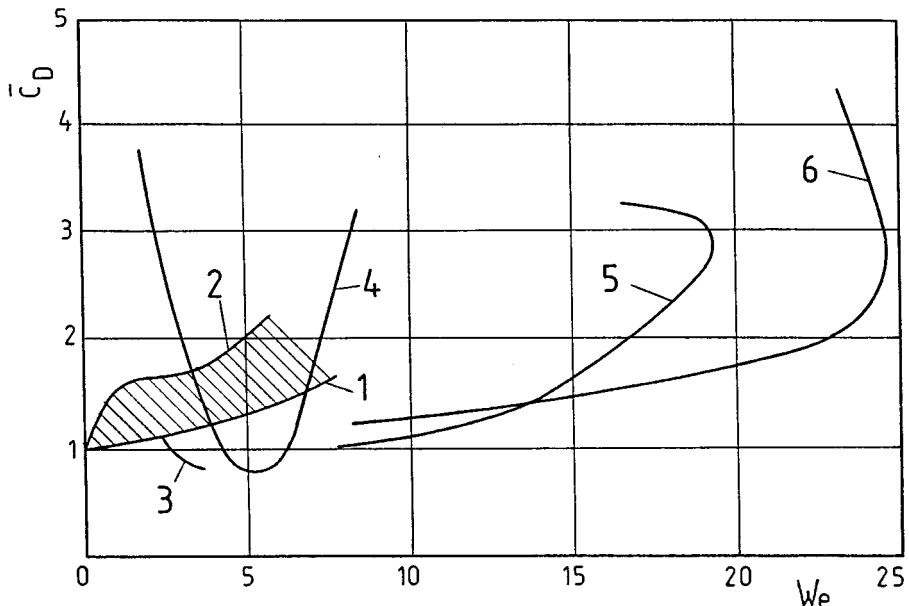


Figure 2-35 Dependence of the relative drop drag coefficient \bar{C}_D on Weber number We .

where V_D denotes the drop velocity. The shaded area between curves 1 and 2 contains the results obtained by various authors for the case of falling water drops in air. The coefficients of drag for drops are higher than those for equivalent (volumewise) spherical particles.

Curve 3 refers to the fall of drops of distilled water in air; the influence of the circulation inside the drop on the decrease of \bar{C}_D ($C_D < 1$) is noticeable. Curve 4 corresponds to the injection of a single drop of water of diameter 2 mm into a motionless gaseous environment; the unsteady motion of the drop, assisted by deformation into the form of a flattened ellipsoid, causes the shape of the curve to be different than for the steady motion. Curves 5 and 6 refer to the unsteady motion of a drop in a Venturi tube; curve 5 refers to drop diameter 104 μm and $P_{\min}/P_t = 0.814$ (P_{\min} denotes the static pressure in the minimum cross section of the tube and P_t the total pressure); and curve 6 refers to drag diameter 166 μm . The character of the two latter curves indicates the inertial delay of drop deformation and the increase of the drag coefficient until the onset of the drop disintegration.

The following equations are presented in [11]:

$$C_D \text{We} \left(\frac{K_F \rho_G}{\rho_L - \rho_G} \right)^{0.15} = \frac{4}{3} \left[\text{Re} \left(\frac{\rho_L - \rho_G}{K_F \rho_G} \right)^{0.15} + 0.75 \right]^{1.275} \quad (2-124)$$

$$C_D \text{We} \left(\frac{K_F \rho_G}{\rho_L - \rho_G} \right)^{0.15} = 0.045 \left[\text{Re} \left(\frac{\rho_L - \rho_G}{K_F \rho_G} \right)^{0.15} + 0.75 \right]^{2.37} \quad (2-125)$$

where the Weber number follows from Eq. (2-121); K_f is a dimensionless index:

$$K_f = \frac{\rho_G \sigma^3}{g \mu_G^4} \quad (2-126)$$

Equations (2-124) and (2-125) are shown in Fig. 2-36. For the point of intersection of lines 1 and 2 we have

$$\frac{\text{Re}}{\text{We}} = 0.41 \left(\frac{K_F \rho_G}{\rho_L - \rho_G} \right)^{0.27} \quad (2-127)$$

This intersection point corresponds to the minimum value of C_D , i.e., to the maximum of the drop fall velocity $(V_D)_{\max}$. This velocity follows from Eq. (2-127):

$$(V_D)_{\max} = 2.44 \frac{\sigma}{\mu_G} \left(\frac{K_F \rho_G}{\rho_L - \rho_G} \right)^{0.42} \quad (2-128)$$

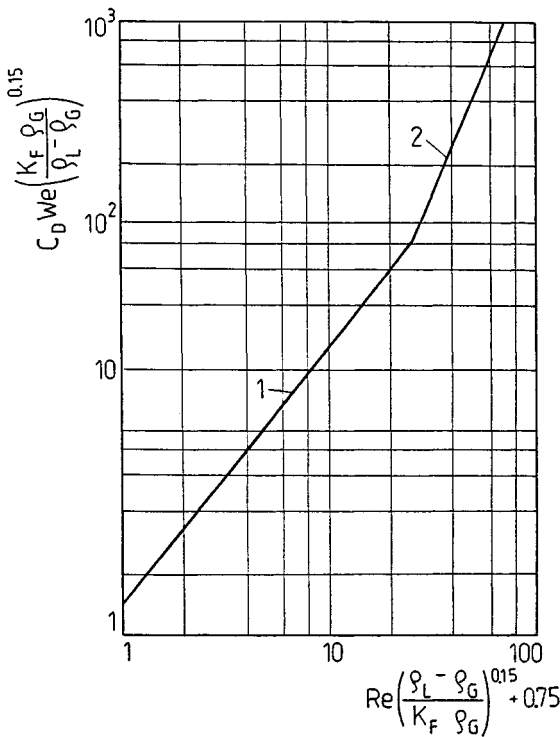


Figure 2-36 Graphic representation of the equations corresponding to the drag coefficient of a drop C_D ; 1, Eq. (2-124); 2, Eq. (2-125).

The maximum drop diameter D_{\max} corresponding to this velocity is given by

$$D_{\max} = 8.88 \frac{\mu_G^2}{\rho_G \sigma} \left(\frac{K_F \rho_G}{\rho_L - \rho_G} \right)^{0.42} \quad (2-129)$$

because larger drops disintegrate. The simplified equation can also be applied to determine the diameter D_{\max} .

$$D_{\max} = 0.1205 \left(\frac{\sigma}{\rho_L - \rho_G} \right)^{1/2} \quad (2-130)$$

The *motion of a drop in a gas jet* can proceed in a different ways. First, we consider the case in which the drop is introduced with an infinitesimal velocity into the stream of gas, which flows with constant velocity. The gas accelerates the drop, which is subjected to a varying aerodynamic force F . This is similar to the initial period of drop fall in a stationary gas.

The following simplifying assumptions are made [38]: one-dimensional flow, absence of gravity forces, no drop evaporation, and the drop is spherical and nondeformable. Newton's second law is

$$\frac{d(mV_D)}{dt} = F \quad (2-131)$$

where m is the mass of the drop

$$m = \frac{\pi D^3}{6} \rho_L$$

and F is the varying aerodynamic force, which carries the drop with a relative velocity $w = V$ between the gas and the drop

$$w = v - u$$

Here $v = V_G$ is the gas velocity, and $u = V_D$ is the drop velocity. The force F is derived from Eq. (2-107), where instead of the velocity V_∞ we substitute the velocity W . The same applies to Eq. (2-110). The drag coefficient was derived from the formula

$$C_D = \pi \left(0.128 + \frac{12.8}{\text{Re}} \right) \quad (2-132)$$

which ensures good agreement of results in the range of Reynolds numbers $\text{Re} = 2$ to 1×10^4 . After substituting and simplifying, we obtain the differential equation

$$\frac{dw}{dt} = -(Aw^2 + Bw) \quad (2-133)$$

where

$$A = 0.096 \frac{\pi \rho_G}{\rho_L D}, \quad B = 9.6 \frac{\pi v_G \rho_G}{\rho_L D^2}$$

Taking into account that for $v = \text{constant}$,

$$\frac{du}{dt} = - \frac{dw}{dt}$$

Multiplying Eq. (2-133) by dx , we obtain

$$dx = - \frac{dw(v - w)}{Aw^2 + Bw} \quad (2-134)$$

since the absolute drop velocity equals

$$u = \frac{dx}{dt} = v - w$$

The integration has to be carried out within the limits of a drop path from $x = 0$ to x and relative drop velocity from v to w .

Finally, we obtain the distance traveled by the drop:

$$\begin{aligned} x &= - \int_v^w \frac{dw(v - w)}{w(Aw + B)} = \left| \left(\frac{v}{B} + \frac{1}{A} \right) \ln(Aw + B) - \frac{v}{B} \ln w \right|_v^w \\ &= EvD^2 \left[\left(1 + \frac{C}{v} \right) \ln \frac{w + C}{v + C} - \ln \frac{w}{v} \right] \end{aligned} \quad (2-135)$$

where

$$C = 100 \frac{\nu_G}{D}, \quad E = \frac{\rho_L}{9.6\pi\mu_G}$$

Coordinate x is the path on which the relative drop velocity W decreases from velocity v to an arbitrary velocity w ; i.e., the absolute drop velocity increases from $u = 0$ to $u = v - w$. For the onset of drop motion ($w = v$) it follows from Eq. (2-135) that $x = 0$, and for complete drop drifting ($w = 0$) theoretically the path $x = \infty$ is needed. It is also seen that path x is proportional approximately to the gas velocity ν and the square of drop diameter D .

Figure 2-37 shows the relationship between the path length x and the relative velocity w of drops with various diameters D for several velocities of the air flow ν following from Eq. (2-135). As seen, the relative velocity between the small drops and the high-velocity air decreases very rapidly.

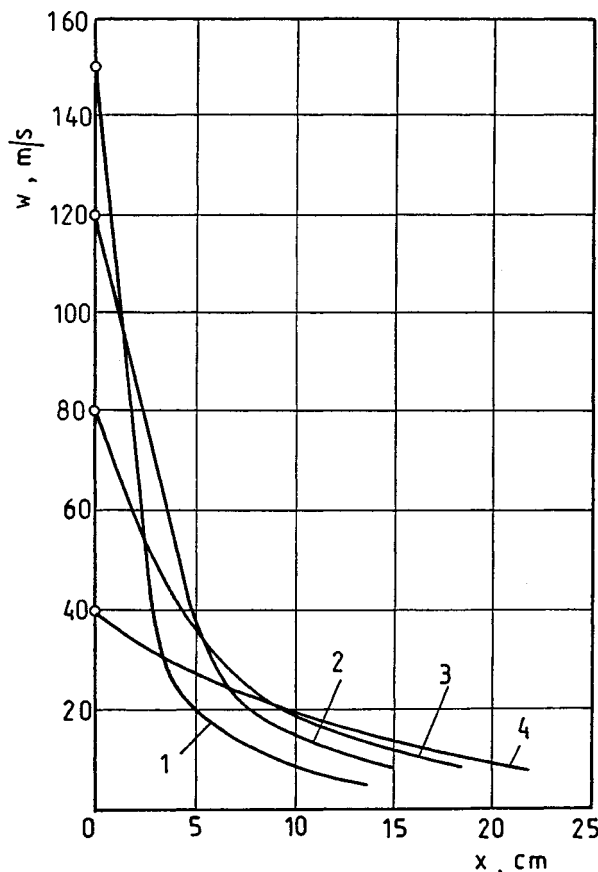


Figure 2-37 Path length of a drop in air flow; 1, $D = 39 \mu\text{m}$; 2, $D = 49 \mu\text{m}$; 3, $D = 70 \mu\text{m}$; 4, $D = 131 \mu\text{m}$.

The relative velocity for an arbitrary distance x can be derived from Eq. (2-135):

$$w - a(w + C)^b = v \left[1 - \frac{x^c(v + C)}{C} \right] \quad (2-136)$$

where

$$a = \frac{v(v + C)^{(v - C)/v}}{C}, \quad b = \frac{C}{v}, \quad c = \frac{9.6\pi\mu_G x}{v\rho_G D^2}$$

From these analytical or graphical relations, we can also determine the time corresponding to the particular path length.

The drop acceleration requires a certain time depending on the drop diameter. For very small drops this time is very short; for example, drops of an oil mist with a diameter 2 μm in an air jet with velocity 50 to 150 m/s require a velocity equal to 90% of the air velocity at a distance smaller than 1.32 mm [5]. When drops are introduced into an accelerating gas flow, this time is longer. For example, when large drops of $D = 2$ to 4 mm were injected into a Venturi tube, the velocity attained in the smallest cross section was only 20 to 30% of the gas velocity (10 to 35 m/s) [38].

Now the reverse case of decelerated motion of the drop will be discussed. This takes place when the drops are discharged from an atomizer into the stationary environment. In that way, the range of the drop can be determined. Making assumptions similar to the previous ones and assuming the drag coefficient for the drop is

$$C_D = \frac{n}{Re^{0.5}} \quad (2-137)$$

we obtain the simplified equation for the drop path length L_D [6].

$$L_D = \frac{8\rho_L D^{3/2}}{3n\rho_G \sqrt{v_G}} \sqrt{V_D} \quad (2-138)$$

where V_D is the velocity of the drop leaving the atomizer. For example when $n = 11$, $V_D = 40$ m/s, and $D = 131 \mu\text{m}$ the path length of water drops in stationary air (atmospheric pressure) is $L_D \approx 50$ cm.

Now the motion and the range of drops discharging from an atomizer in the horizontal direction will be considered. Two cases will be examined: a *jet atomizer* and a *swirl atomizer* (Fig. 2-38). The following assumptions hold [43]: stationary gaseous environment, small drop sizes, and buoyancy force neglected. The equilibrium condition has the form (Fig. 2-38a)

$$\mathbf{S} = -\mathbf{F} + \mathbf{G} \quad (2-139)$$

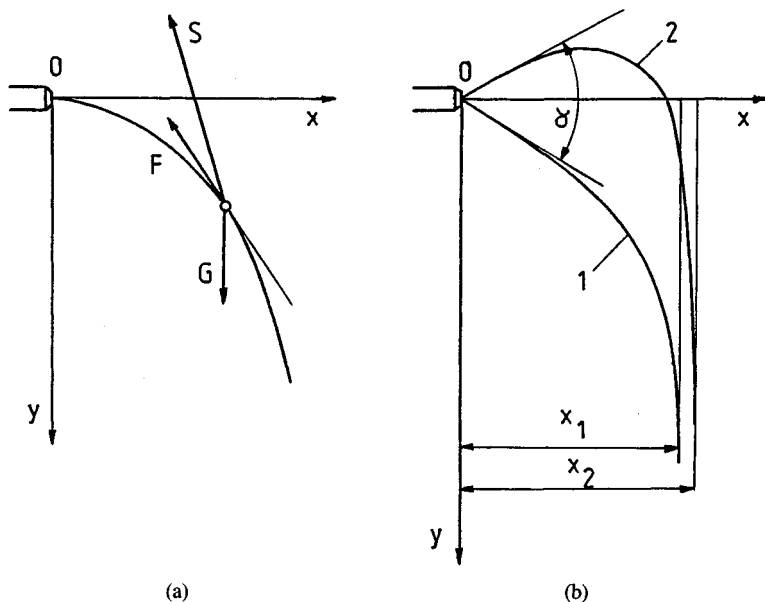


Figure 2-38 Drop trajectory: (a) swirl-less jet; (b) swirled jet; 1, trajectory with a positive vertical component of the initial velocity; 2, trajectory with a negative vertical component of the initial velocity.

where S, F, G are vectors of the inertial force, aerodynamic force, and gravity force, respectively,

$$S = \frac{\pi D^3}{6} \rho_L \frac{dw}{dt}$$

$$F = C_D \frac{\pi D^2}{4} \frac{\rho_G w^2}{2}$$

$$G = \frac{\pi D^3}{6} \rho_L g$$

and $V_D = w = \sqrt{u^2 + v^2}$ is the drop velocity with horizontal component $u = dx/dt$ and vertical component $v = dy/dt$.

The drop passes through all types of motion: turbulent, transient, and laminar. The following ranges of Reynolds numbers and resistance coefficients were assumed: turbulent motion $\text{Re} > 500$, $C_D = 0.44$; transient motion $5 \leq \text{Re} \leq 500$, $C_D = 14/\sqrt{\text{Re}}$; and laminar motion $\text{Re} < 5$, $C_D = 24/\text{Re}$, where

$$\text{Re} = \frac{wD}{\nu_G}$$

From Eq. (2-139) we obtain according to Fig. 2-38 the following sets of equations of motion for the x and y directions:

For turbulent motion:

$$\left. \begin{aligned} \frac{du}{dt} &= -0.33 \frac{\rho_G}{\rho_L} \frac{1}{D} \sqrt{u^2 + v^2} u \\ \frac{dv}{dt} &= -0.33 \frac{\rho_G}{\rho_L} \frac{1}{D} \sqrt{u^2 + v^2} v + g \end{aligned} \right\} \quad (2-140)$$

For transient motion:

$$\left. \begin{aligned} \frac{du}{dt} &= -10.5 \frac{\rho_G}{\rho_L} \frac{\nu_G^{0.5}}{D^{1.5}} (u^2 + v^2)^{0.25} u \\ \frac{dv}{dt} &= -10.5 \frac{\rho_G}{\rho_L} \frac{\nu_G^{0.5}}{D^{1.5}} (u^2 + v^2)^{0.25} v + g \end{aligned} \right\} \quad (2-141)$$

For laminar motion:

$$\left. \begin{aligned} \frac{du}{dt} &= -18 \frac{\rho_G}{\rho_L} \frac{\nu_G}{D^2} u \\ \frac{dv}{dt} &= -18 \frac{\rho_G}{\rho_L} \frac{\nu_G}{D^2} v + g \end{aligned} \right\} \quad (2-142)$$

These equations together with the initial condition $u = u_0$ and $v = v_0$ for $t = 0$, represent the Cauchy problem, which, due to the nonlinearity of the differential equations, can be solved using the numerical Runge-Kutta method. It follows from the solution that for trajectories 1 and 2 (Fig. 2-38b) $x_1 \approx x_2$, which means that the influence of gravity forces on the drop path length is small. Accounting for this fact and recognizing that the turbulent and laminar segment of the drop path is small compared to the transient segment, we derive the following equations for drop path length:

For a jet atomizer:

$$x = 0.195 \frac{\rho_L}{\rho_G} \frac{1}{\nu_G^{0.5}} \sqrt{w_0} D^{1.5} \quad (2-143)$$

For a swirl atomizer:

$$x = 0.195 \frac{\rho_L}{\rho_G} \frac{1}{\nu_G^{0.5}} \sqrt{w_0} \cos \frac{\alpha}{2} D^{1.5} \quad (2-144)$$

where w_0 is the initial drop velocity.

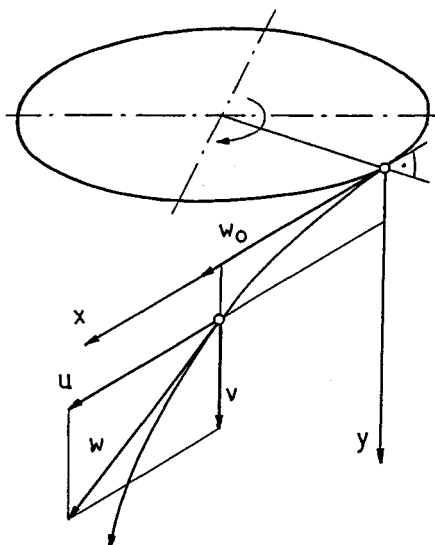


Figure 2-39 Trajectory of a drop discharging from a rotary atomizer.

Similarly, we can describe the motion of a drop discharging from a *rotary atomizer*, which has the form of a rotating horizontal disk [38]. The equilibrium of the inertial force, aerodynamic drag force, and gravity force in the *x* and *y* directions can be written as follows (according to Fig. 2-39):

$$\left. \begin{aligned} m \frac{du}{dt} &= -F_x \\ m \frac{dv}{dt} &= -F_y + mg \end{aligned} \right\} \quad (2-145)$$

where m = drop mass

$V_D = w$ = drop velocity with horizontal component u and vertical component v

F_x, F_y = horizontal and vertical components of the aerodynamic drag force, respectively

The component F_x of the aerodynamic drag force follows from Eq. (2-107), where the velocity V_∞ should be replaced by velocity w , and the drag coefficient C_D can be derived from

$$C_D = \frac{24}{Re} + \frac{4}{Re^{1/3}} \quad (2-146)$$

which refers to the range $3 < Re < 400$. The component F of the resistance force is taken from Eq. (2-112).

Substituting and integrating Eqs. (2-145), we obtain equations from which the time t and corresponding coordinates x and y can be determined:

$$t = a \ln \frac{u}{w_0} \left(\frac{1 + bu^{2/3}}{1 + bw_0^{2/3}} \right)^{3/2} \quad (2-147)$$

$$x = \frac{3a}{b} \left[w_0^{1/3} - u^{1/3} + \frac{1}{b^{1/2}} (\operatorname{arc tg} w_0^{1/3} b^{1/2} - \operatorname{arc tg} u^{1/3} b^{1/2}) \right] \quad (2-148)$$

$$y = ga \left\{ t - a \left[1 - \exp \left(-\frac{t}{a} \right) \right] \right\} \quad (2-149)$$

where w_0 = initial drop velocity equal to the circumferential velocity of the disk
 a, b = parameters

$$a = \frac{\rho_L D^2}{18 \rho_G v_G}, \quad b = 0.167 \left(\frac{D}{v_G} \right)^{2/3}$$

This case is simplified because it does not take into consideration the radial velocity of the drop. The radial component, however, is much smaller than the circumferential component w_0 . A comparison of the theoretical and experimental results showed that the mean-square error of the drop path length did not exceed 9.2%. In the experimental investigation the conditions were disk diameter 70 mm, rotation frequency 4000 to 16,000 rpm, atomized liquids diesel oil and transformer oil.

2-5.2 Motion of a Jet of Drops

The simplest case of motion of a jet of drops is the *fall of a jet (cloud)* of uniform drops or drops with similar diameters in the vast region of the motionless gas. Such a fall can proceed in two limiting regimes. The type of regime depends mostly on the concentration and diameters of drops and on the densities of the liquid and gas. These regimes have the following character:

1. *Entrainment regime*. If there is a significant hydrodynamic interaction between drops, the drops entrain the gas, which fills the space between drops. In this case the velocity of fall of the patch of drops is higher than the velocity of free fall of a single drop with the same diameter.
2. *Filtration regime*. If the hydrodynamic interaction between drops is small, the drop cloud falls more slowly than a single drop; the drops are “filtered” by the motionless gas.

The behavior of a cloud of particles moving in a viscous liquid was examined in [1].

Knowledge of the motion of the drop jet is important when considering *jet atomizers* applied in diesel engines. A literature survey [7] showed that no

mathematical model accounting for all processes occurring in the jet of drops has yet been elaborated. The existing models are based on the theory of the drawn turbulent jet using the Prandtl hypothesis of a mixing path. A model has also been developed based on the two-phase unstable turbulent jet. All of these models assume the existence of an isobaric layer of mixing between drops and ambient gas, but they do not contain equations describing the transverse motion of the gas.

Such an approach does not account for the fundamental fact that a dense front of drops develops in the front part of the jet. This causes rarefaction to appear behind the drop front, and as a result the gas is ejected from the environment through the side surface of the jet, the velocity of ejection can reach 0.657 of the axial velocity of the gas. Simultaneously, the drops move in the opposite direction with a velocity equal to approximately 0.1 of this axial velocity. For such intense transverse flows of the gas and the drops, the applicable equations of motion of a two-phase medium cannot be neglected. In addition, the presence of a negative pressure in the jet of drops makes the isobaric motion hypothesis doubtful.

A two-dimensional mathematical model of a turbulent jet of fuel drops is presented in [7]. This model incorporates the fundamental equations of motion of a two-phase medium. In order to solve simultaneously the equations of motion of the two-phase medium and the $k-\epsilon$ model of turbulence, the Godunov method was applied. The model refers to the average quantities that describe the unsteady axisymmetric motion in the jet of drops. The model consists of a system of 11 complex equations adopted for numerical solution. It is beyond the scope of this book to present this system of equation, all the more so as it also accounts for the processes of heating up and evaporation of drops.

Simplified models of drop jets generated by jet atomizers are based on the assumption that such jets can be treated as a *free turbulent jet*. Such models cannot be solved in a theoretical way without being supplemented by an experiment, which leads to very simple equations. A free turbulent jet and a jet of drops are similar in the following ways:

The boundary of the jet is of a conical shape.

The volume of the jet increases significantly because of gas ejection from the environment.

Thorough mixing of drops and gas ensures that the jet has varying density.

All exchange processes (mass, momentum, and heat) proceed due to intensive turbulence.

A scheme of the drop jet is shown in Fig. 2-40. Two segments can be distinguished in the jet: the initial segment L_1 , which is characterized by a very high concentration of drops already developed or just developing, and the main segment L_2 , characterized by the relatively low concentration of drops moving along with the ejected gas. The length of the initial segment is [29]

$$L_1 = 8.25d_0 \text{We}^{0.25} \text{Lp}^{-0.4} M^{-0.6} \quad (2-150)$$

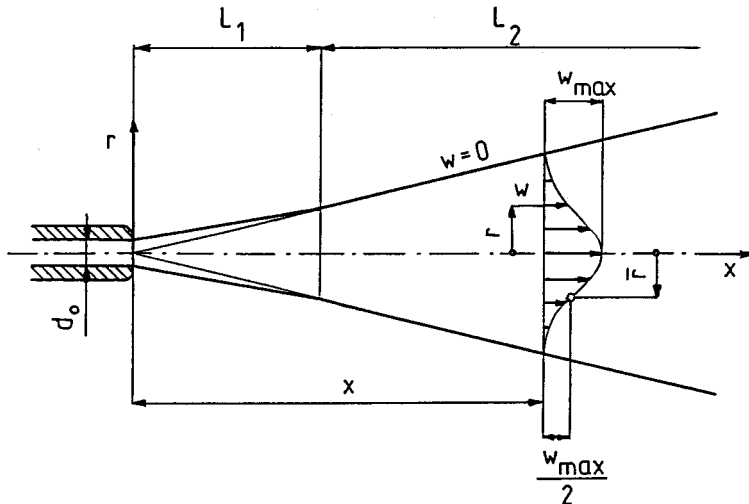


Figure 2-40 Scheme of a jet atomized in a stationary medium; L_1 , initial segment; L_2 , main segment.

The further considerations refer to the main segment. The starting point is the principle of conservation of momentum of the elementary mass of the jet. The impulses of gravity forces and pressure forces were neglected; only the impulses of the forces arising during the turbulent mass exchange between the jet and ambient gas were considered. These impulses were determined from the components of the turbulent stress tensor using the turbulent viscosity. The turbulent viscosity replaces the dynamic viscosity in Eq. (1-9) and characterizes the state of motion instead of fluid property. For simplicity, it was assumed that the turbulent viscosity is constant in the whole region of the jet.

Considering the motion of the jet as stable, the differential equation of motion was obtained. After accounting for the equation of continuity and integrating, an equation stating that the momentum along the jet is constant is obtained. The momentum remains constant because together with the decrease of jet velocity, the mass of the jet increases by the gas supply from the outside. Assuming constant jet density and making transformations, the following equation is obtained for the velocity distribution in the jet:

$$w = \frac{d_0 w_0}{2\sqrt{2} a_u x} \exp\left(-\frac{r^2}{4(a_u x)^2}\right) \quad (2-151)$$

where d_0 = diameter of the outlet orifice of the atomizer

w_0 = initial velocity of the drop jet

a_u = coefficient of free turbulence (experimental coefficient)

The velocity of the jet axis (maximum velocity in a given cross section of the

jet) follows from Eq. (2-151) after substituting $r = 0$:

$$w_{\max} = \frac{d_0 w_0}{2\sqrt{2} a_u x} \quad (2-152)$$

Since $w_{\max} = dx/dt$, after substituting w_{\max} from Eq. (2-152) and integrating we obtain the coordinate of the jet front:

$$x = \sqrt{\frac{d_0 w_0 t}{\sqrt{2} a_u}} \quad (2-153)$$

The integration constant is zero because for $t = 0$, $x = 0$. Denoting the radius of the jet as $r = \bar{r}$ for $w = w_{\max}/2$ (Fig. 2-40), we obtain from Eqs. (2-151) and (2-152)

$$\bar{r}^2 = 4(a_u x)^2 \ln 2 \quad (2-154)$$

Then substituting Eq. (2-154) into (2-151), we obtain the *generalized equation of velocity distribution in a jet*:

$$\frac{w}{w_{\max}} = \exp \left[-0.693 \left(\frac{r}{\bar{r}} \right)^2 \right] \quad (2-155)$$

In order to use this equation it is necessary to know \bar{r} , the value of a_u .

Equation (2-155) has been confirmed experimentally. It will be used in further considerations (Chapter 6). Now the experimental coefficient a_u will be discussed. This coefficient for free gas jets depends on the design of the nozzle, the velocity distribution at the nozzle outlet, and the intensity of turbulence. In the case of the spray, the dependence of a_u is more complex and can be expressed in the form of the function

$$a_u = f(\text{We}, \text{Lp}, M, N) \quad (2-156)$$

The term N accounting for the viscosity effect can be neglected, since the drop motion takes place in the range $\text{Re} = 10^3$ to 2×10^5 . The function (2-156) will be described in detail in Chapter 6.

Liquid atomization occurs most commonly not in a stationary environment but in a gas flow, examples of which are the processes of the combustion of atomized fuel, cooling, and drying. An analytical model presented in [14] is used to describe the motion of a jet of water drops during the cocurrent air flow. The model was based on Prandtl's mixing-length hypothesis by treating the liquid particle motion through the Lagrangian description. The finite-difference method and marching integration technique were used to solve the problem. The flow field was divided into cells, each of which served as a control volume registering the exchange of momentum between the drops and air. Consideration was limited to the case of the spray generated by a jet atomizer, which by its nature is characterized by a small atomization angle.

Measurements of the drop spectrum served as a basis for calculating drop velocities, drop locations, gas flow field, and gas entrainment into the spray.

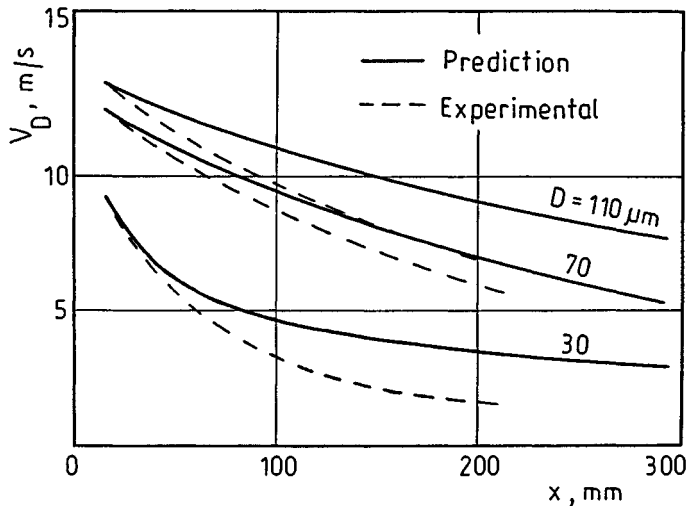


Figure 2-41 Velocity of drop V_D for drops with various diameters D as a function of distance x from the nozzle.

Figure 2-41 compares the predicted and measured changes of drop velocity. In real conditions the drop velocity decays faster than predicted because of the interaction of the entrained air. Figure 2-42a shows a streamline (1) without the spray and a streamline (2) with the spray. The rate of air flow through the cross section A-B increases from G_0 to $(G_0 + G_e)$. Figure 2-42b shows the value G_e of the entrained air and the ratio $G_e/(G_0 + G_e)$ for increasing distance x from the atomizer.

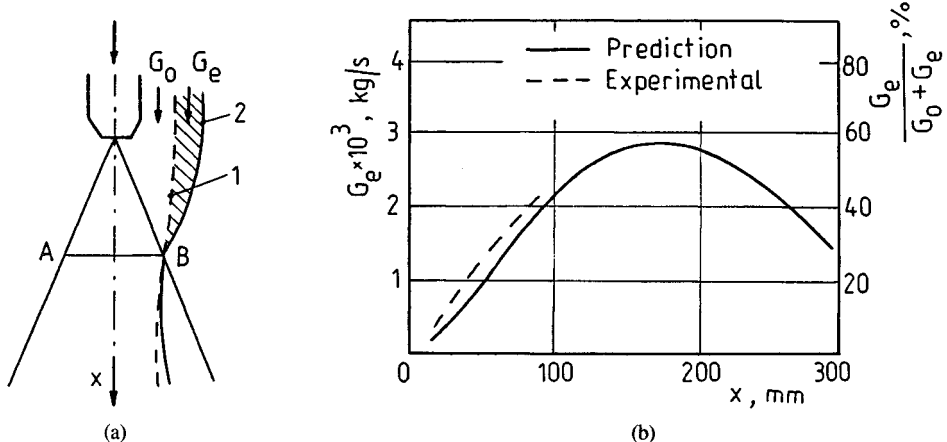


Figure 2-42 Mechanism of air entrainment by a jet of drops: (a) air streamlines; (b) flow rate of the entrained air.

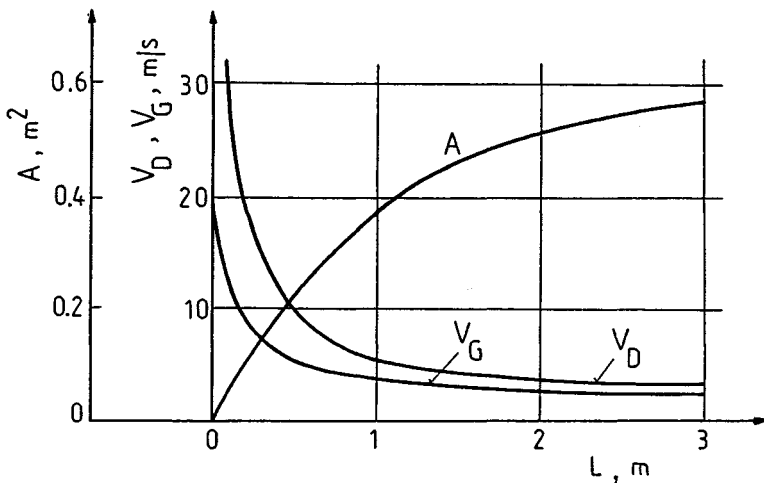


Figure 2-43 Change in cross-sectional area of a jet of drops A , drop velocity V_D , and gas velocity V_G along the jet height L .

In [17] the vertical motion of spray in a cocurrent flow of ambient air was explored. The equilibrium of the elementary volume of the spray acted upon by the inertial forces, gravity forces decreased by the buoyancy and resistance forces, was explored. The resistance force was determined from a semiempirical Ergun equation, which is commonly used for determining the resistance of flow through granular and porous layers. Independently of this, the air flow in the spray was taken into consideration. As a result, a system of differential equations was obtained that can be solved only numerically using the Runge-Kutta method. An example of the results for the basic spray parameters is shown in Fig. 2-43.

Now the motion of a drop jet from a *swirl atomizer* in a jet of air will be considered [6]. Making the same assumptions as in the case of deriving Eq. (2-138), we obtain for $n = 12$ the relative drop velocity u and the coordinates x and y of the drop trajectory as a function of time (Fig. 2-44):

$$u = \frac{u_0}{(t\sqrt{u_0}/AD^{3/2} - 1)^2} \quad (2-157)$$

$$x = \frac{w_0 \cos \alpha/2 \pm v}{\sqrt{u_0}/AD^{3/2} + 1/t} + vt \quad (2-158)$$

$$y = \frac{w_0 \sin \alpha/2}{\sqrt{u_0}/AD^{3/2} + 1/t} \quad (2-159)$$

where u_0 = relative velocity between gas and drops discharging from an atomizer (Fig. 2-44a),

w_0 = velocity of discharging drops

v = gas velocity

α = atomization angle

A = parameter

$$A = \frac{8\rho_L}{3n\rho_G\sqrt{v_G}}$$

In Eq. (2-158) the positive sign refers to *cocurrent atomization* and the negative sign to *countercurrent atomization*. The drop trajectories shown in Fig. 2-44 are schematic and simplified; because of the air flow additional drop selection occurs. The selection relies on the fact that the large drops are deflected from the initial direction less than the small drops, which results clearly from Eq. (2-159). As a result, the trajectories of large drops fall in the outer part of the jet.

The *maximum radial range of the spray* (spray diameter) y_{\max} follows from Eq. (2-159) after substituting $t = \infty$:

$$y_{\max} = AD_{\max}^{3/2} \frac{w_0}{\sqrt{u_0}} \sin \frac{\alpha}{2} \quad (2-160)$$

In order to determine y_{\max} it is necessary to know the maximum drop diameter D_{\max} in given spray, since the large drops will move on the outermost trajectories. To a rough approximation $D_{\max} \approx 2.1\bar{D}$. If one calculates the coordinate \bar{y} for the mean diameter, then

$$\frac{y_{\max}}{\bar{y}} = \frac{D_{\max}^{3/2}}{\bar{D}^{3/2}}$$

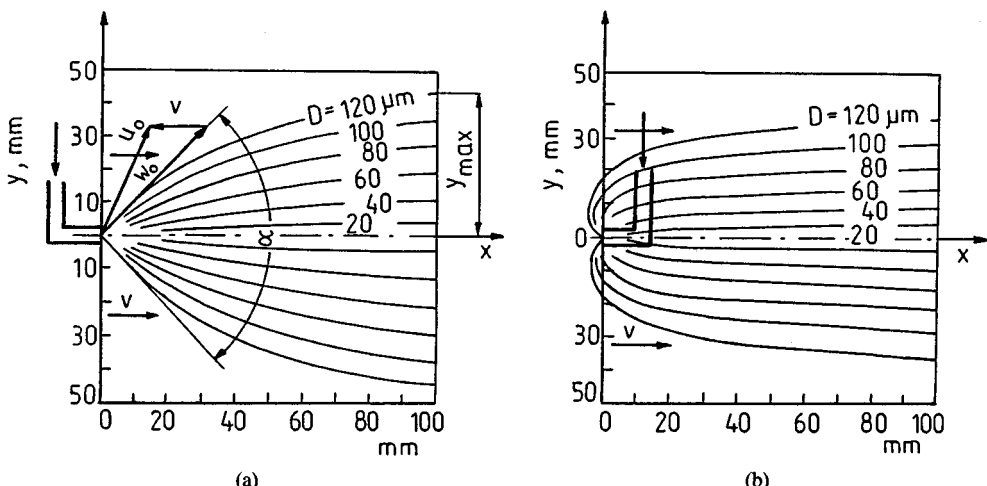


Figure 2-44 Drop trajectories in a jet generated by a swirl atomizer: (a) cocurrent motion; (b) countercurrent motion.

and

$$y_{\max} = \left(\frac{D_{\max}}{D} \right)^{3/2} \bar{y} \approx 2.1^{3/2} \bar{y} \approx 3\bar{y} \quad (2-161)$$

The predicted drop trajectories do not coincide with the measured ones. In Fig. 2-45 the full lines represent the predicted trajectories and the dashed lines represent the measured ones. As seen, the measured trajectories for cocurrent atomization fall closer to the spray axis and for countercurrent atomization farther from the axis than the predicted trajectories. This follows from the specifics of drop motion in a spray. The cocurrent jet of drops represents a well-streamlined elastic body, which converges during the flow. The countercurrent spray is a poorly streamlined body, which causes the flowing air to be deflected outward, which is not taken into consideration when calculating the drop trajectories.

Countercurrent atomization is particularly useful in the process of spray drying [32]. During countercurrent atomization, as seen in Fig. 2-45b, large drops moving on the outer part of the spray have easy contact with the drying air.

As seen from Fig. 2-45, the real contour of the spray differs significantly from the theoretical one, which is based on calculating the trajectories of individual drops. Also, as will be shown in Sec. 6-2, in a real spray the selection of drops based on their diameters (as seen in Fig. 2-45) is not so well developed. This means that drops with a given diameter move in a certain region of the spray. The problem of drop trajectories in the spray is so far poorly explored.

Equally poorly explored, although very important, is the problem of a drop jet in an air vortex, which develops in a combustion chamber. The main characteristic of this motion is the spatial dispersion of the spray accompanied by drop selection, similar to that taking place during the motion of drops in

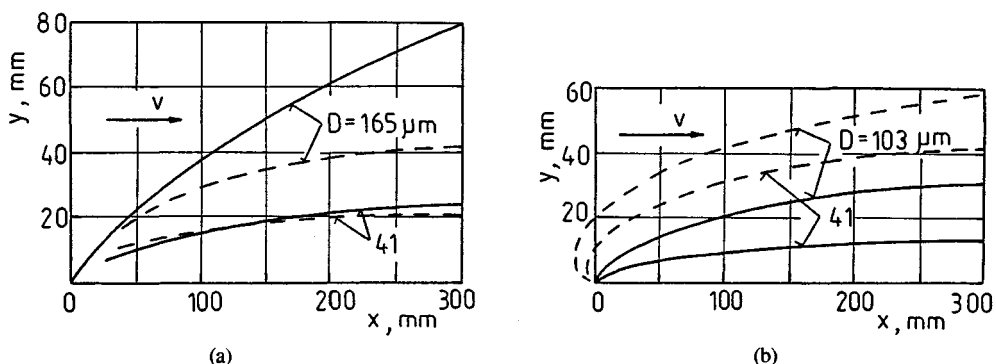


Figure 2-45 Comparison of predicted and measured drop trajectories (swirl atomizer): (a) cocurrent motion, $V = 66.4 \text{ m/s}$, $\Delta P \approx 0.8 \text{ MPa}$, $G_L = 23 \text{ kg/h}$; (b) countercurrent motion, $V = 58 \text{ m/s}$, $\Delta P \approx 0.5 \text{ MPa}$, $G_L = 19 \text{ kg/h}$.

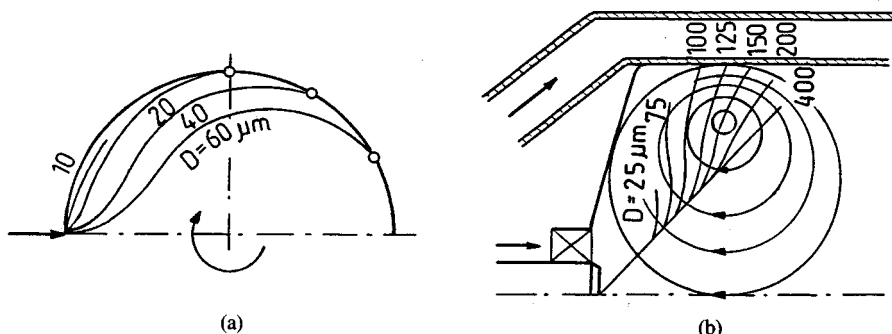


Figure 2-46 Drop trajectories in a vortex: (a) plane vortex in the combustion chamber of a piston engine; (b) toroidal vortex in the combustion chamber of a gas turbine.

cocurrent and countercurrent air flow (Fig. 2-44). Examples of drop selection in a vortex are shown in Fig. 2-46. Both examples are approximate because they were developed for the motion of individual drops and not for a spray. The motion of a spray differs significantly from the motion of individual drops, which is clearly noticeable in Fig. 2-45.

2-6 UNIFORM DROPS

Uniform drops, i.e., drops of the same size, are generated during so-called *monodisperse atomization*. In practice, the term uniform drops refers to drops with a very narrow size distribution. Uniform drops are needed for experimental research on the motion, evaporation, drying, combustion, etc. of atomized liquid. In addition, uniform drops or jets of uniform drops are used in various practical applications, mostly in agricultural spraying and, what is particularly important, in airborne spraying. Other applications, which require very small uniform drops (aerosols), are inhalation therapy, disinfection, and protection against radioactive contamination.

Monodisperse atomization is feasible only in static processes, e.g., in capillaries; in dynamic processes turbulence occurs, which leads to a drop size distribution. Static processes have only limited application, however, because they generate only small quantities of individual drops. Because of these problems nonuniform drops are used; the term median drop diameter is used.

There are several methods for generating uniform drops and numerous types of generators. Uniform drops are generated by standard atomizers or by atomizing installations specially adopted for this purpose. A good generator of uniform drops should ensure not only control of drop dimensions but also, independently, control of the drop velocity and frequency of generation. Such generators are being tested and improved [53].

The simplest way to generate uniform drops is with a *vertical capillary*, in which the liquid flows due to gravity forces. Almost uniform drops develop at the outlet of the capillary. A modification of this method relies on the application of thin needles or vertical plates on which the liquid flows. Threads of liquid develop on the bottom edge and, after breaking off, transform into drops. The diameter of these drops, according to Eq. (2-2), should equal $D \geq 1.5d_0$, where d_0 is the inner diameter of the capillary. In practice, drops of diameter $D > 2.1d_0$ are obtained. For very small flow rates, satellite drops do not develop. However, this method is not applied because of the static and inefficient means of drop generation.

Among other methods that find limited application are drop generation through condensation of supersaturated gas and drop generation as a result of bursting of bubbles at an air-water interface.

Methods that find wider applications will be discussed hereafter. These methods are based on utilization of the following phenomena:

Centrifugal force acting on the liquid (rotary atomization)

Acoustic vibrations acting on the spray

Pressure pulses acting on the liquid (pulsed-jet system)

Longitudinal and transverse vibrations of capillaries

Aerodynamic separation of drops

In *rotary atomizers* centrifugal force acts on the liquid. In such atomizers the process of development of uniform drops can be intensified by using centrifugal acceleration instead of acceleration due to gravity. A characteristic feature of this method is the development of small satellite drops, which occurs even for very low flow rates.

One type of rotary atomizer is a perforated drum rotating in the horizontal plane. The liquid is pressed out through the orifices on the drum perimeter (Fig. 2-47). A drop separates when the centrifugal force exceeds the force of surface

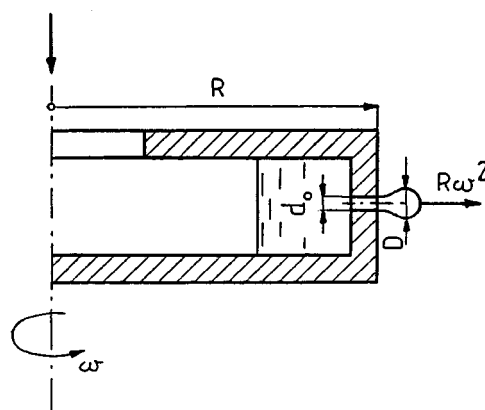


Figure 2-47 Development of a drop on the periphery of a perforated rotating drum.

tension acting on the drop, where the equilibrium condition can be written as

$$\frac{\pi D^3}{6} \rho_L R \omega^2 = \pi d_0 \sigma \quad (2-162)$$

where R = drum radius

d_0 = orifice diameter

ω = angular velocity

The diameters of drops generated in this way are given by

$$D = \left(\frac{6d_0 \sigma}{\rho_L R \omega^2} \right)^{1/3} \quad (2-163)$$

In [12], the generation of water drops using this method was investigated under the following conditions: drum radius $R = 25$ mm, orifice diameter $d_0 = 0.5$ mm, angular velocity $\omega = 157$ s⁻¹, water flow rate 0.004 cm³/s. It was established that the measured drops and drops predicted from Eq. (2-163) differed by only 9 to 10%. The drop sizes were very similar; the standard deviation from the mean value was only 0.84 to 1.5%.

Uniform drags with the possibility of drop size control in a wide size range of 0.015 to 3 mm can also be generated by the application of a *disk rotating* around a vertical axis. Such a drop generator should have a smooth surface and a sharp and even edge. The liquid should be supplied in small amounts in a continuous way into the center of the disk to ensure uniform spreading of the liquid on the disk surface. The specific character of drop generation in such conditions will be discussed in detail in Sec. 4-5.1.

The diameter of the drop can be calculated approximately in the following way. The drop will separate from the edge of the disk (Fig. 2-48) when the centrifugal force is higher than the surface tension force. Similarly to the case shown in Fig. 2-47 we can write

$$\frac{\pi D^3}{6} \rho_L R \omega^2 = \pi D \sigma \quad (2-164)$$

Therefore the drop diameter is given by

$$D = \frac{C}{\omega} \left(\frac{\sigma}{\rho_L R} \right)^{1/2} \quad (2-165)$$

From Eq. (2-164) we obtain $C = 2.36$. For mineral oils the value $C = 2.7$ was obtained experimentally. In general, the constant C falls in the range 1.9 to 4.6 for the following range of parameters [12]: $\rho_L = 900$ to 13,600 kg/m³, $\sigma = (29-465) \times 10^{-3}$ N/m, $\mu_L = (0.1-260) \times 10^{-2}$ Pa · s, $D = 0.03$ to 4 mm, $R = 2$ to 11 cm, $\omega = 30$ to 10,000 s⁻¹.

When uniform drops are generated using this method, satellite drops with significantly smaller diameters develop. After separating from the disk edge, all drops fall down and develop concentric rings depending on the drop size on a

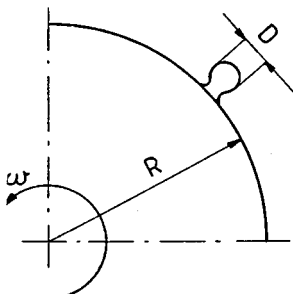


Figure 2-48 Development of a drop on the edge of a flat rotating disk.

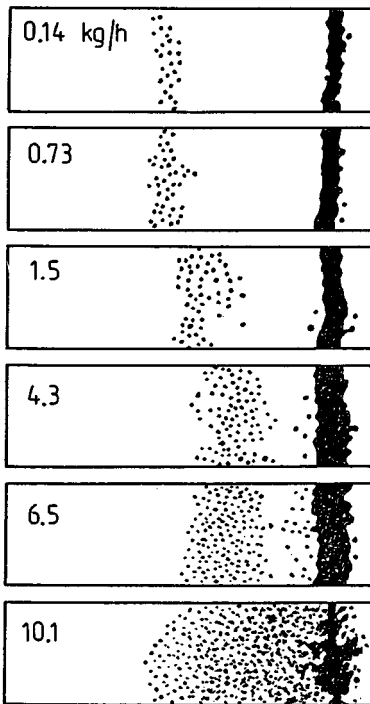


Figure 2-49 Pictures of drops caught from a rotating disk (six segments from an annular space).

horizontal plane. The satellite drops can be easily eliminated because the distance of their fall from the disk edge is much smaller than that for larger drops. The number and diameters of satellite drops increase as the liquid flow rate increases, which follows clearly from Fig. 2-49. After a critical flow rate is reached, a continuous spectrum of drops develops and hinders the separation of uniform drops. Figure 2-50 shows the critical flow rates for three disk diameters as a function of rotation frequency.

Another type of rotary atomizer is the *porous rotor*. In these generators uniform drops develop on the whole outer surface of the rotor. Figure 2-51 shows a porous rotor made of sintered bronze powder of grain size 0.75 mm. Inside the atomizer several layers of filter paper were inserted to ensure uniform fluid supply. Porous rotors must have high strength because for the number of revolutions per minute applied (5000 to 50,000 rpm) the centrifugal acceleration is 10^5 times higher than the acceleration due to gravity. Powders of bronze, stainless steel, glass, aluminium, etc. are used for the porous material. These above requirements are also satisfied by abrasives (grinding wheels).

An analysis of the operation of porous rotors showed that uniform drops are generated only if the porous material has a regular structure, i.e., equal grain

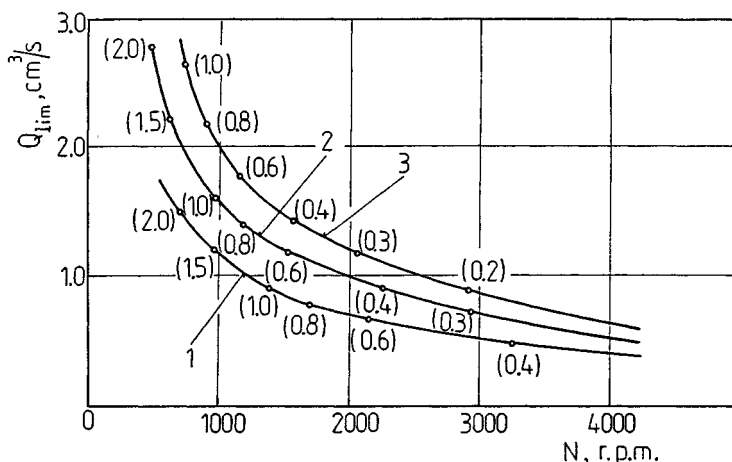


Figure 2-50 Limiting volumetric flow rates of water as a function of rotational speed N for various disk radii R : 1, $R = 1$ cm; 2, $R = 2$ cm; 3, $R = 4$ cm. Numbers adjacent to the dots denote drop diameters in millimeters.

sizes and equal pore sizes. Three regimes of the development of uniform drops can be distinguished: annular, threadlike, and droplike. The annular regime occurs for rotor circumferential velocities of 0.8 to 1.2 m/s and is characterized by the presence of a liquid annulus on the rotor perimeter. The threadlike regime has many variations, depending on the circumferential velocity. The droplike regime begins for circumferential velocities higher than 12 to 20 m/s. The threads of liquid disappear and drops appear. The uniformity of drops is

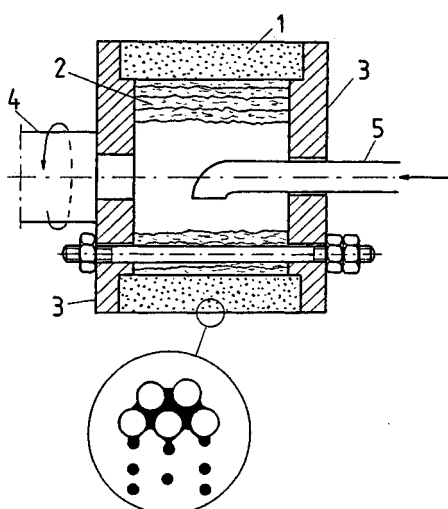


Figure 2-51 Rotary porous atomizer; 1, porous matter; 2, filter paper; 3, side disks; 4, drive shaft; 5, liquid supply.

good: $D_{\max}/D_{\min} \leq 2$. In the case of wetting liquids the drops develop on the surfaces of grains, and in the case of nonwetting liquids they develop in the pores; in both cases the drop size depends on the sizes of grains and pores, respectively.

The drop diameter can be calculated in this case from the modified Eq. (2-163) [41]:

$$D = 0.52 \left(\frac{6d_g \sigma}{\rho_L R \omega^2} \right)^{1/3} \quad (2-166)$$

where d_g denotes the grain diameter and R is the rotor diameter. The flow rate is given by

$$Q_L = 0.24KA(1 - \epsilon) \omega (d_h D)^{0.5} \frac{D}{d_g} \quad (2-167)$$

where A = outer surface of the rotor

d_h = pore diameter

ϵ = porosity (the ratio of the volume of pores to the volume of the rotor)

K = a constant depending on grain size:

For $d_g = 250 \mu\text{m}$:

$$K = (0.11R\omega^2 - 137.8)10^{-3}$$

For $d_g = 400 \mu\text{m}$:

$$K = (0.052R\omega^2 - 206.5)10^{-3}$$

A completely different method of generating uniform drops is based on using the energy of *high-frequency vibrations*. Drops with various diameters can be generated; in particular very small drops (aerosols) with diameters ranging from 0.001 to 5 μm . Such atomizers are basically the only source of very small uniform drops. Acoustic waves in the sound frequency band of 16 to 20,000 Hz as well as ultrasonic waves are used. The generation of those vibrations and the generators will be discussed in Sec. 4-6.

Here we will discuss the action of the acoustic vibrations on the spray (Fig. 2-52) [23, 27]. The liquid discharges from a rectangular nozzle of width $h = 0.130$ to 0.657 mm, length $l = 2.92$ to 6.82 mm, and depth = 0.5 mm. Uniform drops with diameters ranging from 1 to 4 mm were obtained. A loudspeaker generated vibrations with frequencies from 0.3 to 8 kHz at a distance of 20 cm from the spray.

During discharge without the acoustic vibrations the liquid jet deforms and assumes a chainlike form. During disintegration each chain segment can create one drop, but this process is unstable. Uniform drops develop in the range $We \approx 5$ to 16 and for the ratio $a = 1/h \approx 5$ to 40, and the equation

$$We = 21.1 - 1.24a + 0.0289a^2 \quad (2-168)$$

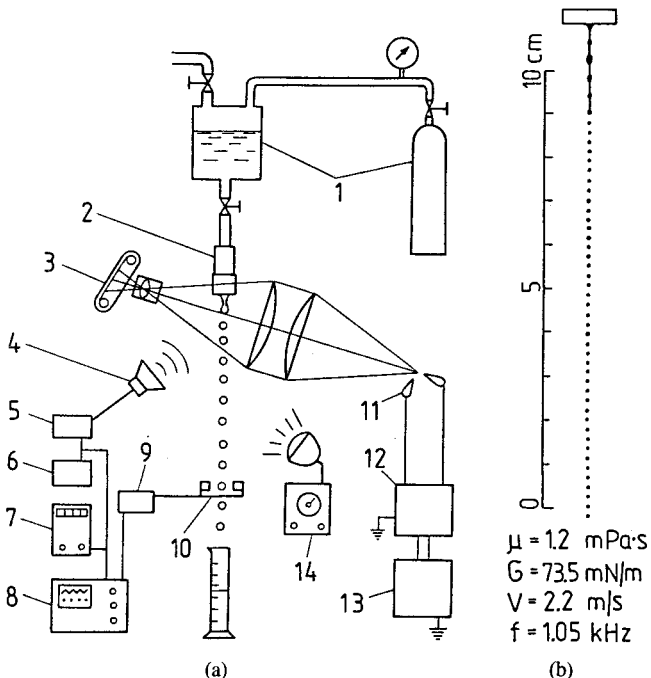


Figure 2-52 Uniform drop generation using acoustic vibrations: (a) scheme of the system; (b) picture of drops; 1, pressurized tank; 2, drop generator; 3, camera; 4, conventional speaker; 5, amplifier; 6, signal generator; 7, electronic counter; 8, oscilloscope; 9, amplifier; 10, optical sensor consisting of a photodiode and a phototransistor; 11, spark gap; 12, high-voltage capacitor circuit; 13, high-voltage DC power supply; 14, stroboscope.

holds, where the Weber number follows from

$$We = \frac{\rho_L V_L^2 d_e}{\sigma} \quad (2-169)$$

and the orifice equivalent diameter is

$$d_e = \frac{4A}{S}$$

where A is the cross-sectional area and S is the perimeter of the rectangular nozzle.

The presence of acoustic waves significantly stabilizes the process of uniform drop development and increases the range of unstable wavelengths λ as follows:

$$2d_a < \lambda < 8d_a$$

Uniform drops were obtained even for $\lambda \approx 25d_e$, but in this case for small liquid velocities. The relationship between the frequency f (kHz) and velocity V_L (m/s) has the form

$$f = 0.2V_L^{1.33} \quad (2-170)$$

The lower limit of velocity V_L is 1 to 2 m/s; the upper one depends on the nozzle geometry. The influence of viscosity is such that when it increases, the range of uniform drop development narrows down.

Uniformity of drops generated in this way is very high. The number of drops coincides with the frequency of acoustic vibrations. The electric power of the speaker is much lower than 1 W. Because of the low energy consumption and simplicity of the instrumentation, this method is suitable for industrial generation of uniform drops.

The effect of the *pressure pulsation* on the liquid has been discussed in [56, 57]. This new method of generating uniform drops was developed for monodisperse spraying of pesticides from the ground and the air. The system for the ground spraying contains an impulse chamber with a ceramic piezoelectric element. The chamber is connected by a conduit to a transverse pipe with discharging orifices. Sprays of uniform drops were generated with a diameter range from 144 to 803 μm . The liquid velocity was 2.22 m/s. The system for air spraying contains magnetostriction drive generating impulses, which act on the liquid through an injection sprayer containing 121 orifices of diameter 125 μm . This system, in motionless air, generated almost uniform drops, which had a diameter of 260 μm right after the discharge. These drops, during experiments in a wind tunnel with an air velocity of 160 km/s, were subjected to coalescence as well as to secondary disintegration.

Longitudinal and transverse vibrations of the capillary were used by different authors [2, 47, 49]. The *vibrating capillary method* has the advantages that it uses simple instrumentation, allows easy control of sizes and quantities of drops, and does not depend on the type of liquid used. It was experimentally established that uniform drops can be generated within the range bounded by the lower and upper limits of frequency and liquid velocity and above the lower limit of the vibrational amplitude.

In [2], emphasis was placed on explaining such fundamental problems as the effect of the velocity and jet diameter, frequency, amplitude, and direction of vibrations on the uniformity of spraying. It was established that the minimum unstable wavelength is

$$\lambda_{\min} = \pi d \quad (2-171)$$

and from the Rayleigh relation the optimum condition is defined as $\lambda = 4.508d_0$. In this case the jet diameter d is considered, which during the downward motion of the jet is a function of the diameter d_0 and the shape of the nozzle, Weber number, liquid velocity, and distance from the nozzle.

It was established that the number of drops produced was equal to the frequency of capillary vibrations. The diameter of the uniform drops is then

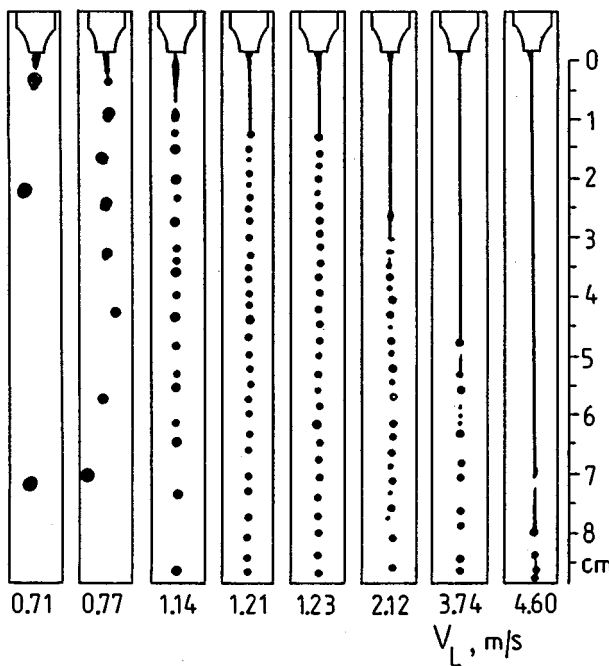


Figure 2-53 Various types of disintegration of a jet as a function of liquid velocity V_L ; $d = 0.41$ mm, $f = 500$ Hz, vibration amplitude = 5 μm .

given by

$$D = \left(\frac{6Q_L}{\pi f} \right)^{1/3} = \left(\frac{3d^2V_L}{2f} \right)^{1/3} \quad (2-172)$$

where Q_L = liquid flow rate

d = jet diameter

f = vibration frequency

V_L = liquid velocity

Equation (2-172) is in good agreement with experiments [49]; the mean error is $\pm 4.4\%$. Figure 2-53 shows the registered picture of drops developing during the longitudinal capillary vibrations.

In [47] the conditions of generating uniform-size drops by using longitudinal vibrations of the capillary were investigated, using Newtonian liquids with low and high viscosities as well as non-Newtonian slimes. The longitudinal acoustic waves were generated with a speaker, inside which the capillary nozzle was placed. The speaker was amplified and generated the sinusoidal waves.

Figure 2-54 shows an example of the region of uniform-size drops as a function of vibration frequency and velocity of the liquid of low viscosity. The following equations for the vibration frequency f were found.

For the upper frequency limit:

$$\frac{fd_0}{V_L} = 0.18 \text{Re}^{0.031} \text{We}_L^{0.12} \quad (2-173)$$

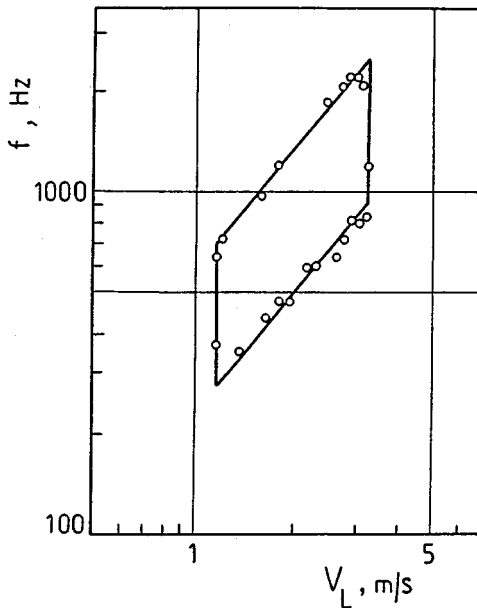


Figure 2-54 Region of generation of uniform water drops; jet diameter $d = 0.46$ mm.

For the lower frequency limit:

$$\frac{fd_0}{V_L} = 0.11 \text{Re}^{0.066} \text{We}_L^{0.17} \quad (2-174)$$

where the Reynolds number Re and Weber number We_L follow from Eqs. (2-5) and (2-6), respectively. The ranges in which Eqs. (2-173) and (2-174) hold are

$$\text{Re} = 1.3 \times 10 \text{ to } 2.1 \times 10^3$$

$$\text{We}_L = 5.0 \text{ to } 8.1 \times 10^2$$

$$d_0 = 0.25 \text{ to } 0.46 \text{ mm}$$

$$\mu_L = 1.33 \times 10^{-3} \text{ to } 50.7 \times 10^{-3} \text{ Pa} \cdot \text{s}$$

$$\sigma = 23.8 \times 10^{-3} \text{ to } 77.8 \times 10^{-3} \text{ N/m}$$

$$\rho_L = 846 \text{ to } 1283 \text{ kg/m}^3$$

The following equations were found for the liquid velocity V_L

For the upper velocity limit:

$$\text{Re} = 300Z^{-0.33} \quad (2-175)$$

For the lower velocity limit:

$$\text{Re} = 1.4Z^{-1.33} \quad (2-176)$$

where the Ohnesorge number Z follows from Eq. (2-7). Equations (2-175) and (2-176) are valid for $Z = 4.4 \times 10^{-3}$ to 2.7×10^{-2} , and the validity of other parameters is the same as for Eqs. (2-173) and (2-174).

Similar equations have been established for Newtonian liquids with high viscosity and for non-Newtonian liquids.

Uniform aerosols are used for the calibration of measuring instrumentation. Methods for generating such aerosols with a very narrow distribution of droplet diameters, i.e., so-called standard aerosols, are discussed in [44]. To produce aerosols with diameters of 0.5 to 50 μm , one uses generators with a vibrating discharge orifice of diameter of 5, 10, or 20 μm and with additional disintegration caused by the turbulent jet of air. Colloidal aerosols with diameters of 0.1 to 1.0 μm are generated by spraying and classification in an electrostatic field. Colloidal aerosols can be also produced by using the Wright principle, which is based on disintegration by an air jet and collision with a spherical target. Such a generator (TSI, Thermo-systems Inc.) generates aerosols with diameters of 0.3 μm , which are used for the evaluation of filters. Subcolloidal aerosols with diameters ranging from 0.003 to 0.01 μm are generated by rapid condensation.

We should also mention the generation of *uniform oil mists*, which are transmitted long distances to lubricating points [5, 52]. The generators are available commercially (e.g., Alemite) and are based on pneumatic atomization; uniformity of the oil mist is achieved by *aerodynamic separation*. Separation is achieved by directing the drops onto a target, where drops with diameters larger than a certain critical diameter develop and smaller drops flow around the target.

REFERENCES

1. Adachi, K., Kiriyama, S., Yoshioka, N. The behavior of swarm of particles moving in viscous fluid. *Chem. Eng. Sci.*, Vol. 33, No. 1, 1978.
2. Araki, N., Masuda, A. Production of droplets of uniform size by vibration. *Proceeding of ICLASS-78*, Tokyo, 8-1, 173-180, 1978.
3. Arkhipov, V. A., Bushlanov, V. P., Vasenin, I. M., Rusakov, V. V., Trokhimov, V. F. Equilibrium forms and stability of rotating drops. *Mekh. zhidkosti i gaza*, No. 4, 1982 (in Russian).
4. Bazarov, V. G. *Dynamics of Liquid Atomizers*. Mashinostroenie, Moscow, 1979 (in Russian).
5. Bednarek, K. Method of evaluation of the influence of selected parameters of oil mist on oil film development on active face of a gear. Ph.D. thesis, Academy of Mining and Metallurgy, Crakow, Poland, 1980 (in Polish).
6. Beloshkurskaya, O. N., Klyachko, L. A. Motion of a deformed drop in a gaseous medium. *Inzh. Fiz. Zh.* Vol. 47, No. 6, 1984 (in Russian).
7. Berevin, S. R. A model for calculating the development of a turbulent fuel cone in diesel engines. *Izv. Vuzov Mashinostr.*, No. 3, 1985 (in Russian).
8. Borysov, A. A., Gel'fand, B. E., Natanzon, M. S., Kossov, O. M. Modes of drop disintegration and criteria of their existence. *Inzh. Fiz. Zh.*, Vol. 11, No. 1, 1981 (in Russian).
9. Borysov, A. A., Gel'fand, B. E., Polenov, A. N., Tymofelev, E. I., Tsyanov, S. A. Disintegration of drops of liquid in the rarefied waves, *Mekh. zhidkosti i gaza*, No. 1, 1986 (in Russian).
10. Borodin, V. A., Dityakin, Yu. F., Klyachko, L. A., Yagodkin, I. *Liquid Atomization*. Moscow, 1967 (in Russian).

11. Brauer, H. *Fundamentals of Single and Multiphase Flows*, Verlag Sauerlander, Aarau and Frankfurt on Main, 1971 (in German).
12. Dunskii, V. F., Nikitin, V. V. Drop sizes in a monodisperse disintegration of liquids. *Inzh. Fiz. Zh.* Vol. 31, No. 2, 1976 (in Russian).
13. Eisenklam, P. Atomisation of liquid fuel for combustion. *J. Inst. Fuel*, Vol. 34, No. 243, 1961.
14. El-Emam, S. H. Experimental and theoretical study on liquid atomisation into a gas stream. *Proceedings of ICLASS-85*, London, LP/VIIIC/3/1-13, 1985.
15. Filyand, L. V. Instability and disintegration of the capillary liquid jets in a moving air stream. *Mekh. zhidkosti i gaza*, No. 3, 1981 (in Russian).
16. Gel'fand, B. E., Gubin, S. A., Kogarko, S. M. Various modes of drop disintegration in the shock waves and their characteristics. *Inzh. Fiz. Zh.*, Vol. 27, No. 1, 1974 (in Russian).
17. Gel'perin, N. I., Basargin, B. N., Zvezdin, Yu. G., Vlasov, V. V. Liquid atomization using mechanical atomizers. *Teor. Osn. Khim. Tekhnol.*, Vol. 8, No. 3, 1974 (in Russian).
18. Giffen, E., Muraszew, A. *The Atomisation of Liquid Fuels*. Chapmen & Hall, London, 1953.
19. Girin, A. G. Hydrodynamical instability and modes of drop disintegration. *Inzh. Fiz. Zh.*, Vol. 48, No. 5, 1985 (in Russian).
20. Goering, C. E., Smith, D. B., Bode, L. E. Transport of agricultural pesticide sprays. *Proceedings of ICLASS-78*, Tokyo, 14-1, 341-346, 1978.
21. Gonor, A. L., Zolotova, N. V. Breaking and deformation of a liquid drop in a stream of gas. *Mekh. zhidkosti i gaza*, No. 2, 1981 (in Russian).
22. Iciek, J. The hydrodynamics of a free, liquid jet and their influence on direct contact heat transfer—I, II. *Int. J. Multiphase Flow*, Vol. 8, No. 3, 1982.
23. Karasawa, T., Shiga, S., Kurabayashi, T. Production of uniform-size drops by a rectangular nozzle. *Proceedings of ICLASS-85*, London, VII B (b)/1/1-9, 1985.
24. Kawase, Y., Shirotsuka, T. Atomization of viscoelastic fluids. *Proceedings of ICLASS-78*, Tokyo, 1-4, 21-28, 1978.
25. Kitamura, Y., Takahashi, T. Influence of nozzle on breakup of a liquid jet. *Proceedings of ICLASS-78*, Tokyo, 1-1, 1-7, 1978.
26. Krzeczkowski, S. Measurement of liquid droplet disintegration mechanisms. *Int. J. Multiphase Flow*, Vol. 6, 1980.
27. Kurabayashi, T., Karasawa, T. Production of uniform droplets by non-circular nozzles. *Proceedings of ICLASS-82*, Madison, Wisconsin, 2-3, 55-61, 1982.
28. Loparev, V. L. An experimental evaluation of liquid drop disintegration in the conditions of gradually increasing internal forces. *Mekh. zhidkosti i gaza*, No. 3, 1975 (in Russian).
29. Lyshevskii, A. S. *Processes of Fuel Atomization in Diesel Nozzles*. Mashgiz, Moscow, 1963 (in Russian).
30. Mahoney, T. J., Sterling, A. M. The breakup length of laminar Newtonian liquid jets in air. *Proceedings of ICLASS-78*, Tokyo, 1-2, 9-12, 1978.
31. Malloggi, S., Tognotti, L., Zanelli, S. An experimental study on the mechanism of jet breakup. *Proceedings of the Two Day Meeting on Sprays and their Applications*, Milan, Italy, 1986.
32. Masters, K. *Spray Drying Handbook*. George Godwin, London, 1985.
33. Matsumoto, S., Takashima, Y. Design criteria of hollow cone nozzle and prection of drop size distribution. *Proceedings of ICLASS-78*, Tokyo, 4-1, 79-84, 1978.
34. Milkin, A. S., Galustov, V. S., Chufarovskii, A. I. Increase of the efficiency of liquid spraying. *Teploenergetika*, No. 12, 1986 (in Russian).
35. Nagaosa, S., Matsui, H., Tokuoka, N., Sato, G. T. A study of the disintegration of a liquid jet in an air flow. *Proceedings of ICLASS-78*, Tokyo, 2-1, 29-36, 1978.
36. Novikov, A. A. Non-linear capillary waves on the surface of a jet of a viscous liquid. *Mekh. zhidkosti i gaza*, No. 2, 1977 (in Russian).
37. Okhotskii, V. B. A criterion of drops and jet disintegration. *Inzh. Fiz. Zh.*, Vol. 49, No. 3, 1985 (in Russian).
38. Orzechowski, Z. *Liquid Atomization*. WNT, Warsaw, 1976 (in Polish).
39. Orzechowski, Z. *Two-Phase Flow*. Warsaw 1990 (in Polish).
40. Pazhi, D. L., Galustov, V. S. *Liquid Atomizers*. Khimiya, Moscow, 1979 (in Russian).

41. Pazhi, D. L., Galustov, V. S. *Liquid Atomization*. Khimiya, Moscow, 1984 (in Russian).
42. Petela, R., Zajdel, A. Calculation of a mean droplet diameter of an atomized mixture of dust and liquid. *Fuel*, Vol. 59, November, 1980.
43. Petela, R., Wilk, R. Determination of the drop size distribution in an atomized liquid on the basis of the sediment mass distribution. *Arch. Thermodyn. Combust.*, Vol. 7, No. 4, 1967 (in Polish).
44. Pui, D. Y. H., Liu, B. Y. H. Aerosol generation and calibration of instruments. *TSI Quarterly*, May/June, 1979.
45. Rowinski, R. Problems of the drifting of the chemical compounds spraying from the air, *Acta Acad. Agric. Tech. Olstenensis, Aedificatio et Mechanica*, No. 16, 1987.
46. Rutland, D. F., Jameson, G. J. Theoretical prediction of the sizes of drops formed in the breakup of capillary jets. *Chem. Eng. Sci.*, Vol. 25, No. 11, 1970.
47. Sakai, T., Sadakata, M., Saito, M., Hoshino, N., Senuma, S. Uniform size droplets by longitudinal vibration of Newtonian and non-Newtonian fluids. *Proceedings of ICLASS-82*, Madison, Wisconsin, 2-1, 37-45, 1982.
48. Sato, H., Saito, M. Non-linear wave propagation and disintegration of a circular liquid jet. *Proceedings of ICLASS-82*, Madison, Wisconsin, 1-3, 19-27, 1982.
49. Schummer, P., Tebel, K. H. Production of monodispersed drops by forced longitudinal vibration of a liquid jet. *Proceedings of ICLASS-82*, Madison, Wisconsin, 2-2, 47-54, 1982.
50. Spalding, D. B. Computational fluid dynamics and its application to liquid-atomisation and spray systems. *Proceedings of ICLASS-85*, London, IP/3/1-18, 1985.
51. Swithenbank, J., Ewan, B. C. R., Swithenbank, J. R., Taylor, D. S. Aerial agricultural spray drift minimization. *Proceedings of ICLASS-85*, London, IV B/2/1-17, 1985.
52. Szydlo, Z. Investigation of the influence of stream velocity of oil mist on precipitation of oil drops in pipes with a circular cross section. Ph.D. thesis, Academy of Mining and Metallurgy, Crakow, Poland, 1984 (in Polish).
53. Tokuoka, N., Honoki, H., Yagi, M., Sato, G. T. A piezoelectric generator of evenly spaced, homogeneous drops of liquid. *Proceedings of ICLASS-85*, London, VII B(b)/3/1-9, 1985.
54. Volynskii, M. S., Lipatov, A. S. The deformation and drop disintegration in an air flow. *Inz. Fiz. Zh.*, Vol. 18, No. 5, 1970 (in Russian).
55. Voronin, V. V. Analysis of the liquid drop deformation in a gas flow. *Inz. Fiz. Zh.*, Vol. 50, No. 5, 1986.
56. Yates, W. E., Akesson, N. B. Monodisperse atomization systems for pesticide sprays. *Proceedings of ICLASS-78*, Tokyo, 8-2, 181-192, 1978.
57. Yates, W. E., Cowden, R. E., Akesson, N. B. Influence of some unique nozzle designs on uniformity of drop size produced by agricultural aircraft. *Proceedings of ICLASS-82*, Madison, Wisconsin, 7-4, 201-207, 1982.
58. Zajdel, A. Investigation of dust-liquid fuel. Ph.D. thesis, Silesian Polytechnic, Gliwice, Poland, 1979 (in Polish).



Taylor & Francis
Taylor & Francis Group
<http://taylorandfrancis.com>

PARAMETERS OF ATOMIZED LIQUID

3-1 FLOW RATE OF ATOMIZED LIQUID

Flow rate is the only parameter concerning the quantity rather than the quality of atomized liquid. If the flow rate is known, one can determine the dimensions of an atomizer. This refers, however, to the types of atomizers for which the design methods exist. All theoretical calculations require some experimental corrections. The flow rate measured as a function of liquid pressure drop is a fundamental characteristic of an atomizer.

3-1.1 Atomizers with Continuous Operation

The operation of continuous atomizers is based on discharge through an orifice (nozzle) assisted by an adequate pressure drop ΔP , where $\Delta P = P_1 - P_2$ is the pressure difference on both sides of the orifice (Fig. 3-1). Rotary atomizers are the exception because their operation is based on a different principle; however, some types of rotary atomizers are based on discharge through orifices.

From the Bernoulli equation for cross section 1 in front of the orifice and cross section 2 behind the orifice it follows that

$$\frac{\rho V_1^2}{2} + P_1 = \frac{\rho V_2^2}{2} + P_2 \quad (3-1)$$

Therefore

$$V = V_2 = \sqrt{\frac{2(P_1 - P_2)}{\rho} + V_1^2} \approx \sqrt{\frac{2\Delta P}{\rho}} \quad (3-2)$$

since velocity V_1 is usually very small compared to velocity V_2 . The velocity V calculated in (3-2) is the theoretical liquid velocity.

Volumetric flow rate Q (m^3/s) is equal to

$$Q = \mu A_0 V = \mu A_0 \sqrt{\frac{2\Delta P}{\rho}} \quad (3-3)$$

and mass flow rate G (kg/s) is equal to

$$G = \rho Q = \mu A_0 \sqrt{2\rho \Delta P} \quad (3-4)$$

where μ = discharge coefficient (ratio of actual to theoretical flow rate)

$A_0 = \pi d_0^2/4$ is the cross section of the outlet orifice (for continuous atomizers $A_0 = \text{const}$)

Discharge coefficient μ is determined experimentally. It depends on the Reynolds number. However, for large Reynolds numbers occurring during atomization the value of μ remains approximately constant. For a given atomizer and given liquid it follows from Eqs. (3-3) and (3-4) that

$$Q = f(\sqrt{\Delta P}) \quad \text{and} \quad G = f(\sqrt{\Delta P}) \quad (3-5)$$

Functions (3-5) have a parabolic shape. They are called *continuous operation atomizer characteristics* and express the relationship between the flow and pressure drop (Fig. 3-2).

Because the discharge coefficient μ does not change significantly, it is often used as a parameter characterizing a particular atomizer. The concept of *flow number* FN originates from such an approach.

$$FN = \frac{Q}{\sqrt{\Delta P}} \quad (3-6)$$

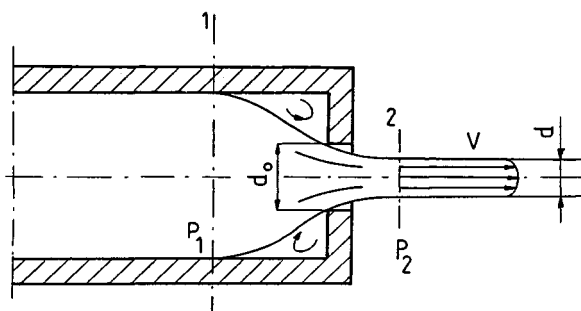


Figure 3-1 Liquid discharge from an outlet orifice.

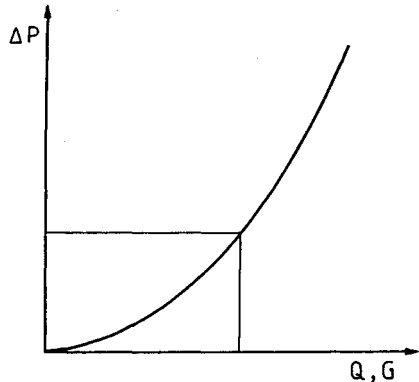


Figure 3-2 Characteristics of a continuous atomizer.

The flow number is a denounce number. If two states of atomization are denoted by indices 1 and 2, the following relation is obtained:

$$\frac{Q_1}{\sqrt{\Delta P_1}} = \frac{Q_2}{\sqrt{\Delta P_2}} \quad (3-7)$$

from which, knowing P_1 and Q_1 for a particular atomizer, one can calculate Q_2 for an arbitrary P_2 .

3-1.2 Atomizers with Intermittent Operation

Jet atomizers with intermittent operation work totally differently from continuous atomizers. They are used exclusively in piston engines (diesel engines). Intermittent atomizers are used to supply a fuel charge to a combustion chamber in an intermittent manner. The cross section of the discharge orifice varies ($A_0 \neq \text{const}$). The variation of the cross section is due to the motion of a needle, which in the extreme position blocks the fuel flow.

Mean fuel charge is defined as the mass or volume of fuel per cylinder per work cycle of the engine. This fuel charge is injected in the form of a single jet or several simultaneous jets, depending on the design of the atomizer. The mean fuel charge V_w (mm^3/cycle) is given by

$$V_w = \frac{10^6 Q_h i}{60 n N} \approx 16.7 \times 10^3 \frac{Q_h i}{n N} \quad (3-8)$$

where Q_h = fuel consumption per hour (L/h)

$i = 1$ for a two-stroke engine

$i = 2$ for a four-stroke engine

n = number of cylinders

N = rotational speed (rpm)

The mean mass fuel charge G_w (g/cycle) can be determined in a similar way. Mean charge is being determined experimentally from a large number of injections (e.g., 1000).

Not only the value of the fuel charge but also the manner in which the fuel is fed to the engine is important. An *injection characteristic* is the volume of injected fuel q_w (mm^3/deg) per degree of rotation of the camshaft of a fuel pump

$$q_w = \frac{dV_w}{d\varphi} \quad (3-9)$$

where φ is the angle of rotation of the camshaft. The injection characteristics can also be expressed as a function of the angle of rotation of the crankshaft or time. Similarly, we can present the injection characteristic in terms of mass instead of volume.

The injection characteristic has a fundamental influence on the processes of development of the fuel mixture and combustion. It has to satisfy the following requirements (Fig. 3-3):

During the self-ignition delay, the quantity of fuel supplied should not be more than 20% of the total fuel charge.

The fuel injection should not have a pulsating character in order to avoid pressure pulsation in a cylinder or a break in the fuel supply.

Additional injections should not follow the main injection because they might cause improper combustion and fuel deposition in atomizer orifices.

The injection characteristic depends on the fuel pump and injection nozzle. The operation of the fuel pump is determined by the shape of the cam, velocity of

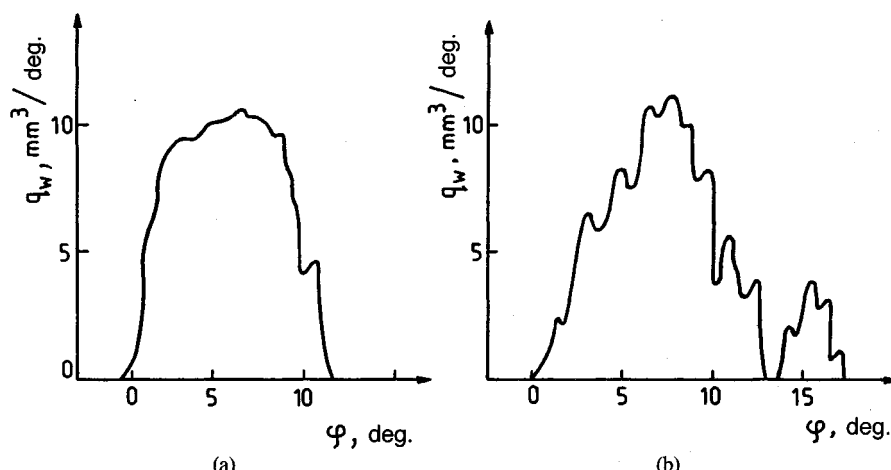


Figure 3-3 Injection characteristic of a pulsed atomizer: (a) correct; (b) incorrect.

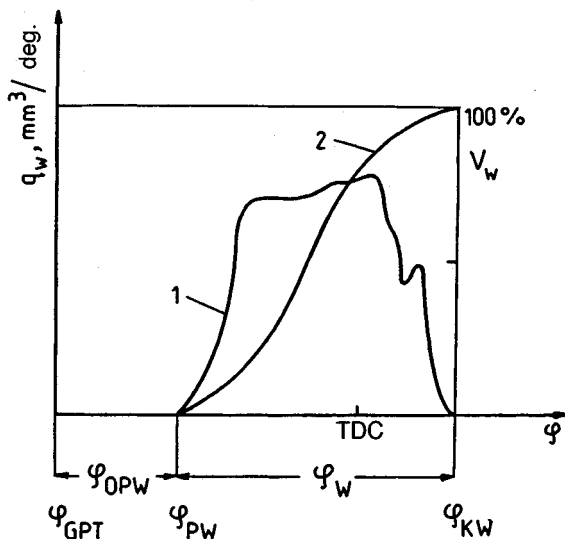


Figure 3-4 Injection characteristic for a constant rotational speed ($N = \text{const}$): φ_{GPT} , angle of geometric onset of compression; φ_{PW} , angle of injection onset; φ_{KW} , angle of injection end; φ_{OPW} , angle of injection onset delay; φ_W , angle of injection duration; TDC, top dead center of the piston.

the pump piston, and relation between the effective stroke and the total stroke of the piston, which determines the beginning and end of pumping. Fuel injection starts when a pressure wave from the fuel pump reaches the injection nozzle, which takes place at the end of the compression stroke, typically 20° to 30° before the top dead center of the piston. The pulsating character of the injection is caused by the presence of pressure waves in the liquid in the fuel conduits. Pulsations can be suppressed by a stiff spring in the nozzle, the needle mass, and the geometry of the nozzle and atomizer. The process of injection is determined experimentally but can also be estimated theoretically.

Figure 3-4 shows an example of the injection characteristic in two forms (curves 1 and 2). Differential curve 1 shows the instantaneous value of fuel charge, and curve 2 shows the total value of the fuel charge injected from the beginning of injection. Curve 2 is generated by the summation of curve 1. The areas under the curves 1 and 2 are equal to the mean charge V_w in volume units or in percent.

The relationship between the pressure and flow rate, i.e., the *characteristic of an atomizer* $P = f(Q)$, is very complex in the case of intermittent atomizers. This relationship will be derived for two basic types of atomizers: a multiorifice atomizer and a pintle nozzle.

Multiorifice atomizer (Fig. 3-5). In the static conditions the balance of forces acting on the needle has the following form:

$$F_s + k_s x = \frac{\pi(D^2 - d^2)}{4}P + \frac{\pi d^2}{4}P_1 \quad (3-10)$$

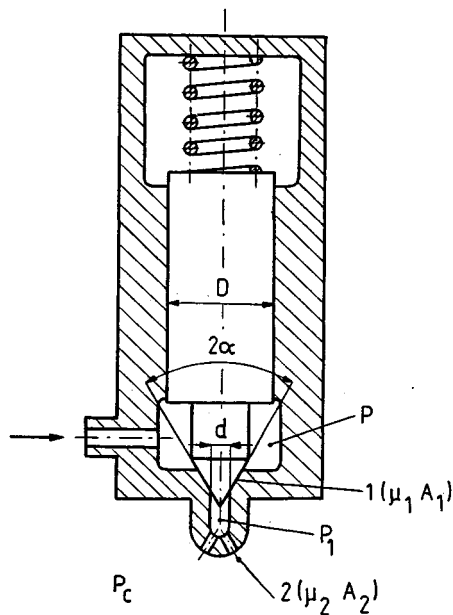


Figure 3-5 Schematic diagram of multiorifice atomizer.

where F_s = initial force of the spring

K_s = spring constant

x = needle lift

For $x = 0$, $P = P_0$, $P_1 = P_c$ the initial force of the spring is given by

$$F_s = \frac{\pi(D^2 - d^2)}{4}P_0 + \frac{\pi d^2}{4}P_c \quad (3-11)$$

where P_0 = opening pressure (pressure at the onset of fuel injection)

P_c = pressure in the combustion chamber

A multiorifice atomizer has two throttling cross sections; cross section 1 has surface $\mu_1 A_1$ in the region of the needle seat and is variable, and cross section 2 has surface $\mu_2 A_2$ representing the discharge orifices and is constant. From the Bernoulli equation and the continuity equation for those two cross sections it follows that

$$P - P_1 = \frac{\rho Q^2}{2(\mu_1 A_1)^2} \quad (3-12)$$

where $A_1 = \pi x d \sin \alpha$

Q = volumetric flow rate

and

$$P_1 = P_0 = \frac{\rho Q^2}{2(\mu_2 A_2)^2} \quad (3-13)$$

From these equations, after eliminating x and P_1 first and P and P_1 next, we obtain

$$P_0 + \frac{4k_s Q \sqrt{\rho/2}}{\pi(D^2 - d^2) \mu_1 \pi d \sin \theta \sqrt{(P_0 - P_c) - \frac{\rho Q^2}{2(\mu_2 A_2)^2}}} = P + \frac{\rho Q^2}{2(\mu_2 A_2)^2} \frac{d^2}{D^2 - d^2} \quad (3-14)$$

$$1 + \frac{4k_s x}{\pi(D^2 - d^2)(P_0 - P_c)} = \frac{\rho Q^2}{2(\mu_2 A_2)^2(P_0 - P_c)} \frac{D^2}{D^2 - d^2} + \frac{\rho Q^2}{2(\mu_1 \pi d \sin \alpha)^2(P_0 - P_c)x^2} \quad (3-15)$$

From Eq. (3-14) we obtain the characteristic $P = f(Q)$ and from Eq. (3-15) the function of the needle lift $x = f(Q)$, which is shown in Fig. 3-6.

As seen, during the initial stage of the injection the pressure P drops slightly, the needle rises a little, and the fuel discharge is unstable. Starting from pressure P_{\min} and critical rate Q^* , stable discharge begins. The fuel throttling in the needle seat decreases as the needle lift increases, which causes pressure P_1 under the needle to increase and approach pressure P asymptotically. The curve $P_1 = f(Q)$ is similar to the curve in Fig. 3-2.

Pintle nozzle (Fig. 3-7). In static conditions the balance of forces acting on the pintle has the following form:

$$F_s + k_s x = \frac{\pi(D^2 - d^2)}{4} P + \frac{\pi(d^2 - d_x^2)}{4} P_1 + \frac{\pi d_x^2}{4} P_c \quad (3-16)$$

where d_x is the instantaneous needle diameter corresponding to a given lift x , and F_s, k_s are as in Eq. (3-10). For $x = 0$, $P = P_0$, $P_1 = P_c$, $d_x = 0$ the initial spring force is equal to

$$F_s = \frac{\pi(D^2 - d^2)}{4} P_0 + \frac{\pi d^2}{4} P_c \quad (3-17)$$

A pintle nozzle has three throttling cross sections, 1, 2, and 3, for which, according to Eq. (3-3), we can write the following equation of continuity:

$$\begin{aligned} Q &= \mu_1 A_2 \sqrt{\frac{2}{\rho}(P - P_1)} = \mu_2 A_2 \sqrt{\frac{2}{\rho}(P_1 - P_2)} \\ &= \mu_3 A_3 \sqrt{\frac{2}{\rho}(P_2 - P_c)} = \mu A \sqrt{\frac{2}{\rho}(P - P_c)} \end{aligned} \quad (3-18)$$

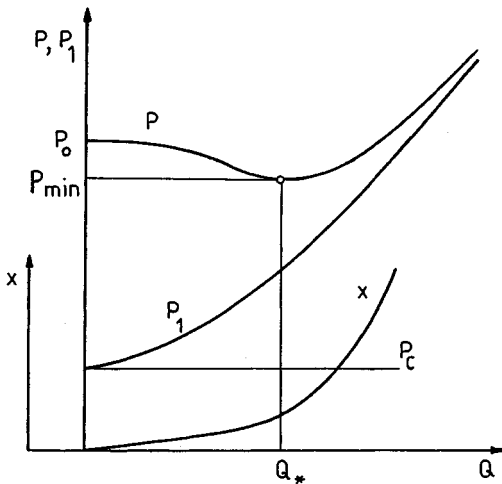


Figure 3-6 Characteristic of the atomizer shown in Fig. 3-5.

The throttling in cross section 1 is much smaller than in cross sections 2 and 3; therefore, assuming $P_1 = P$, we can calculate from the three last terms of Eq. (3-18) the *surface of an equivalent flow cross section*:

$$\mu A = \mu_2 A_2 \sqrt{\frac{1}{1 + (\mu_2 A_2 / \mu_3 A_3)^2}} \quad (3-19)$$

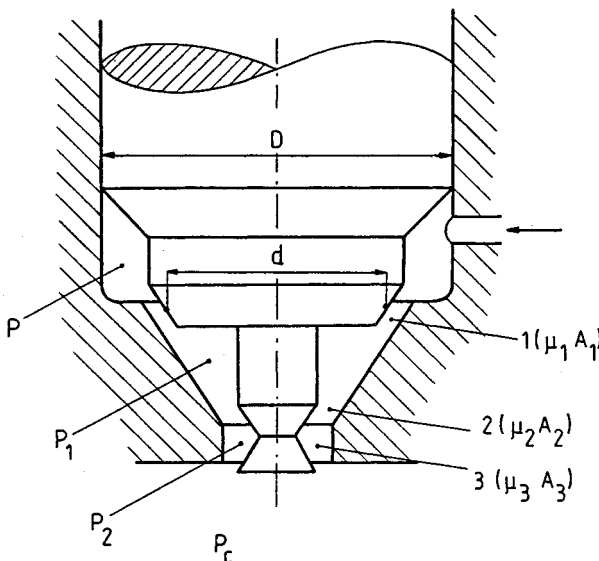


Figure 3-7 Schematic diagram of pintle nozzle.

From the Bernoulli equation and from the continuity equation one obtains

$$P - P_1 = \frac{\rho Q^2}{2(\mu_1 \pi x d \sin \alpha)^2}, \quad (3-20)$$

$$P_1 - P_c = \frac{\rho Q^2}{(\mu A)^2} \quad (3-21)$$

From the above equations after eliminating first x and P_1 and then P and P_1 one obtains

$$\frac{\pi}{4}(D^2 - d^2)(P - P_0) = \frac{\pi}{4}(d^2 - d_x^2) \frac{\rho Q^2}{2(\mu A)^2} + \frac{k_s Q}{\mu_1 \pi d \sin \alpha \sqrt{\frac{2}{\rho}(P - P_c) - \frac{Q^2}{(\mu A)^2}}}, \quad (3-22)$$

$$k_s x - \frac{\pi}{4}(D^2 - d^2) \frac{\rho Q^2}{2(\mu_1 \pi d \sin \alpha)^2} \cdot \frac{1}{x^2} = \frac{\pi}{4}(D^2 - d_x^2) \frac{\rho Q^2}{2(\mu A)^2} - \frac{\pi}{4}(D^2 - d^2)(P_0 - P_c). \quad (3-23)$$

From Eq. (3-22) we obtain the characteristic $P = f(Q)$, and from Eq. (3-23) we obtain the function of the needle lift $x + f(Q)$, which is shown in Fig. 3-8. The flow rate depends mostly on the surface of the equivalent flow cross section μA . A proper shape of the pintle allows control of the flow rate in all stages of the injection, because it follows from the character of the curve $x = f(Q)$ that in a certain range of x there is a decrease of the flow rate. Such a decrease during the initial stage of the injection is advantageous for the process of combustion in the engine. Curves $P = f(Q)$ and $x = f(Q)$ are smooth because of the shape of the pintle.

3-2 MACROSTRUCTURE OF ATOMIZED LIQUID

Macrostructure encompasses the external shape and the internal structure of the spray. The external shape of a drop jet is characterized by the spray angle and the range of the jet; the internal structure refers mostly to the distribution of the liquid in the spray.

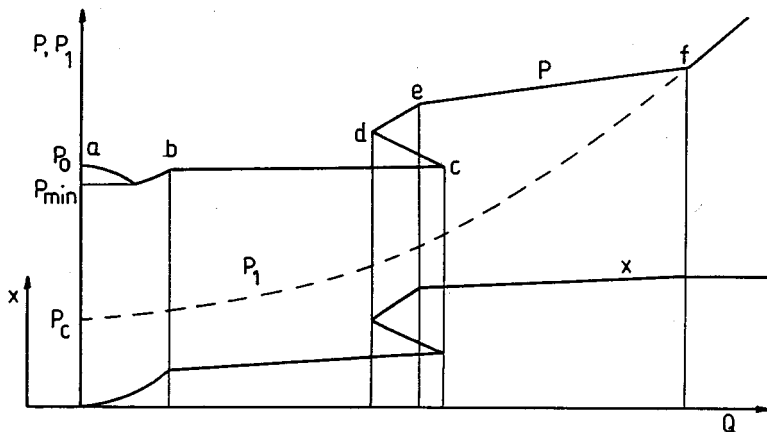


Figure 3-8 Characteristic of the nozzle shown in Fig. 3-7; symbols a-f correspond to the positions of the pintle in Fig. 5-8.

3-2.1 Spray Angle

Spray angle (injection angle) α is an apex angle of the spray. Figure 3-9 shows a jet discharging into a stationary environment. The jet narrows with increasing distance x from the nozzle. The narrowing of the jet is caused mainly by the action of the ambient gas, which starts to move as the jet is ejected. The angle α can therefore be uniquely determined only in a vacuum. In some cases the spray angle is defined as α' , which can be measured more accurately than angle α .

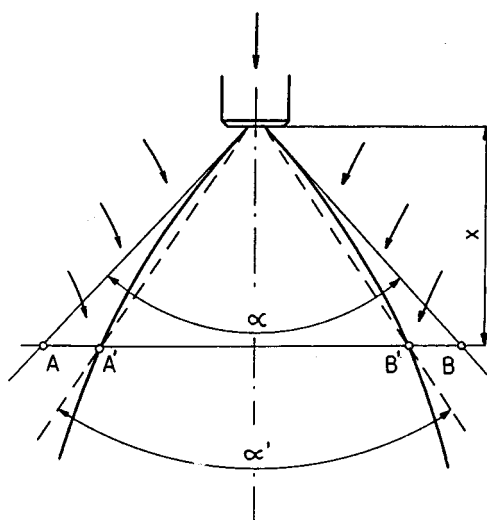


Figure 3-9 Contraction of a jet in a stationary environment.

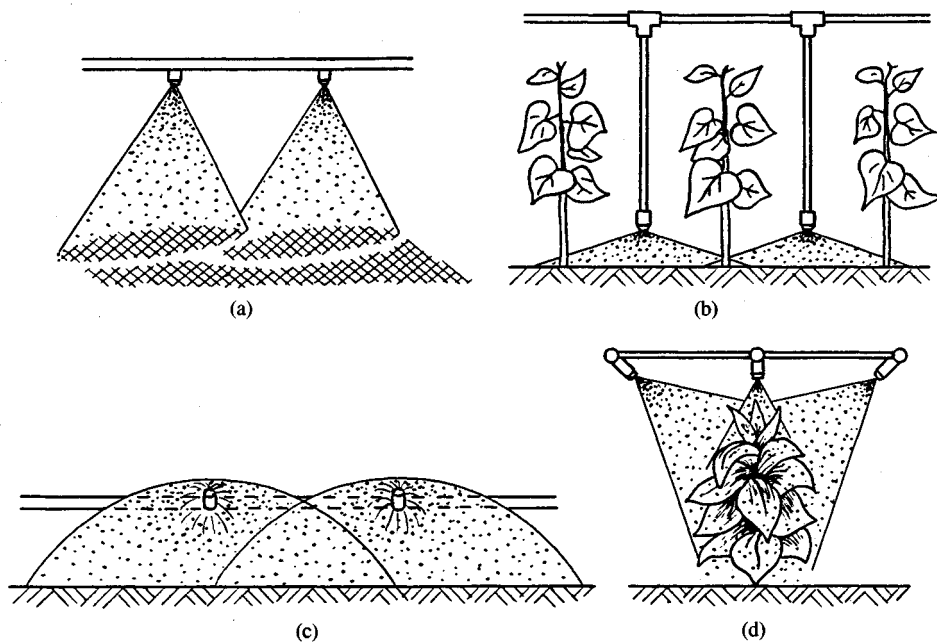


Figure 3-10 Clustered nozzles in agricultural treatments; dependence of the distance between nozzles on the shape of drop jets.

Such measurements make sense when the relation between the segments A–B and A'–B' is known for a given distance x , i.e., when the relationship between α and α' is known.

The spray angle characterizes the shape of the drop jet. In many cases it is necessary to predict the spray shape because it guarantees proper utilization of the jet. It is important mostly in cases in which atomizers occur in groups—for example, during agricultural treatments (Fig. 3-10); knowledge of the shape of an individual atomizer makes it possible to select correctly the distance between atomizers.

Figure 3-11 shows schematic diagrams of some atomizers and their spray angles α . These angles can be significantly different. Jet atomizers (continuous and intermittent), which have a circular discharge orifice, have very small angles α . Swirl and pneumatic atomizers have significantly larger angles α , depending on their internal geometry. Rotary atomizers generate drops in the plane perpendicular to the atomizer axis. It is hard therefore to define the spray angle. However, in the case of forced gas flow around the atomizer, the desired spray angle can be achieved (Fig. 3-11d).

Only two of the most characteristic cases of the spray angle will be discussed. They refer to jet atomizers with discontinuous operation and to simplex swirl atomizers.

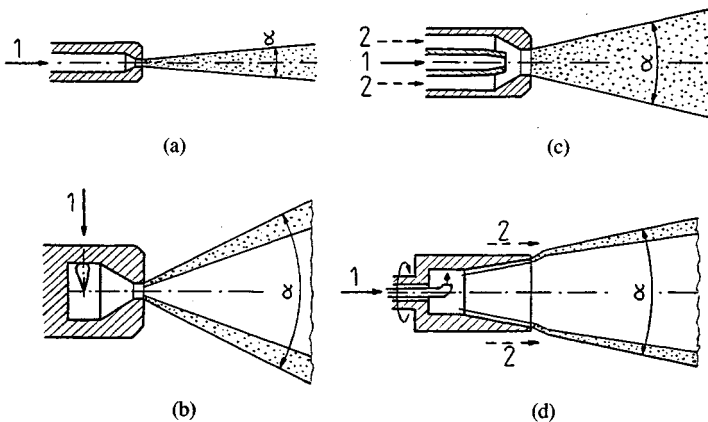


Figure 3-11 Spray angle α of various atomizers: (a) continuous jet nozzle; (b) swirl atomizer; (c) pneumatic atomizer; (d) rotary atomizer; 1, liquid; 2, gas.

Jet atomizers with the intermittent operation (diesel nozzles) are characterized by very small spray angles that do not exceed several degrees. Further information regarding the spray angle will be given while discussing the range of the jet of these atomizers, since these problems are interrelated.

Swirl atomizers are characterized by a very broad range of spray angles, $\alpha = 15^\circ - 120^\circ$. The angle α can be determined when the axial component u and the circumferential component w of the liquid velocity are known at the discharge orifice (Fig. 3-12):

$$\operatorname{tg} \frac{\alpha}{2} = \frac{v}{u} \quad (3-24)$$

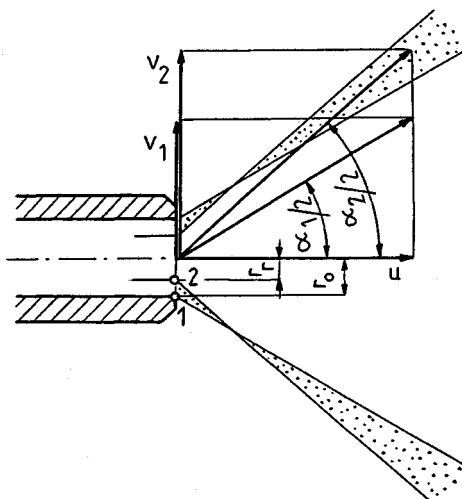


Figure 3-12 Spray angle α of a swirl atomizer.

The following simplifying assumptions were made: the liquid is a nonviscous one, there is no radial velocity component, and there is no interaction with the environment.

Not all of the liquid elements in the outlet cross section move identically. Element 1 on radius r_0 deflects less than element 2 on radius r_r , where r_r is the radius of an air vortex. Angle $\alpha_1/2$ between the trajectory of element 1 and the atomizer axis is smaller than the corresponding angle $\alpha_2/2$, where

$$\operatorname{tg} \frac{\alpha_1}{2} = \frac{v_1}{u}, \quad \operatorname{tg} \frac{\alpha_2}{2} = \frac{v_2}{u}$$

This follows from the assumption that the liquid elements move according to the equation of a *free vortex*.

$$r_0 v_1 = r_r v_2 = \text{const} \quad (3-25)$$

Because $r_0 > r_r$, then $v_1 < v_2$; therefore $\alpha_1/2 < \alpha_2/2$, hence $\alpha_1 < \alpha_2$.

It follows from the above that the drop trajectories cross and the drops collide. As a result, some mean angle α_m is established, which is approximately equal to

$$\alpha_m = \frac{\alpha_1 + \alpha_2}{2} \quad (3-26)$$

The mean angle α_m can also be derived from another approximation:

$$\operatorname{tg} \frac{\alpha_m}{2} = \frac{(v_1 + v_2)/2}{u} = \frac{v_m}{u} \quad (3-27)$$

Other methods of averaging α in a swirl atomizer will be discussed in Chapters 5 and 7.

Knowledge of the mean spray angle is necessary for the proper design of various devices. Examples are the combustion chambers of gas turbines (Fig. 3-13). Combustion in these chambers proceeds with high velocities of air flow and is possible due to the swirling of the air used for combustion. Because of the swirling, stagnation zones develop, which are necessary for stabilization of the flame. The mean spray angle is selected to match the stagnation zones present in the centers of the vortices.

The spray angle of swirl atomizers depends on the internal geometry of the atomizers. This problem will be discussed in Sec. 5-2. Here the effect of external factors on α will be discussed briefly. The effect of liquid properties is such that the lower the density and viscosity of the liquid, the larger is the spray angle. The effect of the pressure is such that, according to Fig. 3-12, the circumferen-

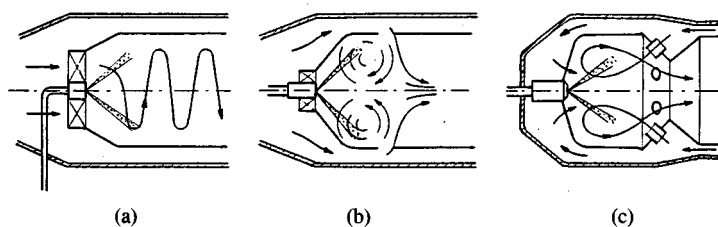


Figure 3-13 Combustion chambers of gas turbines: (a) chamber with a spiral vortex; (b) chamber with a toroidal vortex; (c) chamber with a loop vortex.

tial velocity component increases as the pressure increases and therefore angle α also increases. This increase is observed only in the pressure range 0.7–2.1 MPa [9]. Above 2.1 MPa, the angle α does not change.

3-2.2 Spray Penetration

The range of drop jet (penetration) l is the length of the jet in the axial direction. The spray penetration is not a unique parameter, because in many cases (e.g., during plant spraying or spray painting) the spray is used right after it formed. In these instances one cannot refer to spray penetration. In some cases, however, spray penetration has a unique or conditional meaning (Fig. 3-14).

Figure 3-14 shows several stages of an intermittent injection of fuel; in the final stage the spray has a defined range, which can be observed only when combustion is not present. In the case of continuous injection, spray penetration can be defined in terms of the horizontal or vertical (upward) motion of the spray. During horizontal motion (Fig. 3-14b), spray penetration is defined as the distance from the discharge orifice to a vertical line that passes through the point of intersection of the median streamline with a plane located at a distance h below the atomizer. During vertical injection (Fig. 3-14c), spray penetration, l_{99} , is defined as the height reached by at least 99% of the liquid [8].

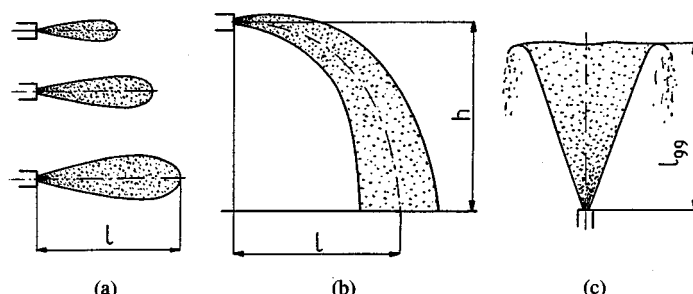


Figure 3-14 Drop jet range: (a) pulsed injection; (b) continuous horizontal injection; (c) continuous upward injection.

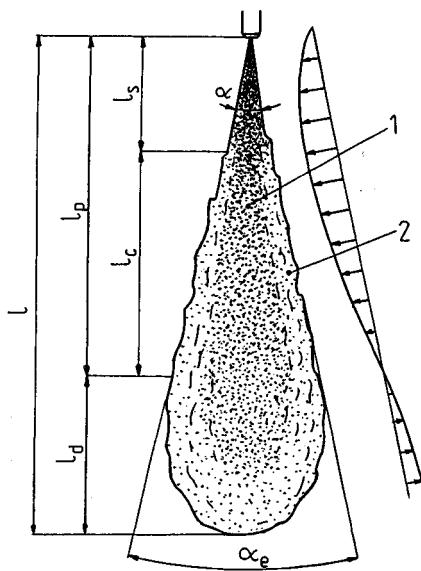


Figure 3-15 Structure of a jet of drops generated by a diesel nozzle.

In air-conditioned chambers, penetration of a horizontal spray is estimated as the distance from the discharge orifice to the vertical plane in which drop fall begins. Such penetration is defined uniquely only in stagnant air or for a known air velocity. In the case of direct water spraying in air-conditioned rooms, the term spray penetration is understood to mean the distance between the atomizer and the place where drops disappear because of evaporation.

Jet atomizers with intermittent operation are characterized by the fact that the spray penetration changes in time but has a definite limiting value. The penetration should be such that the spray reaches the end of the combustion chamber but does not hit the walls or piston. If there is intense air swirling in the chamber, the problem of spray penetration is less significant. The process of combustion in a piston engine and the concentration of fumes and nitrogen oxide depend mostly on the shape and penetration of the spray. It has been established that, in principle, the spray penetration is proportional to the square root of the time counted from the start of injection [3]. The details will be discussed in Chapters 5 and 6.

A spray generated in an intermittent manner in stagnant ambient air is shown in Fig. 3-15 [10]. The shape of the spray is known only from experiments because no mathematical model is available. The jet can be divided into two regions: main jet region 1 and mixing flow region 2. Region 1 contains the jet core and is characterized by a higher concentration and higher velocity of large drops; therefore this region has a significantly lower temperature even when the ambient temperature is high. Region 2 is located outside region 1 and is characterized by a high intensity of turbulent mixing.

The total spray penetration of length l can be divided into the following segments:

Initial segment of length l_s ; this segment is located directly behind the nozzle and has a distinct shape with a spray angle α .

Mixing flow segment of length l_c ; this segment is located behind the initial segment and refers to the part of the spray with an equivalent angle α_e , where the process of the turbulent mixing occurs.

Penetration segment of length l_p ; this comprises the initial and mixing segments; in this region the spray is similar to one generated in a continuous manner, and this similarity includes the process of ambient air supply to the spray.

Stagnation segment of length l_d ; this segment comprises the front of the spray, which is flattened by aerodynamic drag and is characterized by instability and outward air flow.

Spray penetration, the lengths of the segments, and the values of the angles are given by

$$l = 27.1V^{0.5}d_0^{0.5}\rho^{0.09} \log t - 0.41t^{0.38} \quad (3-28)$$

$$\left. \begin{array}{l} l_s = 10 \text{ to } 15 \text{ mm} \\ l_p = 0.7l \end{array} \right\} \quad (3-29)$$

$$\left. \begin{array}{l} \alpha = 0.35\rho \\ \alpha_e = 0.17\rho^{0.3} \end{array} \right\} \quad (3-30)$$

where V = mean fuel velocity at outlet of nozzle (m/s)

d_0 = discharge orifice diameter (m)

ρ = spray density (kg/m^3)

t = time counted from start of injection (ms)

Figure 3-15 shows direction of the motion of ambient air with respect to the jet. Velocity of the air entrained by the jet increases on the initial segment and reaches a maximum on the border between the initial and mixing segments. This velocity then decreases and changes its sense of direction between the mixing and stagnation segments.

3-2.3 Liquid Distribution in a Drop Jet

The liquid distribution in a drop jet is best characterized in terms of the *density of the liquid jet*, $q = q_v$ defined as the ratio of the volumetric flow rate ΔQ to the surface ΔA perpendicular to the axis of the atomizer:

$$q = q_v = \frac{\Delta Q}{\Delta A} \left[\frac{\text{m}^3/\text{s}}{\text{m}^2} \right] \quad (3-31)$$

The density of the liquid jet can also assume the form

$$q_m = \frac{\Delta G}{\Delta A} \left[\frac{\text{kg/s}}{\text{m}^2} \right] \quad (3-32)$$

However, the first form, $q = q_v$, is applied more because the measurement of the liquid jet density is based principally on a volumetric method.

The density is in principle nonuniform; i.e., there is a certain distribution of the liquid jet density and one can consider a three-dimensional density distribution q in a spray, in the radial, circumferential, and axial directions:

The radial density distribution $q = f(r)$ of the spray is most important because of the high nonuniformity of density in this direction,

The circumferential liquid density distribution of the spray $q = f(\varphi)$ is used for assessment of the spray symmetry with respect to its axis.

The axial liquid density distribution $q = f(x)$ is rarely considered because it can be replaced by radial distributions for several distances x from the nozzle.

The *radial liquid density distribution* $q = f(r)$ is by nature nonuniform for all types of atomizers. Only two types of atomizers, swirl-jet atomizers and pneumatic atomizers, can ensure a uniform liquid density distribution $q = f(r)$ if certain conditions are satisfied. Lack of nonuniformity is a big disadvantage that hinders or even prevents rational use of atomizers in processes of heat and mass exchange (chemical reactors, steam attemperation, scrubbers, air-conditioned chambers, etc.)

The characteristic liquid density distributions $q = f(r)$ are distinguished for jet atomizers, swirl atomizers, and swirl-jet atomizers (Fig. 3-16). To describe

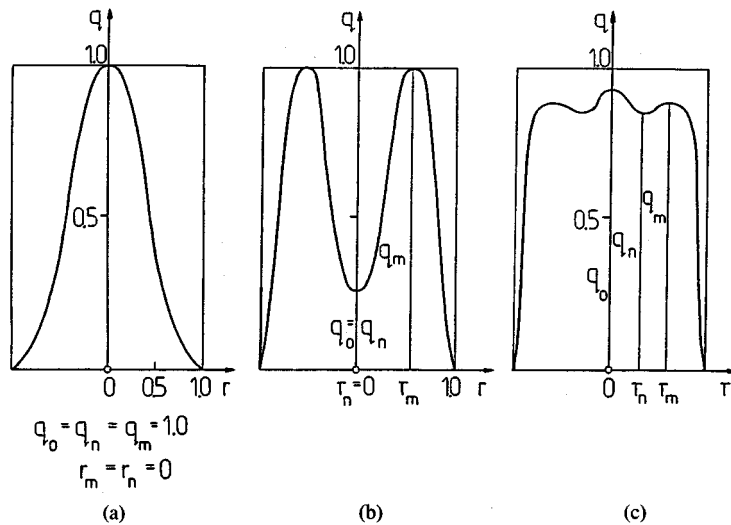


Figure 3-16 Parametric description of the density distribution $q = f(r)$ for (a) jet atomizers; (b) swirl atomizers; (c) jet-swirl atomizers.

these distributions, we introduce the following relative parameters:

- q_0 —liquid density in the spray axis
- q_m —maximum density outside the axis
- q_n —minimum density between two maximum values
- r_m, r_n —radii on which q_m and q_n occur

An attempt at an analytic representation of the curves shown in Fig. 3-16 has been undertaken [8]. The foregoing parameters are interrelated and therefore can change independently only in a certain (however adequate for practical applications) region. Because of the large number of parameters, the analyses have been restrained to the basic interrelationships between these parameters.

The liquid density distribution $q = f(r)$ of *jet atomizers* is highly nonuniform because it is characterized by high values of q in the spray axis (Fig. 3-16a). Such a state exists in all transverse cross sections of the spray and the subsequent distribution curves are similar (Fig. 3-17). It can therefore be assumed that the liquid density distribution is governed by a law similar to this one for the velocity distribution.

Based on this assumption, Lyshevskii [4] treated a spray as a free turbulent jet, and Eq. (2-155) assumes the form

$$\frac{q}{q_{\max}} = \exp \left[-0.693 \left(\frac{r}{\bar{r}} \right)^2 \right] \quad (3-33)$$

where q_{\max} is the liquid density at the spray axis and \bar{r} is the radius corresponding to the value $q_{\max}/2$.

$$\bar{r} = 2a_c^2 x^2 \ln 2 \quad (3-34)$$

Coefficient a_c can be determined experimentally based on the function

$$a_c = f(\text{We}, \text{Lp}, M, N) \quad (3-35)$$

where the term N is usually neglected as nonsignificant. The experimental results will be presented in Chapter 6.

Sprays generated by jet atomizers are characterized by the fact that large drops are located in the core of the spray. Especially complex is the structure of sprays generated by jet atomizers with discontinuous operation (Fig. 3-15). Measurements in the core of these jets are difficult, but they indicate that the process of disintegration is not complete [12]. The length of the core depends strongly on the pressure of the ambient gas; for example, for a pressure of 0.5 MPa it is 60 mm and for 5 MPa it is only 20 mm. This fact affects the radial liquid density distribution.

In the region surrounding the core, i.e., in the flow mixing region (Fig. 3-15), the concentration of drops is much lower, which enables measurement of their

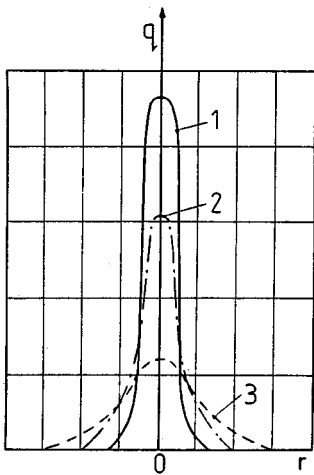


Figure 3-17 Density distribution $q = f(r)$ for a jet atomizer; curves 1, 2, and 3 correspond to increasing distance x from the atomizer.

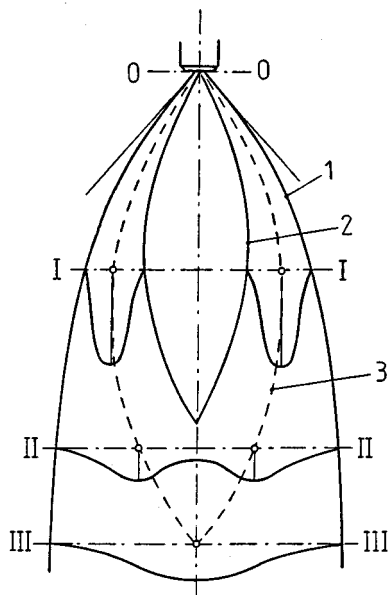


Figure 3-18 Density distribution $q = f(r)$ of a swirl atomizer; 1 and 2, external and internal borders of the jet; 3, line of maximum liquid density in consecutive cross sections of the jet.

sizes. The drop Sauter diameter is 30–40 μm [10]. There is a linear relationship between the mean drop velocity and drop diameter.

The density distribution $q = f(r)$ for *swirl atomizers* is highly nonuniform, with small values of q occurring in the spray axis and high values present at its periphery (Fig. 3-16b). Such a state exists in the intermediate cross sections of the spray, for instance, in cross section II-II in Fig. 3-18. As seen, a characteristic feature is lack of similarity of the density distribution curves in the transverse cross sections of the spray. In the initial cross section I-I there are no drops in the vicinity of the spray axis; in the final cross section III-III the maximum density q occurs on the axis. The spray shown in Fig. 3-18 is a free jet, which moves downward in an unlimited space.

The radial liquid distribution of a swirl atomizer can be represented by a cumulative curve (Fig. 3-19). This curve is generated by measuring the volume of the liquid collected at different places along the spray diameter and relating it to the total volume of the collected liquid. The integral curve can be approximated by the *Rosin-Rammler equation*

$$Y = 1 - \exp \left[-0.693 \left(\frac{r}{\bar{r}} \right)^n \right] \quad (3-36)$$

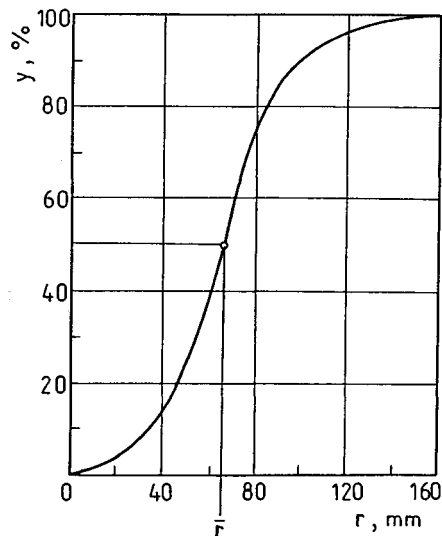


Figure 3-19 Cumulative curve of the radial liquid distribution—swirl atomizer.

where Y = fraction of the collected liquid

\bar{r} = spray diameter, which separates the collected liquid volume into halves

$n = 2-5$ is an experimental exponent

In principle, the circumferential liquid density distribution $q = f(\varphi)$ is uniform for all types of atomizers. However, due to technological and assembly errors, significant distortion of the spray can occur. Circumferential nonuniformity can also occur during the operation of an atomizer because of erosion or contamination of nozzles. In small atomizers a uniform circumferential liquid distribution is hard to achieve.

The circumferential nonuniformity I is given by

$$I = \frac{q_{\max} - q_{\min}}{\bar{q}} \times 100 [\%] \quad (3-37)$$

where q_{\max} , q_{\min} , and \bar{q} denote the maximum, minimum, and mean liquid density, respectively. These densities are determined by measuring the volume of the liquid collected for certain angles φ along the spray perimeter. The nonuniformity I should be determined at a given distance from the atomizer, because as this distance increases so does the tendency of the spray to be more uniform.

Limits of acceptable nonuniformity I are established individually depending on needs. In some cases there is no need for any limits, but in most cases atomizers having the nonuniformity $I > 30-40\%$ are not accepted for operation. In the case of the aircraft gas turbines, too much circumferential nonuniformity of the fuel can cause a burn through the wall of a combustion chamber, and $I < 20-35\%$ is required.

Measurements of the nonuniformity I are made using vessels of the same cross-sectional area. Then in order to calculate I it suffices to determine the volume of collected liquid or even the head of liquid in the measuring vessels. This will be discussed more in Chapter 7.

In the case of group atomizers, we are concerned with the liquid distribution that develops as a result of partial superposition or separation of adjacent jets. This occurs, for example, in air-conditioned chambers with a large number of water atomizers. A similar situation arises during aerial and ground spraying.

Installations for plant protection should ensure a uniform liquid distribution on the surface being sprayed. The proper liquid distribution depends on the distance between atomizers, the height of atomizers above the surface, and their ability to maintain a constant flow rate.

During field spraying an important parameter is the *transverse liquid distribution*. In order to assess this distribution we introduce an *indicator of the nonuniformity of the transverse liquid distribution*

$$\delta = \frac{(1/n) \sum_{i=1}^n (V_i - \bar{V})^2}{\bar{V}} \times 100 [\%] \quad (3-38)$$

where V_i is the liquid volume collected from the i th groove, \bar{V} is the mean liquid volume per groove, and n is the number of active grooves. Parallel grooves are made on a measuring table (see Chapter 7). The indicator of nonuniformity should satisfy the condition $\delta \leq 20\%$. It should be pointed out that this indicator refers to a group of atomizers mounted properly on the beam of field atomizers; the indicator of nonuniformity for an individual atomizer is much higher.

Surface coating during the spraying operation should be achieved using the minimal amount of liquid. Not only the drop diameters but also the diameters of the traces of drops are important. In order to increase the coated surface, the largest drop traces are desired. This is achieved by lowering the surface tension of pesticides, which leads to better smearing of drops on the surface. In this way the coated surface can be increased 3.5-fold.

The degree of surface coating, i.e., the ratio of the cumulative area of the drop traces to the surface being sprayed, depends (as mentioned in Sec. 1-2.4) on the type of spraying operation. The surface of a plant is approximately five times larger than the surface on which the plant grows. The concentration of drops is determined by measuring the number of drop traces on an area of 1 cm².

3-3 MICROSTRUCTURE OF ATOMIZED LIQUID

3-3.1 Concept of Atomization Quality

The drops in a spray constitute a typical nonuniform system (polydisperse), which is characterized by a large scatter of drop diameters. An even larger

scatter is observed in the case of surfaces and masses of drops. For example, a spray with drop diameters ranging from 10 to 200 μm has a diameter scatter of 20:1 and a mass scatter equal to this ratio to the third power, i.e., 8000:1. In most cases this is a disadvantage, and the generation of an approximately uniform drop distribution (as follows from Sec. 2-6) is very difficult.

During atomization large numbers of drops are produced. For example, in a piston engine, for a mean fuel charge $V_w = 50 \text{ mm}^3/\text{cycle}$ and a mean drop diameter $D = 10 \mu\text{m}$, a very large number of drops N is obtained:

$$N = \frac{6V_w}{\pi D^3} = \frac{(6)(50)}{(\pi)(0.01)^3} \approx 10^8$$

Under real conditions the number of drops will be different due to the scatter in drop diameters.

Atomization quality is a general term that has two specific meanings: degree of atomization and uniformity of atomization. *Degree of atomization* refers to the mean drop diameter, with a higher degree of atomization denoting a smaller mean drop diameter. *Uniformity of atomization* describes the scatter of drop diameters, with a higher uniformity of atomization denoting smaller scatter. In this way we can formulate the requirements regarding the quality of atomization in the following fields.

In combustion processes the drop size plays a fundamental role. A jet of small drops ($D \leq 25 \mu\text{m}$) evaporates quickly, creating a gas mixture, which leads to combustion of the kinematic type. A jet of larger drops ($D = 25\text{--}250 \mu\text{m}$ and larger) undergoes a complex process of fuel mixture development, which leads to much slower combustion of the diffusion type. Very large drops ($D \geq 2.5 \text{ mm}$) undergo surface combustion in a protracted manner.

Drop diameter scatter has a versatile influence on the combustion process. A large scatter of drops leads to incomplete combustion of large drops. In installations operating under highly changing loads, as in the combustion chambers of gas turbines, greater scatter of drop diameters ensures higher stability of combustion.

A similar effect of drop size scatter exists during combustion in piston engines. When the nozzle needle is open, large drops with high size scatter develop, which makes self-ignition and drop penetration easier. The same atomization condition exists at the end of injection, but in this case there are disadvantages because they result in incomplete combustion of large drops.

In air conditioning various degrees of atomization are required, depending on the operating process. During air humidification small drops are desired, whereas during the simultaneous processes of humidification, cleaning, and heating or cooling of the air large drops are desired. These are general requirements, because more specific recommendations do not exist. In this case, drop diameter scatter does not play as important a role as it does in other fields.

Table 3-1 Evaporation time of a water drop as a function of temperature and relative humidity of the air

Drop diameter (μm)	Temperature ($^{\circ}\text{C}$)	Relative humidity (%)	Drop evaporation time (s)
200	15	40	63
100	15	40	16
	20	70	20
		40	9
50	15	40	4
	20	70	5
		40	2

In *agricultural treatments* the following classification of drop diameters is used:

- Aerosol generation, 0–50 μm
- Small drop spraying, 25–125 μm
- Medium drop spraying, 50–250 μm
- Coarse drop spraying, 150–600 μm

The sizes of drops change because of evaporation. Effects of climatic factors on the “lifetime” of a drop are presented in Table 3-1. The degree of atomization depends on the type of treatment (Sec. 1-2.4); the uniformity of atomization should be as high as possible, since small drops evaporate quickly or drift with the wind.

There are other applications in which atomization uniformity plays an important role. Among them are spray drying of various substances in the chemical, pharmaceutical, and food industries, and medical treatment (inhalations, disinfection).

3-3.2 Drop Size Spectrum in a Spray

The size of drops depends on both controllable quantities (e.g., nozzle geometry, type of liquid) and uncontrollable quantities (e.g., liquid turbulence, vibrations). As a result, drops with various diameters develop, and the process of their generation itself has a statistical character. Theoretical prediction of drop number and size based on the disintegration mechanism itself is not feasible. However, some attempts have been made to make such predictions. These attempts are by nature limited to a certain type of atomizer.

For example, a method has been proposed for determining the characteristic of the drop diameter distribution for a swirl atomizer [5]. The starting point is knowledge of the geometry of the nozzle and the operating conditions of the

atomizer. The method contains a three-stage procedure that is based on assessment of the initial thickness and velocity of the sheet discharging from the nozzle, assessment of the separated liquid fragment developed as a result of sheet instability, and assessment of drop size.

The drops then represent a statistical set in which the variable is the drop diameter D . The distribution of drop diameters creates the spectrum of drop sizes. According to the principles of statistics, this term represents the relationship between the number of drops Δn_i having a diameter in the range

$$\left\langle D_i - \frac{\Delta D}{2}, D_i + \frac{\Delta D}{2} \right\rangle$$

and the diameter D_i , which corresponds to the center of each i th range, and ΔD is the constant width of the range. The spray spectrum is determined on the basis of measurements of drop diameters. These measurements are based on classification of each diameter into the proper *diameter range*. The size of the range, e.g., $\Delta D = 10 \mu\text{m}$, is based on the measuring method and required accuracy.

The *total number of drops* (size of the set) is equal to

$$N = \sum_{i=1}^m \Delta n_i \quad (3-39)$$

where m is the number of diameter ranges. The number of drops Δn_i in each range related to the total number of drops N in the set considered represents the number fraction of drops in a given range.

$$\Delta \bar{n}_i = \frac{\Delta n_i}{N} \quad (3-40)$$

Figure 3-20 shows a histogram of the number fraction of drops $\Delta \bar{n}_i$, which is prepared as a result of measurements. The resultant height of all fractions is

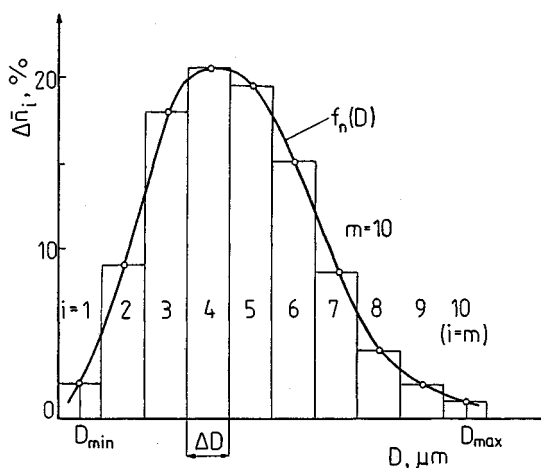


Figure 3-20 Drop size distribution curve.

equal to 100%. A histogram can be substituted by a continuous curve, i.e., the frequency curve of the probability density of the number fraction of drops, which will be referred to as the *number distribution curve*.

The *function of the number distribution* of drops is given by

$$f_n(D) = \frac{\Delta \bar{n}_i}{\Delta D_i} = \frac{\Delta n_i / \Delta D_i}{\sum_l^m \Delta n_i} \quad (3-41)$$

Treating the diameter D as a continuous variable in the range $\langle 0, \infty \rangle$ or $\langle D_{\min}, D_{\max} \rangle$, we can write

$$f_n(D) = \frac{d\bar{n}}{dD} = \frac{dn/dD}{\int_0^\infty (dn/dD) dD} \quad (3-42)$$

Experiments show that using either of these ranges does not lead to significant errors.

The *cumulative distribution function* of the variable D , or the cumulative function of the number distribution of drops in this case, is equal to

$$\Phi_n(D) = \sum_l^i \Delta \bar{n}_i \quad (3-43)$$

or

$$\Phi_n(D) = \int_0^D f_n(D) dD = \int_0^D \frac{d\bar{n}}{dD} dD = \frac{\int_0^D (dn/dD) dD}{\int_0^\infty (dn/dD) dD} \quad (3-44)$$

The function $\Phi(D)$ is obtained by the summation of function $f_n(D)$, and for the total range of diameters we obtain

$$\sum_l^m \Delta \bar{n}_i = 1, \quad \int_0^\infty \frac{d\bar{n}}{dD} dD = 1 \quad (3-45)$$

Figure 3-21a shows curves of the cumulative distribution functions of drop sizes. The curves were obtained by summing the corresponding ordinates of the curve $f_n(D)$ in Fig. 3-20 (points on both curves correspond). They show the number fraction of drops with diameters lower than D in the total number of drops. A curve represented on a logarithmic scale and probability scale is a straight line (Fig. 3-21b). The advantage of the linearity is that one can correct all measuring errors and employ simplified extrapolation and interpolation using a minimum number of measuring data.

Everything that has been said about the distribution of drop number also refers to the surface and volume (mass) distributions. For example, the volumetric (mass) distribution follows from the number distribution:

$$\frac{d\bar{V}}{dD} \sim D^3 \frac{d\bar{n}}{dD} \quad (3-46)$$

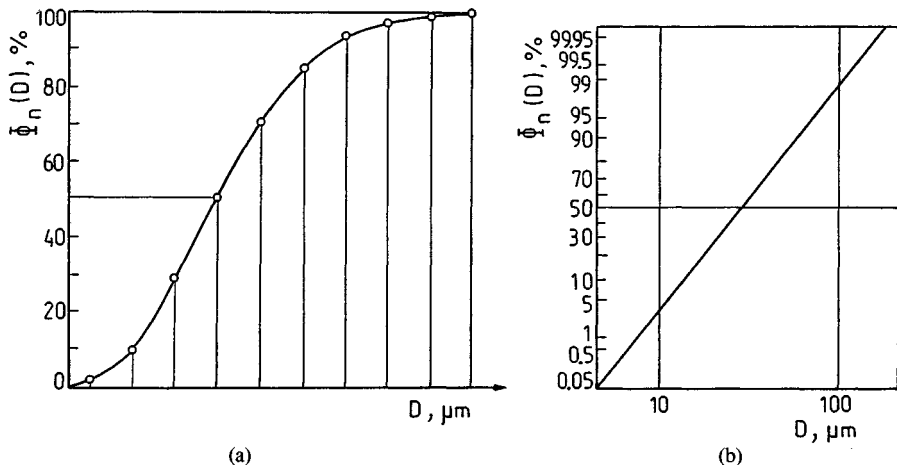


Figure 3-21 Cumulative drop size distribution curve $\Phi_n(D)$: (a) standard system; (b) system on a logarithmic scale and a probability scale.

where $d\bar{V}$ denotes the volume fraction of drops in a particular range. We can thus write instead of Eqs. (3-42) and (3-44) the following equations:

$$f_a(D) = \frac{(dn/dD)D^a}{\int_0^\infty (dn/dD)D^a dD} \quad (3-47)$$

and

$$\Phi_a(D) = \frac{\int_0^D (dn/dD)D^a dD}{\int_0^\infty (dn/dD)D^a dD} \quad (3-48)$$

Value $a = 0$ refers to the number distributions $f_0(D)$ and $\Phi_0(D)$, value $n = 2$ to the surface distribution $f_2(D)$ and $\Phi_2(D)$, value $n = 3$ to the volume (mass) distribution $f_3(D)$ and $\Phi_3(D)$.

To describe the functions $f(D)$ and $\phi(D)$ various equations are employed, which approximate the experimental size spectra of drops in a spray. Among the most commonly used are the Rosin-Rammler equation, the Nukiyama-Tanasawa equation, and the log-normal distribution equation. Each of these equations contains two experimental parameters and can be used to calculate mean drop diameters.

The *Rosin-Rammler equation* describes the cumulative volume or mass distribution function

$$\Phi_3(D) = 1 - \exp \left[- \left(\frac{D}{X} \right)^\delta \right] \quad (3-49)$$

where $\Phi_3(D)$ = fraction of the total volume contained in drops of diameter less than D

X = size parameter

δ = distribution parameter (spray uniformity parameter)

Figure 3-22a shows the curve of the cumulative distribution function of drop volume for $X = 90 \mu\text{m}$ and $X = 120 \mu\text{m}$ for the same value of δ . As seen, larger fractions of small drops correspond smaller values of X . In this particular case approximately 0.52 (52%) drops with diameters smaller than $D = 80 \mu\text{m}$ correspond the value $X = 90 \mu\text{m}$. Only approximately 0.285 (28.5%) drops correspond the value $X = 120 \mu\text{m}$. From Eq. (3-49) it follows that for $D/X = 1$:

$$\Phi_3(D) = 1 - e^{-1} = 0.632$$

and therefore parameter X represents the diameter D for which $\phi_3(D) = 0.632$ (points A and B in Fig. 3-22a). In other words, size parameter X indicates, that 63.2% of the volume of atomized liquid consists of drops with diameters smaller than X , and 36.8% of the volume liquid of drops with diameters larger than X .

Figure 3-22b shows the function $\Phi_3(D)$ for various distribution parameters $\delta = 0, 1, 2, 3, \infty$. The lower the parameter δ , the more nonuniform the drop distribution becomes, which is manifested by the lower slope of the distribution function. For $D/X = 1$ all curves cross at one point, for which $\phi_3(D) = 0.632$. Under real conditions of atomization, parameter δ falls in the range $\delta = 2-4$.

Equation (3-49) can be differentiated, yielding (according to what has been said) a function of the volume distribution $f_3(D)$:

$$f_3(D) = \frac{d\Phi_3(D)}{dD} = \frac{\delta}{X^\delta} D^{\delta-1} \exp\left[-\left(\frac{D}{X}\right)^\delta\right] \quad (3-50)$$

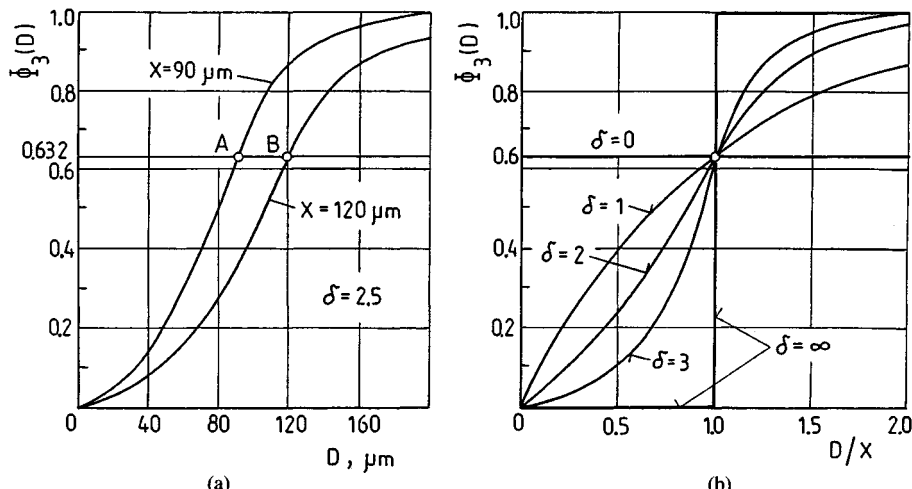


Figure 3-22 Interpretation of the parameters X and δ in the Rosin-Rammler distribution function.

From Eq. (3-49) one can derive the remaining distribution functions. It has been demonstrated experimentally that the functions of the volume distribution $f_3(D)$ and surface distribution $f_2(D)$ are in good agreement with experimental data [4], but not the number distribution function. In the latter case better results are given by the equation proposed by Y. Tanasawa and T. Tesima [1].

The character of volume distributions $f_3(D)$ and $\Phi_3(D)$ indicates that there are two characteristic drop diameters (Fig. 3-23). One of them is defined as a *modal diameter* D_M , which corresponds to the maximum of curve $f_3(D)$ or to the point of inflection of curve $f_3(D)$. It is the diameter of the largest number of drops in the spectrum. The second is the *median diameter* $D_m = D_{0.5} = \text{MMD}$, which divides the volume of the drops into two halves.

The latter diameter can be determined from Eq. (3-49) by substituting $\Phi_3(D) = 0.5$ and $D = D_m$.

$$D_m = 0.693^{1/\delta} X \quad (3-51)$$

The drop diameter D_m is determined from parameters X and δ . Using the term diameter D_m , one can transform the Rosin-Rammler equation. Substituting X from Eq. (3-51) into Eq. (3-49), we have

$$\Phi_3(D) = 1 - \exp\left[-0.693\left(\frac{D}{D_m}\right)^\delta\right]. \quad (3-52)$$

This equation has the same form as Eq. (3-36) and in this case D_m denotes the diameter for which $\Phi_3(D) = 50\%$.

The uniformity of spraying can be characterized by two diameters, for example, $D_{0.1}$ and $D_{0.9}$, as shown in Fig. 3-23. These diameters denote that 10%

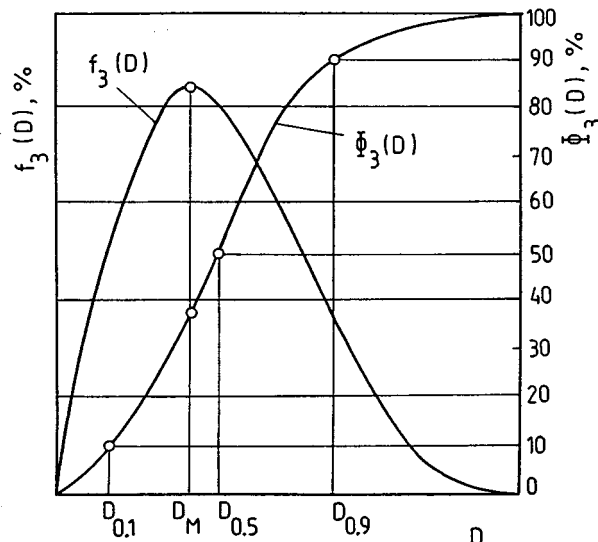


Figure 3-23 Drop volume distribution curves.

or 90% of the liquid volume consists of drops with diameters smaller than $D_{0.1}$ or $D_{0.9}$, respectively. The difference $D_{0.9} - D_{0.1}$ indicates the inclination of the curve of the volumetric distribution. This inclination is a measure of spraying uniformity. Independently, diameter $D_{0.1}$ (or $D_{0.05}$) characterizes the ignition properties of an atomized fuel, and diameter $D_{0.9}$ (or $D_{0.95}$) determines the required length of a combustion chamber because it is related to the maximum diameter D_{\max} of drops that should burn in the chamber.

In order to determine the drop distribution using the Rosin-Rammler equation, we can substitute the diameter $X = D_{0.632}$ with an arbitrary characteristic diameter, i.e., $D_{0.1}, D_{0.5} = \text{MDM}$, $\text{SMD} = D_{32}, D_M, D_{0.9}$. Chin and Lefebvre demonstrated [2] that for combustion of liquid fuels, substitution of the Sauter mean diameter $\text{SMD} = D_{32}$ provides the best assessment of spraying quality.

The *Nukiyama-Tanasawa equation* refers to the number drop distribution:

$$f_0(D) = \frac{d\bar{n}}{dD} = BD^2 \exp(-bD^\delta) \quad (3-53)$$

where B is a constant, b is the size parameter, and δ is the distribution parameter. Constant B can be evaluated from the condition (3-45) using the gamma function Γ . Parameter b is a dimensional quantity (dimension $\mu\text{m}^{-\delta}$). It is difficult to determine the parameters b and δ . Experiments show that for each type of distribution (number, surface, and volume) b and δ must be determined independently [4].

The *log-normal distribution equation* refers to the volume distribution of drops

$$f(y) = \frac{d\bar{V}}{dy} = \frac{h}{\sqrt{\pi}} \exp(-h^2 y^2) \quad (3-54)$$

where $d\bar{V}$ = volume fraction of drops in a given range

$y = \ln(D/\bar{D})$, i.e., $D = \bar{D}e^y$

h = mean standard deviation of y (and D)

\bar{D} = mean drop diameter

Equation (3-54) is based on the normal Gauss distribution, in which the variable D is replaced by the logarithm of D .

In conclusion, the real drop distribution is best described by the Rosin-Rammler equation. This equation has a relatively simple form, and its two parameters can easily be determined by a graphic method. The only disadvantage of this equation is that it does not describe the number drop distribution with sufficient accuracy.

It should be added that the maximum entropy law has been applied for prediction of the drop size distribution [11]. A law was formulated that predicts the most probable distribution based on the equations of conservation of mass, momentum, surface energy, and kinetic energy. The results are in accordance

with the empirical distributions, especially with the distribution expressed by the Rosin-Rammler equation.

3-3.3 Mean Drop Diameters

A *mean drop diameter* is a conventional quantity that characterizes a set of uniform drops substituted for the real set (drop size spectrum in a spray). Depending on the way it is calculated, the mean drop diameter determines such characteristics as number, diameter, surface, and volume of drops. The selection of a mean diameter depends on the field of application of the atomized liquid. The mean diameter does not supply information about the drop set itself; nevertheless, it is the most informative quantity for atomization quality assessment. It can be used in calculations related to drop motion and heat and mass exchange. Use of the mean diameter is satisfactory for engineering applications.

All definitions of mean diameter originate from one formula [6]:

$$D_{pq} = \sqrt[p+q]{\frac{\sum_{i=1}^m D_i^p \Delta n_i}{\sum_{i=1}^m D_i^q \Delta n_i}} \quad (3-55)$$

p and q are used simultaneously for the determination of a particular diameter (Table 3-2).

The *arithmetic mean diameter* D_{10} is the diameter of a uniform equivalent drop set with the same number of drops and sum of diameters as in the real set. Figure 3-24 shows as an example a set of 10 drops with diameters ranging from 1 to 10 in conditional units replaced by a set of 10 drops with the same length and a mean diameter of 5.5 units. From Eq. (3-55) we obtain

$$D_{10} = \frac{\sum D \Delta n}{\sum \Delta n} \quad (3-56)$$

Table 3-2 Mean drop diameters

Mean diameter				
p	q	Symbol	Name	Application
1	0	D_{10}	Arithmetic	Comparison of disperse systems
2	0	D_{20}	Surface	Surface area control, surface phenomena, e.g., absorption, vaporization
3	0	D_{30}	Volume	Volume control, volumetric phenomena
2	1	D_{21}	Relative surface	Drop disintegration, absorption
2	1	D_{31}	Relative volume, Probert's	Evaporation, molecular diffusion, combustion
3	2	D_{32}	Volume-surface, Sauter's	Drop range, mass transfer, heat transfer
4	3	D_{43}	Mass, de Brouckere's or Herdan's	Drop fractionation, combustion

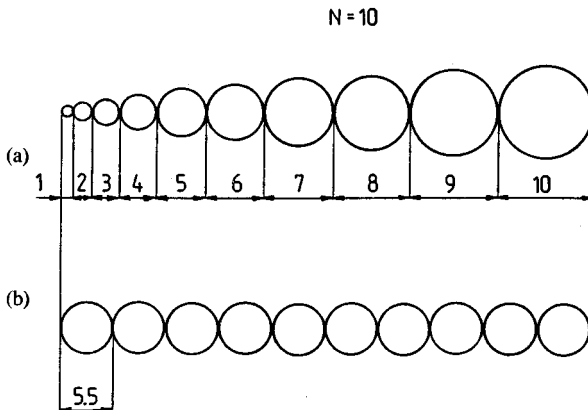


Figure 3-24 Sets of drops: (a) nonuniform set; (b) set equivalent with respect to drop number and size.

where index 10 denotes, that in the numerator the drop diameter D has the power of one, and in the denominator—the power of zero. In this notation, as well as in the following, the index i has been omitted.

The *area mean diameter* D_{20} is the drop diameter of an equivalent set with the same number of drops and the same total surface of all drops as in the real set.

$$D_{20} = \sqrt{\frac{\sum D^2 \Delta n}{\sum \Delta n}} \quad (3-57)$$

The *volume mean diameter* D_{30} is the drop diameter of a uniform equivalent set with the same number of drops and the same total volume of all drops as in the real set.

$$D_{30} = \sqrt[3]{\frac{\sum D^3 \Delta n}{\sum \Delta n}} \quad (3-58)$$

The *relative surface diameter* D_{21} is the drop diameter of a uniform equivalent set with the same sum of diameters and the same total surface of all drops as in the real set.

$$D_{21} = \frac{\sum D^2 \Delta n}{\sum D \Delta n} \quad (3-59)$$

This diameter characterizes drop disintegration because it can be represented as the ratio of the aerodynamic drag forces to the forces of surface tension.

$$\frac{\sum C_D (\pi D^2 / 4) \cdot (\rho_G V^2 / 2) \Delta n}{\sum \pi D \sigma \Delta n}$$

From this ratio and Eq. (3-59) it follows that

$$D_{21} \sim \frac{\sigma}{\rho_G V^2}$$

which means that diameter D_{21} is the characteristic linear dimension in the Weber number, which is the criterion of secondary drop disintegration.

The *relative volume diameter* D_{31} is the mean drop diameter of a uniform equivalent set with the same sum of drop diameters and the same total volume of all drops as in the real set.

$$D_{31} = \sqrt{\frac{\sum D^3 \Delta n}{\sum D \Delta n}} \quad (3-60)$$

This diameter characterizes the identical evaporation rate or combustion rate per unit volume. The evaporation rate expressing the volume (mass) of evaporated liquid per unit time is proportional to the initial diameter.

The *volume-to-surface-area mean diameter* D_{32} or *Sauter mean diameter* (SMD) is the diameter of a uniform equivalent drop set with the same total volume and the same surface of all drops as in the real set.

$$D_{32} = \text{SMD} = \frac{\sum D^3 \Delta n}{\sum D^2 \Delta n} \quad (3-61)$$

The Sauter mean diameter is used most commonly because it characterizes a number of important processes involving drop penetration or heat and mass transfer.

The penetration of drops is a measure of the ratio of the forces of inertia to the forces of aerodynamic drag.

$$D_{32} \sim \frac{\sum \rho_L (\pi D^3 / 6) a \Delta n}{\sum C_D (\pi D^2 / 4) (\rho_G V^2 / 2) \Delta n}$$

where ρ_L and ρ_G are the density of the liquid and ambient gas respectively, and a is the drop acceleration. The heat exchange between drops and the ambient gas is a measure of the ratio of the heat necessary to increase the temperature of the drop by ΔT to the heat taken up by the drops from the ambient gas with temperature difference ΔT :

$$D_{32} \sim \frac{\sum c_L \rho_L (\pi D^3 / 6) \Delta T \Delta n}{\sum \alpha \pi D^2 \Delta T \Delta n}$$

where c_L = specific heat capacity of the liquid

α = thermal conductivity

The mass exchange between the drops and the environment is a measure of the ratio of the mass of drops to the mass of liquid evaporated per unit time:

$$D_{32} \sim \frac{\sum \rho_L (\pi D^3 / 6) \Delta n}{\sum \pi D^2 \beta (C_0 - C) \Delta n}$$

where β = mass exchange coefficient

C, C_0 = liquid concentration in the ambient gas far away from and close to the drop surface, respectively

The *mean mass diameter* D_{43} follows from the formula

$$D_{43} = \frac{\sum D^4 \Delta n}{\sum D^3 \Delta n} \quad (3-62)$$

D_{43} is used in cases in which the drops are fractionated by the sieve method (substitute liquid method, freeze drop method) or the sedimentation method.

The mean diameters derived from these formulas for the same drop set have different values. This will be shown in Example 3-1. It can be generally stated that the smaller the difference of the drop diameters is (smaller scatter of drop diameters), the smaller is the difference between various mean diameters. It is worth adding that these differences increase as the liquid viscosity increases [7].

Mean diameters are very convenient because they make it possible to carry out various calculations. However, in many cases their use can lead to excessive simplification. An example is the results presented in [7], where for the drop diameter range 10 to 600 μm the Sauter mean diameter $D_{32} = 331 \mu\text{m}$ was obtained. In this spray drops with diameters larger than D_{32} constituted 49.4% of the total surface area and 71.6% of the total volume of drops. Half of the surface and much more than half of the liquid volume was represented by drops larger than the Sauter mean diameter D_{32} .

The calculation of mean diameters from the spectrum of drop sizes in a spray is tedious. It is more convenient to use equations that approximate the drop distribution, e.g., the Rosin-Rammler equation. The general equation (3-55) can be written as follows:

$$D_{pq} = \sqrt[p-q]{\frac{\int_0^\infty D^p (d\bar{n}/dD) dD}{\int_0^\infty D^q (d\bar{n}/dD) dD}} \quad (3-63)$$

and using the volume distribution and Eq. (3-46) we can write

$$D_{pq} = \sqrt[p-q]{\frac{\int_0^\infty D^{p-3} (d\bar{V}/dD) dD}{\int_0^\infty D^{q-3} (d\bar{V}/dD) dD}} \quad (3-64)$$

In both of these equations the integration limits were expanded to the range $\langle 0, \infty \rangle$.

Using the distribution described by the Rosin-Rammler equation and integrating Eq. (3-64), we obtain

$$D_{pq} = X \sqrt[p-q]{\frac{\Gamma[(p-3)/\delta + 1]}{\Gamma[(q-3)/\delta + 1]}} \quad (3-65)$$

Table 3-3 Relations between mean drop diameters, Example 3-1

Diameter symbol	D_{10}	D_{20}	D_{30}	D_{21}	D_{31}	D_{32}
Diameter value (conditional units)	5.50	6.21	6.71	7.00	7.43	7.87

For example, the Sauter mean diameter ($p = 3, q = 2$) is given by

$$D_{32} = \frac{X}{\Gamma(1 - 1/\delta)} \quad (3-66)$$

Example 3-1 Using the drop set shown in Fig. 3-24, determine the mean diameters $D_{10}, D_{20}, D_{30}, D_{21}, D_{31}, D_{32}$.

SOLUTION Since the number of drops in individual ranges is equal to $\Delta n = 1$, the total length, surface, and volume (mass) of drops are equal, respectively, to

$$\sum D \Delta n = 1 \cdot 1 + 2 \cdot 1 + \cdots + 10 \cdot 1 = 55$$

$$\sum D^2 \Delta n = 1^2 \cdot 1 + 2^2 \cdot 1 + \cdots + 10^2 \cdot 1 = 385$$

$$\sum D^3 \Delta n = 1^3 \cdot 1 + 2^3 \cdot 1 + \cdots + 10^3 \cdot 1 = 3025$$

The total number of drops in the set is $N = \sum \Delta n = 10$. Using Eqs. (3-56)–(3-61) yields the values of mean diameters (Table 3-3). It is seen that the values of mean diameters expressed in conditional units are different. They increase according to the sequence shown in Table 3-3.

3-3.4 Various Indicators of Spray Quality

The *maximum drop diameter* is an essential indicator of spray quality. The diameter D_{\max} has been considered by numerous authors, but results obtained have not found practical application. D_{\max} is determined from the spray spectrum (Fig. 3-20), but an adequately large number of drops must be considered. In practice, the diameters $D_{0.9}, D_{0.95}, D_{0.999}$, etc. and the drop volume distribution curve are used (Fig. 3-23).

In [2], the relationship between the diameter $D_{0.999}$ and the median diameter $D_{0.5}$ was considered and the dispersion boundary factor (DBF) was established:

$$\text{DBF} = \frac{D_{0.999} - D_{0.5}}{D_{0.5}} \quad (3-67)$$

This factor is a function of the diameter distribution parameter δ only:

$$\left. \begin{array}{ll} \delta = 2 & D_{0.999} = 3.16D_{0.5} \\ \delta = 3 & D_{0.999} = 2.15D_{0.5} \\ \delta = 4 & D_{0.999} = 1.77D_{0.5} \end{array} \right\} \quad (3-68)$$

From experiments [7] it follows that for the majority of swirl atomizers the following relationship exists:

$$\frac{D_{0.95}}{D_{0.5}} \approx 2 \quad (3-69)$$

The maximum diameter is important. The design of numerous installations should be based not on the mean drop diameters but on the maximum diameter because only then is there a guarantee that the processes will be completed within the given installation. This refers to such processes as evaporation, combustion, and spray drying. In practice, 100% efficiency is not required, which allows a decrease in the dimensions of the installation.

The *specific surface of drops* A_D is the surface corresponding to a unit volume of the atomized liquid. Knowledge of this surface is necessary for all processes occurring on the drop surface. The area A_D can be calculated from the drop size spectrum in a spray, but because this is tedious the Sauter mean diameter D_{32} is used. The diameter D_{32} refers to a set of drops that has the same volume-to-surface ratio for all drops as for one drop with diameter D_{32} . We can then write

$$A_D = \frac{A_1}{V_1} = \frac{\pi D_{32}^2}{\pi D_{32}^3/6} = \frac{6}{D_{32}} \quad (3-70)$$

where A_1 and V_1 denote the surface area and volume of one drop. Expressing D_{32} in centimeters yields A_D in cm^2/cm^3 .

For the determination of the specific area A_D the Rosin-Rammler equation can also be used. In order to do so, one should use the equation

$$A_D = 6 \frac{\int_{\max}^{\min} D^2 (dn/dD) dD}{\int_{\max}^{\min} D^3 (dn/dD) dD} \quad (3-71)$$

and after using the Rosin-Rammler equation one obtains

$$A_D = \frac{6 \times 10^4}{X} \frac{\Gamma(2 - 1/\delta)}{1 - 1/\delta} \left[\frac{\text{cm}^2}{\text{cm}^3} \right] \quad (3-72)$$

The specific surface of uniform drops for the diameter range 50 to 1000 μm is presented in Table 3-4. The presented values have a comparative meaning only, since the specific surfaces in the cases of monodisperse and polydisperse

Table 3-4 Specific surface A_0 of uniform drops

Drop diameter D (cm)	0.005	0.01	0.02	0.03	0.04	0.05	0.06	0.08	0.1
Specific surface A_D (cm^2/cm^3)	1200	600	300	200	150	120	100	75	60

(real) spraying can be significantly different. For swirl atomizers the real specific surface is of the order of $1000 \text{ cm}^2/\text{cm}^3$, i.e., has a value 200 times larger than the surface of a sphere of volume 1 cm^3 .

A *relative diameter span factor*

$$\text{RSF} = \frac{D_{0.9} - D_{0.1}}{D_{0.5}} \quad (3-73)$$

characterizes the drop diameter span with respect to the median diameter. Factor RSF is a function of the diameter distribution parameter δ only [2]. It has been established that this factor correctly characterizes the combustion process in gas turbines.

A method for analyzing drop size distribution data to obtain the “best” fit to standard distributions and distribution parameters is described in Sec. 7-6. It provides the best fit to any postulated standard distribution as expressed by the smallest variance. From the given equations, a very simple computational package can be designed that provides the means and their variances of some standard distributions that are fit to a given input distribution. The choice between them can then be made on strictly statistical grounds.

REFERENCES

1. Abou-Ellail, M. M. M., Elkotb, M. M., Rafat, N. M. Effect of fuel pressure, air pressure and air temperature on droplet size distribution in hollow-cone kerosene sprays. *Proceedings of ICLASS-78*, Tokyo, 1978, 4-2, 85-92.
2. Chin, J. S., Lefebvre, A. H. Some comments on the characterization of drop-size distribution in sprays. *Proceedings of ICLASS-85*, London, 1985, IV A/1/1-12.
3. Hiroyasu, H., Kadota, T., Arai, M. Supplementary comments: Fuel spray characterization in diesel engines. *Proceedings of the Symposium on Combustion Modeling in Reciprocating Engines*. Plenum Publishing, New York, 1980.
4. Lyshevskii, A. S. *Processes of Fuel Atomization in Diesel Nozzles*, Mashgiz, Moscow, 1963 (in Russian).
5. Matsumoto, S., Takashima, Y. Design criteria of hollow cone nozzle and prediction of drop size distribution. *Proceedings of ICLASS-78*, Tokyo, 1978, 4-1, 79-84.
6. Mugele, R. A., Evans, H. D. Droplet size distribution in sprays. *Ind. Eng. Chem.*, June, 1951.
7. Orzechowski, Z. *Liquid Atomization*. WNT, Warsaw, 1976 (in Polish).
8. Pazhi, D. G., Galustov, V. S. *Fundamentals of Liquid Atomization*. Khimiya, Moscow, 1984 (in Russian).
9. Sankaran, Kutty P., Narasimhan, M. V., Narayanaswamy, K. Design and prediction of discharge rate, cone angle and aircore diameter of swirl chamber atomisers. *Proceedings of ICLASS-78*, Tokyo, 1978, 4-3, 93-100.
10. Sato, G. T. Structure of diesel spray. *Proceedings of ICLASS-85*, London, 1985, IP/1/1-10.
11. Sellens, R. W., Brzustowski, T. A. A prediction of the drop size distribution in a spray from first principles. *Atomisation Spray Technol.*, Vol. 1, No. 2, pp. 89-102, 1985.
12. Yule, A. J., Mo, S.-L., Tham, S. Y., Aval, S. M. Diesel spray structure. *Proceedings of ICLASS-85*, London, 1985, II B/2/1-15.

CHAPTER
FOUR

TYPES OF ATOMIZERS

The problem of atomizer design is based on the classification principles presented in Fig. 1-1. Atomizer designs are highly diverse; for example, Spraying Systems Co. produces 16,000 standard atomizers.

The operation of atomizers requires a vast amount of auxiliary instrumentation, including:

Liquid pumps, gas compressors, etc.

Water supply installations

Gas supply installations for pneumatic atomizers

Drive systems for rotary atomizers

Power supply systems for acoustic, ultrasonic, and other atomizers

Flow stabilizers, pressure regulators, valves, etc.

Instrumentation (pressure gauges, flowmeters)

Filters

Auxiliary instrumentation will not be discussed here. In the final part of this chapter the problems of materials, technology, and operation of atomizers will be discussed briefly.

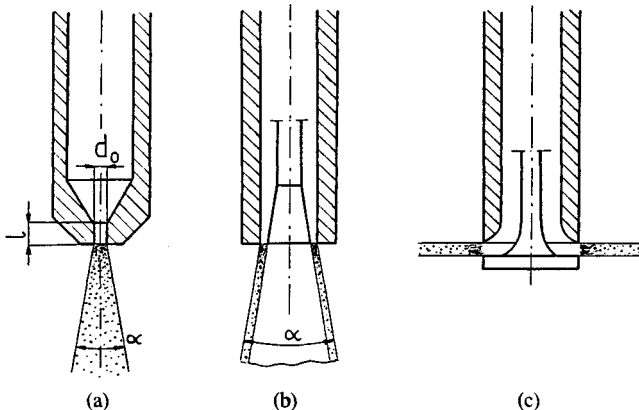


Figure 4-1 Singular jet atomizer: (a) cylindrical jet; (b) annular jet; (c) radial jet.

4-1 JET ATOMIZERS

4-1.1 Jet Atomizers with Continuous Operation

Jet atomizers with continuous operation are the simplest of all atomizers in design. They are divided into simple atomizers, group atomizers, impinging jet atomizers, blast atomizers, and fan atomizers.

Simple atomizers. The simple atomizer is, in the simplest case, a manifold terminated with an orifice (nozzle) through which liquid is discharged in the form of a cylindrical jet (Fig. 4-1a). The main advantage of such an atomizer is its simplicity of design; the main disadvantages are difficult jet disintegration and the small spray angle α .

In the case shown in Figure 4-1b liquid discharges through a coaxial annular slot. The advantages of this atomizer are that liquid discharging from a narrow slot disintegrates more easily than a cylindrical jet and the desired angle α can be achieved by deflecting the jet. The disadvantage is that the slot clogs easily.

Figure 4-1c shows discharge of liquid in a radial direction. Such an atomizer has the characteristics of a jet atomizer only if the whole slot is filled with fluid; otherwise a blast atomizer is created.

Jet disintegration into drops occurs at a certain distance from the atomizer, depending on the type of orifice and the discharge conditions. The discharge conditions follow basically from the pressure drop ΔP . The drop pressure is generally small and falls in the range $\Delta P = 0.3\text{--}1.0 \text{ MPa}$, which corresponds to the water discharge velocity range $V_L = 25\text{--}45 \text{ m/s}$ and drop diameter range $D = 200\text{--}500 \mu\text{m}$. As discussed earlier (Sec. 2-2.1), the velocity has to be high enough, $V_L = 100 \text{ m/s}$, to ensure high quality of atomization, which, however, requires the drop pressure to be of order $\Delta P = 5 \text{ MPa}$.

The spray angle does not exceed $\alpha = 10\text{--}15^\circ$ and in most cases falls in the range $\alpha = 2\text{--}10^\circ$. Such small angles do not allow proper spatial distribution of the atomized liquid. Larger angles α can be achieved by using other types of jet atomizers.

The discharge orifice of an atomizer is most commonly a cylindrical orifice of diameter $d_0 = 0.5\text{--}2.5$ mm. Orifices with diameters smaller than 0.5 mm clog easily, and jets with diameters larger than 2.5 mm disintegrate into drops that are too large. The liquid discharge has a turbulent character, which is why the discharge coefficient μ is more or less constant. The value of the discharge coefficient μ depends on many factors and will be discussed in Chapter 6.

Figure 4-2 shows some shapes of outlet orifices. The inlet edge of the orifice can be beveled or rounded in order to increase the discharge coefficient μ to a value that corresponds to a conical orifice with an almost optimum angle β (optimum angle $\beta = 13\text{--}14^\circ$). An orifice with a very streamlined inlet (Fig. 4-2e) has a smaller value of μ than an orifice with the rounded edge (Fig. 4-2c). The problem of the ratio l/d_0 will be discussed in Chapter 6.

Simple atomizers are used mostly because of the compact and strong liquid jet they produce. Such jets are applied in cleaning and washing of tanks; in black and slag removal from boiler furnaces; in ice, frost, and snow removal from airplanes and so forth. For this purpose, high-pressure guns with pressures of several or tens of MPa are used.

Group atomizers. The jet group atomizers have not one but many outlet orifices. They are used for large flow rates; by using a large number of small orifices one can achieve satisfactory spray quality. Examples of their application are in steam attemperators and small and medium rocket engines. Higher liquid pressures are used to obtain strong compact liquid jets that are suitable for washing the inner surfaces of barrels, cylinders, and other closed vessels. A group atomizer in the form of a spherical head is shown in Fig. 4-3.

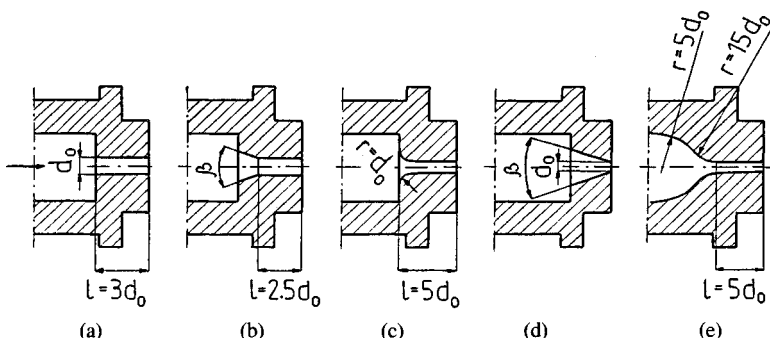


Figure 4-2 Various shapes of discharge orifices and corresponding values of the discharge coefficient μ . (a) $\mu = 0.625$; (b) $\mu = 0.87$ for $\beta = 20^\circ$, $\mu = 0.775$ for $\beta = 60^\circ$; (c) $\mu = 0.85$; (d) $\mu = 0.865$ for $\beta = 11^\circ 40'$; (e) $\mu = 0.79$.

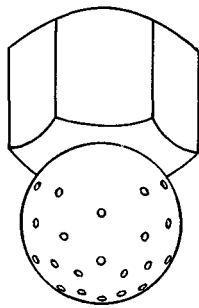


Figure 4-3 Head of a multiple-orifice jet atomizer (Lechler) [24].

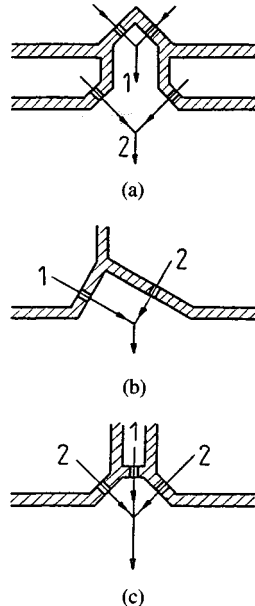


Figure 4-4 Various setups for atomizers with colliding jets. 1, Fuel; 2, oxidizer.

Atomizers with impinging jets. Jet atomizers with the impinging jets are used to accelerate the disintegration of the jet. The collision of opposite jets produces atomization as shown in Fig. 2-11—completely different from that in the case of simple atomizers. A similar situation occurs when two jets directed at an arbitrary angle collide. Jet collision causes very intensive mixing of liquid, which is very important in the case of rocket engines using liquid propellants.

Atomizers in rocket engines are regular orifices drilled in the injection head. There are many ways in which the jets can collide (Fig. 4-4); among them are two basic ways:

Collision of fuel jets 1 and collision of oxidizer jets 2 (Fig. 4-4a)

Collision of fuel jet 1 with oxidizer jet 2 (Fig. 4-4b, c)

The flow rate of the fuel is two to four times smaller than the oxidizer flow rate. Hence the system shown in Fig. 4-4c is advantageous compared to the system shown in Fig. 4-4b, since the diameters of the jets are more alike. The injection heads have various shapes and dimensions depending on the size of the engine, and the number of the nozzles varies from several to several thousand.

Jets with the shapes other than cylindrical can also collide. Figure 4-5 shows the collision of two flat jets, which results in the generation of a flat jet with a rectangular cross section.

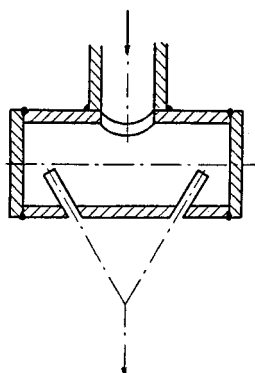


Figure 4-5 Collision of two liquid sheets.

Blast atomizers. In blast atomizers the liquid jets collide with a solid object. Blast atomizers can be divided into two groups: deflection atomizers and cascade atomizers.

Deflection atomizers are characterized by the fact that the liquid jet impinges on the deflector, which can be of arbitrary shape and orientation (Fig. 4-6). These atomizers operate with low pressures, so even for low flow rates they do

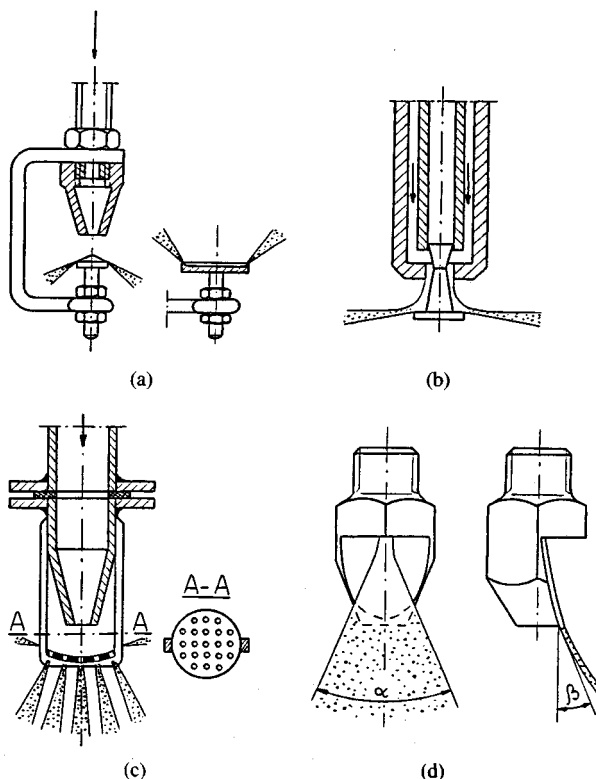


Figure 4-6 Schematic diagram of collision atomizers with various deflectors: (a) conical deflector or flat deflector with a bent-out edge; (b) conical disk-like deflector; (c) perforated deflector; (d) blade deflector.

not achieve proper atomization. The atomizers shown in Fig. 4-6a and b generate a hollow liquid jet. The atomizer with the perforated deflector (Fig. 4-6c) produces a different liquid distribution because approximately 70% of the liquid passes through the orifices. The atomizer with a blade deflector (Fig. 4-6d) generates a flat jet, for which the angle α varies in a very large range depending on the liquid pressure; the deflection angle β depends on the shape of the blade.

Cascade atomizers have complicated designs. Figure 4-7 shows one example of such an atomizer. The liquid passes into the deflectors through annular slots. This occurs due to the shearing off of the outermost layers of the liquid jet. The deflectors are connected by bolts. The spray quality can be improved by reducing the size of the slots (i.e., minimizing the thickness of the liquid layers), but this can cause the gaps to clog. For large flow rates the number and diameters of the deflectors increase. The distribution of atomized liquid can be controlled by selection of the shape angle of the deflectors.

Fan atomizers. Fan atomizers are based on the same principle as atomizers with impinging jets. The difference is that the jets impinge inside rather than outside the atomizer. This is shown in Fig. 4-8. As a result of the collision of liquid flowing from two opposite directions, the transverse components of velocity annihilate and the liquid discharges through the outlet as a flat jet in the shape of a fan. The thickness and angle of the fan jet depend on the internal dimensions of the atomizer.

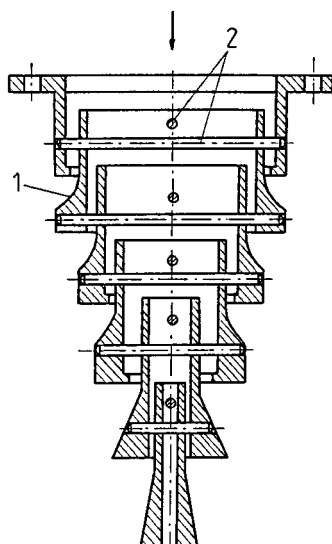


Figure 4-7 Cascade atomizer. 1, Coaxial deflector; 2, bolts.

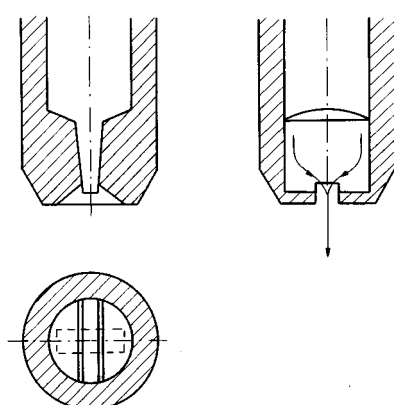


Figure 4-8 Schematic of diagram fan atomizer.

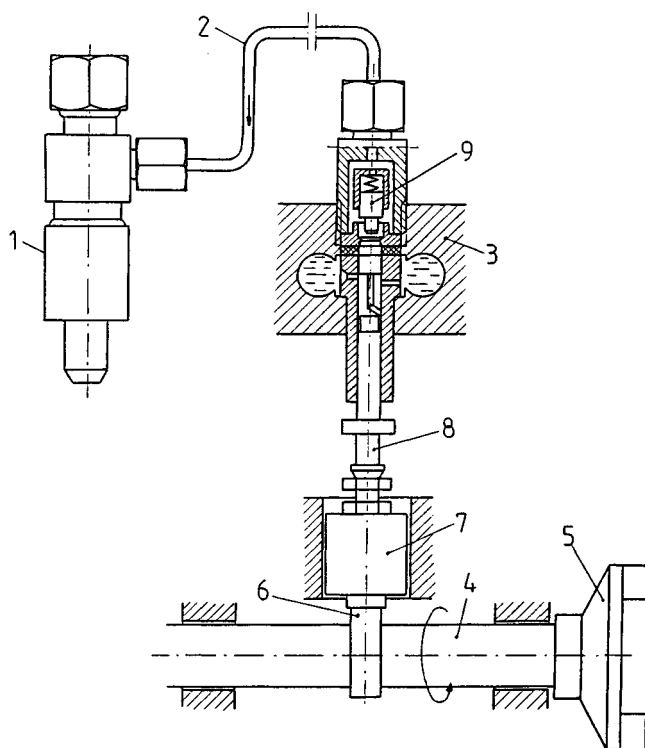


Figure 4-9 Injection system of a piston engine.

Fan atomizers find vast application in agriculture treatment, fire protection, in cooling of machine elements, washing and cleaning, drying, and so forth.

4-1.2 Jet Atomizers with Intermittent Operation

Jet atomizers with intermittent operation are used in piston engines with self-ignition [15]. The discontinuous atomizers constitute a whole unit with the injection system (Fig. 4-9). The injection system comprises an injector (1), manifold (2), and injection pump (3). The camshaft of injection pump 4 is driven using the clutch (5), and in a four-stroke engine two rotations of the crankshaft correspond to one rotation of the camshaft.

The operation of the injection system is as follows. Cam 6 acts through the follower (7) on the pump piston (8), which causes the compression of fluid. After a pressure of several tenths to several MPa is reached, the bucket valve (9) opens and the fuel flows to the injector. The pressure wave arrives at the injector and raises the needle of the nozzle. The opening pressure of the nozzle is in the range 12 to 22 MPa. During the injection a pressure increase occurs and, in the case of combustion chambers with direct injection, reaches values of

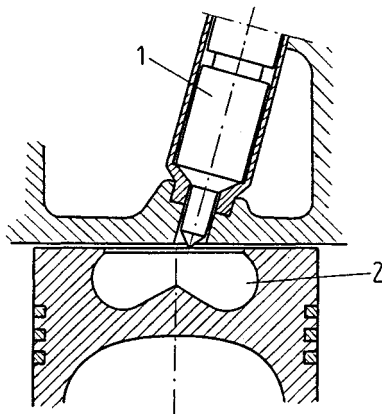


Figure 4-10 Combustion chamber with direct injection.
1, Injector; 2, chamber in a piston.

60 MPa or more. The fuel pumping lasts until the edge of the pump piston reaches the overflow orifice. The pressure then drops and the bucket valve closes, and as a consequence the nozzle closes abruptly.

The atomizer is placed in the engine head, and its operation depends on the type of combustion chamber. Two types of combustion chambers are distinguished: chambers with direct injection (i.e., nondivided chambers), and chambers with indirect injection (i.e., chambers divided into two or more parts).

Chambers with direct injection (Fig. 4-10) are characterized by the fact that the fuel is injected into a chamber in the piston. During the direct injection, very good atomization and fuel distribution in the chamber are required. The advantages of engines with direct injection are:

Low fuel consumption

Easy start

Adaptation to supercharging is possible

The disadvantages of engines with direct injection are:

High toxicity and smokiness of the fumes

High noise level due to high rates of pressure built up above the piston

Limitation on the engine rotational speed (to about 3000 rpm) due to the relatively high ignition lag

Limitation on medium and high power, where fuel economy plays an important part

Chambers with indirect injection are characterized by the fact that fuel is injected into an auxiliary chamber, in most cases the initial chamber or a swirl chamber, as shown in Figure 1-11. Gas exchange takes place between the auxiliary chamber and the main chamber, which is located in the cylinder above the piston. The atomizer plays a less important role in this case, because there is

intensive swirling in the auxiliary chamber that accelerates the generation of the mixture and its ignition. The advantages of the engines with indirect injection over direct injection engines are:

Lower toxicity of fumes due to division of the combustion process into two phases; in the auxiliary chamber the combustion proceeds with insufficient air, in the main with excess air

Lower noise level

High rotational speed (up to 5000 rpm)

The disadvantage of indirect injection is higher fuel consumption, which is why this type of injection is applied mainly in car engines. The requirements for the injection nozzles are tough:

Fuel charge adjusted to the instantaneous engine load

Moderate rates of fuel feed in the first phase of injection and high rates in the second phase, i.e., controlled injection

Proper macrostructure of the atomized fluid (spray angle, spray penetration, jet angle with respect to the chamber)

Proper microstructure of the atomized fuel limiting the combustion time; for mean drop diameters in the range 5–20 μm the combustion time is 0.5–2 ms

Short injection time; for example, for an engine with a rotational speed of 1500 rpm it is about 3 ms, 25–35° of the revolution of the crankshaft

Resistance to cyclic changing of the conditions in the combustion chamber, where the injection itself occurs in air compressed to 2.8–6.0 MPa at 520–700°C.

Precise shutoff of the fuel feed

A typical *injector* is shown in Fig. 4-11. The most important part of the injector is the *nozzle*, which influences the shape of the spray and the spray quality. The fuel flows to the injector chamber through a channel in the housing of the injector and then through two or three channels in the body of the nozzle. The latter channels are located symmetrically on the perimeter in order to improve the cooling conditions of the nozzle. The pressure acting on the needle overcomes the resistance of the spring and friction resistance of the needle and, as a result, the needle rises up. The force of the spring is controlled by the replacement of the washers under the adjusting screw. The stroke of the needle is very small, usually several tenths of a millimeter. The stroke should be limited to prevent excessive decompression of the fuel in the nozzle chamber. This limitation is realized in most cases by means of a special bumper. The limitation of the needle lift and subsequent limitation of the cross section of the flow cause a significant increase of the fuel pressure, and as a result the mean injection pressure is 2 to 2.5 times higher than the pressure at which the needle separates from the seat.

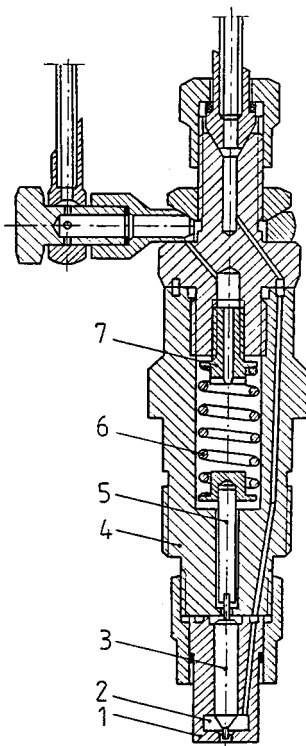


Figure 4-11 Injector. 1, Atomizer; 2, atomizer chamber; 3, needle; 4, body; 5, follower; 6, spring; 7, adjusting screw.

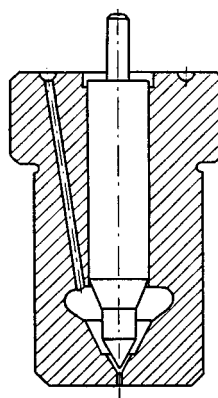


Figure 4-12 Single-orifice atomizer.

The nozzle is a replaceable element because of the unification of injectors. In general, nozzles can be divided into orifice nozzles and pindle nozzles. The former are used for direct injection, the latter for indirect injection. The particular classification of nozzles is as follows: single-orifice nozzles, multiorifice nozzles, cylindrical pindle nozzles, conical pindle nozzles, and flat seat nozzles.

Single-orifice nozzles. Single orifice atomizers have a needle with a conical ending and a conical seat face (Fig. 4-12). As a result of the atomization, a spray is generated with small spray angle $\alpha = 4-15^\circ$ and large spray penetration. The flow section in the initial phase depends on the needle lift. However, in the following phases it is constant. Single-orifice nozzles are cheaper than other types of nozzles and are more reliable because of the relatively large diameter of the outlet orifice, which reduces the probability of clogging.

Multiorifice nozzles. In multiorifice nozzles the needle closes the nozzle well in which the injection orifices are located (Fig. 4-13). The cross section of the well

should be at least twice as large as the cross section of the orifices; however, correct injection for low load or high rotational speed of the engine requires that the volume of the well be small. The diameters of the orifices are very small, commonly 0.2–0.6 mm; however, there are orifices with diameters as small as 0.05 mm, which ensures good atomization. Such small orifices are sensitive to clogging, which is a disadvantage of multiorifice nozzles. The number of orifices varies from 2 to 12. If the injector is located vertically in the central position in the combustion chamber, the orifices are drilled symmetrically with respect to the injector axis; for oblique placement of the injector they are symmetrical with respect to the axis of the chamber. In the latter case the unique positioning of the nozzle with respect to the injector housing is achieved with a dowel pin.

Cylindrical pintle nozzles. These nozzles produce a compact spray with large penetration and small spray angle. The needle is terminated by a cylindrical pintle with a conical seat face (Fig. 4-14a). The pintle passes loosely through the outlet orifice, and coaxiality of the pintle and the orifice is required with a radial clearance of 10–20 μm . The fuel discharges through a narrow annular slot if the pintle does not stick out of the orifice. Because of this, in the initial phase a small amount of well-atomized liquid is injected. The outlet orifice diameter is large and varies from 1 to 3 mm, depending on the dimensions of the nozzle. The motion of the pintle results in self-cleaning of any carbon deposition, which is an important advantage of these nozzles.

Conical pintle nozzles. These nozzles generate spray with an increased spray angle and lower penetration than that generated by nozzles with a cylindrical pintle. This stems from the characteristic shape of the pintle, which comprises a cylindrical gland and a conical sprinkler (Fig. 4-14b). Adjusting the length of the pintle to its stroke results in flow cross sections that ensure the most convenient division of the fuel charge between the individual phases of injection.

A variation of the conical pintle nozzle is the Ricardo-Pintaux nozzle (Fig. 4-15a) which has an auxiliary orifice. In the first phase of injection to the swirl

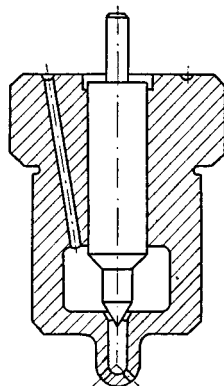


Figure 4-13 Multiorifice atomizer.

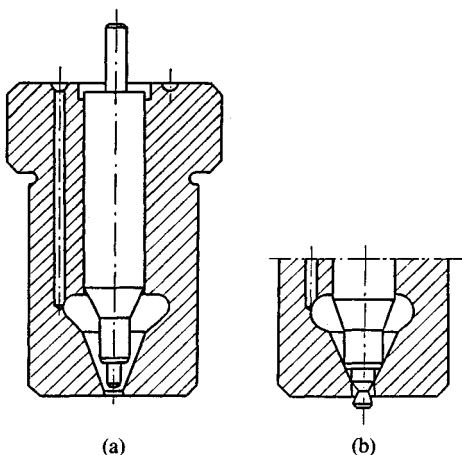


Figure 4-14 Pintle nozzles: (a) with a cylindrical pintle; (b) with a conical pintle.

chamber of an engine, throttling of the fuel occurs in the main orifice and the fuel is injected through the auxiliary orifice (Fig. 4-15b). Later, the opposite occurs; the main injection proceeds through the main orifice (Fig. 4-15c). This makes the ignition of the first fuel charge easier; the fuel charge moves countercurrently with respect to the swirl and has good conditions for evaporation and ignition in the central, hottest part of the swirl chamber. Most of the fuel charge is injected cocurrently, since this direction of injection is most advantageous. A state similar to the injection phase exists for small loading and for idle running.

Flat seat nozzles. In certain applications better results are obtained when, instead of an annular spray, one uses a jet discharging in the form of a cloud of

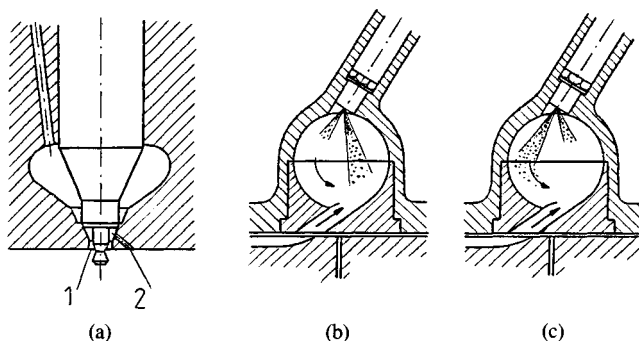


Figure 4-15 Ricardo-Pintaux atomizer. 1, Main orifice; 2, additional orifice.

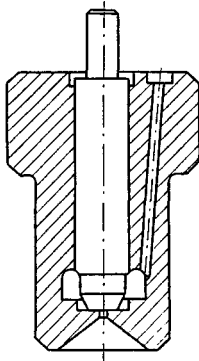


Figure 4-16 Atomizer with a flat seat.

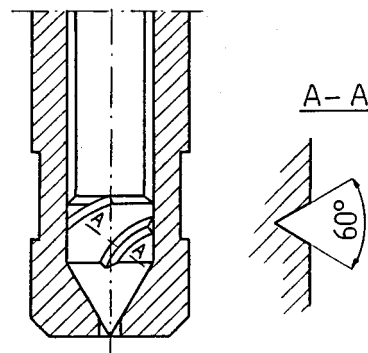


Figure 4-17 Pulsed swirl atomizer.

drops from a flat seat nozzle. In these nozzles the pintle closes the flow with a flat surface (Fig. 4-16). The flow cross section is not dependent on the pintle lift to the degree that it is in a single-orifice atomizer. The leaktightness worsens faster than for other atomizers.

Stricter requirements for nozzles with intermittent operation concern first of all reduction of toxicity and smokiness of fumes and noisiness of the engine. Research on improvement of nozzles has focused on this problem for a long time. The research directions include: ensuring controllable injection, reducing the temperature of the nozzle, decreasing the mass of the moving elements, decreasing the pintle lift and decreasing the nozzle diameter.

Other attempts at improving atomization have also been undertaken. One is based on the application of *liquid swirling* [31]. Swirling results in significantly smaller drop diameters. Figure 4-17 shows a single-orifice swirl atomizer, which has two screw grooves on the conical terminal.

Attempts to apply continuous nozzles in piston engines have encountered difficulties. The intermittent injection in these atomizers is realized in such a way that the fuel flows only during the delivery stroke of the pump; in the remaining time the fuel pressure is too low to overcome the resistance to flow. However, there is no definite cutoff of the fuel after the injection is completed, since the compressed fuel decompresses and causes "afterinjections" and dribbles of individual drops. This leads to carbon deposition and clogging of the nozzle which forces to connect directly a continuous nozzle with a piston injection pump into one assembly called *injection unit* (e.g., General Motors Corp., Cummins Engine Co.).

It should be added that intermittent atomizers are not only used in piston engines. An example would be the simple jet atomizers used for manual plant spraying. The fluid injection is self-controlled by means of valves that open or close according to the motion of the piston. The injection occurs once per two strokes of the manual driving lever and per two lifts of the pump piston.

4-2 SWIRL ATOMIZERS

Swirl atomizers are most commonly used because they have essential advantages compared to other nozzles. The advantages of swirl atomizers are as follows:

- Relatively simple design
- High reliability
- Good spraying quality
- Small power required

This last advantage follows from the property of a free vortex that the circumferential velocity is relatively small on the chamber perimeter, which ensures small friction loss. The circumferential velocity increases toward the chamber axis, which causes the liquid to discharge with a high velocity, ensuring good atomization quality.

A schematic diagram of the simplest swirl atomizer is shown in Fig. 4-18. The characteristic parameters of swirl atomizers are represented by the *geometric constant K*:

$$K = \frac{Rr_0}{ir_p^2} = \frac{2Rd_0}{id_p^2} = \frac{\pi Rr_0}{iA_p} = \frac{2\pi Rd_0}{4iA_p} \quad (4-1)$$

where R is the swirl radius, r_p and d_p are the radius and diameter of the tangential orifice, respectively, r_0 and d_0 are the radius and diameter of the discharge orifice, respectively, i is the number of tangential inlet orifices, and A_p is the cross section of the tangential inlet orifice with an arbitrary transverse shape.

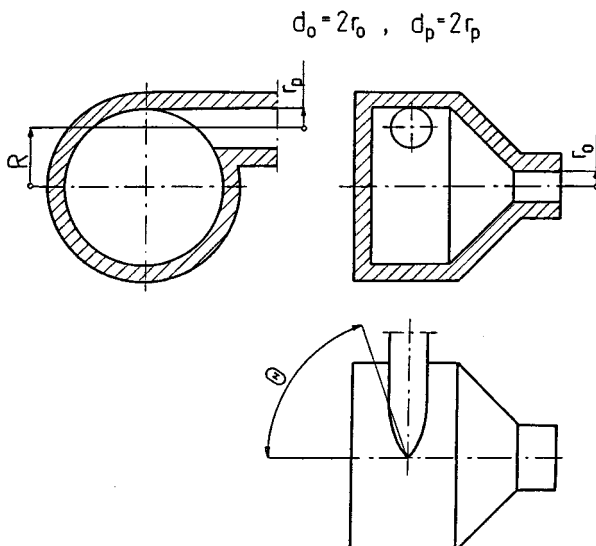


Figure 4-18 Characteristic geometric parameters of a swirl atomizer.

If tangential inlet orifices are inclined to the swirl chamber axis at angle Θ , then Eq. (4-1) assumes the form

$$K = \frac{Rr_0}{ir_p^2} \sin \Theta = \dots \quad (4-2)$$

Swirl atomizers have the two following disadvantages:

Limited use for atomization of very viscous fuels

Small range of regulation, where the range of regulation is understood as the ratio of the maximum and minimum flow rates

The second disadvantage, which applies to all pressure atomizers, stems from the fact that for large changes of flow rate the spray quality deteriorates. The large range of flow rates is necessary in many cases, especially in aircraft gas turbines. In these turbines the fuel consumption varies 20 to 30 times, but the requirements are twice this much; according to Eqs. (3-3) and (3-4) the pressure drop should change 400 to 900 times.

Under real conditions satisfactory atomization of aircraft fuels can be achieved for a minimum pressure drop of $\Delta P = 0.3\text{--}0.4$ MPa. The maximum pressures of the pumps used are 7.5–8 MPa. So the pressure drop changes approximately 25 times and the flow rate approximately 5 times. In most cases, however, the range of the flow rate changes does not exceed 2–2.5. Hence, it is necessary to use controllable swirl atomizers, whose flow rate changes more than with the square root of the pressure drop.

As follows from Eqs. (3-3) and (3-4), the flow rate Q or G also depends on the area of the inlet orifice A_0 and on the discharge coefficient μ . The design of controllable atomizers is then based on the changes in A_0 and μ . The area A_0 can be adjusted by means of a movable needle, but such solutions have not been applied in practice because of design, technologic, and exploitational difficulties. Another solution in the form of a dual nozzle has found application. The discharge coefficient μ is a function of the geometric constant K [see Eq. (4-1)] and therefore the change of μ is related to changes of the quantities incorporated in K .

Swirl atomizers are classified as simplex atomizers, duplex atomizers, spill-return atomizers, variable-geometry atomizers (atomizers with controllable inlet orifice area). Of these, only simplex atomizers belong to the group of noncontrollable atomizers. Among the remaining atomizers combined solutions are also possible, for example, a two-stage atomizer with bleeding control.

4-2.1 Simplex Atomizers

Simplex atomizers are the most common swirl atomizers. These atomizers can be divided into two groups: angular atomizers and axial atomizers. This division stems from the fact that in the first case there is a right angle between the

direction of the liquid supply and liquid discharge, and in the second case the inlet and outlet directions coincide with the axis of the atomizer.

Simplex atomizers can also be divided into atomizers with tangential inlet orifices and atomizers with a swirling insert. In atomizers with tangential inlet orifices the fluid enters the swirl chamber with only one velocity component, i.e., with circumferential velocity, and in atomizers with a swirling insert the fluid enters the chamber with two or three velocity components. Two velocity components, i.e., circumferential and axial, apply to a cylindrical insert, and three velocity components, i.e., circumferential, axial, and radial, apply to a conical insert.

The kinematics of the liquid at the inlet to the swirl chamber does not have a decisive influence on the shape of spray, especially on the spray angle. This is because the swirl chamber itself can have a cylindrical or conical shape, and in the case of the cylindrical chamber a conical interface exists between the chamber and the outlet orifice. The angle of opening of this conical interface also influences the shape of the spray.

Angular atomizers. Figure 4-19 shows a very simple design of a swirl angular atomizer with a tangential inlet orifice [24]. This atomizer has only two parts: body and nozzle. A single tangential inlet orifice has a relatively large diameter, which prevents deposition of contaminants. Because of their simplicity, such atomizers are applied in cases in which a large number of atomizers are needed, for example, in air conditioning. In most cases the following data are valid: inlet orifice diameter $d_0 = 2\text{--}6 \text{ mm}$, discharge coefficient $\mu = 0.35\text{--}0.45$, pressure drop $\Delta P = 0.12\text{--}0.25 \text{ MPa}$, spray angle $\alpha = 45\text{--}90^\circ$, water flow rate $Q = (0.05\text{--}0.1) \times 10^{-3} \text{ m}^3/\text{s}$. This atomizer can be easily adapted for various air-conditioning tasks (humidification, cleaning, heating, or cooling) by replacing the nozzle.

In spray chambers, direct contact between the atomized water and air occurs at an air velocity of 2–3.5 m/s. The spray chamber is characterized by

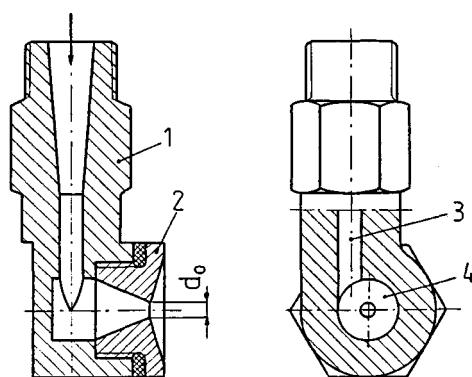


Figure 4-19 Swirl atomizer (angular) with a tangential inlet orifice. 1, Body; 2, nozzle; 3, tangential inlet orifice; 4, swirl chamber.

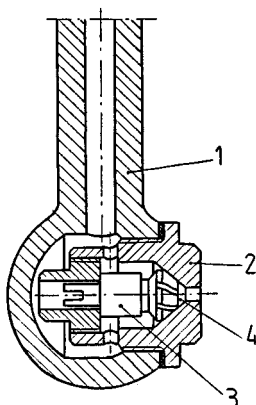


Figure 4-20 Swirl atomizer with a conical swirler. 1, Body; 2, sprayer; 3, conical swirler; 4, swirl chamber.

the *spray ratio*

$$B = \frac{G_L}{G_G} \quad (4-3)$$

which represents the ratio of the water mass flow rate G_L to the mass flow rate G_G of the air through the chamber. The spray ratio falls in the range $B = 0.2\text{--}1.0 \text{ kg/kg}$, which is the starting point for determining the flow rate and number and localization of the nozzles. One uses 10 to 30 atomizers per 1 m^2 of the chamber transverse cross section; altogether, the atomizers generate water at $1.1\text{--}1.4 \text{ kg/s}$.

Figure 4-20 shows another angular atomizer that has a conical swirling insert [24]. The liquid is swirled in grooves machined on the conical surface of the insert. Insert 3 is fitted on the conical surface to the sprayer (2) by means of lapping and therefore it constitutes an integrated assembly; the lapping is facilitated by the incision at the end of the insert. The nozzle can easily be dismounted, which is an advantage of angular atomizers. The main disadvantage is nonuniform atomization, which stems from errors in machining small grooves and the fact that they clog easily.

Axial atomizers. Figure 4-21 shows an atomizer with tangential inlet orifices [24]. The three tangential orifices of circular cross section are located in insert 2, which also includes the swirl chamber (4) and discharge orifice (3). The liquid flows to the tangential orifices through longitudinal grooves on the surface of the screw plug (6). This atomizer was used in small burners with a diesel oil flow rate $Q = (0.55\text{--}25) \times 10^{-6} \text{ m}^3/\text{s}$ and pressure drop $\Delta P = 0.7 \text{ MPa}$, and it ensured satisfactory atomization for the nominal pressure drop $\Delta P = 0.21 \text{ MPa}$. By changing the dimensions included in the geometrical constant K , spray angles in the range $\alpha = 45\text{--}80^\circ$ were obtained.

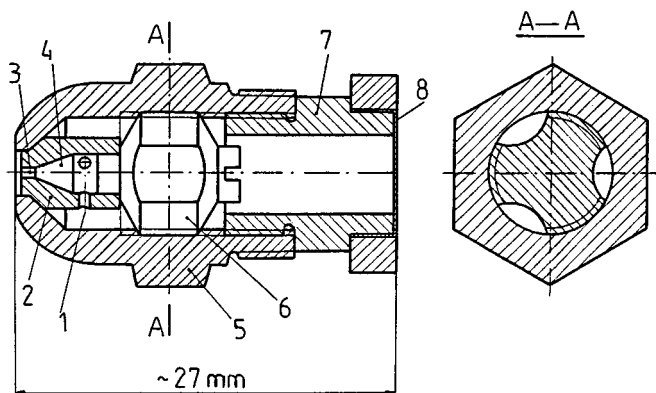


Figure 4-21 Swirl atomizer (axial) with tangential inlet orifices (Lucas). 1, Tangential inlet orifice; 2, insert; 3, discharge orifice; 4, swirl chamber; 5, body; 6, screw plug; 7, threaded fastener; 8, filter gauze [24].

Another example of an axial atomizer is shown in Fig. 4-22. This atomizer consists of only two parts, i.e., the body and the nozzle. The front part of the body has three tangential incisions of rectangular cross section, through which the liquid flows to the swirl chamber. This atomizer has found vast application in air conditioning because of its simple design. The discharge coefficient of this atomizer falls into the broad range $\mu = 0.3\text{--}0.45$, depending on the geometric constant K . The spray angle $\alpha = 45\text{--}80^\circ$.

One more example of an axial atomizer is shown in Fig. 4-23. The injection assembly consists of three adjacent circular plates. The middle one contains orifices tangential to the swirl chamber, which is located in the axis of the plate. The tangential orifices have a rectangular or square cross section. The front plate has an outlet orifice and the rear plate has axial orifices through which the liquid flows to the tangential orifices. The surfaces of the plates must be parallel

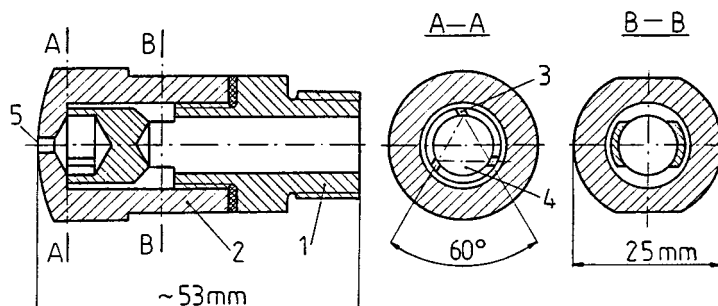


Figure 4-22 Axial atomizer with tangential cutouts. 1, Body; 2, sprayer; 3, tangential cutout; 4, swirl chamber; 5, discharge orifice.

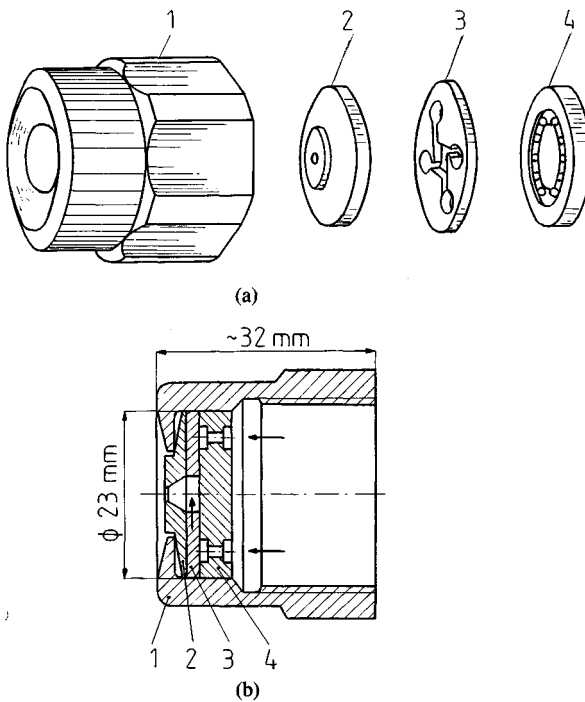


Figure 4-23 Swirl atomizer (axial) with a plate with tangential inlet orifices (Lucas): (a) before assembly, (b) assembled. 1, Body; 2, front plate; 3, plate with tangential orifices; 4, rear plate [24].

and smooth, but the assembly is simple because the plates can be rotated with respect to each other arbitrarily. The plates can be replaced and adjusted to particular needs.

This atomizer has found implementation in boiler burners using heating oil of viscosity less than $\nu = 15 \times 10^{-6} \text{ m}^2/\text{s}$ [24]. It creates a series of types in the range $G \approx 0.02\text{--}0.5 \text{ kg/s}$ and spray angles $\alpha = 60^\circ, 70^\circ, \text{ and } 80^\circ$. The pressure drop for small flow rates should be $\Delta P = 0.7 \text{ MPa}$ and for large flow rates $\Delta P = 2.8 \text{ MPa}$.

It should be added that the shape of the cross section of the tangential inlet orifice affects the friction losses [24], which is important during spraying of heavy fuels in boilers. The losses in rectangular orifices are larger than in circular ones and are equal to 25–30% of the total pressure drop in the atomizer.

In addition to atomizers with a conical swirl insert (Fig. 4-20), there are others with cylindrical inserts. One of the oldest atomizers of this type, the Körting atomizer (1902) had a long multturn screw insert. Contemporary inserts have threaded grooves with trapezoidal or rectangular cross sections. The grooves are short—one fourth to one third of the insert perimeter—which suffices to swirl the liquid without an unnecessary increase in flow resistance. The scheme of an atomizer with such an insert is shown in Fig. 4-24.

Figure 4-25 shows an axial atomizer with a spiral insert, which is located

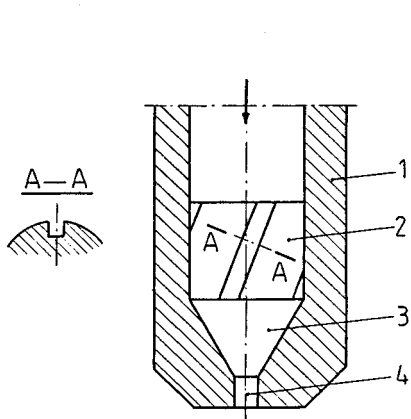


Figure 4-24 Swirl atomizer with a cylindrical swirl. 1, Body; 2, cylindrical insert; 3, swirl chamber; 4, discharge orifice.

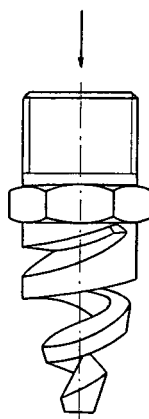


Figure 4-25 Spiral atomizer (Lechler) [24].

outside and not inside the atomizer. Such an atomizer does not have any internal parts and has high flow capacity. This atomizer sprays (splashes) the liquid in the form of a hollow conical jet, which is why it is used in scrubbers, splashing columns, cooling towers, etc.

Simplex swirl atomizers, like single-jet atomizers, can be used as *multiple spray nozzles*. The division of the total flow rate between several atomizers ensures better spray quality, and the proper location of nozzles makes it possible to achieve a desired spray angle of the whole jet. Multiple spray nozzles find various applications, e.g., in humidification, cooling, and scrubbing. Figure 4-26 shows a group atomizer whose head consists of seven swirl nozzles.

4-2.2 Duplex Atomizers

Duplex atomizers are controllable atomizers with two stages of feeding. These atomizers enlarge the range of flow changes by 5 to 10 times and in some cases

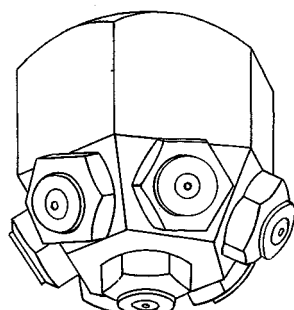


Figure 4-26 Compound atomizer (Spraying Systems Co.) [24].

by 25 times, which is why they are applied primarily in aircraft gas turbines. The design, technology, and exploitation of duplex atomizers are, however, more complex than in the case of simplex atomizers. Duplex atomizers have been developed by Joseph Lucas Ltd., Birmingham. These atomizers come in two main design types: two-manifold duplex atomizers and dual-orifice atomizers.

Two-manifold duplex atomizers [24]. A schematic of a dual-range atomizer is shown in Fig. 4-27. Self-closing control valve 1 is placed between the main control valve and collectors, which are used to feed the group of atomizers. The control valve is composed of a seat and a needle, which is spring loaded. When the fuel pressure is low the needle closes the valve and the fuel flows through the collector (2) and the manifold (4). This is the first stage (range) of feeding (I) through an inlet orifice with a small cross section.

When fuel pressure increases, the needle lifts and the fuel also starts to flow through the collector (3) and manifold (5). The second stage (range) of feeding through the inlet orifice with a large cross section is activated. The fuel from two stages of feeding mixes in the common swirl chamber and discharges through the outlet orifice.

In the range of small flow rates the fuel is fed through the orifices with the small radius r_{p1} , and according to Eq. (4-1) the geometric constant K_1 assumes the high value

$$K_1 = \frac{Rr_0}{i_1 r_{p1}^2} \quad (4-4)$$

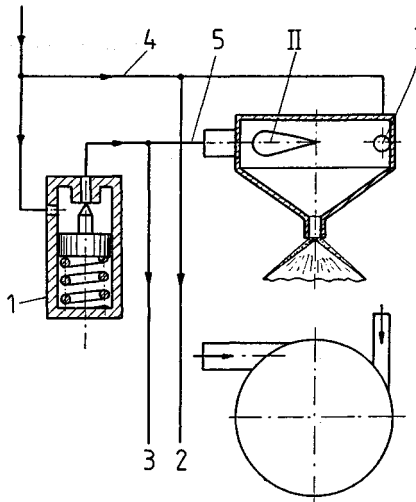


Figure 4-27 Schematic diagram of duplex atomizer. 1, Control valve; 2, 3, liquid collectors; 4, 5, manifolds of primary and secondary range of supply.

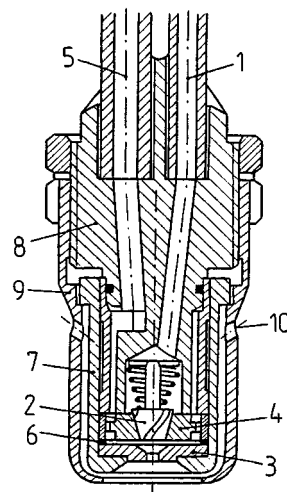


Figure 4-28 Duplex atomizer.

The high value of K_1 denotes a small value of the discharge coefficient μ_1 (see Fig. 5-11). The pressure drop is sufficient to ensure good atomization.

In the range of high flow rates the fuel is fed through the orifice with small radius r_{p1} and large radius r_{p2} , and therefore the constant K_2 is smaller and is given by

$$K_2 = \frac{Rr_0}{i_1 r_{p1}^2 + i_2 r_{p2}^2} \quad (4-5)$$

The smaller value of K_2 corresponds to the higher flow ratio μ_2 and higher spray angle α .

Figure 4-28 shows the design of a duplex atomizer (Duplex 1). The first stage of feeding consists of manifold 1, conical swirling insert 2, a plate 3 with a swirl chamber and outlet orifice. Insert 2 is pressed with a conical spring against the seat in plate 4. The second stage of feeding consists of manifold 5, plate 4 with axial orifices, a plate with tangential orifices (6), and the same swirl chamber with the discharge orifice. Plates 4 and 6 are similar to plates 4 and 3 in Fig. 4-23. The body (9) has 8 to 12 orifices (10) through which air flows into the annular space between the sleeve (7) and body (9). This air insulates the atomizer thermally and removes soot from the atomizer end.

An example of the characteristics of a duplex atomizer is shown in Fig. 4-29. Curve 1 refers to the primary fuel supply. Point B marks the moment when the control valve starts to open; in this particular example it occurs at $P_1 = 1$ MPa.

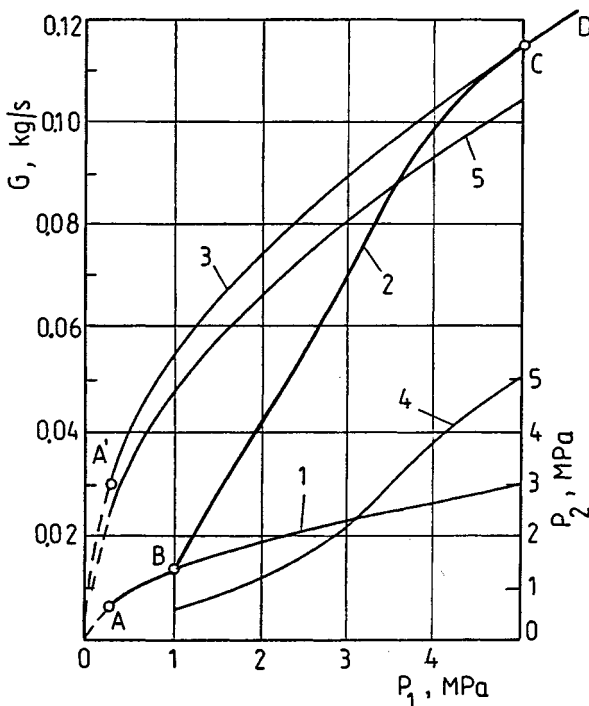


Figure 4-29 Characteristics of a duplex atomizer.

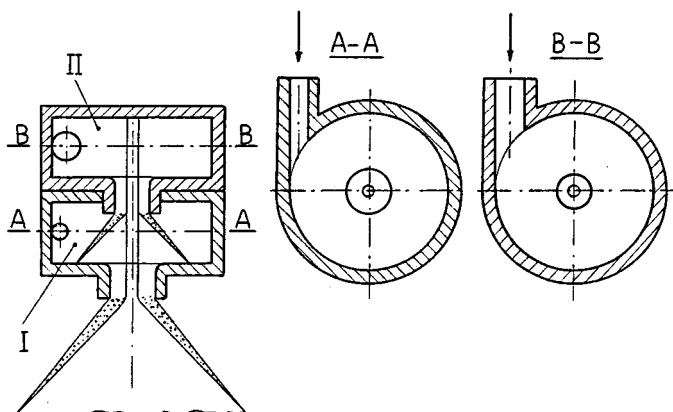


Figure 4-30 Schematic diagram of a two-chamber atomizer. I, Primary range; II, secondary range.

Curve 2 characterizes the operation of the atomizer in the transient region that corresponds to partial opening of the valve. The character of curve 2 depends on the pressure change P_2 behind the control valve. The pressure change follows from the characteristics of the control valve (curve 4). At point C, in this example for $P_1 = 5$ MPa, the control valve is completely open. Curve 3 is characteristic of the atomizer during the joint operation of both fuel supply systems for the same pressure. The working characteristic of a duplex atomizer has the shape of the curve ABCD. In the range of pressures from 0.3 to 5.0 MPa the flow rate G changes approximately 15 times. Had the atomization followed curve 3 from the beginning, one would obtain point A' instead of A , and the flow rate would change less than four times.

Curve 5 is characteristic of the secondary fuel supply. It is easy to see that the total flow (curve 3) is smaller than the sum of the primary (curve 1) and secondary (curve 5) fuel supplies. This follows from the interaction of both flows. The total flow rate is almost equal to the flow rate of the secondary supply system, since the geometric constants of the atomizer in these instances differ only slightly.

The disadvantage of a duplex atomizer is, as mentioned, the change of the spray angle α . This angle decreases significantly at the moment when the secondary supply system is activated. Another disadvantage, which occurs in the case of a group of atomizers connected parallel to the collector, is that the flow rates of these atomizers are not uniform. Because of certain differences of the flow resistance that can occur in the orifices of the primary supply systems of individual atomizers, the pressures in the swirl chambers can also be different. When the pressure in a certain chamber is lower, the flow rate increases after the control valve opens. Since curve 2 is very steep, small pressure differences give the large differences of flow rates.

The nonuniformity of the flow rates of a group of atomizers is reduced by using *two-chamber atomizers* (Fig. 4-30) [24], which are a variation of duplex

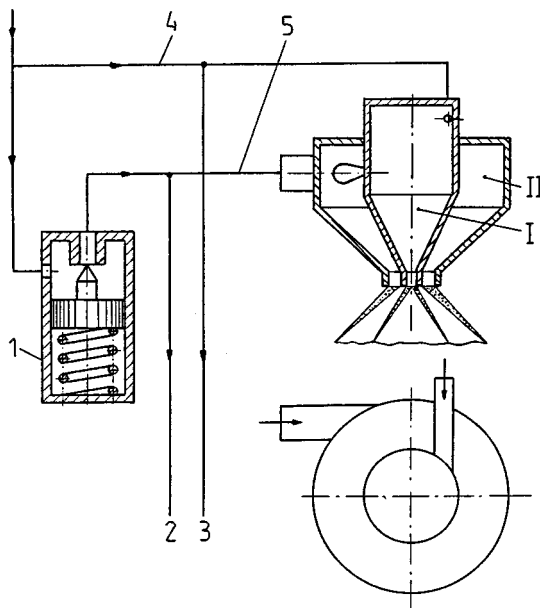


Figure 4-31 Schematic diagram of a two-orifice atomizer: Legend as in Fig. 4-27.

atomizers. The two-chamber atomizer consists of two simplex atomizers connected in series; hence it contains two swirl chambers. The fuel flows through the tangential orifices to each chamber independently. From the first chamber, I, the fuel discharges to the environment; from the second chamber, II, it flows to chamber I. The existence of two chambers causes the pressure variation in the first chamber to affect the pressure in the second chamber less than in a duplex atomizer.

Mixing of liquid jets in the first swirl chamber proceeds at high velocities, accompanied by high energy losses. This occurs especially at the moment when the second chamber is activated. As a result, the spray quality deteriorates. In general, the spray quality of two-chamber atomizers is better than the quality of duplex atomizers but worse than that of two-orifice atomizers.

Two-orifice atomizers [24]. A schematic diagram of a two-orifice atomizer is shown in Fig. 4-31. A two-orifice atomizer consists of two simplex atomizers connected in parallel. The two coaxial swirl chambers fed separately are terminated by two coaxial orifices (nozzles). The outer swirl chamber and the outer discharge orifice have annular cross-sections. For small pressures and low flow rates, the fuel flows only to the inner chamber, creating the primary supply system, I. When the pressure increases, the control valve opens and the fuel also starts to flow to the outer chamber, which constitutes the secondary supply system, II. The flows do not interact until they reach the inside of the atomizer, generating a single conical spray.

The flow rate is controlled through the variation of the discharge orifice cross section. The range of the flow rate control, according to Eq. (3-4), equals

$$\frac{G_{\max}}{G_{\min}} = \frac{\mu_1 A_1 + \mu_2 A_2}{\mu_1 A_1} \sqrt{\frac{\Delta P_{\max}}{\Delta P_{\min}}} \quad (4-6)$$

where A_1, A_2 = cross sections of the inner and outer discharge orifices,

μ_1, μ_2 = discharge coefficients

$\Delta P_{\max}, \Delta P_{\min}$ = maximum and minimum pressure drop.

Figure 4-32 shows the design of a two-orifice atomizer (Duplex 3). At low pressure the fuel flows through manifold 1 to the conical swirling insert 2 and then to the inner swirl chamber and discharge orifice, which are located in plate 3. Insert 2 is pressed by a conical spring against the seat in plate 4. After the control valve opens, the fuel also flows through manifold 5 to the axial orifices in plates 4 and 3 and then through the tangential orifices in plate 6 to the outer swirl chamber and to the outer discharge orifice in plate 7.

An example of the characteristic of a two-orifice atomizer is shown in Fig. 4-33. Curve 1 represents the characteristic of the primary supply system, curve 5 the characteristic of the secondary supply system, and curve 3 the characteristic of the total supply. As seen, the total flow rate is the sum of the flow rates during the independent flow through both systems. The above summation condition was not satisfied in Fig. 4-29. The interaction between the two systems relies on the fact that when the control valve opens, the two jets of drops with completely different spray qualities start to mix.

During partial opening of the control valve the fuel flows through both systems with different pressures. The dependence of the pressure behind the

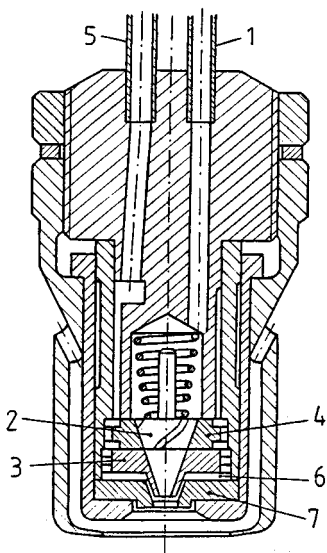


Figure 4-32 Two-orifice atomizer.

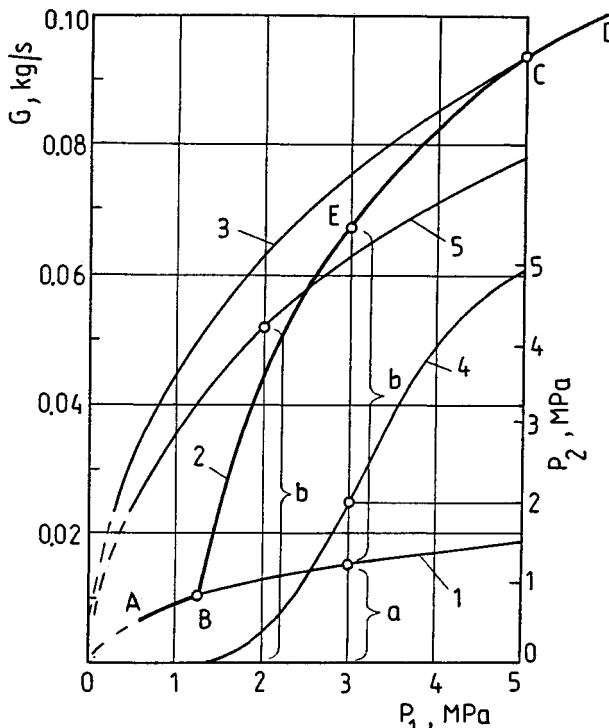


Figure 4-33 Characteristic of a two-orifice atomizer.

secondary stage, P_2 , on the pressure in front of the primary stage, P_1 , is represented by curve 4. Curve 2 characterizes the total flow through both stages during partial opening of the control valve. Curve $ABCD$ is a characteristic of a two-orifice atomizer. Curve 2 was generated by summation of the ordinates of curves 1 and 5. For example, for pressure $P_1 = 3$ MPa, on curve 4 the pressure $P_2 \approx 2$ MPa, so segments a and b must be added to obtain point E on curve 2.

The advantages of the two-orifice atomizers are as follows:

The range of flow rate changes is larger than for two-manifold atomizers and for variable geometry atomizers.

Flow rate is uniform.

Spray angle α is practically constant.

The disadvantages of the two-orifice atomizers are as follows:

During the opening of the control valve, high flow rate nonuniformity develops if the atomizers are located at different altitudes; the overpressure of fuel in front of the second stage is very small and comparable to the hydrostatic fuel pressure.

When the control valve opens the spray quality deteriorates but it improves as the pressure increases.

There are also *three-orifice atomizers*, for which a vast range of flow rate changes can be achieved (e.g., 240 times). The design of these atomizers is very complex.

4-2.3 Spill-Return Atomizers

The first spill-return atomizer was patented in 1921 and was initially used in the burners of ship boilers and later in other fields, especially in aircraft gas turbines. The spill-return atomizer is a simplex swirl atomizer that atomizes only a part of the liquid being supplied. The liquid supplied to the chamber is divided into two jets, one of which discharges outside and is atomized while the other is “spilled” away from the atomizer back to the feeding system. The total flow rate G_t of the liquid supplied to the atomizer is given by

$$G_t = G_a + G_d \quad (4-7)$$

where G_a is the flow rate of the atomized liquid and G_d is the flow rate of the returned liquid.

The spill-return atomizer is characterized by means of the *excess liquid coefficient*

$$e = \frac{G_t}{G_a} \quad (4-8)$$

When $G_a \rightarrow 0$ (i.e., $e \rightarrow \infty$), all the liquid is diverted away from the chamber; when $G_t = G_a$ (i.e., $e = 1$), the liquid is not diverted at all and the spill-return atomizer becomes a simplex swirl atomizer.

There are two basic control systems of the liquid flow rate: one-way and two-way. In the one-way system a control valve throttles the liquid flowing through the return manifold and changes the flow rate of the liquid being atomized. The two-way system has two independent circuits, each of which has its own pump (Dowty system). Only the one-way system will be discussed [24].

The simplest *one-way system* is realized with a constant pressure of the fuel pump, $P = \text{const}$. When the liquid is throttled in the control valve, the total flow rate G_t decreases as well as the flow rate of the returned liquid G_d (up to $G_d = 0$); the flow rate of the atomized liquid increases (up to $G_a = G$). The flow rate G_t changes depending on the flow resistance but is always higher than G_a . The disadvantage of this system is a large coefficient e in the whole range of control, especially in the range of small engine loads. This leads to high energy consumption by the fuel pump.

More advantageous in this respect is a one-way system operating at $P \neq \text{const}$ (Fig. 4-34). Control valve 1 operates in such a way that when pressure P increases, pressure P_d in the bleeding manifold in front of the valve also increases, and this increased pressure P_d acts on the piston and closes the valve. When the valve is closed the atomizer operates as a simplex atomizer.

The characteristic of an atomizer controlled in this way is shown in Fig. 4-35. Curve 1 shows the relationship between pressure P_d and pressure P . For

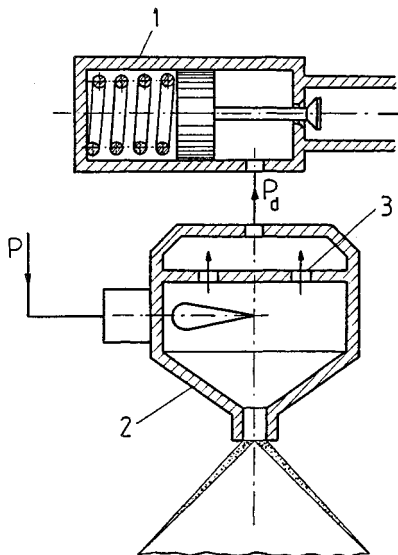


Figure 4-34 Schematic diagram of spill-return atomizer with $p = \text{const}$. 1, Control valve; 2, atomizer; 3, back wall of swirl chamber with bleed orifices.

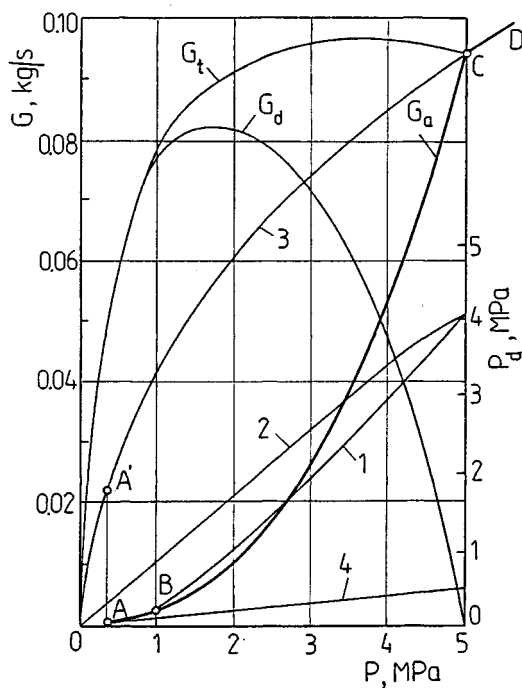


Figure 4-35 Characteristic of a spill-return atomizer operating at $P \neq \text{const}$.

pressures lower than P , which in this case is equal to $P = 1 \text{ MPa}$, the control valve is completely open; for pressures higher than $P = 5 \text{ MPa}$ it is completely closed. Compare this with curve 2, which shows the interrelationship of pressures P and P_d when the control valve is totally closed.

Curves G_t and G_d represent the total flow rate and the flow rate of the returned liquid; the difference is the flow rate of the atomized liquid, G_a . The characteristic of a spill-return atomizer is represented by curve ABCD. Segment CD also belongs to curve 3, which is the characteristic of a simplex atomizer. Curve 4 is the characteristic of a spill-return atomizer with the control valve completely closed.

In the pressure range $P = 0.3$ to 5 MPa , the flow rate of the atomized liquid varies from $G_a \approx 0.0011$ to 0.095 kg/s , which corresponds to points A and C. The flow rate changes in this example approximately 85 times. The same atomizer without the spill-return feature would have only a fourfold flow rate change, which corresponds to points A' and C .

The geometric constant of a spill-return atomizer is

$$K_d = eK \quad (4-9)$$

where K is the geometric constant of the atomizer when the return is closed. The geometric constant determined in this way can be treated as a constant of a simplex atomizer. The discharge coefficient μ of a spill-return atomizer is a function not only of the geometric parameters but also of the flow rate G_d diverted from the chamber. The higher the coefficient e , the smaller the ratio μ . Spill-return atomizers provide good atomization for very low flow rates of the atomized liquid G_a .

The design of spill-return atomizers is based on the design of simplex atomizers. The only essential change is the drain manifold, as shown in Fig. 4-36 [24]. Nozzle 1 contains tangential inlet orifices 2, swirl chamber 3, and discharge orifice 4. The annular slot in the back wall of the swirl chamber serves for draining the fluid. The influence of the dimensions and localization of the drain on the operation of the spill-return atomizer will be discussed in Chapter 6.

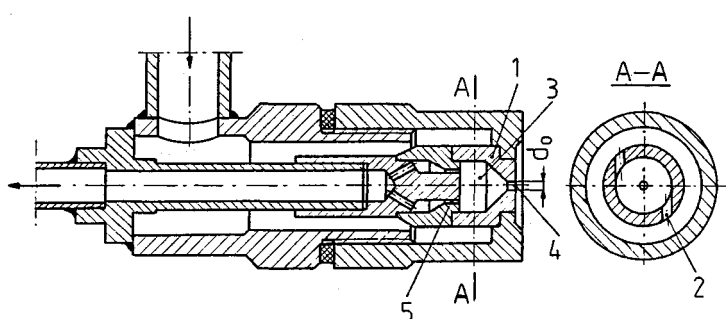


Figure 4-36 Spill-return atomizer.

A variation on spill-return atomizers is the *recirculation atomizer* which is used in oil burners. The essential feature of recirculation relies on the fuel pumping through the feeding and draining channels while the outlet orifice is closed. The outlet orifice is closed by a needle. The goals of recirculation are (1) to warm up the fuel and to decrease its viscosity before the burner starts to operate and (2) to protect the nozzle from overheating after the burner is turned off while the furnace chamber still radiates heat.

Among recirculating atomizers an important role is played by atomizers of the oil that lights up burners. These atomizers are used to light the burners using coal dust and to burn oil during an emergency shutdown of power units. The stand-by type of operation requires continuous recirculation of fuel in these atomizers.

The advantages of the spill-return atomizers are as follows:

- Very good atomization quality in the whole range of flow rates
- Vast range of flow rate changes
- Simplicity of design (as for simplex atomizers)
- High durability in the flame zone due to good cooling conditions
- Small sensitivity to contamination due to relatively large flow cross sections

The disadvantages of the spill-return atomizers are as follows:

- Very high increase of spray angle α (of 20–30°) during the reduction from the nominal to minimal flow rate
- Complex control system
- Additional energy consumption for pumping the liquid
- Excessive temperature increase for large spill-return flow rates

4-2.4 Variable-Geometry Atomizers (Atomizers with the Controllable Area of Inlet Orifices)

The operation of variable-geometry atomizers (*atomizers with a controllable inlet orifices area*, is based on the fact that the tangential orifices are blocked or opened by a needle, which moves axially in the swirl chamber. From Eq. (4-1) it follows that the geometric constant K changes as the total area of the inlet orifices iA_p changes. The change in K results in a change of the discharge coefficient μ , which is the essence of this control.

The first designs of atomizers with this type of control were the Pillard industrial atomizers and the Lubbock aircraft atomizers. In these atomizers the needle movement was caused by fuel pressure. A disadvantage, which prevents the implementation of such atomizers, was the tendency to vibrate or to jam the needle in the sleeve. Only an approach with mechanical needle control found application.

An example of such an atomizer is shown in Fig. 4-37 [26]. Fuel flows through channel 1 to the outlet orifice in two ways. The first supply stage, I, corresponding to small flow rates, consists of orifice 1 in sleeve 4 and orifice 5 in

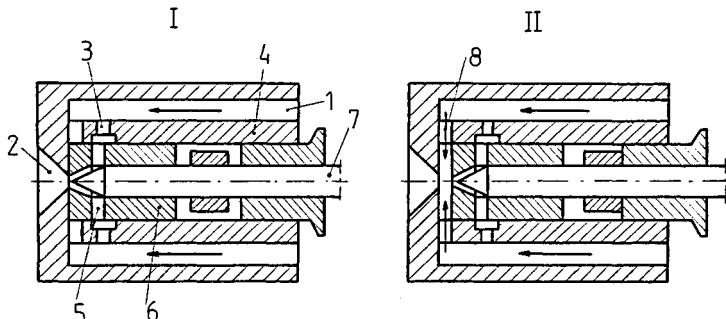


Figure 4-37 Schematic of a boiler atomizer developed by the Central Boiler and Turbine Institute (St. Petersburg, Russia) with regulated area of inlet orifices.

sleeve 6. Needle movement to the right causes further opening of these orifices, and when the needle reaches the right-most position sleeve 6 moves, opening orifice 8 (second stage of supply II). The displacement of the needle during the first stage is 3 mm and the total displacement is 9 mm. The needle can also be used to shut the atomizer.

Advantages of variable-geometry atomizers are as follows:

Advantageous characteristic, since through the proper localization of the inlet orifices one can obtain, for constant feeding pressure, almost linear relationship between the flow rate and the needle displacement.

Good atomization quality.

Large theoretical range of flow rate control; the total area of the tangential orifices is not more than three times larger than the discharge orifice area, since its further increase does not produce the flow rate increase and reduces the atomization quality.

Disadvantages of variable-geometry atomizers are as follows:

Technological difficulties with respect to the needle, sleeve, and tangential orifices in the sleeve.

Increase of the spray angle α with decreasing flow rate.

Difficult manufacturing of a group of identical atomizers.

Difficult simultaneous control of the group of atomizers.

Difficult adaptation of these atomizers to fuel recirculation.

4-3 JET-SWIRL ATOMIZERS

The *jet-swirl atomizer* is a combination of a jet and swirl atomizer. The vortex-free jet flows in the axis of the atomizer and the swirled jet flows next to the wall of the swirl chamber. These jets interact in the swirl chamber and in the discharge orifice, so at the discharge nozzle the *full cone jet* of atomized liquid is

obtained. If the proportions of the orifices are properly selected, the liquid jet has a uniform radial distribution. This eliminates the nonuniform distributions typical of jet and swirl atomizers.

There are approximately 30 different designs of jet-swirl atomizers. One of the oldest is an atomizer produced by the Dowty company for industrial gas turbines. These atomizers can be divided into three groups: atomizers with tangential inlet orifices, atomizers with a swirling insert, and atomizers with special structural components.

Atomizers with tangential inlet orifices. Atomizers in this group have an axial orifice through which a vortex-free jet is fed to a swirl chamber and orifices tangential to the chamber cause the liquid swirling (Fig. 4-38). These atomizers differ mainly in the number and shape of the tangential orifices. The swirl chamber, the conical space, and the discharge nozzle constitute the mixing chamber.

Jet-swirl atomizers have large spray angles, $\alpha = 80\text{--}110^\circ$, which can hardly be controlled by design changes. The biggest change of the angle α can be achieved by changing the swirl radius, i.e., by changing the diameter of the swirl chamber. These atomizers are used for moderate flow rates.

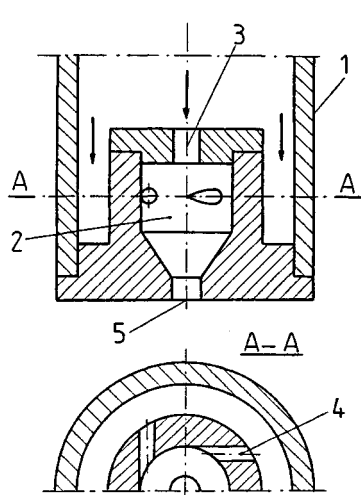


Figure 4-38 Jet-swirl atomizer with tangential inlet orifice. 1, Body; 2, swirl chamber; 3, axial orifice; 4, tangential orifices with circular cross section; 5, discharge orifice.

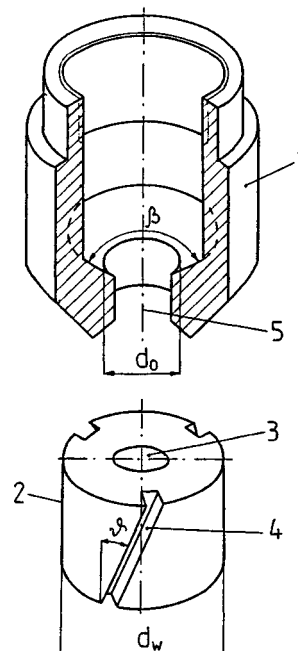


Figure 4-39 Jet-swirl atomizer with an inserted swirler. 1, Body; 2, inserted swirler; 3, axial orifice; 4, groove; 5, discharge orifice.

Table 4-1 Insert diameter d_w for various values of d_0

d_0 , mm	< 2	2–15	> 15
d_w , mm	15	30	$2d_0$

Atomizers with a swirling insert. Atomizers in this group consist of two elements, a body and a swirling insert (Fig. 4-39) [27]. The swirling insert, in this case a cylindrical insert, has an axial channel for the vortex-free jet and grooves producing the swirled jet. The insert diameter d_w is determined depending on the inlet channel diameter d_0 from Table 4-1. The insert length has not yet been precisely established. The swirl chamber (mixing chamber) is located between the insert and the discharge nozzle. The cone angle β of the swirl chamber in most cases is 60 to 120°. The grooves on the insert surface have a rectangular or square cross section. They are inclined with respect to the axial direction by an angle ϑ . The machining of the grooves and the insert itself is relatively simple. Basically the number of grooves is limited to three. The angle of inclination affects the spray angle α (Table 4-2). Angle ϑ is not larger than 30°.

Atomizers with cylindrical swirling insert are applied for lower flow rates. They have relatively small spray angles, not exceeding $\alpha = 70$ –80°. The advantages of these atomizers are simplicity of design and feasibility of replacing the insert. That is why they are used more often than other jet-swirl atomizers. Their disadvantage is their tendency to clog. A calculation method exists for these atomizers.

Other designs of swirling inserts include bladed inserts (curved or flat blades) and worm inserts. However, they are difficult to machine and therefore have lower uniformity of operation.

Atomizers with special structural components. This group of atomizers appeared in recent years. Their principle of operation is based on utilization of the properties of a free vortex. In the outer region of the vortex the circumferential velocity increases and the pressure decreases toward the axis of the vortex. Hence, there is a positive pressure gradient in this region. This gradient is supported by the auxiliary operation of various elements, and therefore the liquid flows toward the axis and an axial jet develops. Three types of liquid motion can be distinguished in the swirl chamber (Fig. 4-40) [27]. The first type of motion (Fig. 4-40a) is based on the fact that the liquid is supplied in the form of swirled and crossing jets, which develop in swirlier channels inclined in the radial direction. Collision of these jets causes partial loss of angular momentum and the development of motion in the axial direction. Such motion is realized in

Table 4-2 Angle ϑ for various ranges of spray angle α

α , deg	30	30–50	50–75	> 75
ϑ , deg	10	15	25	30

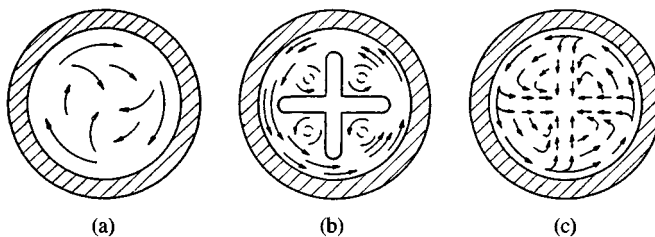


Figure 4-40 Liquid motion in a swirl chamber: (a) first type; (b) second type; (c) third type.

atomizers with cross swirlers (Fig. 4-41). In side view these swirlers have the shape of a cross and the edges mark the direction of swirling.

A swirler of this type can achieve a uniform jet with a square cross section, as shown in Fig. 4-42. A jet with such a cross section develops because of the perpendicular grooves on the front surface of the atomizer.

The second type of motion (Fig. 4-40b) is based on the fact that in the central region the circumferential component of velocity is blocked. This blocking is achieved by placing an element with grooves or blades on the axis. A portion of the liquid moves from the outer region to the central region and has a circumferential-axial motion. As a result of the interaction between the outer and central jets, a jet develops that has a uniform distribution of the liquid.

The third type of motion (Fig. 4-40c) is based on the fact that axial motion develops in the swirl chamber as a result of the impingement of two radial jets. The impingement is realized in the region of the back wall of the swirl chamber by means of such elements as swirl vanes and radial grooves. One portion of the

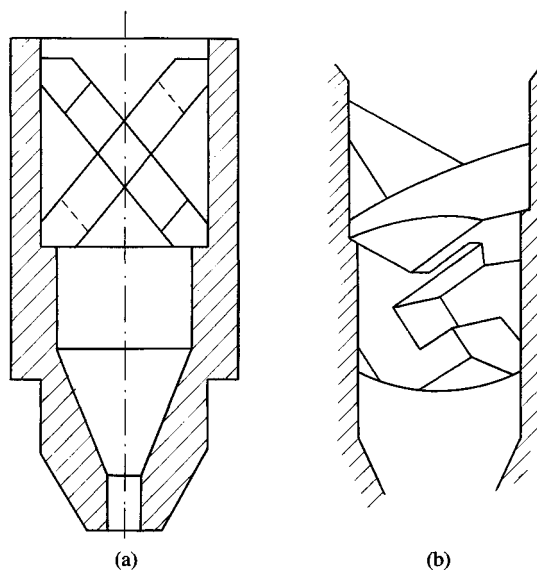


Figure 4-41 Jet-swirl atomizer with a cross insert: (a) body with an insert; (b) perspective view of the insert (Lechler) [24].

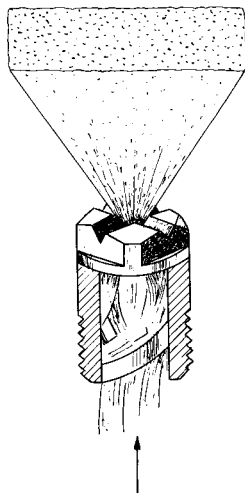


Figure 4-42 Uniform jet of drops generated by a jet-swirl atomizer with a cross swirler (Spraying Systems Co.) [24].

liquid swirling in the chamber flows around these elements, and the second portion falls down into them and moves in the axial direction.

The latter group of atomizers are characterized by generally high flow rates. The basic feature of these atomizers is high turbulence of the liquid motion, the impingement and mixing of the jets. For the reasons stated above, there is no theory that would provide the basis for calculations for these atomizers.

One feature of jet-swirl atomizers is the *mixing of the jets*. If the inlet orifice and the swirling orifices are fed with two liquids supplied separately, the feed control can be used to achieve precise mixing of these liquids in the desired proportions. The mixing of the jets can be internal or external (Fig. 4-43). Internal mixing (Fig. 4-43a) proceeds in a manner typical of jet-swirl atomizers.

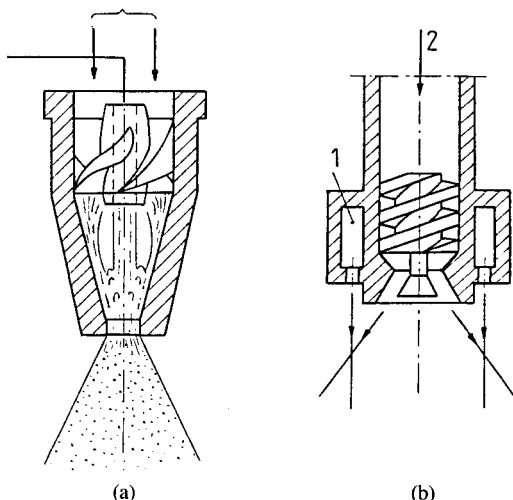


Figure 4-43 Mixing of the jets of two liquids: (a) internal mixing; (b) external mixing. 1, Fuel; 2, oxidizer.

During external mixing (Fig. 4-43b) the central swirled jet mixes with the axial jets that discharge from the orifices in an annular chamber; the atomizers in the well-known Walter-type rocket engine operated on this principle.

4-4 PNEUMATIC (TWIN-FLUID) ATOMIZERS

Pneumatic (twin-fluid) atomizers are atomizers in which the energy of the gas, in most cases air or steam, is used for liquid disintegration. These are the oldest type of atomizers; the first patent for a residual fuel oil–steam boiler atomizer was obtained by V. G. Shukhov in 1880. Pneumatic atomizers are increasingly applied in numerous fields. There has been intensive development of these atomizers for application to very viscous liquids, oil-in-water fuel mixtures, liquid metals, etc.

The principle of pneumatic atomization is based on the high shear stresses that develop at the interface between the liquid and gas. The liquid prior to the contact with gas can assume various shapes. The three basic shapes are liquid column, liquid film, and liquid drop. It is easier to atomize a liquid film than a liquid column with the same volume because in the first case the contact surface between the liquid and gas is much larger. The task is to develop a film or many thin columns of liquid instead of one thick column. A thin column flowing coaxially with the gas disintegrates as early as at the relative liquid-gas velocity of 30 m/s.

There are two mechanisms of gas-assisted liquid atomization: detachment of drops from wave crests of disturbances on a liquid surface and disintegration of a liquid film at the edge of a solid wall. If the liquid occurs in the form of drops, secondary disintegration occurs under the action of the flow.

Pneumatic atomizers have the following advantages:

It is feasible to atomize very viscous liquids (see Table 1-5) if the gas kinetic energy is high enough. If steam or an overheated gas is used, the liquid viscosity decreases.

The atomization quality and the liquid flow rate are less related than for pressure atomizers. The energy supplied by the gas can be arbitrarily high; the only limits are economic. Therefore one can achieve a very high flow rate control range with good atomization quality.

Various atomizer designs provide for the generation of sprays of arbitrary shape (flat, conical) and arbitrary spray angle α .

The spray has a completely different liquid distribution in the transverse cross section compared to swirl atomizers; the most drops with the largest diameters flow in the center of the spray and the small drops are located on its periphery. Such sprays are advantageous in boiler burners because during combustion they ensure the highest radiant heat exchange.

Air-assisted atomization is advantageous because the air, as early as in the atomization process, causes the initial fuel oxidation reactions. The air-fuel mixture discharging from the nozzle makes the flow in the combustion

chamber turbulent, which decreases the combustion time and the flame length.

An arbitrary gas can be used for atomization, depending on need. In the case of nonvolatile liquid fuels the combustion conditions can be improved by using a flammable gas, e.g., natural gas. In producing light metal alloy powders one uses inert gases (helium, argon), which for high gas velocities (Mach number $Ma = 2-3$) allow maintaining the diameters of 90% of the powder volume at a level lower than $44 \mu\text{m}$ [37].

As the relative gas velocity increases the atomization quality improves, but above 80 m/s this improvement is less and less significant. At high gas velocities self-excited pulsations occur. These significantly increase the efficiency of utilization of the gas kinetic energy, allowing production of drops that have 1.7–2.0 times smaller diameters and are more uniform than in the case without pulsations.

Pneumatic atomizers do not tend to clog because the liquid is supplied at low pressure through channels with large cross sections. This is especially important in the case of contaminated liquids and mixtures containing solid particles.

The disadvantages of pneumatic atomizers are as follows:

It is necessary to use gas compressors or other sources of compressed gas.

The energy consumption per atomization of a unit mass is higher than for other atomizers. This results from the additional energy necessary to compress the gas and from the low efficiency of energy transfer. Pneumatic atomizers have a relatively complex structure and therefore are more difficult and expensive to manufacture than pressure atomizers.

The large quantities of steam used for residual fuel oil atomization in the boiler furnace can cause corrosion of the boiler heating surfaces. This takes place for a steam/liquid mass ratio $b = 0.5-1.0$, but in the modern atomizers where $b = 0.05-0.1$ the corrosion is not significant. This is because in the stoichiometric combustion of 1 kg of the heating oil the water content of the generated gas increases from about 1.1 kg to 1.15–1.20 kg, which is insignificant.

Calculation methods do not exist, especially for internal operation atomizers, because of the complexity of the processes occurring during atomization.

Pneumatic atomizers have very diverse processes of atomization and their classification cannot be based on only one of these processes or on one parameter of the atomizer. In this situation, pneumatic atomizers can be classified on the basis of the following features:

Gas pressure drop

Place between liquid and gas

Method of gas and liquid separation

Direction of the gas action on liquid

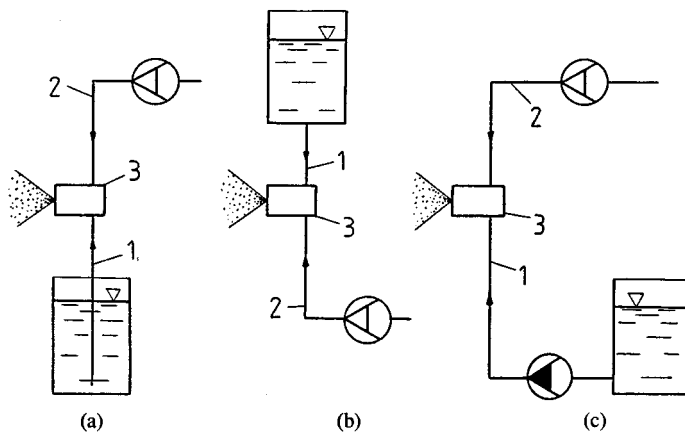


Figure 4-44 Liquid supply for a pneumatic atomizer: (a) suction; (b) gravitation; (c) pressure. 1, Liquid; 2, gas; 3, atomizer.

The classification of pneumatic atomizers according to the *gas pressure drop* is in principle independent of the way in which the liquid is supplied and independent of the liquid pressure. The liquid can be supplied by gravitational flow, ejection with gas or pumping (Fig. 4-44). The liquid pressure is always very low compared to that in pressure atomizers and falls in the range of negative pressures to pressure of order 0.5 MPa. The gas pressure varies depending on the needs and the gas source (fan, blower, compressor, etc.). Table 4-3 shows the classification of the air pressure drop. According to this classification, pneumatic atomizers can be divided into *low-, intermediate- and high-pressure atomizers*. The air/liquid mass ratio b

$$b = \frac{G_G}{G_L} \quad (4-10)$$

depends on the liquid properties, liquid pressure, atomizer design, and required atomization quality. It should be emphasized that b is the ratio of the flow rates and not the ratio of energies, and therefore it is not the only factor that

Table 4-3 Pneumatic atomization—air parameters

Pressure drop	Overpressure value		Air velocity, m/s	Air/liquid mass ratio b , kg/kg
	mm H ₂ O	MPa		
Low	100–500	0.001–0.005	40–90	6–15
Medium	1000–3000	0.01–0.03	120–220	0.2–1.0
High	—	> 0.1	transonic or supersonic	< 0.5

determines the atomization quality. The atomization quality is determined by the gas kinetic energy, which generally depends on the relative gas velocity [1].

Classification of pneumatic atomizers in terms of the *place of contact between the gas and liquid* takes into account two possibilities, i.e., the action of the gas on the liquid inside or outside the atomizer. As a result of such classification we consider atomizers with *internal gas action* and atomizers with *external gas action*. In internal gas action atomizers it is difficult to control the flow of both agents because a change in flow of one agent results in a change in flow of the other. Such an interrelationship does not exist in atomizers with external gas action. The external action of gas jets on liquid is used during the atomization of very viscous and contaminated liquids. The atomization quality of internal and external atomizers has been discussed in [8].

Classification of pneumatic atomizers considering the *way in which the liquid and gas masses are separated* takes into account two types of atomizers, *single-jet atomizers* and *multijet atomizers*. In the first case, one gas jet of arbitrary shape acts on one liquid jet. This can take place inside or outside of the atomizer. In the case of multijet atomizers, there are two design solutions. In the first, a liquid jet flowing through an annular channel is surrounded on both sides by gas jets—these are the *two-sided atomizers*. In the second case a gas jet interacts with several liquid jets and there are many stages of mixing—these are the *multistage atomizers*.

The classification of pneumatic atomizers considering the *direction of gas action on the liquid* represents the design features of atomizers most generally, since it accounts for the gas interaction. One can divide the atomizers into those with parallel, cross, and swirl flow. Our further discussion will be based on this classification, while accounting for other design features related to the other classifications.

4-4.1 Parallel Flow Atomizers

Pneumatic atomizers with parallel flow are characterized by the fact that the gas and the liquid flow in the same direction at the moment of their contact. Large shear forces develop along the surface of contact and cause disintegration of the liquid jet.

Figure 4-45 shows the simplest atomizer with parallel flow. This atomizer is used for air humidification directly in rooms. Water in the quantity of 4.5 kg/h is sucked through an orifice with a large diameter and discharges through an orifice with a diameter of 0.6–1.0 mm. The air pressure drop is 0.1 MPa, the air flow rate is 7.3 kg/h, and the orifice diameter is 2–4 mm. A spray with an angle $\alpha = 30^\circ$ has deep penetration of 1.5–2 m due to the high air pressure drop [24].

Atomizers of this type (air-water nozzles) suck in water from a level located at a distance H below the discharge nozzle. This prevents a water leak from the atomizer when the air does not flow and provides easy control of the water flow rate through the change of height H . Such atomizers provide good atomization only for small water flow rates, and one should expect small spray angles α which are typical for jet atomizers.

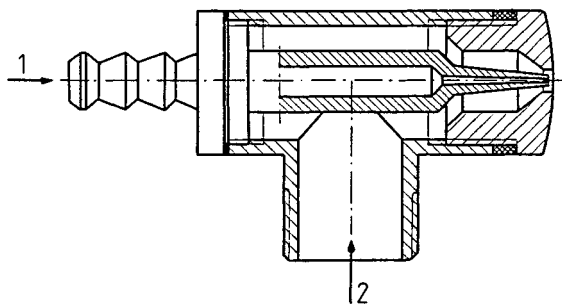


Figure 4-45 Pneumatic atomizer with parallel flow and external gas operation. 1, Water; 2, air.

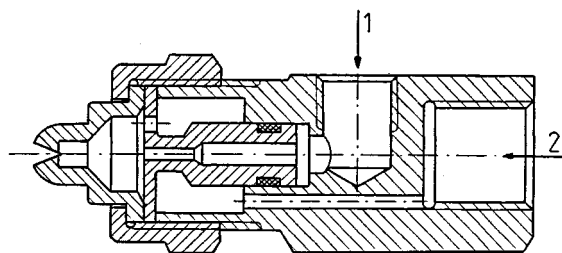


Figure 4-46 Pneumatic atomizer generating a fanlike jet of drops (Delavan). 1, Liquid; 2, gas [34].

The pneumatic atomizers, as mentioned, are able to provide liquid jets with arbitrary shapes and spray angles. An example of an atomizer with an elliptical discharge orifice that generates a fan spray is shown in Fig. 4-46. The fan spray has an angle of approximately 80° , depending on the ambient conditions and the distance from the atomizer. This is an atomizer with internal gas operation [34].

Figure 4-47 shows the nozzle of a pneumatic atomizer with a conical deflector. The liquid discharges through an annular gap (4) on the surface of the deflector (3) whose cone angle is $100\text{--}150^\circ$. In gap 5 with height $h = 3 \text{ mm}$ the liquid film encounters the air, which flows with velocity $80\text{--}300 \text{ m/s}$. As a result of the gas action a hollow conical spray develops. The maximum water flow rate is 0.05 kh/s . The air pressure drop equals 0.2 MPa [21].

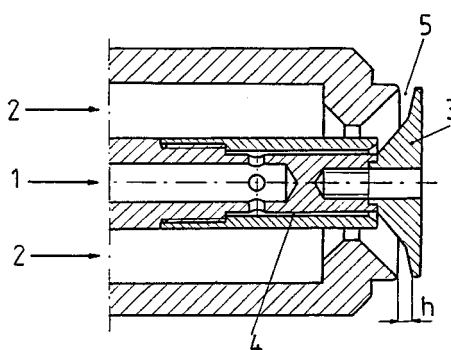


Figure 4-47 Pneumatic atomizer with a large spray angle. 1, Water supply; 2, air supply; 3, deflector; 4, annular slot; 5, discharge slot.

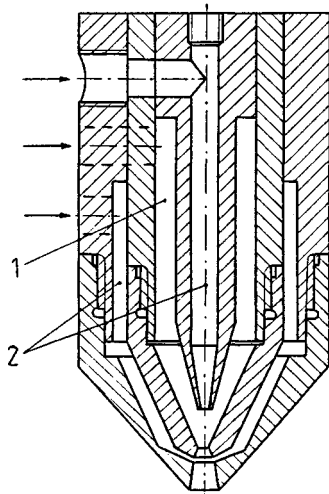


Figure 4-48 Pneumatic atomizer with a two-sided gas action.
1, Liquid channel; 2, gas channels [24].

An example of a pneumatic multijet atomizer is shown in Fig. 4-48. This is a two-sided atomizer in which the annular liquid jet is subjected to a two-sided action of the gas; it involves a combined internal-external action. This atomizer has a complex design, but its advantage is increased energy exchange, which is essential during the atomization of viscous liquids. This atomizer can easily be transformed to an atomizer with swirl flow if the liquid and gas are supplied tangentially to the flow channels in order to develop a countercurrent swirl [13].

A carburetor of a piston engine with spark ignition operates on the principle of ejection, i.e., the principle of the simplest pneumatic atomizer with liquid suction. During the action of the piston a negative pressure develops in the throttle; its value depends on the degree of opening of the choke for a given rotational frequency of the engine. For complete opening of the choke a negative pressure of approximately 0.008 MPa (800 mm H₂O) develops, which corresponds to an air velocity of about 120 m/s. The fuel is sucked in from the carburetor jet with a diameter approximately 5% of the throttle diameter. The fuel is atomized and flows to the engine cylinder; the atomization quality is such that about 50% of the fuel evaporates.

4-4.2 Cross-Flow Atomizers

Pneumatic atomizers of cross-flow type operate on a principle similar to that of jet atomizers of the impinging jet type. The operation is based on the formation of thin liquid jets that are introduced into the gas flow. The liquid jets can be introduced at various angles, most commonly at 90°. The impingement of liquid jets with the flowing gas leads to intensive jet disintegration, and the thinner the jets are, the better the atomization is. This mechanism of impingement of liquid and gas jets can also proceed in a different way.

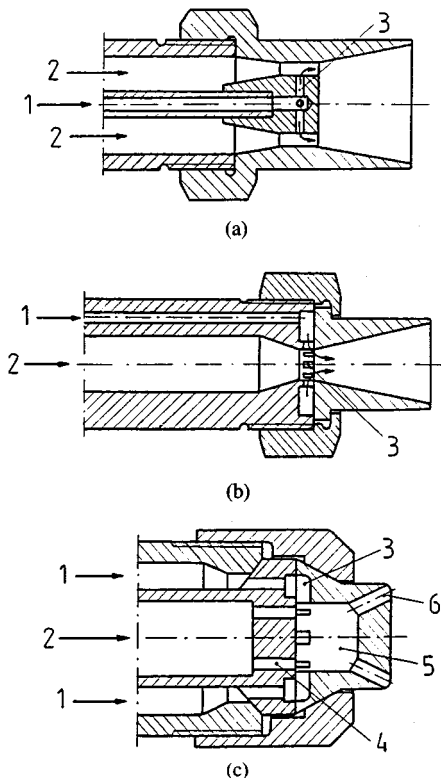


Figure 4-49 Pneumatic atomizers with a cross-flow and internal operation: (a) outward flow of liquid; (b) inward flow of liquid; (c) collision of gas and air jets. 1, Liquid; 2, gas; 3, liquid orifices; 4, gas orifices; 5, mixing chamber; 6, outlet orifices.

The problem of liquid jet disintegration due to the dynamic action of the gas has been poorly explored, despite the significant progress in the development of pneumatic atomizers in recent years. In general, the liquid and gas impinge in two ways, namely inside and outside the atomizer. In both cases the liquid can be fed at a negative pressure or overpressure.

Atomizers with internal operation can have various designs. Figure 4-49a shows a liquid discharge from the orifices outside to the gas that flows in an annular space. In Fig. 4-49b the direction of the liquid flow is opposite and the gas flows in the channel along the axis of the atomizer. Figure 4-49c shows yet another development in which the liquid and gas jets impinge at an angle of 90°.

The atomizer shown in Fig. 4-49c is known in the United States as an “internal mix” atomizer and is used in boiler furnaces. The fuel is atomized by means of steam. The atomizer has an additional mixing chamber. The number of fuel and steam nozzles located at an angle of 90° varies from 4 to 20 and the number of discharge nozzles from 4 to 30. The steam pressure is always higher than the pressure of the fuel by approximately 0.1 MPa.

Figure 4-50 shows a popular *atomizer of the Y type* (Y-jet nozzle), which was patented by I. Fletcher in 1944 (United States). Numerous publications discuss these atomizers [20, 24, 25, 28]. The Y-jet nozzle has been applied in boiler

burners, e.g., the burner produced by Babcock. The heating oil pressure is 1.3–1.5 MPa and the pressure of the steam used for atomization is higher by 0.2–0.3 MPa. Approximately 5% of the steam generated in the boiler is used for atomization.

The principle of operation of the Y-jet nozzle is based on the fact that the process has two stages (Fig. 4-51):

1. The liquid and gas flow to the discharge nozzles, where they impinge at a certain angle. The discharge nozzles act as mixers in which the expanding gas develops a thin annular film of liquid. Drops are sheared off the tops of the wavy films and carried by the gas.
2. The liquid film discharges from the nozzles and is subjected to wavy perturbations, which cause the disintegration into annuli and subsequently into drops. A hollow conical spray develops. The lengths of segments L_1 and L_2 are equal to about 5 and 40 diameters of the discharging nozzle.

Discharging nozzles are located in the atomizer head. The number of nozzles is 5–18, most commonly 6–12. The angle β between the nozzles is arbitrary and therefore one can shape the spray depending on the need; asymmetric sprays can also be generated. The liquid flows through the channels located at the periphery of the atomizer and the gas flows through the channel in the atomizer axis; however, the opposite can take place.

A pneumatic atomizer used for the atomization of coal-water slurries (CWS) has been evaluated [3, 18]. This atomizer has two places in which the liquid and gas mix. The first place is similar to the Y-jet nozzle (Fig. 4-50) and the second to the atomizer shown in Fig. 4-49c. It follows from experiments that small drops in the spray are located closer to the spray axis and large ones are located on the spray periphery. For pressure 1 MPa and air/liquid mass ratio $b = 0.07–0.15$, the mean drop diameter was $D_m = 40–180 \mu\text{m}$.

For very viscous liquids (above $2 \text{ Pa} \cdot \text{s}$) an atomizer with internal operation can have a simple design such as that shown in Fig. 4-52. This atomizer is based on the operating principle of the Y-jet nozzle and has the additional advantage that the relative air velocity is increased by the countercurrent-oblique liquid feeding. Liquid feeding into the center of the gas jet ensures better contact

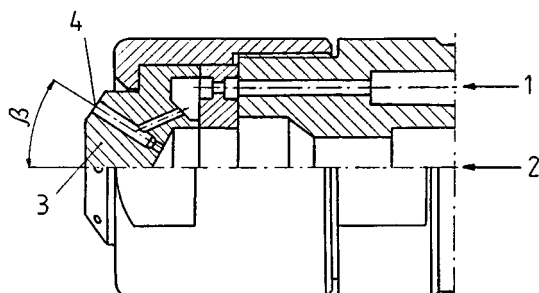


Figure 4-50 Pneumatic atomizer of the Y type. 1, Liquid; 2, gas; 3, atomizer head; 4, discharge orifice.

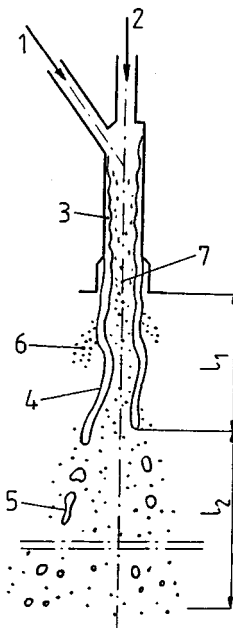


Figure 4-51 Model of liquid atomization in a discharge orifice of a Y-type atomizer. 1, liquid; 2, gas; 3, liquid film with a wavy surface; 4, liquid film subjected to wavy disturbances; 5, drops developed as a result of film disintegration; 6, small drops developed on crests of wave; 7, small drops developed as a result of tearing action of gas.

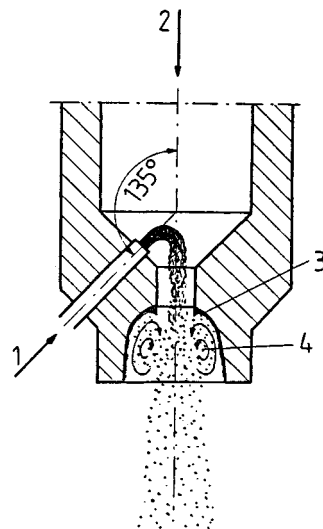


Figure 4-52 Schematic diagram of pneumatic atomizer with internal operation for very viscous liquids. 1, Liquid; 2, air; 3, liquid film; 4, vortex.

between gas and liquid. A dome-shaped discharge nozzle causes the liquid film that develops on the orifice wall to be removed by intense vortex motion. During experiments for $b = 1.0$ mean drop diameters smaller than $100 \mu\text{m}$ were obtained [32].

Atomizers with external operation will be presented by means of two examples. The first example is shown in Fig. 4-53. An annular air jet discharging with a high velocity from nozzle 1 impinges at a right angle to the liquid jets that discharge from six nozzles (2) with a velocity of 3–35 m/s [30]. A conical deflector (3) placed in front of the air nozzle changes the shape of the spray and disintegrates the droplets. For proper pressure drops the air behind the nozzle can expand further, corresponding to the air velocity expressed by Mach number $\text{Ma} = 1-2$. This atomizer can serve a heavily loaded burner in a boiler. Such an atomizer generates a very good atomized spray (4). In region 5 some large drops appear due to the inertial flow in the radial direction. The disadvantage of this design is the presence of large droplets in region 6; these drops develop as a

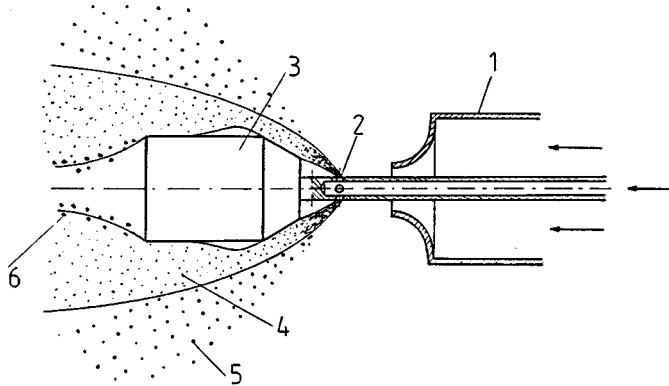


Figure 4-53 Schematic diagram of injection sprayer of a pneumatic atomizer with a cross-flow with external gas operation.

result of the disintegration of the liquid film produced during the flow around the cylindrical part of the deflector.

The second example of an atomizer with external operation is shown in Fig. 4-54 [33]. Jets of gas impinge with jets or sheets of liquid. The use of impinging jets improves the atomization of heavy heating oils. Advantages are a low air/liquid mass ratio and the possibility of building large burners with increased numbers of air and fuel nozzles.

The effects of the impingement of air and liquid jets have been investigated and the results will be presented in Chapter 6. It should be stated here that the operation of the atomizer shown in Fig. 4-54 depends mainly on the distance between the air nozzle and the point of collision, on the angle of the impingement, and on the air/liquid mass ratio l . The basic results are as follows:

1. The mean drop diameter increases as the distance between the air nozzle and the point of collision increases.

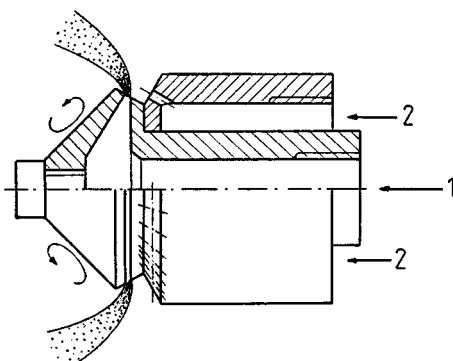


Figure 4-54 Schematic diagram of pneumatic atomizer with a cross-flow and perpendicular directions of colliding jets of gas and liquid. 1, Liquid; 2, gas.

2. The angle of jet impingement does not significantly affect the atomization quality if the air velocity is much higher than the liquid velocity.
3. Drop diameters smaller than $100 \mu\text{m}$ can be obtained during the atomization of a liquid of viscosity $0.25 \text{ Pa} \cdot \text{s}$ if $b = 1.0$.

4-4.3 Swirl-Flow Atomizers

Pneumatic atomizers with swirl flow are characterized by the fact that at least one medium (liquid or gas) is subjected to swirling. Introducing a thin film or thin jets of liquid into the swirled gas jet results in very high atomization quality. The interaction between the gas and liquid can take place inside or outside the atomizer.

Because of design limitations, one medium flows in the axis and the other one far from the axis of the atomizer. Either gas or liquid can swirl and in some cases both swirl. This leads to at least six design variations; however, the total number of solutions is higher because the swirling can be cocurrent or countercurrent and the gas can act on the liquid from one or two sides.

Atomizers with the internal operation are most commonly used. Figure 4-55 shows the two simplest designs of pneumatic atomizers with the swirl flow. The atomizer shown in Fig. 4-55a is in principle similar to the jet-swirl atomizer shown in Fig. 4-38. The atomizer shown in Fig. 4-55b has a conical-disk deflector that generates a hollow conical spray used in the chamber of a gas turbine [24].

Figure 4-56 shows an atypical pneumatic atomizer with an open swirl chamber [1]. This atomizer is designed for *steam attemperation* in a boiler. The circular water guide plate has six to nine orifices inclined at an angle of $15\text{--}45^\circ$ to the guide axis. The steam guide has four to six orifices tangential to the swirl chamber. The calculation method developed for this atomizer will be presented in section 5.4. A separate group of pneumatic atomizers—due to their high requirements—are those designed for combustion chambers of *gas turbines*. The basic feature of these atomizers is low air energy, which stems from the low air pressure drop because the air is taken from the engine circulation. For these

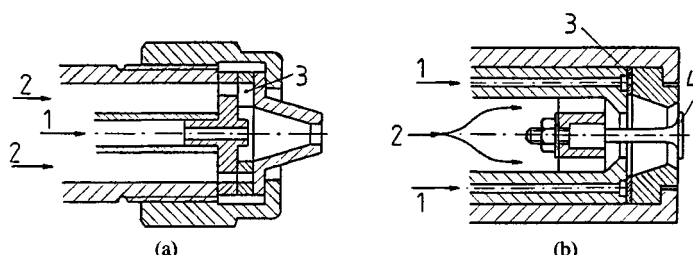


Figure 4-55 Two typical pneumatic atomizers with swirled flow: (a) swirled gas motion and axial liquid motion; (b) swirled liquid motion and axial gas motion. 1, Liquid; 2, gas; 3, plate with tangential orifices; 4, deflector.

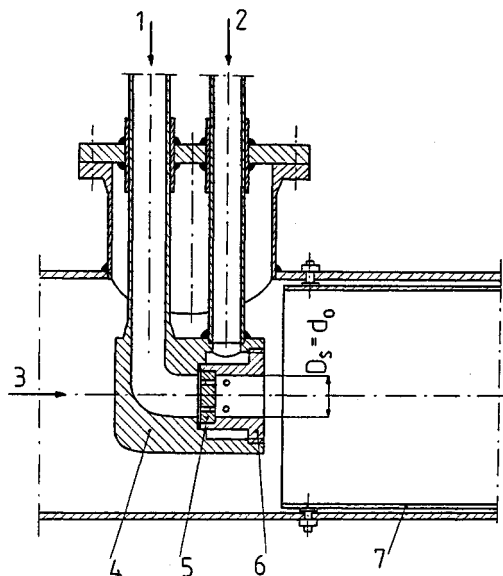


Figure 4-56 Pneumatic atomizer of water-steam type with an open swirl chamber. 1, Water; 2, atomizing steam; 3, attemperated steam; 4, atomizer head; 5, water orifices; 6, steam orifices; 7, shield.

reasons, attention is focused on the development of thin jets or films of the liquid.

In recent years research has been devoted to the development of two types of such atomizers. One is the plain-jet atomizer. The second is the prefilming atomizer, which has been developed by Lefebvre and is widely used.

Figure 4-57 shows a plain-jet atomizer [29]. This atomizer is used in the combustion chamber of an aircraft gas turbine. Liquid jets flow from 16 nozzles in the direction transverse to the swirled air jet. Extensive evaluation of these types of atomizers has been conducted in the following range of parameter

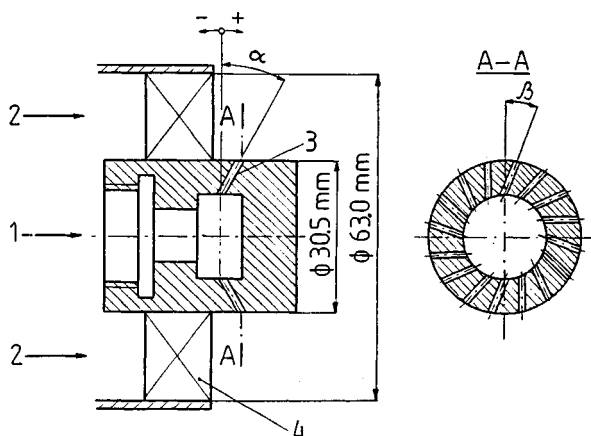


Figure 4-57 Schematic diagram of pneumatic jet atomizer. 1, Liquid; 2, air; 3, liquid orifices; 4, air swirler.

changes: liquid nozzle diameter 0.5–1.8 mm, angles of nozzle inclination $\alpha = -30$ to $+45^\circ$ and $\beta = 0$ – 60° , air velocity 35–80 m/s, and air/liquid mass ratio $b = 1$ –10. Results of the research of this atomizer will be presented in Chapter 6. It is possible to state that the inclination of orifices in the longitudinal and transverse cross sections affects the Sauter mean diameter (SMD). The SMD decreases as the air velocity increases and depends insignificantly on air/liquid mass ratio b . Increasing the liquid nozzle diameter results in an increase in SMD.

Figure 4-58 shows a pneumatic atomizer of the prefilming type. Its operation is based on the fact that one air jet flows along the liquid film and generates waves on its surface. The second air jet acts on the liquid film at the edge of the atomizer; this action proceeds in the region of very high shear stresses between the air jets that swirl in opposite directions. Such a countercurrent interaction allows reduction of the air flow rate.

It was established [2] that the thickness of the liquid film does not have a significant effect on the atomization quality. The liquid film thickens at the edge of the atomizer until the aerodynamic force becomes higher than the surface tension force; then separation and disintegration of the film occur. The droplet diameters decrease as the air velocity increases. When the fuel flow rate reaches a certain critical value, the wave structure of the film changes and drops start to separate from the film before the discharging edge. This critical flow rate is 0.6–0.8 m³/s per 1 m of perimeter of the atomizer's edge and in some instances can be much higher.

Figure 4-59 shows an atomizer that is used in the combustion chambers of

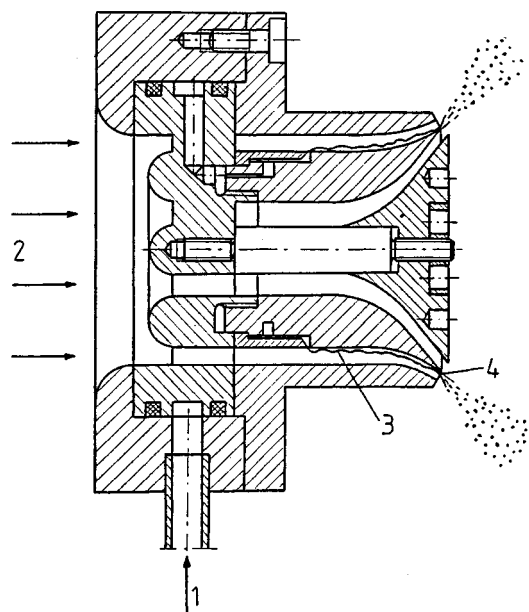


Figure 4-58 Prefilming atomizer (pneumatic atomizer operating on the principle of tearing off the liquid film from the outlet edge). 1, Liquid inlet; 2, air inlet; 3, wavy liquid film; 4, outlet edge.

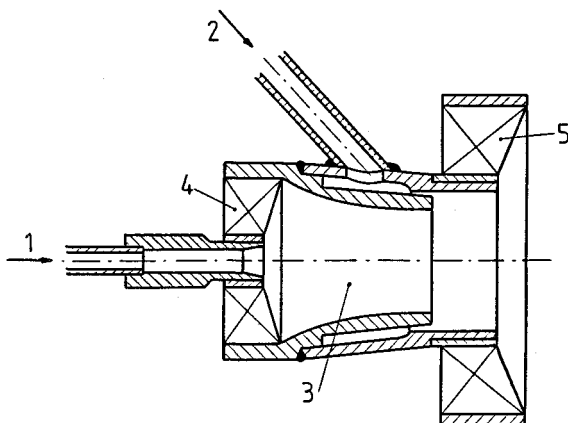


Figure 4-59 Design of an atomizer with two-stage fuel supply. 1, Stage I of fuel supply; 2, stage II of fuel supply; 3, mixing chamber; 4, internal air swirl; 5, external air swirl.

stationary gas turbines. This atomizer has two stages of fuel feed; stage I is the jet atomizer, and stage II has the form of an annular slot of 0.3 to 0.5 mm. In stage I the fuel is atomized by means of an internal air swirl and in stage II it is atomized by means of an external air swirl. Both vane swirlers are fed with the air from the gas turbine circulation and operate in the countercurrent regime. The atomizer of stage I operates during the starting of the engine; then in the nominal operating condition it is turned off.

Such a system of fuel feeding allows a lower fuel pressure and extends the failure-free running time of the system. Higher combustion efficiency and lower concentration of nitrogen oxide combustion products are achieved. It was determined that for an air velocity behind the swirl lower than 40 m/s the atomization is unsatisfactory and for air velocities higher than 80 m/s the flow resistance increases excessively. The air/liquid mass ratio is in the range $b = 2-8$.

In [16] the design of an atomizer used in the combustion chamber of a gas turbine is presented. The design is complex but allows reduction of air/liquid mass ratio to the value to $b = 0.3-0.5$. The fuel flows in the form of a film from a swirl atomizer and enters a region of two air jets swirling countercurrently. An additional annular air jet flows around the spray and forms its cone angle. Research showed that the efficiency of the operation depends on the mutual positions of the fuel and air jets.

The use of a pneumatic atomizer for the atomization of fuels in the form of the coal-water slurries as well as coal-heating oil and coal-heating oil-water slurries has been evaluated [17]. The coal-water slurry contained 70% of coal by weight and had an apparent viscosity of 0.5–0.75 Pa · s. A fuel film is subjected to an inner air jet swirled cocurrently and an outer air jet countercurrently. The fuel film thickens and that discharged from the atomizer was 1.0 or 1.4 mm, the fuel velocity was 3.1 or 2.3 m/s, and the largest size of the coal particles was 80 μm . The evaluation was conducted for air pressure up to 1.3 MPa and $b = 0.3$.

4-5 ROTARY ATOMIZERS

Rotary atomizers appeared about 100 years ago. The first patent application in the United States for an atomizer for the humidification and cooling of air was submitted in 1890 and the first rotary atomizer used in boiler furnaces appeared in approximately 1900. The atomization in the rotary atomizers occurs because of the mechanical energy supplied by a rotating element. Design efforts are directed toward ensuring effective transfer of this energy to the liquid. The general *advantages of rotary atomizers* are as follows:

Very viscous (see Table 1-5) and contaminated liquids can be atomized.

Liquid can be fed with low pressure.

Good atomization can be assured, in some instances close to monodisperse atomization.

Possibility of flow rate control without affecting the atomization quality (atomization is moderately insensitive to feed rate).

Rotary atomizers display minimal flow blockage.

High flow rates can be used.

Rotary atomizers can readily be cleaned.

Power consumption is relatively low.

The general *disadvantages of rotary atomizers* are as follows:

Design is complex, including a rotating element, drive with a transmission, bearings, and lubrication system.

High rotational speed is required to ensure high atomization quality.

High rotational speed reduces the reliability and requires appropriate protections.

Rotary atomizers generate large lateral spray cloud dispersion. In many instances this hinders spray utilization.

Rotary atomizers have an air pumping effect.

Rotary atomizers reached a high level of design development and found wide industrial application, mainly in spray drying, boiler furnaces, air conditioning, etc. Rotors with diameters up to 0.44 m or more are built with rotational speed up to 32,000 rpm and flow rate up to 100 m³/h [14].

Based on the method of fuel supply to the rotating element, rotary atomizers are classified as follows (Fig. 4-60):

1. Atomizers with direct axisymmetric liquid feed; the feeding system can be gravitational or pressurized.
2. Atomizers with a partially submerged rotating element where the liquid is fed due to the viscosity.

Direct liquid feeding to the rotating element is the usual method. Liquid feeding by means of a submerged rotating disk is rarely used. This is because

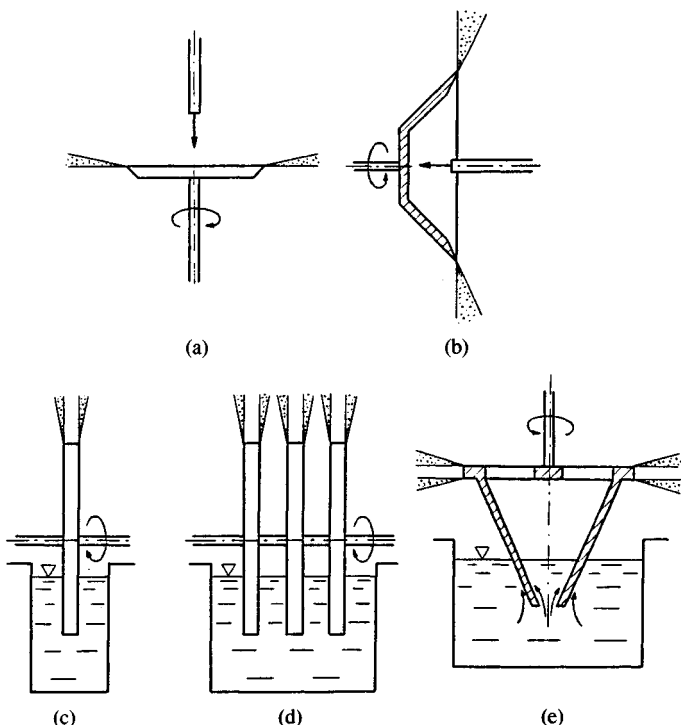


Figure 4-60 Various methods of liquid supply to rotary atomizers: (a, b) direct liquid supply to the rotating element; (c, d, e) liquid supply by submerging the rotating element.

(Fig. 4-60c and d) the liquid smears on the surface and then is centrifuged off the disk edge; three disintegration regimes discussed in Sec. 4-5.1 can occur, i.e., drop, ligament, and film type. This disintegration does not proceed uniformly on the disk perimeter [10]. In the rotating one (Fig. 4-60e) the liquid rises because of the centrifugal force on the inside and outside surfaces of the cone and subsequently separates from both edges.

Atomizers with submerged rotating elements are useful in cases in which the atomized liquid can be reused repeatedly, for example, in air washers during the humidification, cooling, and cleaning of the air.

Traditionally, rotary atomizers are divided into two groups: disk atomizers and impeller atomizers. Further considerations will be based on this classification.

4-5.1 Disk Atomizers

Disk atomizers are divided into (Fig. 4-61) flat disk atomizers, bowl atomizers, and cup atomizers. The term “disk” is a conventional one that comprises both

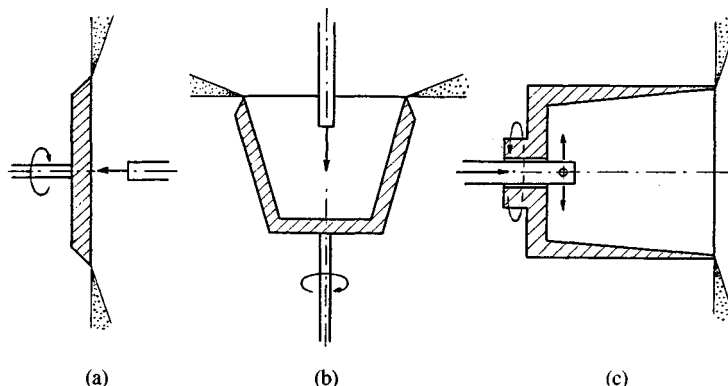


Figure 4-61 Schematic diagrams of disk atomizers: (a) disk atomizer; (b) bowl atomizer; (c) cup atomizer.

rotating flat and nonplanar elements. A common feature of these rotating elements is a smooth surface on which the liquid creates a thin film. The liquid film separates from the edge of the atomizer and disintegrates into droplets.

Depending on the liquid flow rates, three regimes of drop development are distinguished (Fig. 4-62):

1. Drop regime (Fig. 4-62a). For very low liquid flow rates a liquid annulus develops at the edge. Its thickness is controlled by the equilibrium of the centrifugal and surface tension forces. As a result of the disturbances, local thickenings develop from which single drops separate.
2. Ligament formation regime (Fig. 4-62b). As the flow rate increases, liquid ligaments form at the edge and disintegrate into drops.
3. Sheet formation regime (Fig. 4-62c). As the flow rate increases further a sheet forms and at a certain distance from the edge disintegrates into jets and drops. The drop sizes are less uniform than in the two previous regimes.

Flat disk atomizers. Flat disk atomizers are widely used because of the simplicity of the rotating element. The range of flow rate control is $\pm 50\%$ without any significant change in atomization quality. Flow rates of disk atomizers are small and can be increased only by implementation of a multidisk system.

Good atomization requires a high velocity of the film flowing off the disk edge. Atomization achieved in this way is not always satisfactory, so additional atomization using the air jets or the collision of drops with a solid object is often used. These are called hybrid atomizers.

An example of additional atomization using air jets is the atomization of water in a *humidifier*. A humidifier contains a rotating disk and an air fan, which constitutes an *air-assisted rotary atomizer*. Humidifiers are used for direct air

humidification in rooms. Disk diameters do not exceed 0.35 m. The rotational speed is in the range 3000 to 50,000 rpm (the highest speeds are related to disks of very small diameter). The water flow rate varies from a couple to several kg/h [24].

Figure 4-63 shows a schematic diagram of a humidifier (mist generator) [24]. The water is fed onto the inner surface of the conical disk. Water leaving the disk is atomized into a mist by an air jet. Mist is entrained by the air jet and blown into the room; a significant portion, however, deposits on the humidifier body and is returned to the water system.

Modern humidifiers have small dimensions. Energy consumption per kilogram of atomized water is in the range 0.01 to 0.06 kWh/kg. Humidifiers can operate independently or supplement central air conditioning. High quality and uniformity of atomization are required, since the drops should evaporate within a certain distance. Water should be chemically and physically treated.

Improvement of atomization can be achieved by the collision of drops with a splash ring located at the periphery of the humidifier (Fig. 4-64). The splash ring disintegrates the liquid into the drops with diameters of about 50 μm , which ensures that the drops can evaporate completely. It is worth mentioning that the mean drop diameters generated in the air washers using rotary atomizers are 200–500 μm and therefore the drops cannot evaporate. To supply the same

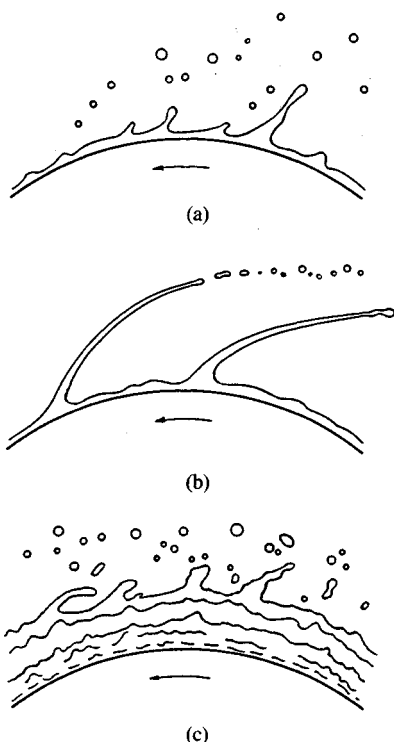


Figure 4-62 Three regimes of drop formation in disk atomizers: (a) drop regime; (b) ligament regime; (c) sheet regime.

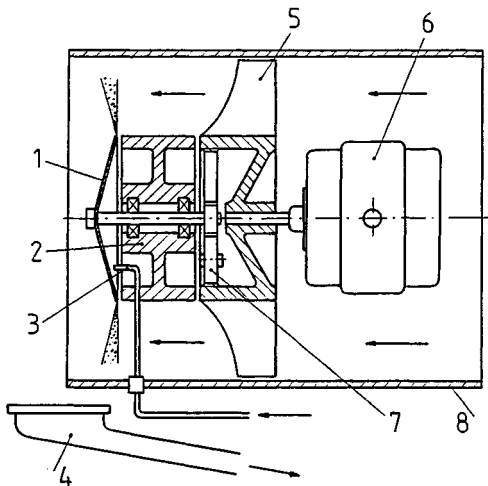


Figure 4-63 Schematic diagram of humidifier. 1, Atomizing disk; 2, stationary bearing mounting; 3, water supply; 4, water outlet; 5, axial-flow fan; 6, electric motor; 7, step-up gear; 8, body.

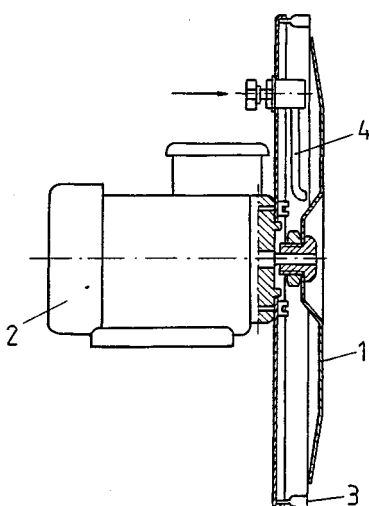


Figure 4-64 Humidifier with a splash ring. 1, Rotating disk; 2, electric motor; 3, stationary splash ring; 4, water supply.

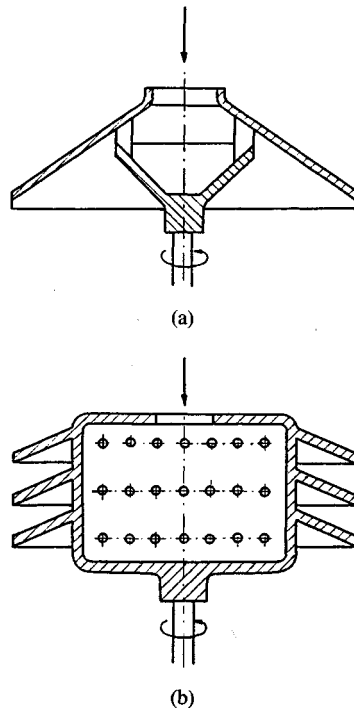


Figure 4-65 Bowl (conical) rotary atomizers. 1, Single-layer type; 2, multiple-layer type.

amount of moisture to the air in the latter case, one must repeat the atomization process 40 times [24].

Experimentally, the best results have been obtained for a disk with a diameter of 0.3 m and a rotational speed of 3000 rpm (circumferential velocities are of the order of 50 m/s). Maximum water flow rate of the humidifier was 300 kg/h and provided humidification of air flowing at 25000 m³/h in a channel with a cross section of 0.7 × 0.77 m.

Bowl atomizers. Bowl atomizers most commonly have the form of a truncated cone. They differ from cup atomizers only in the larger cone angle. Figure 4-65 shows examples of single-layer and triple-layer cone atomizers. Multilayered atomizers have higher flow rates and a wider spray. In order to distribute the liquid uniformly, the liquid layer should develop at the perforated inner surface. Liquid flows through the small orifices to the surface of the conical elements, where a liquid film develops, is centrifuged off the edge, and disintegrates [27].

The influence of surface smoothness on the film motion has not been investigated in detail. It is estimated that this influence is significant because of the small film thickness. Experiments show that the film thickness is less than 150 μm for a liquid of viscosity 45×10^{-6} m²s⁻¹ and the following parameters: bowl diameter $D = 0.05$ m, flow rate $G = 23$ kg/h, rotational speed $N = 4500$ rpm or $D = 0.1$ m, $G = 45$ kg/h, $N = 5600$ rpm [24].

The condition of the edge is important because edge irregularities are a source of drop nonuniformity. Uniformity of the film also depends on vibrations generated by the eccentricity of the bowl or by vibration of the drive. Drive vibrations are most effectively eliminated by using a belt drive.

Cup atomizers. Rotary atomizers in the form of a cup were applied mainly in oil boiler burners. The first design of such a burner was developed by the Ray Company (United States) in 1914. In Europe, the best-known manufacturer is Saacke. Both companies manufacture burners of their own design; the production of other companies is based mainly on licensing.

Cup atomizers enable the combustion of heating oils, residual fuel oil, paraffin wastes, used lubricating oils, etc. These fuels, in most cases waste fuels, are cheap and plentiful. The efficiency of operation of these atomizers depends basically on the fuel viscosity, and it is possible to warm the fuel by 100–200°C in the atomizer itself during the motion of the film on the cup surface. This warm-up proceeds mainly due to the furnace radiation.

An example of a burner with a cup atomizer is shown in Fig. 4-66 [6]. Fuel flows inside the hollow shaft to the rotating fuel distributor and subsequently flows into the cup through the radial orifices. Fuel flows on the inside surface of the cup to the lip, where it impinges with an air jet flowing through the annular slot outside the atomizer. As seen, this is a *hybrid atomizer of the pneumatic-rotary type*.

Another example of a pneumatic-rotary atomizer used in industrial spray drying is shown in Fig. 4-67 [13]. The liquid film discharging from the cup

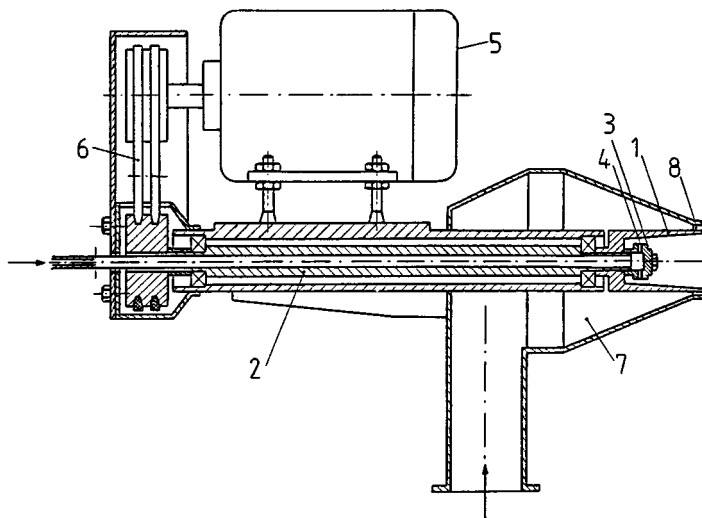


Figure 4-66 Schematic diagram of burner with a cup atomizer. 1, Atomizer; 2, hollow drive shaft; 3, fuel distributor; 4, radial orifices; 5, electric motor; 6, transmission; 7, air channel; 8, annular air slot.

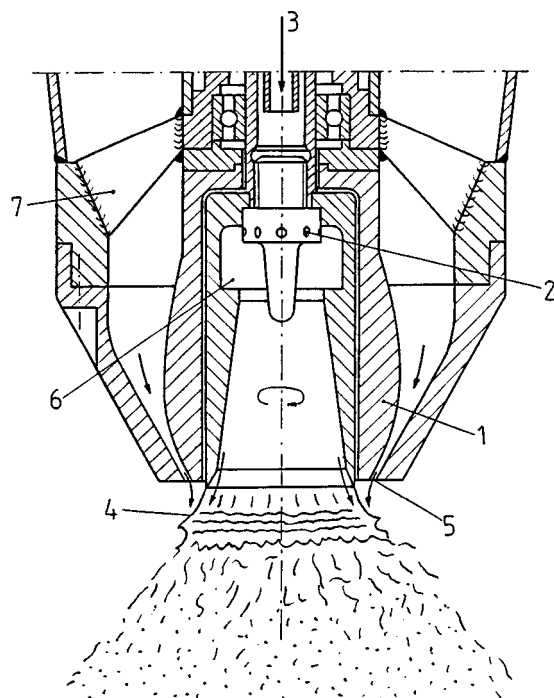


Figure 4-67 Spray nozzle of a rotary-pneumatic atomizer and mechanism of liquid sheet disintegration. 1, Cup; 2, liquid distributor; 3, liquid supply; 4, liquid sheet; 5, annular gas slot; 6, overflow; 7, blades [24].

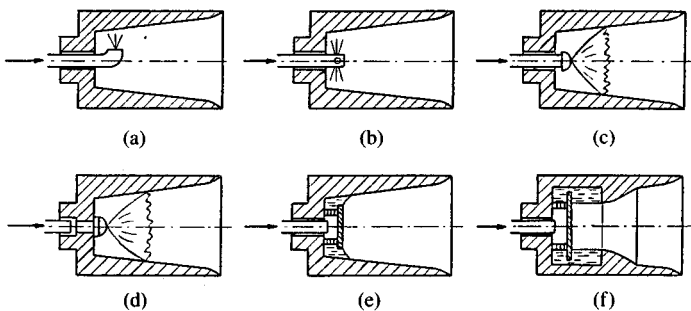


Figure 4-68 Various methods of liquid supply to a rotating cup: (a–c) Stationary liquid distributor; (d–f) liquid distributor rotating with the cup.

impinges, similarly to the case shown in Fig. 4-66, with a gas jet. Usually cold or warmed-up air and steam are used. The gas can be swirled initially. The air/liquid mass ratio is generally higher than $b = 2 \text{ kg/kg}$. The cone angle of the spray is small.

Pneumatic-rotary atomizers are used when atomization of very viscous liquids or very good atomization of less viscous liquids is to be achieved. The design of these atomizers is more complex than that of pneumatic and rotary atomizers but the operating costs are lower because liquid pumps, filters, heating systems, etc. are not necessary.

The liquid feed onto the cup surface can be achieved (Fig. 4-68) with a stationary liquid distributor or a distributor that rotates with the cup. Figure 4-68 shows the simplest design, with the liquid fed in the form of a single jet. The local increase of the film thickness at the location where the liquid is fed moves toward the cup edge, which impairs atomization uniformity. A significant improvement is achieved by feeding the liquid uniformly on the cup perimeter using radial orifices in the separator (Fig. 4-68b) or the swirl atomizer (Fig. 4-68c). In this latter case, coarse atomization takes place.

A distributor rotating with the cup has the advantage that at the points of contact between the liquid and the cup tangential forces, which would cause distortions of the film motion, are not present. In Fig 4-68d liquid is fed by a swirl atomizer. In Fig. 4-68e liquid is supplied by a stationary manifold to the chamber, from which it discharges through an annular slot between the rotating disk and the cup. Figure 4-68f shows a frequently used design with overflow in which the liquid rotates with the atomizer before it flows around the overfall edge.

4-5.2 Impeller Atomizers

Impeller atomizers found wide application in the dairy industry, paint industry, manufacturing of pharmaceuticals, ceramic industry, etc. Impeller atomizers have a large variety of designs (Fig. 4-69): vaned atomizers, atomizers with radial

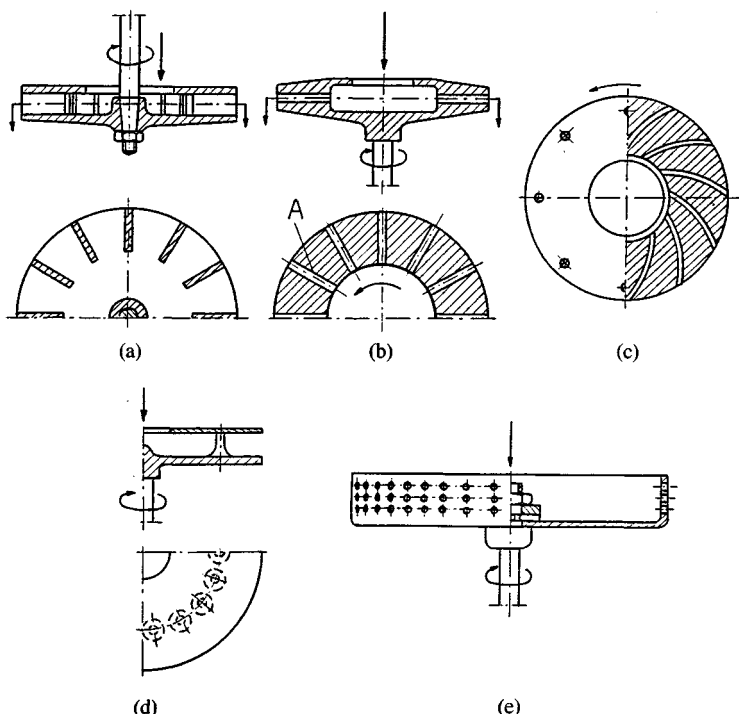


Figure 4-69 Centrifugal atomizers: (a) vaned atomizer; (b) atomizer with radial channels; (c) reaction blade atomizer; (d) atomizer with pin-type wheels; (e) atomizer with perforated rim.

channels, reaction atomizers, atomizers with pin-type wheels, atomizers with a perforated periphery, and porous atomizers.

Vaned atomizers (Fig. 4-69a). Vanes reduce slippage of the liquid on the impeller surface and increase the velocity of flow off the impeller edge, improving atomization quality. The simplest vaned atomizers have impellers with *straight vanes*. The vane passages usually have a rectangular cross section. Such passages are contamination resistant. The number of blades is in the range of 18–36.

Vaned atomizers can be single-impeller or multiimpeller types. Larger flow rates and larger spray widths are achieved in multiimpeller atomizers, but the feeding is less uniform in these atomizers. Liquid jets discharging from two adjacent impellers can impinge (NIRO Atomizer), which improves the atomization quality.

A variation with straight vanes is shown in Fig. 4-70. Liquid is fed into the impeller well and is centrifuged off on the internal wall. The liquid achieves a circumferential velocity almost equal to that of the impeller and therefore reaches the edge of the vane without impact. This allows improvement of the

uniformity of atomization, which generally is lower than for disk atomizers. The design shown in Fig. 4-70 is somewhat similar to the design shown in Fig. 4-68f, since it provides uniform development of the liquid film.

Impellers can have *curved vanes*. Such vanes provide impactless feeding of the liquid into the vane passages. The curved trajectory allows separation of dissolved gases, which in the case of spray drying results in high-density products [13].

Flow rates can be increased by increasing the length of the vanes. However, there is a problem with uniform liquid distribution along the whole vane length. This distribution can be realized by using throwers with sharp edges as shown in Fig. 4-71 (NIRO Atomizer).

Disadvantages of vaned atomizers are: manufacturing problems, especially in the case of multiimpeller atomizers; increased weight of the impeller (maximum diameter 0.22 m); and an air pumping effect.

The *air pumping effect* is a source of energy losses. These losses for small impellers are comparable to the atomization energy. Figure 4-72 shows the air circulation in the vicinity of a vaned atomizer used in industrial spray drying [24]. Because of the negative pressure at the inlet to the vane passages, air is sucked in and then blown out of the atomizer together with drops. The air pumping effect can be decreased by decreasing the height of the slot.

Atomizers with radial channels (Fig. 4-69b). These atomizers operate similarly to atomizers with straight vanes except that the rectangular passages are replaced by vane passages with a circular cross section. Diameters of the orifices are 3–10 mm, and the maximum number of orifices depends on their diameter and the impeller diameter. The impeller diameter is generally lower than 0.25 m. The radial channel can turn into nozzles at the outlet, creating so-called *nozzle atomizers*. Liquid does not flow through the whole passage cross section but along the back wall (A) with respect to the direction of rotation (Fig. 4-69b).

Atomizers with radial channels can be single or multilayered, and the latter have several layers of orifices depending on the required flow rate. Atomizers

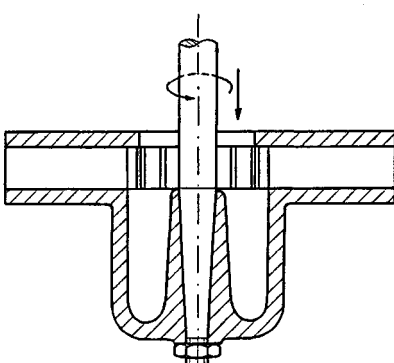


Figure 4-70 Atomizer with straight blades and pocket impeller.

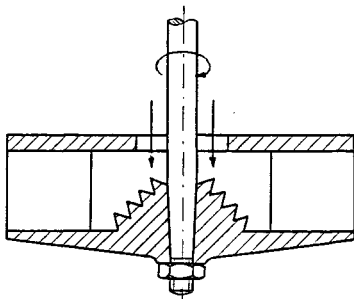


Figure 4-71 Impeller atomizer with a liquid thrower [24].

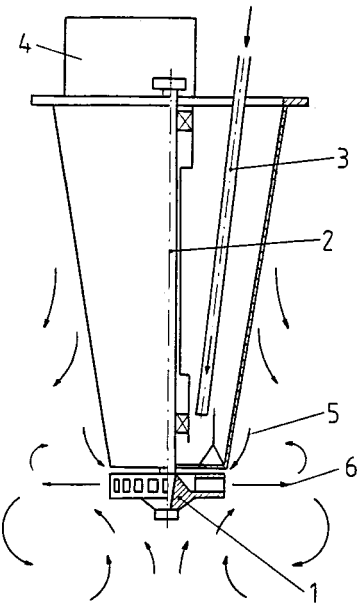


Figure 4-72 Air circulation around a blade impeller. 1, Impeller; 2, drive shaft; 3, liquid supply; 4, drive; 5, air sucked in the impeller gap; 6, jet of drops and air [24].

with radial channels have found wide application in industrial spray drying, where they operate with pressureless liquid feeding. These atomizers tend to clog, however.

Atomizers with radial channels have also been used in aircraft gas turbines with annular combustion chambers (Société Turboméca and others). A schematic diagram of such an atomizer is shown in Fig. 4-73 [24]. Fuel discharges from channels with a high velocity, which corresponds to the pressure drop $\Delta P = 13\text{--}16 \text{ MPa}$. Good atomization is also ensured for much smaller pressure drops. The rotary motion of the atomizer provides uniform fuel distribution in the combustion chamber. The channel cross sections are not filled with fuel completely and therefore can be large.

Straight radial orifices generate a spray similarly to jet atomizers. The radial channels can have screw inserts at the outlet which cause the liquid discharge to be similar to the discharge from a swirl atomizer. The screw channels can be used only for clean liquids.

Reaction atomizers (Fig. 4-69c). These atomizers can have numerous designs, varying from those with bent pipe channels of the Segner type to atomizers with bent slot channels as shown in Fig. 4-69c. Torque is determined by the reaction forces at a certain distance from the axis of rotation. The reaction results from

the liquid discharge from the channels. Reaction atomizers do not require mechanical drive. Liquid disintegration proceeds in a similar way as for jet atomizers.

Atomizers with pin-type wheels (Fig. 4-69d). These atomizers use the effect of the collision of liquid with solid objects inside the impeller. Pins, which can be of various shapes, are usually located along several concentric circles. These atomizers have a large scatter of drop diameters with large diameters prevailing. The wheel has high strength and therefore the diameters can be larger than the aforementioned value of 0.44 m.

Atomizers with a perforated periphery (Fig. 4-69e). These are rotary atomizers with an impeller in the form of a semiclosed or closed drum with a large number of orifices in the outer wall. Instead of a rotating perforated drum, mesh drums can be used. The axis of rotation is usually vertical but in some cases can be horizontal. Examples of the latter case are the fan atomizers with rotating wire mesh drums used for orchard spraying.

Atomization in a perforated impeller proceeds differently than in the cases discussed earlier. The liquid film flows to the perforated periphery and moves upward on the wall. Centrifugal force presses the film through the orifices, outside which it disintegrates into small droplets. The thinner the film and the higher the angular velocity of the impeller, the smaller the droplets are.

In perforated impellers a different atomization mechanism can also take place when the thick liquid film adjacent to the orifices rotates along with the drum. The liquid discharges in the form of thin jets, which disintegrate into drops [36]. Such atomizers or splashers do not ensure proper atomization and

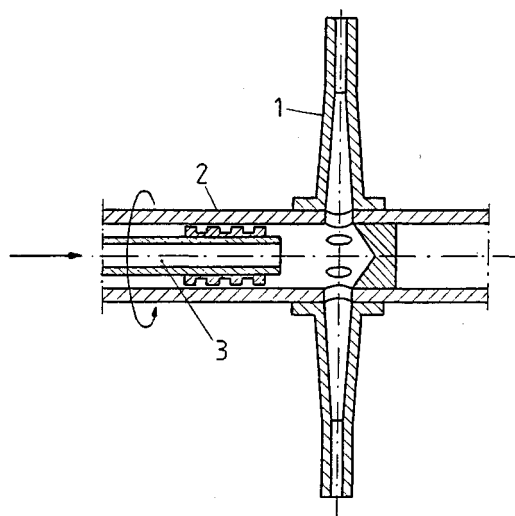


Figure 4-73 Rotary atomizer with radial channels. 1, Impeller atomizer; 2, turbine shaft; 3, stationary fuel manifold.

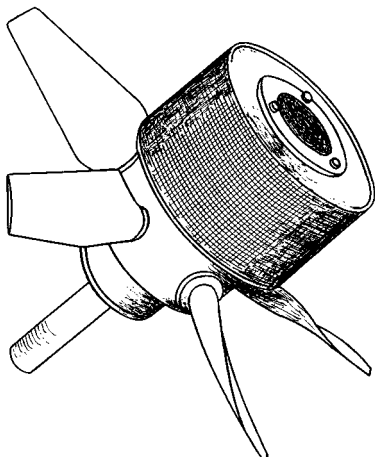


Figure 4-74 Atomizer with a rotating mesh drum (Micro-nair AU 4000) [38].

are used in the production of granules, e.g., fertilizers. Calculations for such an atomizer will be presented in Chapter 5.

Yet another atomization mechanism is present in atomizers with rotating wire mesh drums [38]. Such atomizers supplemented by a fan are used in agricultural treatments in which the spray has to be directed onto the object. An example of such an atomizer is shown in Fig. 4-74. This is an aerial atomizer for spraying pesticides in a narrow range of drop diameters, $15\text{--}55 \mu\text{m}$. For a rotational speed of 14,000 rpm and a flow rate of 2 l/min, the experiments showed that 80% of drops by volume had diameters in this range. The experiments were conducted in a wind tunnel for wind velocity 49 m/s, i.e., a velocity typical for an aircraft.

A drum of diameter 0.127 m made of a 20 mesh (number of orifices per inch) screen is attached to a hub with five adjustable fan blades. The whole system is mounted on a hollow shaft through which the liquid is fed from a stationary distributor. The distributor, in the form of a perforated pipe, atomizes the liquid preliminarily and supplies it uniformly to the rotating drum, where the final atomization takes place as the liquid passes through the screen.

Porous atomizers (Fig. 2-51). Rotary atomizers with porous wheels have the important advantage that they generate drops with a small scatter of diameters and are therefore used as monodispersive generators. This has been discussed in Sec. 2-6.

4-6 MISCELLANEOUS ATOMIZERS

Industry imposes new requirements that cannot always be satisfied by the atomizers described so far. Here are some examples of these requirements:

1. Atomization of very small quantities of a liquid in inhalation chambers, closed circuit climatic chambers, etc. In these cases the desired orifice diameters are too small. For example, for atomization of 5 l/h of water at a pressure of 0.2 MPa, a rotary atomizer with a discharge orifice diameter as small as 0.25 mm is required.
2. Atomization of very large quantities of liquid, e.g., the atomization of hundreds or even thousands of cubic meters of water in the cooling towers of power plants. In this case, the economic aspect of the atomization process should be considered.
3. Atomization of contaminated liquids or chemically aggressive liquids; an example is gas cleaning with water recirculation.
4. Atomization of very viscous non-Newtonian liquids with multichain molecular structures.

To satisfy these requirements, new methods of atomization are sought. Additional forms of energy can be used for liquid atomization, such as energy of vibrations or electric energy. Based upon these possibilities the following types of atomizers have been developed: acoustic atomizers, ultrasonic atomizers, electrostatic atomizers, and pulsary atomizers.

These atomizers do not represent all of the possibilities. For example, the process of liquid saturation with a gas can be used. Gas supplied prior to the atomizer or inside the atomizer increases significantly the surface energy of the liquid and decreases its effective viscosity. Gas in the form of bubbles is compressed inside the atomizer to the pressure of liquid and during the discharge expands rapidly, causing the drops to be smaller than in pressure atomizers. The quantity of gas can be significantly smaller than in pneumatic atomizers.

4-6.1 Acoustic Atomizers

Acoustic atomizers operate on the principle of superposition of the acoustic vibrations generated by a gas flowing with supersonic velocity on the fluid. The vibration frequency in the audible range equals 0.016–20 kHz. Acoustic atomizers require that the gas be used as in pneumatic atomizers, but there are the following differences between those two types:

Acoustic atomizers use a different form of gas energy than pneumatic atomizers. Acoustic atomizers ensure better quality and uniformity of atomization for the same conditions.

Acoustic atomizers are more economic and have better prospects in the future. Design of acoustic atomizers is more complex.

There are two hypotheses about action of the gas on the discharging jet or film of the liquid, but neither of them completely explains the mechanisms of this action [27]. The first hypothesis explains the atomization in terms of

capillary waves that develop at the liquid surface; the tips of the waves separate in the form of drops. The second hypothesis (cavitation) is based on the assumption that the acoustic waves (expansion and compression) are involved: during the cycle of expansion regions of evaporated liquid develop and their blowout during the compression causes liquid atomization.

It follows from experiments that cavitation plays a role at very high vibration frequencies, which are very rare in acoustic atomizers. In this situation the capillary wave hypothesis is relevant. However, the following calculation shows that the acoustic waves cannot directly cause the development of drops. If one assumes that the wavelength is comparable to the drop diameter ($\lambda \approx D$), then in order to generate drops of diameter $D = 20 \mu\text{m}$ ($2 \times 10^{-5} \text{ m}$) the following frequency of vibrations is needed:

$$f = \frac{c}{\lambda} = \frac{1000}{2 \times 10^{-5}} = 50 \text{ MHz}$$

where $c \approx 1000 \text{ m/s}$ is the wave velocity.

As seen, a very high frequency of vibrations is required for atomization, whereas for frequencies as low as several kHz it is possible to generate drops with diameters of several micrometers in acoustic atomizers. Hence, the mechanism of disintegration is more complex and depends strongly on the relative velocity of the gas and the liquid. Quantitative information on acoustic atomization can be derived only empirically.

Acoustic atomizers have various *generators of acoustic vibrations*. Atomizers with a Hartmann generator are used most and will be discussed in detail, whereas atomizers with static, dynamic, and swirl generators will be only mentioned.

Acoustic atomizers with a Hartmann generator. The Hartmann generator is a mechanical transducer that is used to generate acoustic waves (Fig. 4-75). Gas leaving the nozzle with high velocity is subjected to the wavy disturbances caused by a *resonator* located in front of the nozzle. The frequency of acoustic waves depends on the diameter d and the depth h of the cavity of the resonator and on the distance l between the nozzle and the resonator. In order to obtain

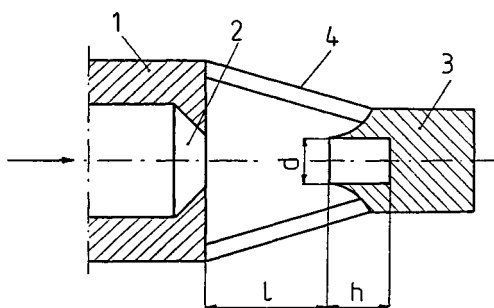


Figure 4-75 Hartmann generator. 1, Body; 2, gas nozzle; 3, resonator; 4, resonator holder.

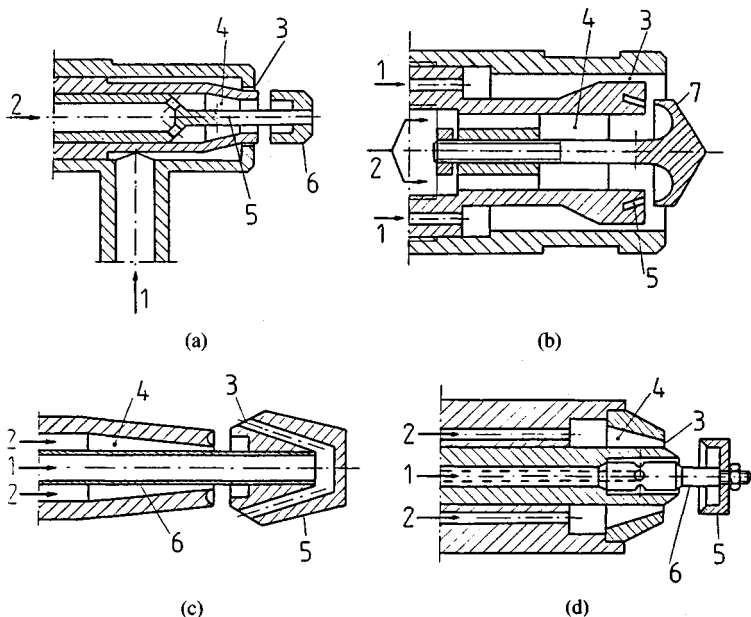


Figure 4-76 Acoustic atomizers with Hartmann generator: (a) with liquid supply through a slot; (b) with reversed gas supply; (c) with reversed liquid supply; (d) with liquid-gas mixture supply to the resonator. 1, Liquid; 2, gas; 3, liquid slit; 4, gas nozzle; 5, resonator; 6, resonator stem; 7, deflector.

an acoustic atomizer one must supplement this gas system with a liquid system. The liquid system should form thin jets or a film of the discharging liquid; the most desirable is a swirled film. The problem of film stability has been discussed extensively [9].

Commonly used designs of acoustic atomizers are shown in Fig. 4-76. These are the atomizers with a stem-type Hartmann generator, as opposed to the generator without a stem shown in Fig. 4-75.

An atomizer with slit liquid feed (Fig. 4-76a) seems to be the most established design, since the very thin liquid film generated in this atomizer disintegrates easily in the field of the acoustic vibration. Liquid can also be swirled, which allows disintegration of even very viscous liquids. A design in which thin jets of liquid are fed to the atomizer is also used.

An atomizer with returnable gas feed (Fig. 4-76b) is characterized by the fact that the gas jet is returned by a deflector (7) which is placed at the end of the stem. This jet enters the annular space in resonator 5, which is located in the atomizer's housing, not at the end of the stem.

An atomizer with returnable liquid feed (Fig. 4-76c) operates on the following principle. The liquid flows in through the hollow stem to the back side of the resonator, where it changes the direction of flow, and through the annular slit it enters the region of atomization.

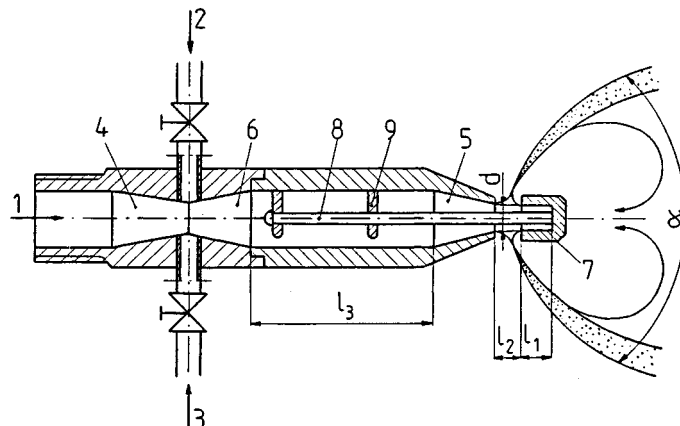


Figure 4-77 Two-liquid acoustic atomizer with a liquid-gas mixture supply to the resonator. 1, gas; 2, 3, two different liquids; 4, first nozzle; 5, second nozzle; 6, mixing chamber; 7, resonator; 8, resonator stem; 9, stay. $d = 5$ mm; $l_1 = l_2 = 2.5$ mm; $l_3 = 50$ mm.

An atomizer in which the liquid-gas mixture is fed to the resonator (Fig. 4-76d) has channels with relatively large cross sections and slots through which the liquid flows, which protects them from clogging. Another feature of this atomizer is that it has a swirl chamber where the liquid-gas mixture is initially produced.

Figure 4-77 shows a variation of the atomizer in Fig. 4-76d. This device is used to atomize mixtures of heavy heating oils with water in boilers [22, 23]. Both liquids are subjected to initial atomization and mixing with gas in the first nozzle (4). Further mixing occurs in the mixing chamber (6), and initial disintegration of the mixture is caused by collisions with the stays (9) of the resonator stem. The final atomization occurs in the resonator region. It has been established that the optimum ratio of the depth and the diameter of the cavity of the resonator is $l_1/d = \frac{1}{3}$ to $\frac{1}{2}$. Under these conditions a spray with a large spray angle α develops. A certain portion of small drops is entrained to the region of recirculation behind the resonator.

This atomizer in its industrial version has a flow rate of 3 t/h and is used in a boiler producing 16 t/h of steam. Heavy heating oil (U.S. No. 2 to No. 6) was mixed with water and the steam was used as a gas in the quantity $R = Q_G/Q_L = 250$, where Q_G and Q_L are the volumetric flow rates of steam and liquid, respectively. Very good atomization was achieved. By adding water the emission of NO_x was reduced. Maximum water content was 24%.

Acoustic atomizers with a static generator. Operation of this type of atomizer is similar to that of a static acoustic horn in which compressed gas is supplied to a dual toroidal space with sharp edges. Part of the gas jet reflects and crosses with the remaining part of the jet, which leads to intermittent gas discharge

and the development of vibrations. Liquid supplied to this region undergoes disintegration.

Acoustic atomizers with a dynamic generator. The operation of such an atomizer is based on mechanical breaking up of gas jet by a rotating disk, as takes place in a dynamic acoustic horn. In this particular case, the compressed gas drives the turbine with a disk mounted on the shaft. The gas jets leaving the turbine are cut off by the disk, which generates strong acoustic vibrations that cause liquid disintegration.

Acoustic atomizers with a rotating generator. In design these are similar to swirl atomizers. Compressed gas flows in through the tangential channels to the swirl chamber, where it creates a vortex. Negative pressure develops in the vortex core and causes the gas flow. This cycle is repeated, generating pressure pulsations in the core of the vortex and therefore generating acoustic vibrations. These vibrations are used for liquid atomization.

4-6.2 Ultrasonic Atomizers

Ultrasonic atomizers operate on the principle that the liquid in contact with the element of the generator vibrating with ultrasonic frequency (over 20 kHz) disintegrates into drops with diameters of order 30–60 μm and with a small size scatter. This is due to an increase in the surface energy of the jet or film of liquid. An essential role in the process of atomization, as mentioned in Sec. 4-6.1, is played by cavitation.

An advantage of these atomizers is low electric power consumption, approximately 30 W. As opposed to other atomizers, the liquid does not have to be supplied under pressure, which is advantageous in the case of viscous and contaminated liquids. A disadvantage of these atomizers is their low flow rate, but in the most recent developments the flow rate is as high as 50 l/h (Lechler). Another disadvantage is that a complex and expensive ultrasound generator is necessary.

The development of ultrasonic atomizers is discussed in [19]. The evaluation of the ultrasonic atomizer shown in Fig. 4-78 is also presented. Vibrations with a frequency of approximately 26 MHz are generated using the Hartley oscillator. This oscillator is connected to the vibrating stem with a horn. The stem vibrates vertically in the axial direction and the liquid flowing down along the stem and the horn disintegrates.

In practice, vibration energy is supplied to the liquid jet or sheet by using either a magnetostrictive vibrator or a piezoelectric transducer.

A *magnetostrictive vibrator* operates on the principle that if a stem or a pack of stems made of a magnetostrictive material (nickel, nickel alloys with aluminum and iron, ferrite, etc.) is placed in an alternating magnetic field, the dimensions of the stem will change. These changes occur during the two half-periods of the alternation of the magnetic field; i.e., the vibration frequency

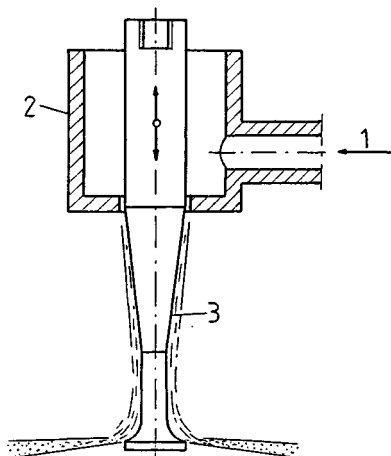


Figure 4-78 Ultrasonic atomizer. 1, Liquid supply; 2, well; 3, vibrating stem with a horn.

of the stem will be twice as high as the frequency of the magnetic field. The maximum amplitude of the stem vibrations occurs at resonance, when the frequency of free vibrations is equal to the frequency of alternation of the magnetic field.

Magnetostrictive vibrators applied to the ultrasonic atomizers are not sufficiently developed. Generators with frequencies up to 60 MHz are used at present. The evaluation of such a generator equipped with a ferrite vibrator operating at 30–35 MHz is discussed in [7]. The process of atomization is a function of many variables. It has been established that the flow rate and the mean drop diameter decrease with increasing vibration frequency.

A piezoelectric transducer operates on the principle that a piezoelectric element connected to a high-frequency electric field vibrates in accordance with the oscillations of the electric field. If the piezoelement is in contact with a liquid, it generates ultrasonic waves in the liquid. The maximum effect occurs at resonance, when the frequency of oscillations of the electric field is equal to the frequency of free vibrations of the piezoelement. The piezoelement has practically no inertia, so very high frequencies of vibration, up to 10^5 – 10^6 kHz can be obtained. The application of a piezoelectric transducer to the generation of uniform drops is discussed in [35].

4-6.3 Electrostatic Atomizers

Electrostatic atomizers have been the subject of intensive research in the past 25 years. Electrostatic atomization is applied in various fields, such as paint spraying, rocket propulsion, emulsion component production, thin film coating, meteorological experiments, and pollution research [5].

A new technique for generating thin sprays whose disintegration proceeds in a controllable manner has been developed. These sprays can be deflected

electrostatically to a precise position on a target (for example, in ink jet printing). By using a proper design of the nozzle and controlling the flow rate and the electric field, liquid can be disintegrated into many jets that generate drops with a very small size scatter that are used in agricultural treatment.

Production of fine metal powders can be based on electrostatic atomization. A wire is introduced into a region where it is bombarded by electrons generated in a thermoionic emitter. The wire melts and is atomized into particles of the desired sizes. Particles with diameters smaller than $0.01 \mu\text{m}$ as well as particles with diameters of $10\text{--}100 \mu\text{m}$ can be generated. Use of many such atomizers allows the production of 0.5 ton of powder per day [4].

The mechanism of atomization is as follows. When liquid in the form of a jet or a film enters a strong electrostatic field, a certain distribution of pressure develops on the liquid surface and causes deformation and disintegration into drops. The generated drops take up an electric charge, and as a result their internal pressure and surface tension decrease. In this situation the effectiveness of the aerodynamic forces acting on the drops and their tendency to monodisperse atomization increase. If the liquid prior to or during the discharge experiences a strong electric charge it disintegrates into drops with sizes such that the disintegrating forces are balanced by the forces of surface tension.

There are two different cases of electrostatic atomization:

1. Electrostatic forces are too small to atomize the liquid but the drops receive a large electric charge. The electric charge transfer to the liquid is achieved by ionized-field particle charging, i.e., corona charging or induction charging.
2. Electrostatic forces are large enough to atomize the liquid and drop charging is not relevant. The transfer of the electric charge to the liquid proceeds through direct contact (contact charging).

The first case is represented by so-called hybrid atomizers in which the liquid is atomized basically in pressure, pneumatic, or rotary atomizers and the drop charging ensures their better use. For example, during agricultural treatment the charged drops are more resistant to drift and cover the plants better; unfortunately, only some pesticides can be electrically charged.

Law developed an electrostatic atomizer for agricultural treatment (Fig. 4-79) [4]. This is a hybrid pneumatic atomizer in which air flowing with transonic velocity atomizes liquid. The electrode potential is relatively small, of the order of several hundred volts. The median diameter of drops is in the range $30\text{--}50 \mu\text{m}$ for a liquid flow rate of approximately 1 ml/s . For low voltage the electric field between the atomizer and the plant is weak and therefore the drops are driven by air.

Electrostatic atomization depends on the electrical resistivity of liquid. One distinguishes conducting liquids, such as water, water solutions, and metals, which have resistivity lower than about $10^4 \Omega\text{-m}$; semiconducting liquids, which have resistivity of $10^4\text{--}10^6 \Omega\text{-m}$; and nonconducting liquids (isolators).

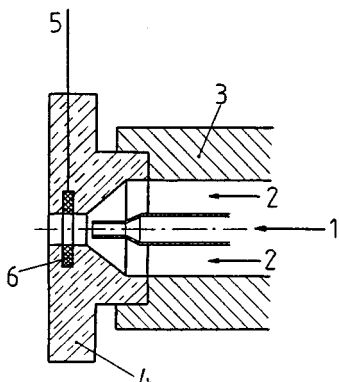


Figure 4-79 Electrostatic atomizer. 1, Liquid; 2, compressed air; 3, metal body; 4, insulator; 5, HV connection; 6, embedded electrod.

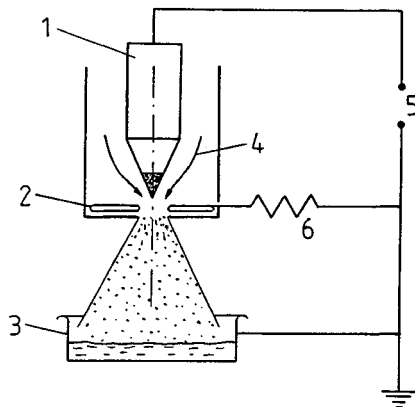


Figure 4-80 Schematic diagram of spray triode atomizer. 1, Emitter electrode; 2, blunt electrode; 3, collector electrode; 4, liquid supply; 5, voltage source; 6, resistor.

In 1952, B. Novvegut and L. Neubauer proposed an idea that is applied in modern theories of electrostatic atomization. According to this idea, the energy of the drop system consists mainly of the surface energy and electric energy tends to reach a minimum during atomization. This idea was further developed by Bailey [4].

Liquid atomization by electrostatic forces only takes place in “electrodynamic” atomizers. An example of such an atomizer is Electrodyn (manufactured by ICI) used for plant spraying [4]. This atomizer generates a strong electric field between two concentric electrodes. The inner electrode has a voltage of 15–25 kV. The liquid consumption is 0.5–2 l/ha and the flow rate is 0.1–0.2 ml/s. Drop diameters are 40–200 μm . The drop size scatter is about five times less than for pressure atomizers.

Atomization of hydrocarbon fuels, which are liquids with high electrical resistivity, has been investigated by Kelly [12]. Figure 4-80 shows a schematic diagram of a spray triode atomizer. Operation is based on the fact that a potential difference exists between the central electrode (1) submerged in the fuel and electrode 2. The electrodes represent an electron gun. Fuel flows around electrode 1 and to the discharge orifice. Charge is transported to the electric circuit by electrode 3, which in the combustion system has the form of the flame front and the combustion chamber walls. The fact that electrode 1 is submerged in fuel (isolating liquid) prevents the formation of a corona discharge.

This type of atomizer has low power input and provides well-atomized fuel drops with diameters of 10–100 μm . The fuel viscosity should be lower than 25×10^{-4} Pa · s. One can atomize fuels with flow rates higher than 0.1–0.2

ml/s, which is considered to be the minimum value in practical applications. Attempts to use this type of atomizer in diesel engines were made.

4-6.4 Pulsatory Atomizers

Pulsatory atomizers operate on the principle that additional disturbances are super-imposed on the atomized jet of liquid and these disturbances are the pulsations of the flow or the liquid pressure—in most cases both of them. The result is acceleration of loss of stability of the liquid and improvement of atomization quality. The advantage of pulsatory atomizers is the improvement of the quality and uniformity of the atomization, which does not require increased power input and does not complicate the atomizer's design.

Atomizers operating only on the principle of pulsation do not exist, but pulsations can be used in all the methods of atomization we have discussed. Thus there are pulsatory jet atomizers, pulsatory swirl atomizers, etc., that is, typical hybrid atomizers. The frequency of pulsations is low and does not exceed 200 Hz. Two different methods of pulse generation exist [27]:

1. *Throttling pulsation*, i.e., pulsation of liquid flow due to instantaneous blocking of the flow channels.
2. *Induced pulsation*, i.e., pulsation of pressure in the feed channel induced by a piston pulser.

Information about the influence of pulsations on atomizer operation is limited. Experiments showed that the effect is significant but different for both methods of pulse generation. For example, in jet-swirl atomizers during throttling pulsations a small decrease of the flow rate is observed accompanied by a significant improvement of the atomization quality, which is not observed in the case of the induced pulsations.

Figure 4-81 shows schematic diagrams of three pulsatory atomizers based on the design of jet, swirl, and pneumatic atomizers.

Pulsatory-jet atomizers (Fig. 4-81a) operate using a spring and a valve. Because of liquid pressure the spring bends and the valve opens. When the valve is open the liquid pressure drops rapidly, which causes valve closure, and the cycle repeats.

Pulsatory-swirl atomizers (Fig. 4-81b) generate a pulsating flow by means of a rotating breaker. The flow is disrupted when liquid jets flowing from the grooves of a screw swirler are blocked by the rotating breaker. The pulsation frequency can be controlled by changing the rotational speed of the breaker stem or by changing the number of breaker orifices. The breaker shown in Fig. 4-81b rotates because of liquid flow.

Pulsatory-pneumatic atomizers (Fig. 4-81c) operate by using pulsations of gas and liquid. The pulsator has the form of a membrane (1) that separates liquid chamber 2 from gas chamber 3. Increased pressure causes bending of the

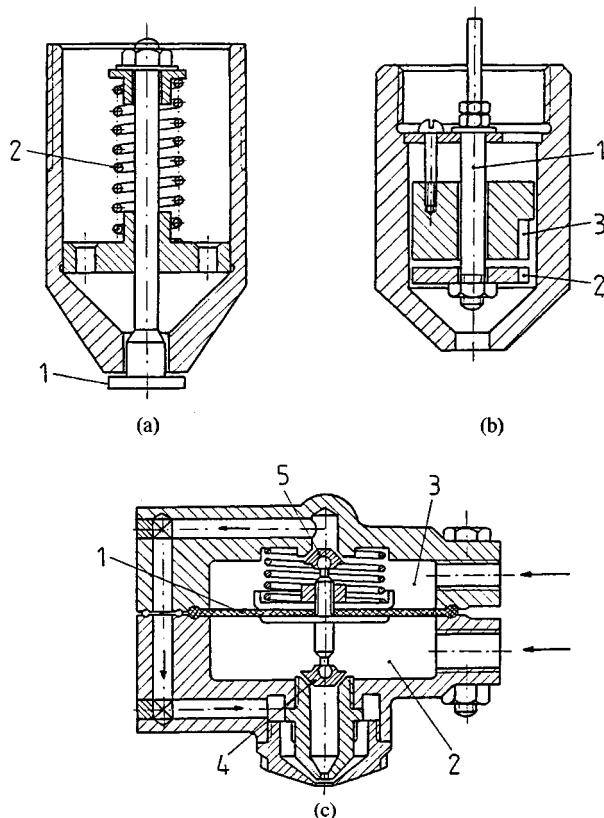


Figure 4-81 Pulsatory atomizers. (a) Pulsatory jet atomizer; 1, valve; 2, spring. (b) Pulsatory swirl atomizer; 1, stem; 2, rotary breaker; 3, screw swirler. (c) Pulsatory pneumatic atomizer; 1, membrane; 2, liquid chamber; 3, gas chamber; 4, 5, valves.

membrane and the closure of valve 5 and opening of valve 4. At this stage the liquid pressure drops rapidly, which causes the membrane to assume the initial position, and the cycle repeats.

4-7 MATERIAL, TECHNOLOGICAL, AND MAINTENANCE PROBLEMS

Our considerations of material, technological, and maintenance problems encompass only diesel atomizers and swirl atomizers. This is because these types of atomizers are most commonly used and the requirements imposed on them are high.

4-7.1 Materials

The catalogs supplied by atomizer manufacturers, i.e., Spraying Systems, Lechler, Delavan, G. Schlick, and others, show that over 100 different materials are used in atomizer production. These are nonferrous metals, carbon steels, alloy

steels, plastics, ceramics, etc. The type of material depends primarily on the atomizer application. Since high precision is required for the atomizer elements, the materials used should be easy to machine.

Diesel atomizers are composed of many elements, each of which requires different material. The two most important elements, the nozzle and the pintle, require materials with proper hardness and heat treatment. The nozzle can be made of, for example, carbon steel with 1% Cr, and the pintle is made of stainless steel containing 3–5% Cr, 2% V, and 18% W. The pintle is hardened in oil at 1200°C and tempered at 550°C [24].

Swirl atomizers are characterized by high liquid velocity in the swirl chamber and therefore require wear-resistant materials. Atomizers used in industrial spray drying and during powder production are made of alloy steels, tungsten carbide, silicon carbide, alumina, etc. [13]. Wear resistance of these materials is 10 times higher than that of steel.

In the swirl atomizers incorporated in boiler burners operating on residual fuel oil, ceramic metal materials based on temperature-resistant tungsten carbides, titanium carbides, chromium carbides, etc. are used. Application of such materials in stationary gas turbines with 100 MW power can increase their lifetime to 8000 to 10,000 hours, i.e., by 10-fold compared to steel atomizers.

Low-pressure swirl atomizers exposed to moisture are usually made of brass. Atomizers exposed to corrosive liquids or operating in a corrosive environment require corrosion-resistant materials such as stainless steel, titanium, tantalum, and plastics (polyvinyl chloride, polypropylene, polytetrafluoroethylene, etc.).

4-7.2 Atomizer Technology

The toughest technological requirements are imposed on atomizers with intermittent operation. This is dictated by their complex design and specific operating conditions. Production of atomizers is in general large-scale and therefore requires specialized machines.

Atomizers should have leaktight pintles and seats as well as general tightness at a pressure of tens of megapascals. The clearance between the pintle and the guide in small piston engines is 2–3 μm and in big ship engines is 3–6 μm . The cone of the pintle should fit to the seat on the narrow annular surface because the cone angle of the pintle is usually larger by 1° than the cone angle of the seat, and the coaxiality of the cone is approximately 0.25 μm .

Thermochemical treatment consists mainly of hardening and carburizing. In order to improve wear resistance, gas nitriding is used. The pintle seat is usually chrome plated (galvanic treatment). Grinding and lapping are used as the finishing treatment. After lapping, the pintle and nozzle are a precise pair.

Discharge orifices also require very precise machining. The inside edges of these orifices must be rounded off, for which purpose electrochemical treatment is used. Unfinished edges can cause a variation in the fuel flow of tens of percent, whereas acceptable variations should be at maximum 5–10%. It is

especially difficult to drill deep orifices, whose depth in some instances exceeds 50 diameters.

High technological requirements regarding both dimensional tolerances and surface roughness result in more precise quality control techniques. The most difficult to control is the conical shape of the pintle and seat. In addition to control of the individual operations in the production process, the final product is subjected to quality inspection.

Production technology for swirl atomizers is simpler. Attention is directed mostly to the coaxiality of the discharge orifice and the swirl chamber. For a swirl atomizer of the design shown in Fig. 4-23 the disk surfaces should be ground and lapped. Atomizers used in combustion chambers of gas turbines contain elements made of hard metal ceramics, for which special techniques of pressing and sintering with minimum grinding allowances are required. Orifices in this case are drilled using the electroerosion method.

Inaccuracies in finishing swirl atomizers result in incorrect circumferential distribution of the liquid density $q = f(y)$. As mentioned in Sec. 3-2.3, circumferential nonuniformity is especially important in the case of combustion chambers of aircraft gas turbines. The higher the flow, the smaller is the effect of technological errors on the circumferential nonuniformity.

All dimensional deviations, including the allowable deviations, result in significant variations in flow rate. In boiler atomizers the allowable dimensional deviations can cause as much as 15% flow rate variation, which necessitates control measurements and selection of atomizers. In industrial driers the variations of the flow rate and spray angle should not exceed 3–6% [13]. Powder metallurgy allows for manufacture of atomizers with flow rate variations lower than $\pm 3\%$.

4-7.3 Maintenance of Atomizers

Atomizers with discontinuous operation have especially severe operating conditions: cyclic mechanical loading, cyclic temperature changes of the environment, chemical interaction with fumes. The conical surfaces of the pintle and the seat wear out most rapidly. This results in loss of tightness, leaking of the nonatomized fuel, and penetration of the hot gases into the atomizer. Carbon deposits develop, causing thermal damage as shown in Fig. 4-82. The only countermeasure is to maintain the atomizer at a temperature lower than 250°C. The injection orifices in piston engines can become enlarged due to the erosive action of the fuel, but most commonly they become smaller or even clog due to deposition of the products of fuel coking. Multiorifice atomizers wear out most rapidly.

Swirl atomizers have equally severe operating conditions in the burners and in combustion chambers of gas turbines. In some cases the temperature of the nozzles exceeds 550°C, which causes large temperature gradients to exist between the inner and outer elements resulting in loss of leaktightness.

Most damage to and failures of fuel atomizers are caused by the fuel itself.



Figure 4-82 Intermittent atomizer tip damage caused by improper operation.

The effect of the fuel is of both a physical and chemical nature. Mechanical impurities in the fuel cause erosive damage, development of depositions, and clogging of the flow channels. The origins of mechanical impurities are diverse. Some impurities such as dust, fibers, and rust from tanks are supplied from outside; others precipitate from the fuel installation in the form of metal chips. The heavier the fuel, the more inorganic impurities it contains.

Impurities are removed by filtration. The allowable contamination of diesel oil is 0.005%, i.e., approximately 4 g per 100 l of oil, and that of heating oils is as much as 2.5% [24]. One has to remember also about the powdered additives which are sometimes present in heating oils. In piston engines, preliminary and final filtrations are used. The first retains impurities larger than 60–70 μm ; the second should retain 98–99% of impurities larger than 2–2.5 μm . For multi-orifice intermittent atomizers, removal of impurities of approximately 1 μm is desired.

Fuels at temperatures higher than 100°C show a lack of thermal stability that is manifested as a tendency to precipitate solids. Small and large particles are formed, depending on the condition and type of fuel. The most undesirable particles are those larger than 100 μm , which clog the atomizers. The highest tendency toward precipitation is displayed by fuels containing sulfur.

Operation of water atomizers requires proper water treatment and conditioning. Observations of humidifiers show that many atomizer malfunctions or failures are caused by impurities or erosion. Figure 4-83 shows the inside of a jet-swirl atomizer whose wall was perforated by erosion. Water contains organic and inorganic substances and microorganisms, which occur in the form of suspensions, colloids, or chemical compounds. In small atomizers the quantity of small suspensions should not be higher than 1–2 mg/l.

Chemical compounds present in water precipitate in atomizers. These are compounds of calcium and magnesium, whose content is the measure of water hardness. Hardness should be much lower than 56 mval/l, which is the upper limit for water hardness for industrial purposes. The pH of water should be close to neutral ($\text{pH} \approx 7$) in order to reduce corrosion.

Chemical compounds are often compounds of iron and manganese. In contact with air, these turn into compounds that are insoluble in water and precipitate in the form of flakes causing clogging of the atomizer. The content of these compounds should not exceed 0.2–0.3 mg/l, including not more than 0.1 mg/l of manganese compounds. Water used in direct air humidification should be softened and deironed. Similar operation problems can be caused by air locks. Such air locks occur in installations for aerial spraying and cause partial or total clogging of the atomizers. The countermeasure is implementation of



Figure 4-83 Atomizer damaged by erosion. 1, Swirl chamber; 2, erosion grooves and perforation of chamber wall.

overflow manifolds and deaerators. Agricultural atomizers require cleaning after each usage and operation check prior to usage.

REFERENCES

1. Adamowicz, K., Orzechowski, Z. Design of a pneumatic atomizer for steam attemperation. *Teploenergetika*, No. 1, 1978 (in Russian).
2. Aigner, M., Witting, S. Swirl and counterswirl effects in prefilming airblast atomizers. *Trans. ASME J. Eng. Gas Turbines Power*, Vol. 10, January 1988.
3. Andreussi, P., Tognotti, L., Graziadio, M., Morelli, F. Preliminary investigation on CWS-air flow within a twin fluid atomizer. Proceedings of the Two Day Meeting on Sprays and Their Applications, Milan, 1986.
4. Bailey, A. G. The theory and practice of electrostatic spraying. *Atomisation Spray Technol.*, Vol. 2, No. 2, pp. 95-134, 1986.
5. Balachandran, W. Electrostatic atomization in liquids. Proceedings of the Two Day Meeting on Sprays and Their Applications, Milan, 1986.
6. Brykowski, L. Effect of the geometrical dimensions and operating parameters on the limiting shape of the atomization in the rotary atomizers in burners, Ph.D. thesis, Łódź Polytechnik, Poland, 1974 (in Polish).
7. Chiba, C., Oda, M., Ono, Y. Atomization of a liquid by an improved vibratory atomizer. *Proc. ICLASS-82*, Madison, Wisconsin, 6-2, 173-180, 1982.
8. Deysson, J. Y., Karian, J. Approximate sizing of single fluid and pneumatic atomizers. *Proc. ICLASS-78*, Tokyo, 10-2, 243-249, 1978.
9. Dityakin, J. F., Klyachko, L. A., Novikov, B. V., Yagodkin, V. I. *Liquid Atomization*. "Mashinostroenie," Moscow, 1977 (in Russian).
10. Gupta, J. P., Vijayraghvan, K., Mohan, R. Disintegration of a liquid film by a vertically rotating disk. *Proc. ICLASS-78*, Tokyo, 6-2, 139-144, 1978.
11. Hurley, J. F., Doyle, B. W. Design of two-phase atomisers for use in combustion furnaces. *Proc. ICLASS-85*, London, Vol. 1, IA 3/1-13, 1985.
12. Kelly, A. J. The electrostatic atomization of hydrocarbons. *Proc. ICLASS-82*, Madison, Wisconsin, 57-65, 1982.
13. Masters, K. *Spray Drying Handbook*. George Godwin, London, 1985.
14. Matsumoto, S., Belcher, D. W., Crosby, E. J. Rotary atomizers: Performance understanding and prediction. *Proc. ICLASS-85*, London, Vol. 1, IA/1/1-21, 1985.
15. Melaniuk, M., Orzechowski, Z. The influence of surface tension on liquid atomization. *Rozpr. Inzy.-Eng. Trans.*, Vol. 26, No. 1, pp. 41-50, 1978.
16. Melenchuk, A. I. Pneumatic atomizer for gas turbines. *Izv. Vyssh. Uchebn. Zaved. "Mashinostroenie"* No. 9, 1982 (in Russian).
17. Meyer, P. L., Chigier, N. Characterization of the atomization process in coal-water slurry sprays. *Proc. ICLASS-85*, London, Vol. 2, IV B(b)/1/1-23, 1985.
18. De Michele, G., Graziadio, M., Morelli, F., Tognotti, L. Atomisation of some commercial coal-water slurries. Proceedings of the Two Day Meeting on Sprays and Their Applications, Milan, 1986.
19. Mochida, T. Ultrasonic atomization of liquids. *Proc. ICLASS-78*, Tokyo, 8-4, 193-199, 1978.
20. Mullinger, P. J., Chigier, N. A. The design and performance of internal mixing multijet twin fluid atomizers. *J. Inst. Fuel*, December 1974.
21. Nagai, N., Inamura, T. Atomization of liquid flowing over a solid surface by high speed air. *Proc. ICLAS-82*, Madison, Wisconsin, 5-2, 153-160, 1982.
22. Nagai, N., Kumazawa, T., Hayakawa, Y., Okazaki, H. Combined twin-fluid atomizer with cavity fluid disperser. *Proc. ICLASS-78*, Tokyo, 9-1, 209-216, 1978.
23. Nagai, N., Kumazawa, T., Hayakawa, Y., Okazaki, H. Emulsion formation by atomization, mixing

236 LIQUID ATOMIZATION

- and dispersion with a combined twin-fluid atomizer and cavity fluid disperser. *Proc. ICLASS-82*, Madison, Wisconsin, 8-2, 215–219, 1982.
- 24. Orzechowski, Z. *Liquid Atomization*. WNT, Warsaw, Poland, 1976 (in Polish).
 - 25. Patel, S. L. Development of Aspec Micronizer Nozzle for controlled droplet application with motorised mist blower. *Proc. ICLASS-78*, Tokyo, 9-3, 225–234, 1978.
 - 26. Pazhi, D. G., Galustov, V. S. *Liquid Atomizers*. "Khimiya," Moscow, 1979 (in Russian).
 - 27. Pazhi, D. G., Galustov, V. S. *Fundamentals of Liquid Atomization*. "Khimiya," Moscow, 1984 (in Russian).
 - 28. Sergeant, M. Blast atomiser developments in the Central Electricity Generating Board. *Proc. ICLASS-82*, Madison, Wisconsin, 4-4, 131–136, 1982.
 - 29. Shaw, S. G., Jasuja, A. K. Effect of injector geometry variables upon the spray performance of a plain-jet airblast atomizer. *Atomisation Spray Technol.*, Vol. 3, No. 2, pp. 107–121, 1987.
 - 30. Takehira, A., Kawashima, T., Morita, S. Spray characteristics of the atomizer using a high speed gas flow. *Proc. ICLASS-78*, Tokyo, 10-3, 251–258, 1978.
 - 31. Tanasawa, Y., Muto, N., Saito, A. Injection valve of swirl flow type used for electronic fuel injection. *Proc. ICLASS-78*, Tokyo, 5-2, 117–124, 1978.
 - 32. Tanno, S., Miura, T., Ohtani, S. Atomisation of high viscosity liquid by pneumatic nozzle. *Proc. ICLASS-85*, London, Vol. 2, LP/VB/6/1-8, 1985.
 - 33. Tanno, S., Miura, T., Ohtani, S. Development of a crossflow type pneumatic nozzle. *Atomisation Spray Technol.*, Vol. 2, No. 1, pp. 17–34, 1986.
 - 34. Tate, R. W. Droplet size distribution data for internal-mixing pneumatic atomizers. *Proc. ICLASS-85*, London, Vol. 1, II C 1/1-13, 1985.
 - 35. Tokuoka, N., Honoki, H., Yagi, M., Sato, G. T. A piezoelectric generator of evenly spaced, homogeneous drops of liquid. *Proc. ICLASS-85*, London, Vol. 2, VII B(b)/3/1-9, 1985.
 - 36. Troshkin, O. A. Hydraulic calculation of the centrifugal cylindrical splasher, *Khim. Neft. Mashinostr.*, 1984, No. 5 (in Russian).
 - 37. Unal, A., Robertson, D. G. C. Inert gas atomiser for liquid metals. *Proc. ICLASS-85*, London, Vol. 2, P/4/1-2, 1985.
 - 38. Van Vliet, M. W., Picot, J. J. C. Drop spectrum characterization for the Micronair AU 4000 spray atomizer. *Atomisation Spray Technol.*, Vol. 3, No. 2, pp. 123–134, 1987.

DESIGN OF ATOMIZERS

The least progress in the development of atomizers has been made in the field of their design methods. This follows from the complexity of the flow phenomena occurring in atomizers and from the difficulties in establishing proper computational models.

The design of atomizers involves the determination of their basic geometric dimensions and some flow parameters such as spray angle and liquid film thickness. The design of jet atomizers with continuous operation is simplest. The most developed theory exists for swirl atomizers, so the design of these atomizers will be presented most extensively. The design of pneumatic and rotary atomizers will be presented in a fragmentary manner because of the lack of satisfactory data.

5-1 DESIGN OF JET ATOMIZERS

5-1.1 Jet Atomizers with Continuous Operation

Atomizer with a circular orifice (Fig. 4-1a). Design of such an atomizer consists of determining the diameter d_0 from the Eq. (3-3)

$$d_0 = \sqrt{\frac{4Q}{\pi_\mu \sqrt{2\Delta P/\rho}}} \quad (5-1)$$

or from Eq. (3-4)

$$d_0 = \sqrt{\frac{4G}{\pi_\mu \sqrt{2\rho \Delta P}}} \quad (5-2)$$

for a given flow rate Q (m^3/s) or G (kg/s), pressure drop ΔP (Pa), and liquid density ρ (kg/m^3). The only problem is presented by determining the discharge coefficient μ .

The discharge coefficient μ depends on the orifice geometry and the flow conditions. During the discharge from the outlet orifice the jet contracts (Fig. 3-1). The *coefficient contraction* φ is defined as the ratio of the areas of the contracted jet A and the orifice A_0 :

$$\varphi = \frac{A}{A_0} = \left(\frac{d}{d_0} \right)^2 \quad (5-3)$$

The jet contraction is a result of the liquid inertia. The effect of liquid viscosity is manifested by the fact that, due to the friction, a certain velocity profile develops whose mean value V is lower than the theoretical value V_{th} . It is represented by the *coefficient of velocity loss* β

$$\beta = \frac{V}{V_{\text{th}}} \quad (5-4)$$

The discharge coefficient is given by

$$\mu = \varphi\beta \quad (5-5)$$

Coefficients μ , ρ , and β are the functions of the Reynolds number

$$\text{Re} = \frac{Vd_0}{\nu} \quad (5-6)$$

Figure 5-1 shows the character of these functions for a sharp-edged orifice in a thin wall. Three regions are distinguished: laminar, transient, and turbulent. In

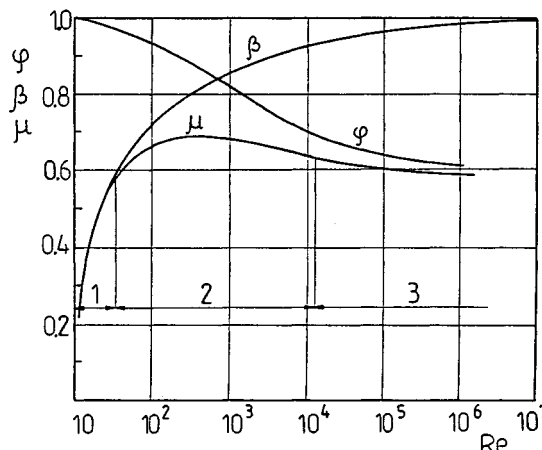


Figure 5-1 Dependence of coefficients φ , β , μ on Reynolds number Re . 1, Laminar range; 2, transient range; 3, turbulent range.

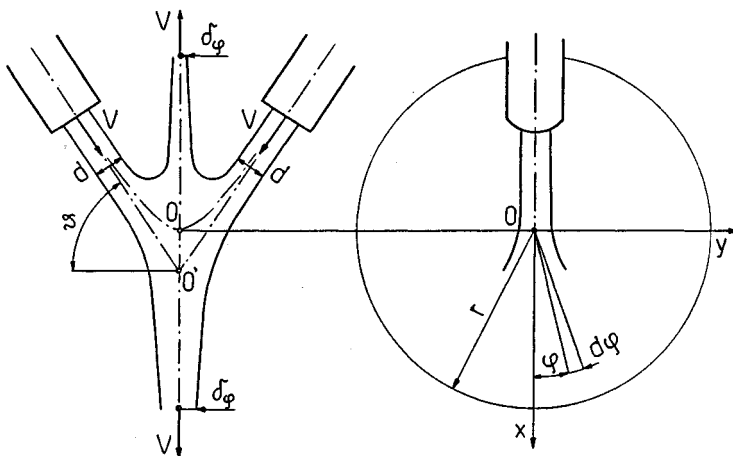


Figure 5-2 Liquid motion during impingement of jets.

the laminar region μ is the same as coefficient β , and in the turbulent region it is the same as the coefficient φ . In the turbulent region, which is essential in the case of atomization, one assumes $\mu = \text{const}$ for a particular atomizer.

In some instances, instead of the coefficient of velocity loss β , the relative loss of kinetic energy ξ is used:

$$\xi = \frac{V_{\text{th}}^2 - V^2}{V^2} \quad (5-7)$$

From Eqs. (5-4) and (5-7) it follows that β and ξ are related as follows:

$$\beta = \frac{1}{\sqrt{1 + \xi}} \quad (5-8)$$

Atomizer with impinging jets (Fig. 5-2) [4, 16]. In the case of two impinging jets with identical diameter d , a thin film of variable thickness develops and at a certain distance disintegrates into drops (Fig. 2-11). In the case of impingement of two countercurrent jets ($\vartheta = 0^\circ$) the liquid divides symmetrically; in the case of $0^\circ < \vartheta < 90^\circ$ this division is asymmetric and the film assumes the shape of an ellipse instead of a circle. The velocity V of an ideal liquid (according to the Bernoulli equation) is identical in the jets and in the film.

The origin of the coordinate system is located at point 0, where the liquid is completely motionless. Our further discussion concerns a single jet and the half-thickness of the liquid film δ_φ . The volumetric flow ratio of liquid is given by

$$Q = V \frac{\pi d^2}{4} \quad (5-9)$$

The volumetric flow ratio in an elementary sector of the film with diameter r and angle $d\varphi$ is

$$dQ_\varphi = V\delta_\varphi r d\varphi \quad (5-10)$$

From this equation it follows that there is a hyperbolic relationship between δ_φ and r .

From the equation of flow continuity in the jet and the film it follows that

$$\frac{\pi d^2}{4} = r \int_0^{2\pi} \delta_\varphi d\varphi \quad (5-11)$$

The equation of conservation of momentum in the $0x$ and $0y$ directions has the form

$$\frac{\pi d^2}{4} \sin \vartheta = r \int_0^{2\pi} \delta_\varphi \cos \varphi d\varphi \quad (5-12)$$

$$\int_0^{2\pi} \delta_\varphi \sin \varphi d\varphi = 0 \quad (5-13)$$

From Eqs. (5-11) to (5-13),

$$\delta_\varphi = \frac{\delta_0 \cos^2 \vartheta}{1 - 2 \sin \vartheta \cos \varphi + \sin^2 \vartheta} \quad (5-14)$$

where $\delta_0 = 0.125d^2/r$.

From Eq. (5-14) it follows that the *liquid film thickness* in an arbitrary cross section with diameter r does not depend on the liquid velocity V ; it is a function of the jet diameter d and angle of impingement ϑ . The maximum thickness of the film follows from Eq. (5-14) for $\varphi = 0$:

$$\delta_{\max} = \frac{\delta_0 \cos^2 \vartheta}{(1 - \sin \vartheta)^2} \quad (5-15)$$

The relative film thickness $\bar{\delta}_\varphi$ follows from Eqs. (5-14) and (5-15):

$$\bar{\delta}_\varphi = \frac{\delta_\varphi}{\delta_{\max}} = \frac{(1 - \sin \vartheta)^2}{1 - 2 \sin \vartheta \cos \varphi + \sin^2 \vartheta} \quad (5-16)$$

The thickness of the liquid film during the impingement of two jets is twice as large. The results of the calculations are in agreement with experimental results.

Impact atomizer—perpendicular impingement with a flat deflector (Fig. 5-3). A liquid jet with diameter d after it impinges with the flat surface develops a film that flows off the deflector's edge and disintegrates into drops [17]. A boundary layer develops on the deflector's surface whose thickness δ_L increases and the *liquid film thickness* δ decreases. At point M these thicknesses are equal. The region of flow can be divided into potential flow region 1 and viscous flow region 2.

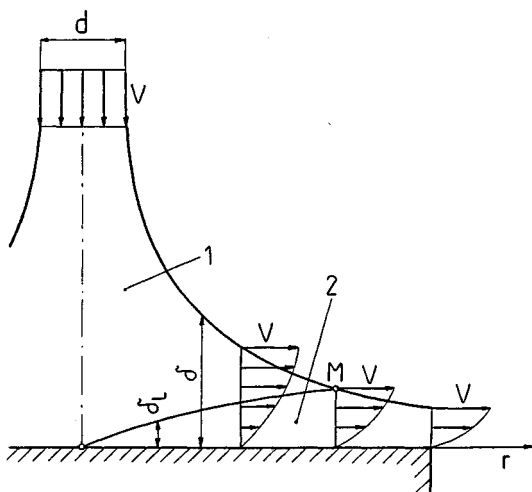


Figure 5-3 Impingement of a liquid jet at a flat surface.

The velocity of a liquid jet in impact atomizers in most cases is $v = 15\text{--}30 \text{ m/s}$. This velocity does not change on the jet boundary and afterwards on the film boundary. The mean velocity of the liquid film depends on whether the boundary layer is of a laminar or turbulent character. The film thickness at radius r is given by following equations [4].

For a laminar jet:

$$\frac{2\delta}{d} = 1.22\text{Re}^{-1}\eta^2 + 0.696\eta^{-1} \quad (5-17)$$

For a turbulent jet:

$$\frac{2\delta}{d} = 0.0158\text{Re}^{-0.25}\eta^{1.25} + 0.511\eta^{-1} \quad (5-18)$$

where

$$\begin{aligned} \text{Re} &= \frac{Vd}{2\nu} \\ \eta &= \frac{2r}{d} \end{aligned}$$

The critical Reynolds number is $R = 2.57 \times 10^4$.

From Eqs. (5-17) and (5-18) it follows that the relative liquid film thickness is minimal at distances corresponding to

$$\eta = 0.656\text{Re}^{0.333}$$

$$\eta = 4.20\text{Re}^{0.111}$$

Therefore, as a result of the impingement of the jet and the horizontal surface, a liquid film develops with the following minimum thickness.

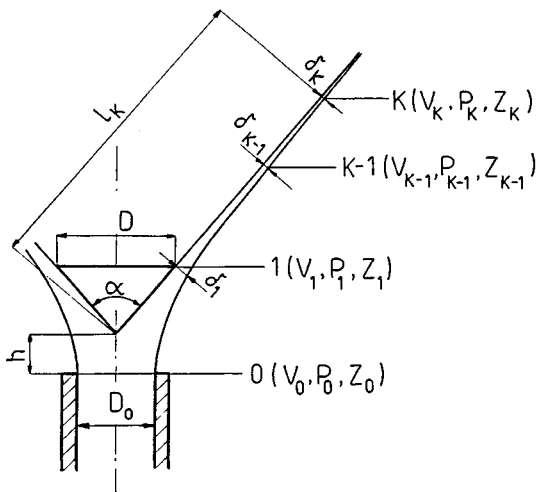


Figure 5-4 Shape of jet during the impingement at a conical deflector.

For a laminar jet:

$$\frac{2\delta_{\min}}{d} = 1.59 \text{Re}^{-0.333} \quad (5-19)$$

For a turbulent jet:

$$\frac{2\delta_{\min}}{d} = 0.210 \text{Re}^{-0.111} \quad (5-20)$$

Impact atomizer—impingement with a conical deflector with cone angle α and base diameter D (Fig. 5-4). The flow continuity equation for cross sections 0 and 1 has the following form:

$$V_0 A_0 = V_1 A_1 \quad (5-21)$$

where

$$A_0 = \frac{\pi D_0^2}{4}, \quad A_1 = \pi \left(\delta_1 D + \delta_1^2 \cos \frac{\alpha}{2} \right)$$

The Bernoulli equation for cross sections 0 and 1 has the following form:

$$\frac{V_0^2}{2} + \frac{P_0}{\rho} + gZ_0 = \frac{V_1^2}{2} + \frac{P_a}{\rho} + gZ_1 \quad (5-22)$$

where $P_1 = P_a$ is an atmospheric pressure
 Z_0, Z = heights above a horizontal level
From Eq. (5-22) follows

$$V_1 = EV_0 \quad (5-23)$$

where

$$E = \left[1 + \frac{2(P_0 - P_a)}{\rho V_0^2} + \frac{2g(Z_0 - Z_1)}{V_0^2} \right]^{1/2} \quad (5-24)$$

The coefficient of the velocity increase E is greater than unity, which indicates that the liquid accelerates after it discharges from the orifice. The values of E given in [11] fall in the range 1.04–1.18 depending on h .

From the above equations we can calculate the relative *liquid film thickness* in cross section 1:

$$\frac{\delta_1}{D} = \frac{-1 + \left[1 + \cos(\alpha/2)(D_0/D)^2/E \right]^{1/2}}{2 \cos(\alpha/2)} \quad (5-25)$$

As the film moves away from the deflector it becomes thinner and thinner. Its velocity in cross section K equals

$$V_K = [V_{K-1}^2 + 2g(Z_{K-1} - Z_K)]^{1/2} \quad (5-26)$$

The flow continuity equation has the following general form:

$$Q = V_{K-1} A_{K-1} = V_K A_K \quad (5-27)$$

where

$$A_K = \pi \left(2\delta_K l_K \sin \frac{\alpha}{2} + \delta_K^2 \cos \frac{\alpha}{2} \right) \quad (5-28)$$

From Eqs. (5-27) and (5-28) we obtain the film thickness in an arbitrary cross section K :

$$\delta_K = -l_K \operatorname{tg} \frac{\alpha}{2} + \left[\left(l_K \operatorname{tg} \frac{\alpha}{2} \right)^2 + \frac{Q}{\pi V_K \cos(\alpha/2)} \right]^{1/2} \quad (5-29)$$

Fan atomizers. Liquid film discharges from a slot with length a_0 and width b_0 . The film thickness δ decreases gradually. The flow rate of such an atomizer should be calculated from Eq. (3-3) or (3-4). $A = a_0 \times b_0$, and flow ratio μ appears from Fig. 5-5 [4].

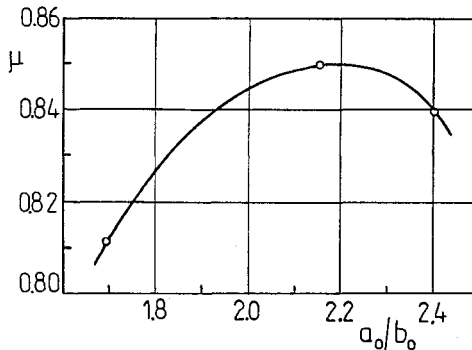


Figure 5-5 Relation $\mu = f(a_0/b_0)$ for fan atomizer.

5-1.2 Jet Atomizers with Intermittent Operation

The design of diesel atomizers, i.e., nozzles used in piston engines, is a very difficult one. The process of injection depends not only on the atomizer but also on the system fuel pump–high pressure manifold–nozzle. The goal of a design is first of all to determine the injection characteristic. This characteristic was discussed in Sec. 3-1.2 and an example was shown in Fig. 3-4. In order to calculate this characteristic, knowledge of various experimental quantities, mainly discharge coefficients, is needed.

Literature dealing with calculation methods for the injection process is extensive. In addition to methods presented in [15] we should mention [2], which describes numerous calculation methods. A simplified calculation method for computer analysis will be presented briefly here [15]. This method is based on the following assumptions:

1. Fuel properties, i.e., elasticity modulus, viscosity, and velocity of the pressure wave propagation as a function of pressure, are variable.
2. Input data contain the actual values of the discharge coefficients of all orifices (pump cylinder, bucket valve, nozzle).
3. Calculations take into account for the resistance coefficients of the pintle and the bucket valve head.
4. The possibility of lack of tightness in the pumping elements is taken into account.
5. Deformation of the pump driving system is taken into account.

The calculation process was divided into the phases and periods for which different equations hold. These equations are of dual character: they are equations of continuity and equations of equilibrium of forces acting on the

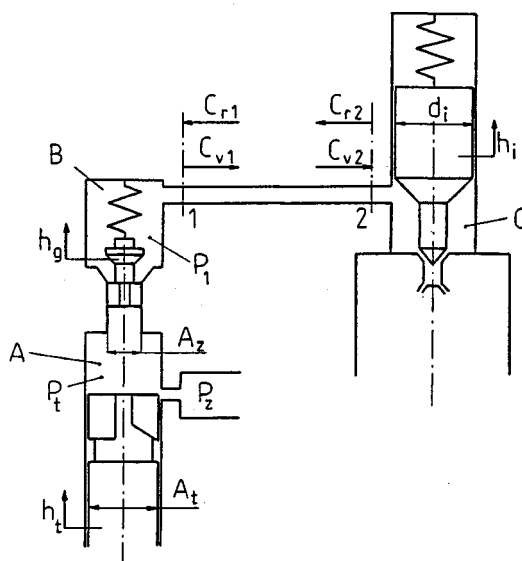


Figure 5-6 Calculation scheme for an injection system. A, Fuel pump chamber; B, bucket valve head chamber; C, nozzle.

movable elements of the bucket valve and nozzle. After fuel compression starts in the high-pressure system, the calculations are done alternately for a pump and a nozzle. The calculation procedure is changed when the pressure wave from the pump reaches the nozzle and vice versa.

The process of pumping in the fuel pump was divided into two phases:

Phase I of pumping—from the onset of pumping to the beginning of fuel compression in the high-pressure system.

Phase II of pumping—from the beginning of fuel compression to the moment when the bucket valve closes.

The region of high pressure in the pumping section consists of chamber A of the cylinder of the fuel pump and chamber B of the bucket valve (Fig. 5-6). The equation of flow continuity for chamber A has the form

$$A_t \left[v_t - \lambda(\varphi) A_t \frac{dP_t}{dt} \right] = s \mu A'_0 j \sqrt{\frac{2}{\rho} |P_t - P_z|} + s \mu_z A_z \sqrt{\frac{2}{\rho} |P_t - P_1|} + A_z \frac{dh_g}{dt} + \frac{V_A - A_t h'_0}{E} \frac{dP_t}{dt} + q_u \quad (5-30)$$

The left-hand side of Eq. (5-30) represents the instantaneous flow rate of fuel pumping for the given angle φ of the camshaft rotation at time t , and the term in square brackets expresses the actual velocity of the piston corrected for the elastic deformation of the shaft. The other symbols are A_t , area of the active cross section of the pump piston; V_t , piston velocity; $\lambda(\varphi)$, compliance coefficient for the camshaft. The right-hand side of Eq. (5-30) represents the following:

The first term determines the fuel flow through the orifices in the cylinder. $(P_t - P_z)$ is the pressure difference between chamber A and the feeding chamber, $\mu A'_0$ is the area of the active flow cross section, j is the number of orifices prior to geometric onset of pumping, ρ is the fuel density, $s = 1$ for $(P_t - P_z) > 0$, and $s = -1$ for $(P_t - P_z) < 0$.

The second term determines the fuel flow through the bucket valve. $(P_t - P_1)$ is the pressure difference between chambers A and B, $\mu_z A_z$ is the area of the active cross section, which is a function of the valve head lift, h_g , $s = 1$ for $(P_t - P_1) > 0$, and $s = 1$ for $(P_t - P_1) < 0$.

The third term determines the fuel flow to the space created by the valve head lift (cross section A_z).

The fourth term determines the cumulative fuel flow in chamber A due to the pressure increase. V_A is the volume of chamber A, h'_0 is the distance of the piston edge from the center of the orifice or orifices in the cylinder, and E is the elasticity modulus for fuel.

The fifth term determines fuel leakage $q_u = f(t)$ due to piston looseness.

A similar flow continuity equation for chamber B has the form

$$A_1 C_1 + \frac{V_B}{E} \frac{dP_1}{dt} = s \mu_z A_z \sqrt{\frac{2}{\rho} |P_t - P_1|} + A_z \frac{dh_g}{dt} \quad (5-31)$$

The left-hand side of Eq. (5-31) represents the following:

The first term describes the fuel flow to the pressure manifold due to the initial velocity and the backward pressure wave. A_1 is the area of cross section 1, C_1 is the fuel velocity in cross section 1.

The second term describes the cumulative fuel flow in chamber B due to the change of pressure P_1 . V_B is the volume of chamber B.

The right-hand side of Eq. (5-31) has already been discussed.

The equation of equilibrium of forces acting on the bucket valve has the form

$$A_z(P_t - P_1) = (F_s + k_s h_g) + (k_v + k_{vs}) \frac{dh_g}{dt} + m_z \frac{d^2 h_g}{dt^2} \quad (5-32)$$

The left-hand side term in Eq. (5-32) represents the force acting on the valve head. The right-hand side terms represent the following:

The first term describes the spring force. F_s is the force of initial deflection of the spring; K_s is the spring constant.

The second term describes the damping force of the valve head. K_v is the damping coefficient of the valve; K_{vs} is the damping coefficient for the valve seat.

The third seat describes the inertia force. m_z is the mass of the valve head and the reduced mass of the spring.

Pressure waves propagate in the pressure manifold with very small friction losses, and therefore the *Allievi equations* can be applied because they refer to unsteady flow of the liquid. It follows from these equations that for cross section 1

$$\left. \begin{aligned} C_1 &= C_{v1} = C_{r1} \\ C_{v1} &= k P_{v1} \\ C_{r1} &= -k P_{r1} \\ P_1 &= P_{v1} + P_{r1} + P_0 \\ k &= \frac{1}{a \rho} \end{aligned} \right\} \quad (5-33)$$

where C_{v1}, C_{r2} = fuel velocities due to the changes of the initial and backward pressure waves

P_{v1}, P_{r1} = pressures of the initial and backward waves

P_0 = pressure in the conduit at the onset of pumping (between two consecutive injections)

a = velocity of pressure wave propagation

Fuel discharge from the nozzle begins when the pressure wave from the pump reaches the nozzle, i.e., when pressure P_2 reaches the valve, which is sufficient to lift the pintle. The injection stops when the pressure under the pintle drops down. The flow continuity equation in cross section 2 has the following form:

$$\frac{v_p}{E} \frac{dP_2}{dt} = A_2 C_2 - A_n \frac{dx}{dt} - s\mu A \sqrt{\frac{2}{\rho} |P_2 - P_c|} - q_n \quad (5-34)$$

where V_p = volume of the pressure conduit

A_2 = area of cross section 2

C_2 = fuel velocity in cross section 2

A_n = cross section area of the pintle

x = pintle lift

μA = area of an equivalent flow cross section

P_c = pressure in the combustion chamber during fuel injection

q_n = fuel leakage

s = as in Eqs. (5-30) and (5-31)

The equation of the equilibrium of forces acting on the nozzle pintle has the form

$$m_a \frac{d^2x}{dt^2} + F_s + k_s x + (k_d + k_{ds}) \frac{dx}{dt} - P_2 A_n z - A_a P_c = 0 \quad (5-35)$$

where m_a = mass of the movable parts of the nozzle

x = pintle lift

F_s = force of the initial deflection of the spring

k_s = spring constant

k_d = coefficient of damping of the pintle

k_{ds} = damping coefficient for the pintle seat

z = coefficient taking into account the effect of the discharging fuel on the nozzle closure pressure

A_a = area of the discharge orifices of the nozzle

From Allievi's equations the flow velocities and pressures in cross section 2 follow:

$$\left. \begin{aligned} C_2 &= C_{v2} + C_{r2} \\ C_{v2} &= kP_{v2} \\ C_{r2} &= -kP_{r2} \\ P_2 &= P_{v2} + P_{r2} + P_0 \\ k &= \frac{1}{a\rho} \end{aligned} \right\} \quad (5-36)$$

The symbols are similar to those in Eq. (5-33).

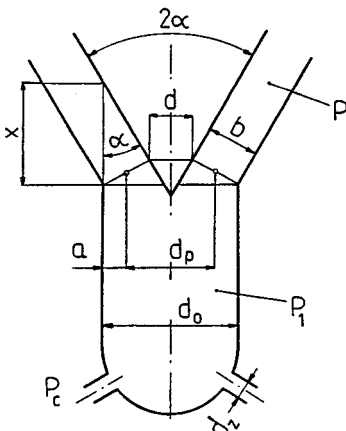


Figure 5-7 Calculation scheme for a multiorifice atomizer;
 $2\alpha = 60^\circ$.

The *area of an equivalent flow cross section* μA appearing in Eq. (5-34) has the form of a function (flow characteristic)

$$\mu A = f(x) \quad (5-37)$$

This function is determined computationally and experimentally.

Function $A = f(x)$ for a *multiorifice atomizer* will be calculated using Figs. 3-5 and 5-7. This atomizer has the following throttling cross section: in the region of the pintle seat and in the discharge orifices. For flow in the pintle seat region the following equation holds:

$$Q = \mu_1 A_1 \sqrt{\frac{2}{\rho} (P - P_1)} \quad (5-38)$$

From Fig. 5-7 the geometric relationships follow:

$$a = \frac{b}{2} \cos \alpha$$

$$b = x \sin \alpha$$

$$d_p = d_0 - 2a = d_0 - \frac{x}{2} \sin 2\alpha$$

The area of the flow cross section for the seat is

$$A_1 = \pi \left(\frac{d_0}{2} + \frac{d}{2} \right) b = \pi \left(d_0 - \frac{x}{2} \sin 2\alpha \right) x \sin \alpha$$

For $2\alpha = 60^\circ$ we obtain

$$A_1 = \frac{\pi}{2} \left(d_0 - \frac{\sqrt{3}}{4} x \right) x$$

Equation (5-38) assumes the following form after A_1 is substituted:

$$Q = \frac{\pi}{2} \mu_1 \left(d_0 - \frac{\sqrt{3}}{4} x \right) x \sqrt{\frac{2}{\rho} (P - P_1)} \quad (5-39)$$

For the flow through the discharge orifices the following equation holds:

$$Q = \mu_2 \frac{\pi d_2^2}{4} n \sqrt{\frac{2}{\rho} (P_1 - P_c)} \quad (5-40)$$

where n denotes the number of orifices. For the discharge from an atomizer we can write

$$Q = \mu A \sqrt{\frac{2}{\rho} (P - P_c)} \quad (5-41)$$

From Eqs. (5-39)–(5-41) follows the expression for calculation of the area of an equivalent flow cross section for a multiorifice atomizer with angle $2\alpha = 60^\circ$.

$$\mu A = \frac{\pi}{2} \cdot \frac{\mu_1 (d_0 - (\sqrt{3}/4)x)x}{\left\{ 1 + [(2/\mu_2 d_2^2 n) \mu_1 (d_0 - (\sqrt{3}/4)x)x]^2 \right\}^{1/2}} \quad (5-42)$$

For a different angle 2α and for a different nozzle the calculations would be similar. Equation (5-42) shows good agreement with experiments.

Function $\mu A = f(x)$ for a *pintle nozzle* is shown schematically in Fig. 5-8b. The area of an equivalent flow cross section follows from Eq. (3-19). This function depends on the characteristic positions of the pintle in the discharge

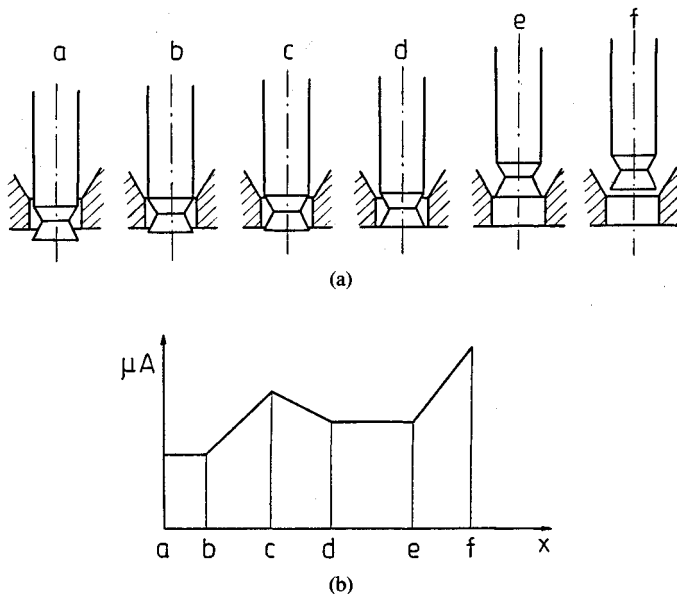


Figure 5-8 Equivalent area of the flow cross section for a pintle nozzle: (a) characteristic positions of the pintle; (b) function $\mu A = f(x)$.

orifice (Fig. 5-8a). In region $c-d$ the function decreases. From Fig. 3-8 it also follows that in this region flow rate Q decreases.

Example 5-1 Analyze the fuel injection in a high-speed piston engine [8]. Atomizer data:

Single-orifice nozzle of Bosch type

$d_0 = 0.8 \text{ mm}$ —discharge orifice diameter

Data characterizing the injection conditions:

$P_0 = 20 \text{ MPa}$ —pressure at the onset of pumping

$P_{\max} = 15.5 \text{ MPa}$ —maximum injection pressure

$\bar{P} = 0.675 P_{\max} = 10.5 \text{ MPa}$ —mean injection pressure

$V_w = 304 \text{ mm}^3/\text{cycle}$ —mean fuel charge

Data characterizing the combustion chamber:

$P_c = 1.5 \text{ MPa}$ —pressure

$\varphi_G = 18.1 \text{ kh/m}^3$ —air density

Fuel data:

$\rho_L = 860 \text{ kg/m}^3$ —density

$\nu = 6.5 \times 10^{-6} \text{ m}^2/\text{s}$ —kinematic viscosity

$\mu = 56 \times 10^{-6} \text{ Pa}\cdot\text{s}$ —dynamic viscosity

$\sigma = 27 \times 10^{-3} \text{ N/m}$ —surface tension

Determine the following parameters of the spray:

- (a) Length L of the initial segment of the spray
- (b) Coordinate x of the spray front at time $t = 3 \text{ ms}$
- (c) Spray angle α of the main spray segment
- (d) Sauter drop diameter D_{32}
- (e) Drop surface A_D

SOLUTION

- (a) Length L of the initial segment of the spray.

Maximum $w_0 = w_{\max}$ and mean \bar{w} velocities of discharge without losses follow from Eq. (3-2):

$$w_{\max} = \sqrt{\frac{2(P_{\max} - P_c)}{\rho_L}} = \sqrt{\frac{2(15.5 - 1.5)}{860} \cdot 10^6} = 180.5 \text{ m/s}$$

$$\bar{w} = \sqrt{\frac{2(\bar{P} - P_c)}{\rho_L}} = \sqrt{\frac{2(10.5 - 1.5)}{860} \cdot 10^6} = 149 \text{ m/s}$$

The Weber numbers according to Eq. (2-5) are equal for w_{\max} and w , respectively:

$$\text{We}_{\max} = \frac{\rho_L w_{\max}^2 d_0}{\sigma} = \frac{860 \times 180.5^2 \times 0.8 \times 10^{-3}}{27 \times 10^{-3}} = 842,000$$

$$\overline{\text{We}} = \frac{\rho_L \bar{w}^2 d_0}{\sigma} = \frac{860 \times 149^2 \times 0.8 \times 10^{-3}}{27 \times 10^{-3}} = 574,000$$

The Laplace number according to Eq. (2-79) is

$$\text{Lp} = \frac{\rho_L \sigma d_0}{\mu^2} = \frac{870 \times 27 \times 10^{-3} \times 0.8 \times 10^{-3}}{(56 \times 10^{-4})^2} = 585$$

The density ratio is

$$M = \frac{\rho_G}{\rho_L} = \frac{18.1}{860} = 0.02115$$

Length L of the initial segment of the spray according to Eq. (2-150) and Fig. 2-40 equals L_1 given by

$$L_1 = 8.25 d_0 \text{We}_{\max}^{0.25} \text{Lp}^{-0.4} M^{-0.6}$$

$$= 8.25 \times 0.8 \times 842,000^{0.25} \times 585^{-0.4} \times 0.02115^{-0.6} = 156 \text{ mm}$$

(b) Coordinate x of the spray front at time $t = 3 \text{ ms}$.

The coefficient of the free turbulence a'_u follows from Eq. (6-13) assuming $C_1 = 2.9$:

$$a'_u = 2.9 \text{We}_{\max}^{-0.21} \text{Lp}^{0.16} M$$

$$= 2.9 \times 842,000^{-0.21} \times 585^{0.16} \times 0.02115 = 0.0097$$

The coordinate x of the spray front follows from Eq. (2-153):

$$x = \sqrt{\frac{d_0 w_{\max} t}{\sqrt{2} a'_u}} = \sqrt{\frac{0.8 \times 180.5 \times 10^{-3} \times 0.003}{\sqrt{2} \times 0.0097}} = 176 \text{ mm}$$

(c) Spray angle α of the main segment of the spray.

This angle follows from Eq. (6-10) assuming $C = 0.0089$:

$$\tan \frac{\alpha}{2} = 0.0089 \text{We}_{\max}^{0.32} \text{Lp}^{0.07} M^{0.5}$$

$$= 0.0089 \times 842,000^{0.32} \times 585^{0.07} \times 0.02115^{0.5} = 0.159$$

Hence $\alpha = 18^\circ$.

(d) Sauter drop diameter D_{32} .

The Sauter diameter D_{32} can be determined from Eq. (2-39):

$$D_{32} = 1.44 d_0 (\text{We} M)^{-0.266} \text{Lp}^{-0.0733}$$

$$= 1.44 \times 0.8 \times 10^3 (574,000 \times 0.02115)^{-0.266} \times 585^{-0.0733}$$

$$= 59.2 \mu\text{m}$$

Value $K = 1.44$ is approximately two times smaller than in Table 6-3.

(e) Drop surface.

Specific drop surface A_D follows from Eq. (3-70):

$$A_D = \frac{6}{D_{32}} = \frac{6}{0.00592} = 1010 \text{ cm}^2/\text{cm}^3$$

The drop surface equals

$$A = A_D V_w = 1010 \times 0.304 = 307 \text{ cm}^2/\text{cycle}$$

5-2 DESIGN OF A SWIRL ATOMIZER

There is an extensive literature devoted to calculation methods for swirl atomizers, especially simplex atomizers. There are two main approaches to the calculations. The first uses the so-called principle of the maximum flow, the second the equation of conservation of momentum. The first approach is historically older and more popular than the second. Both approaches differ with respect to the methodology used, but they consider the establishment of relationships between the same characteristic dimensions of an atomizer, such as d_0 , A_p , R , i.e., geometric constant K , as well as spray parameters μ , ϵ , α .

A literature survey and a comparison of results obtained by different calculation methods are presented in [15]. The comparison shows that some discrepancies do exist; however, they are of less importance when it comes to the design of the atomizers for practical applications. In such cases, simplicity of the calculation method is most important.

Newer work on the design of swirl atomizers has appeared, including [4, 16, 17]. Methods based on the Navier-Stokes equations are considered critically in [6]; however, new work on this subject was published more recently [14]. A calculation method based on the principle of maximum flow with the modified free vortex equation is presented in [18, 19] and a method based on the principle of conservation of momentum in [13].

Special attention must be paid to [20, 21]. The analysis is based on the theoretically calculated liquid film thickness in the discharge orifice. This thickness was related to spray angle α and to the value of the conventional velocity coefficient K_v . Knowledge of this coefficient and its changes caused by the atomizer dimensions, liquid properties, and atomization conditions is the basic condition that allows the design of an atomizer.

5-2.1 Simplex Atomizers

Ideal liquid theory [15]. A model of the design a simplex atomizer is presented in Fig. 5-9. The liquid is fed through tangential orifice 1 with diameter d_p and cross-sectional area A_p to swirl chamber 2 with diameter $D_s = 2R + d_p$, and

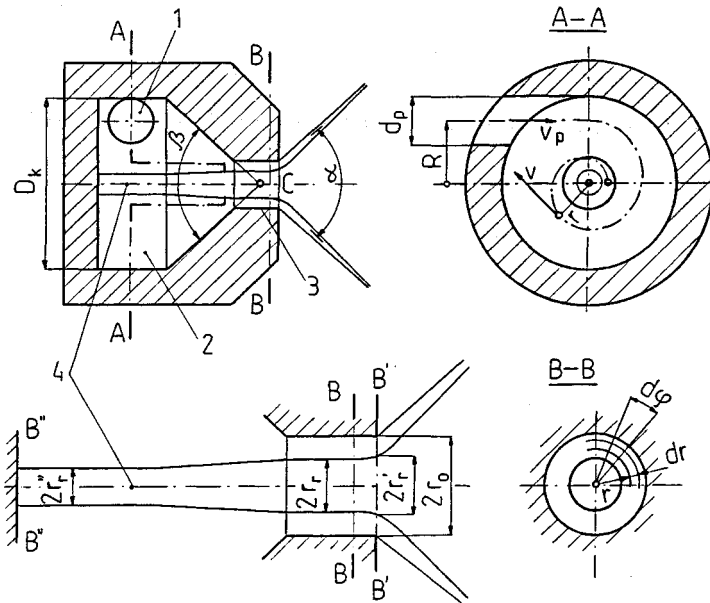


Figure 5-9 Design model for a simplex swirl atomizer. 1, Inlet orifice; 2, swirl chamber; 3, discharge orifice; 4, gas core.

the inlet of the tangential orifice is located on radius R . In general, there are several inlet orifices and in this case

$$iA_p = i\pi r_p^2 = i \frac{\pi d_p^2}{4} \quad (5-43)$$

where i is the number of orifices. Tangential orifices often have a shape other than circular, which does not affect the calculation methodology. The liquid discharges from outlet orifice 3 with diameter $d_0 = 2r_0$.

The motion of the liquid inside the atomizer is complex. In the region of the swirl chamber this motion consists of a potential vortex and the motion caused by the negative source whose position coincides with vertex C of the transient cone. In the region of the cylindrical discharge orifice the motion consists of a potential vortex and an axial motion. All velocity components should be considered, i.e. axial u , circumferential v , and radial w ; the last one is significantly lower than the others.

The liquid discharges not through the whole cross section but through an annular one. The central part of the cross section is filled by *gas core* 4, which in Fig. 5-9 is shown in a smaller and larger scale. The area of annular cross section A is

$$A = \pi(r_0^2 - r_r^2) = \epsilon\pi r_0^2 \quad (5-44)$$

hence the efficiency of filling of the discharge orifice ϵ has the following form:

$$\epsilon = \frac{A}{A_0} = \frac{\pi(r_0^2 - r_2^2)}{\pi r_0^2} = 1 - \left(\frac{r_r}{r_0}\right)^2 \quad (5-45)$$

where $A_0 = \pi r_0^2 = \pi d_0^2/4$ is the area of the discharge orifice and r_r is the gas core diameter.

Circumferential velocity component V changes according to the principle of the potential vortex, which is represented by the equation

$$vr = \text{const} \quad (5-46)$$

A free vortex has a singular point at $r = 0$, for which $V = +\infty$ and pressure $P = -\infty$. If so, a free vortex can exist only in the region with radius $r \geq r_r$. The circumferential velocity increases at the core boundary to a certain maximum value v_{\max} .

Axial velocity u occurs inside the swirl chamber at a radius slightly larger than radius r_0 .

This velocity causes the circumferential velocity v to decrease and therefore velocity v_{\max} is lower, as would follow from the free vortex equation. This fact will not, however, be incorporated in the analysis.

In the region of the gas core $r < r_r$, a so-called *rigid vortex* exists in which the gas originating from the atomizer's ambient rotates as a rigid body with constant angular velocity

$$\omega = \frac{v}{r} = \frac{v_{\max}}{r_r} = \text{const} \quad (5-47)$$

Velocity v_{\max} can be calculated from the Bernoulli equation (for $w = 0$)

$$\frac{\rho}{2}(u^2 + v^2) + P = P_t = \text{const} \quad (5-48)$$

if the values u and P are known at the core boundary. The pressure is equal to $P \approx P_0$, where P_0 is the ambient pressure. Axial velocity u varies and is constant only in the region of the outlet orifice. Pressure P_t is the total liquid pressure. According to the equation of conservation of angular momentum with respect to the chamber axis, we can write

$$v_p R = vr = v_{\max} r_r = \text{const} \quad (5-49)$$

The following assumptions will be made for further considerations:

The liquid is ideal.

The velocity field is a potential one in the whole region between the chamber walls and the gas core.

Angular momentum, according to Eq. (5-49), is constant.

There is no gravity.

The flow is stable and axisymmetric.

There is no radial component of velocity ($w = 0$).

According to Fig. 5-9, a liquid element on radius r , with width dr , length $r d\varphi$, and unit thickness is acted on by a pressure force and mass force. The condition of equilibrium of these forces has the form

$$r d\varphi dm = \frac{v^2}{r} dm \quad (5-50)$$

Substituting element of mass $dm = \varphi r d\varphi$ and velocity v from Eq. (5-49),

$$v = \frac{v_{\max} r_r}{r} \quad (5-51)$$

into Eq. (5-50), one obtains

$$dP = \rho v_{\max}^2 r_r^2 \frac{dr}{r^3} \quad (5-52)$$

After integration Eq. (5-52) assumes the following form:

$$P = -\frac{\rho}{2} v_{\max}^2 r_r^2 \frac{1}{r^2} + C \quad (5-53)$$

Constant C follows from the condition that on the gas core boundary, i.e., for $r = r_r$, the overpressure equals zero, hence

$$C = \frac{\rho}{2} v_{\max}^2$$

By substituting C and v_{\max} from Eq. (5-51) into (5-53) we obtain the equation of the pressure distribution in the transverse cross section of the discharge orifice:

$$P = \frac{\rho}{2} (v_{\max}^2 - v^2) \quad (5-54)$$

Substituting pressure P from Eq. (5-54) into Eq. (5-48) one obtains

$$u = \sqrt{\frac{2P_t}{\rho} - v_{\max}^2} = \text{const} \quad (5-55)$$

As seen, axial velocity component u is uniform in the transverse cross section of the discharge orifice, since in the given conditions $P_t = \text{const}$ and $v_{\max} = \text{const}$. This uniformity of velocity u is, however, disturbed between cross sections $B-B$ and $B'-B'$. This is caused by the fact that between these cross sections the static centrifugal overpressure is transformed into the dynamic pressure, since in cross section $B'-B'$ pressure should be constant and equal to the ambient pressure. Therefore velocity u is higher at the wall than at the core boundary. The change of velocity u was not accounted for in Fig. 3-12.

Distribution of axial velocity w in cross section $B'-B'$ can be determined as follows. Velocity v_p from Eq. (5-60) and Q from Eq. (5-62) should be substituted into Eq. (5-49), and after taking into account K from Eq. (4-1) we obtain

$$v = \frac{\mu K r_0}{r} \sqrt{\frac{2P_t}{\rho}} \quad (5-56)$$

Velocity v should be introduced into Eq. (5-48), assuming that overpressure $P = 0$ in cross section $B'-B'$. Hence

$$u = \sqrt{1 - \frac{\mu^2 K^2 r_0^2}{r^2}} \sqrt{\frac{2P_t}{\rho}} \quad (5-57)$$

Equation (5-57) expresses the distribution of axial velocity component W in the discharging cross section, i.e., in the cross section $B'-B'$. It follows from this equation that velocity u increases as radius r increases.

Radius r_r of the gas core changes along the chamber axis in a following way. The smaller the axial velocity component, the higher (according to the Bernoulli equation) the circumferential component. Its increase causes a decrease of radius r_r . The smaller radius r_r'' occurs on the back wall of the swirl chamber (Fig. 5-9), where the axial velocity has its minimum value; the largest radius r_r' occurs on the front wall, where the axial velocity has its maximum value.

Radius r_r' of the gas core can be calculated from the following integral equation using Eq. (5-62):

$$Q = \int_{r_r'}^{r_0} 2\pi r dr u = \mu \pi r_0^2 \sqrt{\frac{2P_t}{\rho}}$$

Substituting velocity u from Eq. (5-57), we obtain the following equation:

$$\mu = \sqrt{1 - \mu^2 K^2} - S \sqrt{S^2 - \mu^2 K^2} - \mu^2 K^2 \ln \frac{1 + \sqrt{1 - \mu^2 K^2}}{S + \sqrt{S^2 - \mu^2 K^2}} \quad (5-58)$$

where $S = r_r'/r_0$ is a dimensionless radius of the gas core in the discharge cross section.

Solving Eq. (5-58) graphically with respect to S , we must assign to each value of K a corresponding value of μ from Fig. 5-11. The solution is shown in Fig. 5-10 as curve 1. In addition, the changes of the dimensionless core r_r/r_0 and r_r''/r_0 (curves 2 and 3) are shown. Curve 1 assumes the highest position since it refers to the larger radius r_r' . The largest differences in the curve positions correspond to small values of constant K .

Volumetric flow rate Q determined by using Eq. (5-44) equals

$$Q = Au = \epsilon \pi r_0^2 u \quad (5-59)$$

On the other hand, the same flow rate can be determined at the inlet to the swirl chamber by using Eq. (5-43):

$$Q = iA_p v_p = i\pi r_p^2 v_p \quad (5-60)$$

Substituting velocity v_{\max} from Eq. (5-49) and velocity v_p from Eq. (5-60) into Eq. (5-55), we obtain

$$u = \sqrt{\frac{2P_t}{\rho} - \frac{R^2 Q^2}{i^2 \pi^2 v_p^2 r_p^2}} \quad (5-61)$$

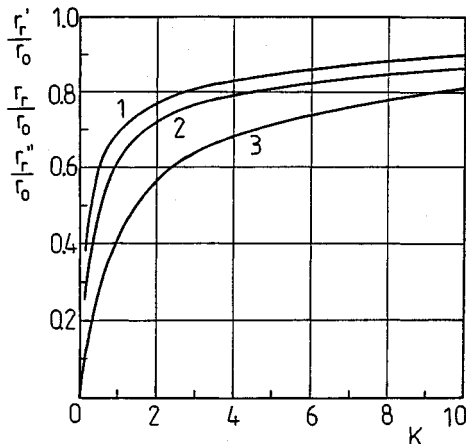


Figure 5-10 Dimensionless radii of the gas core. 1, On the outlet from atomizer r'_r/r_0 ; 2, inside the outlet orifice r_r/r_0 ; 3, on the back wall of swirl chamber r''_r/r_0 .

Comparing this velocity u with velocity u obtained from Eq. (5-59) and taking into account Eq. (5-45) and geometric constant K from Eq. (4-1), we obtain volumetric liquid flow rate Q :

$$Q = \frac{1}{\sqrt{K^2/(1-\epsilon) + 1/\epsilon^2}} \pi r_0^2 \sqrt{\frac{2P_t}{\rho}} = \mu A_0 \sqrt{\frac{2\Delta P}{\rho}} \quad (5-62)$$

or mass liquid flow rate G

$$G = \rho Q = \mu A_0 \sqrt{2\rho \Delta P} \quad (5-63)$$

Equations (5-62) and (5-63) are identical in notation to Eq. (3-3) and (3-4), since the drop of static pressure ΔP in the atomizer is approximately equal to liquid overpressure P_t with respect to ambient pressure P_0 , i.e., $\Delta P \approx P_t$. Discharge coefficient μ of a simplex swirl atomizer is therefore equal to

$$\mu = \frac{1}{\sqrt{K^2/(1-\epsilon) + 1/\epsilon^2}} \quad (5-64)$$

As seen, discharge coefficient μ depends on two quantities: the geometric constant K and the efficiency of filling the discharge orifice ϵ .

Discharge coefficient μ is a complex function of ϵ , since it has small values for both small and large filling efficiency ϵ , passing through a maximum. The explanation is as follows. Small efficiency of filling ϵ corresponds to a large diameter of the gas core, i.e., to a small equivalent flow cross section, and large efficiency of filling ϵ means a small diameter of the gas core and therefore high circumferential velocity v and small axial velocity u .

At the outlet of the atomizer the gas core establishes an efficiency of filling ϵ , that ensures the maximum value of the discharge coefficient μ , i.e., the maximum liquid flow for a given pressure drop. This is the *principle of maximum*

flow. The first author who implemented this principle for swirl atomizers was Abramovich [3]. Only when this principle is satisfied do the conditions of stable flow exist.

Flow in a swirl atomizer has a free liquid surface at the boundary of the gas core and in this respect is similar to the flow in an open channel. The maximum flow principle in a swirl atomizer is equivalent to the principle of the maximum (critical) flow in an open channel; the difference is that in open channels a free surface develops because of gravity forces and in the case of a swirl atomizer because of centrifugal force.

A stable flow occurs when the flow velocity is equal to the velocity of wave propagation on the free liquid surface, in this case on the surface of the gas core. In [3] an equation was derived for the velocity of propagation of waves in a swirl atomizer and it was demonstrated that this velocity is equal to the axial velocity during the maximum flow. However, it follows from experiments [17] that on the vortex surface a transition can occur from supercritical flow ($Fr < 1$) to subcritical flow ($Fr > 1$), where Fr is the Froude number. The liquid energy reaches its maximum when the Froude number is equal to unity ($Fr = 1$).

Efficiency of filling ϵ ensures the maximum value of discharge coefficient μ when

$$\frac{d\mu}{d\epsilon} = 0$$

Differentialtion of Eq. (5-64) gives

$$K = \frac{(1 - \epsilon)\sqrt{2}}{\epsilon\sqrt{\epsilon}} \quad (5-65)$$

From Eqs. (5-64) and (5-65) we have the following expression for the discharge coefficient:

$$\mu = \epsilon\sqrt{\frac{\epsilon}{2 - \epsilon}} \quad (5-66)$$

Figure 5-11 presents function $\epsilon = f(K)$ from Eq. (5-65) and function $\mu = f(K)$ from Eqs. (5-65) and (5-66).

The *spray angle* follows from the ratio of the circumferential and axial velocities (Sec. 3-2.1). Drops circumscribe a hyperboloidal surface of revolution whose asymptote is a conical surface. Angle α can be calculated in a simplified way from the ratio

$$\operatorname{tg} \frac{\alpha}{2} = \frac{\hat{v}}{u} \quad (5-67)$$

where v is the circumferential velocity component on a mean radius r (Fig. 5-12)

$$\hat{r} = \frac{1}{2}(r_0 + r_r) \quad (5-68)$$

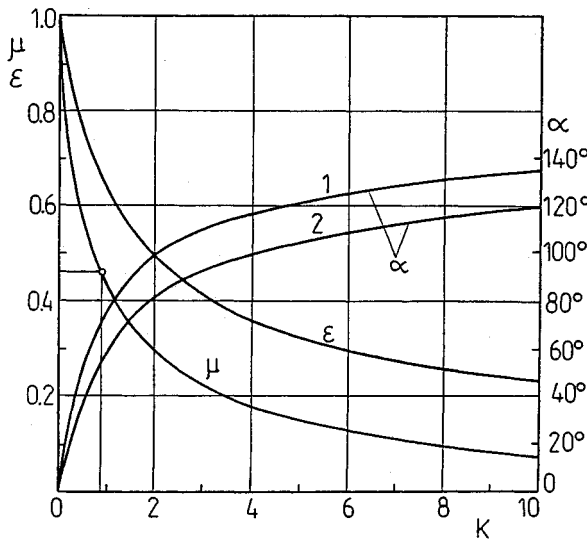


Figure 5-11 Dependence of the discharge coefficient μ , inlet orifice filling efficiency ϵ , and spray angle α on geometric constant of a swirl atomizer K . 1, According to Eq. (5-72); 2, according to Eq. (5-75).

Formula (5-67) differs from formula (3-27) in that in the first case \hat{v} is the circumferential velocity on mean radius r and in the second case v_m is the arithmetic mean of the circumferential components or radii r_0 and r_r . The difference is caused by the fact that the distribution of circumferential component v is not linear but hyperbolic [Eq. (5-49)]. In both cases the same simplification was adopted, namely $u = \text{const}$ in the discharge cross section.

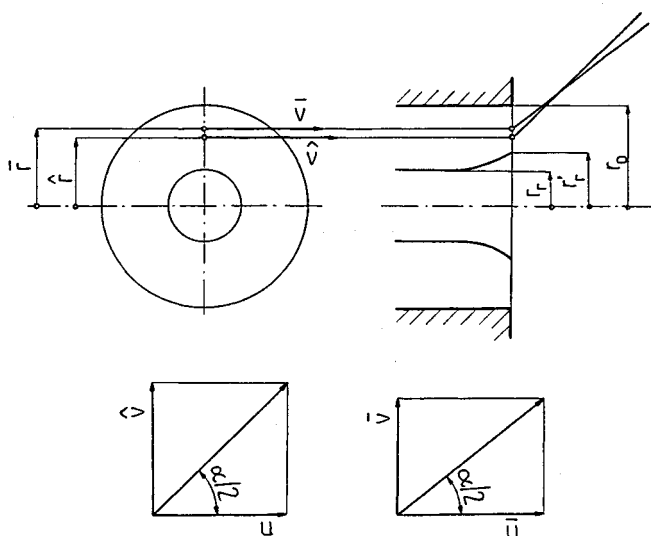


Figure 5-12 Scheme for calculating angle α using Eqs. (5-67) and (5-73).

Circumferential velocity v on the radius \hat{r} can be calculated from the free vortex equation

$$\hat{v}\hat{r} = v_p R \quad (5-69)$$

Taking into account Eq. (5-68), we obtain

$$\hat{v} = \frac{v_p R}{\frac{1}{2}(r_0 + r_r)} \quad (5-70)$$

Axial velocity u can be derived from Eqs. (5-59) and (5-60):

$$u = \frac{v_p r_p^2}{\epsilon r_0^2} \quad (5-71)$$

For simplicity it was assumed that $i = 1$, i.e., one tangential inlet orifice, which does not change the methodology of calculations.

Substituting \hat{v} and u from Eqs. (5-70) and (5-71) into Eq. (5-67) and taking into account

$$K = \frac{Rr_0}{r_p^2}$$

and ϵ from Eq. (5-45) and K from Eq. (5-65), we obtain finally

$$\operatorname{tg} \frac{\alpha}{2} = \frac{2\sqrt{2}(1 - \epsilon)}{\sqrt{\epsilon}(1 + \sqrt{1 - \epsilon})} \quad (5-72)$$

This equation is exceptionally simple because it relates angle α only to the efficiency of filling ϵ . Due to the simplifying assumption ($u = \text{const}$), angle α is too large (Fig. 5-11).

For a more precise calculation one should use the following relationship:

$$\operatorname{tg} \frac{\alpha}{2} = \frac{\bar{v}}{\bar{u}} \quad (5-73)$$

where \bar{v} and \bar{u} are velocity components on the mean radius \bar{r} (Fig. 5-12)

$$\bar{r} = \frac{1}{2}(r_0 + r'_r) = \frac{r_0}{2}(1 + S) \quad (5-74)$$

Substituting $r = \bar{r}$ into Eqs. (5-56) and (5-57), we obtain

$$\bar{v} = \frac{2\mu K}{1 + S} \sqrt{\frac{2P_t}{\rho}}$$

and therefore

$$\begin{aligned} \bar{u} &= \sqrt{1 - \frac{4\mu^2 K^2}{(1 + S)^2}} \sqrt{\frac{2P_t}{\rho}} \\ \operatorname{tg} \frac{\alpha}{2} &= \frac{\bar{v}}{\bar{u}} = \frac{2\mu K}{\sqrt{(1 + S)^2 - 4\mu^2 K^2}} \end{aligned} \quad (5-75)$$

Figure 5-11 shows angle α derived from Eq. (5-75). For $k = 0$, $\alpha = 0$ and for $K \rightarrow \infty$, α tends to 180° . Condition $K = 0$ corresponds to the vortex-free flow that is typical of jet atomizers.

Viscous liquid theory [15]. The effect of viscosity on the operation of a swirl atomizer has been discussed in numerous publications but there are still some controversies. Due to viscosity, friction forces develop at the wall of the swirl chamber which cause the angular momentum to decrease. As a result, the angular momentum in the discharge orifice should be smaller than at the inlet to the swirl chamber, and therefore the radius of the gas core and angle α should decrease and the discharge coefficient μ should increase. Therefore an unexpected situation occurs when the discharge coefficient of a viscous liquid is larger than that of an ideal liquid.

The motion of the viscous liquid was considered in [3] based on the condition of equilibrium of forces acting on a liquid element. As a result, the following approximate value of the flow ratio was obtained:

$$\mu = \frac{1}{\sqrt{K_\lambda^2/(1 - \epsilon) + 1/\epsilon^2}} \quad (5-76)$$

As seen, Eq. (5-76) differs from Eq. (5-64) in the sense that constant K is replaced by K_λ . Equivalent geometric constant K_λ is given by

$$K_\lambda = \frac{K}{1 + (\lambda/2)(B^2/i - K)} \quad (5-77)$$

where

$$B = \frac{R}{r_p} \quad \text{or} \quad B = R \sqrt{\frac{\pi}{A_p}} \quad (5-78)$$

Here λ is a friction coefficient and parameters i, R, r_p, A_p follow from Fig. 5-9.

One can use curve $\mu = f(K)$ from Fig. 5-11, but value K_λ instead of K should be used as the abscissa. Since $K_\lambda < K$, coefficient μ is larger than that for an ideal liquid.

For a viscous liquid Eq. (5-65) has the same form, namely

$$K_\lambda = \frac{(1 - \epsilon)\sqrt{2}}{\epsilon\sqrt{\epsilon}} \quad (5-79)$$

It follows from the condition $K_\lambda < K$ (Fig. 5-11) that for a viscous liquid the efficiency of filling ϵ is higher and the radius of the gas core r_r is smaller than for an ideal liquid. The spray angle can be expressed approximately by an equation similar to Eq. (5-75), namely

$$\operatorname{tg} \frac{\alpha}{2} = \frac{2\mu K_\lambda}{\sqrt{(1 + S)^2 - 4\mu^2 K^2}} \quad (5-80)$$

Since $K_\lambda < K$, from Fig. 5-11 we obtain a smaller value of angle α than for an ideal liquid.

Substituting K and B to Eq. (5-77), we obtain

$$K_\lambda = \frac{Rr_0}{ir_p^2 + (\lambda/2)R(R - r_0)} \quad (5-81)$$

Two cases will be considered: changes of R and r_p for other parameters held constant. When $R \rightarrow \infty$ then for the ideal liquid $K \rightarrow \infty$, i.e., $\mu \rightarrow 0$ and $\alpha \rightarrow 180^\circ$; for a viscous liquid from Eq. (5-81) it follows that K_λ increases to a certain maximum and subsequently decreases to zero. When $r_p \rightarrow 0$, then for the ideal liquid $K \rightarrow \infty$, but for a viscous liquid it follows from Eq. (5-81) that K_λ increases to a certain finite value.

It is seen therefore that the maximum value K_λ depends on how geometric constant K increases, whether it is due to the increase of R or the decrease of r_p . A "viscosity barrier" of some kind develops, which is manifested by the fact that equivalent geometric constant K_λ reaches a maximum to which minimum value μ_{\min} and maximum value α_{\max} correspond.

As opposed to the theoretical consideration of the effect of viscosity, there are many works in which the viscosity is taken into account empirically. This will be discussed in Sec. 6-2.

Design method [15]. The aim of the design is to determine the dimensions of a simplex swirl atomizer for the following data: Q or G , α , ΔP , ρ , and ν . First one calculates the basic dimensions incorporated in geometric constant K and then the other dimensions (Fig. 5-13). As it turns out, it is not a unique problem. The ambiguity is caused by the fact that the same value of constant K can be derived from an appropriate selection of various values R , i , d_p , d_0 . That is why one should follow some recommendations dictated by experience gathered up until now.

The *first phase of calculations* refers to an ideal liquid. For given angle α from Fig. 5-11 (curve 2) we determine geometric constant K and subsequently discharge coefficient μ . From Eq. (5-63) we calculate the discharge orifice diameter

$$d_0 = \sqrt{\frac{4G}{\pi\mu\sqrt{2\rho P_t}}} \quad (5-82)$$

The geometric constant contains now three unknown quantities, R , i , d_p

$$K = \frac{2Rd_0}{id_p^2} \quad (5-83)$$

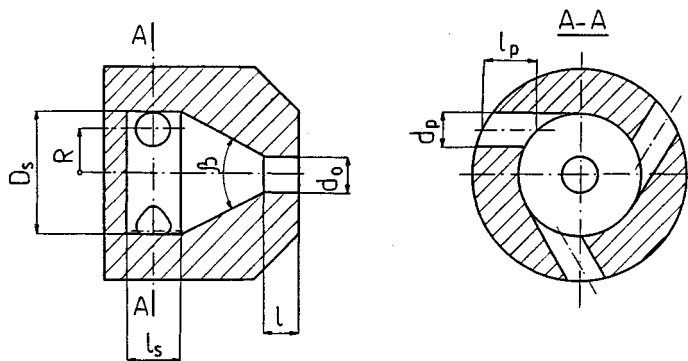


Figure 5-13 Basic dimensions of a simplex swirl atomizer.

two of which have to be assumed. It is most convenient to assume the number of orifices and radius of swirling. Most commonly, $i = 2$ to 4 and $R = (2-5)r_0$ are used. In some instances the dimensions of the atomizer dictate the value of R . From Eq. (5-83) we calculate the diameter of the tangential inlet orifices.

$$d_p = \sqrt{\frac{2Rd_0}{iK}} \quad (5-84)$$

In the case of orifices with a shape other than circular, instead of d_p we determine A_p from Eq. (4-1).

The second phase of calculations refers to the assessment of the viscosity effect. The Reynolds number at the inlet to the atomizers is

$$Re = \frac{v_p d}{\nu} \quad (5-85)$$

where d is the diameter of the equivalent orifice, which can be determined as follows

$$\frac{\pi d^2}{4} = i \frac{\pi d_p^2}{4}$$

hence

$$d = \sqrt{i} d_p$$

Velocity v_p is given by

$$v_p = \frac{4G}{\rho i \pi d_p^2}$$

Substituting it to Eq. (5-85), we obtain

$$Re = \frac{4G}{\pi \rho v \sqrt{i} d_p} \quad (5-86)$$

Friction coefficient λ follows from the formula

$$\lg \lambda = \frac{25.8}{(\lg Re)^{2.58}} - 2 \quad (5-87)$$

Equation (5-87) has been established as a result of extensive investigations of atomizers in the range $Re = 10^3-10^5$. Values λ determined from Eq. (5-87) are significantly larger than would follow from well-known equations used in hydraulics. This is due to by high transverse gradients of pressure in the wall boundary.

The effect of liquid viscosity can be neglected when the following inequality is satisfied:

$$\frac{B^2}{i} - K \leq \frac{2}{\lambda} (\Phi^{1.5} - 1) \quad (5-88)$$

where Φ denotes ratio of discharge coefficients μ for a viscous and an ideal liquid.

Considering the selection of the value of radius R , remember that R should be small and simultaneously the area of the inlet orifices should be small in order to overcome the viscosity barrier. The higher K is, i.e., the larger angle α is required, the smaller radius R should be. Also, the smaller the flow rate and the higher the liquid viscosity, the smaller radius R should be. For liquids with moderate viscosity we should assume

$$B = \frac{R}{r_p} < 4-5$$

which follows from the fact that the following condition should be satisfied:

$$\frac{B^2}{i} - K < 5-10$$

One should not, however, assume too small values of B and R , since this would cause the atomizer's dimensions to be too small.

In tangential inlet orifices, liquid counteraction occurs and therefore the actual area of cross section A' of each inlet orifice should be increased in such a way that the jet has cross section area A_p . From the definition of the *contraction coefficient* [Eq. (5-3)] follows

$$\varphi = \frac{A_p}{A'_p} = \left(\frac{d_p}{d'_p} \right)^2$$

hence

$$d'_p = \frac{d_p}{\sqrt{\varphi}} \quad (5-89)$$

The contraction coefficient is assumed to be $\varphi = 0.85-0.90$.

The *third phase of calculations* concerns the determination of the remaining dimensions of the atomizer (Fig. 5-13). The following recommendations are of a general character; the more detailed recommendations will be given in Sec. 6-2.

The diameter of the swirl chamber D_s is

$$D_s = 2R + d'_p$$

The length of the swirl chamber l_s should be slightly larger than that of the inlet orifice. It suffices for a liquid to make one fourth to one third of rotations, since a long chamber determines the atomization conditions.

The inlet orifices should have the proper length l_s so that jets entering the swirl chamber are not deflected from the tangential direction. We recommend $l_s = (1.5-3.0)d'_p$.

The discharge orifice should not be too long in order not to decrease angle α . For $K_\lambda < 4-5$ we recommend $l = (0.5-1.0)d_0$; for $K_\lambda > 4-5$, $l = (0.25-0.5)d_0$. The angle of the transient cone most commonly equals $\beta = 60-120^\circ$; smaller angles β cause an increase of the discharge coefficient μ and decrease of angle α .

The calculation method presented refers not only to atomizers with tangential orifices but also to atomizers with a swirling insert. In the latter case the radius of swirling R is equal to the radius of the swirling grooves. Geometric constant K follows from Eq. (4-1), where A_p is a cross section of an individual groove and i is the number of grooves.

Example 5-2 Design an atomizer of a gas turbine according to Fig. 5-13 for the following data [3]:

$G = 144 \text{ kg/h} = 0.04 \text{ kg/s}$ is the flow rate of kerosene

$\alpha = 60^\circ$ is the spray angle

$P_t = \Delta P = 3.45 \text{ MPa}$ is the pressure drop

$\rho = 830 \text{ kg/m}^3$ is the density of kerosene

$\nu = 2.2 \times 10^{-6} \text{ m}^2/\text{s}$ is the kinematic viscosity of kerosene

SOLUTION For angle $\alpha = 60^\circ$ from Fig. 5-11 we obtain

$$K \approx 0.9, \quad \mu \approx 0.46$$

From Eq. (5-82)

$$d_0 = \sqrt{\frac{4G}{\pi\mu\sqrt{2\rho\Delta P}}} = \sqrt{\frac{4 \times 0.04}{\pi \times 0.46\sqrt{2 \times 830 \times 3.45 \times 10^6}}} \approx 0.0012 \text{ m} = 1.2 \text{ mm}$$

$$\approx 0.0012 \text{ m} = 1.2 \text{ mm}$$

It was assumed that $i = 3$ and $R = 4r_0 = 2d_0 = 2 \times 1.2 = 1.4 \text{ mm}$. From Eq. (5-84) it follows that

$$d_p = \sqrt{\frac{2Rd_0}{iK}} = \sqrt{\frac{2 \times 2.4 \times 1.2}{3 \times 0.9}} = 1.46 \text{ mm}$$

The Reynolds number from Eq. (5-86) equals

$$\text{Re} = \frac{4G}{\pi \rho v \sqrt{i} d_p} = \frac{4 \times 0.04}{\pi \times 830 \times 2.2 \times 10^{-6} \sqrt{3} \times 1.46 \times 10^{-3}} \\ = 11,080$$

From Eq. (5-87) we obtain

$$\lg \lambda = \frac{25.8}{(\lg \text{Re})^{2.58}} - 2 = \frac{25.8}{(\lg 11080)^{2.58}} - 2 = -1.3$$

Therefore

$$\lambda \approx 0.051$$

After substitution, we obtain from Eq. (5-81)

$$K_\lambda = \frac{Rr_0}{ir_p^2 + (\lambda/2)R(R - r_0)} = \frac{2.4 \times 0.6}{3 \times 0.73^2 + (0.051/2)2.4(2.4 - 0.6)} \\ = 0.843$$

As seen, constant K_λ differs only slightly from constant K and therefore the viscosity effect can be neglected.

Independently, assuming 5% accuracy, i.e., assuming the ratio of flow ratios $\Phi = 1.05$, we obtain from inequality (5-88)

$$\frac{2}{\lambda}(\Phi^{1.5} - 1) = \frac{2}{0.051}(1.05^{1.5} - 1) = 2.9$$

and

$$\frac{B^2}{i} - K = \frac{(2.4/0.73)^2}{3} - 0.9 = 2.7 < 2.9$$

which also indicates that viscosity can be neglected.

Assuming counteraction coefficient $\varphi = 0.9$, we obtain from Eq. (5-89) the corrected diameter of the inlet orifice d'_p

$$d'_p = \frac{d_p}{\sqrt{\varphi}} = \frac{1.46}{\sqrt{0.9}} \approx 1.55 \text{ mm}$$

The remaining dimensions of the atomizer are

$$D_s = 2R + d'_p = 2 \times 2.4 + 1.55 = 6.35 \text{ mm}$$

$$l_s = 2 \text{ mm} > d'_p$$

$$l_p = 2 \times d'_p = 2 \times 1.55 = 3.1 \text{ mm}$$

$$l = 0.5d_0 = 0.5 \times 1.2 = 0.6 \text{ mm}$$

$$\beta = 90^\circ$$

5-2.2 Duplex Atomizers

Duplex atomizers. The design of duplex atomizers is a complex one, since jets interact in a common swirl chamber [15]. The most complex state of flow exists when the control valve is partially open (Fig. 4-27). The Bernoulli equation has the following form.

For primary feeding:

$$P_t = P_{p1} + \frac{\rho v_{p1}^2}{2}(1 + \zeta_1) \quad (5-90)$$

For secondary feeding:

$$P_t = P_{p2} + \frac{\rho v_{p2}^2}{2}(1 + \zeta_2) \quad (5-91)$$

where ζ_1, ζ_2 are the coefficients of local losses in the inlet channels. $\zeta_1 = \text{const}$ for primary feeding. For secondary feeding coefficient ζ_2 varies from $\zeta_2 = \infty$ for the closed valve to $\zeta_2 = 0$ when the control valve is open. Since in the common swirl chamber $P_{p1} = P_{p2} = P_p$, it follows from Eqs. (5-90) and (5-91) that

$$v_{p2} = v_{p1} \sqrt{\frac{1 + \zeta_1}{1 + \zeta_2}} \quad (5-92)$$

The equation of conservation of angular momentum in the swirl chamber has the following form:

$$Gv_p R = G_1 v_{p1} R + G_2 v_{p2} R$$

where G, G_1, G_2 are the mass flow rates and, v_p is the resultant velocity on the radius R .

From the equation of conservation of angular momentum it follows that

$$v_p = \frac{G_1 v_{p1} + G_2 v_{p2}}{G} \quad (5-93)$$

The equation of flow continuity has the following form:

$$G = G_1 + G_2 = \pi \rho (i_1 r_{p1}^2 v_{p1} + i_2 r_{p2}^2 v_{p2}) \quad (5-94)$$

Substituting Eq. (5-92), we obtain

$$G = \pi \rho \bar{r}_p^2 \bar{v}_{p1} \quad (5-95)$$

where

$$\bar{r}_p = \sqrt{i_1 r_{p1}^2 \left(1 + \kappa \sqrt{\frac{1 + \zeta_1}{1 + \zeta_2}} \right)} \quad (5-96)$$

$$\kappa = \frac{i_2 r_{p2}^2}{i_1 r_{p1}^2} \quad (5-97)$$

Equation (5-93), after accounting for Eqs. (5-94) and (5-92), assumes the form

$$v_p = v_{p1} \frac{1 + \kappa(1 + \zeta_1)/(1 + \zeta_2)}{1 + \kappa\sqrt{(1 + \zeta_1)/(1 + \zeta_2)}} \quad (5-98)$$

Denoting

$$\bar{R} = R \frac{1 + \kappa(1 + \zeta_1)/(1 + \zeta_2)}{1 + \kappa\sqrt{(1 + \zeta_1)/(1 + \zeta_2)}} \quad (5-99)$$

then the angular momentum for a unit volume of the liquid equals

$$M = \rho v_p R = \rho v_{p1} \bar{R} \quad (5-100)$$

By the same reasoning as for a simplex atomizer, and using Eqs. (5-95) and (5-100), we arrive at the conclusion that for a duplex atomizer the role of geometric constant K is played by constant \bar{K} :

$$\bar{K} = \frac{\bar{R} r_0}{\bar{r}_p^2} \quad (5-101)$$

Discharge coefficient μ and spray angle α of a duplex atomizer can be determined from Fig. 5-11, if constant K is replaced by constant \bar{K} . Substituting \bar{r}_p from Eq. (5-96) and \bar{R} from Eq. (5-99) in Eq. (5-101), we obtain

$$\bar{K} = \sigma K_1 \quad (5-102)$$

where

$$\sigma = \frac{1 + \kappa(1 + \zeta_1)/(1 + \zeta_2)}{\left(1 + \kappa\sqrt{(1 + \zeta_1)/(1 + \zeta_2)} \right)^2} \quad (5-103)$$

and geometric constant K_1 is expressed by Eq. (4-4). From Eq. (5-102) it follows that when the control valve is closed ($\zeta_2 = \infty$), $\bar{K} = K_1$, and when the valve is completely open ($\zeta_2 = 0$), constant \bar{K} is close to constant K_2 and for $\zeta_1 = 0$, $\bar{K} = K_2$. Geometric constant K_2 is expressed by Eq. (4-5). Constant \bar{K} therefore falls in the range $K_2 \leq \bar{K} < K_1$.

Knowing flow rate G , we can determine flow rate G_1 of the first and G_2 of the second feed system. Implementing Eqs. (5-92), (5-93), (5-94), and (5-98), we

obtain

$$G_1 = \frac{1}{1 + \kappa\sqrt{(1 + \zeta_1)/(1 + \zeta_2)}} G \quad (5-104)$$

$$G_2 = \frac{\kappa\sqrt{(1 + \zeta_1)/(1 + \zeta_2)}}{1 + \kappa\sqrt{(1 + \zeta_1)/(1 + \zeta_2)}} G \quad (5-105)$$

Here the energy loss in the control valve and losses of mixing of the first and second feed jets in the swirl chamber were omitted. These losses in the range $\kappa = 4-10$ do not exceed 15–20% of the total energy of the liquid, so they can be neglected in technical calculations.

Duplex atomizers are used for small liquid viscosities. When it is necessary to take the viscosity into account, the approach is as follows. From Eqs. (5-95), (5-100), and (5-102) it follows that the equivalent geometric constant for a partially open control valve is

$$K_\lambda = \frac{\sigma K_1}{1 + (\lambda/2)\sigma(B_1^2/i_1 + K_1)} \quad (5-106)$$

where $B_1 = R/r_{p1}$.

The Reynolds number equals

$$\text{Re} = \frac{v_p d_p}{\nu}$$

Velocity v_p can be calculated from Eq. (5-98). To do so, we substitute

$$v_{p1} = \frac{4G_1}{\rho i_1 \pi d_{p1}^2}$$

and G_1 from Eq. (5-104) and σ from Eq. (5-103). As a result we obtain

$$v_p = \frac{4\sigma G}{\pi i_1 \rho d_{p1}^2}$$

Diameter d_p equals

$$d_p = \frac{i_1 d_{p1} + i_2 d_{p2}}{i_1 + i_2}$$

After substituting,

$$\text{Re} = \frac{4\sigma G(i_1 d_{p1} + i_2 d_{p2})}{\pi i_1 \rho d_{p1}^2 \nu (i_1 + i_2)} \quad (5-107)$$

Using Eq. (5-107), we calculate friction coefficient λ from formula (5-87). With Eq. (5-106), it is possible to determine geometric constant K_λ .

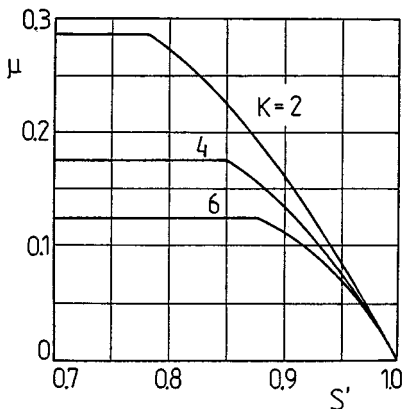


Figure 5-14 Relationship $\mu = f(K, S')$ for the secondary feeding system of a duplex atomizer.

Two-nozzle atomizers. In two-nozzle atomizers, liquid flow through both systems proceeds independently (Fig. 4-31), which significantly simplifies the calculations [15]. The design of a two-nozzle atomizer consists of separate calculations for two systems following the method described for simplex atomizers. The relative position of the two nozzles (discharge orifices) affects the shape of the spray, which will be discussed further in Sec. 6-2. The first feeding system of a two-nozzle atomizer operates at low liquid flow rates, which leads to small Reynolds numbers and high values of $(B^2/i - K)$ due to the small diameter of the inlet orifices. In this situation the calculations for the first feeding system take into account viscosity effects.

During calculations one should pay attention to the diameter of the gas core of the secondary flow system. If the core diameter is larger than the outer diameter of the nozzle of the first system, the design of the secondary system proceeds exactly as for a simplex atomizer. However, if the core diameter is smaller (which leads to disturbances during the flow through the second stage), one should use Eq. (5-58), assume $S = S' = r'/r_0$, where r' denotes the outer diameter of the nozzle of the first stage.

Solving Eq. (5-58) graphically, we obtain the function $\mu = f(K, S')$. The solution is shown in Fig. 5-14. As seen, discharge coefficient μ of the secondary stage of the atomizer starts to decrease rapidly when S' exceeds a certain value. These results have been confirmed experimentally.

5-2.3 Spill-Return Atomizers

This design will concern spill-return atomizers operating in the one-way system regime (Fig. 4-34) [15]. The reasoning will be limited to the case of an ideal liquid.

The flow rate of the liquid discharging through the outlet orifice is

$$G_a = \mu \pi r_0^2 \sqrt{2 \rho P_t} \quad (5-108)$$

Flow rate μ during the return of the liquid is a function not only of geometric constant K but also of the flow rate of the returned liquid G_d , and according to Eq. (4-7) the total flow rate equals

$$G_t = G_a + G_d$$

The geometric constant assumes the form

$$K = \frac{Rr_0}{ir_p^2}$$

Flow rate G_d can be expressed in the same way as in Eq. (5-59), namely

$$G_d = \epsilon \rho \pi r_0^2 u \quad (5-109)$$

Axial component u can be expressed by using Eq. (5-55):

$$u = \sqrt{\frac{2P_t}{\rho} - v_{\max}^2} \quad (5-110)$$

According to Eq. (4-8), the excess liquid coefficient is

$$e = \frac{G_t}{G_a} = 1 + \frac{G_d}{G_a}$$

The total flow rate of the liquid, using Eq. (5-108), is

$$G_t = eG_a = e\mu \pi r_0^2 \sqrt{2\rho P_t} \quad (5-111)$$

When there is no liquid return ($G_d = 0$), the excess liquid coefficient equals $e = 1$ and Eq. (5-111) transforms to Eq. (5-108), i.e., $G_t = G_d$.

Now we should use Eq. (5-49)

$$v_{\max} r_r = v_p R \quad (5-112)$$

Velocity v_p at the inlet to the swirl chamber can be expressed as in Eq. (5-60), namely

$$v_p = \frac{G_t}{\rho i \pi r_p^2} \quad (5-113)$$

From Eqs. (5-111) to (5-113) we obtain

$$v_{\max} = \frac{e \mu R r_0^2}{i r_r r_p^2} \sqrt{\frac{2P_t}{\rho}} \quad (5-114)$$

Equation (5-109), after substitution of Eqs. (5-45), (5-109), (5-110), and (5-114) into it, assumes the following form:

$$G_a = \epsilon \pi r_0^2 \sqrt{\left(1 - \frac{\mu^2 e^2 K^2}{1 - \epsilon}\right) 2 \rho P_t} \quad (5-115)$$

Comparing Eqs. (5-108) and (5-115), we obtain the value of the flow ratio

$$\mu = \epsilon \sqrt{1 - \frac{\mu^2 e^2 K^2}{1 - \epsilon}}$$

and after further transformation

$$\mu = \frac{1}{\sqrt{K_d^2/(1 - \epsilon) + 1/\epsilon^2}} \quad (5-116)$$

As seen, Eq. (5-116) differs from Eq. (5-64) in that, instead of geometric constant K , constant K_d appears. K_d is expressed by Eq. (4-9). The relationship between the filling efficiency ϵ and the geometric constant of a spill-return atomizer K_d can be determined on the basis of the principle of the maximum flow. According to this principle, condition $d\mu/d\epsilon = 0$ should be satisfied. Excess liquid coefficient e is a function of ϵ , but in the range of the maximum flow it is almost constant. In this situation the dependence of discharge coefficient μ on geometric constant K_d has the same character as the dependence of μ on K for a simplex atomizer. The same refers to angle α . As coefficient e increases, coefficient μ decreases and angle α increases.

5-2.4 Variable-Geometry Atomizers

The control of the area of the tangential inlet orifices to the swirl chamber causes the geometric constant of the atomizer to change. During the uncovering of the orifices the geometric constant decreases from K , to K_2 , where

$$K_1 = \frac{Rr_0}{i_1 r_p^2}, \quad K_2 = \frac{Rr_0}{i_2 r_p^2}$$

where i_1 , i_2 are the numbers of uncovered orifices for the initial and final positions of the needle, respectively. It was assumed in this case that the inlet orifices are identical. In the range K_1 to K_2 the values of the discharge coefficient μ and the angle α must be determined from Fig. 5-11.

The needle is acted on by the pressure and spring forces. Using the equations of flow continuity, conservation of momentum, and angular momentum results in the following equation, which expresses the pressure (overpressure) distribution in the swirl chamber:

$$P = P_t \left[1 - \frac{\mu^2 r_0^4}{i_1 r_p^2} \left(\frac{1}{16} + \frac{R^2}{r_p^2} \right) \frac{1}{r^2} \right] \quad (5-117)$$

Assuming $P = 0$, we can determine the radius of the gas core in the swirl chamber, r_r'' (Fig. 5-9):

$$r_r'' = \mu r_0 K \sqrt{1 + \frac{r_p^2}{16 R^2}} \quad (5-118)$$

The expression under the square root is close to unity, hence Eq. (5-118) assumes the form

$$\frac{r''}{r_0} = \mu K \quad (5-119)$$

Function $r''/r_0 = f(k)$ is shown in Fig. 5-10.

Equation (5-117) therefore assumes the form

$$P = P_t \left(1 - \frac{r''^2}{r^2} \right) \quad (5-120)$$

Radius r varies in the range $r'' \leq r \leq R_s$, where R_s is the radius of the swirl chamber. Determining the pressure distribution makes it possible to calculate the force acting on the needle spring:

$$F = \int_{r''}^{R_s} P 2\pi r dr$$

Substituting P from Eq. (5-120) and integrating yield

$$F = 2\pi P_t \left[\frac{1}{2} (R_s^2 - r''^2) - r''^2 \ln \frac{R_s}{r''} \right] \quad (5-121)$$

In order to take into account viscosity, one should use not constant K but equivalent constant K_λ from Eq. (5-77). The viscosity effect is especially visible for low pressures P_t when only some orifices are uncovered.

5-3 DESIGN OF JET-SWIRL ATOMIZERS

5-3.1 Ideal Liquid Theory [16, 17]

In a swirl chamber and especially in the discharge orifice, an interaction occurs between the unswirled (axial) and swirled jets (Fig. 5-15). The *unswirled jet* flows with axial velocity u_a . The *swirled jet* moves along the walls of the swirl chamber with a resultant velocity in which the dominant role is played by the circumferential components of velocity. Both jets enter the discharge orifice, where the swirled jet has circumferential component v and axial component $u < u_a$.

In the discharge orifice on the boundary between two jets a *turbulent boundary layer* develops in which significant shear stresses exist. As a result, equalization of the axial components of both jets occurs and a certain circumferential velocity is set for the unswirled jet. The turbulent processes cause not only energy exchange but also mass exchange. A theoretical solution does not exist for these processes, so empirical-theoretical solutions are used.

The following assumptions will be made:

1. Liquid motion inside the atomizer has a turbulent character, and therefore the velocity distributions are approximately uniform.

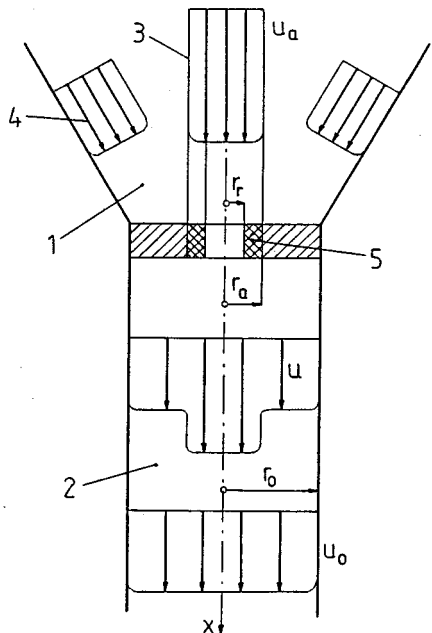


Figure 5-15 Schematic diagram of the interaction of liquid jets in a jet-swirl atomizer. 1, Swirl chamber; 2, discharge orifices; 3, unswirled jet; 4, swirled jet, 5, boundary layer.

2. A common velocity distribution for both jets in the discharge orifice develops at a distance shorter than three diameters of the orifice as measured from the point where the jets meet.
3. The distribution of circumferential velocity v in the discharge orifice satisfies the equation of a straight line (rigid vortex), i.e.,

$$\frac{v}{r} = \frac{v_0}{r_0} \quad (5-122)$$

where v_0 denotes the circumferential velocity component on radius r_0 .

The latter assumption regarding a rigid vortex, instead of a free vortex, simplifies further consideration significantly. It will be shown that this assumption does not cause noticeable errors. From the Bernoulli equation for an arbitrary cross section of inlet orifice 1 and outlet orifice 2 it follows that

$$P_1 = \frac{\rho}{2}(u^2 + v^2) + P_2 \quad (5-123)$$

In this equation the dynamic pressure in cross section 1 was neglected as very small compared to static pressure P_1 . Flow rate G_0 is the sum of the flow rate of the liquid flowing through axial orifice G_a and through swirling grooves G_s (Fig. 5-16)

$$G_0 = G_a + G_s \quad (5-124)$$

Further reasoning is relevant to an *atomizer with a swirling insert*; however, it is also valid for other designs of jet-swirl atomizers.

The terms in Eq. (5-124) are

$$\begin{aligned} G_0 &= \epsilon_0 A_0 u_0 \\ G_a &= \epsilon_a A_a u_a \\ G_s &= u_s \sum (\epsilon_s A_s) \end{aligned} \quad (5-125)$$

For an ideal liquid $u_a = u_s$, A_0 , A_s , and $\sum A_s$ are areas of the cross sections of orifices:

$$A_0 = \frac{\pi d_0^2}{4}, \quad A_a = \frac{\pi d_a^2}{4}, \quad \sum A_s = n a^2 \cos \vartheta$$

where n denotes the number of swirling grooves.

The axial orifice and swirling grooves are completely filled with liquid, hence filling efficiencies are equal to $\epsilon_a = \epsilon_s = 1$. Efficiency of filling $\epsilon_0 = \epsilon$ refers to the case in which a gas core with radius r_r exists in the discharge orifice. According to Eq. (5-45),

$$\epsilon = \frac{r_0^2 - r_r^2}{r_0^2} = 1 - \frac{r_r^2}{r_0^2}$$

In the most typical case for jet-swirl atomizers a gas core does not exist in the discharge orifice, i.e., $\epsilon = 1$. From Eqs. (5-124) and (5-125) we then obtain

$$u_s = \frac{u_0 A_0}{A_a + \sum A_s} \quad (5-126)$$

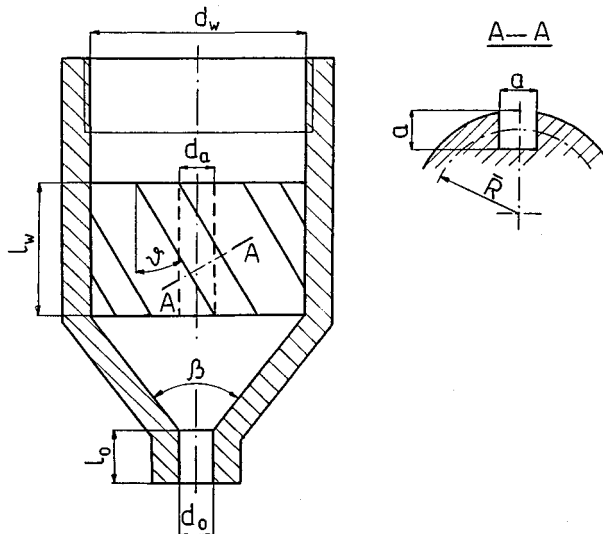


Figure 5-16 Schematic diagram of a jet-swirl atomizer with a cylindrical swirling insert.

From the equation of conservation of the angular momentum of the liquid in the atomizer, it follows that total moment M_s in the swirling channels is equal to the moment M_0 in an arbitrary cross section of the discharge orifice. Moment M_s is given by

$$M_s = G_s u_s \bar{R} \sin \vartheta = \rho u_s^2 \bar{R} \sin \vartheta \sum A_s \quad (5-127)$$

where u_s = liquid velocity in the swirling grooves

\bar{R} = mean radius of swirling (Fig. 5-16)

ϑ = angle of inclination of grooves with respect to the swirler axis

$\sum A_s$ = total area of cross section of swirling grooves

Moment M_0 equals

$$M_0 = 2\pi\rho \int_{r_r}^{r_0} u_0 v r^2 dr \quad (5-128)$$

After substituting Eq. (5-122), integrating and accounting for $u_0 = \text{const}$, and substituting Eq. (5-45), Eq. (5-128) assumes the following form:

$$M_0 = \frac{1}{2} \rho A_0 r_0 u_0 v_0 (2 - \epsilon) \epsilon \quad (5-129)$$

From the condition $M_s = M_0$ and using Eq. (5-126), (5-127), and (5-129), we obtain the ratio of velocity components:

$$\frac{v_0}{u_0} = 2 \frac{\bar{R}}{r_0} \sin \vartheta \frac{A_0 \sum A_s}{(A_a + \sum A_s)^2} \frac{\epsilon}{2 - \epsilon} = \frac{\epsilon}{2 - \epsilon} K_* \quad (5-130)$$

where K_* is the *geometric constant of the jet-swirl atomizer*:

$$K_* = 2 \frac{\bar{R}}{r_0} \sin \vartheta \frac{A_0 \sum A_s}{(A_a + \sum A_s)^2} \quad (5-131)$$

Constant K_* (similar to constant K for the swirl atomizer) takes into account the relationship between the basic dimensions of the jet-swirl atomizer.

According to Fig. 5-17 and Eq. (5-130) *spray angle* α equals

$$\alpha = 2 \arctg \frac{\epsilon K_*}{2 - \epsilon} \quad (5-132)$$

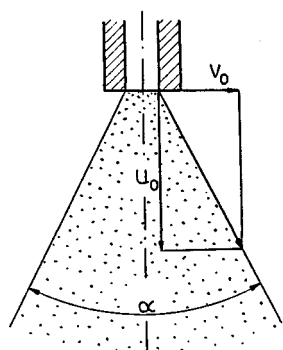


Figure 5-17 Spray angle α .

As experiments show, the value of angle α for all jet-swirl atomizers with a swirling insert does not exceed 90° .

Because of the nonuniform distributions of velocity and pressure in the individual cross sections, Eq. (5-132) for mean parameters assumes the form

$$P_1 = \frac{\rho}{2} (\bar{u}^2 + \bar{v}^2) + \bar{P}_2 \quad (5-133)$$

From this equation one can determine the basic parameters that characterize the flow through the atomizer by calculating mean parameters \bar{v} and \bar{P}_2 .

Mean value \bar{v}^2 can be calculated from the linear distribution of circumferential velocity. The circumferential velocity on radius r_0 equals v_0 and on radius r_r [according to Eq. (5-122)] equals $v_0 r_r / r_0$, hence

$$\bar{v}^2 = \frac{1}{2} \left(v_0^2 + v_0^2 \frac{r_r^2}{r_0^2} \right)$$

Taking into account Eq. (5-45), we obtain

$$\bar{v}^2 = \frac{2 - \epsilon}{\epsilon} v_0^2 \quad (5-134)$$

The difference of the pressure forces acting on the sides of a liquid element of unit height, width dr , length dl , and mass dm , rotating on radius r with respect to the axis of the discharge orifice, is balanced by the centrifugal force:

$$dl dP_2 = \frac{v^2}{r} dm$$

Substituting v from Eq. (5-122) and $dm = \rho dl dr$, we obtain

$$dP_2 = \rho \frac{v_0^2}{r_0^2} r dr$$

Integrating and determining the interaction constant from the condition of zero pressure on the boundary of the gas core, we obtain the distribution of static pressure in an arbitrary cross section of the discharge orifice:

$$P_2(r) = \rho \frac{\bar{v}^2}{2r_0^2} (r^2 - r_r^2)$$

The mean pressure follows from the condition

$$\bar{P}_2 = \frac{F}{\pi(r_0^2 - r_r^2)}$$

where pressure force F equals

$$F = \int_{r_r}^{r_0} dF = \int_{r_r}^{r_0} 2\pi r dr P_2(r)$$

After substituting $P_2(r)$ and integrating,

$$\bar{P}_2 = \frac{1}{4} \epsilon \rho v_0^2 \quad (5-135)$$

From Eqs. (5-130) and (5-133) to (5-135) we obtain the mean value of the axial component of velocity $\bar{u}_0 = u_0$ in the discharge orifice:

$$u_0 = \sqrt{\frac{2P_1}{\rho}} \left[1 + \frac{\epsilon^2 K_*^2}{(2 - \epsilon)^2} \right]^{-0.5} \quad (5-136)$$

The volumetric flow rate of the liquid is

$$Q = \epsilon A_0 u_0 \quad (5-137)$$

On the other hand, we can write

$$Q = u A_0 \sqrt{\frac{2P_1}{\rho}} \quad (5-138)$$

where μ is the atomizer's discharge coefficient. From Eqs. (5-136)–(5-138) it follows that

$$\mu = \left[\frac{1}{\epsilon^2} + \frac{A_*^2}{(2 - \epsilon)^2} \right]^{-0.5} \quad (5-139)$$

In order to establish the relationship between filling efficiency ϵ and geometric constant K_* the *principle of the maximum flow* will be used. In order to do so, we differentiate Eq. (5-139) with respect to ϵ and set it equal to zero and as a result obtain

$$K_*^2 = \left(\frac{2 - \epsilon}{\epsilon} \right)^3 \quad (5-140)$$

For $\epsilon = 1$, i.e., for complete filling of the discharge orifice, we obtain $K_* = 1$. It follows that for $K_* \leq 1$ the cross section of the orifice is completely filled and for $K_* > 1$ a gas core exists in the discharge orifice.

5-3.2 Viscous Liquid Theory [16, 17]

Because of the viscosity of the liquid, discharge coefficient μ and angle α decrease. Experiments show that the value of μ for all types of jet-swirl atomizers does not drop under normal conditions below $\mu = 0.7$.

Losses due to viscosity have the character of friction and local losses. The sources of these losses are the axial orifice, swirling grooves, swirl chamber, and discharge orifice. The loss coefficients depend mainly on the atomizer's design, so calculation of the pressure loss in a general form is impossible. In this situation, the value of the general loss coefficient should be determined for each type of design.

A general loss coefficient $\Sigma\delta$ can be introduced into Eq. (5-139), and the discharge coefficient assumes the following form:

$$\mu = \left[\frac{1}{\epsilon^2} + \frac{A_*^2}{(2 - \epsilon)^2} + \Sigma\delta \right]^{-0.5} \quad (5-141)$$

For the atomizer shown in Fig. 5-16 the general loss coefficient is

$$\Sigma\delta = 1.1K_*^{0.32}Re^{-0.11} \quad (5-142)$$

where the Reynolds number is given by

$$Re = \frac{u_0 d_0}{\nu}$$

5-3.3 Method of Calculations [16, 17]

This method refers to the atomizer shown in Fig. 5-16. The discharge coefficient can be assumed initially in the range $\mu = 0.7\text{--}0.9$. If spray angle α is known, μ can be calculated from the following equation:

$$\mu = \left(1 + \operatorname{tg}^2 \frac{\alpha}{2} \right)^{-0.5} \quad (5-143)$$

In order to check the value of μ for the designed atomizer one can use the equation

$$\mu = 0.9(0.676 - 24d_0)^{0.13} \quad (5-144)$$

where diameter d_0 is expressed in meters. It was established that discharge coefficient μ does not depend on the angle ϑ of inclination of the swirling grooves.

Based on the given volumetric flow rate Q of the liquid, we calculate from Eq. (5-138) the diameter of the discharge orifice:

$$d_0 = \left(\frac{4Q}{\pi\mu\sqrt{\frac{2\Delta P}{\rho}}} \right)^{0.5} \quad (5-145)$$

where $\Delta P = P_1$.

The problem of the spray angle α in the case of jet-swirl atomizers is very complex. Angle α can be calculated from empirical equations. It can also be calculated from Eq. (5-132), which for $\epsilon = 1$ assumes the form

$$\operatorname{tg} \frac{\alpha}{2} = K_* \quad (5-146)$$

The diameter of the axial orifice d_0 follows from the empirical equation

$$d_a = d_0(0.676 - 24d_0)^{0.5} \quad (5-147)$$

where d_0 is expressed in meters. Knowing diameter d_a and area A_a , we can calculate the total cross-sectional area of the swirling grooves, ΣA_s :

$$\sum A_s = 4.3A_a \quad (5-148)$$

Equation (5-148) refers to the most optimal case, where a uniform radial distribution of the jet density exists in the drop jet.

The size of the square swirling grooves is

$$a = \left(\frac{\sum A_s}{n \cos \vartheta} \right)^{0.5} \quad (5-149)$$

The angle of the inclination of grooves, ϑ , can be selected from Table 4-2, and the diameter of the swirling insert from Table 4-1.

5-4 DESIGN OF PNEUMATIC ATOMIZERS

As mentioned, significant progress has been made in the design of pneumatic atomizers. In Sec. 4-4 information was given about both the design and the dimensions of atomizers. Progress in design has not been followed, however, by progress in calculation methods. The development of such methods is still different due to the character of the flow of two and in some instances three phases. The interaction between these phases has not yet been sufficiently studied.

These difficulties do not refer, however, to atomizers with external gas action on the liquid. Depending on the design of such an atomizer, the primary disintegration of drops proceeds similarly to that in a jet or swirl atomizer, and the gas action affects the secondary drop disintegration and the spray shape. Atomizers with external gas operation can be therefore designed by using methods already presented.

5-4.1 Parallel Flow Atomizers

The characteristic features of these atomizers are small liquid velocities and high or very high gas velocities. The liquid velocity usually does not exceed $V_L = 4$ m/s and often is much lower, especially during gravitational liquid feeding or ejection gas action. The liquid velocity follows from Eq. (3-2):

$$V_L = \sqrt{\frac{2\Delta P}{\rho}} = \sqrt{2gH} \quad (5-150)$$

Table 5-1 Polytropic coefficient π and critical pressure ratio β

	Air	Superheated steam	Dry saturated steam
χ	1.4	1.3	1.135
β	0.528	0.546	0.577

where ΔP = liquid overpressure, Pa

H = height above horizontal level, m

Gas velocity V_G follows from

$$V_G = \sqrt{2 \frac{\chi}{\chi - 1} \frac{P'_G}{\rho'_G} \left[1 - \left(\frac{P''_G}{P'_G} \right)^{(\chi-1)/\chi} \right]} \quad (5-151)$$

where χ = a polytropic coefficient (Table 5-1)

P'_G , ρ'_G = pressure and density of gas before expansion, respectively

P''_G = pressure of gas after expansion

Critical pressure ratio β equals (Table 5-1)

$$\beta = \left(\frac{P''_G}{P'_G} \right)_* = \left(\frac{2}{\chi + 1} \right)^{\chi/(\chi-1)} \quad (5-152)$$

The Mach number equals

$$\text{Ma} = \frac{V_G}{a} \quad (5-153)$$

where a is velocity of sound

$$a = \sqrt{\chi \frac{P'_G}{\rho'_G}} = \sqrt{\chi R T_G} \quad (5-154)$$

where R = gas constant, J/kg · K

T_G = gas temperature, K

In the case of the critical pressure ratio β , gas velocity V_G is equal to the velocity of sound, i.e., $V_G = a = a_*$, where a_* is *critical velocity*. For critical conditions the Mach number is $\text{Ma} = 1$. The gas flow can be described as follows:

- | | | | |
|---------------------|-----------------------|----------------------|-----------------|
| $V_G < a_*$, | $\text{Ma} < 1$, | $P''_G/P'_G > \beta$ | subsonic flow |
| $V_G = a_*$, | $\text{Ma} = 1$, | $P''_G/P'_G = \beta$ | critical flow |
| $V_G \approx a_*$, | $\text{Ma} \approx 1$ | | transsonic flow |
| $V_G > a_*$, | $\text{Ma} > 1$, | $P''_G/P'_G < 1$ | supersonic flow |

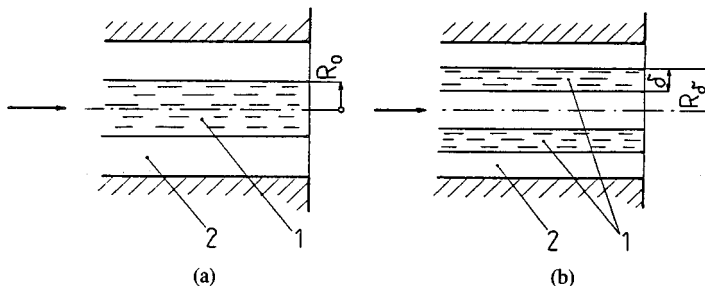


Figure 5-18 Two cases of parallel flow of the liquid and gas: (a) compact liquid jet, (b) annular liquid jet. 1, Liquid; 2, gas.

In pneumatic atomizers all of the types of gas flow described above are used. In the case of supersonic flow, waves of discontinuities develop which improve the liquid atomization.

Figure 5-18 shows two typical cases of cocurrent flow of a liquid and gas, where liquid flows in the form of a compact jet of diameter \$R_0\$ or in the form of an annular jet of inner diameter \$R_\delta\$. The second case is equivalent to the flow of a liquid film of thickness \$\delta\$. Such flows can be considered on the basis of the *similarity criteria*. The quality of atomization can be characterized by using the following criterion [7]:

$$\Pi = \frac{ge_G SR_0}{\nu_L^2} \quad (5-155)$$

where \$e_G\$ = energy of gas/mass of liquid

\$S = 2\pi R_0\$ is the perimeter

\$\nu_L\$ = kinematic viscosity of liquid

$$e_G = b \frac{V_G^2}{2}$$

where \$b\$ = gas/liquid mass ratio (equation (4.10))

\$V_G\$ = initial velocity of gas

For a compact jet (Fig. 5-18a) we obtain

$$\frac{D}{R_0} = B(\bar{\beta}\Pi)^n \quad (5-156)$$

where \$D\$ = mean drop diameter

\$\bar{\beta}\$ = relative coefficient of efficiency of the energy used for liquid atomization (\$\bar{\beta} \approx 0.001\$)

\$B\$ = empirical constant

\$n\$ = empirical coefficient

Disintegration of compact and annular jets caused by the action of the gas proceeds through separation of drops from the liquid surface. It was observed that as the depth from the surface increases, the drop diameters increase. The distribution of drop diameters in the cross section of a jet can be expressed by using the *theory of turbulent jets* proposed by Abramovich [3]:

$$\ln \frac{D_i}{D_{\min}} = K \left(1 - \frac{r_i^2}{r_{\max}^2} \right) \quad (5-157)$$

where D_i = mean drop diameter on radius r_i

D_{\min} = mean drop diameter in the inner layer of the jet

r_{\max} = maximum radius of the liquid jet

K = empirical coefficient (in the case of a compact jet $K = 0.6$)

As a result of the disintegration of the whole jet, a set of drops with different diameters develops. The *mean drop diameter normalized with respect to the total mass* equals

$$D = \frac{\sum_{i=1}^n D_i g_i}{\sum_{i=1}^n g_i} = \frac{\sum_{i=1}^n D_i g_i}{G} \quad (5-158)$$

where g_i = flow rate of an elementary liquid layer encompassing drops with diameter D_i

G = liquid flow rate

Flow rate g_i is given by

$$g_i = \rho_L V_L 2\pi r_i dr_i. \quad (5-159)$$

Substituting Eq. (5-159) into Eq. (5-158) yields

$$D = \frac{\rho_L V_L 2\pi \int_{r_{\min}}^{r_{\max}} D_i r_i dr_i}{G}. \quad (5-160)$$

Substituting D_i from Eq. (5-157) into Eq. (5-160) and noting that r_i changes from 0 to R_0 , we obtain the normalized mean drop diameter for disintegration of the whole jet:

$$D_r = \frac{\rho_L V_L \pi R_0^2 D_{\min} \exp(K_r - 1)}{K_r G} \quad (5-161)$$

In the case of an annular jet or a film of thickness δ (Fig. 5-18), we obtain

$$D_\delta = \frac{\rho_L V_L \pi R_\delta^2 D_{\min} \exp[K_\delta(2\delta/R_\delta) - 1]}{K_\delta G} \quad (5-162)$$

During the gas action on the liquid film, not only do the individual layers disintegrate into drops but also the film deforms, which affects the atomization quality. For this reason coefficients K_r and K_δ have different values.

In the first approximation, expanding $\exp K_r$ and $\exp(K_\delta 2\delta/R_\delta)$ in series and considering only the first two terms of the series, we obtain

$$D_r = \frac{\rho_L V_L \pi R_0^2 D_{\min}}{G} \quad (5-163)$$

$$D_\delta = \frac{\rho_L V_L 2\pi R_\delta \delta D_{\min}}{G} \quad (5-164)$$

Equations (5-163) and (5-154) contain the areas of jet cross sections $A_r = \pi R_0^2$ and $A_\delta = 2\pi R_\delta$, which will be denoted by A_r and A_δ . Equations (5-163) and (5-164) assume the form

$$D_{r,\delta} = \frac{\rho_L V_L D_{\min} A_{r,\delta}}{G} \quad (5-165)$$

For the same values G and the same conditions of gas action, the outer layer of the jet and of the film will disintegrate into identical drops. As a result,

$$\frac{D_\delta}{D_r} = \frac{A_\delta}{A_r} \quad (5-166)$$

That means that under similar conditions of atomization the dimensionless ratio in Eq. (5-156), which contains the mean drop diameter, can be replaced by the ratio $D_{r,\delta}/\sqrt{A_{r,\delta}}$.

Error caused by the approximate series expansion can be compensated for by a correction coefficient ξ . Finally, Eq. (5-156) assumes the form

$$\frac{D}{\sqrt{\xi A}} = B \Pi^n \quad (5-167)$$

For contact jet atomizers $\zeta = 1$, and for atomizers with an annular jet or with a liquid film $\zeta = 2.5$.

5-4.2 Cross-Flow Atomizers

The operation of these atomizers is based on feeding thin liquid jets perpendicular to or at a certain angle with respect to the gas jet. The liquid is disintegrated and entrained, developing a spray with the proper shape. The first subject of calculation is the gas energy consumption. The pressure drop can be determined approximately from the following equation [15]:

$$\Delta P_G = \frac{C}{b} \frac{\rho_G V_G^2}{2} \quad (5-168)$$

where $C = 0.8-0.9$ is an empirical coefficient

b = gas/liquid mass ratio.

Equation (5-168) takes into account only acceleration of gas; it does not account for the liquid disintegration into drops, friction, etc.

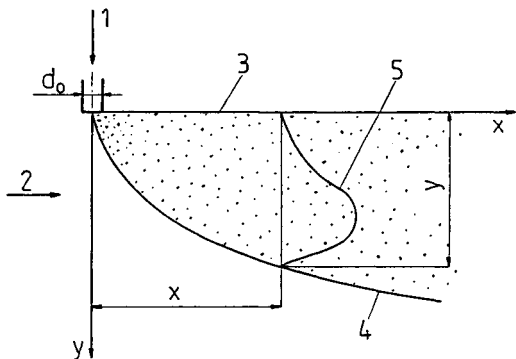


Figure 5-19 Perpendicular liquid feeding to a gas jet. 1, Liquid; 2, gas; 3, 4, inner and outer boundaries of spray; 5, distribution of liquid jet density in spray cross section.

Figure 5-19 shows in a schematic way the shape of the spray during the cross-flow of water and air. Inner border 3 of the spray runs along the streamline passing through the point of water feeding, and outer border 4 is described by the following empirical equation:

$$\frac{y}{d_0} = 1.45 \left(\frac{\Delta P_L}{P_G} \right)^{0.5} \left(\frac{x}{d_0} \right)^{0.5} \quad (5-169)$$

where d_0 = diameter of orifice through which water is fed

ΔP_L = water pressure drop

P_G = dynamic pressure

Equation (5-169) refers to the following conditions:

Uniform distribution of air velocity

Normal conditions (pressure and temperature) of air

Turbulence intensity of air equals 3%

Diameter of water feeding orifice $0.42 \leq d_0 \leq 0.80$ mm

Dimensionless distance, $120 \leq x/d_0 \leq 500$

Pressure ratio $26 \leq \Delta P_1/P_G \leq 300$

5-4.3 Swirl Flow Atomizers

The only published method for a complete design of a pneumatic atomizer with swirl flow will be presented [1]. This method applies to the atomizer shown in Fig. 4-56 with open swirl chamber $D_s = d_0$. The aim of calculations is to determine the dimensions of elements shown in Fig. 5-20. The data given are as follows:

G_L = mass flow rate of water

ρ_L = water density

ΔP_L = water pressure drop

P_G, T_G = initial pressure and temperature of steam used for atomization

P'_G = pressure of attemperated steam (pressure in the swirl chamber)

α = spray angle

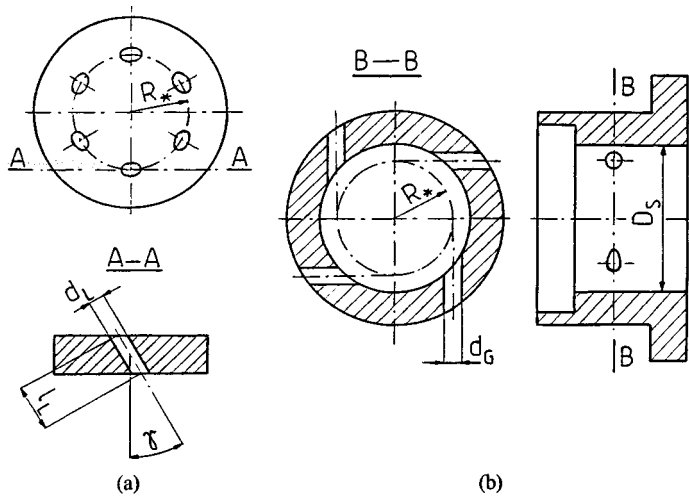


Figure 5-20 Injection elements of atomizer shown in Fig. 4-56: (a) water guide, (b) steam guide with swirl chamber.

The calculation method is based on the following assumptions:

1. The water-steam mixture behaves as a gas because steam constitutes 96–98% of the mixture by volume.
2. The density of the mixture is uniform in the swirl chamber outlet cross section.
3. Axial velocity components of the mixture are equal in the swirl chamber outlet cross section.
4. No heat exchange with the environment occurs.

The total area of cross sections of the water orifices according to Eq. (3-4) is

$$A_L = \frac{G_L}{\mu_1 \sqrt{2 \rho_L \Delta P_L}} \quad (5-170)$$

where μ_1 is the discharge coefficient. For sharp-edged orifices with relative length $l_L/d_L \leq 3.8$, inclination angle $\gamma = 15\text{--}45^\circ$, and Reynolds number $Re = V_L d_L / \nu_L \geq 6 \times 10^4$, one should assume $\mu_1 = 0.63$. The diameter of the water feeding orifices equals

$$d_L = \sqrt{\frac{4A_L}{\pi n_L}} \quad (5-171)$$

where n_L denotes the number of orifices

Steam feeding into the swirl chamber causes throttling of water feeding. The degree of throttling $\lambda = G_L/G_L'$ is the ratio of the water flow rates during

throttling and without throttling. The degree of throttling determined experimentally will be presented in Chapter 6. The calculated diameter of orifices d_L should be corrected by multiplying it by $1/\lambda$.

A flow rate G_G that would ensure good atomization quality should be assumed. It follows from experiments that this can be achieved when the difference in the flux of kinetic energy (power difference) ΔE of the steam and the water is

$$\Delta \dot{E} = \dot{E}_G - \dot{E}_L \geq 2000 \text{ W}$$

where

$$\dot{E}_G = \frac{G_G V_G^2}{2}, \quad \dot{E}_L = \frac{G_L V_L^2}{2}$$

The velocity of water discharge follows from Eq. (3-2):

$$V_L = \sqrt{\frac{2\Delta P_L}{\rho_L}} \quad (5-172)$$

The velocity of steam discharge follows from Eq. (5-151)

$$V_G = \sqrt{2 \frac{\chi}{\chi - 1} \frac{P_G}{\rho_G} \left[1 - \left(\frac{P'_G}{P_G} \right)^{(\chi-1)/\chi} \right]} \quad (5-173)$$

where ρ_G = steam density for P_G and T_G

χ = polytropic coefficient from Table 5-1

The total area of the cross section of steam orifices follows from the equation of flow continuity:

$$A_G = \frac{G_G}{\mu_2 \rho'_G V_G} \quad (5-174)$$

where $\mu_2 \approx 0.63$ is the discharge coefficient for water channels

ρ'_G = steam density in swirl chamber, $\rho'_G = \rho_G (P'_G/P_G)^{1/\chi}$.

The diameter of steam orifices is

$$d_G = \sqrt{\frac{4A_G}{\pi n_G}} \quad (5-175)$$

where n_G is the number of steam orifices.

The cross-sectional area of the jet of the discharge mixture from the swirl chamber equals

$$A = \frac{G}{\rho u} \quad (5-176)$$

where $G = G_L + G_G$,

$$\rho = \left(\frac{G_L}{G} \frac{1}{\rho_L} + \frac{G_G}{G} \frac{1}{\rho_G} \right)^{-1}$$

and u is the mean value of the axial velocity component at the discharge from the swirl chamber. Area A can be also determined in the following way:

$$A = \epsilon \frac{\pi D_s^2}{4} \quad (5-177)$$

where D_s = swirl chamber diameter,

ϵ = efficiency of filling of the inlet cross section which is expressed by an empirical equation

$$\epsilon = 0.99 - 0.00001\Delta E \quad (5-178)$$

The theoretical mean velocity of the mixture, V_t , will be calculated from the condition

$$\dot{E} = \dot{E}_L + \dot{E}_G \quad (5-179)$$

where

$$\dot{E} = \frac{GV_t^2}{2} \quad (5-180)$$

From Eq. (5-179) and (5-180) it follows that

$$V_t = \sqrt{\frac{2(\dot{E}_L + \dot{E}_G)}{G}} \quad (5-181)$$

The real mean velocity of the mixture is $V = kV_t$, where k is the loss coefficient in the swirl chamber. These losses are caused by the impingement of the water and steam jets and therefore depend mainly on ΔE . The following empirical equation has been established:

$$k = \frac{b}{2.67 - \Delta E^{0.05}} \quad (5-182)$$

The value of constant b for investigated water guides fell in the narrow range $b = 1.0-1.03$.

It was established during experiments that for cocurrent swirling of water and steam the velocity ratio $s = u/V$ and the spray angle α depend on angle γ , not on ΔE , which will be discussed further in Chapter 6.

From Eqs. (5-176), (5-177), and (5-181) and taking into account the loss coefficient K and velocity ratio s , we obtain the diameter of the swirl chamber D_s :

$$D_s = 2 \sqrt{\frac{G}{\pi \epsilon \rho u}} = 0.95 \sqrt{\frac{G^{1.5}}{\epsilon \rho k s (\dot{E}_L + \dot{E}_G)^{0.5}}} \quad (5-183)$$

5-5 DESIGN OF ROTARY ATOMIZERS

5-5.1 Disk Atomizers

The liquid is fed in the vicinity of the axis and moves on the surface toward the edge of the disk. The fundamental role in the liquid motion is played by the *slippage* between the liquid and the disk surface. Slippage is an undesirable phenomenon in the process of atomization. For small rotational speed N and small flow rates G , it is assumed that there is no slippage and therefore the circumferential velocity of the liquid spinning off the disk edge is equal to the velocity of this edge. For rotational speeds higher than $N = 1000$ rpm and flow rates higher than $G \approx 0.5 \times 10^{-3}$ kg/s, i.e., the conditions most frequently encountered in practice, the problem of slippage cannot be neglected.

Slippage can be significantly reduced by shaping the disk in the form of a cone or a cup as depicted in Figs. 4-63 and 4-64, which causes increased liquid pressure on the disk surface. However, if the ratio of the flow rate to the disk perimeter increases to a certain value, slippage increases again, which can be expressed by the following inequality:

$$\frac{G}{2\pi R \mu} > 600 \quad (5-184)$$

where G = mass flow rate, kg/s

R = disk radius, m

μ = liquid viscosity, Pa · s

For example, in the case of a disk with radius $R = 63.5$ mm and water flow rate $G = 0.063$ kg/s, the circumferential velocity of water is 0.8 of the velocity of the disk. As the flow rate increases to $G = 0.63$ kg/s, the velocity ratio drops to 0.5. A radical way to decrease or eliminate slippage is to place radial vanes on the disk.

In the vicinity of the disk axis a liquid element has all components of velocity, axial u , circumferential v and radial w (Fig. 5-21). On the disk's edge the liquid has only v and w components. The following forces act on an element of the liquid: centrifugal force, friction force on the disk surface, inertial force, and Coriolis force.

The Coriolis force appears in all types of rotary atomizers, especially in cases of motion of a liquid with small viscosity. The Coriolis force acts perpendicularly to the radius having the sense opposite to the direction of rotation of the atomizer. As a result, the circumferential velocity of the liquid becomes smaller than the velocity of the rotating surface; liquid moves along a spiral trajectory and the liquid thickness increases at the disk edge. This is due to slippage of the liquid.

From the Navier-Stokes equation and the equation of flow continuity, we

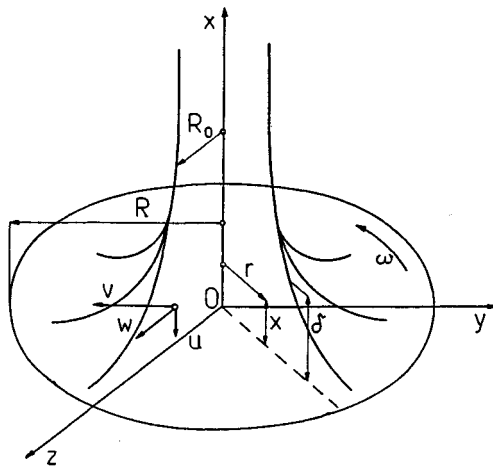


Figure 5-21 Disk atomizer—calculation scheme.

obtain equations for all three velocity components of the liquid element (Fig. 5-21) [17]:

$$u = \left(\frac{3\omega^4 Q}{16\pi\nu^2 r^2} \right)^{1/3} x^2 - \frac{\omega^2}{16\nu} x^3 \quad (5-185)$$

$$v = r\omega \left[1 - \frac{Q}{\pi\nu r^2} x - \left(\frac{\omega^4 Q}{18\pi\nu^5 r^2} \right)^{1/3} x^3 + \frac{\omega^2}{12\nu^2} x^4 \right] \quad (5-186)$$

$$w = \left(\frac{3r\omega^4 Q}{2\pi\nu^2} \right)^{1/3} x - \frac{r\omega^2}{2\nu} x^2 \quad (5-187)$$

Now all three types of drop development using disk atomizers will be considered (Fig. 4-62). The first type, the *drop mode*, applies to low flow rates. Relatively uniform drops develop in this case as well as drop satellites, whose diameter is approximately 2.5 times smaller than the diameter of main drops. The diameter of main drops follows from Eq. (2-165), which has the form

$$D = \frac{C}{\omega} \left(\frac{\sigma}{\rho R} \right)^{1/2} \quad (5-188)$$

where $C = 1.9-4.6$ is a constant

$\omega = 2\pi N/60$ is the disk angular velocity, rad s⁻¹

N = rotational speed, rpm

σ = surface tension, N m⁻¹

$\rho = \rho_L$ = liquid density, kg/m³

R = disk radius, m

In [12] a semi-empirical equation was given:

$$\frac{D}{R} = 2.69 \text{We}^{-1/2} \quad (5-189)$$

where the Weber number is

$$\text{We} = \frac{\rho R^3 \omega^2}{\sigma} \quad (5-190)$$

For $C = 2.69$ Eqs. (5-188) and (5-189) are identical.

Mass fraction e of drops to satellites follows from

$$e = 0.86 \frac{\omega^{0.48} \nu^{0.12}}{R^{0.3}} \left(\frac{\rho Q}{\sigma} \right)^{0.62} \quad (5-191)$$

This fraction is $e = 0.1\text{--}0.2$. From Eqs. (5-188) and (5-191) the disk radius R and angular velocity ω can be calculated.

From the Navier-Stokes equation and flow continuity equation we calculate the film thickness on the disk edge [17]:

$$\delta = \left(\frac{3\nu Q}{2\pi R^2 \omega^2} \right)^{1/3} \quad (5-192)$$

The maximum radial velocity component of the liquid on the disk edge is

$$w_{\max} = \left(\frac{9\omega^2 Q^2}{32\pi^2 \nu R} \right)^{1/3} \quad (5-193)$$

The mean value of the radial velocity component in the liquid film is

$$\bar{w} = \frac{2}{3} w_{\max} = \left(\frac{\omega^2 Q^2}{12\pi^2 \nu R} \right)^{1/3} \quad (5-194)$$

These equations are valid for the laminar flow of the film, which under real conditions is always satisfied.

Assuming that there is no slippage, we can calculate the circumferential velocity component of the liquid v on the disk edge and therefore determine the angle Θ between the total velocity V_L and the tangential direction (Fig. 5-22). For example, for $R = 76$ mm and $N = 10,000$ rpm the circumferential component v is

$$v = \frac{2\pi RN}{60} = \frac{2\pi \times 0.076 \times 10,000}{60} \approx 80 \text{ m/s}$$

For low water flow rates, e.g., $Q = 0.005 \times 10^{-3} \text{ m}^3/\text{s}$, the radial velocity component of water on the disk edge is only $w_{\max} \approx 2.2 \text{ m/s}$. Angle Θ is given by

$$\tan \Theta = \frac{w_{\max}}{v} = \frac{2.2}{80} = 0.0275$$

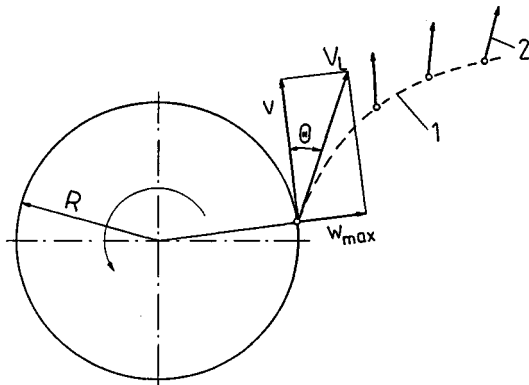


Figure 5-22 Kinematics of a liquid element on the disk edge. 1, Drop trajectory with respect to the disk edge; 2, direction of drop motion with respect to the environment.

hence $\Theta \approx 1^{\circ}30'$. For a water flow rate that is 10 times higher, the radial component is as high as $w_{\max} \approx 46 \text{ m/s}$, and angle $\Theta \approx 30^\circ$.

The second atomization type, the *ligament formation mode*, applies to larger liquid flow rates than in the first regime. The limiting criterion for those regimes is the dimensionless flow rate [12]

$$Q_{1-2} = 0.096 \text{Re}^{0.95} \text{We}^{-1.15} \quad (5-195)$$

where

$$Q_{1-2} = \frac{Q}{2\pi R^2 \sqrt{\nu \omega}} \quad (5-196)$$

$$\text{Re} = \frac{\omega R^2}{\nu} \quad (5-197)$$

and We is given as in Eq. (5-190). Another condition for passing from the first mode to the second one follows from Eq. (5-191) and corresponds to $e = 1$.

In the ligament mode, the number of liquid ligaments at the disk edge increases as the flow rate increases up to a certain limiting value. At a certain distance from the disk edge the ligaments disintegrate into drops. Thin links between ligaments transform into drops-satellites (Fig. 5-23). This mode is the most advantageous because of the technical possibility of use of uniform drops.

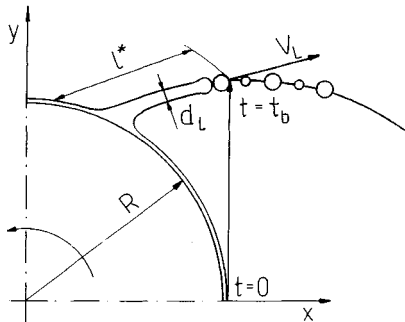


Figure 5-23 Trajectory of a ligament.

A trajectory of a ligament developed at the disk edge is described by the following approximate system of equations [12]:

$$\left. \begin{aligned} x &= R \cos(\omega t) + R \omega t \sin(\omega t) \\ y &= R \sin(\omega t) - R \omega t \cos(\omega t) \end{aligned} \right\} \quad (5-198)$$

and liquid velocity in a ligament is given by

$$V_L = \sqrt{\left(\frac{dx}{dt}\right)^2 + \left(\frac{dy}{dt}\right)^2} = R \omega^2 t \quad (5-199)$$

Assuming time t_b at which the ligament starts to disintegrate, we can write the following equations:

$$V_L = R \omega^2 t_b \quad (5-200)$$

$$l^* = \frac{1}{2} R \omega^2 t_b^2 \quad (5-201)$$

where l^* is the length of the ligament, i.e., length of the ligament until it disintegrates. From Weber theory, it follows that

$$\frac{l^*}{d_l} = C \sqrt{\text{We}_l} \left(1 + \frac{3\mu}{\sqrt{\rho \sigma d_l}} \right) \quad (5-202)$$

while

$$\text{We}_l = \frac{\sigma d_l V_L^2}{\sigma} \quad (5-203)$$

The drop diameter according to Weber theory is approximately (see Sec. 2-2.1)

$$D = 1.88 d_l \quad (5-204)$$

The diameter of the ligament follows from the flow rate balance

$$d_l = \sqrt{\frac{4Q}{\pi N_l V_l}} \quad (5-205)$$

where a number of liquid ligaments follows from a semiempirical equation presented by Hinze and Milborn [10]

$$N_l = 0.574 \text{Re}^{1/3} \text{We}^{1/4} \quad (5-206)$$

where Re and We are the Reynolds and Weber numbers from Eqs. (5-197) and (5-190), respectively.

From Eqs. (5-200)–(5-205), omitting the second term in the brackets in Eq. (5-202), we obtain the equation for drop diameter

$$\frac{D}{R} = C' \left(\frac{1}{N_l} \right)^{2/7} \left(\frac{\rho Q^2}{R^3 \sigma} \right)^{1/7} \text{We}^{-2/7} \quad (5-207)$$

Equation (5-207) was confirmed experimentally for $C' = 1.23$.

A theoretical expression was derived in [5] for a mean drop diameter D for drops that develop as a result of ligament disintegration:

$$D = 5.75 N^{-0.79} Q^{0.32} R^{-0.69} \rho^{0.29} \sigma^{0.26} (1 + 0.23 \mu^{0.65}) \quad (5-208)$$

where individual parameters are expressed as D , cm; N , rpm; Q , cm^3/s ; R , cm; ρ , g/cm^3 ; σ , g/s^2 ; μ , $\text{g}/(\text{cm} \cdot \text{s})$. It was established experimentally that drop diameters derived from Eq. (5-208) are approximately 5% larger than the Sauter mean diameter.

The third atomization type, the *sheet formation mode*, occurs for further flow rate increases. The limiting criterion for the ligament and sheet formation modes is dimensionless flow rate Q_{2-3} , which is expressed as in Eq. (5-195):

$$Q_{2-3} = 0.340 \text{Re}^{0.667} \text{We}^{-0.883} \quad (5-209)$$

The sheet formation mode is characterized by a large scatter in drop diameters, similar to that for atomization using jet, swirl, jet-swirl, and pneumatic atomizers. For this mode neither theoretical nor empirical data exist.

In [12] theoretical expressions were derived for the liquid sheet thickness δ and dimensionless flow rates Q_{1-2} and Q_{2-3} for non-Newtonian liquids. These equations were confirmed by experiments.

5-5.2 Cup Atomizers

On the rim of the cup, as on the disk edge, one of the previously discussed atomization regimes can occur. At an arbitrary point on the cup surface on radius r a liquid film develops with thickness δ (Fig. 5-24):

$$\delta = \left(\frac{3 \nu Q}{2 \pi r^2 \omega^2 \sin \beta} \right)^{1/3} \quad (5-210)$$

For the inlet edge $r = R$ and for the angle $\beta = 90^\circ$, i.e., for $\sin \beta = 1$, Eq. (5-210) assumes the form of Eq. (5-192). This equation neglects gravity, hence it applies to high centrifugal accelerations $r\omega^2 \gg g$. For $\beta = 0^\circ$, $\delta = \infty$, which means that liquid adheres to the cup surface.

The *mean film velocity* \bar{w} along the cup surface is

$$\bar{w} = \left(\frac{\omega^2 Q^2 \sin \beta}{12 \pi^2 \nu r} \right)^{1/3} \quad (5-211)$$

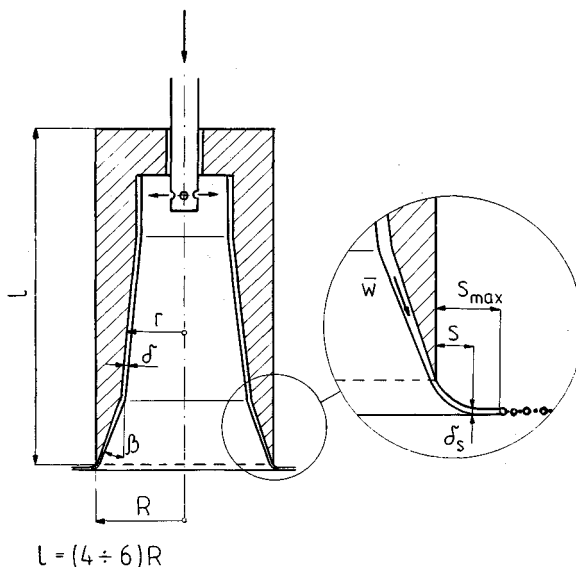


Figure 5-24 Schematic diagram of liquid flow in a cup atomizer.

For the inlet edge $r = R$ and for angle $\beta = 90^\circ$, i.e., for $\sin \beta = 1$, Eq. (5-211) assumes the form of Eq. (5-194). At the edge of the cup the liquid film deflects rapidly in the radial direction.

The thickness δ of the liquid film at radial distance s from the cup edge (Fig. 5-24) is given by [15]

$$\delta_s = \frac{Q}{2\pi\nu} \left(\frac{R^2 \bar{w}^2}{\nu^2} + 2Rs + s^2 \right)^{-1/2} \quad (5-212)$$

where ν is a circumferential velocity component. Film thickness decreases rapidly as distance s increases. Film moving in the radial direction loses stability and at distance s_{\max} disintegrates into drops.

Example 5-3 Determine the liquid film thickness δ on the edge and at distance s from the edge for a cup atomizer (Fig. 5-24). Data: $Q = 0.078 \text{ l/s}$, $R = 50 \text{ mm}$, $N = 4500 \text{ rpm}$, $\nu = 45 \times 10^{-6} \text{ m}^2/\text{s}$, $s = 5 \text{ mm}$.

SOLUTION Liquid film thickness on the edge follows from Eq. (5-210) for $r = R$ and angle $\beta = 90^\circ$, i.e., for $\sin \beta = 1$:

$$\begin{aligned} \delta &= \left(\frac{3\nu Q}{2\pi R^2 \omega^2} \right)^{1/3} = \left(\frac{3 \times 45 \times 10^{-6} \times 0.078 \times 10^{-3}}{2\pi \times 0.05^2 \times 470^2} \right)^{1/3} \\ &\approx 0.00014 \text{ m} = 140 \mu\text{m} \end{aligned}$$

where

$$Q = 0.078 \times 10^{-3} \text{ m}^3/\text{s}$$

$$R = 0.05 \text{ m}$$

$$\omega = \frac{2\pi N}{60} = \frac{2\pi \times 4500}{60} = 470 \text{ s}^{-1}$$

Liquid film thickness can also be calculated from Eq. (5-212) for $s = 0$. We then obtain

$$\delta = \frac{Q}{2\pi R \bar{w}}$$

Velocity \bar{w} on the atomizer edge follows from Eq. (5-211) for $r = R$ and $\beta = 90^\circ$, i.e., for $\sin \beta = 1$:

$$\bar{w} = \left(\frac{\omega^2 Q^2}{12\pi^2 \nu R} \right)^{1/3} = \left[\frac{470^2 (0.078 \times 10^{-3})^2}{12\pi^2 \times 45 \times 10^{-6} \times 0.05} \right]^{1/3} = 1.71 \text{ m/s}$$

As a result of substitutions,

$$\delta = \frac{0.078 \times 10^{-3}}{2\pi \times 0.05 \times 1.71} \approx 0.00014 = 140 \mu\text{m}$$

Liquid film thickness δ_s at a distance s from the cup atomizer's edge follows from Eq. (5-212)

$$\begin{aligned} \delta_s &= \frac{Q}{2\pi\nu\sqrt{R^2\bar{w}^2/v^2 + 2Rs + s^2}} \\ &= \frac{0.078 \times 10^{-3}}{2\pi \times 23.6\sqrt{(0.05^2 \times 1.71^2)/23.6^2 + 2 \times 0.05 \times 0.005 + 0.005^2}} \\ &= 0.000022 \text{ m} = 22 \mu\text{m} \\ &\quad \left(v = \frac{2\pi RN}{60} = \frac{2\pi \times 0.05 \times 4500}{60} = 23.6 \text{ m/s} \right) \end{aligned}$$

5-5.3 Wheel Atomizers

Vaned atomizers. Power consumption in the case of impeller atomizers is higher than for disk atomizers. The theoretical power in kilowatts equals [9]

$$\dot{E} = 3.8 \times 10^{-10} GN^2 (8R^2 - d_d) \quad (5-213)$$

where G = liquid flow rate, kg/h

N = engine rotation speed, rpm

R = impeller diameter, m

d_d = liquid distributor diameter, m

The real power consumption is higher because of the friction losses and air pumping effect. It is difficult, however, to establish an empirical expression taking these losses into account because the design of vaned atomizers is very diverse.

Radial velocity on the outlet edge of the impeller follows from [9]

$$w_{\max} = 0.0024 \left(\frac{2\rho\pi^2 N^2 R Q^2}{\mu h^2 n^2} \right)^{1/3} [\text{m/s}] \quad (5-214)$$

where ρ = liquid density, kg/m³

N = rotation speed of the impeller, rpm

R = impeller diameter, m

Q = liquid flow rate, m³/h

μ = liquid dynamic viscosity, mPa · s

h = height of vanes, m

n = number of vanes

Radial penetration of drops is a complex problem because it concerns the motion of a set of drops for which the initial velocities are not known. Due to air currents and turbulence it is difficult to establish a distinct boundary of the spray. Herring and Marshall presented an expression for $(r_{99})_{0.9}$, i.e., for the radial penetration for which 99% of drops fall 0.9 m lower than the atomizer plane with a vertical axis of rotation [10]

$$(r_{99})_{0.9} = \frac{31R^{0.21}G^{0.25}}{N^{0.16}} [\text{m}] \quad (5-215)$$

where R = impeller radius, m

G = liquid flow rate, kg/s

N = rotational speed of the impeller, rpm

Atomizers with a perforated periphery. A schematic diagram of a perforated drum is shown in Fig. 5-25. Inside the drum, liquid motion establishes according to [22]

$$v = C_1 r^{k+1} - \frac{C_2}{(k+2)r} \quad (5-216)$$

where $v = \omega r$ is circumferential component of liquid velocity

C_1, C_2 = constants

r = radius

$K = Q/2\pi H_\nu$ is a dimensionless parameter

H = height of liquid column

ν = liquid kinematic viscosity

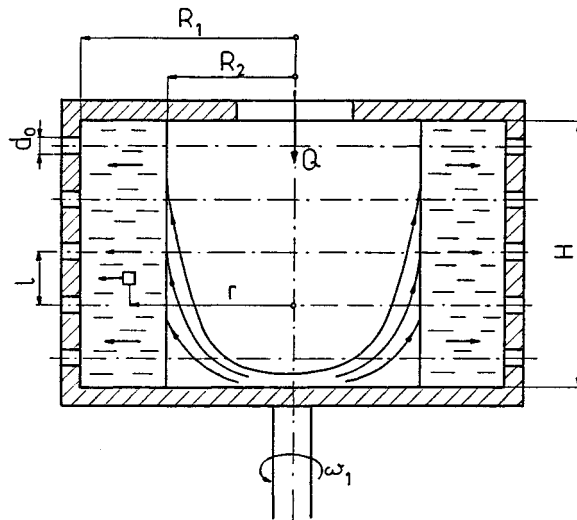


Figure 5-25 Schematic diagram of operation of a perforated drum.

The boundary conditions are as follows.

For $r = R_1$: $v = \omega_1 R_1$

For $r = R_2$: $\tau = 0$

where the latter condition means absence of a stress on the free surface of the liquid. As a result,

$$v = \frac{\omega_1 R_1^2 (r^{k+2} + 0.5kR_2^{k+2})}{r(R_1^{k+2} + 0.5kR_2^{k+2})} \quad (5-217)$$

Figure 5-26 shows the results of calculations of velocity v from Eq. (5-217). Because of liquid feed Q , a radial component of liquid velocity appears that affects significantly the value of the liquid slippage. The higher the value of parameter K , the more the circumferential component of liquid velocity decreases with respect to the transport velocity of the impeller. This can be explained in terms of the increase of the Coriolis force.

From Eq. (5-217) for $v = \omega_2 R_2$ and $r = R_2$ we obtain the expression for ω_2 :

$$\omega_2 = \frac{\omega_1 x^2 (k + 2)}{2x^{k+2} + k} \quad (5-218)$$

where $x = R_1/R_2$. Assuming that the hydraulic pressure of the liquid head equal to H is balanced by the centrifugal force of the vortex with radius R_2 , we obtain

$$\sqrt{2gH} = \omega_2 R_2 \quad (5-219)$$

It follows from Eqs. (5-218) and (5-219) that

$$x = \left[\frac{\omega_1 R_1 (k+2) - (k/x) \sqrt{2gH}}{2\sqrt{2gH}} \right]^{1/(k+1)} \quad (5-220)$$

Quantity x can be calculated using an iteration method assuming as a first approximation $k/x \approx k$.

Mean angular velocity $\bar{\omega}$ of the liquid in region $R_2 \leq r \leq R_1$ equals

$$\bar{\omega} = \frac{1}{R_1 - R_2} \int_{R_2}^{R_1} \omega dr$$

hence

$$\frac{\bar{\omega}}{\omega_2} = \frac{(1 + (\omega_1/\omega_2)x^2)(x^{k+2} - 1) + x(k+1)(x-1)[(k+1)\omega_1/\omega_2 - x^k]}{(k+1)(x-1)(x^{k+2} + k+1)} \quad (5-221)$$

The Navier-Stokes equation for a nonviscous liquid in cylindrical coordinates has the following form:

$$w \frac{dw}{dr} - \frac{v^2}{r} = - \frac{1}{\rho} \frac{dP}{dr}$$

In the absence of slippage resulting from the absence of the radial velocity component, i.e., for $w = 0$ and $V = \omega r$, we obtain

$$P = \rho \omega^2 \int_{R_2}^{R_1} r dr = \frac{\rho \omega_1}{2} (R_1^2 - R_2^2)$$

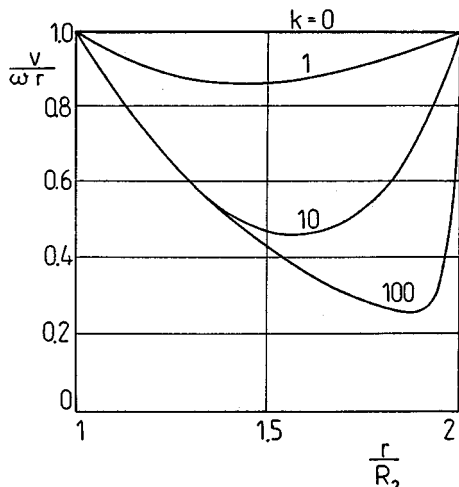


Figure 5-26 Liquid slippage as a result of the radial flow of liquid for $R_1/R_2 = 2$.

where calculated pressure P corresponds to $\omega = \omega_1$. Based on this pressure we can calculate in a simplified way the liquid discharge through a perforated wall. Substituting from the Bernoulli equation

$$P = \frac{\rho u^2}{2}$$

we obtain

$$u = \omega_1 \sqrt{R_1^2 - R_2^2}$$

It follows from the flow continuity equation that

$$Q = Au = \mu n A_0 \omega_1 \sqrt{R_1^2 - R_2^2} \quad (5-222)$$

where $A = \mu n A_0$ is the total area of orifices

μ = discharge coefficient; for $d_0 = 1\text{-}4$ mm and $l/d_0 < 2$, $\mu = 0.53(l/d_0)^{0.45}$, and for $l/d_0 > 2$, $\mu = 0.73$ independent of liquid viscosity

$A_0 = \pi d_0^2/4$ is the cross-sectional area of a singular orifice

n = number of orifices

As seen, flow rate Q increases as radius R_2 decreases and reaches the maximum value for $R_2 = 0$.

Under real conditions, pressure causing the liquid flow through the orifices is a sum of the pressures of the central vortex with radius R_2 and the liquid layer rotating with mean angular velocity $\bar{\omega}$. The liquid flow rate is then equal to

$$Q = \mu n A_0 \omega_2 R_2 \sqrt{1 + \left(\frac{\bar{\omega}}{\omega_2}\right)^2 (x^2 - 1)} \quad (5-223)$$

Example 5-4 Determine the liquid film thickness δ on the edge of an impeller atomizer. Data: $Q = 0.5 \text{ m}^3/\text{h}$, $R = 105 \text{ mm}$, $N = 10,000 \text{ rpm}$, $\rho = 1100 \text{ kg/m}^3$, $\mu = 2 \text{ mPa} \cdot \text{s}$, $n = 24$ vanes, vane height $h = 30 \text{ mm}$ [9].

SOLUTION A uniform liquid distribution in all vane passages was assumed. From Eq. (5-214) the radial velocity of the liquid is

$$\begin{aligned} w_{\max} &= 0.0024 \left(\frac{2 \rho \pi^2 N^2 R Q^2}{\mu h^2 n^2} \right)^{1/3} \\ &= 0.0024 \left(\frac{2 \times 1100 \times \pi^2 \times 10,000^2 \times 0.105 \times 0.5^2}{2 \times 0.03^2 \times 24^2} \right)^{1/3} \\ &= 9 \text{ m/s} \end{aligned}$$

Liquid film thickness δ follows from the flow continuity condition:

$$Q = n \delta h w_{\max}$$

hence

$$\begin{aligned}\delta &= \frac{Q}{n h w_{\max}} = \frac{0.5}{3600 \times 24 \times 0.03 \times 9} \\ &= 0.0000214 \text{ m} = 21.4 \mu\text{m}\end{aligned}$$

REFERENCES

1. Adamowicz, K., Orzechowski, Z. Design of a pneumatic atomizer for steam attemperation. *Teploenergetika*, No. 1, 1978 (in Russian).
2. Astakhov, I. V. *Fuel Supply and Atomization in Diesel Engines*. Mashinostroenie, Moscow, 1972 (in Russian).
3. Borodin, V. A., Dityakin, Yu. F., Klyachko, L. A., Yagodkin, V. I. *Liquid Atomization*. Mashinostroenie, Moscow, 1967 (in Russian).
4. Dityakin, Yu. F., Klyachko, L. A., Novikov, B. V., Yagodkin, V. I. *Liquid Atomization*. Mashinostroenie, Moscow, 1977 (in Russian).
5. Kayano, A., Kamiya, T. Calculation of the mean size of the droplets purged from the rotating disk. *Proc. ICCLASS-78*, Tokyo, 6-1, 133–138, 1978.
6. Klyachko, L. A. Theories of a flow of a real liquid in rotary atomizer. *Teploenergetika*, No. 6, 1980 (in Russian).
7. Kulagin, L. V., Makarov, V. V. A choice of a similarity criterion for evaluation of fuel atomization using pneumatic atomizers with film flow. *Teploenergetika*, No. 6, 1977 (in Russian).
8. Lyshevskii, A. S. *Processes of Fuel Atomization in Diesel Nozzles*. Mashgiz, Moscow, 1963 (in Russian).
9. Masters, K. *Spray Drying Handbook*. George Goodwin, London, 1985.
10. Matsumoto, S., Belcher, D. W., Crosby, E. J. Rotary atomizers: Performance understanding and prediction. *Proc. ICCLASS-85*, London, Vol. 1, IA/1/1–21, 1985.
11. Matsumoto, S., Crosby, E. J. Flow characteristics of impact jet nozzles. *Atomisation Spray Technol.*, Vol. 3, No. 2, pp. 77–88, 1987.
12. Matsumoto, S., Takashima, Y. Atomization characteristics of power law fluids by rotating disks. *Proc. ICCLASS-78*, Tokyo, 6-3, 145–150, 1978.
13. Melodiev, E. A., Sinitsyn, B. D., Shamanaev, V. S. Hydraulic characteristics of a rotary atomizer, *Izv. Vyssh. Uchebn. Zaved. Mashinostr.*, No. 8, 1980 (in Russian).
14. Nieuwkamp, W. C. Flow analysis of a hollow cone nozzle with potential flow theory. *Proc. ICCLASS-85*, London, Vol. 1, III C/1/1–9, 1985.
15. Orzechowski, Z. *Liquid Atomization*. WNT, Warsaw, 1976 (in Polish).
16. Pazhi, D. L., Galustov, V. S. *Liquid Atomizers*. "Khimiya" Moscow, 1979 (in Russian).
17. Pazhi, D. L., Galustov, V. S. *Fundamentals of Liquid Atomization*. "Khimiya" Moscow, 1984 (in Russian).
18. Ranganatha Babu, K., Narasimhan, M. V., Narayanaswamy, K. Design of swirl chamber atomizers. *Proc. ICCLASS-85*, London, Vol. 1, III C/3/1–7, 1985.
19. Ranganatha Babu, K., Narasimhan, M. V., Narayanaswamy, K. Correlations for prediction of discharge rate, cone angle and air core diameter of swirl spray atomizers. *Proc. ICCLASS-82*, Madison, Wisconsin, 3-3, 91–97, 1982.
20. Rizk, N. K., Lefebvre, A. H. Prediction of velocity coefficient and spray cone angle for simplex swirl atomizers. *Proc. ICCLASS-85*, London, Vol. 1, III C2/1–16, 1985.

21. Rizk, N. K., Lefebvre, A. H. Influence of liquid properties on the internal flow characteristics of simplex swirl atomizers. *Atomization Spray Technol.*, Vol. 2, No. 3, pp. 219–233, 1986.
22. Troshkin, O. A., Hydraulic design of a centrifugal cylindrical sprayer. *Khim. Neft. Mashinostr.*, No. 5, 1984 (in Russian).
23. Valeev, R. S., Kudryavtsev, A. V., Kuntsev, G. M. Experimental investigation of atomization of liquid jet fed perpendicular to the gas jet. *Izv. Vyssh. Ucheln. Zaved. "Aviatsionnaya Tekhnika,"* No. 3, 1984 (in Russian).
24. Walzel, P. Advantages and limits in large scale modeling of atomizers. *Proc. ICLASS-82*, Madison, Wisconsin, 7-12, 187–194, 1982.

EXPERIMENTAL RESULTS

The present chapter contains results of experimental investigations. These results show the influence of the design and operational conditions of atomizers on the parameters of the atomized liquid. These parameters are the flow rate, macrostructure, and microstructure of atomized liquid. Basic types of atomizers will be discussed. The experimental data are very extensive because the development of atomizers is based mainly on experimental results, and therefore only selected data will be presented.

6-1 JET ATOMIZERS

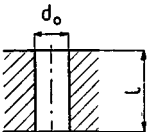
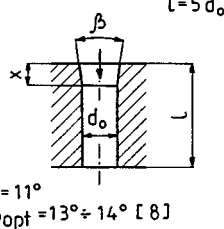
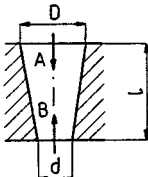
6-1.1 Flow Rate of Atomized Liquid

The flow rate can be calculated from Eq. (3-3) or (3-4) if the discharge coefficient μ is known. In Sec. 3-1 basic information concerning μ was supplied and some quantitative data (Fig. 4-2) for simplex atomizers were given. In Sec. 5-1.2 methods of calculation of μ were presented for two intermittent jet atomizers for the case in which the constituent discharge coefficients are known. Presently, the results of some experiments will be given.

Discharge coefficient μ depends on such factors as the shape of the orifice, length to orifice diameter ratio l/d_0 , pressure drop $\Delta P = P_1 - P_2$, ambient gas pressure P_2 , and properties of liquid.

The effect of the orifice shape on μ is clearly visible in Fig. 4-2. Table 6-1 contains values of μ for orifices with a circular cross section but different

Table 6-1 Discharge coefficient μ for various types of orifices [4]

	l/d_0	0.5–1 0.6–0.65	2–5 0.75–0.85	5* 0.62
*for $\Delta P > 0.3 \text{ MPa}$				
	$x, \text{ mm}$	0.5 0.67–0.69	1–2 ~ 0.9	
for $\Delta P > 0.3 \text{ MPa}$				
	Flow direction μ	A 0.93–0.96	B 0.62	
for $\Delta P > 0.3 \text{ MPa}$				

shapes. As seen, the shape of the orifice has a large influence on the value of μ . Especially the shape of the inlet edge (Fig. 4-2) has a large effect.

The influence of the ratio of length to orifice diameter, i.e., l/d_0 is very complex. Fig. 6-1 shows a liquid jet discharging from a sharp-edged orifice with various lengths l but the same diameter d_0 . The liquid jet *contracts* (see Sec. 5-1.1). In the case of $l/d_0 \geq 2$ (Fig. 6-1b) the jet expands within the orifice, which causes the discharge to have the same character as in the so-called mouthpiece. In the smaller cross section of the jet a negative pressure P_{\min} develops, which causes almost a 40% increase of the flow rate. Under certain conditions, i.e., when velocity V increases (increase of $\Delta P = P_1 - P_2$), the liquid jet can separate from the orifice wall; i.e., jet contraction and a rapid flow rate decrease can occur.

It follows from Table 6-1 that for a cylindrical orifice distinctly different values exist for $l/d_0 = 0.5–1.0$ and $l/d_0 = 2–5$. Cylindrical orifices with $l/d_0 = 2–5$ are most commonly used. For this case μ for a cylindrical orifice with a sharp edge follows from the formula [9]

$$\mu = \left(1.23 + \frac{58}{\text{Re}_H} \frac{1}{d_0} \right)^{-1} \quad (6-1)$$

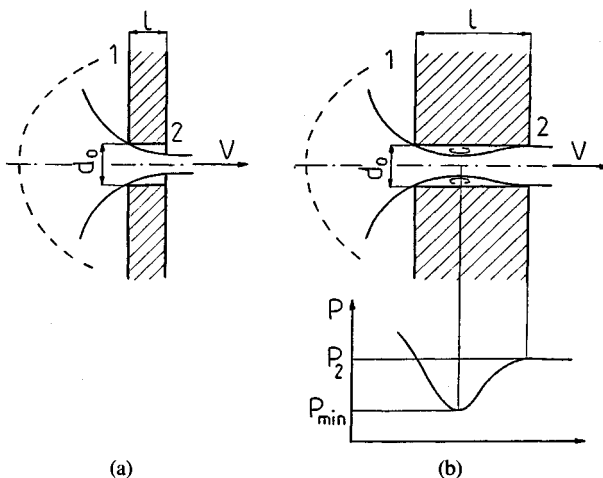


Figure 6-1 Shape of the liquid discharging from a sharp-edged orifice: (a) $l/d_0 < 2$; (b) $l/d_0 \geq 2$.

where the Reynolds number is given by

$$\text{Re}_H = \frac{4Q}{\pi d_0 \nu} \frac{1}{\mu} \quad (6-2)$$

Equation (6-1) applies to the range of Reynolds numbers $\text{Re}_H = 1 \times 10^2$ to 1.5×10^5 .

The increase of ratio l/d_0 leads to an increase in friction losses, i.e., to increased loss of kinetic energy ξ expressed by Eq. (5-7). According to Eq. (5-80), this causes a decrease in the velocity loss coefficient β and therefore a decrease in ratio μ . Figure 6-2 shows an example of the change of μ as a function of l/d_0 for an orifice with a rounded inlet edge [4]. As seen, μ decreases as l/d_0 increases but still has a high value because of the advantageous effect of the inlet edge. From [13] it follows that starting with $r > 0.3r_0$, where $r_0 = d_0/2$, the phenomenon of contraction does not occur.

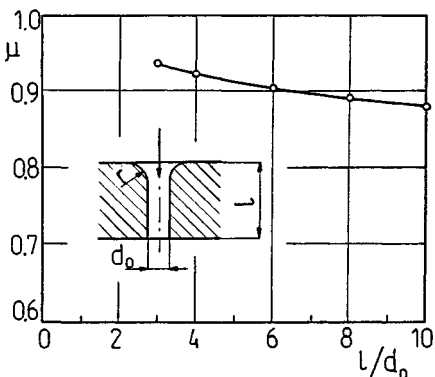


Figure 6-2 Dependence of discharge coefficient μ on ratio l/d_0 ; $\Delta P = 0.7$ MPa, $d_0 = 0.8$ mm, $r = 0.8$ mm.

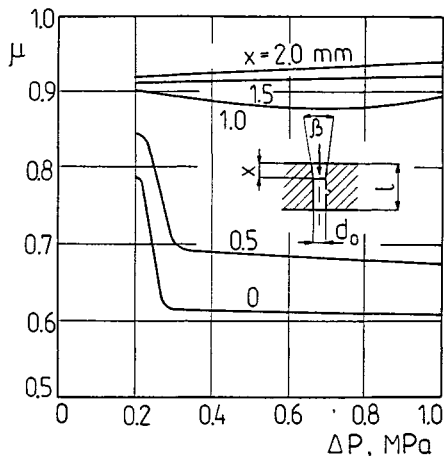


Figure 6-3 Discharge coefficient μ as a function of ΔP for various cone heights x ; $l/d_0 = 5$; $\beta = 11^\circ$.

The effect of pressure drop ΔP on μ is shown in Fig. 6-3 [4]. As seen, for $\Delta P \approx 0.3$ MPa a rapid decrease of μ occurs. This is caused by the separation of the jet from the orifice wall. For a cylindrical orifice ($x = 0$) μ decreases from 0.78 to 0.62. The value $\mu = 0.62$ also appears in Table 6-1 for $\Delta P > 0.3$ MPa. The separation of the jet and rapid decrease of μ should not occur during atomizer operation. However, the lack of sufficient experimental data for various orifices makes it difficult to protect against such phenomena.

The effect of ambient gas pressure P_2 on μ can be considered only when pressure drop $\Delta P = \text{const}$. It follows from (Fig. 6-4), that the increase of P_2 can eliminate the phenomenon of contraction [4]. As seen, even a very short orifice ($l = 0.5 d_0$) can have a high value of μ .

Everything said above applies to continuous and intermittent atomizers. However, intermittent atomizers have more complex flow conditions and therefore a determinant parameter for them is an *equivalent flow cross section* μA as a function of pintle liftoff x [Eqs. (3-19) and (5-42)].

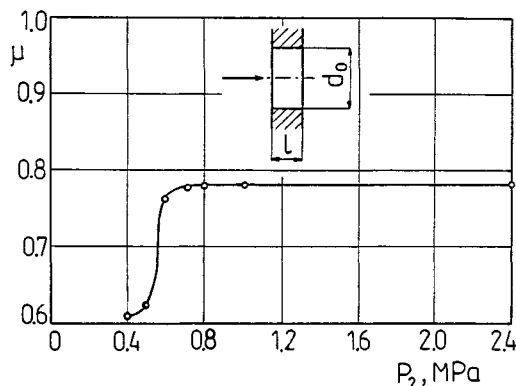


Figure 6-4 Dependence of discharge coefficient μ on back pressure P_2 ; $\Delta P = 1.2$ MPa, $d_0 = 0.8$ mm, $l/d_0 = 0.5$.

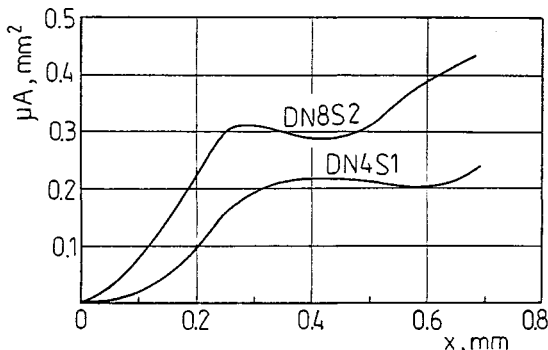


Figure 6-5 Equivalent flow cross sections of a pintle nozzle (Bosch).

Figure 6-5 presents the equivalent flow cross sections that were determined during the evaluation of Bosch pintle nozzles. The curves show the smooth change of cross section μA in the whole range of pintle liftoff x . Similar changes of μA were shown schematically in Fig. 5-8b.

6-1.2 Macrostructure of the Atomized Liquid

Diesel engines are most sensitive to the spray shape. In these engines, open chambers with direct injection, semi-open chambers with direct injection, and divided chambers, i.e., swirl chambers and precombustion chambers (Fig. 6-6), are used. Correct operation of the engines requires that the spray and air be mixed properly.

Operation of older designs of *open chambers with direct injection* (Fig. 6-6a) was based mainly on utilization of the fuel jet energy. Present designs make considerable use of the swirling of air. Circumferential swirling with respect to

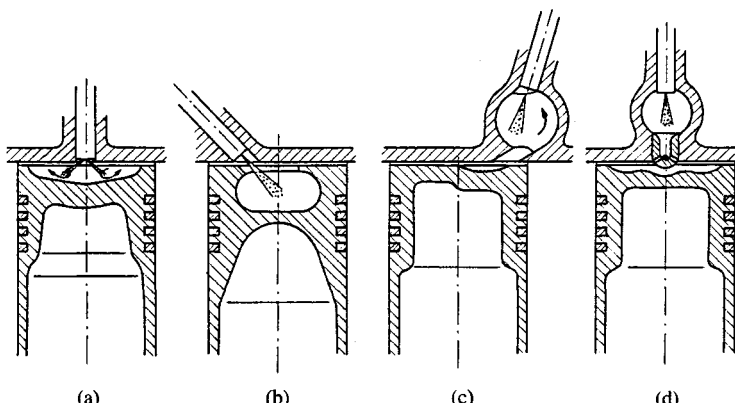


Figure 6-6 Combustion chambers of diesel engines: (a) open chamber with direct injection; (b) semi-open chamber with direct injection; (c) swirl chamber; (d) precombustion chamber.

the chamber is caused by the tangential suction channel or by a strangler on the suction valve, and transverse swirling (toroidal vortex) develops during the compression stroke. *Semi-open chambers with direct injection* (Fig. 6-6b) located in the piston or in the engine head have the goal of developing an intense toroidal vortex during the compression stroke.

Among the divided chambers, we first mention the *swirl chambers* (Fig. 6-6c). A swirl chamber most commonly has the shape of a sphere or a cylinder and is connected with the space above the piston by a tangential channel. During the compression stroke the air flows through this channel to the chamber and causes strong swirling. The fuel is fed in the form of a single jet, usually in the direction of the vortex. The velocity of the vortex is selected so that during the injection the drops make a whole rotation, which ensures the correct fuel distribution in the chamber.

Precombustion chambers (Fig. 6-6d) are smaller than swirl chambers and therefore only part of the fuel combusts there. The pressure increase during combustion forces out the whole burning content through the orifices (a type of pneumatic injection), which causes a strong vortex to develop in the space above the piston and enables mixing with the rest of the air and completion of combustion. In this case the spray shape requirements are insignificant. There are also chambers with an air chamber, which play a similar role to precombustion chambers but they have a nozzle located not inside but outside the air chamber.

Spray angle. The spray angle α of jet atomizers is very small. Knowledge of this angle is most important in piston engines with an open chamber (Fig. 6-6a and b). Angle α is a function of the following parameters:

$$\operatorname{tg} \alpha = f(\rho_L, \rho_G, \mu_L, \sigma, w, d_0, t) \quad (6-3)$$

Based on the analogy with the motion of a turbulent gas jet or using dimensional analysis, one arrives at the same *dimensionless* relationship:

$$\operatorname{tg} \frac{\alpha}{2} = C \operatorname{We}_L^k \operatorname{Lp}^l M^m E^n \quad (6-4)$$

where C = constant depending on the atomizer's design

k, l, m, n = experimental coefficients

We_L = Weber number [see Eq. (2-5)]

$$\operatorname{We}_L = \frac{\rho_L w^2 d_0}{\sigma} \quad (6-5)$$

Lp = Laplace number [see Eq. (2-79)]

$$\operatorname{Lp} = \frac{\rho_L \sigma d_0}{\mu_L^2} \quad (6-6)$$

M = density ratio [see Eq. (2-80)]

$$M = \frac{\rho_G}{\rho_L} \quad (6-7)$$

E = injection instability criterion

$$E = \frac{t^2 \sigma}{\rho_L d_0^3} \quad (6-8)$$

Criterion E plays a role only for the jet developing region L_1 (Fig. 2-40). The length of this segment can be determined from

$$L_1 = C_1 d_0 \text{We}_L^{0.25} \text{Lp}^{0.4} M^m \quad (6-9)$$

where for high back pressures P_2 [i.e., for $M = (0.95-2.8) \times 10^{-2}$] $C_1 = 8.85$, $m = 0.6$, and for small back pressures [i.e., for $M = (0.14-0.95) \times 10^{-2}$] $C_1 = 46.9$, $m = 0.24$.

Figure 6-7 presents the results of measurements of angle α as a function of time t for the atomizer shown in Fig. 2-8. It is seen from Fig. 6-7 that for the jet developing region (to the left of the dashed line) angle α decreases in time and for the main region of the jet $\alpha = \text{const}$ [26]. Angle α is larger for higher back pressures P_2 (Fig. 6-7a), for higher pressure drops ΔP (Fig. 6-7b), and for larger orifice diameters d_0 (Fig. 6-7c). The jet developing region is contained in time interval $t \approx 0.3-1.0$ ms, depending on the injection conditions. This time interval is approximately the same as the ignition delay period [11].

As a result of these measurements, the following formula was obtained for the main region of the jet:

$$\tan \frac{\alpha}{2} = C \text{We}^{0.32} \text{Lp}^{0.07} M^m \quad (6-10)$$

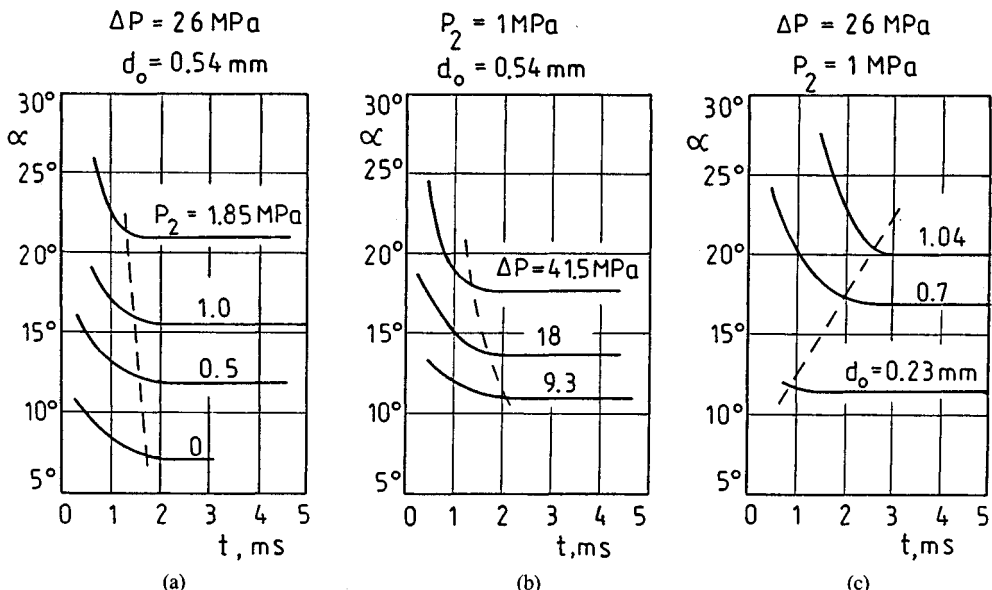
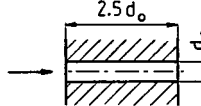
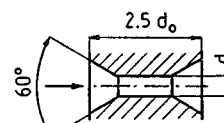
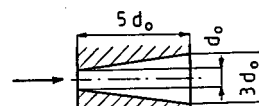
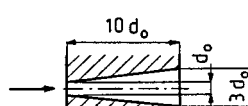
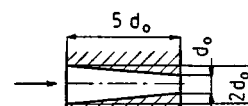
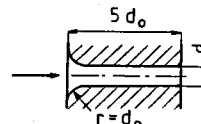


Figure 6-7 Dependence of angle α on time t : (a) for various backpressure (overpressure) drops P_2 ; (b) for various pressure drops ΔP ; (c) for various orifice diameters d_0 .

Table 6-2 Values of constant *C* for various discharge orifices

Shape of the discharge orifice	High back pressure, $M = (0.95-2.8)10^{-2}$	Small back pressure, $M = (0.14-0.95)10^{-2}$
	0.0089	0.0028
	0.0089	0.0028
	0.005	0.00198
	0.00831	0.00261
	0.00513	0.00158
	0.01265	0.00393

while for high back pressures [i.e., for $M = (0.95-2.8) \times 10^{-2}$] $C = 0.0112$, $m = 0.5$ and for small back pressures [i.e., for $M = (0.14-0.95) \times 10^{-2}$] $C = 0.00364$, $m = 0.26$. Formula (6-10) applies to $We_L = (140-725) \times 10^3$ and $L_p = 300-1350$. In general, this formula gives good results for continuous and intermittent injection with an error less than 20%. The results of investigations of other authors lead to the same formula, where only constant C assumes different values (see Table 6-2) [20].

An example is the equation given in [11]:

$$\alpha = 0.05 \left(\frac{\rho_G \Delta P d_0^2}{\mu_G^2} \right)^{1/4} \quad (6-11)$$

When one takes into account Eqs. (2-8), (2-82) and (3-2), then Eqs. (6-10) and (6-11) have an equivalent form, while differences occur only for the values of constants and coefficients.

In [50] the change of angle α as a function of time was measured. The measurements were conducted at a distance of 5 mm from the atomizer, i.e., for the spray developing region. A strong dependence of angle α on back pressure P_2 and a relatively weak dependence on pressure drop ΔP were established, which also follows from Fig. 6-7a and b. The effect of the temperature of the ambient gas in the range 290–673 K was also investigated, and it was found that α decreases as the temperature increases. This takes place because as the temperature increases the gas density decreases, which has the dominant effect. As the temperature increases small drops start to evaporate at the spray periphery, which also affects the decrease of angle α . It should be added that the temperature of the fuel in a piston engine causes a decrease in fuel viscosity that has the oppose effect, i.e., increases the angle α .

Spray penetration. In [12] the length L_c of the compact jet (breakup length) was investigated. Length L_c is especially important in the case of small cars because of the small dimensions of the combustion chamber. Figure 6-8 shows the effect of jet velocity V (discharge velocity) on length L_c . Regions, I, II, and III are, according to Fig. 2-7, the regions of laminar, turbulent, and spray flow. Between regions I and II is a transition flow region.

As seen, in region II length L_c increases and in region III it decreases as velocity V increases. Length L_c also decreases as back pressure P_2 increases. It was established that L_c never vanishes but tends to a constant value of approximately 20 mm. This is a very important conclusion because the radius of the combustion chamber in small cars has approximately the same value.

Figure 6-8 shows two curves for $l/d_0 = 4$ and $l/d_0 = 10$, where l and d_0 are the length and diameter of the orifice, respectively. Ratio $l/d_0 = 4$ is typical

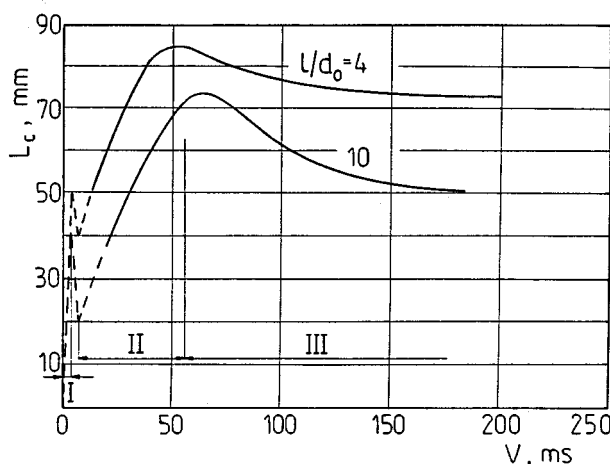


Figure 6-8 Length of compact jet L_c as a function of jet velocity V ; discharge orifice diameter $d_0 = 0.3$ mm, gas back pressure $P_2 = 0.1$ MPa.

for intermittent atomizers. For other ratios l/d_0 the curves have similar character as for $l/d_0 = 4$. Ratio $l/d_0 = 10-20$ is an exception and corresponds to the lowest values of L_c . However, this applies only to small back pressures of the order of $P_2 = 0.1$ MPa; for high back pressures $P_2 = 0.3$ MPa the effect of l/d_0 on L_c is insignificant.

Spray penetration x and velocity of spray front w' depend on many parameters, in particular back pressure P_2 , pressure drop ΔP , and discharge orifice diameter d_0 (Fig. 6-9) [20]. As seen, as time t increases, penetration x increases and velocity w' decreases. From Fig 6-9a it follows that an increase of back pressure P_2 causes a decrease of spray penetration x and velocity w' . From Fig. 6-9b it follows that an increase of ΔP increases x and w' ; however, above a certain limit ΔP the opposite can take place (which is not shown in the figure); i.e., the penetration will decrease as ΔP increases. In this case very small drops develop, which are easier to decelerate. Figure 6-9c shows that an increase in d_0 causes an increase of x and w' .

Additional effects (less important) on spray penetration x are as follows:

Higher liquid viscosity is associated with large drops, resulting in more compact spray with larger penetration x .

Higher surface tension has an effect similar to that of higher viscosity.

Higher gas temperature (higher gas viscosity at the same pressure) causes velocity w' to decrease, but in the temperature range 22–320°C this effect is negligible.

According to Eq. (2-156), the coefficient of free turbulence a'_u of the spray front can be expressed as

$$a'_u = C_1 \text{We}_L^k \text{Lp}^1 M^m \quad (6-12)$$

where C_1, k, l, m are experimental constants. Term N in Eq. (6-12) was neglected as insignificant. It was established that in the jet developing region coefficient a'_u varies and decreases to a certain value, and then it remains constant on the entire length of the main region. This confirms the assumption that the main region of the spray can be treated as a turbulent jet. Equation (6-12) finds application only for the main region of the spray.

All of the constants were determined experimentally and the following equation was obtained [20]:

$$a'_u = C_1 \text{We}_L^{-0.21} \text{Lp}^{0.16} M^m \quad (6-13)$$

while for $M = (0.95-2.8) \times 10^{-2}$ $C_1 = 2.72$, $m = 1$, and for $M = (0.14-0.95) \times 10^{-2}$ $C_1 = 0.202$, $m = 0.45$. Equation (6-13) applies to $\text{We}_L = (140-725) \times 10^3$ and $\text{Lp} = 300-1350$. Constants C_1 correspond to a cylindrical discharge orifice.

The spray front velocity w' equals

$$w' = \frac{dx}{dt}$$

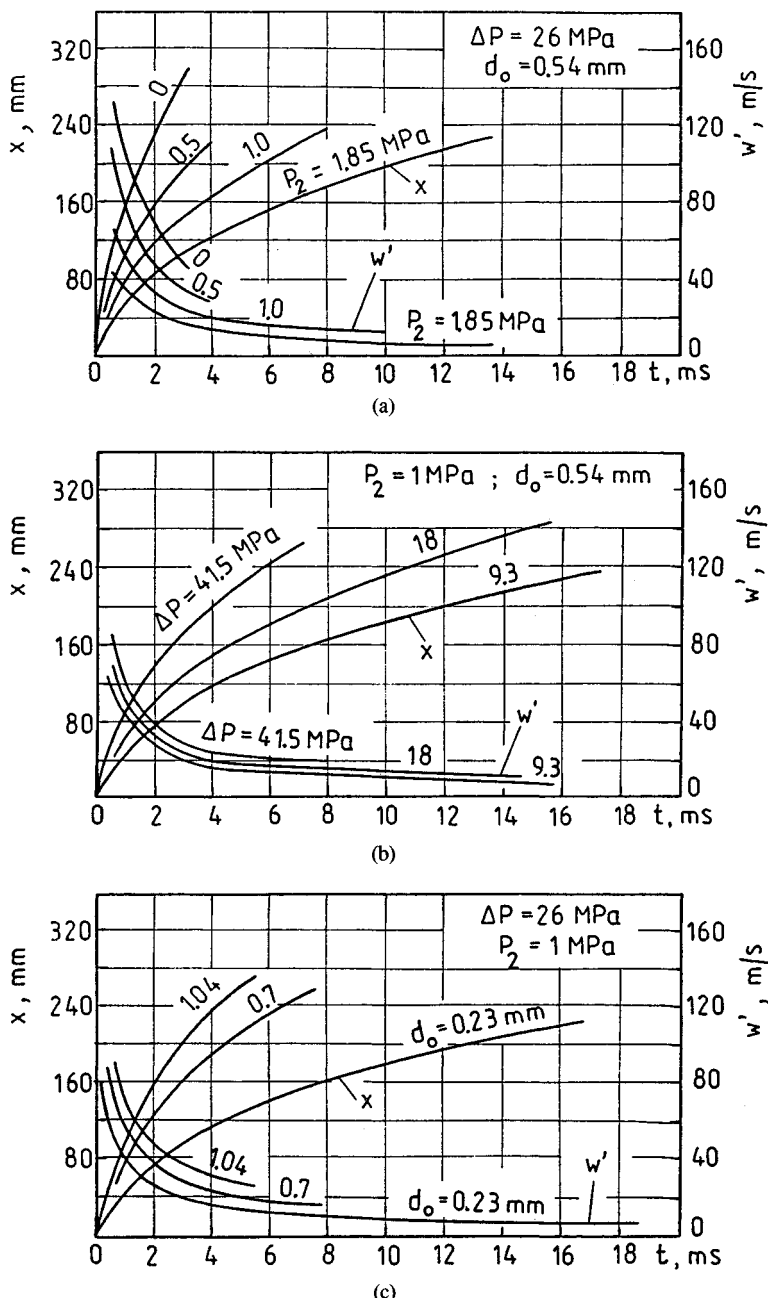


Figure 6-9 Dependence of spray penetration x and spray front velocity w' on time t : (a) for various back pressures P_2 ; (b) for various drop pressures ΔP ; (c) for various orifice diameters d_0 .

Substituting w' instead of w_{\max} in Eq. (2-152), we obtain

$$x dx = \frac{d_0 w}{2\sqrt{2} a'_u} dt$$

After integrating and determining the integration constant from the condition $x = 0$ for $t = 0$, we obtain the equation for the penetration of the main spray:

$$x = \sqrt{\frac{d_0 w}{\sqrt{2} a'_u}} t \quad (6-14)$$

Knowing a'_u one can determine the spray front velocity w' . For the main spray region, after substituting $a'_u = a_u$ in Eq. (2-152), we obtain

$$\frac{w'}{w} = C' \frac{d_0}{x} \text{We}_L^{0.21} \text{Lp}^{-0.16} M^m \quad (6-15)$$

while for $M = (0.95-2.8) \times 10^{-2}$ $C' = 0.13$, $m = -1.0$, and for $M = (0.14-0.95) \times 10^{-2}$ $C' = 1.71$, $m = -0.45$. Velocity $w = w_0$ is the velocity of the liquid discharging from the atomizer.

The foregoing equations apply to continuous injection, but experiments showed that they are also valid for intermittent atomizers.

In [11] the following equations describing penetration were presented.

For $0 < t < t_b$:

$$x = 0.39 \sqrt{\frac{2\Delta P}{\rho_L}} t \quad (6-16)$$

For $t \geq t_b$:

$$x = 2.95 \left(\frac{\Delta P}{\rho_G} \right)^{1/4} \sqrt{d_0 t_b} \quad (6-17)$$

where t_b = spray breakup time, s

P = pressure drop, Pa

t = time, s

ρ_L, ρ_G = liquid and ambient gas densities, kg/m³

d_0 = orifice diameter, m

Breakup time t_b is given by

$$t_b = 28.65 \frac{\rho_L d_0}{\sqrt{\rho_G \Delta P}} \quad (6-18)$$

Experimental data do not exist for the jet development region, i.e., for time period $t \approx 1$ ms from the beginning of injection. This time period is approximately equal to the ignition delay period.

Figure 6-10 shows on a logarithmic scale the spray penetration as a function of time with emphasis on the beginning of penetration. The injection proceeds

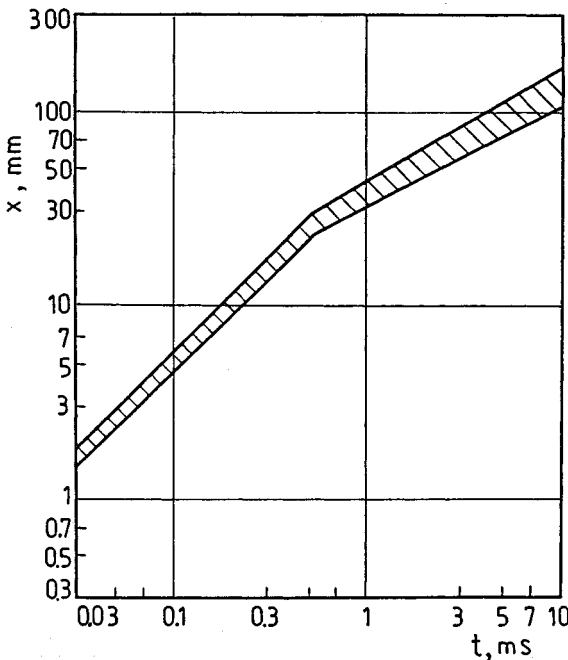


Figure 6-10 Penetration of spray front x ; pressure of pintle opening 10 MPa.

to the space with back pressure $P_2 = 1, 2, 3$ MPa. The results of calculations using Eqs. (6-16) and (6-17) and the experimental results are contained in the hatched area, and according to Fig. 6-9a, higher values of x correspond to higher values of P_2 . Linear relationships with two different slopes are visible: until the spray breakup time the spray velocity is proportional to time, and then the spray velocity is proportional to the square root of time.

It was demonstrated in [35] that the penetration increases in proportion to time up to 0.5–1.0 ms. Strictly speaking, this condition is not exactly satisfied, since $dx/dt \neq \text{const}$. At the beginning dx/dt increases and then decreases due to the air feeding to the spray in the mixing region (see Fig. 3-15).

Liquid distribution in a drop jet. This distribution can be considered in three directions: radial, circumferential, and axial. The most essential is the radial distribution $q = f(r)$, where q is the density of the liquid jet [Eq. (3-31)]. The radial distribution was expressed by Eq. (3-33), which contains an empirical coefficient a_c . Equation (3-33) can be written in the form

$$q = \frac{q_0 d_0^2}{8a_c^2 x^2} \exp \frac{r^2}{2a_c^2 x^2} \quad (6-19)$$

The first term on the right-hand side of Eq. (6-19) represents the value q_{\max} in

the jet axis at distance x from the atomizer:

$$q_{\max} = \frac{q_0 d_0^2}{8 a_c^2 x^2} \quad (6-20)$$

where q_0 is the value of q for $x = 0$, i.e.,

$$q_0 = \rho_L w \quad (6-21)$$

where w is the discharge velocity. The second term on the right-hand side of Eq. (6-19) represents the change of q in the transverse cross section of the jet.

Figure 6-11 contains the results of measurements of radial distribution $q = f(r)$ of a jet atomizer with continuous operation [20]. As seen, an increase of back pressure P_2 causes the distribution to become more uniform. A similar situation takes place when pressure drop ΔP increases; however, this influence is much smaller than that of P_2 . The effect of distance x from the atomizer was shown in Fig. 3-17.

These results were used to determine coefficient a_c . For the jet developing region $a_c \neq \text{const}$, and for the main region $a_c = \text{const}$. For the jet main region the equation has the form

$$a_c = C \text{We}_L^{0.3} \text{Lp}^{0.1} M^m \quad (6-22)$$

while for $M = (0.95-2.8) \times 10^{-2}$ $C = 0.019$, $m = 0.8$, and for $M = (0.14-0.95) \times 10^{-2}$ $C = 0.003$, $m = 0.4$. Equation (6-22) applies for $\text{We}_L = (140-725) \times 10^3$ and $\text{Lp} = 300-1350$. By substituting Eq. (6-22) to Eq. (6-19) we can calculate the density of the liquid jet at the arbitrary place in the jet $q = f(x, r)$. It was assumed that the jet was axisymmetric. Assuming $r = 0$, we can calculate from Eq. (6-19) the density distribution $q = f(x)$ in the axis of the jet.

In [19] the trajectories of drops for a jet atomizer that generates an annular jet were calculated (Fig. 4-1b). The results of calculations are shown in Fig. 6-12.

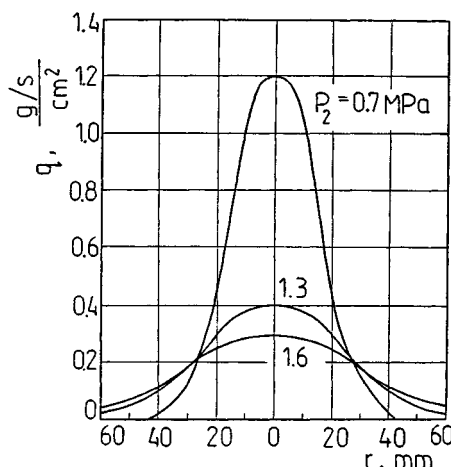


Figure 6-11 Radial distribution of liquid jet density $q = f(r)$ for various air back pressures P_2 ; $\Delta P = 25 \text{ MPa}$, $d_0 = 0.38 \text{ mm}$, $x = 350 \text{ mm}$.

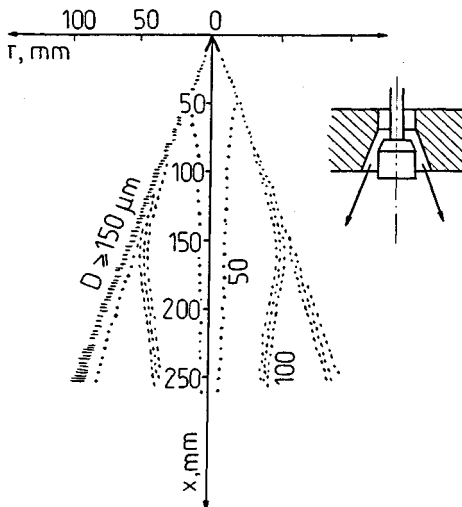


Figure 6-12 Drop trajectories in atmospheric air; water flow rate $G_L = 0.00352 \text{ kg/s}$.

The point of disintegration of the sheet is located at a distance 5–10 diameters of the discharge orifice from the front of the atomizer. After the sheet disintegrates, ambient gas is sucked in, which causes the contraction of the jet and deflection of the trajectories of small drops toward the center of the jet. The results of the calculations were confirmed experimentally.

6-1.3 Microstructure of Atomized Liquid

The *quality of atomization* depends on many factors such as [20]:

discharge orifice diameter d_0 of a jet atomizer,
injection pressure P_1 ,
ambient back pressure P_2 ,
liquid viscosity ν_L ,
surface tension σ .

Discharge orifice diameter d_0 has a distinct effect on the atomization spectrum (Fig. 6-13a). For smaller orifice diameters d_0 the maxima of the distribution curves are higher and shifted to the left, toward smaller drop diameters D , which indicates that the atomization quality improves as well as the atomization uniformity. An increase of injection pressure P_1 (Fig. 6-13b) also causes improvement of the atomization quality. Better atomization means a smaller parameter X , i.e., a larger fraction of small drops, and greater atomization uniformity denotes a higher parameter δ —see the Rosin-Rammler equation.

The effect of back pressure P_2 on the atomization macrostructure is very complex. In [20] it was found that as the back pressure increases the atomization

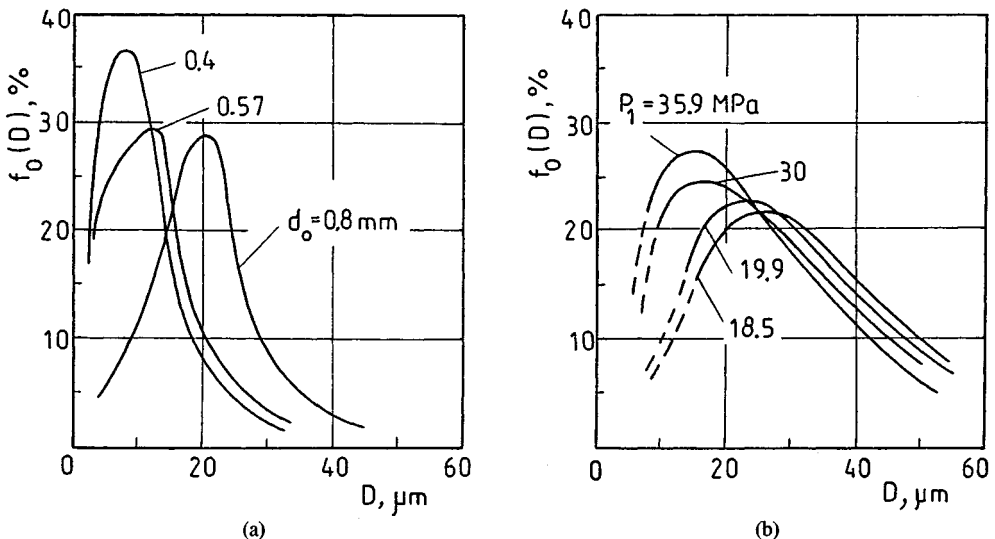


Figure 6-13 Drop size number distribution curve $f_0(D)$: (a) for various orifice diameters d_0 , $P_1 = 28 \text{ MPa}$, $P_2 = 1 \text{ MPa}$; (b) for various injection pressures P_1 , $d_0 = 0.15 \text{ mm}$, $P_2 = 1.4 \text{ MPa}$.

quality also improves, but in [11] it was established that the atomization quality deteriorates. This latter statement can raise reservations, because as P_2 increases the gas density also increases and therefore the dynamic action of the gas on drops increases, which would result in improved atomization. On the other hand, as P_2 increases the pressure drop $\Delta P = P_1 - P_2$ also increases, which decreases the velocity of the liquid and causes the atomization to deteriorate.

Thus two opposing effects exist. Another effect, which is probably important, is that as P_2 increases the drop penetration decreases, which causes drop coalescence, i.e., growth of drop diameters [11].

In [18] investigations were carried out at large changes of P_2 and therefore the air density varied 15-fold. It was determined that when air density increases, the diameters of small drops (of the order of several μm) slightly decrease, diameters of medium-sized drops ($40\text{--}60 \mu\text{m}$ and larger) do not change or slightly increase, and the diameters of large drops ($160 \mu\text{m}$) increase significantly.

The effect of back pressure P_2 on the mean drop diameter was discussed but was not sufficiently explained in [39]. The results are concerned with the change of Sauter mean diameter D_{32} as a function of pressure drop $\Delta P = P_1 - P_2$, and not as a function of injection pressure P_1 (Fig. 6-14). As seen, at small values of ΔP D_{32} decreases as P_2 increases and at large values of ΔP D_{32} increases as P_2 increases. A critical value ΔP exists that separates these two phenomena.

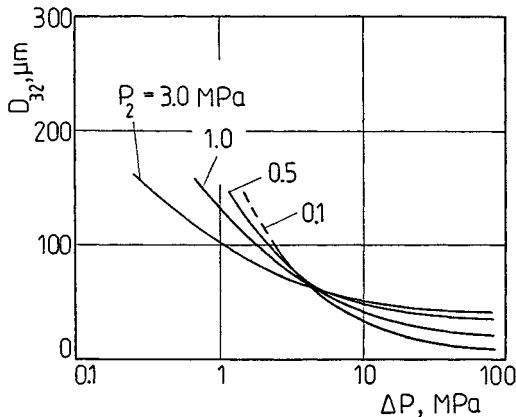


Figure 6-14 Effect of back pressure P_2 on Sauter mean diameter D_{32} ; $d_0 = 0.3 \text{ mm}$, $\nu_L = 1 \times 10^{-6} \text{ m}^2/\text{s}$.

The effect of liquid viscosity ν_L on Sauter mean diameter D_{32} is shown in Fig. 6-15 [39]. As the viscosity increases, D_{32} also increases. When the injection pressure P_1 for a particular fuel decreases, i.e., when $\Delta P = P_1 - P_2$ decreases (for $P_2 = \text{const}$), D_{32} increases gradually, but when P_1 drops below a certain limiting value, diameter D_{32} increases rapidly. In this way the effect of back pressure P_2 on the atomization quality is manifest. The higher the liquid viscosity, the higher this limiting value of pressure P_1 .

The effect of surface tension σ on Sauter mean diameter D_{32} is shown in Fig. 6-16 [39]. Liquids with higher surface tension have larger value of D_{32} but only for relatively small pressures P_1 . For each liquid a certain lower bound of P_1 exists below which diameter D_{32} grows rapidly.

General Eq. (2-39) for mean drop diameter \bar{D} can be expressed in the following form:

$$\begin{aligned}\bar{D} &= K d_0 (\text{We}_L M)^{-0.266} L p^{-0.0733} \\ &= K d_0 \text{We}_G^{-0.266} L p^{0.0733}\end{aligned}\quad (6-23)$$

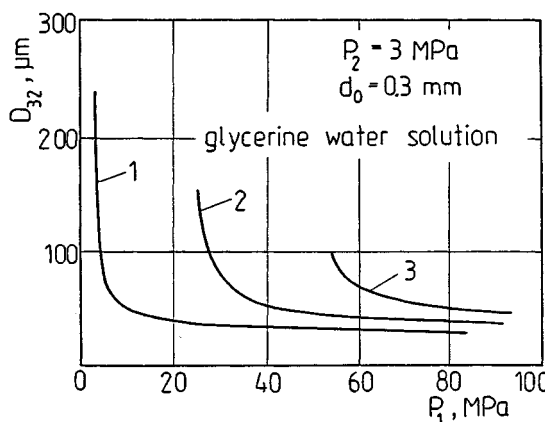


Figure 6-15 Effect of liquid kinematic viscosity on Sauter mean diameter: 1, $\nu_L = (0.7-1.4) \times 10^{-6} \text{ m}^2/\text{s}$; 2, $\nu_L = (23.7-27.4) \times 10^{-6} \text{ m}^2/\text{s}$; 3, $\nu_L = 61.1 \times 10^{-6} \text{ m}^2/\text{s}$.

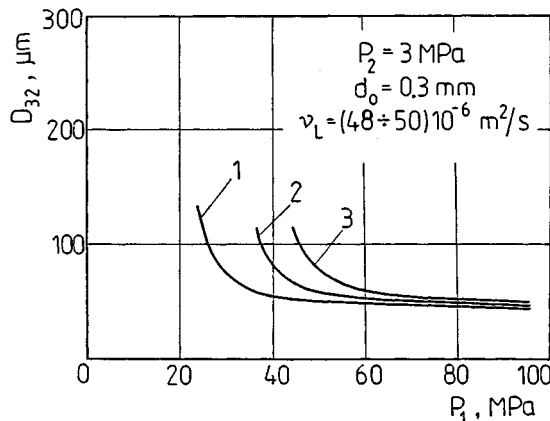


Figure 6-16 Effect of surface tension on Sauter mean diameter: 1, Heavy oil $\sigma = 33.5 \times 10^{-3}$ N/m; 2, glycerine alcohol water solution $\sigma = 51.5 \times 10^{-3}$ N/m; 3, glycerine water solution $\sigma = 66.0 \times 10^{-3}$ N/m.

where \bar{D} = arbitrary mean drop diameter

K = empirical constant

We_L, We_g = Weber numbers according to Eqs. (6-5) and (2-78)

M = density ratio [Eq. (6-7)]

L_p = Laplace number [Eq. (6-6)]

Constant K depends on the jet atomizer's design and on the method used for drop diameter averaging. In [20], continuous atomizers were evaluated for the following conditions:

$$d_0 = 0.15\text{--}0.35 \text{ mm}$$

$$P_1 = 10\text{--}40 \text{ MPa}$$

$$P_2 = 0.1\text{--}2.1 \text{ MPa}$$

$$\rho_L = 852 \text{ kg/m}^3$$

$$v_L = 7.9 \times 10^{-6} \text{ m}^2/\text{s}$$

$$\sigma = 28.4 \times 10^{-3} \text{ N/m}$$

$$We_L = (63\text{--}400) \times 10^3$$

$$L_p = 185\text{--}800$$

$$M = (0.1124\text{--}2.95) \times 10^{-2}$$

Diesel oil was the atomized liquid, and the atomization took place in the air with a constant temperature of 20°C. The values of constant K are presented in Table 6-3.

During the study of intermittent atomizers different authors derived various values of K . Generally speaking, these values are two times smaller. This is explained by the fact that intermittent atomizers have a pintle, which is a source of additional disturbances improving the atomization quality.

Liquid atomization during intermittent injection has the following characteristic features:

During a limited time interval, the velocity of pumping and fuel discharge increases from zero to a certain variable value and subsequently drops to zero. For discharge velocities higher than 180 m/s the drop diameters change only slightly [18].

During the main phase of injection, the discharge velocity varies due to the unsteady motion of the piston of the pump and mostly due to the wavy changes of pressure in front of the discharge orifice.

For the aforementioned reasons, significant deterioration of the atomization quality occurs at the onset and the end of each injection. It was found that during the initial phase of injection individual drops are present in front of the spray, and during the final phase of the injection (when the injection pressure drops) ligaments and large drops are present [17]. During these investigations the drop diameters measured by a holographic method fell in the range 20–60 μm except for the region close to the core of the jet. From measurements reported in [11] it follows that the drop diameters are larger toward the axis of the jet.

Thus, during intermittent injection the drop diameters vary with both time and location in the jet. Drop diameters and velocities have been measured in the mixing region (Fig. 3-15) [36]. The drop diameters are in the range 20–50 μm and have a logarithmic normalized distribution; i.e., they lie on the straight line in Fig. 3-21b. Figure 6-17 shows an example of the relationship between mean drop diameter D and mean drop velocity \bar{V}_D . As seen, this relationship is a linear one. Velocities \bar{V}_D in the mixing region are very low in spite of the velocity of the discharging liquid being equal to 200 m/s. This indicates that an intense mixing process takes place in this region (eddy mixing phenomenon).

Some results of the evaluations of *impact atomizers* will be discussed. During the collision of a jet of diameter d with a flat surface, a film develops (Fig. 5-3) whose diameter d_f before it disintegrates into drops can be calculated from the simplified dimensionless equations for the following ranges of Weber numbers [8].

$$\text{For } \text{We}_L = 100-500: \quad \frac{d_f}{d} = 0.167 \text{We}_L \quad (6-24)$$

$$\text{For } \text{We}_L = 2000-3 \times 10^4 \quad \frac{d_f}{d} = 1250 \text{We}_L^{-0.333} \quad (6-25)$$

Table 6-3 Value of constant K in Eq. (6-23)

Mean diameter K	D_{10}	D_{30}	D_{31}	D_{32}
	1.8	2.21	2.15	2.68

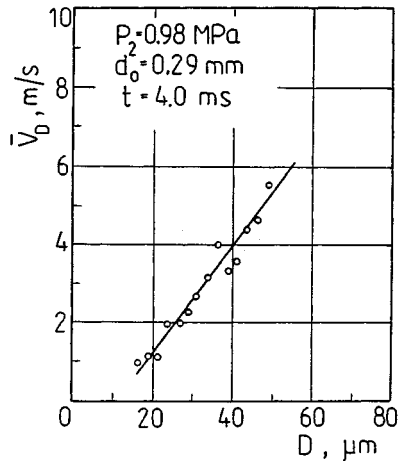


Figure 6-17 Relationship between diameter and velocity of drops in spray mixing region.

where

$$We = \frac{\rho_L V^2 d}{\sigma}$$

In the case of the first Weber number range symmetric waves develop on the film surface and drops develop on the rim of the sheet. In the case of the second range of We_L asymmetric waves develop on the film which lead to disintegration of the film edge into small droplets. Between these ranges is a transient range in which the largest film diameter d_f is observed.

When two jets impinge at a certain angle (Fig. 5-2), then for jets of an ideal liquid one assumes that the center of the sheet is shifted by a distance $00'$. Equations (6-24) and (6-25) change, since their left-hand sides should be divided by $(1 + \sin \vartheta)$. Median diameter D_m is given by

$$D_m = 1.22 d We_L^{-0.25} \sin^{-0.5}(90^\circ - \vartheta) \quad (6-26)$$

The relationship between D_m and d is a linear one. When d increases twice diameter D_m increases approximately 2.7 times. The lower the angle of impingement $(90^\circ - \vartheta)$, the larger the developing drops.

6-2 SWIRL ATOMIZERS

6-2.1 Flow Rate of Atomized Liquid

Simplex atomizers. First, the experimental results will be presented as a supplement to the material contained in Sec. 5-2. Figure 6-18 shows a graph [5], that presents dependence of the ratio μ_{exp}/μ on injection pressure P_1 for atomizers with similar values of geometric constant K and with various values of $B = R/r_p$

[Eq. (5.78)]. Discharge coefficient μ is the theoretical value for an ideal liquid. An atomizer with a single tangential orifice with diameter d_p and swirl chamber with length $l_s = d_p$ was used for the investigation. The evaluations were carried out for kerosene.

As seen from Fig. 6-18, as B increases, i.e., as $(B^2/i - K)$ [Eq. (5.77)] increases, the ratio μ_{exp}/μ increases significantly. This ratio for the ideal liquid should be equal to unity independently of B . It is also seen that the flow ratio decreases as pressure P_1 increases, i.e., as Reynolds number increases. These tendencies to decrease vanish gradually. The decrease of the discharge coefficient follows in this case from the decrease of friction coefficient λ [Eq. (5.87)].

The "viscosity barrier" mentioned in Sec. 5-2.1 can be illustrated by using Fig. 6-19 [5]. For evaluation an atomizer of the following design was used: two tangential inlet orifices of cross section 1.01×1.01 mm, swirl chamber of length $l_s = 1.01$ mm, discharge orifice of diameter $d_0 = 1.21$ mm, swirl radius $R = 0-15$ mm, geometric constant $K = 0-14.0$. Kerosene was the atomized liquid, and the Reynolds number was $\text{Re} = 6 \times 10^3$. As shown by the experimental curve, μ decreases rapidly at the beginning, as K increases, and then increases.

An extreme value μ_{min} is reached. This was predicted analytically, since when R varies according to Eq. (5.81) a certain maximum value of K_λ is reached to which extreme values of μ_{min} and α_{max} correspond. The experimental and theoretical results are in agreement. For $K = 0$, μ is smaller than one and α is higher than zero. This is obvious, since in this case a jet atomizer is created that has certain values of μ and α .

As demonstrated in Sec. 5-2.1, flow rate increases as liquid viscosity increases, which is also seen in Fig. 6-20 [31]. The increase of flow rate G_L is due to the increase of friction and reduction of the circumferential velocity compo-

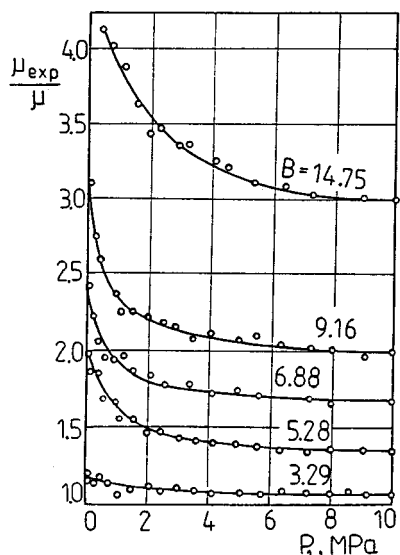


Figure 6-18 Dependence of ratio μ_{exp}/μ on liquid pressure P_1 for various values of B and almost constant value $K = 4.36-5.11$.

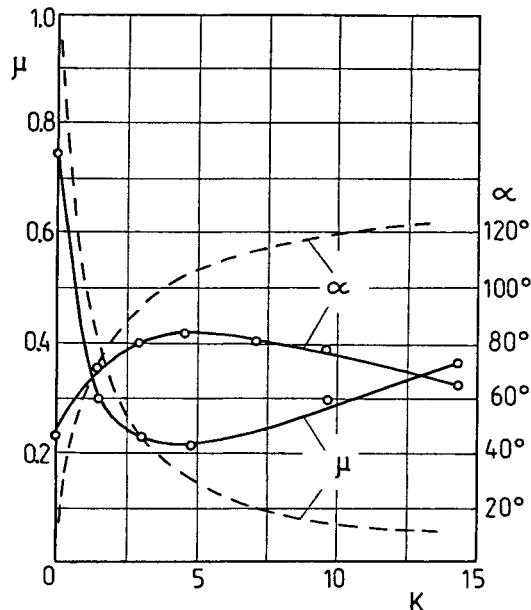


Figure 6-19 Dependence of discharge coefficient μ and spray angle α on geometric constant K during change of swirling radius R ; dashed lines denote theoretical values (see Fig. 5-11).

ment in the atomizer and to the increase of the thickness of the liquid sheet discharging from the atomizer. The gas vortex vanishes then, and the liquid flows through the whole cross-section of the discharge orifice. Further increase of the liquid viscosity causes a decrease in flow rate G_L because of the increase of friction resistance.

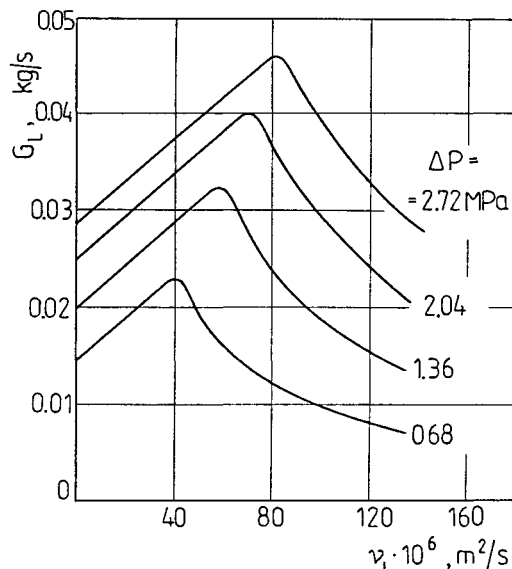


Figure 6-20 Dependence of liquid flow rate G_L on kinematic viscosity ν_L for various values of pressure drop ΔP [31].

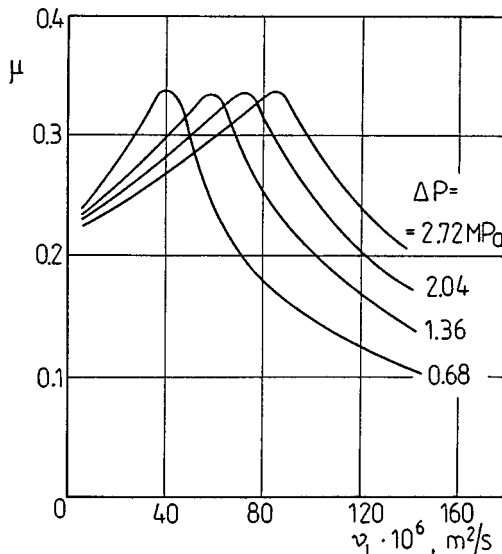


Figure 6-21 Dependence of discharge coefficient μ on liquid viscosity ν_L for various pressure drops ΔP [31].

Liquid flow rate increases with an increase of liquid density ρ_L . However, the sheet thickness decreases slightly as liquid density increases.

Discharge coefficient μ varies with the liquid viscosity similarly to flow rate G_L (Fig. 6-21) [31]. Attention is drawn to the fact that for a given liquid viscosity μ increases as the pressure drop ΔP decreases, but this tendency is clear only for $\nu_L < 40 \times 10^{-6} \text{ m}^2/\text{s}$. Velocity coefficient K_v , which is defined as the ratio of the actual discharge velocity to the theoretical velocity corresponding to the total pressure drop across the nozzle, is given by

$$K_v = \frac{\mu}{(1 - X) \cos \alpha_m / 2} = \frac{\mu}{\epsilon \cos \alpha_m / 2} \quad (6-27)$$

where $X = A_r/A_0 = (r_r/r_0)^2$ is the ratio of the cross section of the gas core to the cross section of the discharge orifice

$\epsilon = 1 - (r_r/r_0)^2 = 1 - X$ is the efficiency of filling of the discharge orifice [Eq. (5-45)]

α_m = mean spray angle [Eq. (3-27)]

Knowledge of the coefficient K_v is necessary in order to calculate the actual discharge velocity.

Figure 6-22 [31] shows that for relatively small liquid viscosities, i.e., below $\nu_L = 12 \times 10^{-6} \text{ m}^2/\text{s}$, a rapid drop in K_v occurs as a result of the joint effects of film thickness $\delta \approx r_0 - r_r$ increase and angle α_m decrease. In this range of liquid viscosity, i.e., for $\nu_L < 12 \times 10^{-6} \text{ m}^2/\text{s}$, the effect of viscosity on flow rate G_L is relatively small (Fig. 6-20).

Getting back to Fig. 6-22, it should be pointed out that for further increase of ν_L the slope of curves decreases because when the liquid film thickness δ

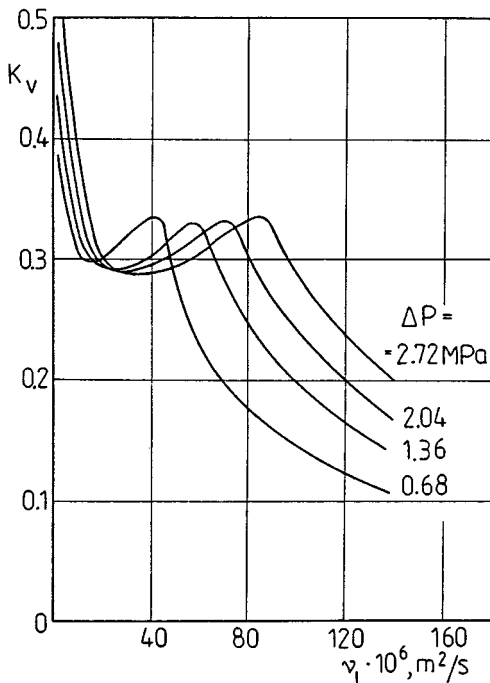


Figure 6-22 Dependence of velocity coefficient K_v on liquid viscosity ν_L for various values of pressure drops ΔP [31].

reaches a certain value, the changes of X and α_m are less important than the increase of μ . In a certain range of viscosities the value K_v even increases slightly until for a certain viscosity the discharge orifice is completely filled with the liquid. In these conditions $K_v \approx 0.34$ and does not depend on ΔP . For a further increase of liquid viscosity K_v decreases due to the decrease of μ .

The results in Figs. 6-20, 6-21, and 6-22 concern a simplex atomizer with the following features: three tangential inlet orifices, $d_0 = 1.6 \text{ mm}$, and nozzle constant K' given by

$$K' = \frac{A_p}{D_s d_0} \quad (6-28)$$

where A_p = cross section of the inlet orifices

D_s = diameter of the swirl chamber

The effect of the atomizer's design and dimensions on the flow rate requires a more extensive discussion [26]. In this case the atomizer is as shown in Fig. 5-13.

Length of the swirl chamber L_s should be equal to or slightly greater than the diameter or the width of the tangential inlet orifice. If chamber length L_s is too long, then the calculation method presented in Sec. 5-2.1 cannot be applied. In this case liquid in the swirl chamber rotates due to the action of the fluid that actively flows through the atomizer. Therefore the angular momentum decreases, accompanied by an increase in μ .

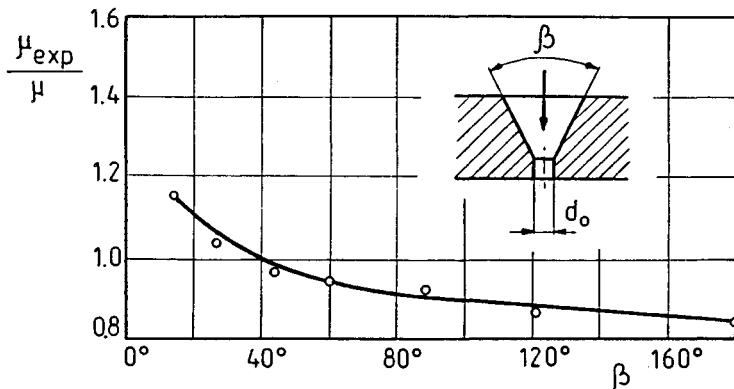


Figure 6-23 Dependence of ratio μ_{exp}/μ on cone angle β ; four tangential inlet orifices 1.01×0.53 mm, $d_0 = 1.5$ mm, $R = 2.2$ mm.

Length of the discharge orifice L does not have any effect on μ . This is because μ depends on the conditions in the initial cross section of the discharge orifice. These conditions do not change along the orifice, since the diameter of the gas core remains the same.

The angle of the transient cone β has some effect on μ . The centrifugal force prevents the contraction of the jet leaving the cone, but on the sharp edge at the end of the cone separation of the jet occurs. The results of investigations show (Fig. 6-23) [5] that the greater the ratio μ_{exp}/μ , the smaller the angle β_0 . This is explained by the fact that smaller β causes smaller jet contraction and as β decreases the height of the cone increases, which causes a decrease of angular momentum and therefore an increase of μ . Of course, the value μ for $b = 0^\circ$ and $\beta = 180^\circ$ should be the same, hence in the range $\beta = 0-15^\circ$ the curve should have a maximum (this is not shown in Fig. 6-23).

The conditions at the entry to the swirl chamber are very important (Fig. 6-24) [5]. The direction of liquid motion should coincide with the direction of the axis of the inlet orifices, which requires proper length of orifices l_p (Fig. 6-24a).

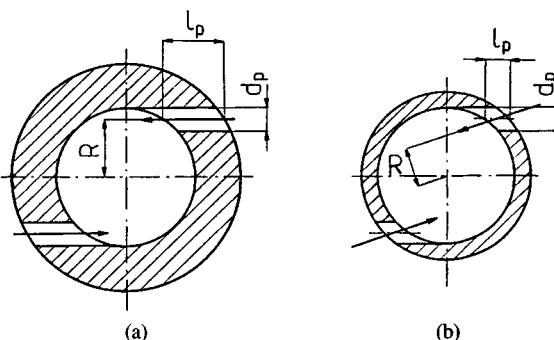


Figure 6-24 Liquid flow to the swirl chamber: (a) correct flow; (b) incorrect flow.

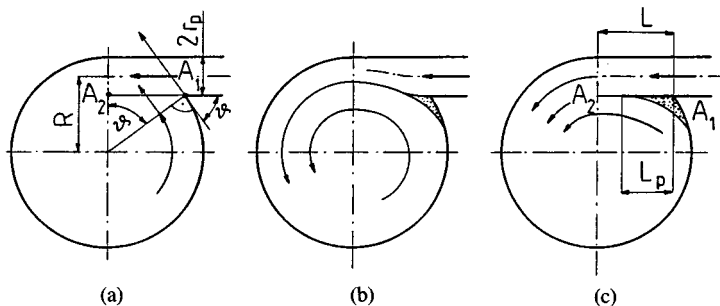


Figure 6-25 Schematic diagram of liquid jet behavior at the entry to the swirl chamber.

If this condition is not satisfied, the liquid flows in the manner shown in Fig. 6-24b and therefore the initial angular momentum decreases. The decrease in angular momentum causes an increase of μ . Length l_p should match orifice diameter d_0 and, in the case of the rectangular orifices, their height. The length of orifices should be greater than $l_p/l_d = 1.5-2.0$, since in the opposite case a rapid increase of μ occurs.

In short inlet orifices jet contraction occurs. The orifice cross-section should then be increased according to the contraction coefficient φ . Coefficient φ depends mainly on the shape of the inlet edge and is on the range $\varphi = 0.60-0.95$. It follows from experiments that for swirl atomizers one should assume $\varphi = 0.85-0.90$ independent of whether the orifice cross-section is circular or rectangular.

Liquid jets flowing in through tangential orifices impinge with the liquid rotating inside the swirl chamber (Fig. 6-25) [5]. If we assume, for simplicity reasons, one orifice through which the liquid flows in the right direction and without contraction, then the angle of impingement at the point A_1 equals (Fig. 6-25a)

$$\cos \vartheta = \frac{R - r_p}{R + r_p} = \frac{B - 1}{B + 1} \quad (6-29)$$

Angle of impingement ϑ is therefore a function of the parameter $B = R/r_0$. As a result of the impingement, jet contraction occurs with a simultaneous increase of swirl radius R (Fig. 6-25b), which leads to a decrease of μ .

The contraction of the jet was confirmed experimentally [5]. The subject of the investigation was a transparent model of an atomizer: one inlet orifice with the cross-section of 10.4×9.5 mm, $d_0 = 6$ mm, $R = 15$ mm. At cross-section A_1-A_2 a partition with a thickness of 0.2 mm and variable length L_p was mounted (Fig. 6-25c). The partition prevents the impingement of jets and jet contraction, which causes flow rate G_L to increase. Experimental results are shown in Table 6-4. As seen, for $L_p > 0.25L$, the flow rate is greater than for an ideal liquid. This is explained by the fact that the angular momentum decreases as a result of disturbances caused by the presence of the partition.

In addition to the pressure drop due to friction in the swirl chamber, other sources of pressure drop are local losses at the entry to the tangential inlet orifices. These orifices have, in general, sharp entry edges. The local losses follow from the equation

$$\Delta P_p = \zeta_p \frac{\rho V_p^2}{2} \quad (6-30)$$

where ζ_p is the coefficient of losses at the entry to tangential orifices. Coefficient ζ_p depends on the type of entry edge and for turbulent flow depends slightly on the Reynolds number. Losses ΔP_p are higher the greater is the portion of pressure drop ΔP across the nozzle which is transformed into dynamic pressure $\rho V_p^2/2$ in the tangential orifices. This depends on the *degree of divergence of the atomizer*

$$C = \frac{R}{r_0}. \quad (6-31)$$

Taking into account the above losses, Eq. (5-48) assumes the form

$$\frac{\rho}{2}(u^2 + v^2 + \zeta_p V^2) + P = P_t \quad (6-32)$$

Following the procedure described in 5-2.1, one obtains an equation similar to Eq. (5-64), namely

$$\mu_\zeta = \frac{1}{\sqrt{K^2/(1 - \epsilon) + 1/\epsilon^2 + \psi}} \quad (6-33)$$

where

$$\psi = \zeta_p \left(\frac{K^2}{C} \right)$$

As seen, ψ does not depend on ϵ , and therefore using the principle of the maximum flow rate one obtains the previous relationship between K and ϵ , viz. Eq. (5-65).

From Eqs. (5-64) and (6-33) follows the ratio of flow ratios with entry losses and without losses:

$$\frac{\mu_\zeta}{\mu} = \frac{1}{\sqrt{1 + \zeta_p(\mu K/C)^2}} \quad (6-34)$$

Table 6-4 Effect of a partition at the entry to the swirl chamber

Relative length of partition L_p/L	0	0.25	0.5	1.0
Relative liquid flow rate G_{exp}/G	0.8	1.09	1.22	1.31

Equation (6-34) indicates that for $K = \text{const}$ the coefficient μ_ζ depends only on the degree of divergence C . The experimental results agree very well with Eq. (6-34) when K is replaced by K_λ [Eq. (5-77)]. For $C < 3$ one should take into account the entry losses, since actual discharge coefficients μ_{exp} are significantly lower than the calculated ones.

In addition to the losses in the tangential orifices and in the swirl chamber, losses also occur in other places within the atomizer. These losses depend on the atomizer design and therefore are not suitable for generalization. It is recommended that the internal flow cross section does not change rapidly and has an area at least twice as large as the area of the tangential orifices.

In [29] the modified equation of a free vortex in the swirl chamber was accounted for and instead of Eq. (5-46) the following equation was used:

$$\nu r^n = \text{const} \quad (6-35)$$

Coefficient n in the range of fuel pressures up to $P_1 \approx 2.76 \text{ MPa}$ is a function of P_1 and the atomizer geometry. For a particular atomizer, coefficient n in this pressure range changes almost linearly with a change of P_1 . For fuel pressures greater than $P_1 \approx 2.76 \text{ MPa}$ n is a function of the atomizer geometry only. The basic dimensions of the atomizer are diameter d_0 or area A_0 of the discharge orifice, diameter d_p or area A_p of the tangential inlet orifices, and diameter D_s or area A_s of the swirl chamber. As a result of experiments, the following expressions for n were derived.

For $P_1 > 2.76 \text{ MPa}$:

$$n = 1.1764 \frac{A_0^{0.1396} A_p^{0.2336}}{A_s^{0.1775}} \quad (6-36)$$

For $P_1 = 0.69 \text{ MPa}$:

$$n = 1.0776 \frac{A_0^{0.1418} A_p^{0.2703}}{A_s^{0.1763}} \quad (6-37)$$

If, for a particular atomizer, n is known for $P_1 \geq 2.76 \text{ MPa}$ and $P_1 = 0.69 \text{ MPa}$, then one can determine n for an arbitrary pressure in the range $P_1 < 2.76 \text{ MPa}$ by interpolation.

Discharge coefficient μ was also determined experimentally:

$$\mu = \xi \left[\frac{1}{\epsilon^2} + \frac{(\pi/4E)^2}{(1-\epsilon)^n} \right]^{-1/2} \quad (6-38)$$

where ξ is the correction factor

$$\xi = 0.6625 \frac{A_0^{0.1373} A_s^{0.0778}}{A_p^{0.0411}}$$

ϵ is the air core coefficient [Eq. (5-45)], E is the nozzle parameter,

$$E = \frac{A_p}{2d_0 R} \left(\frac{2R}{d_0} \right)^{1-n} \quad (6-39)$$

and R is the swirl radius.

Duplex atomizers. There are few publications regarding evaluations of duplex atomizers. Here the results of the study of a fuel two-chamber atomizer that was discussed in Sec. 4-2.2 (Fig. 4-30) will be presented. The study is concerned with the effect of back pressure in the first chamber (feeding system I) on the atomizer's operation.

The pressure in the first chamber is the back pressure for the second chamber and can be calculated based on the material in Sec. 5-2.1. The back pressure in the first chamber is equal to the dynamic pressure of the liquid:

$$P_I = \frac{\rho u_I^2}{2} \quad (6-40)$$

The axial velocity of the fuel in front of the discharge from the first chamber is

$$u_I = \frac{Q}{\pi \epsilon r_0^2} \quad (6-41)$$

The fuel flow rate is given by

$$Q = \mu \pi r_0^2 \sqrt{\frac{2 \Delta P}{\rho}} \quad (6-42)$$

Substituting Eqs. (6-41) and (6-42) into (6-40),

$$P_I = \left(\frac{\mu}{\epsilon} \right)^2 \Delta P \quad (6-43)$$

where ΔP = pressure drop in the first chamber

ϵ, μ = parameters that can be calculated from Eqs. (5-65) and (5-66)

Equation (6-43) can be applied when diameter of the discharge orifice of the second chamber $2r_{0II}$ is greater than the diameter of the gas core of the first chamber $2r_{I1}$. The method of calculation is the same for an ideal and a viscous liquid; the only difference is caused by the fact that either constant K or K_λ is used. In order to confirm Eq. (6-43), experiments were carried out. The conditions of the study of evaluations are as follows: fuel density 843 kg/m^3 , kinematic viscosity $5.5 \times 10^{-6} \text{ m}^2/\text{s}$ at 20°C , surface tension $30.4 \times 10^{-3} \text{ N/m}$, diameter of the discharge orifice of the second chamber $2r_{0II} = 0.5\text{--}5.0 \text{ mm}$, feeding pressure of the first chamber $0.5\text{--}5.5 \text{ MPa}$.

Experimental results are shown in Fig. 6-26 [26]. As seen, the agreement of results is satisfactory only in the range of diameters $2r_{0II}$ greater than the core

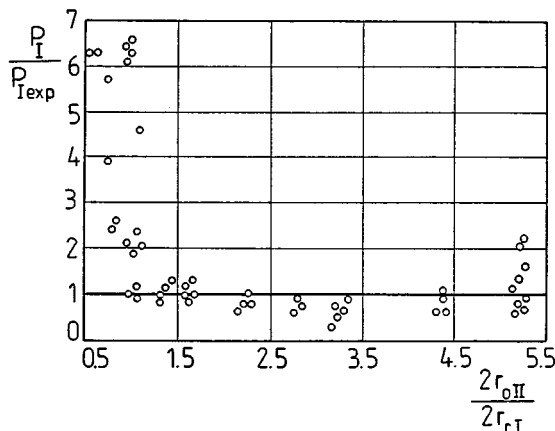


Figure 6-26 Ratio of theoretical and empirical back pressures as a function of the ratio of diameter of the discharge orifice of the second chamber $2r_{oII}$ and diameter of the gas vortex in the first chamber $2r_{rI}$.

diameter $2r_{rI}$. In the opposite case the results are completely in disagreement, which confirms that the limitations of Eq. (6-43) are correct. During the experiments it was established that the back pressure for the flow through the first chamber does not depend on the diameter of the second swirl chamber and on the tangential orifices. The flow rate of both systems equals the sum of slow rates corresponding to the pressure drops corrected for the back pressure. The back pressure is usually 5–20% of the pressure in the first feeding system. In the case of feeding pressures of order 1.5 MPa, $P_1 = 0.075\text{--}0.3$ MPa (above the ambient pressure). Such values of back pressures are in some cases comparable to feeding pressures in the second chamber and therefore it is clearly necessary to take back pressures into account.

Spill-return atomizers. A very important problem regarding spill-return atomizers is the question of the dimensions and location of the return orifices. The liquid return can be realized by a singular axial orifice, by several small orifices placed symmetrically, or by an annular slot. This latter solution, shown in Fig. 4-36, was considered in Sec. 4-2.3 as most useful in terms of flow. However, there are no experimental data on this subject but data do exist for the case of return orifices.

The results presented in [5] can serve as an example. An atomizer with the following features was used for experiments: six tangential inlet orifices with cross section 1.06×1.015 mm, $d_0 = 1.8$ mm, $R = 2.65$ mm, three different disks with the return orifices. These disks constituting the back wall of the swirl chamber are shown in Fig. 6-27 and the data concerning the orifices are presented in Table 6-5. The characteristics of an atomizer with these disks were established as a result of experiments (Fig. 6-28).

Figure 6-28a corresponds to a closed control valve (Fig. 4-3.4). Since there is no liquid return, the characteristics have the same shape as for the simplex atomizers. The dashed line denotes the characteristic for an ideal liquid for

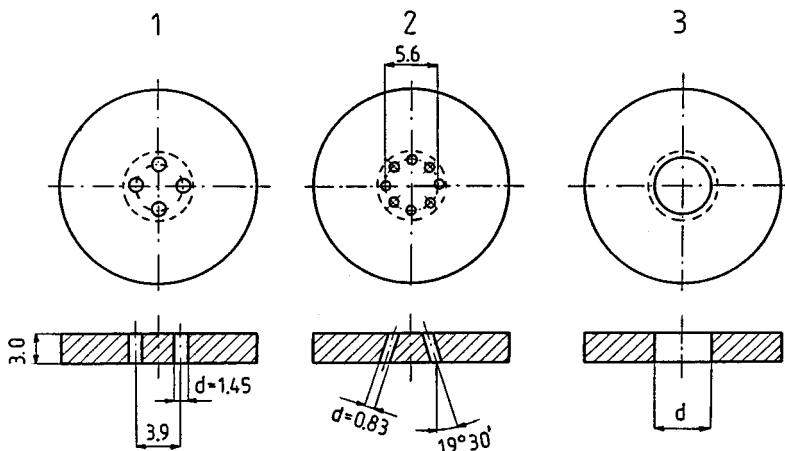


Figure 6-27 Disks with return orifices with diameter d (Table 6-5); dashed line circles show the shape of a swirl chamber.

$\mu = 0.40$. The influence of viscosity can be neglected (see Sec. 5-2.1), since

$$\frac{B^2}{i} - K = \frac{4.55^2}{6} - 1.17 = 2.28$$

This is correct if the length of the swirl chamber is only slightly greater than the diameter (in this case the width) of the inlet orifices. Disk 3b does not satisfy this requirement.

Figure 6-28b shows the results of measurements of the flow resistance through the return orifices. Since the discharge orifice was closed, the liquid flowed only through the return orifices. The experiments were conducted for constant liquid pressure $p = 3.0$ MPa and for variable pressure in the return manifold P_d . The lower the flow rate G for a given pressure P_d , the higher the

Table 6-5 Data concerning return orifices and liquid flow rates (Fig. 6-27)

	Disks			
	1	2	3a	3b
Orifice diameter d , mm	1.45	0.83	2.03	6.65
Number of orifices	4	8	1	1
Total area of orifices A , mm^2	6.70	4.38	3.23	34.7
Flow rate kg/s				
G_a min	0.0036	0.00815	0.0367	0.01615
G_a max	0.074	0.069	0.071	0.10
G_a max/ G_a min	20.55	8.47	1.94	6.2

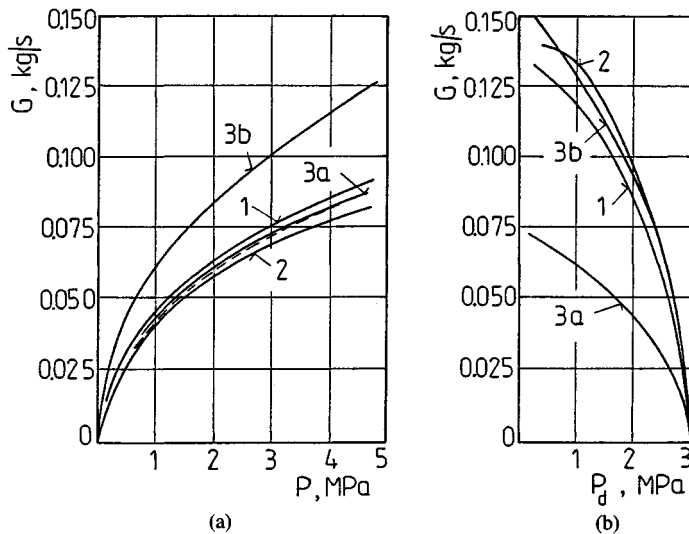


Figure 6-28 Characteristics of an atomizer with various return flow disks: (a) closed control valve (b) closed discharge orifice; curves are labeled according to disk notation in Table 6-5.

resistance of the return orifices. As seen, the smallest resistance is for disk 2 despite the fact that the total cross section of the orifices A (Table 6-5) is not the largest. These orifices are located on the large diameter, so the circumferential velocity is relatively small and does not cause large losses when the velocity direction changes and during flow through the orifices. The highest resistance is for disk 3a due to the presence of an axial orifice through which the liquid flows with high velocity.

Table 6-5 contains flow rates for a completely open $G_{a \min}$ and completely closed $G_{a \max}$ control valve for constant pressure in front of the atomizer $P = 3.0$ MPa. Ratio $G_{a \max}/G_{a \min}$ denotes the range of flow rate changes. The highest flow rate change is ensured by the disk 1, the lowest by the disk 3a. Therefore, in order to reduce the hydraulic resistance, it is advantageous to return the liquid through the orifices located far from the chamber axis. This, however, leads to an increase of the friction of the remaining liquid flowing to the discharge orifice and therefore to an increase of flow rate G_a of the atomized liquid. The optimum solution is to return the liquid through the orifices located approximately on the mean diameter of the swirl chamber. Disk 1 satisfies this condition. Instead of the orifices, an annular slot can be used.

6-2.2 Macrostructure of the Atomized Liquid

In the case of swirl atomizers the shape of the spray is determined by spray angle α and by the liquid distribution; the spray penetration is less important.

Spray angle. Most of the data on angle α concerns the *simplex atomizers*. The relationship between actual angle α and geometric constant K was discussed on the basis of Fig. 6-19. In this case it is seen that an increase of K causes angle α to increase to a certain extreme value α_{\max} and subsequently to decrease. Constant K is changing by changing swirl radius R .

The effect of liquid pressure P_1 on angle α for various geometric dimensions of the atomizer is shown in Fig. 6-29 [34]. As seen, in the range of pressure $P_1 = 0.69$ – 2.07 MPa a linear relationship exists between α and P_1 . The gradient of angle α in this pressure range is approximately 4.6° per 1 MPa. Above $P_1 = 2.07$ MPa angle α is constant ($\alpha = \text{const}$). The same results were obtained for other geometric dimensions of the atomizer, but of course angle α had a different numerical value. Similar results were also obtained in [38].

The effect of the geometric parameters of the atomizer on angle α is diverse. Angle α depends most of all on discharge orifice diameter d_0 , the diameter of the tangential inlet orifices d_p , and the diameter of the swirl chamber D_s (more precisely on swirl radius R), since these parameters are incorporated into geometric constant K [Eq. (4-1)]. Each of these geometric parameters has a different effect. Angle α increases as d_0 increases but decreases as d_p increases. Angle α increases to a certain value as D_s increases and then does not change.

The influence of length l_s of the swirl chamber is such that as l_s increases angle α decreases. A reduction of angle α is caused by a decrease of the angular momentum, since additional frictional drag is caused by an increase of l_s . This effect is significant for high liquid viscosities; for small viscosities it is negligible.

Length of the discharge orifice l has an essential effect on the value of angle α , which is shown in Fig. 6-30 [5]. The longer the orifice, the lower angle α is, since the angular momentum decreases due to friction in the orifice. The

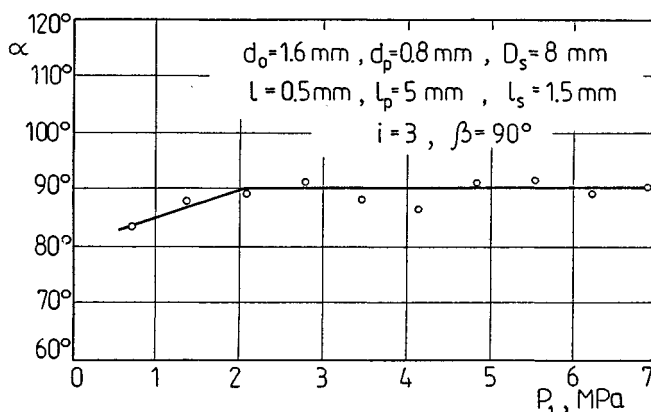


Figure 6-29 Dependence of spray angle α on liquid pressure P_1 ; atomizer dimensions as in Fig. 5-13.

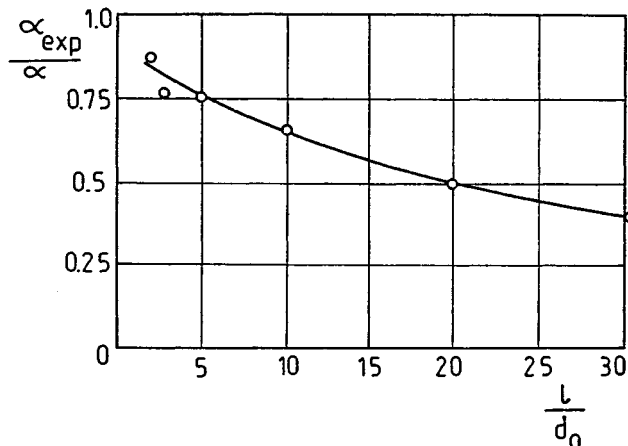


Figure 6-30 Relationship between $\alpha_{\text{exp}}/\alpha$ and l/d_0 ; $A \approx 4.45$, $B \approx 4.44$, liquid is kerosene.

friction effect grows along with the increase of friction coefficient λ and geometric constant K_λ [Eq. (5-77)]. For large values of λ and K_λ even a small increase of the orifice length causes a distinct decrease of angle α .

The phenomena occurring at the entry to the swirl chamber also affect angle α . If length l_p of the inlet orifices is too low, as in Fig. 6-24b, the angular momentum decreases, accompanied by a decrease of angle α . In the case $l_p/l_d < 1.5-2$ a rapid drop of angle α occurs. The opposite situation takes place due to the contraction of jets in the inlet orifices, since together with the increase of the velocity caused by contraction the angular momentum increases and therefore angle α increases. Deformation of the inlet jets and increase of swirl radius R (Fig. 6-25b) also lead to an increase of angle α . The entry losses at the inlet orifices do not, however, have any effect on angle α , since ψ in Eq. (6-33) does not depend on the efficiency of filling ϵ .

In the range of conical angle of the swirl chamber $\beta = 60-90^\circ$, angle α is constant and for $\beta > 90^\circ$ angle α increases.

In [29] an empirical formula was presented that relates angle α to the geometric dimensions of the atomizer:

$$\operatorname{tg} \frac{\alpha}{2} = \frac{k \pi \epsilon}{4E} \quad (6-44)$$

where ϵ, E are as in Eqs. (5-45) and (6-39) and k is the correction factor

$$k = 1.7099 \frac{A_p^{0.0340}}{A_0^{0.1755} A_s^{0.2458}}$$

Figure 6-31 shows the effect of liquid viscosity ν_L on the mean spray angle α_m from Eq. (3-27) [31]. The results correspond to the same atomizer as described

in Fig. 6-20, Fig. 6-21, and Fig. 6-22. As follows from Fig. 6-31, angle α_m drops significantly as viscosity ν_L increases but it increases as ΔP increases; a wide range of viscosities was investigated. For a certain value of ν_L the liquid swirling vanishes and the liquid discharges through the whole cross-section of the discharge orifice ($\alpha_m = 0$). Spray angle α_m increases slightly as liquid density increases.

In [31] a formula was given that allows calculation of the spray angle in the range $\alpha_m = 50\text{--}120^\circ$ for a wide range of values K' , ΔP , d_0 , ρ_L , and μ_L :

$$\alpha_m = 5.63 K'^{-0.15} \text{Re}^{0.11} \quad (6-45)$$

while constant K' follows from Eq. (6-28) and the Reynolds number is

$$\text{Re} = \frac{\rho_L u d_0}{\mu_L}$$

where liquid velocity u follow from pressure drop ΔP across the atomizer.

Duplex atomizers have relatively large variations of angle α , as mentioned in Sec. 4-2.2. This variation corresponds to the transient region of the operation (BC, Fig. 4-29) and particularly to the moment when the secondary feeding system is activated. It follows clearly from Fig. 6-32 that at the moment of opening of the control valve at $P_1 = 1$ MPa a drop of angle α occurs. The theoretical curve calculated according to recommendations in Sec. 5-2.2 is in a relatively good agreement with the experimental curve, since in the limiting case the error does not exceed $\pm 1.5\%$.

Dual-orifice atomizers (Fig. 4-31) have a small variation of angle α . In the operating range when both feeding systems are active, α depends on angles α_1

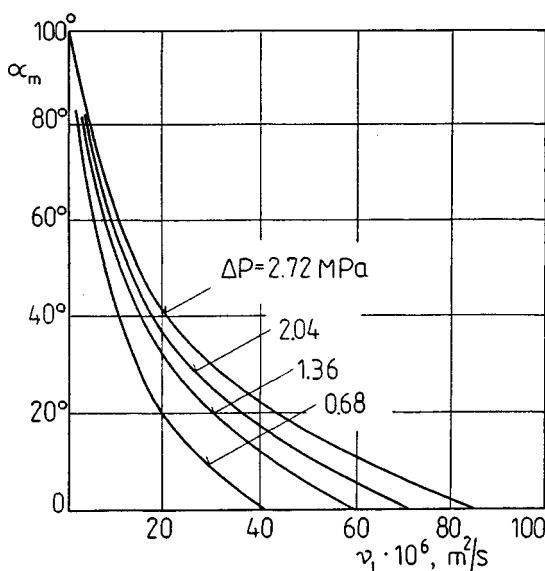


Figure 6-31 Dependence of mean spray angle α_m on kinematic viscosity ν_L for various values of pressure drops ΔP [31].

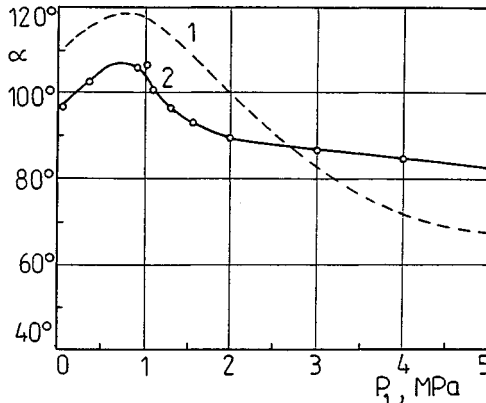


Figure 6-32 Dependence of angle α of a duplex atomizer on feeding pressure P_1 . 1, theoretical curve; 2, experimental curve.

and α_2 of both stages on the relative position of the discharge orifices (nozzles). If the discharge cross sections of both nozzles lie in the same plane and if $\alpha_1 > \alpha_2$, then the resultant spray angle is given by

$$\cos \alpha = \frac{u_1 G_1 \cos \alpha_1 + u_2 G_2 \cos \alpha_2}{u_1 G_1 + u_2 G_2} \quad (6-46)$$

where u_1, u_2 = axial velocity of the liquid at the discharge from the primary and secondary feeding system

G_1, G_2 = mass flow rates of the primary and secondary feeding system
Equation (6-46) has a relatively good experimental confirmation.

The relative position of the nozzles of both stages has a large influence on the resultant angle α , which is seen in Fig. 6-33 [5]. The results shown were obtained for various projections of the secondary nozzle achieved by using

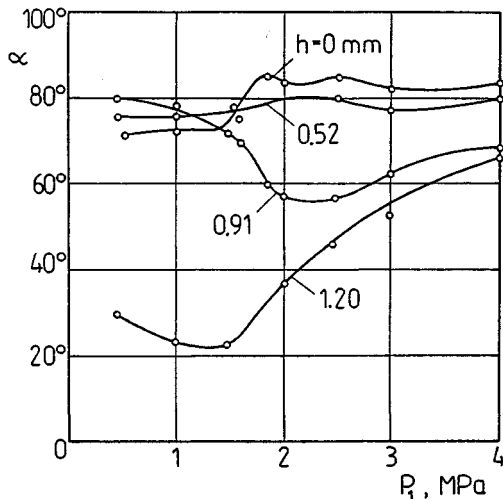


Figure 6-33 Dependence of angle α of a duplex atomizer on feeding pressure P_1 for various nozzle positions.

distance plates with various thicknesses h . It is seen that by changing the position of nozzles one can significantly affect the function $\alpha = f(P_1)$. One can even arrive at the situation where angle α is practically constant, which in this example takes place for $h = 0.52$ mm.

Spill-return atomizers have the larger angle α the greater the excess liquid coefficient e is [Eq. (4-8)]. Along with the increase of coefficient e , geometric constant K_d increases and larger angle α correspond to higher values of K_d (Fig. 5-11). For the atomizer whose characteristic is shown in Fig. 4-35, the change of angle α is similar to that one shown in Fig. 6-32, where pressure P_1 should be replaced by pressure P . The control value starts to close at pumping pressure $P = 1$ MPa, and from this moment a significant change of angle α is observed. The largest spray angle exists for a totally open return orifice, i.e., for the minimum flow rate of the atomized liquid.

Liquid distribution in a drop jet. Experimental results will be given for simplex atomizers only because such data does not exist for other types of swirl atomizers.

The effect of pressure drop ΔP on the radial distribution of the density of the liquid jet is shown in Fig. 6-34 [5]. As ΔP increases, the central part of the jet fills up with liquid and the conical shape of the jet starts to deform as shown in Fig. 3-9. The jet narrows and assumes appropriately a cylindrical shape. This is due to the ejection of the ambient gas. Measurements were carried out regarding the gas ejected by a jet of the atomized liquid with various viscosity, density, and surface tension [45]. The quantity of air at a distance x from the atomizer increases linearly as the Reynolds number increases, where the Reynolds number corresponds to the atomized liquid.

Figure 6-35 shows the effect of discharge orifice diameter d_0 on the dimensionless density q/\bar{q} , where \bar{q} is the mean jet density across the whole area of the transverse cross section of the jet. In the case of small diameter d_0 and small injection pressure $P_1 = 0.5$ MPa, the density distribution differs from a typical radial distribution for swirl atomizers (Fig. 6-34). Generally, it can be

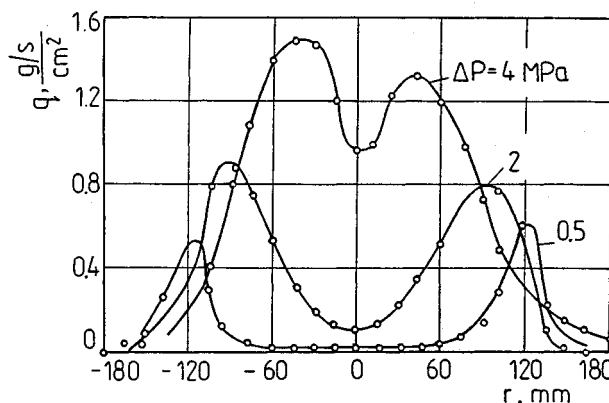


Figure 6-34 Radial distribution of liquid jet density $q = q_m = f(r)$ for a simplex atomizer for various liquid pressure drops ΔP ; $x = 150$ mm.

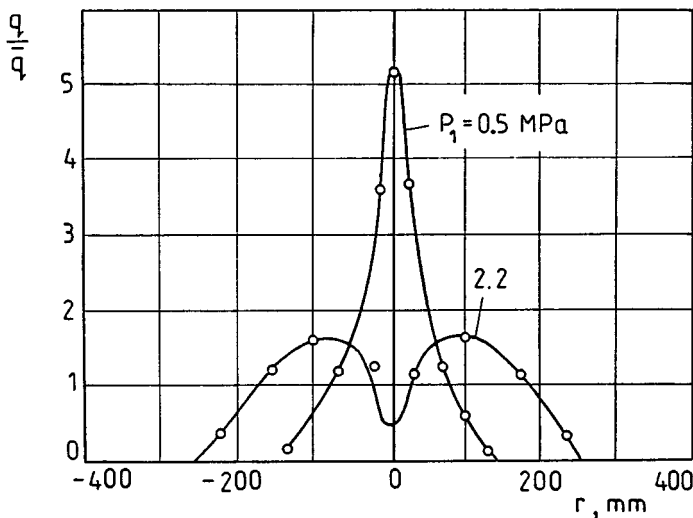


Figure 6-35 Radial distribution of dimensionless liquid jet density for diameter $d_0 = 0.38 \text{ mm}$; $D_s = 7.89d_0$, $K = 3.87$.

stated as d_0 and K decrease, the flow rate of the liquid in the central part of the jet increases.

The radial distribution of liquid jet density also depends on the flow rate and viscosity of the liquid. Figure 6-36a shows the results of the study of an atomizer with the following data [26]: $d_0 = 0.9 \text{ mm}$, $R = 4.86d_0$, $K = 4.40$. As seen, for a liquid with only slightly different viscosity ($\sim 60 \times 10^{-4} \text{ Pa} \cdot \text{s}$) a decrease of the flow rate causes the distribution to become atypical for swirl atomizers. Figure 6-36b shows the results of the evaluations of the same atomizer for similar injection pressures $P_1 = 0.6\text{--}0.95 \text{ MPa}$ but for liquids with various viscosities. An increase of viscosity also leads to a distinct change of the radial density of the liquid jet.

As mentioned in Sec. 3-2.3, the *circumferential distribution of the jet density* $q = f(\varphi)$ is determined experimentally and presented in the form of circumferential nonuniformity I [Eq. (3-37)]. The circumferential nonuniformity of a new atomizer is caused by design asymmetry or by technological or assembly flaws. Circumferential nonuniformity of an operating atomizer can also indicate its failure or contamination. Design asymmetry of an atomizer stems mainly from a limited number of tangential inlet orifices. Technological and assembly flaws include eccentricity of the discharge nozzle with respect to the swirl chamber and poor precision of orifice drilling.

The effect of tangential inlet orifices on circumferential nonuniformity is shown in Fig. 6-37 [5]. The atomizers investigated differ in the number of orifices but the total area of their cross-sections remained constant. The

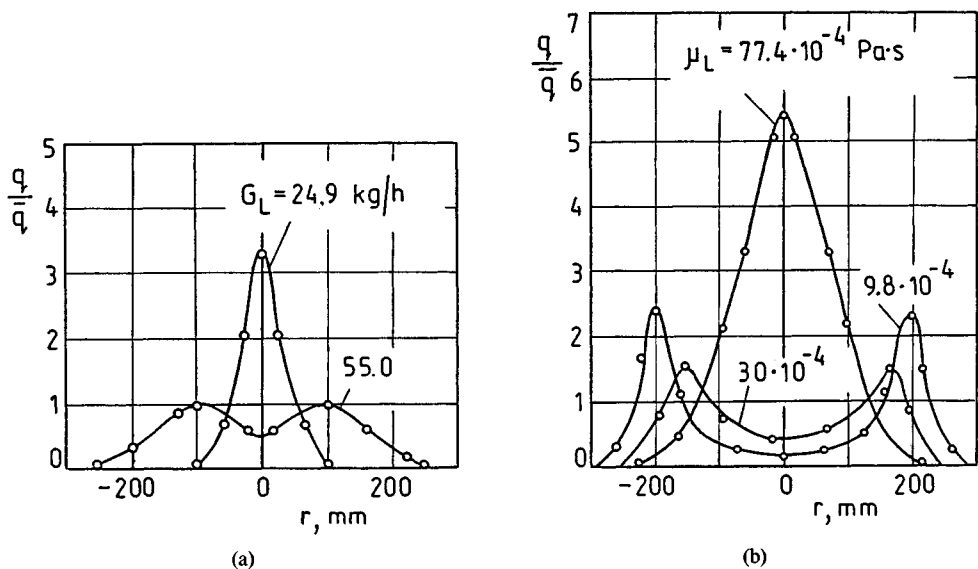


Figure 6-36 Radial distribution of dimensionless liquid jet density: (a) for various flow rates G_L ; (b) for various dynamic viscosities μ_L .

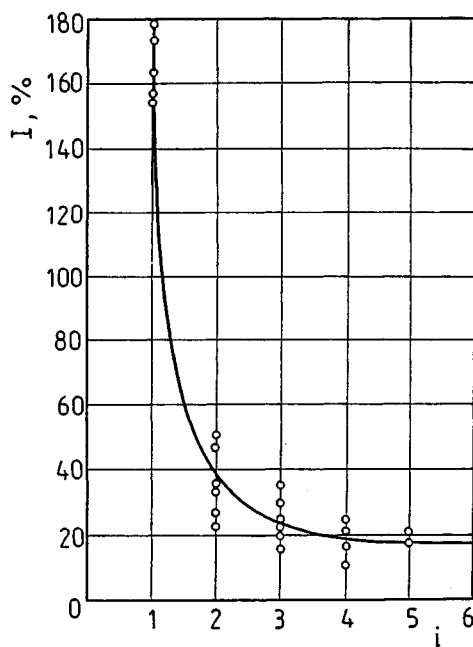


Figure 6-37 Dependence of circumferential nonuniformity I on number of tangential inlet orifices i .

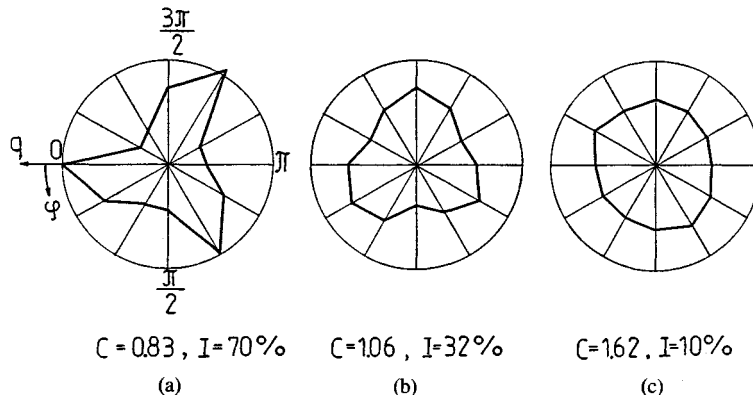


Figure 6-38 Circumferential distribution of liquid jet density $q = f(\varphi)$ for atomizers with various degree of divergence C .

transition from $i = 1$ to $i = 2$ brings an essential improvement, and for $i > 3$ there is no distinct change of nonuniformity I .

For a limited number of tangential inlet orifices the film thickness in the discharge orifice is in general nonuniform, which causes an increase of nonuniformity I . This depends especially on the degree of divergence of the atomizer C [Eq. (6-31)], which is shown in Fig. 6-38 [8] for $i = 3$. The smaller C is, the higher the circumferential nonuniformity I is.

Figure 6-39 shows the empirical relationship $I = f(C)$ [8], which concerns atomizers with different numbers of tangential inlet orifices. The atomizer has a short swirl chamber ($L_s/D_s \leq 0.3$) and during the experiments efficiency of filling $\epsilon = 0.2$ was maintained. It is seen that for a number of orifices $i = 2-8$, there exists in each case a certain value $C = C^*$ such that for $C > C^*$, $I \approx 10\%$. As the number of inlet orifices increases, C^* decreases.

Geometric constant K of the atomizer also affects I . The greater the constant K is, the smaller the filling efficiency ϵ is (Fig. 5-11), i.e., the smaller

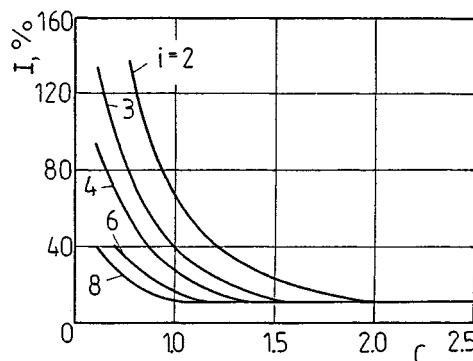


Figure 6-39 Dependence of circumferential nonuniformity I on degree of divergence C for various numbers of inlet orifices.

the liquid film thickness δ is. In this situation nonuniformity I is to a higher extent dependent on the number of inlet orifices, which is confirmed by experiments.

Conical angle β in the swirl chamber and the length of the swirl chamber l_s also have an effect on the circumferential nonuniformity (Fig. 5-13). In the case of small angle β , the length of the path of liquid elements increases, which causes the circumferential distribution to become more uniform. For design reasons, angles β smaller than 60° are not used. On the same base, the effect of length l_s of the swirl chamber can be assessed; the larger l_s , the longer the path of liquid elements.

The effect of parameters discussed above on the circumferential nonuniformity is described by the following empirical equation:

$$I = \frac{23.7}{c^{2.7} i^{1.34} \epsilon^{1.1} (l_s/D_s)^{0.15}} \quad (6-47)$$

As seen, nonuniformity I depends mainly on C , to a lesser extent on i , and insignificantly on l_s .

The manufacturing and assembly faults, as mentioned before, stem mainly from eccentricity of the discharge orifice with respect to the swirl chamber. It follows from experiments [5] that nonuniformity I increases linearly with increasing eccentricity e . In order not to exceed $I = 20\%$, the condition $e/d_0 < 0.075$ must be satisfied. Coaxiality of the discharge orifice and the swirl chamber is easy to achieve when both of these elements constitute an integral unit.

However, in some instances a certain intended circumferential nonuniformity is desired. Investigations of a fuel atomizer [25] which separates the swirled jet into four segments are an example. A reduction of the level of emission of NO_x by 30–40% was achieved because the access of oxygen to drops was improved. Figure 6-40 shows the nozzle of such an atomizer, which has four grooves of triangular cross section on the front surface. The grooves are located tangentially with respect to the discharge orifice and ensure the same direction of swirling as in the swirl chamber. Grooves with different shapes and location were investigated, and no effect on the atomization characteristics was found.

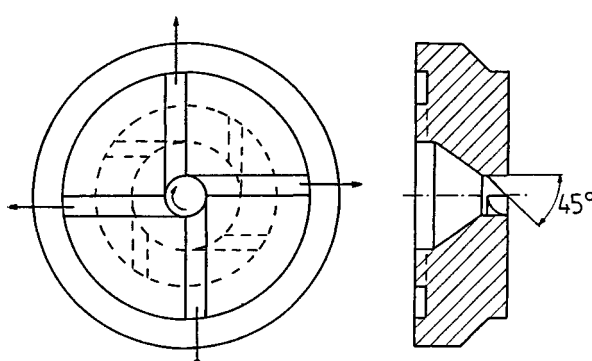


Figure 6-40 Swirl atomizer with grooves on the front surface.

6-2.3 Microstructure of Atomized Liquid

The theoretical basis of the disintegration of a liquid film at the discharge from swirl atomizers was discussed in Chapter 2. It follows from experiments that intensive disintegration of the film (atomization) occurs directly at the outlet from the atomizer. *Liquid film thickness* δ depends on the geometry of the atomizer's elements (diameter d_0 etc.) and on the atomization conditions (discharge velocity liquid properties, ambient properties), so it depends on the values of We , L_p , M , and N . Thickness δ is therefore the most characteristic parameter of swirl atomizers.

Thickness δ can be calculated approximately in the following way (Fig. 6-41). From flow continuity condition it follows that

$$\mu\pi r_0^2 V = AV$$

where μ = discharge coefficient

r_0 = discharge orifice radius

V = discharge velocity

A = film cross-sectional area, equal to the side surface of a truncated cone

$$A = \pi\delta(r_0 + r_r) = \pi\delta\left(2r_0 - \delta \cos \frac{\alpha}{2}\right)$$

where r_r is the gas core radius.

After substitution and transformation, we obtain a quadratic equation with respect to δ/r_0 :

$$\cos \frac{\alpha}{2} \left(\frac{\delta}{r_0}\right)^2 - 2 \frac{\delta}{r_0} + \mu = 0$$

From the two roots only one, $\delta/r_0 < 1$, has a physical meaning, i.e.,

$$\frac{\delta}{r_0} = \frac{1 - \sqrt{1 - \mu \cos \alpha/2}}{\cos \alpha/2} \quad (6-48)$$

In order to calculate δ , values μ and α must be known from measurements.

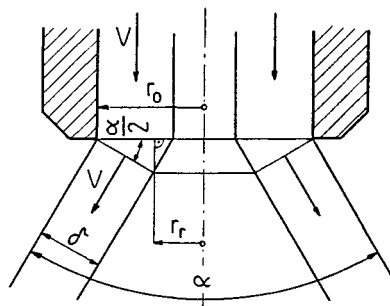


Figure 6-41 Auxilliary schematic diagram for calculating liquid film thickness δ of a swirl atomizer.

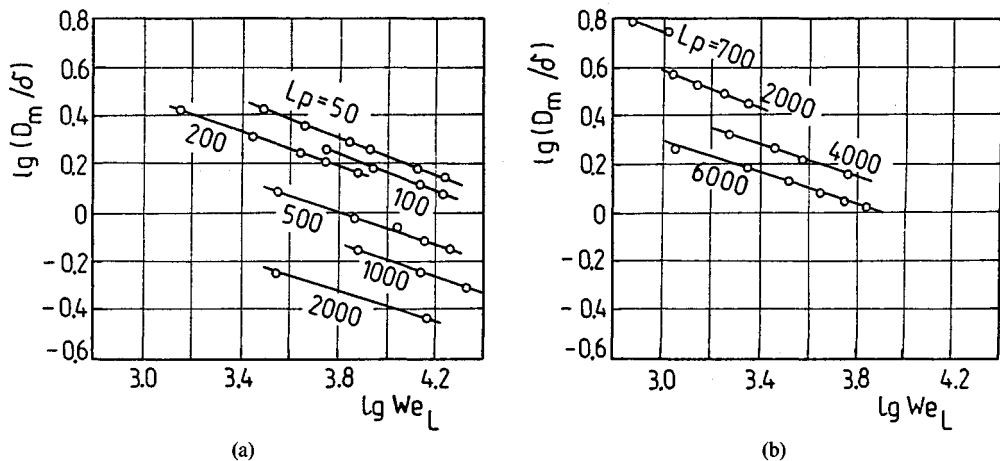


Figure 6-42 Dependence $D_m/\delta = f(\text{We}_L)$ for various values of L_p : (a) kerosene; (b) water and water solutions of glycerine.

Figure 6-42 shows the results of investigations of various simplex atomizers based on the publications of many authors [26]. Two groups of liquids, kerosene and water with water solutions of glycerin were used. Graphs $D_m/\delta = f(\text{We}_L)$ for several values of numbers L_p and for constant M and N are straight lines on a logarithmic scale. Diameter D_m is the median diameter (see Sec. 3-3.2). The Weber number has the same form as in Eq. (6-5), but instead of diameter d_0 , film thickness δ from Eq. (6-48) is used. A similar remark refers to the Laplace number, which follows from Eq. (6-6).

The straight lines in Fig. 6-42 have almost the same slope for different liquids, but these lines are not identical for the same L_p number as seen in the example of $L_p = 2000$. The differences are significant in spite of the fact that the properties of kerosene do not differ much from the properties of water. The diameters of kerosene drops are smaller than the diameters of water drops for the same values of We_L and L_p . It follows that the effect of numbers M and N cannot be neglected. The equations describing the lines in Fig. 6-42 are as follows.

For kerosene:

$$\frac{D_m}{\delta} = 269 \text{We}_L^{-0.35} L_p^{-0.423} \quad (6-49)$$

For water and water solutions of glycerin:

$$\frac{D_m}{\delta} = 1415 \text{We}_L^{-0.35} L_p^{-0.463} \quad (6-50)$$

Equation (6-49) holds for $M = 1.5 \times 10^{-3}$ and $N = 10^{-2}$ and Eq. (6-50) for $M = 1.2 \times 10^{-3}$ and $N = 1.8 \times 10^{-2}$.

The effect of liquid density ρ_L and ambient gas density ρ_G , i.e., the effect of number M on the atomization quality, is not satisfactorily explored, as in the case of swirl atomizers. The experimental results obtained by various authors derived for lowered back pressure of the gas indicated either a decrease or an increase of drop diameters. In [31] it was established that liquid film thickness δ decreases slightly with increasing of liquid density ρ_L , but this effect is small for liquids used in practice.

The effect of viscosities of the liquid μ_L and gas μ_G , i.e., the effect of number N on the atomization quality, is especially distinct for high liquid viscosities. Sauter mean diameter D_{32} and film thickness δ at the discharge from the atomizer are related as follows:

$$D_{32} \sim \delta^{0.39}$$

In [31], the following equation was established for hydrocarbon fuels and for a simplex atomizer:

$$\delta = 3.66 \left[\frac{d_0 F N \mu_L}{(\Delta P \rho_L)^{0.5}} \right]^{0.25} \quad (6-51)$$

where FN, m^2 denotes the flow number according to Eq. (3-6).

Equation (6-51) agrees with results of experiments carried out for the atomizer described in the case presented in Fig. 6-20 and others. In Eq. (6-51) the surface tension is not present, since for the hydrocarbon fuels it varies only about 10%. Figure 6-43 has been prepared to illustrate Eq. (6-51). It is seen that film thickness δ increases significantly as ν_L increases. For a given viscosity, thickness δ decreases as ΔP increases.

In [30] the effect of the swirl atomizer's geometry on Sauter mean diameter D_{32} (SMD) of drops was evaluated. It was established that D_{32} depends mainly

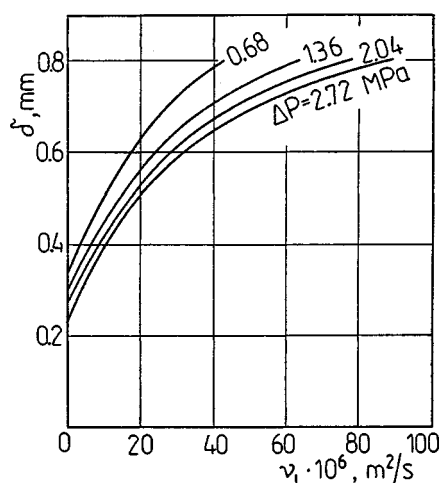


Figure 6-43 Dependence of liquid film thickness δ on kinematic viscosity ν_L for various values of pressure drop ΔP .

on discharge orifice diameter d_0 , diameter of inlet orifices d_p , and swirl chamber diameter D_s , i.e., on the dimensions incorporated in geometric constant K [Eq. (4-1)]. D_{32} increases linearly (especially for higher pressures P_1) with increase of diameter d_0 . D_{32} increases significantly as diameter d_p increases, and the effect of d_p is stronger than that of d_0 . D_{32} decreases as D_s increases.

The drop sizes were measured by the light scattering method, and the following equations were established.

For $P_1 < 2.76$ MPa:

$$D_{32} = 56.7 \frac{A_0^{0.3889} A_p^{0.3211}}{A_s^{0.0541} P_1^{0.2565}} \quad (6-52)$$

For $P_1 \geq 2.76$ MPa:

$$D_{32} = 48.7 \frac{A_0^{0.4246} A_p^{0.2955}}{A_s^{0.0887} P_1^{0.2076}} \quad (6-53)$$

(D_{32} , μm ; A_0, A_p, A_s , mm^2 ; P' , MPa, areas A_0, A_p, A_s correspond to diameters d_0, d_p, D_s).

It was established that D_{32} does not depend on the length l of the discharge orifice, length l_p of the inlet orifices, swirl chamber length l_s , number of tangential inlet orifices i (if the same area A_p is maintained), and conical angle B (see Fig. 5-13).

In [9] the effect of the ratios of various geometric dimensions on D_{32} was investigated. Kerosene was used for atomization. As a result of extensive research for constant conditions of atomization, the following equation was obtained:

$$\frac{D_{32}}{d_0} = 8.343 \frac{\mu^3 (l_s/d_0)^{0.546} (l/d_0)^{0.0673}}{(D_s/d_0)^{0.678} (d_p/d_0)^{1.785}} \quad (6-54)$$

where μ is the discharge coefficient and the remaining symbols are in accordance with Fig. 5-13. It was also found that D_{32} decreases as ratio l_s/D_s increases, but for $l_s/D_s > 2.75$, D_{32} increases.

The effect of pressure drop ΔP on the atomization quality is manifested by the fact that higher ΔP produces higher discharge velocity, which causes a decrease of the drop diameters. The relationship between D_{32} and ΔP is $D_{32} \sim \Delta P^{-1/3}$. This relationship is essential in the range of small values of pressure drop ΔP , but in the range $\Delta P > \sim 2.5$ MPa the effect of ΔP on D_{32} diminishes significantly.

The effect of flow rate G_L , i.e., of the atomizer dimensions, on the Sauter mean diameter is unequivocal; D_{32} increases as G_L increases. This follows from the equation [26]

$$D_{32} = 52 G_L^{0.282} \Delta P^{-0.397} \nu_L^{0.204} \quad (6-55)$$

For the individual terms the following units are used: D_{32} , μm ; G_L , kg/h ; ΔP , MPa ; $\nu_L \times 10^6$, m^2/s . If flow rate G_L increases by 50%, for example, ΔP should increase by 30% in order to preserve the same diameter D_{32} . For high liquid flow rates, several atomizers are often used instead of one in order to reduce the mean drop diameter at the same pressure drop. For D_{32} to decrease twice, pressure drop ΔP should be increased four times.

In [27, 51] the equations for the median diameter D_m during the atomization of coal-liquid mixtures, which are a mixture of oil and coal dust, were derived.

For monodisperse dust in the mixture:

$$\frac{D_m}{\delta} = 9.129 \times 10^{-5} \text{We}^{-0.159} \text{Lp}^{-0.698} M^{-3.17} N^{1.204} B^{-6.41} \quad (6-56)$$

For polydisperse dust in the mixture:

$$\frac{D_m}{\delta} = 5.13 \times 10^{-6} \text{We}^{-0.68} \text{Lp}^{-0.116} M^{-2.922} N^{0.152} B^{-0.545} \quad (6-57)$$

where δ = mixture film thickness from Eq. (6-48)

We = Weber number

$$\text{We} = \frac{\rho_m u^2 \delta}{\sigma},$$

Lp = Laplace number

$$\text{Lp} = \frac{\rho_m \sigma_m \delta}{\mu_m^2},$$

M = dimensionless number

$$M = \frac{\rho_G}{\rho_m},$$

N = dimensionless number

$$N = \frac{\mu_G}{\mu_m},$$

B = parameter representing the influence of the coarseness and concentration of dust in mixture

$$B = \left(1 - \frac{d}{d_0}\right)^g$$

where ρ_m , μ_m , and σ_m are density, viscosity and surface tension of the mixture, respectively, d is the median diameter of dust, and g is the mass fraction of dust in the mixture.

Figure 6-44 shows the result of an investigation of a *two-orifice atomizer* [26] used in the gas turbine "Nene" produced by Rolls-Royce. Curves 1, 2, and 3 in Fig. 6-44 are similar to curves 1, 2, and 5 in Fig. 4-33. The aim of the investigation was to demonstrate the changes of Sauter mean diameter D_{32}

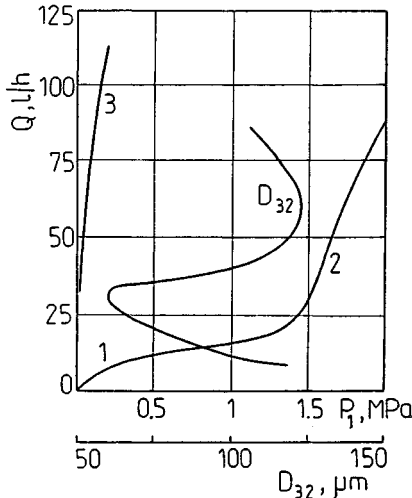


Figure 6-44 Change of Sauter mean diameter D_{32} for a two-orifice atomizer caused by activation of a secondary feeding system [26].

caused by activation of the secondary feeding system, since rapid deterioration of atomization occurs in this case. In this particular case it took place at flow rate $Q = 30 \text{ l/h}$.

Figure 6-45 shows the change of Sauter mean diameter D_{32} of a *spill-return atomizer* during a change of the return flow rate [26]. As seen from this measurement, as the return flow rate increases, i.e., ratio G_a/G_t decreases (Sec. 4-2.3), the ratio of the Sauter mean diameters for the open and closed return circuit D'_{32}/D''_{32} decreases. Therefore, during the return flow the atomization quality improves. Ratio G_a/G_t is the reciprocal of excess liquid coefficient e [Eq. (4-8)]. The case $G_a/G_t = 0$ means a completely open bleeder, and the case $G_a/G_t = 1$ a completely closed bleeder.

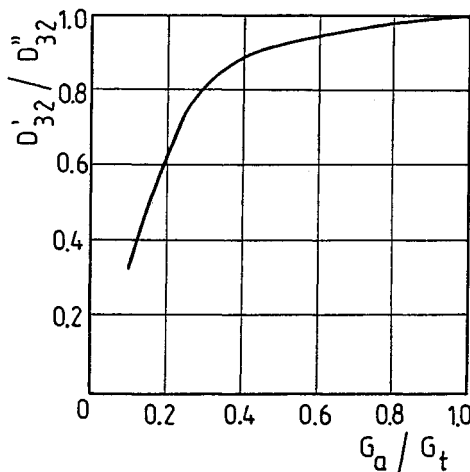


Figure 6-45 Change of Sauter mean diameter D_{32} for a spill-return atomizer as a function of the returned liquid flow rate.

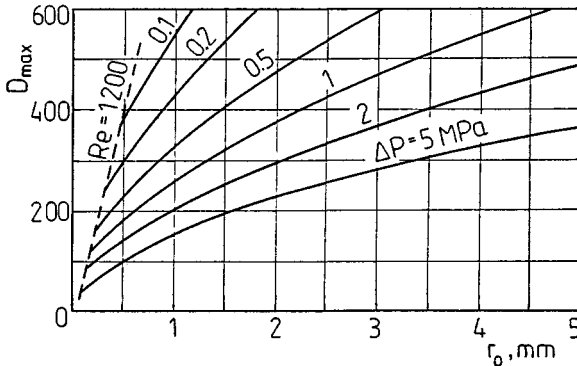


Figure 6-46 Dependence of maximum drop diameter D_{\max} on inlet orifice radius r_0 for various values of pressure drop ΔP .

Maximum drop diameter D_{\max} follows from the empirical equation [26]

$$D_{\max} = 3.72 \times 10^6 \frac{r_0^{0.56} E^{0.11}}{[(\Delta P \sqrt{1 - \epsilon}) / \sigma]^{0.33}} \quad (6-58)$$

where

$$E = \frac{10^6 \mu_L^2}{2 \sigma \rho_L}$$

$(r_0, \text{ m}; \mu_L, \text{ Pa} \cdot \text{s}; \rho, \text{ kg/m}^3; \sigma, \text{ N/m}; \Delta P, \text{ Pa})$. As seen, D_{\max} depends mainly on discharge orifice diameter r_0 and pressure drop ΔP .

Example 6-1 Use Eq. (6-58) to show graphically dependence of maximum diameter D_{\max} on radius r_0 and pressure drop ΔP during the atomization of diesel oil. Data: atomizer's geometric constant $K = 4$, $\epsilon \approx 0.36$ from Eq. (5-11), density $\rho_L = 850 \text{ kg/m}^3$, dynamic viscosity $\mu_L = 42.5 \times 10^{-4} \text{ Pa} \cdot \text{s}$, surface tension $\sigma = 30 \times 10^{-3} \text{ N/m}$.

SOLUTION After substituting Eq. (6-58), we obtain

$$D_{\max} = 1.13 \times 10^6 \frac{r_0^{0.56}}{\Delta P^{0.33}} [\mu\text{m}]$$

For r_0 expressed in mm and ΔP expressed in mPa, this equation assumes the form

$$D_{\max} = 250 \frac{r_0^{0.56}}{\Delta P^{0.33}} [\mu\text{m}]$$

This equation is represented graphically in Fig. 6-46. From Fig. 6-46 we can easily determine the required pressure drop ΔP for assumed allowable diameters D_{\max} . $Re = 1200$ is the limiting value of Eq. (6-58).

6-3 PNEUMATIC ATOMIZERS

As follows from the review of the designs of pneumatic atomizers (Sec. 4-4), the gas can act on the liquid in many different ways and therefore the results of investigations cannot be generalized.

6-3.1 Flow Rate of Atomized Liquid

Figure 6-47 shows the results of an investigation of a *pneumatic atomizer with parallel flow* [26]. This atomizer is used for firing up boilers and uses heating oil. The oil, warmed up to approximately 120°C, is fed gravitationally and atomization is caused by overheated steam with a temperature of about 250°C and a pressure of about 1.2 MPa. The curve in Fig. 6-47 represents steam flow rate G_G as a function of fuel flow rate G_L . It is seen that in the range $G_L = 1350\text{--}2790 \text{ kg/h}$, i.e., 67–139% of the nominal flow rate, the steam/liquid mass ratio falls in the small range $b = 0.40\text{--}0.45 \text{ kg/kg}$ and for small fuel flow rates $b = 0.8 \text{ kg/kg}$. These data supplement the data contained in Table 4-3.

An example of the characteristics of a pneumatic atomizer with cross-flow is shown in Fig. 6-48 [26]. In this case it is a Y-type atomizer (Fig. 4-50). The curves in Fig. 6-48 show fuel flow rate $Q_L = f(P_L)$ for two different atomizing air

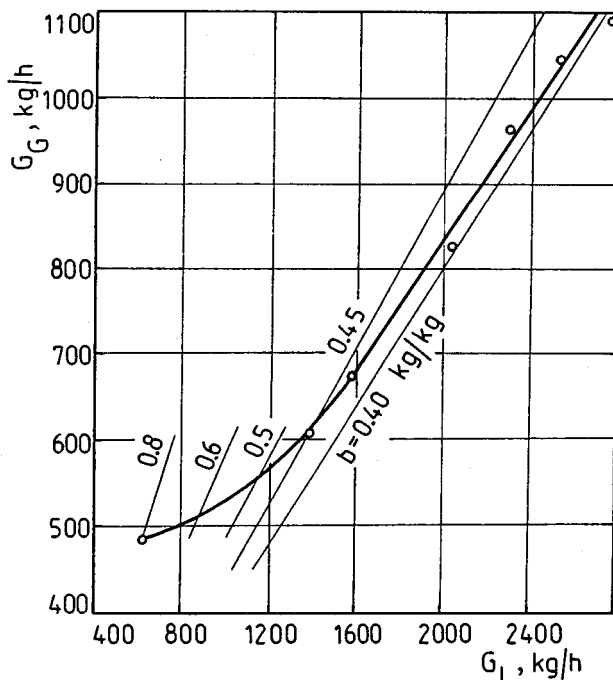


Figure 6-47 Dependence of steam flow rate G_G on fuel flow rate G_L in a boiler atomizer.

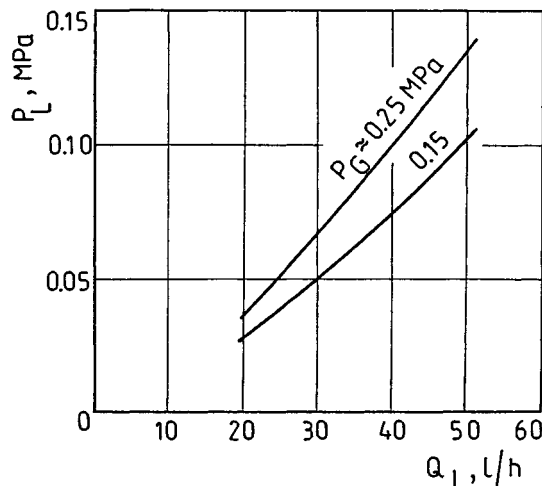


Figure 6-48 Flow characteristics of an Y-type pneumatic atomizer.

pressures P_G . As pressure P_G increases, i.e., as the air flow rate increases, fuel flow rate Q_L decreases for the same value of P_L . This stems from the throttling phenomenon, which is typical for the pneumatic atomizers.

The problem of gas pressure drop ΔP in pneumatic atomizers has not been extensively explored. Figure 6-49 shows schematically a pneumatic atomizer with cross-flow which was investigated in [26]. The design data of this atomizer are minimal diameter of Venturi nozzle $d = 30, 50, 70 \text{ mm}$; length $l_1 = 6-140 \text{ mm}$; length $l_2 = (2-7)d$; angle $\beta = 6^\circ, 8^\circ, 10^\circ$. The air at overpressure $0.00025-0.0125$

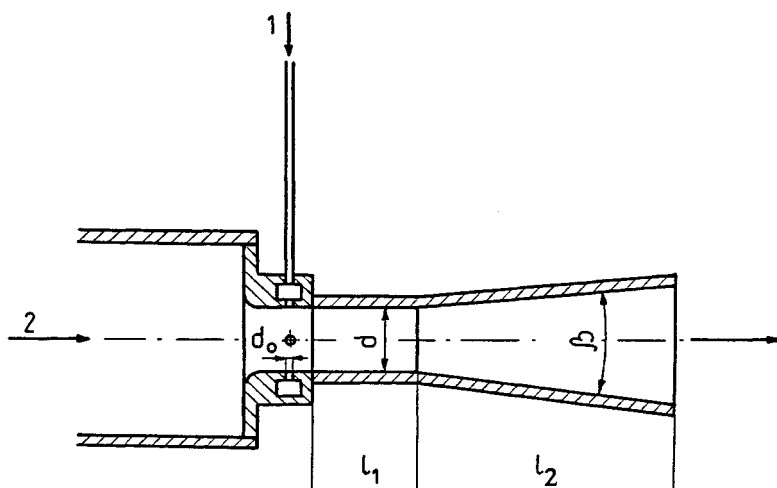


Figure 6-49 Schematic diagram of a pneumatic atomizer used for investigation of air pressure loss ΔP : 1, Water; 2, air.

MPa and temperature 20–35°C flowed through the minimal cross-section with velocity $V_G = 20\text{--}130$ m/s. Water with temperature 10–23°C was fed through $n = 1\text{--}8$ orifices with diameter $d_0 = 0.3\text{--}3.0$ mm with velocity $V_L = 1.5\text{--}17$ m/s. The air/liquid mass ratio varied in a very wide range $b = 0.77\text{--}55$ kg/kg.

The results of the research presented in a dimensionless form are as follows:

$$\text{Eu} = 0.77e^{0.5}\text{We}_G^{0.25}n^{-0.1}C_1^{1.5}C_2^{1.2n^{0.125}} \quad (6-59)$$

where Eu = Euler number

$$\text{Eu} = \frac{\Delta P}{\rho_G v_G^2}$$

e = ratio of dynamic pressures of water and air

$$e = \frac{\rho_L V_L^2}{\rho_G V_G^2}$$

We_G = Weber number

$$\text{We}_G = \frac{\rho_G V_G^2 d_0}{\sigma}$$

$$C_1 = d_0/d$$

$$C_2 = l_1/d_0$$

Terms in Eq. 6-59 varied in the following ranges: $e = 0.6\text{--}90$, $\text{We}_G = 15\text{--}260$, $C_1 = 0.01\text{--}0.1$, $C_2 = 2\text{--}100$. The error in Eq. (6-59) is +12%.

As seen, air pressure drop ΔP is a complex function of many variables. A comparison of the results of calculation by using Eq. (6-59) and simplified Eq. (5-168) shows that the pressure drop calculated in the simplified way constitutes about 63% of the real pressure drop from Eq. (6-59).

Figure 6-50 shows the results of an investigation of water throttling by atomizing steam in the atomizer shown in Fig. 4-56. The throttling was expressed by means of a degree of throttling [1]:

$$\lambda = \frac{G_L}{G'_L} < 1 \quad (6-60)$$

where G_L and G'_L are water flow rates during throttling and without throttling, respectively. λ is expressed as a function of power E_G of the atomizing steam for various velocities V_L and flow rates G_L of water. The ranges of velocities $V_L = 10.9\text{--}22.2$ m/s and flow rates $G_L = 0.33\text{--}6.82$ kg/s correspond to those used in practice in steam attemperators. It is seen that λ decreases as E_G increases and water velocity V_L decreases. Considerable effect is also caused by water flow rate G_L , and the higher velocity V_L is, the smaller is the influence of G_L . Because of the water throttling, the area of the water orifices should be increased to A'_L :

$$A'_L = \frac{A_L}{\lambda} \quad (6-61)$$

where A_L is the area at flow rate G_L .

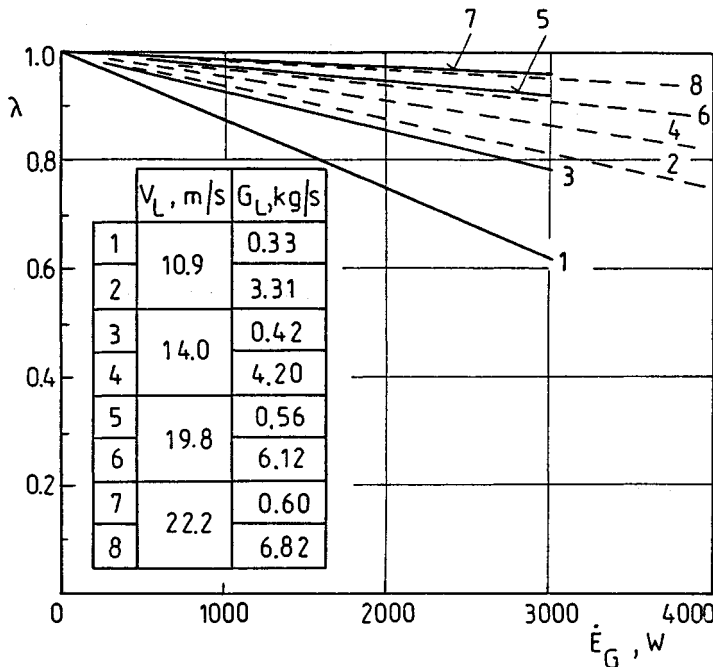


Figure 6-50 Experimental results of water throttling by atomizing steam in the atomizer shown in Fig. 4-65.

6-3.2 Macrostructure of the Atomized Liquid

The *spray shape* and *spray angle* α of pneumatic atomizers depend mainly on the type of interaction between gas and water. Atomizers with the parallel flow and cross-flow have small angles α , a result of the discharge of a free turbulent jet. Atomizers with the swirled flow can have angles α adjusted to needs. Small angle α can be significantly increased by the application of a deflector. In the case of a conical deflector, as shown in Fig. 4-47, a spray with angle $\alpha = 120^\circ$ or higher was obtained, but this spray was hollow.

Examples of spray formation in the case of *atomizers with the parallel flow* are shown in Fig. 6-51 [26]. The contours of the spray are the straight lines. Point A (Fig. 6-51a) lies at distance x from the gas nozzle:

$$x = \frac{3.25}{\lg(\rho_1/\rho_2)} d_2 \quad (6-62)$$

where ρ_1 and ρ_2 are the densities of the liquid and the gas. Points A' and A lie in the same plane perpendicular to the axis, which ensures better utilization of the gas energy. Angle ϑ is approximately $25^\circ 30'$, hence $d_1 \approx 1.2d_2$. Distance x is the conventional distance of liquid atomization. If liquid flows in the atomizer's

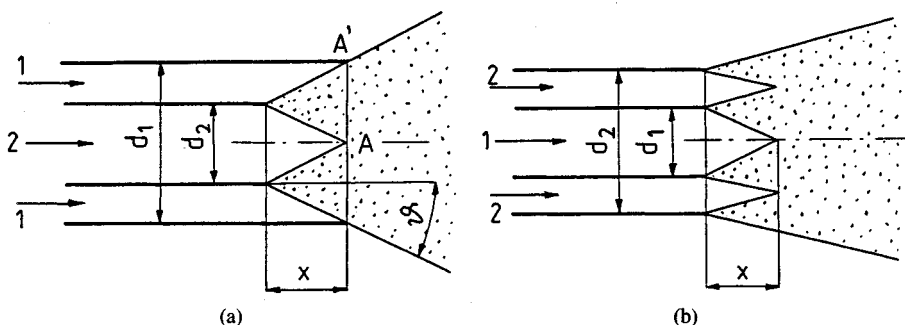


Figure 6-51 Schematic diagram of pneumatic atomizers with parallel flow: (a) gas flows in the atomizer's axis; (b) liquid flows in the atomizer's axis: 1, Liquid; 2, air.

axis (Fig. 6-51b), then distance x is

$$x = \frac{d_1}{0.61 \lg(\rho_1/\rho_2)} \quad (6-63)$$

The sprays in *atomizers with cross-flow* are formed in diverse ways. In [42] trajectory of jets of very viscous liquid, i.e., malt syrup with viscosity 1 Pa · s, is calculated. The liquid is fed in the transverse-countercurrent direction to an atomizer with the internal gas action (Fig. 4-52). Figure 6-52 shows schematically the results of calculations for various values of the air/liquid mass ratio b . These trajectories were confirmed experimentally. It is seen that the spray penetration decreases as b increases. For $b = 3.3$, liquid deflects totally and adheres to the wall of the liquid injection side.

Figure 6-53 shows the results of an investigation of spray angle α for a pneumatic atomizer with cross-flow and external air action [14]. The change of angle $\alpha/2$ is shown as a function of air/liquid momentum ratio. The continuous lines represent the results of calculations done under the assumption that the

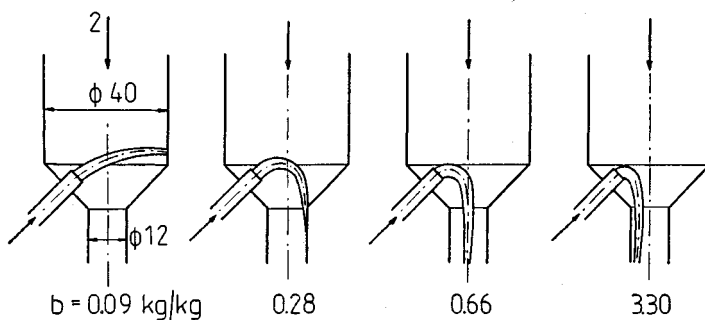


Figure 6-52 Change of the trajectory of a liquid jet during the increase of the air/liquid mass ratio. 1, Liquid; 2, air.

sum of the air and liquid momenta does not change after impingement. As seen, these lines agree well with the experimental results.

In [40] the effect of various parameters on the spray shape for a pneumatic atomizer with cross-flow and external gas action (Fig. 4-53) is investigated. The shape of the spray depends first of all on air/liquid mass ratio b . However, in the range of high values of b it also depends on some geometric parameters of an atomizer (Fig. 6-54). This atomizer has a nonuniform radial distribution of the liquid jet density $q = f(r)$ and a nonuniform distribution of drop diameters D_{32} . These distributions can be corrected by proper selection of the dimensions of a conical deflector.

Atomization angle α depends mainly on b ; for $b > 0.3 \text{ kg/kg}$ angle α is constant and close to zero; i.e., the spray shape is close to cylindrical. For $b < 0.3 \text{ kg/kg}$ angle α increases rapidly. The effect of geometric dimensions of the atomizer on angle α is as follows: For $x_c/b_N \geq 3$ angle α is constant and

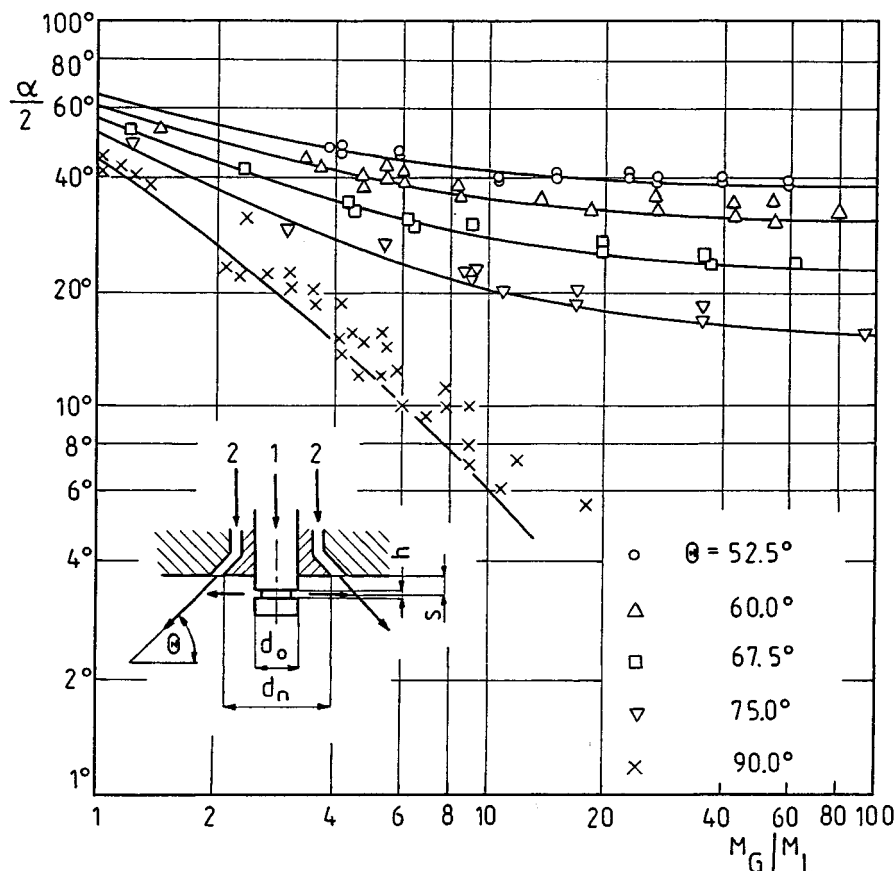


Figure 6-53 Dependence of spray angle α on the air/liquid momentum ratio. 1, Liquid; 2, air.

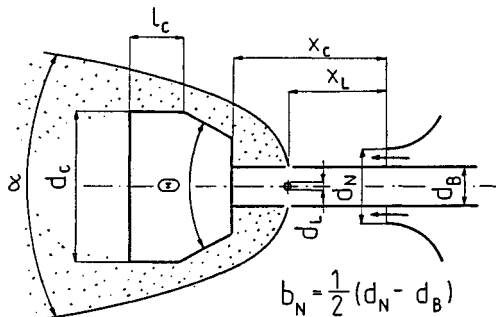


Figure 6-54 Geometric parameters of the atomizer shown in Fig. 4-53.

for $\Theta > 100^\circ$ angle α increases rapidly (the investigation was carried out for the range $\Theta = 30-180^\circ$). For $\Theta = 180^\circ$ the direction of the drop jet is reversed. Angle α does not depend on diameter d_0 .

During the study of an *atomizer with swirled flow* and internal gas action shown in Fig. 4-56 it was established that angle α depends on the direction of water and steam swirling, angle γ of the inclination of water orifices (Fig. 5-20), and the difference of kinetic energy ΔE of the atomizing steam and atomized water. For the same swirling directions for water and steam, angle α does not depend on ΔE but increases slightly as γ increases, and for $\gamma = 30^\circ$, $\alpha = 50^\circ$. For the opposite direction of swirling of steam and water an increase of ΔE causes an increase of γ . This increase is higher the smaller angle α is. Generally speaking, angles α of this atomizer are small due to the presence of walls of the attemperator housing.

The *radial liquid distribution* of pneumatic atomizers depends on their design. It was confirmed by numerous experiments that this distribution can be adjusted according to needs and one can even obtain a uniform distribution. An example is the atomizer shown in Fig. 4-56. It was established during the experiments that maximum density of the liquid jet q occurs in the axis of the atomizer. Such a state exists when water is fed through the axial orifices, but when the water flows through the inclined orifices an equalization of the water distribution takes place.

6-3.3 Microstructure of the Atomized Liquid

Liquid disintegration in pneumatic atomizers proceeds because of the gas action. We may therefore suspect that the atomization quality for a particular liquid would depend only on the relative velocity between gas and liquid V , which leads to the critical drop diameter expressed by Eq. (2-95). However, experimental results of evaluations of pneumatic atomizers do not confirm this equation.

The reason, among others, is that as the Weber number increases the wavelengths of the disturbance waves decrease. These wavelengths become very small compared to the jet diameter or the liquid film thickness. The liquid disintegration proceeds through ablation, i.e., by the separation of drops from

the liquid surface. The disintegration of the liquid in pneumatic atomizers is also caused by the forces of inertia, which are generated during the turbulent pulsations.

For *atomizers with parallel flow and internal gas action* an empirical equation established by S. Nukiyama and Y. Tanasawa is used:

$$D_{32} = \frac{0.585}{V} \sqrt{\frac{\sigma}{\rho_L}} + 53.2 \left(\frac{Q_L}{Q_G} \right)^{1.5} \left(\frac{\mu_L}{\sqrt{\sigma \rho_L}} \right)^{0.45} \quad (6-64)$$

All terms, including Sauter diameter D_{32} , are expressed in the SI system. Velocity V is the relative velocity between the gas and the liquid at the discharge from the atomizer. Equation (6-64) was established as a result of investigation of small atomizers with water nozzle diameter in the range 0.2–1.0 mm and an air nozzle diameter of 2–5 mm. It is seen that D_{32} decreases as velocity V increases and ratio Q_L/Q_G decreases. This equation does not take into account the dimensions of the atomizer or the density and viscosity of the gas. Figure 6-55 shows the dependence of mean diameter D_{32} on air velocity V_G for an atomizer with parallel flow and internal gas action [14]. In the case of the atomizer shown schematically in Fig. 6-55 the mechanism of drop generation is twofold.

The first mechanism is that drops separate from the crests of waves that develop on the surface of the liquid film, discharging from an annular slot with a width of 1 mm, and flow on the inner wall of the discharge nozzle of length 50 mm. The second mechanism relies on atomization of the liquid at the

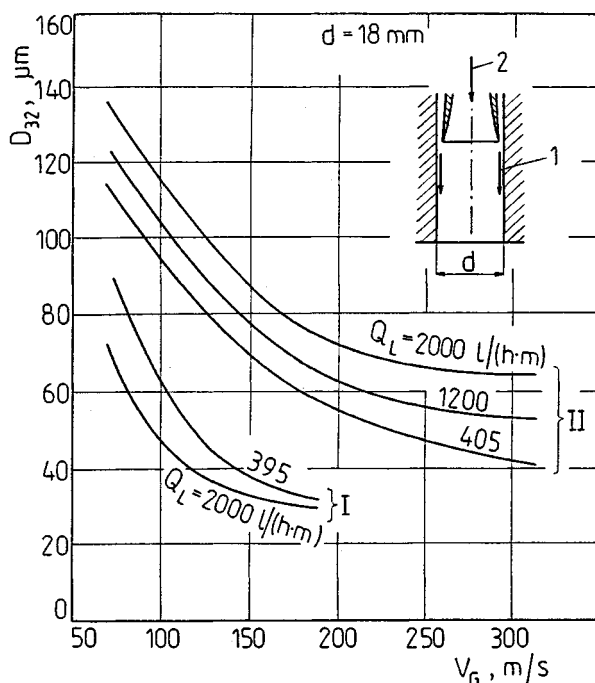


Figure 6-55 Dependence of Sauter mean diameter D_{32} on air velocity V_G : 1, Liquid; 2, air.

discharge from the atomizer. The ratio of the flow rate of the liquid atomized by the first mechanism to the total flow rate, E , depends on air velocity V_G . For $V_G > 150$ m/s, E increases rapidly, and for $V_G = 300$ m/s it reaches the value $E \approx 30\%$.

The drop diameters corresponding to the first atomization mechanism correspond to the group of curves I in Fig. 6-55, and diameters corresponding to the second atomization mechanism group II. Volumetric flow ratio of the liquid Q_L refers to a unit width of the liquid film.

The dependence of drop diameter D_{32} on air/liquid mass ratio b for different air velocities V_G has a similar character to that shown in Fig. 6-55.

In [44] a simplified equation for drop diameter D_{32} was derived as a result of the study of an atomizer shown in Fig. 4-46.

$$D_{32} = 81.0 - 91.0 \lg b [\mu\text{m}] \quad (6-65)$$

It was established that for atomizers with parallel flow and internal gas action the main parameter affecting the atomization quality is the air/liquid mass ratio b .

It was found on numerous occasions [32] that for atomizers with the internal gas action a certain disadvantageous phenomenon occurs. For certain values of b in the mixing chamber, pressure fluctuations occur that cause fluctuating discharge of the mixture of liquid and gas.

In order to design the atomizer with parallel flow and external gas action shown in Fig. 4-47, extensive research was carried out regarding the disintegration of the liquid film in a wind tunnel and in an air nozzle [24]. Waves develop on the liquid film surface for air velocities higher than 20 m/s. Even for high air velocity only several percent of the liquid undergoes atomization because of the wave effects inside the nozzle. Investigation of film atomization on the edge of the nozzle showed that wave effects also occur, causing thin films to disintegrate directly into drops and thick films to disintegrate with difficulty, while liquid ligaments develop initially.

Drop diameter D_{32} decreases exponentially with air velocity, and above velocity 150 m/s it practically does not change. The mean diameter of drops that develop inside the nozzle is smaller than the mean diameter of all the drops.

In Sec. 5-4 calculations were presented based on two models of an atomizer with parallel flow and external operation (Fig. 5-18). As a result of an investigation of the atomization of a mixture of glycerine and water and the atomization of heated paraffin, Fig. 6-56 was obtained. The measurement points can be approximated by one line. D_m is the median diameter. For an atomizer with a filled liquid jet (Fig. 5-18a) and with an annular liquid jet (Fig. 5-18b) the same values of $B = 18.0$ and $n = 0.27$ were obtained in Eq. (5-167). The measurements were done for the following range of parameters:

Cross-sectional area of liquid jets 0.2–36 mm²

Cross-sectional area of gas jets 2.9–44 mm².

Liquid flow rate 25–586 kg/h

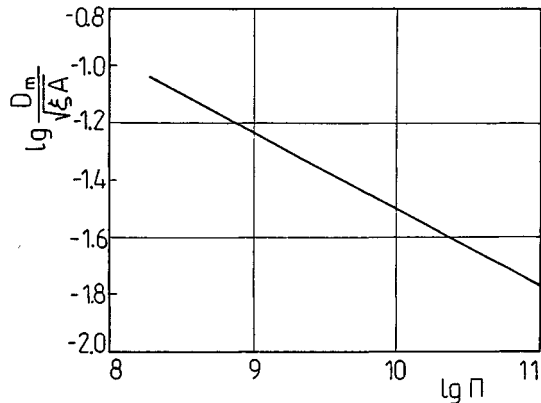


Figure 6-56 Dependence of $\lg(D_m/\sqrt{\zeta} A)$ on $\lg \Pi$ for atomizers shown schematically in Fig. 5-18.

Air/liquid mass ratio 0.05–3.14 kg/kg

Gas velocity 43–310 m/s

Liquid density 745–1120 kg/m³

Liquid viscosity $(3.7\text{--}6.5) \times 10^{-6}$ m²/s

In [3] mean drop diameters for the atomizer shown in Fig. 6-57 were measured. This is an atomizer with parallel flow and external gas operation. The water flows under constant hydrostatic pressure with velocity 1–2 m/s with flow rate $G_L = (1158\text{--}2314) \times 10^{-3}$ kg/s. The air flows under pressure $P_1 = 0.1068\text{--}0.1319$ MPa with velocity $V_G = 100\text{--}140$ m/s. The following equation was derived:

$$D_{32} = 1.06 \times 10^5 V_G^{-3.0} \left(\frac{P_2}{P_1} \right)^{-4.1} G_L^{0.83} \quad (6-66)$$

where D_{32} = Sauter mean diameter, m

V_G = air velocity, m/s; this velocity follows from Eq. (5-151)

P_1, P_2 = air pressure in front of the atomizer and ambient pressure, Pa

G_L = water flow rate, kg/s

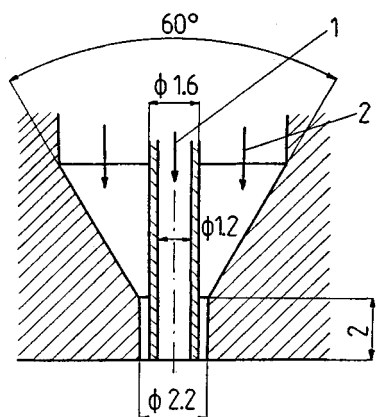


Figure 6-57 Nozzle of a pneumatic atomizer used for dust granulation.

The measured Sauter mean diameters fell in the range $D_{32} = 197\text{--}445 \mu\text{m}$, and the drop size was $3.7\text{--}1036 \mu\text{m}$.

Atomizers with cross-flow have often been subjects of investigation. In [28] an investigation of a Y-type atomizer (Figures 4-50 and 4-51), i.e., an atomizer with internal gas operation was carried out. The aim of investigation was to establish a relationship between median diameter D_m and geometric parameters of the atomizer (Fig. 6-58). The measurements were carried out for water and light diesel oil and for air.

The radial distribution of drop diameters in a discharging jet is not symmetric. This stems from the fact that liquid 1 flows to the mixer (discharge nozzle) from one side, so drops on this side are larger than on the opposite side. The axial distribution of drop diameters is nonuniform because drop diameters increase with distance from the atomizer, but in this particular investigation this increase at distances larger than $l_1 + l_2 = 26 \text{ cm}$ was insignificant (Fig. 4-51).

Median diameter D_m decreases with an increase of air/liquid mass ratio b . During the measurements the flow rate of the liquid was constant, and value b was increased by increasing the air pressure from 0.25 to 0.85 MPa. The mean drop diameter was calculated from Wigg's empirical correlation

$$D_m = 200 \nu_L^{0.5} G_L^{0.1} \left(1 + \frac{1}{b}\right)^{0.5} r_0^{0.1} \sigma^{0.2} \rho_G^{-0.3} V^{-1.0} \quad (6-67)$$

where D_m = median diameter, μm

ν_L = kinematic viscosity of the liquid, $\times 10^6 \text{ m}^2/\text{s}$

G_L = liquid flow rate, $\times 10^3 \text{ kg/s}$

$b = G_G/G_L$ is the gas/liquid mass ratio

$r_0 = d_0/2$ is the radius of the discharge orifice, cm

σ = surface tension, $\times \text{mN/m}$

ρ_G = air density, $\times 10^{-3} \text{ kg/m}^3$

V = relative velocity of the air and the liquid, m/s

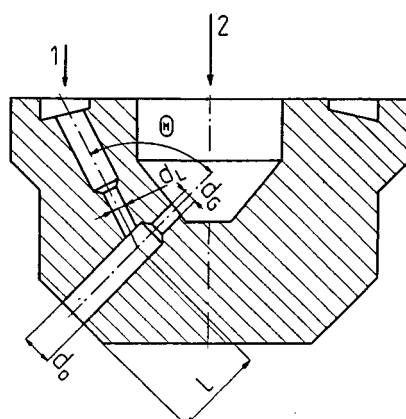


Figure 6-58 One discharge orifice of a Y-type atomizer. 1, Liquid; 2, gas.

D_m has a minimum value at

$$\frac{d_0}{\sqrt{d_L^2 + d_G^2}} \approx 1$$

and at $d_L \approx d_G$. D_m decreases with increasing angle of jet impingement Θ and subsequently increases, and minimum D_m corresponds to angle $\Theta = 75^\circ$. The ratio of length l of the discharge orifice to its diameter d_0 does not have a distinct effect on diameter D_m . Length l , however, should ensure exchange of momentum between the gas and the liquid and therefore it should not be smaller than $l = 2d_0$.

Figure 6-59 shows the relationship between mean diameter D_{32} and gas/liquid mass ratio b for the atomizer shown in Fig. 4-52. For $b > 3.3$, liquid adheres to the wall of the orifice (Fig. 6-52) and therefore cannot be effectively atomized [42].

The results of extensive experiments on the impingement at various angles between a flat gas jet and a flat liquid jet are reported in [46]. This is especially important in the case of cross-flow atomizers with external gas operation. Experiments carried out for various gas and liquid velocities made it possible to determine the length of the film before it disintegrated into drops. Results of the investigation of the atomization quality during the transverse feeding of liquid into the air jet, are shown schematically in Fig. 5-19 [49]. As a result of a study of atomization of water and heated paraffin, a simple formula for the median diameter was obtained:

$$D_m = 0.91d_0We^{-0.5} \quad (6-68)$$

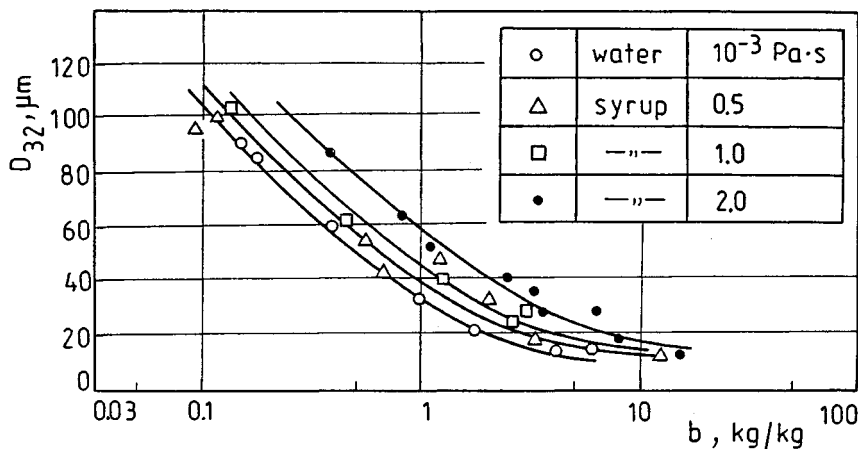


Figure 6-59 Dependence of Sauter mean diameter D_{32} on gas/liquid mass ratio b for the atomizer shown in Fig. 4-52.

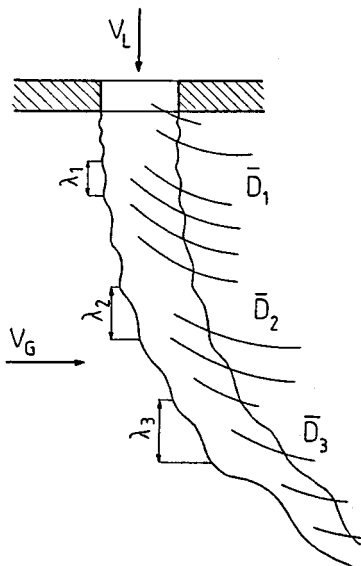


Figure 6-60 Schematic diagram of liquid jet disintegration in transverse air flow; $\lambda_1 < \lambda_2 < \lambda_3$ = wavelength; $\bar{D}_1 < \bar{D}_2 < \bar{D}_3$ = mean drop diameter.

where the Weber number equals

$$We = \frac{\rho_G V_G^2 d_0}{\sigma}$$

and V_G is air velocity.

Figure 6-60 shows schematically the disintegration of a liquid jet fed perpendicularly to an air jet with atmospheric pressure [15]. In the case of short-wavelength disturbances relatively small drops develop, and as the wavelength increases drop diameter also increases. For the range $We Re < 10^6$ the formula obtained was

$$D_{32} = 3.9d_0(We Re)^{-0.25} \quad (6-69)$$

and for $We Re > 10^6$

$$D_{32} = 37d_0(We Re)^{-0.4} \quad (6-70)$$

where

$$We = \frac{\rho_G V^2 d_0}{\sigma}$$

$$Re = \frac{Vd_0}{\nu_L}$$

where V is relative air/liquid velocity.

The dependence D_{32} on air/liquid mass ratio b for various air velocities V_G is shown in Fig. 6-61 [14]. It refers to a cross-flow atomizer with external gas operation, shown schematically in Fig. 6-53. When the value b drops a gradual

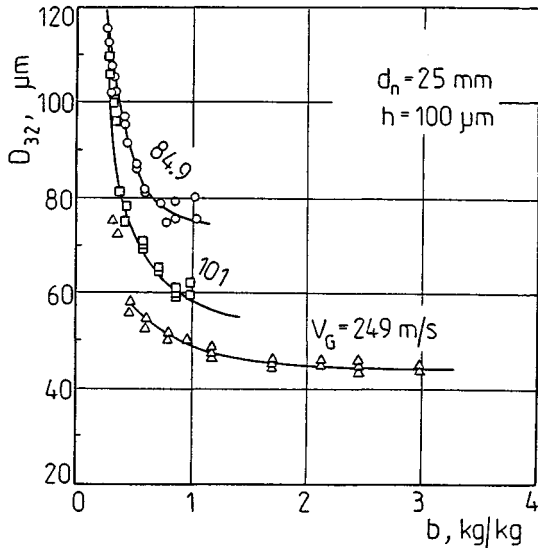


Figure 6-61 Dependence of Sauter mean diameter D_{32} on air/liquid mass ratio b for various air velocities V_G .

increase of D_{32} occurs, but for $b < 0.5 \text{ kg/kg}$ the increase of D_{32} is rapid. For $b > 1.0 \text{ kg/kg}$ diameter D_{32} changes insignificantly since the liquid film thickness for constant slit width h is independent of the flow rate.

The empirical equation has the following dimensionless form:

$$D_{32} = \frac{d_0 h}{d_n} \left(1 + \frac{16,850 \text{St}^{0.25}}{\text{We}(\rho_L/\rho_G)} \right) \left(1 + \frac{0.065}{b^2} \right) \quad (6-71)$$

where the *stability number* is

$$\text{St} = \frac{\mu_L^2}{\rho_L \sigma (d_0 h / d_n)} \quad (6-72)$$

and the Weber number in this case is

$$\text{We} = \frac{\rho_G (V_G - V_L \cos \Theta)^2}{\sigma} \frac{d_0 h}{d_n}$$

The first term on the right-hand side in Eq. (6-71) represents the liquid film thickness at the place where it impinges with the air jet. This equation is valid in the range $h < 220 \mu\text{m}$. The mean scatter of the theoretical and measured results was 7.6%.

A similar relationship to the one shown in Fig. 6-61 was found for D_{32} by changing air velocity V_G . D_{32} changes slightly in the range $V_G > 100 \text{ m/s}$ but increases rapidly for $V_G < 100 \text{ m/s}$.

In [40] an atomizer (Fig. 4-53) with cross-flow and external gas operation was investigated. The results show that mean diameter D_{32} depends only on the air/liquid mass ratio b if the following conditions are satisfied: pressure of

compressed air $P_G \geq 0.3$ MPa, number of water orifices $i_L \geq 3$, $x_C/b_n \geq 3.3$ (Fig. 6-54). The detailed results of this study are as follows (Fig. 6-54):

D_{32} decreases as pressure P_G increases, but for $P_G \geq 0.3$ MPa it practically does not change. For pressure $P_G \approx 0.19$ MPa the air at the discharge reaches the velocity of sound.

D_{32} does not depend on the width b_N of the annular nozzle.

Diameter D_{32} does not depend on the number of water orifices i_L , their diameter d_L , and water velocity V_L ; however, the condition $i_L \geq 3$ should be satisfied.

The effect of x_L on D_{32} is insignificant in the case of large values of b .

A conical deflector causes the atomization quality to deteriorate but its presence ensures the proper shape of the spray.

Distance x_L should be slightly smaller than distance x_c ; distance x_c is changed in the range from 2 to 14 mm.

The liquid atomization occurs directly after the liquid discharges from orifices.

The cross-flow atomizer with the external gas operation shown in Fig. 4-59 was investigated in [43]. It was established that the angle between the liquid axial gas jets does not affect Sauter mean diameter D_{32} because the air velocity is much higher than the liquid velocity. However, D_{32} depends significantly on air velocity V_G and the gas/liquid mass ratio b . Figure 6-62 shows the relationship $D_{32} = f(V_G)$ for the following conditions: liquid orifice diameter $d_L = 0.87$ mm, liquid velocity $V_L = 1.0$ m/s, orifice diameter or air slit width $d_G = 0.47$ mm, distance from air orifices to the point of impingement practically equal to zero ($l \approx 0$). It is seen that for $V_G < 130$ m/s, D_{32} grows rapidly. The effect of the gas/liquid mass ratio on D_{32} is distinct. As mentioned in Sec. 4-4.2 for a modified version of this atomizer $D_{32} < 100 \mu\text{m}$ was obtained for $b = 1.0 \text{ kg/kg}$ in the case of a liquid with viscosity $0.25 \text{ Pa} \cdot \text{s}$.

Distance l and diameter of liquid orifices d_L have an essential effect on D_{32} (Fig. 6-63). Figure 6-63 corresponds to the following conditions: air velocity

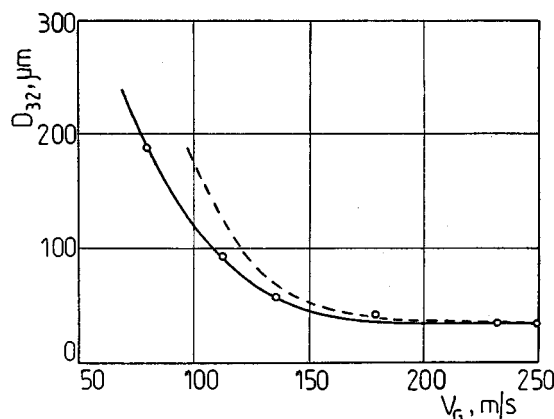


Figure 6-62 Dependence of Sauter mean diameter D_{32} on air velocity V_G ; dashed line refers to Eq. (6-64).

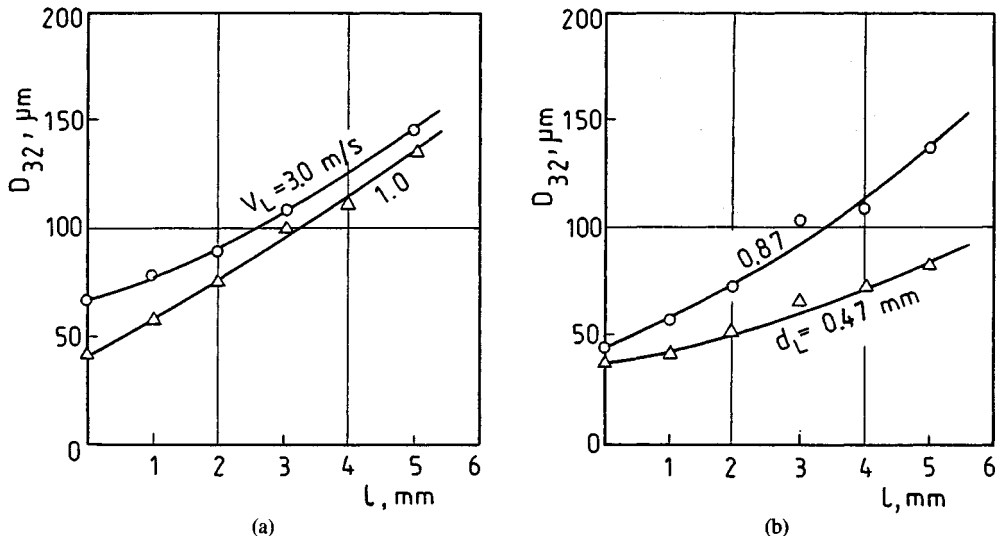


Figure 6-63 Dependence of Sauter mean diameter D_{32} on distance l : (a) for various liquid velocities V_L and $d_L = 0.87 \text{ mm}$; (b) for various orifice diameters d_L and $V_L = 1.0 \text{ m/s}$.

$V_G = 153 \text{ m/s}$, air orifice diameter $d_G = 0.2 \text{ mm}$. As seen, D_{32} increases as distance l increases, since the increase of l is accompanied by a decrease of the kinetic energy of the air jets.

In [16] the atomization quality at the discharge of an open wind tunnel was investigated. The liquid was fed in the following forms: (1) as a flat film generated by the impingement of two liquid jets, (2) as a radial jet generated by the impingement of liquid with the perpendicular deflector, (3) as a conical spray generated by liquid swirling. These methods of feeding liquid into an air jet are used in the combustion chambers of gas turbines and rocket engines. As the result of measurements, a series of simple correlations for mean drop diameter was established.

In [37] the atomizer shown in Fig. 4-57 was investigated. It is a cross-swirled flow atomizer with the external air operation. The investigations concerned the relationship between D_{32} and the air/liquid mass ratio b , air velocity V_G , angles α and β , and water orifice diameters d_0 . It was established that diameter D_{32} decreases as b increases according to the relationship

$$D_{32} \sim \left(1 + \frac{1}{b}\right)^{0.9}$$

For $b > 2-3 \text{ kg/kg}$ D_{32} practically does not change. D_{32} decreases with increasing air velocity V_G according to the relation

$$D_{32} \sim \frac{1}{V_G^{1.09}}$$

in the velocity range $V_G = 35-80 \text{ m/s}$.

Figure 6-64 shows the effect of radial and axial inclination of water orifices, i.e., the effect of angles α and β , on Sauter mean diameter D_{32} . As follows from Fig. 6-64a, the best atomization occurs for perpendicular water feeding to the air jets ($\alpha = 0$). From Fig. 6-64b it follows that as angle β increases D_{32} decreases, but this corresponds to small air velocities V_G . Angle β was changed in the range $\beta = 0\text{--}60^\circ$. The effect of cocurrent or countercurrent feeding of water jets with respect to the air swirling direction was not explained.

D_{32} increases as orifice diameter d_0 increases according to the relationship $D_{32} \sim d_0^x$, where coefficient x varied from 0.692 to 0.230 during change of velocity V_G from 57 to 80 m/s. This relationship refers to $\alpha = \beta = 0$ and $d_0 = 0.5\text{--}1.8$ mm. The mean value of x is 0.43.

Information regarding the mean drop diameters of swirled flow atomizers is limited. In [21] aerodynamic structure of the region located several centimeters from the discharge of a pneumatic atomizer with swirled flow was measured with high accuracy. Drop diameters and the axial velocity of drops and air were measured. It was found that the initial drop acceleration and spray dispersion cause an initial decrease of axial mean drop diameters, and subsequent drop deceleration causes an increase of mean drop diameters.

In [2] the operation of air jets inside the atomizer shown in Fig. 4-58 was analyzed. Special attention was paid to the influence of air swirling on the drop size spectrum. It was found that countercurrent swirling of air jets gives better

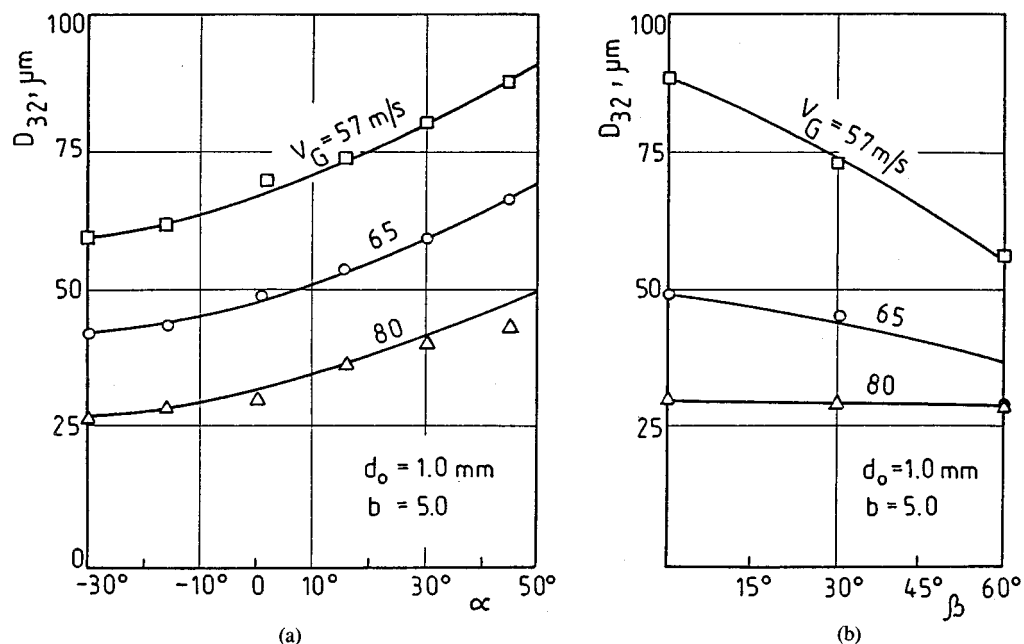


Figure 6-64 Dependence of Sauter mean diameter D_{32} on angles α and β .

results than cocurrent swirling. Various vane types in the inner and outer air channel were considered. In all cases swirling significantly reduced the air/liquid mass ratio b .

On the basis of investigations of the atomizer shown in Fig. 4-59 a relation that allows the calculation of median diameter D_m was established [48]:

$$D_m = 15.3 \times 10^3 d \text{We}^{-1.5} \left(1 + \frac{1}{b}\right)^{0.5} N^{-0.065} \quad (6-73)$$

where $\text{We} = \rho_G V_G^2 d / \sigma$ is the Weber number

d = outer diameter of the mixing chamber, i.e., inner diameter of the annular slit (Fig. 4-59)

V_G = velocity of air discharging from the swirler

$b = G_G/G_L$ is the air/liquid mass ratio

$N = \mu_G/\mu_L$

Equation (6-73) was derived for the following conditions: air velocity $V_G = 40\text{--}90$ m/s, liquid flow rate $G_L = 100\text{--}500$ kg/h, liquid viscosity $\nu_L < 12 \times 10^{-6}$ m²/s. D_m can be calculated with accuracy $\pm 25\%$. In the range of air velocity $V_G = 70\text{--}80$ m/s it was found that $D_m = 120\text{--}150$ μm , while in pneumatic atomizers without swirling $D_m = 100\text{--}200$ μm for the critical air velocity, i.e., for a pressure drop of approximately 0.1 MPa. The atomizer investigated is used in a gas turbine with overpressure of order 1.5–4 kPa.

In [33] the problem of mean drop diameters of various *mixtures of liquid and dust*, i.e., coal-oil mixtures, coal-water suspensions, etc., was studied. Investigations were carried out for pneumatic atomizers with internal gas operation. Based on the “equal distribution model,” a very simple relation was established:

$$\bar{D} = \alpha^{-1/3} \bar{D}_L \quad (6-74)$$

where \bar{D} = mean drop diameter of the mixture

\bar{D}_L = corresponding mean diameter of the liquid producing the mixture

α = liquid volume fraction

Good agreement was found between the theoretical and experimental results.

6-4 ROTARY ATOMIZERS

The experimental results regarding rotary atomizers will be presented according to the classification of these atomizers (Sec. 4-5). Most experimental data concern the microstructure of atomized liquid in cup atomizers.

6-4.1 Flow Rate of the Atomized Fluid

Atomization quality depends mostly on the liquid film thickness, i.e., on the liquid flow rate. Figure 6-65 shows the regions in which various mechanisms of drop development operate [5]. These are the mechanisms discussed in Sec. 5-5,

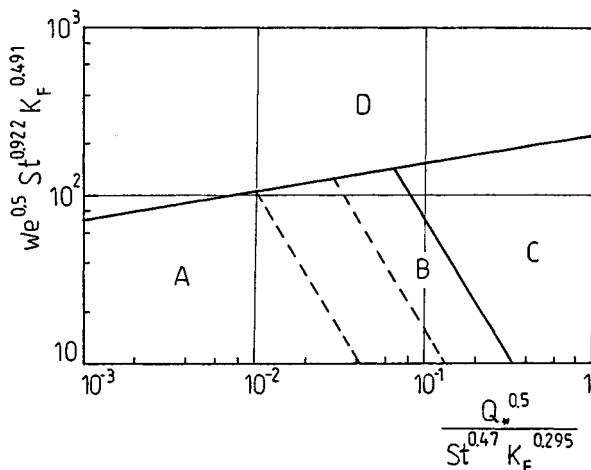


Figure 6-65 Map of drop development regions for disk atomizers: A, Drop formation mode; B, ligament formation mode; C, sheet formation mode; D, atomization.

namely the drop formation mode, ligament formation mode, sheet formation mode, and atomization mode. This last mode is based on direct film disintegration on the disk edge, which generally occurs for circumferential velocities of the disk higher than 50 m/s. This disintegration is caused by the dynamic action of the ambient gas, by a different mechanism than in the case of the drop, ligament, and sheet formation modes.

Figure 6-65 concerns disk atomizers, but to a certain extent it also concerns bowl or cup atomizers. The coordinates in Fig. 6-65 are combinations of the following dimensionless parameters

$$We = \frac{\rho_L \omega^2 R^3}{\sigma}$$

$$St = \frac{\mu_L^2}{2 \rho_L \sigma R}$$

$$Q_* = \frac{Q^2 \rho_L}{\sigma (2R)^3}$$

$$K_F = \frac{\rho_L \sigma^3}{g \mu_L^4}$$

where R = disk radius

$$\omega = 2\pi N/60$$

$$Q = \text{liquid volumetric flow rate}$$

It follows from Fig. 6-65 that the border between the drop and ligament formation modes is not unique.

For practical purposes we can use the following approximate relation:

$$N_{\text{lim}} = 36.6 g^{0.54} \frac{Q^{0.17} \rho_L^{0.2} \nu_L^{0.17}}{(2R)^{0.75} \sigma^{0.2}} \quad (6-75)$$

where N_{lim} is the limiting rotational speed above which the liquid is atomized directly on the disk edge. For a given liquid flow rate, the following combinations can be used: small disk radius and high rotational speed or large disk radius and small rotational speed.

The range of control, i.e., the ratio of the maximum and minimum liquid flow rates, can be easily adjusted to needs. The only limitation follows from the change of atomization quality, and therefore much attention is devoted to information regarding drop diameters. It must be remembered that many rotary atomizers operate as pneumatic-rotary atomizers in which atomization proceeds mainly due to the action of gas jets.

One example is the burner cup atomizer shown in Fig. 4-66. The range of flow rate is usually 27–1360 kg/h and most commonly 45–680 kg/h. Other data are rotational speed 3000–10000 rpm (usually 5000 rpm), cup diameter 25–100 mm, circumferential velocity on the cup edge 9–30 m/s, air overpressure 0.75–7.5 kPa, air velocity 30–11 m/s, fuel viscosity $(7.5-50) \times 10^{-6}$ m²/s. The flow rate of the air used for atomization is usually 7–20% of the total flow rate of air fed to combustion.

6-4.2 Macrostructure of Atomized Liquid

Spray angle. The actual spray angle α of cup atomizers (Fig. 6-66) depends on the liquid film deflection caused by the air jet. This deflection is a function of many variables and therefore is very difficult to describe analytically. For particular conditions, e.g., fuel viscosity $\nu_L = 45 \times 10^{-6}$ m²/s and distance from

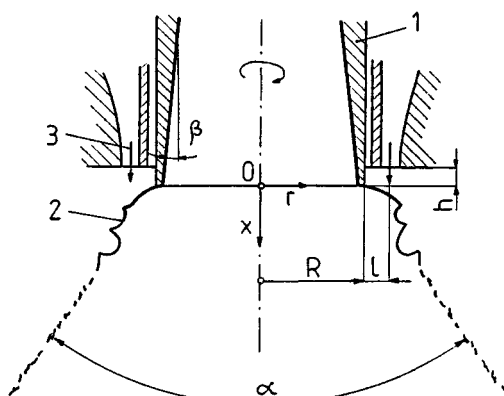


Figure 6-66 Deflection of liquid film and formation of spray angle α . 1, Cup atomizer; 2, liquid film; 3, annular gas jet.

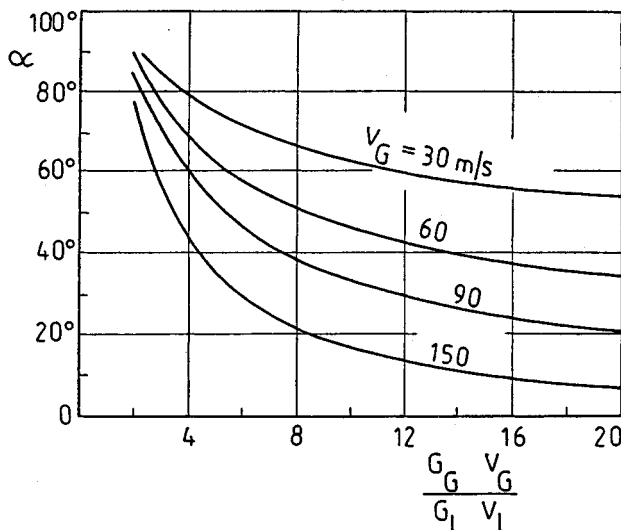


Figure 6-67 Dependence of spray angle α of cup atomizer on the ratio of momenta of gas and liquid for various gas velocities V_G .

atomizer $x = 38$ mm, an empirical equation was derived [26]:

$$\operatorname{tg} \frac{\alpha}{2} = 0.508 V_G^{0.2} b^{0.34} \left(\frac{G_G V_G}{G_L V_L} \right)^{-0.0244 V_G^{0.75}} \quad (6-76)$$

where V_L, V_G = velocity of liquid and air, m/s

b = air/liquid mass ratio, kg/kg

G_L, G_G = mass flow rates of liquid and air

The error of Eq. (6-76) is $\pm 13\%$.

Equation (6-76) is illustrated in Fig. 6-67 for $b = 2$ kg/kg and various air velocities V_G . It is seen that angle α depends on velocity V_G , but for small velocities the curves become flatter. Equation (6-76) does not take into account the liquid viscosity effect on angle α . This effect is significant and can be described as follows. For small liquid viscosities the film disintegrates very close to the point where it impinges with air. For high viscosities the film deflects and simultaneously elongates and becomes thinner before it disintegrates, which causes the decrease of angle α . Therefore an increase of gas velocity and an increase of liquid viscosity cause the decrease of angle α .

Spray penetration. The spray penetration of rotary atomizers is not an unequivocal term since these atomizers operate basically in moving ambient gas. This takes place during air humidification, spray drying, fuel combustion, etc. In most cases drops evaporate, dry out, or burn out, so it is important to know the spray penetration. For example, water drops with mean diameter 50 μm atomized in a

climatic chamber have penetration 14 m before they evaporate if the air velocity in a climatic chamber is 2 m/s. These data correspond to an initial air temperature of 24°C and relative humidity 20%.

The air flowing along the cup atomizer (Fig. 4-66) deflects and breaks the fuel film leaving the cup edge, as shown in Fig. 6-66. If the action of the air jet is not efficient, the spray shape changes because a large number of large drops appears. A certain *limiting state* occurs which separates the proper spray shape from the improper one.

For a particular gas jet this limiting state depends on the fuel flow rate. The limiting fuel flow rate Q_L^* was determined experimentally [7]:

$$Q_L^* = 3.3 \times 10^{-8} V_G^{2.91} d^{0.79} N^{0.52} \quad (6-77)$$

where Q_L^* = fuel flow rate, l/h

V_G = air velocity in the discharge slit, m/s

d = diameter of the cup rim, mm

N = rotational speed, rpm

Equation (6-77) corresponds to the following conditions: $V_G = 100\text{--}200$ m/s, $d = 57\text{--}115$ mm, $N = 1260\text{--}4910$ rpm, heating oil viscosity 19.5×10^{-6} m²/s.

Liquid distribution in the drop jet. In [5] the results of measurements of liquid distribution discharging from a disk atomizer were presented. On the basis of measurements, curves of the total radial liquid distribution were prepared as shown in Fig. 3-19. From these curves radius r_{99} , which is the radius of a spray encompassing 99% of the liquid, was derived. Results were presented in the form of dimensionless expressions r_{99}/\bar{D} as a function of Re , Fr and M . Mean drop diameter \bar{D} should be found experimentally or derived from proper empirical relationships.

The equations obtained have different forms depending on the absolute liquid velocity V on the disk edge.

For $V = 37\text{--}60$ m/s:

$$\frac{r_{99}}{\bar{D}} = 0.25 \times 10^5 Re^{-0.53} Fr^{-0.033} M^{-0.5} \quad (6-78)$$

For $V = 60\text{--}68$ m/s:

$$\frac{r_{99}}{\bar{D}} = 25 Re^{-0.53} Fr^{0.45} M^{-0.5} \quad (6-79)$$

For $V = 68\text{--}105$ m/s:

$$\frac{r_{99}}{\bar{D}} = 0.37 Re^{-0.51} Fr^{0.7} M^{-0.5} \quad (6-80)$$

where Reynolds number

$$Re = \frac{V\bar{D}}{\nu_L}$$

Froude number

$$\text{Fr} = \frac{V^2}{gD}$$

ratio of densities of the ambient gas and the liquid

$$M = \frac{\rho_G}{\rho_L}$$

6-4.3 Microstructure of the Atomized Liquid

As a result of the dimensional analysis and experiments in [41], the following equations were obtained for maximum and mean diameters of drops that develop in three modes of drop formation (Sec. 4-5.1, Fig. 4-62).

For the drop formation mode:

$$D_{\max} = \frac{43.2}{Nd^{0.5}} \left(\frac{\sigma}{\rho_L} \right)^{0.5} \left(1 + 0.003 \frac{Q}{\nu_L d} \right) \quad (6-81)$$

For the ligament formation mode:

$$D_{32} \approx \frac{D_{\max}}{1.6} \quad (6-82)$$

$$D_{\max} = 32 \frac{Q^{0.1}}{Nd^{0.5}} \cdot \frac{\sigma^{0.5}}{\rho_L^{0.4} \mu_L^{0.1}} \quad (6-83)$$

$$D_{32} \approx \frac{D_{\max}}{1.7} \quad (6-84)$$

For the sheet formation mode:

$$D_{\max} = 105 \frac{Q^{0.5}}{Nd^{0.8}} \left(\frac{\sigma}{\rho_L} \right)^{0.4} \quad (6-85)$$

$$D_{32} \approx \frac{D_{\max}}{1.7} \quad (6-86)$$

where D_{\max} , D_{32} = maximum and Sauter diameter, respectively, cm

N = rotational speed, rpm

d = disk diameter, $\times 10^2$ m

σ = surface tension, $\times 10^3$ N/m

ρ_L = liquid density, $\times 10^{-3}$ kg/m³

μ_L = liquid viscosity, $\times 10$ Pa · s

Q = liquid flow rate, $\times 10^6$ m³/s

For disk atomizers used in spray drying the following relationships were found between the mean drop diameter and basic parameters.

Relationship between mean drop diameter D and rotational speed N :

$$\frac{D_1}{D_2} = \left(\frac{N_2}{N_1} \right)^p \quad (6-87)$$

Coefficient p is in the range $p = 0.77\text{--}0.82$. For normal conditions of industrial spray drying, i.e., for circumferential velocity on the disk edge $v = 85\text{--}115 \text{ m/s}$ and liquid flow rate $G' < 1200 \text{ kg/(h*m)}$, one assumes $p = 0.82$. Flow rate G' is related to the unit of disk circumference.

Relationship between mean drop diameter D and liquid flow rate G :

$$\frac{D_1}{D_2} = \left(\frac{G_1}{G_2} \right)^q \quad (6-88)$$

Coefficient q is in the range $q = 0.12\text{--}0.2$, while for normal industrial conditions one assumes $q = 0.2$.

Relationship between mean drop diameter D and liquid viscosity μ :

$$\frac{D_1}{D_2} = \left(\frac{\mu_1}{\mu_2} \right)^r \quad (6-89)$$

Coefficient r is approximately $r = 0.2$.

Relationship between mean drop diameter D and liquid density ρ :

$$\frac{D_1}{D_2} = \left(\frac{\rho_2}{\rho_1} \right)^s \quad (6-90)$$

Coefficient s is approximately $s = 0.5$.

Relationship between mean drop diameter D and surface tension:

$$\frac{D_1}{D_2} = \left(\frac{\sigma_1}{\sigma_2} \right)^t \quad (6-91)$$

Coefficient t is approximately $t = 0.1$.

The atomization quality of *disk atomizers* was evaluated for a vast range of parameter changes. As a result the following dimensionless equation was obtained [5].

$$\frac{\bar{D}}{\delta} = C \text{We}^{-0.5} \text{Lp}^{-0.04} M^{0.5} \quad (6-92)$$

where

$$\text{We} = \frac{\rho_G V_L^2 \delta}{\sigma}$$

$$\text{Lp} = \frac{\rho_L \sigma \delta}{\mu_L^2}$$

where δ = liquid film thickness at disk edge

V_L = absolute velocity of the liquid spinning off the disk (velocity V_L is approximately equal to the circumferential velocity of the disk edge)
Constant $C = 81.5$ for $\bar{D} = D_{32}$; $C = 8.5$ for $\bar{D} = D_m$.

Another equation for a disk atomizer was given by S. Matsumoto and Y. Takashima, also in a dimensionless form [23]:

$$\frac{D_{32}}{R} = 11.1 \text{Re}^{-0.5} \text{We}^{-0.1} Q_0^{0.2} \quad (6-93)$$

where R is the disk radius

$$\text{Re} = \frac{\omega R^2}{\nu_L}$$

$$\text{We} = \frac{\rho_L \omega^2 R^3}{\sigma}$$

The dimensionless liquid flow rate is

$$Q_0 = \frac{Q}{2\pi R^2 (\nu_L \omega)^{1/2}}$$

ω is the angular velocity, rad/s, and Q is the liquid flow rate, m³/s.

In [10] the conditions of liquid film development in atomizers with a partially submerged rotating disk were investigated (Fig. 4-60c). Three liquids with different viscosity and surface tension were used: water, glycerol, and oil. Liquid film thickness was measured. Three modes of drop formation were observed—drop, ligament and sheet. At certain rotational speeds more than one mode of drop formation occurred. The following empirical equation was derived for dimensionless film thickness δ_* :

$$\delta_* = \frac{7.998 R^{5.225} * T^{0.148} \Omega^{2.929}}{\Phi^{0.024} \psi^{3.089}}, \quad (6-94)$$

where $\delta_* = \delta(\rho g / \mu \omega r)^{1/2}$

$R_* = R - R_0/R$ is the dimensionless disk radius

$T = \sigma(g\nu)^{-1/3}/\rho$ is a dimensionless number

$\Omega = \mu \omega r / \sigma$ is a dimensionless capillary number

$\Phi = \omega^2 R / g - \sin \Theta$ is a dimensionless number

$\psi = \mu \omega R_0 / \sigma$ is a dimensionless capillary number based on R_0

g = acceleration of gravity, m/s²

δ = liquid film thickness, m

r = radial coordinate, m

R = disk radius, m

R_0 = radius of unwetted disk, m

θ = angular position

ω = angular velocity of disk, radian/s

μ = liquid dynamic viscosity, Pa · s

ν = liquid kinematic viscosity, m²/s

ρ = liquid density, kg/m³

σ = surface tension, N/m

Hinze and Milborn considered the conditions of the formation of a diesel oil film on the rim of a *cup atomizer*. They established the following semiempirical relation for the sheet formation mode of drop development [26]

$$\frac{\nu_L^{0.34} G_L^2 N^{1.2}}{\rho_L^{0.23} d^{1.37} \sigma^{1.77}} > 0.197 \quad (6-95)$$

where ν_L = diesel oil viscosity, $\times 10^4$ m²/s

G_L = diesel oil flow rate, $\times 10^3$ kg/s

N = rotational speed, 1/s

ρ = diesel oil density, 10⁻³ kg/m³

d = cup rim diameter, $\times 10^2$ m

σ = surface tension, $\times 10^3$ N/m

It follows from relation (6-95) that viscosity effect is small. Substituting typical values for diesel oil, we can calculate the minimum liquid flow rate $G_{L\ min}$ corresponding to the sheet formation mode. The results of calculations are presented in Table 6-6, where it was assumed $d = 0.1$ m, $\nu_L = 45 \times 10^{-6}$ m²/s, $\rho_L = 820$ kg/m³, and $\sigma = 32 \times 10^{-3}$ N/m.

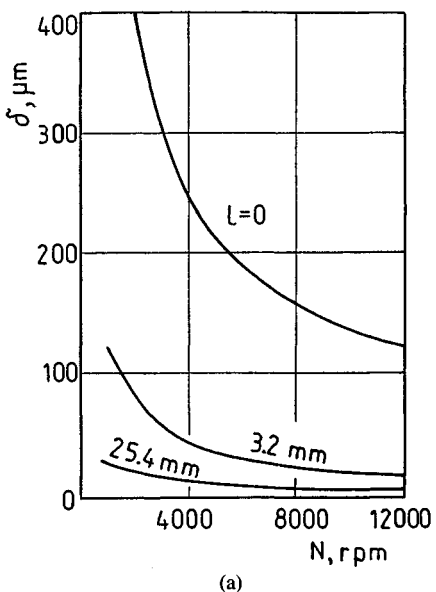
Figure 6-68 shows the influence of different parameters on film thickness δ for a *cup atomizer* in a stationary ambient [26]. Figure 6-68a shows that with increasing rotation speed N the film thickness δ decreases significantly, but this is relevant to small distances (Fig. 6-66). Figure 6-68b shows that with increasing cup rim diameter d the film thickness decreases substantially, but as close as distance $l = 25.4$ mm thickness δ is almost the same for diameter range $d = 50-100$ mm. Figure 6-68c shows that with the increasing liquid viscosity ν_L the film thickness δ decreases substantially, but this is relevant only to the vicinity of the cup rim ($l \approx 0$) because at distances larger than $l = 3.2$ mm the effect of liquid viscosity is negligible. Figure 6-68d shows that with increasing liquid flow rate G_L the film thickness δ decreases significantly, but this is relevant to small distances l only.

Angle of flare β of the cup (Fig. 6-66) also affects film thickness δ . Small angles β cause an increase of δ , but for angle $\beta \approx 40^\circ$ the film thickness decreases rapidly, reaching a minimal value for $\beta = 90^\circ$. At distance $l \geq 3.2$ mm the effect of angle β on thickness δ vanishes.

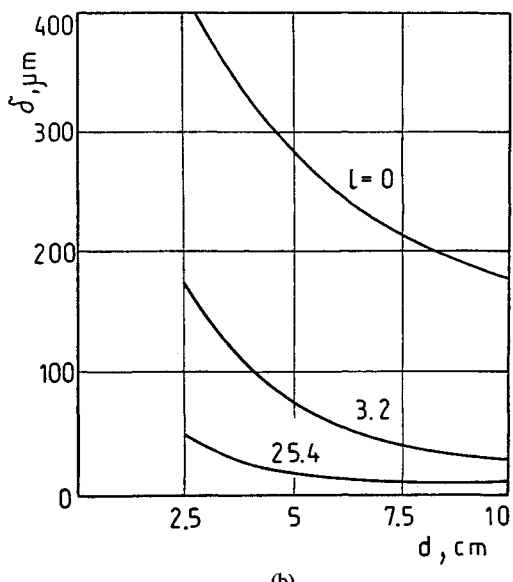
Figure 6-66 shows that during the impingement of air jets with the liquid film, drops do not develop directly. The impingement causes liquid annuli with width equal to the disturbance wavelength to separate initially, and subsequently they disintegrate into drops. The drop diameter is dictated mostly by liquid film thickness δ . The relationship between Sauter mean diameter D_{32} and liquid

Table 6-6 Minimum diesel oil flow rate $G_{L\ min}$ ensuring the sheet mode of drop formation on the cup rim

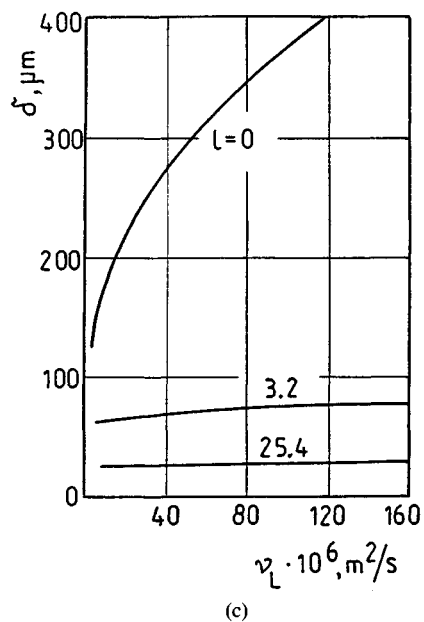
N , rpm	1500	3000	4500	6000	12000
$G_{L\ min}$, kg/h	26.2	17.2	13.7	11.6	7.6



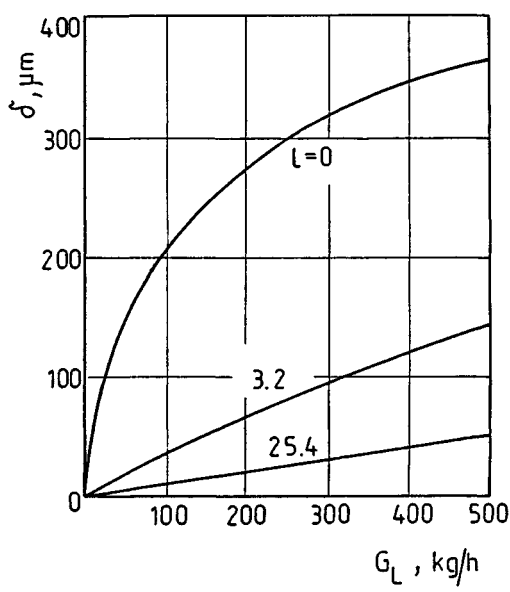
(a)



(b)



(c)



(d)

Figure 6-68 Dependence of liquid film thickness δ on rotational speed N , cup diameter d , liquid viscosity ν_L , and fuel flow rate G_L for various radial distances l from the cup rim.

film thickness δ and other parameters follows from the empirical equations [26]

$$D_{32} = 6 \times 10^{-4} + \frac{1.4\sigma^{0.5}\nu^{0.21}}{\rho_G^{0.5}} \left(1 + \frac{0.065}{b^{1.5}}\right) \left[\frac{\delta}{V_L^2(0.5W^2 - W + 1)} \right]^{0.5} \quad (6-96)$$

or

$$D_{32} = 6 \times 10^{-4} + \frac{0.59\sigma^{0.5}\nu^{0.21}}{\rho_G^{0.5}(ld + l^2)^{0.25}} \left(1 + \frac{0.065}{b^{1.5}}\right) \left[\frac{Q_L}{V_L^3(0.5W^2 - W + 1)} \right]^{0.5} \quad (6-97)$$

where $\nu = \nu_L/\nu_G$ is the ratio of viscosities of heating oil and water

$W = V_G/V_L$ is the ratio of velocities of air and heating oil, where velocity

$$V_L \approx v = \pi dN/60,$$

$d = 2R$ is the cup rim diameter (Fig. 6-66)

In Eqs. (6-96) and (6-97) D_{32} and δ are expressed in cm, V_L in cm^{-1} , σ in $\times 10^3 \text{ Nm}^{-1}$, and ρ in g cm^{-3} . In Eq. (6-96) one should use film thickness $\delta = \delta_s$ from Eq. (5-212). Equation (6-97) is valid for distance $l \geq 5 \text{ mm}$. Equations (6-96) and (6-97) were derived for a cup atomizer (diameter $d \approx 10 \text{ cm}$) at the following conditions:

Diesel oil flow rate $G_L \approx 110\text{--}450 \text{ kg/h}$

Diesel oil viscosity $\nu_L = (5\text{--}165) \times 10^{-6} \text{ m}^2/\text{s}$

Air velocity $V_G \approx 30\text{--}200 \text{ m/s}$

Air flow rate $G_G \approx 23\text{--}450 \text{ kg/h}$

Liquid/air mass ratio $b = 0.17\text{--}3.8 \text{ kg/kg}$

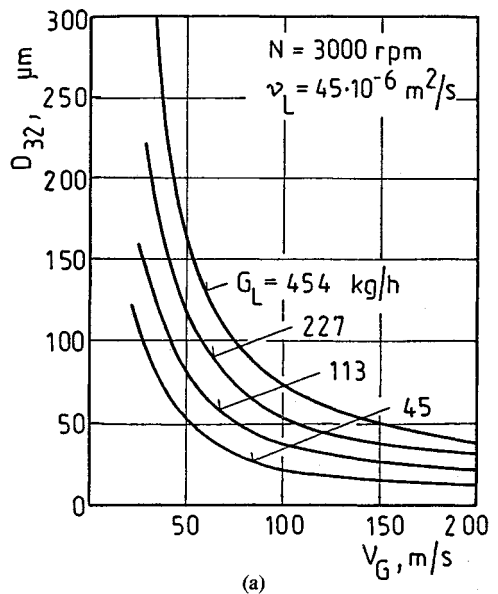
Rotational speed $N = 1500\text{--}1600 \text{ rpm}$

Axial distance $h = 5 \text{ mm}$ (optimum distance in this investigation)

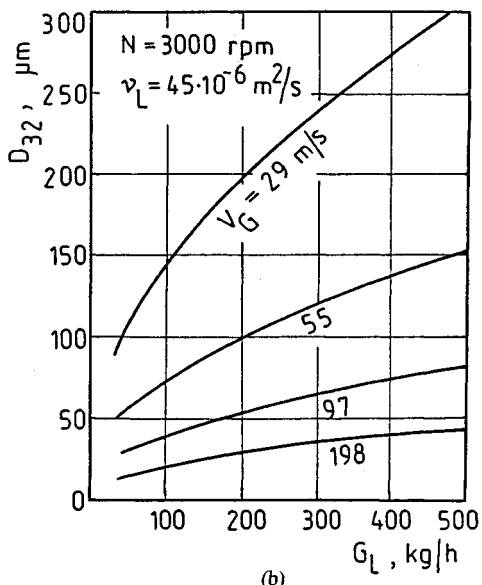
Radial distance $l = 0\text{--}14 \text{ mm}$, and as l increases diameter D_{32} decreases slightly.

Figure 6-69 shows the effect of various parameters on Sauter mean diameter D_{32} [26]. It follows from Fig. 6-69a that the increase of air velocity up to $V_G = 60\text{--}90 \text{ m/s}$ causes a decrease of D_{32} . It follows from Fig. 6-69b that as liquid flow rate G_L increases D_{32} increases, and this increase is especially pronounced for small velocities V_G . It follows from Fig. 6-69c that with the increase of rotational speed N of the cup D_{32} decreases, but in this particular range of N this effect is insignificant. From Fig. 6-69d it follows that with the increase of the liquid viscosity D_{32} increases, but this increase becomes slower for higher viscosities.

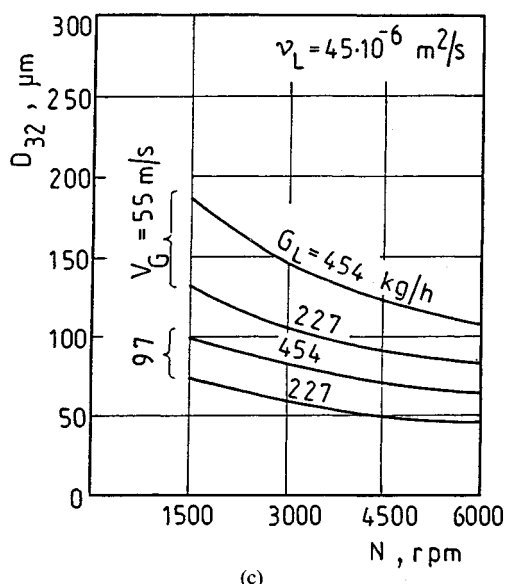
Figure 6-70 shows the change of Sauter mean diameter D_{32} as a function of air/liquid mass ratio b for various air velocities V_G [26]. The conditions of investigations were as follows: $N = 3000 \text{ rpm}$, $\nu_L = 45 \times 10^{-6} \text{ m}^2/\text{s}$, $\sigma = 30 \times 10^{-3} \text{ N/m}$, $G_G = 454 \text{ kg/h}$ except for curves 1 and 2, for which flow rates were respectively $G_G = 45 \text{ kg/h}$ and $G_G = 113 \text{ kg/h}$. The liquid film thickness at the



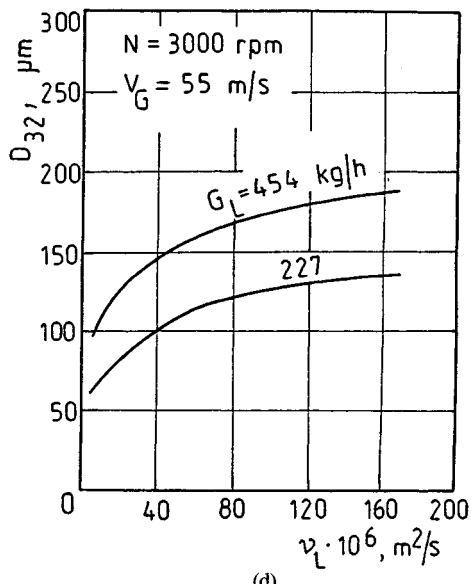
(a)



(b)



(c)



(d)

Figure 6-69 Dependence of Sauter mean diameter D_{32} on air velocity V_G , fuel flow rate G_L , cup rotational speed N , and fuel viscosity ν_L ; diameter $d = 10 \text{ cm}$, distance $l = 5 \text{ mm}$, and air/liquid mass ratio $b = 2.45 \text{ kg/kg}$.

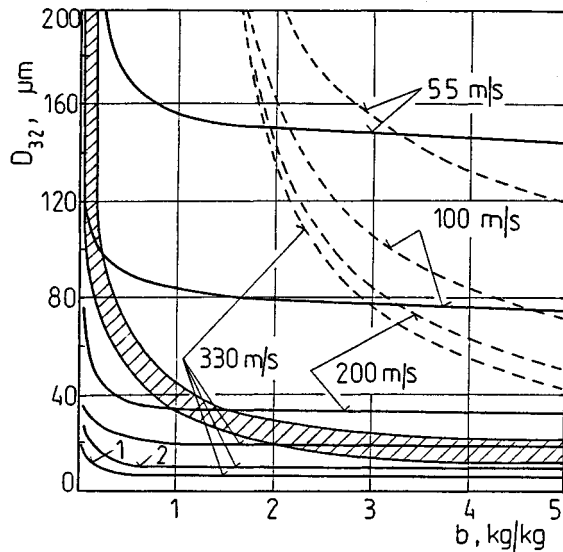


Figure 6-70 Comparison of values of the Sauter mean diameter D_{32} for pneumatic-rotary atomizers with various values of b and V_G .

point of impingement with air was (Fig. 6-66) $\delta = 7 \mu\text{m}$ for $G_L = 45 \text{ kg/h}$, $\delta = 17 \mu\text{m}$ for $G_L = 113 \text{ kg/h}$, and $\delta = 64 \mu\text{m}$ for $G_L = 454 \text{ kg/h}$. The continuous lines show that for b higher than 2 kg/kg improvement of the atomization quality was not observed. For high air velocities V_G this limit is reduced to $b = 0.5 \text{ kg/kg}$.

For comparison, Fig. 6-70 is supplemented with the results for atomization with pneumatic atomizers. The shaded region refers to two atomizers with internal air operation in which the liquid in the form of a film impinged with air flowing with the velocity of sound. The properties of the liquid were as follows: $G_L = 123 \text{ kg/h}$, $\nu_L = (0.7-40) \times 10^{-6} \text{ m}^2/\text{s}$, $\sigma = (20-23) \times 10^{-3} \text{ N/m}$. The comparison shows that above $b = 2 \text{ kg/kg}$ the pneumatic-rotary atomizer generates smaller drops than the pneumatic atomizer. The advantage of rotary atomizers is that the liquid film thickness before disintegration is self-controlled, which is not the case in pneumatic atomizers.

The dashed lines in Fig. 6-70 correspond to the values obtained from Eq. (6-64). This equation corresponds to conditions in which the liquid jet with diameter $0.2-1.0 \text{ mm}$ and flow rate $G_L \approx 4.5 \text{ kg/h}$ is atomized by an annular gas jet. The following data were used for calculations: $\nu_L = 45 \times 10^{-6} \text{ m}^2/\text{s}$ and $\sigma = 30 \times 10^{-3} \text{ N/m}$. It is seen that the atomization of a liquid jet gives much worse results than the atomization of a liquid film.

On the basis of investigation of cup atomizers it was established that the results agreed best with the Rosin-Rammler equation [Eq. (3-49)]. It was found that $\delta = 2.6$ and $X = 320 \mu\text{m}$ for the following conditions: $G_L = 113 \text{ kg/h}$, $\nu_L = 45 \times 10^{-6} \text{ m}^2/\text{s}$, $N = 3000 \text{ rpm}$, $G_G = 256 \text{ kg/h}$, $V_G = 29 \text{ m/s}$. The value $\delta = 2.6$ indicates the relatively wide atomization spectrum. The relationship between Sauter mean diameter D_{32} and maximum drop diameter D_{\max} was

established for these conditions [26]:

$$\frac{D_{\max}}{D_{32}} = 0.6 + 43(D_{32} - 11.5)^{-0.612} \quad (6-98)$$

where diameters D_{32} and D_{\max} are expressed in μm .

Masters [22] considered various equations for diameter D_{32} in the case of *vaned atomizers*, which are used in spray drying. He found the best agreement with experimental results for the equation proposed by Herring and Marshall:

$$D_{32} = 1.4 \times 10^4 G_L^{0.24} (Nd)^{-0.83} (nh)^{-0.12} \quad (6-99)$$

where D_{32} = Sauter mean diameter, μm

G_L = liquid flow rate, kg/h

N = rotation speed, rpm

d = disk diameter, m

n = number of vanes

h = height of vanes, m

The best agreement of Eq. (6-99) with the experimental results is for the circumferential velocity of the cup rim lower than 110 m/s and the liquid flow rate lower than 800 kg/h. For high velocities and flow rates accuracy of Eq. (6-99) deteriorates significantly and therefore the exponent of G_L should be reduced to 0.12. To improve the accuracy, the value of the numerical constant in Eq. (6-99) should be determined experimentally for particular atomization conditions.

For an *atomizer with a perforated periphery* as shown in Fig. 5-25 an empirical equation was found that refers to the mean surface diameter [47]:

$$D_{20} = 19.7d_0 \text{We}^{-0.5}, \quad (6-100)$$

where $\text{We} = \rho_G V^2 d_0 / \sigma$

ρ_G = density of ambient gas

V = absolute velocity of liquid discharging from the orifices; this velocity is approximately $\omega_1 R_1$

Equation (6-100) holds for Weber number $\text{We} \leq 2000$.

In closing, it should be pointed out that rotary atomizers, especially some types of these atomizers, can generate drops with small diameter scatter under specific conditions. This problem was extensively discussed in Sec. 2-6, where methods of uniform drop generation were considered.

REFERENCES

1. Adamowicz, K., Orzechowski, Z. Design of a pneumatic atomizer for steam attemperation. *Teploenergetika*, No. 1, 1978 (in Russia).
2. Aigner, M., Wittig, S. Swirl and counterswirl effects in prefilming airblast atomizers. *Trans. ASME J. Eng. Gas Turbines Power*, Vol. 10, January 1988.

3. Antkowiak, W., Heim, A. Investigation of characteristics of a pneumatic nozzle used for wetting of the granulated dust. *Inz. Chem. Proces.*, Vol. 8, No. 1, 1987 (In Polish).
4. Barré, M., Jaumotte, A., de Veubeke, B. F., Vandenerckhove, J. *Rocket Propulsion*. Elsevier, Amsterdam, 1960.
5. Borodin, V. A., Dityakin, Yu F., Klyachko, L. A., Yagodkin, V. I. *Liquid Atomization*. "Mashinostroenie," Moscow, 1967 (in Russia).
6. Brauer, H. *Fundamentals of Single and Multi-Phase Flows*. Verlag Sauerlander, Aarau and Frankfurt am Main, 1971 (in German).
7. Brykowski, L. Influence of the geometrical dimensions and operational parameters on critical atomization in the rotary atomizers in burners. Ph.D. thesis, Lodz, Poland, 1974 (in Polish).
8. Dityakin, J. F., Klyachko, L. A., Novikov, B. V., Yagodkin, V. I. *Liquid Atomization*. "Mashinostroenie," Moscow, 1977 (in Russia).
9. Elkotb, M. M., Rafat, N. M., Hanna, M. A. The influence of swirl atomizer geometry on the atomization performance. *Proc. ICCLASS-78*, Tokyo, 5-1, 109–115, 1978.
10. Gupta, J. P., Vijayraghavan, K., Mohan, R. Disintegration of a liquid film by a vertically rotating disk. *Proc. ICCLASS-78*, Tokyo, 6-2, 139–144, 1978.
11. Hiroyasu, H., Kadota, T., Arai, M. Supplementary comments: Fuel spray characterization in diesel engines. *Proceedings of the Symposium on Combustion Modeling in Reciprocating Engines*. Plenum Publishing, New York, 1980.
12. Hiroyasu, H., Shimizu, M., Arai, M. The breakup of high speed jet in a high pressure gaseous atmosphere. *Proc. ICCLASS-82*, Madison, Wisconsin, 2-5, 69–74, 1982.
13. Iciek, J. The hydrodynamics of a free, liquid jet and their influence on direct contact heat transfer—I, II. *Int. J. Multiphase Flow*, Vol. 8, No.3, 1982.
14. Inamura, T., Nagai N. The relative performance of externally and internally mixed twin-fluid atomisers. *Proc. ICCLASS-85*, London, II C/2/1–11, 1985.
15. Ingebo, R. D. Liquid fuel spray processes in high-pressure gas flow. *Proc. ICCLASS-85*, London, VI A/4/1–1, 1985.
16. Ingebo, R. Hydrodynamic and aerodynamic breakup of liquid sheets. *Proc. ICCLASS-82*, Madison, Wisconsin, 1-2, 9–17, 1982.
17. Ishikawa, M., Murakami, T. Characteristics of intermittent sprays generated by an orifice atomizer. *Proc. ICCLASS-82*, Madison, Wisconsin, 3-1 (Reu), 85–92, 1982.
18. Kutovoi, V. A. *Fuel Injection in Diesel engines*, "Mashinostroenie," Moscow, 1981 (in Russian).
19. Lee, S. Y., Tankin, R. S. Study of liquid spray (water) in a non-condensable environment (air)—paper I. Study of liquid spray (water) in a condensable environment (steam)—paper II. *Int. J. Heat Mass Transfer*, Vol. 27, No. 3, pp. 351–361, 363–374, 1984.
20. Lyshevskii, A .S. *Processes of Fuel Atomization in Diesel Nozzles*. Mashgiz, Moscow, 1963 (in Russian).
21. Mao, C.-P., Wang, G., Chigier, N. The structure and characterization of air-assisted swirl atomizer sprays. *Atomisation Spray Technol.*, Vol. 2, No.2, pp. 151–169, 1986.
22. Masters, K. *Spray Drying Handbook*. George Godwin, London, 1985.
23. Matsumoto, S., Belcher, D. W., Crosby, E. J. Rotary atomizers: Performance understanding and prediction. *Proc. ICCLASS-85*, London, IA/1/1–21, 1985.
24. Nagai, N., Inamura, T. Atomization of liquid flowing over a solid surface by high speed air. *Proc. ICCLASS-82*, Madison, Wisconsin, 5-2, 153–160, 1982.
25. Nakayama, M., Ohono, T. Experimental investigation of atomizing characteristics of grooved swirl nozzle. *Proc. ICCLASS-78*, Tokyo, 4-4, 101–108, 1978.
26. Orzechowski, Z. *Liquid Atomization*. WNT, Warsaw, 1976 (in Polish).
27. Petela, R., Zajdel, A. Atomization of coal-liquid mixtures. *Fuel*, Vol. 59, July 1980.
28. Prasad, K. S. L. Spray characterisation of air blast atomisers. *Proc. ICCLASS-82*, Madison, Wisconsin, 4-3, 123–130, 1982.
29. Ranganadha Babu, K., Narasimhan, M. V., Narayanaswamy, K. Correlations for prediction of discharge rate, cone angle and air core diameter of swirl spray atomizers. *Proc. ICCLASS-82*, Madison, Wisconsin, 3-3, 91–97, 1982.

30. Ranganadha Babu, K., Narasimhan M. V., Narayanaswamy, K. Prediction of mean drop size of fuel sprays from swirl spray atomizers. *Proc. ICLASS-82*, Madison, Wisconsin, 3-4, 99–106, 1982.
31. Rizk, N. K., Lefebvre, A. H. Influence of liquid properties on the internal flow characteristics of simplex swirl atomisers. *Atomisation Spray Technol.*, Vol. 2, No.3, pp. 219–233, 1986.
32. Sakai, T., Kito, M., Saito, M., Kanabe, T. Characteristics of internal mixing twin-fluid atomizer. *Proc. ICLASS-78*, Tokyo, 10-1, 235–241, 1978.
33. Sakai, T., Sadakata, M., Saito, M. Mean diameters and drop size distribution of suspension sprays. *Atomisation Spray Technol.*, Vol. 1, No. 2, pp. 147–164, 1985.
34. Sankaran Kutty, P., Narasimhan, M. V., Narayanaswamy K. Design and prediction of discharge rate, cone angle and aircore diameter of swirl chamber atomisers. *Proc. ICLASS-78*, Tokyo, 4-3, 93–100, 1978.
35. Sato, G. T. Structure of diesel spray. *Proc. ICLASS-85*, London, IP 1/1–10, 1985.
36. Sato, G. T., Tanabe, H., Fujimoto, H. An investigation of diesel spray. *Proc. ICLASS-82*, Madison, Wisconsin, 9-2, 229–235, 1982.
37. Shaw, S. G., Jasuja, A. K. Effect of injector geometry variables upon the spray performance of a plain-jet airblast atomizer. *Atomisation Spray Technol.*, Vol. 3, No. 2, pp. 107–121, 1987.
38. Simmons, H. C. Initial spray formation in simplex swirl-atomizers (fuel nozzles). *Proc. ICLASS-82*, Madison, Wisconsin, 3-2, 83–90, 1982.
39. Tabata, M., Arai, M., Hiroyasu, H. Effect of fuel viscosity and surface tension on diesel spray drops. *Proc. ICLASS-85*, London, II B/1/1–8, 1985.
40. Takehira, A., Kawashima, T., Morita, S. Spray characteristics of the atomizer using a high speed gas flow. *Proc. ICLASS-78*, Tokyo, 10-3, 251–258, 1978.
41. Tanasawa, Y., Miyasaka, Y., Umehara, M. Effect of shape of rotating disks and cups on liquid atomization. *Proc. ICLASS-78*, Tokyo, 7-3, 165–172, 1978.
42. Tanno, S., Miura, T., Ohtani, S. Atomisation of high viscosity liquid by pneumatic nozzle. *Proc. ICLASS-85*, London, LP/VB/6/1–8, 1985.
43. Tanno, S., Miura, T., Ohtani, S. Development of a crossflow type pneumatic nozzle. *Atomisation Spray Technol.*, Vol. 2, No. 1, pp. 17–34, 1986.
44. Tate, R. W. Droplet size distribution data for internal-mixing pneumatic atomizers. *Proc. ICLASS-85*, London, II C/1/1–13, 1985.
45. Tishkoff, J. M. Air entrainment into sprays from swirl chamber atomisers. *Proc. ICLASS-85*, London, VII C/4/1–10, 1985.
46. Tokuoka, N., Nagaosa, S., Hora, S., Sato, G. T. Study on the disintegration of a liquid film by air impingement. *Atomisation Spray Technol.*, Vol. 1, No. 2, pp. 103–123, 1985.
47. Troshkin, O. A. Hydraulic design of the centrifugal cylindrical sprayer. *Khim. Neft. Mashinostr.*, No. 5, 1984 (in Russian).
48. Tumanovskii, A. G., Semichastnyi, N. N., Akhrameev, V. I. Application of air assisted atomizers for fuel atomization in stationary gas turbines. *Teploenergetika*, No. 11, 1984 (in Russian).
49. Valeev, R. S., Kudryavtsev, A. V., Kuntsev, G. M. Experimental investigation of atomization of a liquid jet fed perpendicularly to the gas jet. *Izv. Vyssh. Uchebn. Zaved. "Aviatsionnaya Tekhnika,"* No. 3, 1984 (in Russian).
50. Yule, A. J., Mo, S.-L., Tham, S. Y., Aval, S. M. Diesel spray structure. *Proc. ICLASS-85*, London, II B/2/1–15, 1985.
51. Zajdel, A. Investigation of dust-liquid fuel. Ph.D. thesis, Silesian Polytechnic, Gliwice, Poland, 1979 (in Polish).



Taylor & Francis
Taylor & Francis Group
<http://taylorandfrancis.com>

EXPERIMENTAL TECHNIQUES AND MEASURING DEVICES

7-1 SCOPE OF INVESTIGATION OF ATOMIZERS

There are two types of atomizer investigations: quality control tests and laboratory investigations.

Quality control. These tests are conducted by manufacturers and users of atomizers. The inspections in the factories are to verify the specifications of atomizers and detect production defects. These inspections are very difficult to carry out because of mass production and strict requirements imposed on atomizers. Mass production is especially typical in the case of intermittent atomizers (diesel engine nozzles), whose production reaches millions of items per year. The strict requirements concern aircraft engines, on whose flawless performance flight safety depends.

Inspections conducted by users are done within the frames of in-service inspections of the devices—diesel engines, boiler burners, spray driers, and so forth. These inspections have as an aim detection and elimination of defects caused by contamination or wear of atomizers. The scope of these inspections and type of measuring devices are different in the case of intermittent and continuous atomizers.

Inspections of *intermittent atomizers* include the following tests:

Tightness of atomizer

Injection pressure

Spray angle
Quality of spray
Volume of mean fuel charge
Pintle lift
Injection advance angle
Atomizer's opening pressure, etc.

Some of these tests are simple; others related to measurements of pressure and pintle motion are complex. The inspection tests have a dynamic character because they deal with pintle motion. Only the tightness tests are static.

Inspections of *continuous atomizers* are simpler than those of intermittent atomizers.

These tests encompass the microstructure and macrostructure of the atomized liquid, that is, liquid flow rate, spray angle, liquid distribution in the jet, and atomization quality. Tests of the macrostructure of the atomized liquid are simple, but the microstructure measurements require special instrumentation.

Laboratory investigations. Knowledge about atomizers is obtained through laboratory investigations. These are conducted in scientific laboratories or at factories. These investigations require special test stands equipped with modern instrumentation that allows the measurement of various high-speed phenomena. Laboratory investigations are conducted by qualified scientific and technical staff.

The laboratory investigations of intermittent atomizers include:

Nonrepeatability of injection
Pressure changes
Pintle motion
Injection characteristics
Spray motion in a combustion chamber
Injection penetration
Atomization quality, etc.

The tests are carried out on special stands or properly equipped piston engines. The tests using engines are more valuable because they represent the real conditions better.

Laboratory investigations of *continuous atomizers* are very diverse because they concern atomizers of various types. Emphasis is put on investigation of atomization quality. The goal of these tests is to determine the effect of such parameters as liquid properties, atomizer geometry, and flow dynamics on atomization quality. The laboratory tests are also concentrated on such problems as:

Motion of single drops and drop jets
Motion of liquid film
Secondary drop disintegration

Interaction between liquid jets and gas
Impingement of liquid with surface of solid bodies
Testing of new materials

The most important aim of the laboratory investigations is to improve existing atomizers and develop new varieties and types of atomizers (acoustic, ultrasonic, electrostatic, pulsating, and other).

7-2 MEASUREMENT OF THE FLOW RATE OF THE ATOMIZED LIQUID

The flow rate of atomized liquid is usually measured together with other parameters. Measurements of flow rate of continuous and intermittent atomizers will be discussed separately, because the measuring methods are completely different.

7-2.1 Atomizers with Intermittent Operation

Various measuring instruments are used for investigation of intermittent atomizers (diesel nozzles) [74]. These instruments are built commercially by specialized manufacturers because these atomizers are widely used.

The instrument most commonly used for investigation of diesel atomizers is a *tester*, which is used to assess the correctness of operation of new atomizers, repaired atomizers, and atomizers under preventional control. The tester, despite its simple design, is a relatively multipurpose device that measures the mean fuel charge as well as injection pressure, spray angle, tightness control, and spray quality. This device is needed in every workshop as well as in production plants.

Testers can be hand operated or power driven. Figure 7-1 shows a hand-operated Testmaster (model HH6d) tester produced by Hertridge Company. The characteristic feature of this tester is an additional valve called a stabilizer, which makes it possible to achieve a constant fuel (testing oil) flow rate.

Figure 7-2 shows a tester driven pneumatically, also produced by Hertridge Company. The testing oil is fed from a tank by using a pneumatic-hydraulic pump driven by compressed air. The oil flows through the throttle valve, which controls flow to the atomizer, and in parallel flows to the assisting accumulator, which equalizes the pressure in the system when the pump is not working.

The testing method using a tester is not standardized, which hinders the comparison of results. Operation of atomizer in the tester and in the engine differs significantly. This is seen clearly in graphs of pressure changes and pintle lift as functions of time. The pintle lift during investigations with a tester is much smaller than during tests with an engine because of the weaker pressure wave. The conditions of fuel throttling in the pintle seat and in the atomizer's orifices are also different. As a result, the instantaneous fuel charge is significantly smaller than in the engine. Differences also occur in pressure changes

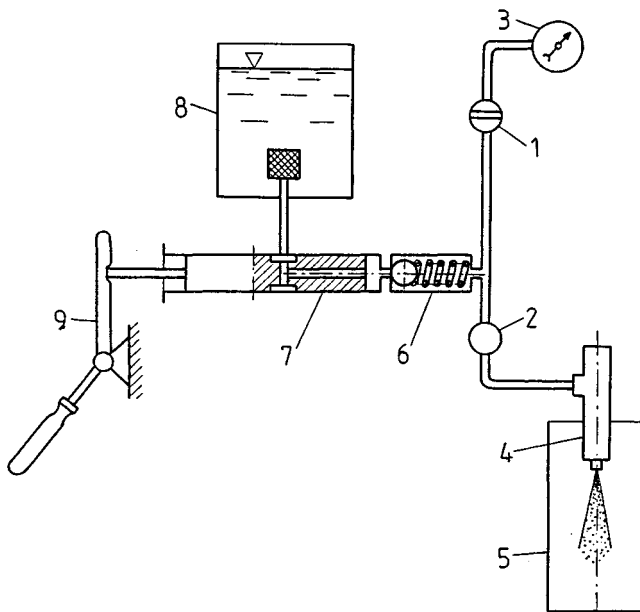


Figure 7-1 Schematic diagram of a hand-operated tester. 1, Stop valve; 2, stabilizer; 3, pressure gauge; 4, injector; 5, vessel; 6, piston valve; 7, pump piston; 8, tank with a filter; 9, hand lever [74].

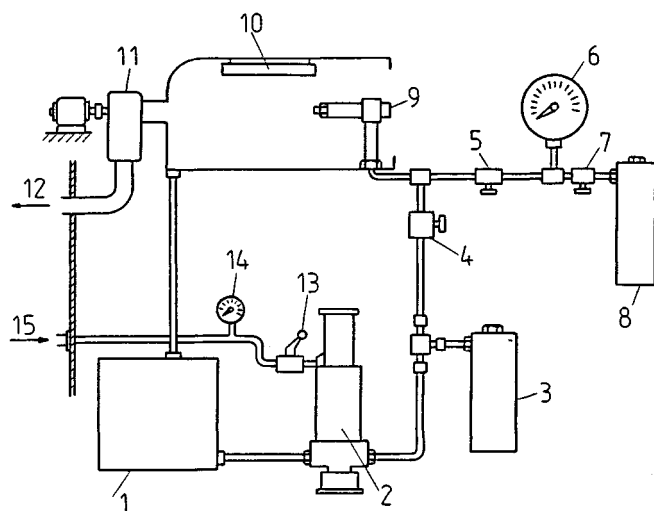


Figure 7-2 Schematic diagram of a mechanical tester. 1, Tank, 2, hydraulic-pneumatic pump; 3, accumulator; 4, throttle valve; 5, pressure gauge stop valve; 6, pressure gauge; 7, stop valve; 8, assisting accumulator; 9, injector; 10, lamp; 11, ventilating fan; 12, polluted air outlet; 13, stop valve; 14, pressure gauge; 15, compressed air feeding.

because during measurements on the tester there is no pressure increase at the onset of injection and no pressure drop after the injection.

These caveats do not eliminate the use of testers. In some instances measurements on a tester are advantageous compared to measurements on an engine. For example, for an arbitrary increase of pressure on the tester one can easily determine the opening pressure of the atomizer, the tighteners of the pintle seat is easily detectable, and so forth. Through application of auxiliary equipment, for example, a hydraulic accumulator (high-pressure accumulator), one can improve test conditions or standardize them.

A larger and more universal device than the tester is the so-called *testing stand*. It can be used to check the correctness of interaction of all elements of the injection system—*injection pump, nozzles, regulators, and feeding pumps*. Testing stands are used by the specialized service stations and research laboratories. The most popular manufacturers are Bosch, Friedmann-Maier, Hartridge, and others.

Mean fuel charge (Sec. 3-1.2) V_w (mm^3/cycle) or G_w (g/cycle) can be determined in a simple way, namely by measuring the fuel volume corresponding to a known number of injections. Proper operation of a multicylinder piston engine requires that injectors with identical flow rates be used. Used for this purpose is a *standard injector* (testing injector), which is custom made or selected from a large number of injectors. Flow rate deviation is determined for each type of engine. It can be stated approximately that for the same series of atomizers the deviation should not exceed 2–5%, while in practice one encounters deviations of 25–30%.

Determination of mean flow charge from many measured charges does not give full information about engine operation because the phenomenon of *injection nonrepeatability* often occurs. Injection nonrepeatability can be total or partial. For total nonrepeatability fuel is injected every other stroke of the pump. For partial nonrepeatability fuel is injected in various quantities. The first type of nonrepeatability is easy to detect, but the second requires special measuring instruments. Nonrepeatability of injection is most pronounced for low rotation speed of the pump and for small flow rates.

Selection of atomizers with identical flow rates and injection repeatability is a secondary solution. The primary solution is to ensure equal flow rates as early as during production. Control is done by measuring the fuel flow. As a result of measurements, flow characteristics are prepared in the form of functions:

$$\mu A = f(x) \quad \text{for } P = \text{const}$$

or

$$\mu A = f(P) \quad \text{for } x = \text{const}$$

The first type of function was shown in Figs. 5-8 and 6-5. The second type has a relatively flat shape (except for the low-pressure region) and represents the typical dependence of flow on the Reynold number.

Characteristics of an atomizer in the form $P = f(Q)$ for various needle lifts $x = \text{const}$ are also prepared (Sec. 3-1.2). The shape of these characteristics is obviously exactly the same as for continuous atomizers due to $x = \text{const}$.

The practical application of these characteristics is as follows. On the basis of the characteristics, we can initially assess the suitability of an atomizer for a particular engine type. The characteristics make it possible to monitor the divergence of atomizer parameters during production. Knowledge of the characteristics is necessary for theoretical prediction of the process of injection [see Eq. (5-37)].

Figure 7-3 shows a device for measuring the function $\mu A = f(x)$, where μA is the area of the equivalent flow cross section (Sec. 5-1.2). Measurement of the flow rate is carried out by a pneumatic method. For measurements compressed gas (usually compressed air) is used with reduced and constant pressure that is maintained by a pressure stabilizer. Gas is carefully purified. The gas flow rate is measured by means of a pneumatic sensor for a constant needle lift. This method is very convenient but is mainly of a comparative character.

Measurement of pressure is carried out in different ways. The pressure is measured on a tester by means of a spring pressure gauge. Measurement of pressure can be omitted when standard and tested injections are connected in parallel to detect all abnormalities of the operation of the tested injector. For measurements of rapidly changing pressure electronic sensors, usually piezoelectric (Vibrometer, Kistler), are used. The measuring system consists of a sensor, amplifier, and recording instrument (cathode-ray or loop oscilloscope). The frequency of pressure oscillations was high, for example, when sensors with frequencies up to 150 kHz were used [27].

Pressure measurement inside the injector itself is impossible because of lack of space, so pressure is measured in front of the injector. The pressure graph usually has a nonuniform character. Pressure fluctuations are caused by needle vibrations. Pressure fluctuation graphs enable the detection of so-called *afterinjection*, an additional injection of a small fuel charge after the regular injection is completed.

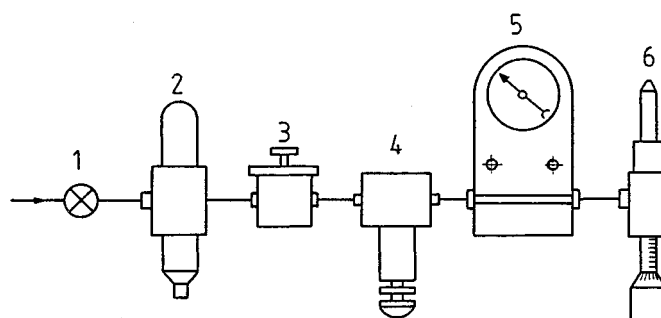


Figure 7-3 Schematic diagram of a stand for measuring the function $\mu A = f(x)$. 1, Stop valve; 2, filter; 3, pressure regulator; 4, pressure stabilizer; 5, pneumatic sensor; 6, tested injector with the micrometer screw for adjustment of needle lift x .

The velocity of the needle caused by the fuel pressure change (i.e., the needle lift as a function of time) is used to assess dynamic properties of the atomizer. Dynamic properties can be also assessed on the basis of the *stroke* (maximum lift) of the needle and the fuel charge. There are various ways to measure the needle stroke.

A simple method of stroke measurement is based on the use of a dial gauge that is screwed into the injector housing in place of the screw pressing on the spring. Such a measurement can be used for needle strokes higher than 50 μm . The needle stroke can be measured by means of an induction transducer that operates with an electric bridge with high frequency (of the order of 100 kHz) and with a cathode-ray oscilloscope or a peak impulse meter.

Needle lift measurement as a function of time is done by means of sensors that are used for measurements of small linear displacements. Usually these are capacitance or inductive sensors, rarely tensometric ones because of their high inertia. Such sensors are placed on the injector housing, and they measure the needle lift by measuring the follower's lift. In [27] a sensor based on the Hall effect and produced by Wolff Controls Corp. was used.

Proper combustion in a piston engine requires that the *characteristic of injection* [Eq. (3-9)] be known. There are several methods of determining these characteristics [74]:

Rotary method

Indicator method

Stroboscope method

Hydrodynamic thrust method

Injection to a constant-volume chamber

Injection to a constant-pressure chamber

Empirical-analytical method

Rotary method. The rotary method is based on measuring the fuel captured by chambers located on the periphery of a wheel that rotates around a vertical axis (Fig. 7-4). The small-diameter chambers are located close to each other and therefore the fuel charge is distributed into several consecutive chambers. Knowing the fuel volume V (expressed in mm^3) in a particular chamber, the angular spacing ϑ of chambers, the transmission ratio ω between the camshaft of the pump, and the number of injections n , we can determine the mean fuel flow rate \bar{q} ($\text{mm}^3/\text{degree of cam rotation}$) during the rotation of the camshaft by angle ϑ/n :

$$\bar{q} = \frac{V\omega}{\omega\vartheta} \quad (7-1)$$

For precise measurement, injection of several hundred charges is required.

The measuring device is usually placed on the testing stand. The rotary method is used most because of the simplicity of measurements. However, it has the following disadvantages: it is highly laborious, is suitable for single-orifice injectors only, has a large error of fuel scatter, and is not suitable for back pressure tests.

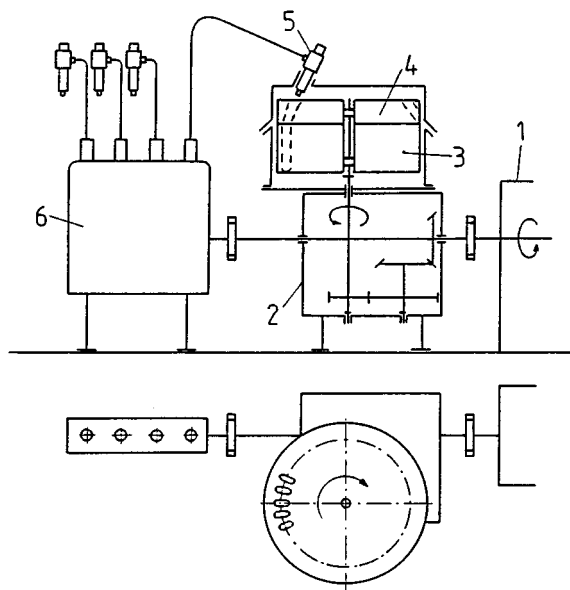


Figure 7-4 Schematic diagram of a rotary device for injection measurement. 1, Stand drive; 2, step-up gear; 3,4, lower and upper parts of the rotating wheel with chambers; 5, injector; 6, injection pump.

Indicator method. The indicator method is based on the phenomenon of hydraulic hammer, during which the increase of liquid pressure in the manifold is proportional to the increase of liquid velocity. The proportionality coefficient is the acoustic impedance, the product of velocity of sound in liquid, c , and liquid density ρ . Using the continuity equation for the liquid we obtain the equation

$$\frac{dV_w}{d\varphi} = A \frac{P}{c\rho} \quad (7-2)$$

from which it follows that the velocity of the liquid flow in a particular manifold cross section of area A is directly proportional to pressure P in this cross section. The measurement of flow velocity is in this case replaced by measurement of the instantaneous value of pressure.

Figure 7-5 shows a schematic diagram of an indicator produced by the Bosch Company. Injector 1 is placed at the beginning of the measuring manifold (3) filled up with fuel. This manifold is sufficiently long (5 m) to ensure that the time of flight of the pressure wave from the measurement point to the end of the tube and back is longer than the duration of injection. The pressure sensor 2 consists of two strain-gauge transducers (resistance and compensating ones). Throttler 4 has an aim to throttle the reflected waves. Behind the throttle a pressure tank (5) with a pressure gauge (6) is located. Back pressure control valve 7 has the aim of maintaining the pressure in the measuring manifold at the

level of the compression pressure in the engine. By using valve 8 and volumeter 9, the fuel flow can be monitored. Valve 10 is a safety valve.

The pressure wave as a function of time is photographed on the oscilloscope screen, and the whole measurement takes place on the testing stand. The indicator method is modern, fast, accurate, and gives the characteristic of each individual measurement. A disadvantage is the need to adjust the measuring manifold to the fuel flow rate and injection duration, otherwise the measurement errors increase significantly.

Stroboscope method. The stroboscope method is based on the principle of fuel injection on the surface of a rotating drum with a slit. The slit width and rotational speed are chosen so that the fuel volume passing through the slit corresponds to the angle $\varphi = 1^\circ$, where φ is the angle of rotation of the camshaft of the fuel pump. The measurements are done so that the position of the drum with respect to the camshaft is adjusted by an angle that corresponds to the slit width. The fuel is captured by a volumeter for the same number of injections. This measurement is simple but very laborious and is not accurate because of the fuel scatter.

Dynamic head method. This method uses the kinetic energy of the liquid jet. The action of the jet is measured by a high-frequency indicator during the impingement of the jet with a smooth membrane placed perpendicular to it. The value of the dynamic head is used to determine the fuel flow rate. Only injectors that give a strong single jet can be evaluated.

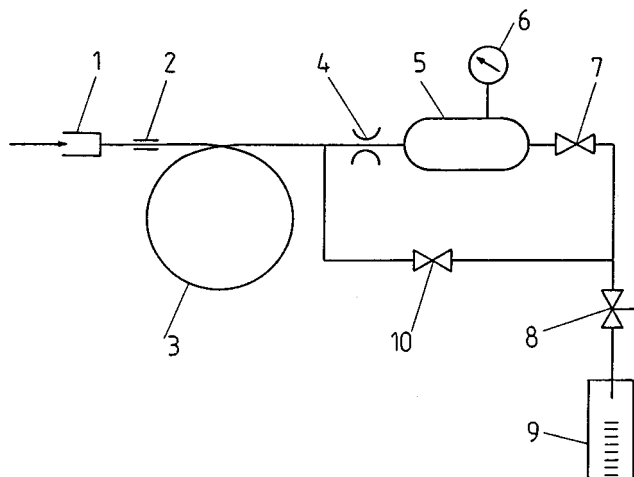


Figure 7-5 Schematic diagram of the injection measurement using the indicator method [74]. 1, Injector; 2, pressure sensor; 3, measuring manifold; 4, throttler; 5, pressure tank; 6, pressure gauge; 7, back pressure control valve; 8, valve; 9, volumeter; 10, safety valve.

Injection to a constant-volume chamber. During injection to an inelastic chamber of volume V_k filled with the liquid, an increase of pressure dP occurs which is proportional to the volume of the injected liquid:

$$dP = E \frac{dV_w}{V_k} \quad (7-3)$$

where E is the modulus of volume elasticity of the liquid. In this case V_w is the fuel volume supplied from injection onset to the moment considered. The pressure increment is measured with a piezoelectric transducer and registered on the screen of an oscillograph as a function of angle φ . The graph $P = f(\varphi)$ obtained presents the increment of flow rate $V_w = f(\varphi)$ (curve 2 in Fig. 3-4) on the appropriate scale.

This method gives a picture of each single measurement at the back pressure that exists in the combustion chamber at the onset of injection. After each injection a fuel volume is removed from the chamber that corresponds to the injected charge due to which the pressure in the chamber is reduced to the previous value. This operation requires very precise moving elements; therefore tightness and accuracy of measurements are difficult to achieve.

Injection to a constant-pressure chamber. In this method the chamber is closed from the top by a piston with a constant pressure. During the injection the piston moves in proportion to the charge volume. The piston displacement is measured by a sensor and registered as a function of angle φ , which gives the injection characteristic.

Empirical-analytical method. This method is related to measurement of injection pressure and needle lift. According to Eq. (3-3),

$$\frac{dV_w}{d\varphi} = \mu A \sqrt{\frac{2\Delta P}{\rho}} \quad (7-4)$$

where $\Delta P = P_1 - P_2$. In order to use this equation, injection pressure $P = P_1$ and needle lift x must be measured as a function of angle φ . During laboratory experiments the back pressure P_2 is constant and equal to atmospheric pressure, but during tests on an engine P_2 is variable and is measured. An equivalent flow cross section μA is measured under static conditions, and a graph such as that shown in Fig. 6-5 is prepared. This method is laborious but the most accurate one.

7-2.2 Atomizers with Continuous Operation

Atomizers with continuous operation comply (except for rotary atomizers) with Eqs. (3-3) and (3-4). These equations describe liquid discharge through an orifice for pressure drop ΔP . Measurement of liquid flow rate is reduced to the

determination of *atomizer characteristics*, namely functions (3-5), that is $Q = f(\Delta P)$ or $G = f(\Delta P)$. Graphical representation of these functions is shown in Fig. 3-2. Discharge coefficient μ is also measured as in the example shown in Fig. 5-1.

Measurements of flow rates of continuous atomizers are much easier than the measurement for intermittent atomizers. This refers especially to *pressure atomizers*, i.e., jet, swirl, and jet-swirl atomizers. To measure flow rates in these atomizers it suffices to use an arbitrary pressure device such as liquid pump or compressed air tank that pumps the liquid under an arbitrary pressure. Measuring devices are also simple since they include a pressure gauge and a flowmeter. This is done in case of urgency, but the producers of injectors and research laboratories have permanent test stands.

Figure 7-6 shows a schematic diagram of a stand for measuring flow rates of swirl chambers [74]. Atomizer 1 is placed at the top of closed chamber 2. Liquid is pumped from lower tank 3 to upper tank 4 by auxiliary pump 5. From tank 4 liquid flows through filter 6 to main pump 7 and from there through control valve 8 to the atomizer. Bypass 9 is used for additional flow control, especially for low liquid flow rates. Liquid flow rate is measured by a rotameter (10) and pressure by a pressure gauge (11). Fan 12 removes mist, which enables observation of the atomized liquid.

Such a measuring stand usually has a universal character because it is equipped with additional devices for measuring both microstructure and macrostructure of the atomized liquid. Accurate measurements require that the liquid temperature be known and controllable, and therefore the stands are equipped

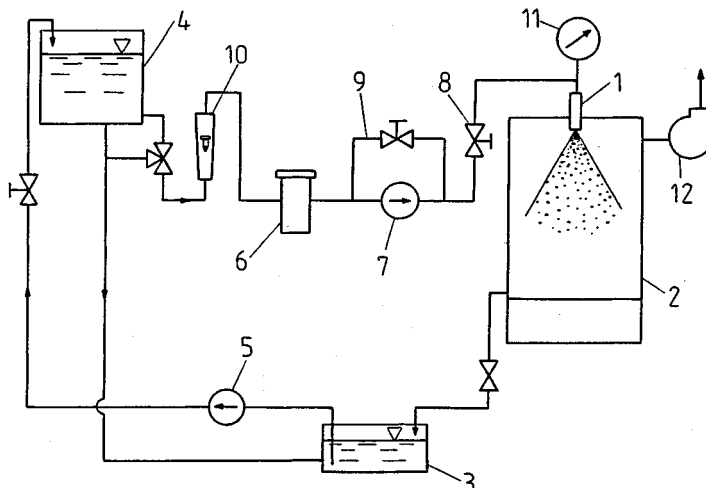


Figure 7-6 Schematic diagram of a test stand for liquid flow rate measurement. 1, Atomizer; 2, closed chamber; 3, lower tank; 4, upper tank; 5, auxiliary pump; 6, filter; 7, main pump; 8, control valve; 9, bypass; 10, rotameter; 11, pressure gauge; 12, fan.

with electric or steam heaters. In the case of liquid flowing in a closed circuit system and for constant increase of its temperature, cooling using water coolers is often necessary.

Pumps of two types are used: high-pressure main pumps and low-pressure auxiliary pumps (feed pumps). The high-pressure main pumps used are centrifugal pumps, gear pumps, and plunger pumps (multipiston pumps). The last are convenient because they have flow rate control through change of the stroke of the plunger. The pumps cause flow pulsation, which is damped by means of compensating tanks.

Liquid flow rate is measured by various methods. Most commonly, Venturi tubes, rotameters, and flowmeters of all kinds are used. Venturi tubes can be used for highly accurate measurements. Most accurate is the volumetric method, which is based on measuring the liquid volume captured in a measuring vessel with a specified volume. The gravimetric method has a similar character.

Measurement of liquid flow rate in the case of *pneumatic atomizers* proceeds in a similar manner. The test stand is more complex, however, since it contains a compressed gas installation; usually gas or steam is used. Pneumatic atomizers are used for atomization of viscous liquids, and therefore the test stand should include a heater and a cooler for the liquid. In addition the gas flow rate must be measured and its flow controlled to ensure the required gas/liquid mass ratio.

In the case of *rotary atomizers* the flow rate measurement depends on whether or not the atomizers use compressed gas.

7-3 MEASUREMENT OF MACROSTRUCTURE OF THE ATOMIZED LIQUID

Measurements of macrostructure of the atomized liquid, i.e., of spray angle, spray shape, spray penetration, and liquid distribution in a spray, are carried out on universal and special stands. Such stands and measuring devices are very diverse.

7-3.1 Measurement of Spray Angle and Spray Shape

Measurement of spray angle α is simple but the experimental results are not unequivocal. This is due to the various definitions of angle α (Sec. 3-2.1) and to measurement errors. The measurement errors depend on the method used. The main source of errors is the deformed and unsharp shape of the spray. The following methods are used for angle measurement: mechanical method, optical method, and photographic method.

Mechanical method. Angle α can be calculated from the equation

$$\operatorname{tg} \alpha = \frac{d}{2x} \quad (7-5)$$

where d is the liquid jet diameter at distance x from the atomizer. Diameter d can be measured in many ways. In the case of a single-orifice intermittent atomizer it suffices to place a screen made of paper or blotting paper and induce a single injection that produces an approximately circular fuel stain with diameter d .

Angle α can be measured directly using a protractor. This measurement, however, is inaccurate and subjective because the spray undergoes contraction (Fig. 3-9).

In the case of jet multiorifice atomizers (intermittent atomizers) a template is used to check the correctness of the axis angles of sprays (Fig. 7-7). The template is part of the test stand and is placed at a known distance from the atomizer. The correctness of angles is assessed by comparison with the positions of steady pins. These pins are placed symmetrically or asymmetrically, depending on the type of atomizer.

Optical method. During investigations of intermittent atomizers, chambers are often used for injection visualization. Chambers have stroboscopic lamps controlled by signals of the position of the camshaft of the fuel pump, and angle α

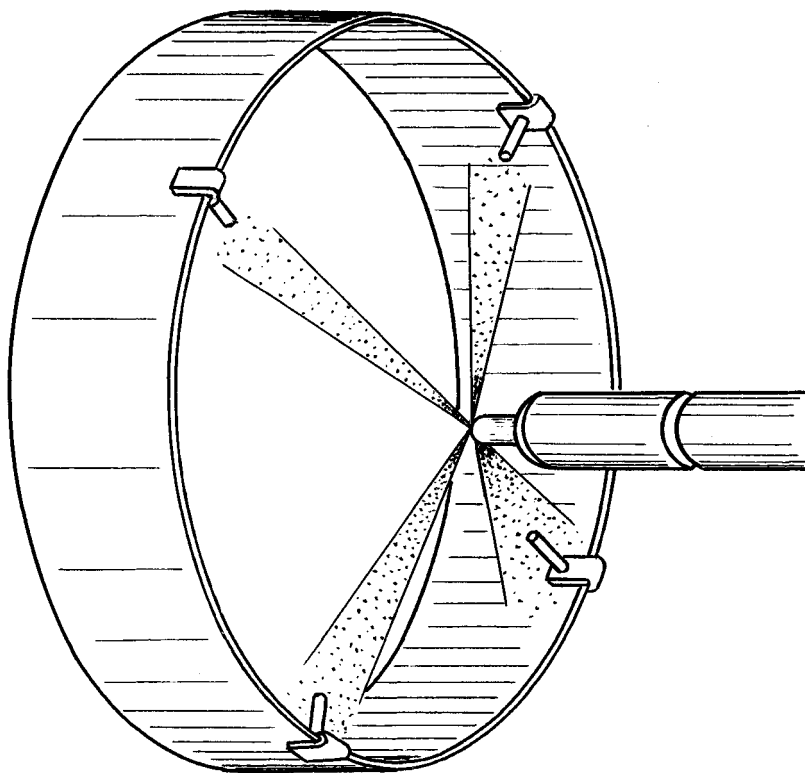


Figure 7-7 A template for checking the direction of liquid sprays.

is evaluated directly or indirectly by comparison with a standard spray. During investigations of continuous atomizers an optical system is used to project the spray contour on a screen and measure the angle α to compare it with the contour of a standard spray.

Photographic method. This is the most accurate method because a picture of the spray is obtained and subsequently enlarged and measured. A good picture can be obtained by photographing the jet against a background in the form of a screen made of black velvet. A flashlight is used for illumination. The error of reading small injection pressures is $\pm 2\%$ and high pressures is $\pm 5\%$. This error can be reduced by improving the image sharpness. Such conditions are assured by a flashlight with a very short exposure time of order $1 \mu\text{s}$.

Figure 7-8 shows the results of photographic measurements of the angle of a swirl atomizer carried out by using a spark light source and a flashlight for various injection pressures P or Reynolds numbers (corresponding to the discharge) [74]. In the case of the spark light source the measurement error is relatively high, especially for higher injection pressures; for the flashlight the error is smaller because of the shorter and better illumination.

Also shown are the results of measuring angle α_m for the same swirl atomizer. Angle α_m corresponds to the contour of a spray with the maximum liquid density $q = q_{\max}$. The method of measuring α_m follows from Fig. 7-11a. Knowledge of angle α_m is necessary for some processes, as follows from Fig. 3-13. It is seen that the measurement of α can be carried out with high accuracy. The process of change of angles α and α_m as a function of P is different. This stems from the fact that the photographic measurement registers the contour of small drops, whose number increases as pressure P increases, and the spray contour expressed by angle α_m decreases because as the injection pressure (velocity) increases the drag forces increase.

The measurements just described concern atomization in a stationary environment. In [79] a single-orifice diesel injector was investigated during injection

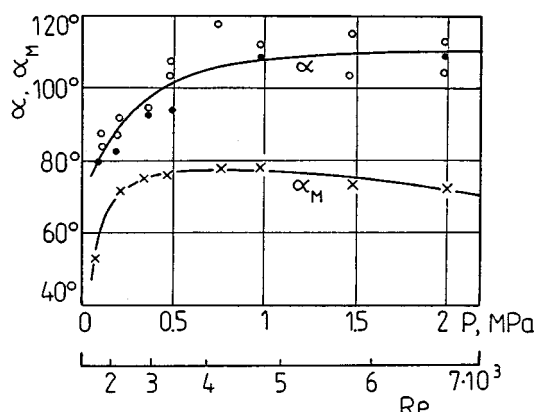


Figure 7-8 Comparison of the results of measurements of angles α and α_M as a function of pressure P or Reynolds number Re ; angle α_M corresponds to a distance from the atomizer of 100 mm; diesel oil with temperature 20°C. \circ Flashlight; \bullet spark light source.

in air flow. The change of air velocity causes a change of spray angle and liquid jet shape and accelerates jet disintegration. This effect is manifested for injection pressures less than 33 MPa. Some results were discussed in Sec. 6-1.2. Liquid jet was injected into a chamber. The pressure could be varied between 8 and 80 MPa. Maximum back pressure in the chamber was 6 MPa. Spray was photographed through quartz windows during a light flash of duration 0.5 μ s. The duration of injection was 3 ms. During this time a jet of compressed air was introduced into the pressure chamber.

7-3.2 Measurement of Spray Penetration

Knowledge of the spray penetration is especially important in the case of intermittent atomizers.

Extensive investigations of spray motion were discussed in [64]. Tests were carried out in a pressure chamber of diameter 200 mm and length 400 mm. The windows of the chamber were made of organic glass and allowed illumination and photographing of the spray. The jet atomizer shown in Fig. 2-8 was used for the investigation. This atomizer operated in an intermittent mode controlled by an electromagnetic valve blocking the discharge orifice. The spray was photographed with a high-speed camera (4700 frames per second). The camera was synchronized with the electromagnetic valve.

Experimental results were shown in Figs. 6-7 and 6-9. From curves $x = f(t)$, graphs of spray front velocity w' were obtained by graphic differentiation. Results of these investigations made it possible to derive the equations presented in Sec. 6-1.2. Further research of the author of [64] on intermittent atomizers confirmed the correctness of these evaluations.

In [108] spray penetration and spray angle of single-orifice diesel injectors during changes of back pressure and gas temperature were investigated. Special attention was directed toward the initial stage of the injection. Investigations were carried out during transverse injection in a wind tunnel. Spray was photographed during a light flash of duration 0.1 μ s. A high-speed camera (Hadland) with 11000 frames per second was also used.

At a later stage of the work [108] a new technique was used to measure the spray penetration. A small area of the flow was focused on a photodiode by a lens system, using a collimated light beam to illuminate the spray. When the shadow of the front edge of the spray passes over the photodiode the output voltage drops. The difference between the time of the initial rise of the needle lift signal and the initial drop of the photodiode signal gives the penetration time, and the distance of penetration is known from the position of the photodiode in the spray.

In [50] the length L_c of a compact jet in a high-pressure chamber filled with nitrogen (from atmospheric pressure to 5 MPa) was investigated. The injection pressure was changed in the range 0.1 to 70 mPa. The maximum velocity of the water jet was 190 m/s, which corresponds to Reynolds number $Re = 6.4 \times 10^4$. Investigations were carried out using the stand shown in Fig. 7-9.

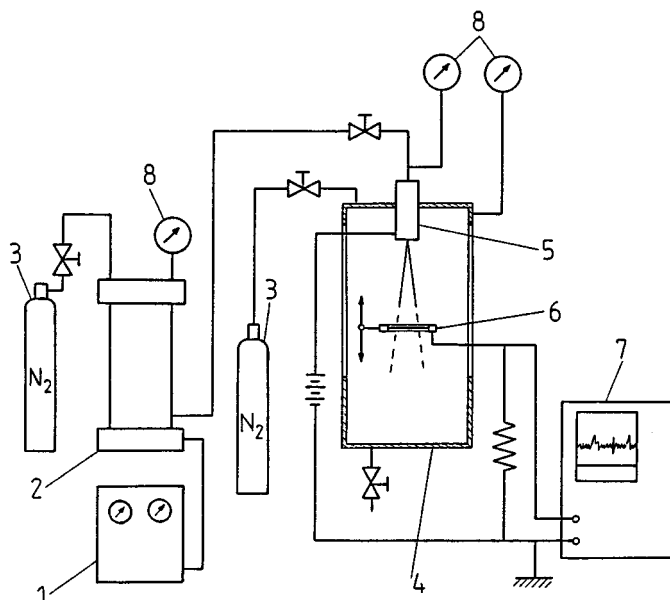


Figure 7-9 Schematic diagram of a stand for measurements of a compact jet of water. 1, Pump; 2, pressure accumulator; 3, gas cylinder; 4, test chamber; 5, injector; 6, wire electrode; 7, oscilloscope; 8, pressure gauge.

The measurement of length L_c was based on measuring the electrical resistivity of the jet between the atomizer and the detector, which had a form of a fine wire screen. The DC voltage was 30 V. The wire electrode was moving up and down. The voltage in the water jet was observed on the oscilloscope screen. When the wire screen was placed in the compact jet region the signal showed low resistance, but when the screen was moved to the drop region the resistance increased significantly.

The length of the compact jet and the disintegration conditions were the subjects of research reported in [65]. Investigations were carried out using a high-speed photographic system with a flashlight source of original design. Fig. 2-3 shows pictures of such sprays.

Liquid films as well as liquid jets have been the subject of investigations. Measurements include the film penetration and the conditions of its disintegration. The most commonly measured parameter is the *film thickness* δ , since it is inversely proportional to the film penetration, i.e., to distance x from the atomizer:

$$\delta = \frac{K}{x} \quad (7-6)$$

The simplest way to measure liquid film thickness is to use a dial gauge. In this way, the liquid film thickness during the operation of the *jet blast atomizer*

shown in Fig. 5-4 was measured [68]. Velocity of the film at the edge of the cone deflector was measured by means of a Pitot tube with inside diameter 0.5 mm and outside diameter 1.0 mm. The measurement of the film thickness was done by observing the standing waves when the needle just reached the liquid surface.

Figure 7-10 shows a schematic diagram of a stand for measuring the penetration distance of a water film during its impingement with a gas jet at various angles φ [99]. Such conditions of motion and disintegration of a liquid film are present in *pneumatic atomizers* with external gas operation. The liquid film was generated by a fan spray nozzle and the flat air jet was discharged from a rectangular nozzle. In this measurement the distance between the air nozzle and film surface was constant and equal to $s = 3$ mm. The water film thickness at the point of impingement with the air jet varied depending on distance x .

The film penetration, amplitude of vibrations, and wave frequency were measured by a contact needle method. The liquid film and the needle constitute part of an electric circuit. The number of closed circuits per unit time indicates the frequency of the waves.

A similar measurement system containing a platinum electrode in the form of a micrometric needle was employed in [69]. The film thickness on the edge of a rotary disk atomizer was measured. Such a measurement system is accurate enough when the film thickness is of the order of several hundred micrometers.

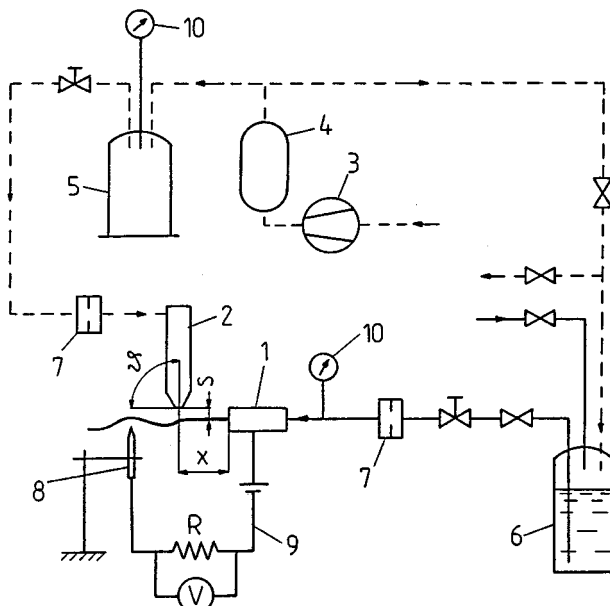


Figure 7-10 Schematic diagram of a stand for the measurement of liquid film thickness. 1, Atomizer; 2, air nozzle; 3, air compressor; 4, surge tank; 5, air reservoir; 6, liquid reservoir; 7, metering orifice; 8, contact needle; 9, electric circuit; 10 pressure gauge.

7-3.3 Measurement of the Liquid Distribution in a Spray

As mentioned in Sec. 3-2.3, the liquid distribution is determined only experimentally. The radial distribution $q = f(r)$ and circumferential distribution $q = f(\varphi)$, where q is the density of the liquid jet, are most important. In aerial spraying for agricultural purposes the transverse liquid distribution is also measured. Measurements of liquid distribution are simple and do not require complex instrumentation.

Radial distribution of liquid jet density $q = f(r)$. The measurement is realized by collecting the spray into vessels whose inlet surfaces are placed perpendicular to the atomizer's axis (Fig. 7-11). The measuring vessels can have various forms. The principle of measurements is that the liquid has to be collected on known radii by means of vessels with the same areas.

Most commonly a number of identical cylindrical vessels are used. They are placed along the diameter or along two perpendicular diameters of the jet to improve the accuracy of measurements (Fig. 7-11a). In most cases glass tubes of

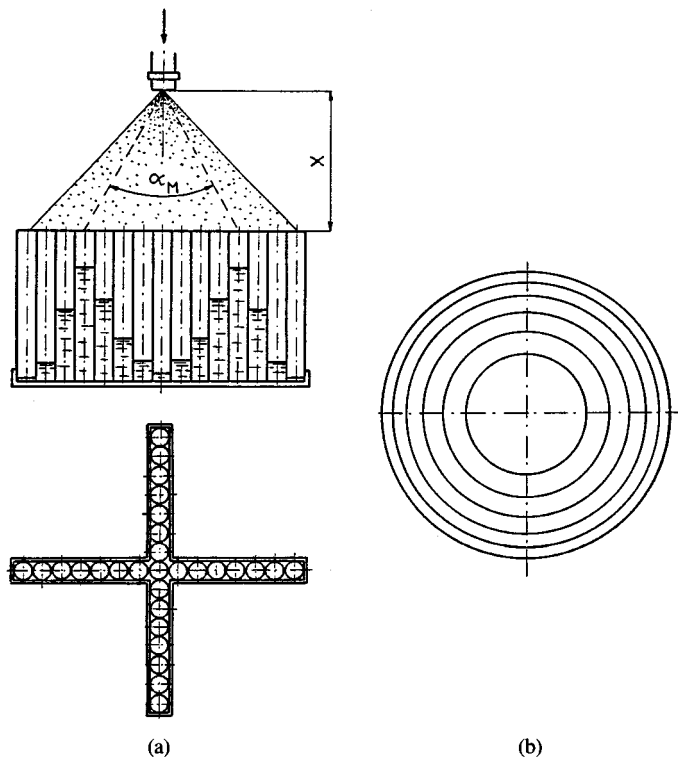


Figure 7-11 Measurement of radial distribution of liquid jet density $q = f(\varphi)$. (a) Set of cylindrical vessels; (b) vessels with concentric segments.

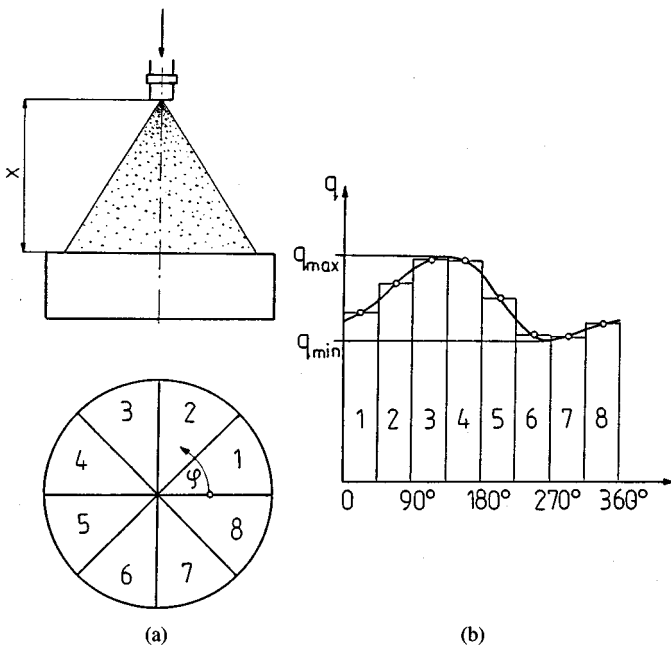


Figure 7-12 Measurement of circumferential liquid jet density $q = f(\varphi)$: (a) measuring vessel; (b) graph $q = f(\varphi)$.

diameter 6 mm and length 10 cm are used. The liquid level in tubes can be read directly or from a photograph. In modern test stands the liquid level in tubes is recorded by an electronic scanner system and transmitted to a computer, and liquid distribution diagrams are printed out. Figure 7-11a shows angle α_m , which was discussed in Sec. 7-3.1.

The tin vessel shown in Fig. 7-11b is composed of several concentric segments of the same area. Liquid is drained through the holes at the bottom of each segment to the glass measures. The whole spray is collected by the vessel, which improves the accuracy of measurements.

Circumferential distribution of liquid jet density $q = f(\varphi)$. The measurement is done by collecting the spray to a segmented vessel as shown in Fig. 7-12a. In this case the vessel has $n = 8$ identical circumferential segments from which the liquid is drained through the holes at the bottom of each segment to glass measures. A graph $q = f(\varphi)$ is obtained, as shown in Fig. 7-12b.

Circumferential nonuniformity I expressed by Eq. (3-37) assumes the form

$$I = \frac{(l_{\max} - l_{\min})n}{\sum_{i=1}^n l_i} \times 100 [\%] \quad (7-7)$$

where l_{\max} , l_{\min} , and l_i are the maximum, minimum, and instantaneous liquid

heights in glass measures in arbitrary units of length. In Eq. (7-7) densities of the liquid jet were replaced by corresponding liquid heights, which is understandable for this measuring technique.

It follows from Eq. (7-7) that nonuniformity I increases as the number n of segments increases. Usually $n = 12$ is used. In order to ensure comparability of results, the liquid should be collected at the same distance x from the atomizer and for the same pressure drop ΔP . Experiments [74] show that for small distances x ($x \approx 50$ mm or less) the value I is almost independent of ΔP . For larger distances x the interaction of the gas being ejected is so high that nonuniformity I increases significantly.

Transverse liquid distribution. The transverse distribution of liquid and an indicator of the nonuniformity of the transverse liquid distribution δ were discussed in Sec. 3-2.3. These are of interest in relation to the liquid distribution on the sprayed surface of plants. The transverse liquid distribution is related to a group of pressure atomizers (fan, swirl) or rotary atomizers during their uniform horizontal motion. The transverse distribution is measured on a stand equipped with a grooved table as shown in Fig. 7-13. The width of grooves is for example, 25 mm.

In discussing the measurement of the liquid distribution earlier we referred to atomization in a stationary environment. The liquid distribution in a liquid jet during concurrent flow of an air jet was the subject of measurements in [35]. Figure 2-42 shows the interaction between the spray and the drifting air and a

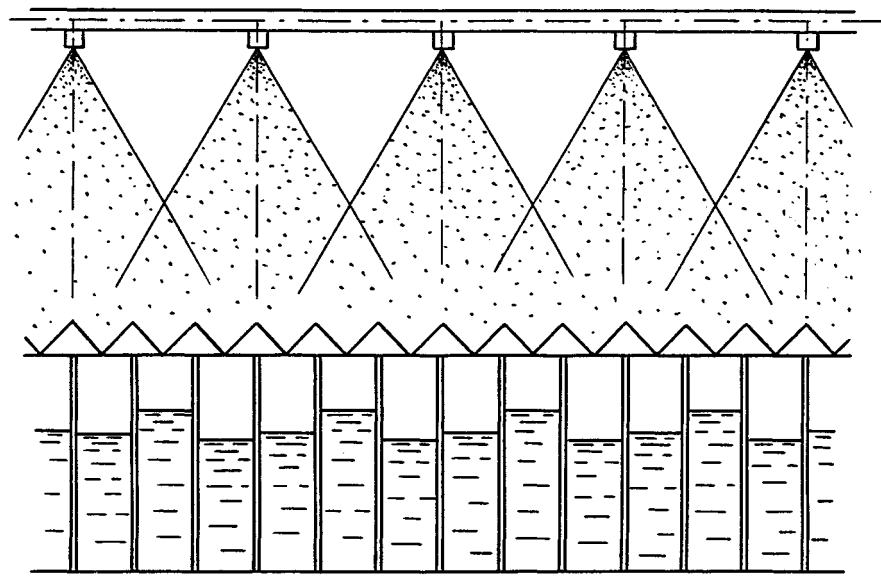


Figure 7-13 Grooved table for measurements of the transverse distribution of liquid.

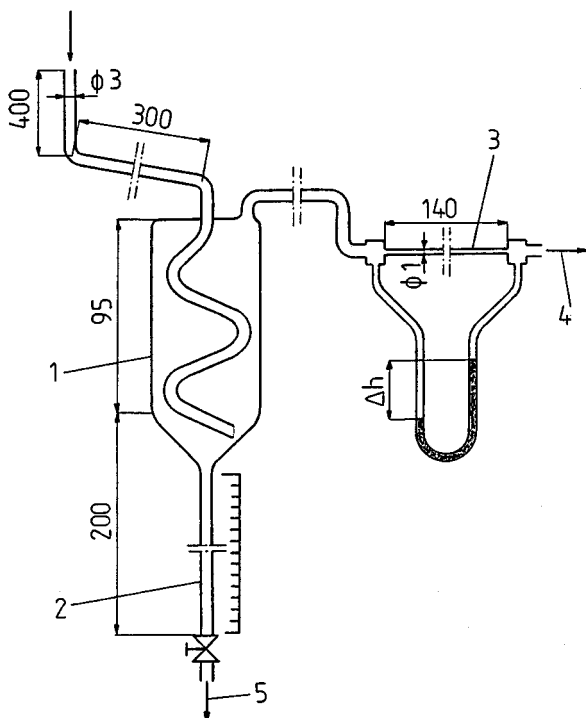


Figure 7-14 Isokinetic probe for sampling the gas-liquid mixture. 1, Separation vessel; 2, metering tube; 3, capillary tube; 4, to suction system; 5, drain. All dimensions are in mm.

graphic representation of the air streamlines. A similar state exists during spraying in a stationary environment, but the effect of the air sucked in by the jet is much smaller.

An isokinetic two-phase sampling apparatus (Fig. 7-14) has been designed to measure drop fluxes, from which gas/liquid mass flux ratios have been calculated. A simple optical arrangement has been developed and used to photograph spray drops in flight. A double-flash technique has been adopted to make measurements of drop size distributions, drop velocities, and directions of drop trajectories. The interval period between two flashes was 10–50 μ s. By separating each pair of images, it was possible to deduce drop velocity and drop flight direction.

7-4 DROP SIZING METHODS BASED ON DROP SAMPLING

7-4.1 General Remarks

Not too long ago, liquid atomizers were characterized and judged primarily on the basis of their capacities and spray patterns. Now, however, the significance of droplet size distribution in most applications is appreciated. The need to form

droplets with controlled size distributions, spray patterns, and flow rates and to correlate this information with the associated phenomena spans a broad range of applications. In oil burners, flame stability, combustion efficiency, and emissions are drastically affected by the quality of atomization. For example, in a gas turbine combustor, the droplet spectrum is a key indicator of ignition and burning characteristics that are affected by fuel properties. Droplet size is of considerable interest to those who design and operate evaporative coolers, spray driers, and flue gas desulfurization plants. In such processes, the drop surface area must be known to calculate heat and mass transfer. In spray drying there is direct relationship between the size spectrum of the liquid droplets and the powder product. In agricultural spraying, drop drift and coverage of crops and weeds are directly affected by droplet size, and similar considerations are involved in spray painting and other coating operations.

Driven by the need to perform drop size measurements in a spray accurately and rapidly, instrumentation based on many different concepts has been developed. The ideal drop sizing technique should not interfere with a spray pattern or liquid breakup process, have good size discrimination over the entire range of drop size distribution measured, tolerate variations in the liquid and ambient gas properties, and permit determination of both the spatial and temporal drop size distributions. Other requirements are high accuracy, short measurement time, suitability for both laboratory and field measurements, and ease of processing the results of measurements. Clearly, it is not possible to fulfill all of these requirements simultaneously. The user of the methods and instruments for drop size measurements must be aware of the capabilities and limitations of the measuring technique applied. Before 1977, methods of drop size measurement based on sampling were widely used. Individual liquid droplets were collected for subsequent observation or counting. In some methods drops were preserved long enough for counting. In others they created stains or impressions on sampling cards or coated slides. In certain sampling methods droplets are frozen or cooled and sized as solid particles. There are methods in which droplets are sorted on the basis of inertial or velocity differences. Depending on its size, a droplet may strike or fail to strike on a solid surface or may follow a different trajectory. The kinetic behavior within a spray may be used to differentiate between droplet size ranges. Other methods include hot-wire anemometry and electrostatic charging of droplets. Detailed surveys of drop size measuring

Table 7-1 Accuracy of Determination of the Sauter Mean Diameter D_{32} as a Function of the Quantity of Drops

Number of drops	Accuracy (%)
500	±17
1400	±10
5500	±5
35000	±2

techniques were presented by Azzopardi [4], Bachalo [6], Chigier [29–31], Hirleman [46]. Drop sizing techniques should provide large representative samples to ensure required accuracy of measurements. The relation between the accuracy of determination of the Sauter mean diameter D_{32} and the quantity of drops in the sample can be seen in Table 7-1 [4]. For example, to achieve a reasonably accurate measurement of size distribution (5%), the sample should contain at least 5500 drops.

7-4.2 Drop Sizing Methods Based on Drop Sampling

In this section the following methods will be discussed:

Drop collection on slides or in cells

Frozen drop techniques

Substitute liquid techniques

Gravitational classification

Drop evaporation technique

Sedimentation

Contact electrode method

Charged wire method

Slide sampling method. This method is based on drop deposition on a flat surface with a suitable structure. Such a surface might be a plate covered with a suitable filter paper. In experiments the best results were obtained with a layer of magnesium oxide or a layer of soot. A layer of magnesium oxide can easily be deposited uniformly but has poor adhesion. Soot has much better adhesion but is more difficult to deposit uniformly. The best results are obtained using a layer of soot with a thin layer of magnesium oxide on top. A layer of soot is deposited by burning a wick soaked in petroleum or kerosene. Magnesium oxide is deposited by burning a magnesium ribbon.

A drop deposited on such a layer creates a trace (crater). The drop trace is usually larger than the drop diameter D , and the relationship between these diameters is described by an empirical equation given by A. Stocker [25]:

$$\frac{d}{D} = 0.77 \text{ We}^{0.2}, \quad (7-8)$$

where the Weber number is equal to

$$\text{We} = \frac{\rho_L V_D^2 D}{\sigma},$$

and V_D is the drop velocity before a collision.

Equation (7-8) does not take into account the soot layer thickness h . For $\text{We} > 1500$ and $h/D > 1.5$, ratio d/D does not depend on h any more and therefore one can assume $d = D$. For drops with diameter $D = 200 \mu\text{m}$ the

thickness of the soot layer should be $h \approx 300\text{--}500 \mu\text{m}$. This method is applicable for drop diameters $D = 30\text{--}500 \mu\text{m}$. Drops smaller than $30 \mu\text{m}$ do not puncture the soot coating and do not create a trace. Drops larger than $500 \mu\text{m}$ require a coating layer of thickness 1 mm, but such a layer is not stable.

During the drop sampling the plate is placed perpendicular to the drop motion. If the drops drift with a gas jet, smaller drops flow around the plate with the gas. This leads to distortion of the measured drop spectrum. The increase of plate dimensions does not improve the effectiveness of drop deposition. Plate width s can be calculated from the following condition [74]

$$\frac{\rho_L V_G D^2}{9\mu_G s} > 50 \quad (7-9)$$

where V_G is the velocity of undisturbed gas flow at a certain distance from the plate.

Condition (7-9) was obtained from the theory of the flow around the plate under the following assumptions:

Velocity of gas and velocity of drops in front of the plate are the same.

Drop drag is described by the Stokes equation [Eq. (2-112)].

Length of the plate is much larger than its width.

Velocity of gas flow around the plate is small compared to the velocity of sound.

It follows from inequality (7-9) that the plate width s is very small, particularly for measurements of drops with small diameters and small flow velocities. For practical reasons the environment plate width cannot be smaller than $s = 2 \text{ mm}$. Drop sampling in a stationary environment is not difficult in this respect.

Probes used for drop sampling are designed to capture on a plate or rod a relatively small number of drops in order to prevent their traces from overlapping. The exposure time of the plate should be short, which is achieved by using various revolving or sliding shutters.

Rotary shutters usually have the form of a concentric tube with a slit. Due to the tube rotation the drops pass through the slit and are deposited on the soot film. Sliding shutters have the form of a tube with a slit through which drops pass and are deposited on a sliding shuttle with a plate. The problem of probes will be discussed further in the description of the immersion liquid method of drop sampling.

In conclusion, we should list the following disadvantages of the method. The capturing layer should be properly prepared and selected for the drop sizes. Sampling drops in a jet of gas and drops from a pneumatic atomizer eliminates a portion of small drops due to the flow around the probe. Total error, including the drop trace measuring error, can be as high as $\pm 30\%$ [25]. Among other disadvantages there is a high labor demand, for preparation of probes, taking

numerous samples of drops, photographing and preparing blowups, drop counting, and processing the results.

Despite these disadvantages, the slide sampling method using soot has had vast application. It is a natural method that does not require expensive instrumentation.

This method has been used among others in [36] for investigation of the atomization quality of a swirl atomizer. A probe with a revolving shutter consisted of a small-diameter cylinder with 10 holes of 5 mm diameter located along its length. The cylinder was placed perpendicular to the spray axis, so it was possible to sample drops at different radial distances from the atomizer axis. A soot-coated glass slide was mounted on an axle fitted inside the cylinder and could be rotated around the cylinder axis by a wheel. The probe was placed 60 mm from the atomizer.

Examples of measurements conducted under field (real) conditions are those made during aerial agriculture spraying. This type of spraying should take into account the flight conditions (velocity, altitude), atmospheric conditions (wind, humidity), etc. For the measurements a dyed liquid is used and drops are captured on equally spaced (1–3 m) measuring devices such as plates, glass vessels, or ribbons of white paper. The drop traces are highly enlarged with respect to drop sizes, and drop diameters are determined by calibrating the trace development phenomenon. For such measurements specially equipped vehicles are often used instead of more expensive aerial measurements.

Immersion liquid sampling method. This has many features in common with the previous method but the properties of the sampling layer are different. The probe used for drop sampling usually contains a small transparent vessel of diameter 3–9 mm (Petri dish). The immersion liquid should have the following features:

Chemically neutral

Transparent

Have density lower than the density of the liquid being atomized

Immiscible with the atomized liquid

Low evaporation pressure

Low surface tension

Requirements regarding the viscosity of the immersion liquid will be discussed separately. Generally speaking, oils with high viscosity are used for measurements of large drops.

Drops embedded in the immersion liquid are clearly visible and give sharp photographic images. This refers particularly to drops of water and water solutions, but there are some difficulties in selecting immersion liquids for hydrocarbon fuels. During the drop sampling, various errors occur. The error due to the flow of small drops around the probe is the same as in the slide

sampling method. Other errors include drop coalescence, secondary drop disintegration caused by collision with the liquid surface, and drop evaporation.

Drop coalescence causes an increase of drop diameters. The coalescence occurs at the surface or inside the immersion liquid. In [133] the effect of various factors on drop coalescence was investigated. It was established that increasing number of droplets, higher viscosity of immersion liquid, and smaller droplet diameter have a tendency to increase the mean diameter due to the droplet coalescence. For example, a four times prolonged interval of drop sampling results in a double increase of Sauter mean diameter D_{32} due to drop coalescence.

The increase in drop coalescence with increasing immersion liquid viscosity is due to the greater time needed for submerging the droplets. The sampling period should be adjusted to the optimum concentration of droplets in the immersion liquid. For given atomization conditions, the concentration of drops is a function of distance from the atomizer. In general, drops are sampled at distances 10–50 cm.

Drop disintegration during collision with the immersion liquid surface involves large drops. It was established that the discharge velocity of the jet does not affect droplet coalescence remarkably. Drop evaporation does not occur as long as drops are completely submerged in the immersion liquid. The velocity of submerging is higher the lower the immersion liquid viscosity. For example, water drops of diameter 10 μm evaporate in 60 seconds after their capture.

Immersion liquids such as mineral oils, glycerin, and its water solutions are used. All of them have similar surface tensions. Immersion liquids with high viscosities of 0.3–1.0 $\text{Pa} \cdot \text{s}$ hinder drop submergence. Widely used immersion liquid is silicone oil, which has a low surface tension of $19\text{--}21 \times 10^{-3}$ N/m and viscosity 0.05–1.0 $\text{Pa} \cdot \text{s}$ or higher. The thickness of the liquid layer is usually 0.5–1.0 mm.

The immersion liquid method has been used in [49]. The distribution of diameters of drops of diesel oil was measured at various stages of injection. The fuel was fed by the injection system of a high-speed diesel engine. An element of spray was sampled with an instantaneously sliding shutter. The test stand is shown in Fig. 7-15.

Sliding shutters operated with a DC solenoid has a stroke of 16 mm. The shutter velocity was calibrated by lamp 11 and phototransistor 10. In order to obtain a synchronizing signal an impulse generator was installed on the axle of the injection pump, which had a disk (17) with a slit, lamp (18), and phototransistor (19). A signal from the injection pump was transmitted to the shutter. The drops fell into the immersion liquid in a small transparent vessel (14), which was placed 16 cm below the atomizer. A special immersion liquid selected for fuel drops was used.

A sliding shutter was also used in [91]. A cylindrical shield 15 mm in diameter and with a slit was moved axially driven by a spring. The drops were sampled into a silicone oil. The measurements were carried out for the pneumatic atomizer shown in Fig. 4-53.

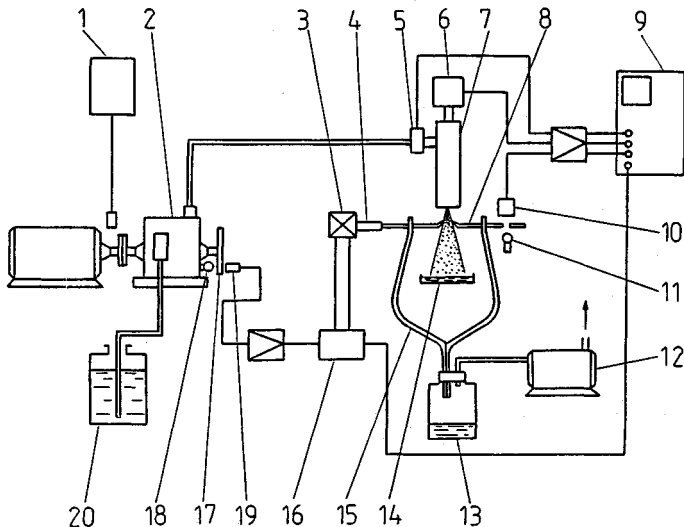


Figure 7-15 Test stand for drop sampling by immersion liquid. 1, Tachometer; 2, injection pump-Bosch type; 3, DC solenoid coil; 4, DC solenoid plunger; 5, semiconductor strain-gauge transducer; 6, light beam chopping-type needle lift detector; 7, injector; 8, sliding shutter; 9, oscilloscope; 10, phototransistor; 11, lamp; 12, vacuum pump; 13, vessel; 14, sampling cell; 15, Teflon tube; 16, SCR switching element; 17, disk for pulse generator, 18, lamp; 19, phototransistor; 20, fuel tank.

In [1] measurements done by means of revolving shutters were considered. Stand design, instrumentation, and sources of errors including the error of breaking of drops by the shutter operation and by the edge of the slit are described. A system for measuring drops smaller than $400 \mu\text{m}$ was built. The drops were sampled into silicone oil by a slit with dimensions $3 \times 5 \text{ mm}$ or $2.7 \times 5 \text{ mm}$ (Fig. 7-16). A reflecting aluminum foil was placed at the bottom of the cell with silicone oil in order to take microphotographs of drops.

In [80] a cylindrical rotary shutter was used for the measurements of drops of a pulverized coal-water mixture, pulverized coal-oil mixture, etc. The mixture was atomized by a pneumatic atomizer. During the atomization of water mixtures silicone oil with viscosity $1 \text{ Pa} \cdot \text{s}$ was used as the immersion liquid. During atomization of oil mixtures an ethylcellulose-ethanol solution was used. The exposure interval of the shutter was 14.7 ms, which allowed sampling of 700–1400 drops per cm^2 of the cell.

Measurement of atomization quality of a pneumatic atomizer was carried out in [92], also by immersion liquid method. The drops were sampled into a cell with a glass bottom using silicone oil as the immersion liquid.

The Delavan Corporation also used the immersion sampling method. In experimental procedures, spray droplets are collected in a solvent medium. These droplets quickly settle to the bottom of the cell, where they remain suspended as nearly perfect spheres. Photographs are taken at high magnifica-

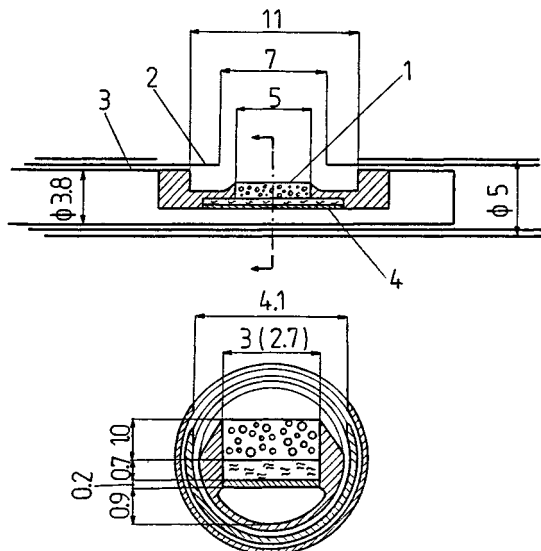


Figure 7-16 Drop sampling system with a tubular shutter. 1, Drop sampling cell; 2, tubular shutter, 3, tubular holder; 4, aluminum foil. All dimensions are in mm.

tion using a photomicrographic camera. Magnified drop images are scanned, and a photomultiplier receives a series of light pulses whose duration corresponds to the size of the drop. The final computer printout shows the droplet volume distribution. This technique is restricted to water or aqueous solutions that are immiscible with the sampling solvent. Fuel sprays cannot be measured by this method.

Drop freezing method. Drop freezing was one of the earliest methods used to measure spray microstructure. This method was originally used at the Massachusetts Institute of Technology to measure atomized diesel oil. Drops fell into cooled spirit and were sorted by sieving. The method of drop freezing is still used but in a completely different form.

The drop freezing method using liquid nitrogen is discussed in detail in [61]. The authors developed and demonstrated designs of five versions of the measuring instruments and the final version, which is based on the following principles:

Cold room should be airtight in order to prevent mist development.
In order to completely freeze the drops, room height should be 2 m.
Cold room should be thermally insulated.

Initially, microphotography of frozen drops through the transparent bottom of the chamber was used. The camera was placed outside the chamber, which was illuminated from inside. In the final version a direct photography technique,

i.e., a photograph method, was applied. In this method frozen droplets are placed on the film surface and their shadows are photographed directly without using a camera. The test of this apparatus was carried out on a gasoline spray. In [77] an isokinetic sampling probe for drop sampling (Fig. 7-17) was developed. The probe could determine the number and the sizes of the drops in the sample. The probe was cooled with gaseous nitrogen to a temperature lower than the freezing point of the atomized liquid. The temperature of the gaseous nitrogen was 140 K and the temperature of frozen drops 195 K. These techniques are intended for measurements in flowing, not stationary, gas.

Isokinetic conditions in the sampling probe can be maintained by adjusting the velocity and static pressure in the flow stream ahead of the probe. A static pressure hole was provided at the probe mouth for this purpose.

Frozen drops of aircraft kerosene were transferred to a transparent vessel filled with liquid nitrogen and photographed. The water drop diameters tend to increase during the freezing process by about 2% and the drops of kerosene decrease by about 5–7%.

Substitute liquid method. This method is based on replacing the actual liquid with another one which, after atomization, solidifies immediately in air. The substitute liquid is under normal conditions a solid body, which has to be melted and heated to the proper temperature. The temperature is selected to achieve properties of the substitute liquid similar to those of the real liquid. The substance used as the substitute liquid should have a low melting point, low partial vapor pressure in the molten state, and a small contraction coefficient during solidification.

As substitute liquids, paraffin, ceresin, wax, etc. are used. For example, paraffin heated to 90–91°C has properties similar to those of kerosene, and heated to 70°C has properties like diesel oil. Benzene carboxylic acid

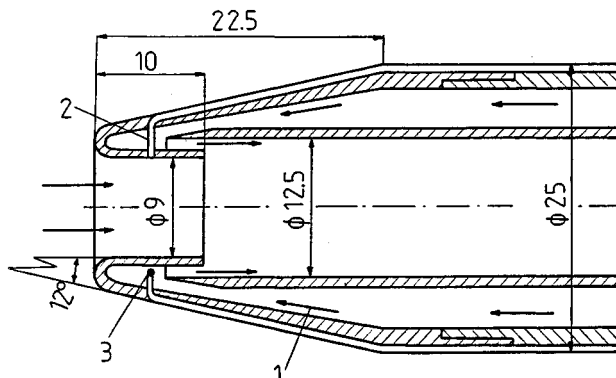


Figure 7-17 Probe head for drop sampling and freezing. 1, Cold nitrogen gas; 2, static pressure tube; 3, thermocouple. All dimensions are in mm.

(C₆H₅COOH), melting point 121.5°C, after solidification produces hard, non-sticking balls, which is not the case for ozocerite.

Solidified drops (balls) are captured from the water or other liquid to prevent them from conglutination. For paraffin drops the most suitable liquid is ethanol. The balls together with the liquid are sieved through a series of screens with different mesh sizes. During this *screen analysis*, balls larger than the mesh deposit on the screen. Each fraction of balls is weighed and counted. Balls smaller than about 60 μm cannot be sieved and therefore are measured by the sedimentation method.

The advantage of this method is the simplicity of determining the number of drops in each diameter fraction. The drop sample is representative, since it contains several millions of drops. Repeatability of measurements is very high because the error of measurements of the mean diameter does not exceed 5–7% [25]. The measurement time is approximately 10 times shorter than the measurement time of the slide sampling method. The basic disadvantage of this method is that the drop diameters differ from those obtained under identical conditions for the actual liquid. For swirl atomizers the drops of the substitute liquid are smaller but a quantitative relation has not been found. This method is not suitable for pneumatic atomizers since it does not take into consideration the gas operation during drop development.

Gravitational classification method. This method has several variations but its principle is based on the analysis of differential penetration of drops during their fall in a stationary environment. When a pressure atomizer (jet or swirl) or a pneumatic one is placed horizontally, a natural classification of drops takes place, since large drops will fall farther from the atomizer than small ones. The drops can be sampled and weighed, and small drop samples can be measured by means of a microscope. By dividing the mass of captured drops by the calculated mass of a single drop, the number of drops in each diameter range can be determined.

Such a classification is unequivocal when drops have the same initial velocity and direction. This condition is satisfied best by jet atomizers, worse by pneumatic atomizers, and worst by swirl atomizers with a large spray angle.

Gravitational classification is particularly suitable for rotary atomizers with vertical axle of rotation. The drops centrifuged off the atomizer's edge fall along the trajectories shown in Fig. 2-39. They generate coaxial annuli consisting of drops with the same diameters, which is clearly visible in Fig. 2-49.

Drop evaporation method. This method uses the fact that the drop evaporation time under particular conditions depends on the drop's initial size. The measurement is based on capturing the drops on a mica plate and then continuously measuring drop mass loss by using a microanalytic balance. On the basis of the evaporation law for a single drop with a known diameter it is possible to determine a curve of the mass loss of the drop sample with a polydisperse character.

Sedimentation method. This method uses different times of sedimentation of drops depending on their sizes. The time of falling from an arbitrary height H is equal to $t = H/V_\infty$, where velocity of falling V_∞ in the laminar range follows from Eq. (2-117). Drop diameter is therefore

$$D = \frac{K}{\sqrt{t}} \quad (7-10)$$

where K is a constant for a particular measuring condition. By measuring time and simultaneously weighing falling drops, one obtains the distribution of the mean mass diameter. The sedimentation can proceed in air or in a selected liquid. Despite its very simple principle, this method is rarely used because of its poor accuracy.

The gravitational classification method can be considered a variation of the sedimentation method.

Contact electrode method. Wicks And Dukler [134] established a relationship between the frequency of registered pulses and the distribution of drop diameters using a system in which two sharp needles (electrodes) with a gap between them are placed in a spray. They are connected to a voltage source and a pulse counter, and each short circuit between needles is registered by the counter. A short circuit is caused by drops with diameters larger than the separation between the needles. During measurements this separation can be changed, which enables classification of drops into a certain diameter range. Also, it is possible to apply a system that contains several pairs of electrodes. Each pair with a different separation between the needles is connected to a separate pulse counter.

The contact probe method has several limitations. A very small voltage must be used because of the possibility of breakdowns between the electrodes. The circuit is closed during an interval one order of magnitude longer than the time in which a drop passes between the needles which is due to the phenomenon of bridging the electrodes by drops caused by the adhesive forces.

Charged wire method. The principle of measurements is based on the fact that a drop colliding with a wire connected to a voltage source removes an amount of charge depending on the drop size. As a result, information is obtained about the drop mean diameter. The measuring system must be calibrated with drops of uniform size or known mean diameter. The probe should be connected to the high-voltage source through a $10 \text{ M}\Omega$ resistor and to the meter and pulse counter by a condenser with a capacitance of 100 pF .

Generally speaking, methods based on sampling are not desirable for implementation in spray measurements. Drops are deformable and break up under aerodynamic forces and collision with probes. Nonintrusive (optical) methods are definitely preferable for drop size measurements.

7-5 OPTICAL DROP SIZING METHODS

During the past 20 years optical methods and instruments for drop sizing have been developed by W. D. Bachalo, L. P. Bayvel, K. Bauckhage, N. Chigier, G. Dodge, P. G. Felton, C. F. Hess, E. D. Hirleman, D. J. Holve, A. R. Jones, R. G. Knollenberg, A. H. Lefebvre, H. C. Simmons, J. Switzenbank, R. W. Tate, B. J. Thompson, J. M. Tishkoff, D. J. Watson, M. L. Yeoman, A. Yule, and others.

Optical drop sizing techniques can be subdivided into three categories: imaging (photography, cinematography, and holography), single drop counting, and ensemble multidrop sizing. On the other hand, all optical drop sizing methods can be divided into two classes, one representing spatial averaging (imaging techniques and ensemble drop sizing) and the second temporal averaging (single drop counting). The choice of a technique and an instrument for drop size distribution measurement that are most appropriate for a particular spray system depends on the application.

7-5.1 Imaging Techniques

Nonintrusive imaging techniques include photography, cinematography, video-based systems, shadowgraphy, and holography. Imaging methods are accurate and reliable. The longest established and most inexpensive imaging method is photography. This technique essentially involves direct photography of a spray followed by analysis of the processed film. After development, the negative can be projected at greatly increased magnification to obtain a direct measurement of particle size.

Microphotography with focus discrimination has been used for many years for characterization of sprays. The number of drops that can be examined is limited by the field of view, the depth of field, the frequency of taking photographs, and the tedium of direct measurement of size of individual drops. Advantages of the photographic technique are simplicity, relatively low cost of photographic apparatus, flexibility, relative insensitivity to the optical properties of the particles, and derivation of drop velocity by using double exposures. As a consequence of the imperfections of optical systems (geometric and chromatic aberrations), it is impossible to measure size drops smaller than $10 \mu\text{m}$.

In order to reduce image blur, short-duration sparks are used as the source of illumination for moving drops. Unfortunately, the shortest duration produced by conventional units is approximately $0.5 \mu\text{s}$, which for fine, fast moving drops would introduce considerably elongation of the image blurs, making analysis difficult. Attempts have been made [54, 56] to use a pulsed laser as the source of illumination; use of a considerably reduced pulse duration (20 ns) would effectively freeze all the drops. These attempts were unsuccessful because the high coherence of the laser gave rise to speckle. The highly variable background intensity had the effect of engulfing small drops altogether and made it difficult to identify clear outlines of the remaining drops. These photographs were of

such poor quality that any attempt at automatic analysis would have been futile. Tests have been made using an argon jet spark light source. In this device four $0.01-\mu\text{F}$ capacitors surrounding a gap produced by two tungsten electrodes were first enlarged to a potential of 11 kV and then discharged rapidly across the gap through which argon was flowing. The pulse duration was about 260 ns. The general quality of the argon jet photograph is such that the background is of more uniform intensity, allowing identification of small particles. When considered for automatic analysis, however, the general improvement in image quality is offset by the existence of image blur.

Jones and Sargeant [56] have developed a photographic system. The camera is a 35-mm Nikon Photomic complete with motor drive. After the film is loaded, the motor drive winds the film and sets the shutter each time the shutter release is pressed. This, combined with a remotely controlled shutter release, ensures that once in position the camera cannot be moved inadvertently during the series of exposures. Synchronization with the spark light source can be done at a camera speed of 1/80s, ensuring minimum exposure to the ambient light. A double-spark argon jet light source manufactured by Lunartron was used. Integrated with it was a delay generator designed and built at Joseph Lucas, Burnley, which enabled time intervals between pulses to be varied between 4 μs and 70 ms. Compared with this single-pulse unit, the sparks of the double-pulse unit were some 35% shorter, 170 ns as opposed to 260 ns. The reduced duration of the sparks from the double-pulse unit was found to produce good-quality photographs and no derating of the unit was required, thus allowing sparks of maximum intensity to be produced. A significant improvement in the amount of light available for photography was obtained by replacing the Lunartron unit by a 2.5-J single argon stabilized spark gap manufactured by Pulse (Instrumentation Controllers) Ltd. This unit is designed to collect as much of the available spark energy as possible.

Chella *et al.* [28] described a high-speed photographic system that was applied in spray diagnosis. In this system a flashlight source of original design is used, and very short duration sparks (half width 20 ns) with high irradiated energy are obtained. The spark is focused in a certain region of spray with an achromatic condenser. An electronic systems controls the double-flash light source of variable interspark interval (0.5–15 ps). The sequence of events consists of operating the camera shutter, firing the first spark, firing the second spark after a short and variable time interval, and closing the camera shutter. This procedure results in photographic recording of the drops in a given position within the spray image at two points. Knowing the time interval between the sparks makes it possible to calculate the velocity of drops.

Yule *et al.* [111] used a photographic technique to study pulsed, nonburning sprays produced by single-hole diesel injectors. They used a technique similar to that in [108] with $12 \times$ magnification and a spark duration of 0.1 ps. Polaroid type 52 film was used with a 5 \times 4 inch technical camera back. The timing of spark photographs of the sprays must be synchronized with respect to the commencement of each spray pulse, and this was achieved by deriving a

triggering voltage pulse from the commencement of the needle lift signal. A time delay circuit enabled the spark to be fired at a controlled time after the beginning of injection. The optical system could be traversed so that the first 200 mm of sprays could be examined.

High-speed cinephotography was also applied to sprays using a Hadland camera capable of a maximum rate of 11,000 frames per second. Continuous backlighting of the sprays was used and a computerized film analyzer system was used to measure spray parameters from images on the frames.

The major drawback associated with photographic techniques for measuring drop sizes is the requirement for tedious, time-consuming, manual analysis of photographs. It is difficult to identify true diameters on a blurred image, and the analyst must use judgment in order to select only in-focus drops. Because the transition from in focus to out of focus is gradual, there is a range of image qualities over which it is difficult to assess the condition of the image. Therefore it is difficult to apply a consistent focus criterion. Before the photographic technique can be seriously considered as a tool, the analytical procedure must be substantially speeded up and at least some of the subjectivity must be removed. The speed of analysis can to some extent be increased by using a semiautomated analysis technique based on an image analysis computer such as the Quantimet 720 series, manufactured by Cambridge Instruments. In this technique the drop field is fed via an epidiascope and scanner to a display screen, where the drop images can be measured automatically. However, in-focus and out-of-focus images alike are processed unless the operator preeditsthe drop fields to remove what is considered to be out of focus. Therefore, this technique still necessitates operator involvement, which makes analysis not only slow but also potentially erroneous.

Yule *et al.* [108] have developed a totally automated analytical procedure with a minimum requirement for operator involvement. This involves imposing a focus criterion predetermined from a calibration experiment and obviates operator judgment. Although manual analysis of drop photographs is very time consuming and subject to operator fatigue and bias, automatic computer analysis of photographic prints provides rapid drop analysis at a very significant increase in cost. Photographic techniques still have an important role to play in spray analysis, particularly in studies of spray formation mechanisms, which involve detection of nonspherical structures, such as sheets, ligaments, or more complex forms of various dimensions, as well as studies in which information is required about the spray angles and structure of spray just being formed.

Simmons and Lapera [81] developed a TV image scanning system for analysis of fuel nozzle spray, which was used by Parker Hanciffin Corporation. This spray analyzer is based on the synchronous operation of an illumination source (0.5-ns xenon flashlamp) and a closed-circuit TV camera with a photo-sensitive vidicon tube. A scanning technique is used to count and measure the size of drop images on the vidicon. A detection circuit is used to establish whether a drop is in focus by monitoring the scanning line voltage change. After drops are classified as being in focus they are electronically identified to the

counting circuit, which sizes and places drops in the appropriate storage group. Observed date are reduced to a common unit volume basis before being displayed. The vidicon is scanned to obtain drop size information and then erased to prepare for the next cycle of measurements (15 times per second) using a telemicroscope with $6 \times$ magnification; the usable area of the vidicon space is 2 mm^2 , providing a resolution of $4 \mu\text{m}$. The fuel nozzle could be sprayed into a large chamber (1 m^3) while the instrument was focused on a small "view" volume (4 mm^3). This instrument performed satisfactorily for many years [82–84]. In 1984 it was modified [103] for use in analyzing sprays produced by the latest generation of air-atomizing nozzles, which typically have fine sprays with wide distributions and high droplet velocities. In this version of the instrument a pulsed nitrogen laser was chosen as the illumination source for improved resolution and contrast made possible by coherent ultraviolet light with a wavelength of 337.1 nm .

To prevent droplet diffraction rings or the speckle pattern created by a coherent beam, a diffusing filter has been placed between the laser and the back-lighted spray. The short pulse duration of 10 ns eliminated concern about velocity smear for almost all drops. The minimum and maximum drop sizes that the system can measure are 6 and $1200 \mu\text{m}$. The maximum drop concentration the system can handle is 10^{10} m^{-3} . The system presents drop size histograms with any size class intervals. The minimum resolution is the video scan line spacing, $3 \mu\text{m}$. After user entry of test parameters, the instrument is capable of running the entire test automatically.

Skifstad [85] has developed a video-based imaging-type system for spray analysis for measuring drops in the size range 8 – $512 \mu\text{m}$. The system has a spray along the optical axis and the experimental data are processed by a special mathematical analysis to yield the local drop size distribution. The spatial resolution is about 1 mm . The analysis of the measured data is not contingent on "quality" images in the usual sense; rather, the signals from drops of different sizes at different positions in the spray must be distinct. Therefore the method offers considerable flexibility in its implementation.

Hotham [52] described a new laser video device for spray characterization developed by laser holography. This imaging device displays drops in real time on a TV monitor at high magnification. The mechanics of atomization; formation of ligaments, hollow spheres, and drops; and processes of evaporation, agglomeration, combustion of liquid drops, and impingement are shown via slide projection and active video reply on a 45-cm monitor. In addition to the straight optical imaging technique, there is a video control circuit that is a focus selector. This selector passes only in-focus images of droplets located in a thin section of the spray and rejects all out-of focus images of droplets not in this section. Hence, a thin section may be selected at the center of the spray. Another section may be closer to the edge. This device produces the drop size distribution at each of the three sections recorded. The system can resolve 5 pm at a distance of 60 cm . The spherical drop size range covered is from $5 \mu\text{m}$ to 1 cm . The device is capable of dealing with irregularly shaped ligaments and filaments

with aspect ratio up to 1:500. After sq. 10 spraying the instrument immediately produces a size distribution plot on the video display terminal.

Yates *et al.* [105] and the Delavan Corporation [87] used a PMS probe [59] for drop size measurement. The probe utilizes a 2-mW He-Ne laser. The beam is directed across an open area 6.1 cm wide and onto a 64-element linear photodiode array. The photodiode array senses the shadowing of array elements by drops passing through the field of view. The droplets are illuminated by laser light and are imaged as shadowgraphs on the array. Drop diameters are computed from the number of occulted elements, the size of each element, and the magnification of the optical system. Four levels of light intensity are sequentially measured at a frequency up to 4 million times per second. The data acquisition system can measure particles from 28 to 2062 μm and classify them into 62 size classes. Each drop that is in focus within the laser sampling area generates a count unless there is drop coincidence or severe distortion that activates the "coincidence reject" mode. Routines based on light intensity measurements reject out-of-focus drops. The drop size distribution measurement time is 30–60 seconds. This instrument is portable and may be used with various laboratory test stands or in the field. Yates *et al.* [105] used it for drop size distribution measurement when the nozzle was airborne during actual flight conditions. The spraying and measuring system was installed on an aircraft that can operate over a range of air speed from 100 to 200 km h^{-1} .

Optical holography is a recording technique in which all of the coherent optical information that passes through or is reflected from a volume is stored. Holography provides "frozen" images of drops in three-dimensional sections of the flow field. After reconstruction of the hologram, drop size and shape analysis is done at various planes along the line of sight, during which focus discrimination is required.

Holography has two important advantages for recording the images of drops: there is little restriction on depth of field, and a reconstructed hologram may be projected so that the magnification is constant, independent of the longitudinal position.

Thompson [95, 96] used far-field holography to measure particle sizes in the range 5 to 300 μm , using a pulsed ruby laser. Webster [102] has also used holography to measure particles in the size range 20 to 500 μm moving at up to 70 mm s^{-1} . He used a chemically switched double-pulse ruby laser. A specially constructed spatial filter reduced interference from noise. Webster points out that permissible subject movement is 10% of its diameter; i.e., for a pulse width of 2×10^{-8} s the maximum permissible velocity of a 20- μm -diameter particle is 100 m s^{-1} . This particle velocity is certainly greater than that which could be tolerated by conventional double-spark photography. The depth of field in laser holography is related to the particle size and the optical resolution of the system. This has been empirically assessed to be of the order of $100 d^2/\lambda$, where d is particle diameter and λ is the wavelength of the incident light. Empirical assessment shows that the depth-of-field criterion, important in the photographic assessment of particle velocity, does not apply to holography.

Holography has been used successfully in a variety of dilute systems such as aerosols and erosion simulators, but its extension to denser systems has been beset with problems. The major problem has been that of obtaining holograms of sufficiently good quality. It appears that the large flux of droplets gives rise to multiple scattering, with the result that the holograms are very noisy. Clearly defined holograms are necessary because analysis is carried out automatically in a similar manner to that described for photography. Holographic quality could be improved by reducing the sample thickness but the uncertainties associated with sampling a thin slice of a particle system make this an unrealistic solution.

Jones *et al.* [55] have investigated the possibility of measuring drop sizes in high-density systems. The basic experimental system for recording in-line holograms is as shown in Fig. 7-18a. Coherent light illuminates the object, and a photographic emulsion at a distance Z from the object records variations in light intensity. The information recorded on the emulsion is a pattern produced by the interference between the light diffracted by the object and the reference light that passes undisturbed through the object. When $Z > d^2/\lambda$, which is termed the Fraunhofer or far-field condition (where d is a characteristic particle diameter within the particle system and λ is the wavelength of light), the pattern is known as a Fraunhofer pattern. The advantage of Fraunhofer in-line holography over side-band holography, in which a reference beam is routed around the object, lies not only in relative ease of reconstruction but also in the fact that the reconstructed hologram is essentially a shadowgraph of the object. Therefore, the characteristics of the system and the quality of the recording can be assessed without necessarily reconstructing the hologram.

Reconstruction of an in-line hologram is best accomplished by placing the processed negative into a continuous beam of coherent light of wavelength similar to that of the original illuminating beam (Fig. 7-18b). The effect is to recreate the original wave front that was propagated from the subject of the exposure. Hence a real, albeit negative, image of the subject is produced. The dimensions of the image can be related to those of the object from a knowledge of the relative divergences and wavelengths of the recorded and reconstructed beams.

Jones *et al.* [55] found that holography for measuring particle sizes can be applied when the obscuration is less than 10%.

An off-axis laser holographic system for the study of sprays was developed at the United Technology Research Centre [70]. In this system a Q-switched ruby laser beam is split into an object beam and a reference beam by a beam splitter. The object beam passes through a lens to a diffuser, which causes the light to be transmitted to the spray over a large range of angles relative to the optical axis. Light from each point in the spray reaches all points on the holographic plate. The reference beam passes through an expander and a collimator, which adjusts the beam so that wave fronts emanating from the lens of the collimator are planar. The holograms are reconstructed using an He-Ne laser and an expander collimator to illuminate the holographic plate, which is mounted in an articulated holder to facilitate precise orientation of the hologram relative to the

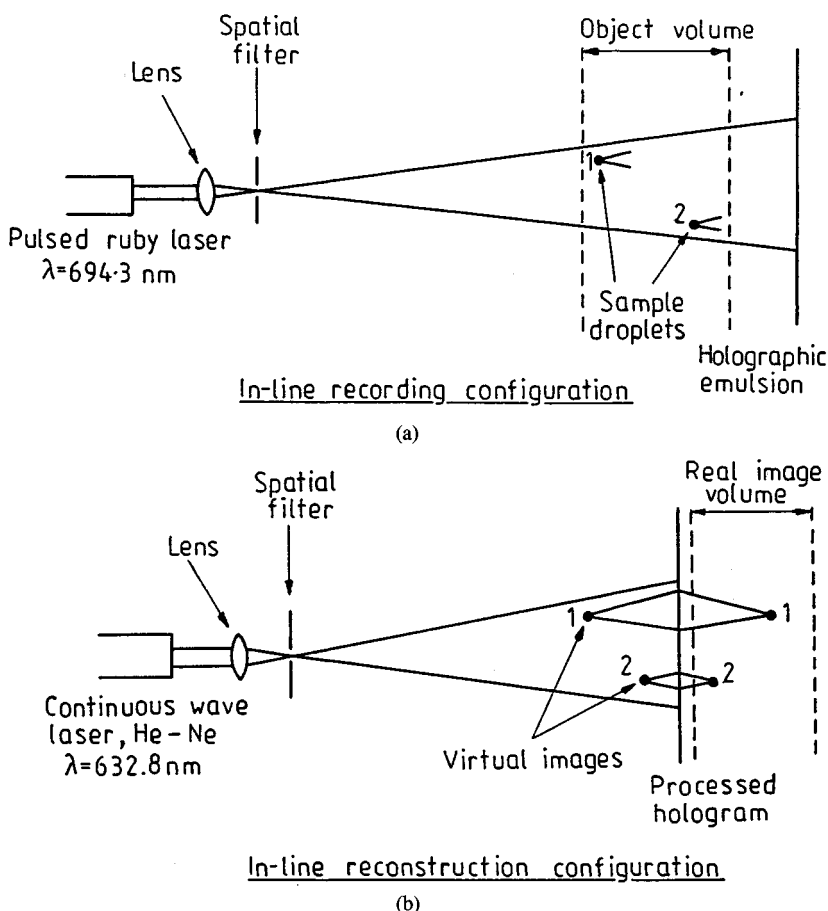


Figure 7-18 Optical system for in-line holography.

incident laser beam. Light diffracted from the hologram forms a real image of the spray.

Double pulsing allows simultaneous measurement of drop size and velocity. Spectron [104] has developed a holographic camera using a 2-ns pulse laser with 50 mJ power and a double-pulse capability with adjustable pulse separations from 1 to 500 μs . Lenses are used to magnify drop images 15-fold before recording, yielding a resolution of 2.5 μm .

The holographic method of spray analysis has considerable potential as a research diagnostic. Its major drawback has been the lack of an automated system for analysis of the large amounts of data that may be present even in a single hologram. The hologram presents data in the form of images. Although the images can be recognized and interpreted readily by humans, manual analysis of holograms can be tremendously time-consuming and tedious.

Aerodyne Research Inc. [88] developed a method for analyzing droplet holograms that is readily adaptable to automation using modern image digitizers and analyzers for the determination of drop size distribution. They have devised a means of determining the true size from measurements made in out-of-focus planes, which drastically reduces the information storage required compared with purely in-focus methods. This approach reduces considerably the number of image processing and analysis steps required, improves the accuracy of measurement of drop size and location, and automatically excludes hologram artifacts (background noise) that are not associated with particles.

An instrument called the Optomax V image analyzer was developed to measure directly the size of droplets of a pesticide spray deposited on leaf surfaces by using fluorescent tracers in the pesticide formulation [130–132]. The fluorescent tracer deposits are visualized using an ultraviolet lamp and a video camera. For droplets smaller than $50 \mu\text{m}$ an epifluorescence microscope equipped with an appropriate filter combination is used. A low-power objective (e.g., $1.6 \times$) gives the largest possible field of view. Finely milled Tinopol CBS-X (Ciba Geigy dyestuff) is recommended as a tracer; when viewed with a 1-inch Newvicon tube camera it provides excellent detection of spray droplet deposits on leaves. The Optomax V with an IBM PC AT provides a wide range of spray deposition parameters, including droplet number, size, distribution, and density. Image analysis provides accurate measurement of spray droplet deposition in a fraction of the time it would take to do it manually.

7-5.2 Single-Drop Counters

One of the advantages of using single-drop counters is that they can provide information rapidly on the size distribution at a specified spatial position as individual drops pass through a defined measurement volume. Ambiguities arise when more than one drop is found inside the measurement volume, which restricts their application to concentrations lower than approximately 10^9 m^{-3} .

Delavan Corporation used a single-drop counter manufactured by Particle Measuring Systems, Inc. of Boulder, Colorado [87]. In this instrument individual droplets passing through a narrow laser beam scatter light, which is sensed by a photodetector. The size of the droplet determines the intensity of scattered light. Hence, the droplets may be sorted into various size classes according to their diameters. Delavan's instrument is designed with four alternative size ranges: 1–16, 2–32, 2–47, and 5–95 μm . Each range contains 15 uniform size channels, and the operator may select any one of the ranges. For a typical flux of drops, coincidence errors are small; i.e., there are relatively few exaggerated counts due to simultaneous intersection of the measuring volume by more than one drop. To ensure accurate sizing drops must pass through the laser beam at a certain velocity.

Tate [93] proposed a procedure for calculating combined drop size distribution when more than one instrument or technique is required to cover the

complete spectrum of drop diameters at a given location. It may be necessary to use one instrument for smaller droplets and another instrument for large droplets. To facilitate the combination, it is necessary to have a region of overlap that is common for both instruments. The percent (or volume) of droplets that lies within the overlap region in each of the separate distributions is then calculated. The ratio of percentages establishes a proportionality factor that may be used to adjust the percentages in the size classes that are combined. It is sensible to choose as a reference distribution one that represents a large portion of the overall size spectrum. This procedure was applied, for example, to the combined data produced by two drop size instruments used by Delavan to measure drop sizes in the same spray. One instrument is a single-particle counter based on forward light scattering and covering the range 5–95 μm ; the other is an imaging device that measures the size of drops larger than 50 μm [83, 97]. The respective drop counts within the overlap region (50–95 μm) established the factor required to combine the size classes for the two instruments.

Polytec Company developed a single-particle counter [113] suitable for drop size measurements. This instrument is also based on light scattering by drops passing through an illuminated measurement volume. The scattered light intensity is related to the drop diameter. A drop passing through the measurement volume scatters light, which is received by a photodetector. Each optical signal is converted into an electrical pulse, which is processed electronically. The signal processor produces a drop size histogram. This instrument measures drop sizes in the range 0.4 to 100 μm . The maximum concentration of drops is $2.8 \times 10^9 \text{ m}^{-3}$.

Holve and Annen [51] developed a nonintrusive particle-counter-sizer velocimeter (PCSV) that is available commercially [73]. The instrument is based on an original system of light scattering data processing known as intensity deconvolution. It covers the drop size range 0.2–300 μm , velocity range 1–80 m s^{-1} , and concentration range up to 10^{13} m^{-3} and can be used on nonuniform backgrounds.

An interesting and original approach to drop size measurement was reported by Beretta *et al.* [21–24], who determined the size of coal particles and water drops in a coal-water slurry by measuring the angular distribution of the polarized components of scattered light and applying the Lorentz-Mie theory.

7-5.3 Ensemble Analyzing Instruments

Ensemble analyzing instruments for particle and drop size measurements were developed commercially only in the past 15 years. They are so called because the light scattering or extinction integrated over the contributions from a large number of particles is used to determine their size distribution. Calculating this distribution from measurement of transmitted or scattered light can be reduced in general to finding a solution to the Fredholm integral equation of the first

kind:

$$I(t) = \int_0^\infty K(t, a)f(a) da$$

where a is the particle radius, $f(a)$ is the particle size distribution function, $I(t)$ is the light intensity measured as a function of the scattering angle or wavelength, and $K(t, a)$ is a kernel defining the general relationship between intensity $I(t)$ for a particle of radius a and is known from light scattering theory.

In most ensemble particle sizers Fraunhofer diffraction theory is the theoretical basis. According to this theory, the intensity of light scattered by a particle of radius a is found from the Airy formula

$$I(\theta) = I_0 \frac{a^2 J_1^2(x, \theta)}{\theta^2} \quad (7-11)$$

where I_0 is the light intensity of incident light, $x = 2\pi a/\lambda$, λ is the wavelength, θ is the scattering angle, and $J_1(x, \theta)$ is a Bessel function of the first kind. The Airy formula can be used if θ is close to zero and $x \gg 1$.

For a system of particles with a number distribution $f(a)$

$$I(\theta) = \frac{I_0}{\theta^2} J_1^2(x, \theta) a^2 f(a) da \quad (7-12)$$

This equation must be inverted in order to find $f(a)$ and its kernel is $J(x, \theta)a^2$. Several methods can be used to find $f(a)$ from the experimentally determined scattering pattern $I(\theta)$. These methods are used in instruments for particle and drop size measurements developed during the 1970s and 1980s [10, 12, 124].

There are many instruments for ensemble particle sizing based on Fraunhofer light scattering but so far there is only one instrument suitable for drop size distribution measurement, namely the Malvern drop sizer [66]. This instrument was initially developed by Swithenbank *et al.* in 1977 [89] and was later modified several times, additional facilities being added.

In this instrument (Fig. 7-19) a 5 mW He-Ne laser ($\lambda = 632.8$ nm) is used as the light source. A spatial filter produces a collimated 9 mm-diameter beam. The light beam passes through the spray, and the light scattered by the drops in the near forward direction is focused by a Fourier transform lens onto a light detector. An array of 31 semicircular coannular photodetectors is used to measure the scattered light intensity as a function of scattering angle.

The scattering pattern measured does not depend on the position of the droplet or the refractive index of the liquid sprayed. The intensity of the scattered light is highest near the beam axis and decreases up to three orders of magnitude with increasing θ . In order to avoid the dynamic range of the instrument being too high, the photo detectors' light-sensitive areas are gradually increased with increasing radial distance of the detectors from the optical

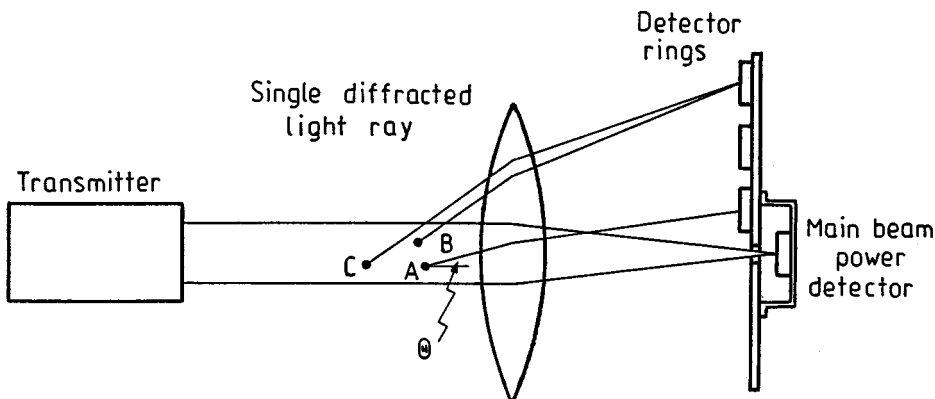


Figure 7-19 Schematic optical configuration of the 2600 Malvern drop sizer.

axis (the largest diode area is $1900 \times$ the area of the innermost ring) to compensate for the reduction in intensity.

The inversion technique used in the Malvern drop sizer is based on matching the scattered light energy profile. The scattered light energy and the drop volume distribution are related by $\bar{S} = \bar{C}\bar{V}$, where \bar{S} is the normalized scattered light energy vector, which contains 15 independent measurements, \bar{C} is the instrument function matrix, and \bar{V} is the particle volume distribution vector of dimension 15, which presents the 15 normalized independent size classes. The nature of \bar{V} is determined by the user-selected size distribution. Initially the Malvern particle sizer had three programs corresponding to the three size distribution functions assumed, namely the Rosin-Rammler, normal, and log-normal, which are two-parameter distributions.

The volume distribution of the drops in a spray is determined by systematically varying the parameters of \bar{V} to reconstruct the experimentally measured light energy distribution. The iterations conclude when a minimum least squares error value is achieved between the measured and predicted (according to the drop size distribution selected) angular light energy distribution.

Later a new facility was added by the manufacturers, a so-called model-independent program. This program does not assume a particular drop size distribution function. Instead it has 15 adjustable parameters corresponding to the 15 size bands of the volume distribution. These parameters are varied systematically until the best fit to the experimental data is obtained.

The Malvern drop sizer provides a normalized volume distribution over a range of size bands. The result represents the volume size distribution of all the drops contained in the cylindrical measurement. Generally, no further spatial resolution is possible. However, if a series of measurements is made traversing a cross section of a symmetrical spray, tomographic techniques can be applied to yield a drop size distribution at each point in the spray cross section.

The Fraunhofer diffraction theory on which the Malvern instrument is based assumes single scattering. This means that an instrument for drop size measurement can be used only if the drop concentration is not too large. When Malvern concentration instruments were used in dense particle clouds, light guides, tubes, cones, and slits were inserted in the drop flow to decrease observations to a level at which no multiple scattering takes place [2, 71, 72, 97]. Such measures compromise the nonintrusive attribute of optical measurements. Multiple scattering effects are usually not significant for obscurations less than 0.4–0.5. At obscurations higher than 0.5, multiple scattering effects become significant.

Several authors have evaluated the effect of multiple scattering on the scattering pattern [32, 39, 40]. Some of them proposed corrections for the parameters of the two most popular two-parameter distributions, the Rosin-Rammler and lognormal, to allow for multiple scattering. This means that the Malvern particle sizer can in principle be supplied with additional software to enable accomplish drop size measurement with obscuration up to 95% while using the Rosin-Rammler or log-normal program. The correctional factors can be presented as a function of obscuration [32, 39, 40]. This approach was used successfully to measure the drop size distribution in a spray formed by an impinging jet in a liquid rocket injector [26] and a coal-water slurry spray [72].

The Malvern instrument for drop size measurement has certain limitations [72]. Among them are ambient light level restrictions, beam steering caused by density gradients, and coarse resolution due to the line of sight of measurement. Efforts have been made to overcome the limitations connected with spatial resolution. Yule *et al.* [109, 110] proposed a procedure for converting the "line integral" data from a Malvern instrument into "point" measurements. One scan of the spray by the laser light beam produces a droplet size distribution along a chord of the spray cross section (for an axisymmetric spray). The light distributions for a large number of scans with systematic variations of the scan position can be converted into drop size distributions for elementary volumes within the spray, i.e., "pocket" measurements. This is analogous to the tomographic technique used by x-ray brain scanners. Using the method of laser tomography, as Yule *et al.* called it, they carried out detailed measurements of drop sizes in vaporizing sprays and found excellent agreement with photographic data. This method is somewhat complicated [112] because it is carried out in two stages. Zhu *et al.* [112] proposed a simplified method that directly transforms Malvern line integral data into point measurements of the drop size distribution and liquid volume concentration distribution. This was applied to the investigation of three types of nozzles. Tomographic transformation of the results obtained using the Malvern instrument revealed different structures of the spray. This method extends the applicability of the Malvern drop sizer and in principle can be developed for use with asymmetric sprays.

In most cases the Malvern instrument is used in continuous processes where a spray has a stable size distribution with time. It can also be used in transient spray conditions. Sprays that are time varying are of two types: repetitive spray

pulses such as those from a diesel injector and single pulses such as that produced by an inhaler. With a pulsed spray a free-running integration of the spray size distribution will give a smoothed-out result of little use to the researcher. It is necessary to trigger the capture of the scattering pattern from the spray generator so that with successive pulses the instrument integrates data from a consistent single time after the spray delivery. To be useful, the process of capturing the data must be fast to allow good time resolution. These specific requirements have been met in the special facilities of the Malvern drop sizer [100, 101]. These beams have an added trigger input to the receiver board. The measurement electronics are adapted to be used for such a purpose. Each photodetector in the array has an individual high-bandwidth amplifier and sample and hold circuit. The gates of all sample and holds are common and are fired by a sweep trigger signal. The electronics transfer the sampled light scattering data at high speed through an analog-to-digital converter and store the results digitally for later computer readout. The computer detects that a sweep has been captured and unloads it for analysis, freeing the electronics to capture another sweep. The sample gate is open for only 10 μs to capture all the photodetector data on a single sweep. The rise time of the electronic amplifiers to a step change in light level is 15 μs , allowing very fast scattering changes to be captured accurately. The repetition time of the measurement is 35 ms. This does not limit the spray pulse repetition rate. If it exceeds 35 ms, the instrument ignores every second pulse, or two out of three, etc., preserving the full timing accuracy on the pulses used.

It is common in a spray produced by a diesel injector system for small particles to be in the forward part of the spray and large ones lagging behind. A mechanical-optical sensor provides a source of timing information about the coming spray pulse. As the pulse requires time to traverse the distance to the laser beam of the Malvern instrument, a delayed trigger must be generated from the initial trigger. At a fixed distance between the injector and the beam, the user can vary the delay time to determine the section of the pulse (e.g., the leading edge, main body, or tail) captured by the detector.

Bayvel *et al.* [11, 14] developed an instrument for drop size measurement based on Shifrin's inversion technique. (Shifrin's theory is described in great detail in [10].) Shifrin's inversion algorithm provides an exact analytical solution of Eq. (7-12), which yields the number size distribution $f(a)$ from the experimentally measured scattering pattern $I(\theta)$. $f(a)$ is obtained independently of any prior assumption about or modeling of the distribution. The solution is very stable. From $f(a)$ it is easy to calculate the volume distribution, $v(a)$, cumulative undersize $G(a)$, and various means of the distributions function (volume mean diameter, Sauter mean diameter, etc.).

In this instrument a helium-neon laser with a spatial filter is used as a light source. A linear array of photodiodes spaced at 0.1-mm intervals, thus forming a long narrow slit, is used as a photodetector. Each photodiode receives light scattered at a particular angle. In this mode the circuit provides a voltage/time waveform closely representing the light intensity profile along the array, i.e., the

scattering pattern. Fraunhofer diffraction measurements require a detector with an extremely high dynamic range. To limit the required detection range, an optical "stop" to block the high-intensity laser beam is placed in front of the central laser beam. Neutral density filters bring the scattered light to a level suitable for the array. Spatial resolution of the linear photodiode array is higher than that of the semicircular photodiode array. Because of the uniform photodiode area, the responsivity is more uniform and calibration is relatively easy. The recorded measured value of light intensity versus scattering angle is processed by a microcomputer. The computer printout produces the drop size distribution with the desired increment within the size range. A software package was developed which uses the number or volume size distribution values determined from the experimentally measured scattering pattern to obtain the best fit to any of so-called standard distribution functions (Rosin-Rammler, log-normal, upper limit, Nukiyama-Tanasawa, root-normal, etc.) as well as various means and parameters of these distributions together with their variances. (By "best" is meant the distribution that has a smallest variance of its means.) A graphic software package provides a visual display of the particle size distribution (see Sec. 7-6.6).

Shifrin's inversion technique was also used by Kouzelis *et al.* [60], who found an instrument based on this analytical inversion, using a linear array of photodiodes as a detector and similar to that developed by Bayvel *et al.* [14], superior to that manufactured by Malvern. Instruments of this type have the advantages of simplicity and lower cost. Bayvel *et al.* [18, 19] applied Shifrin's analytical inversion technique to the Malvern particle sizer. They showed that light scattering data recorded using the hardware of the Malvern instrument can be successfully processed using the Shifrin technique to obtain the particle size distribution. The use of Shifrin's inversion algorithm has a number of advantages over Malvern's proprietary model-independent program. It provides the research worker with a simple and mathematically elegant alternative method of processing the light scattering data.

Bayvel *et al.* [11, 17, 20] developed a method and an instrument for drop size distribution measurement in the submicrometer size range based on numerical inversion of light extinction data. According to the Bouguer-Lambert-Beer law

$$I = I_0 e^{-K_{\text{ext}} L} \quad (7-13)$$

where I_0 is the intensity of the incident light, I is the intensity of the light beam passing through the spray, K_{ext} is the extinction coefficient, and L is the path length of the light in the spray. K_{ext} can be found experimentally from Eq. (7-13):

$$K_{\text{ext}} = \frac{1}{L} \ln \frac{I_0}{I} \quad (7-14)$$

K_{ext} is a function of the wavelength λ if the particle radius a is below 1 μm .

K_{ext} is related to the number size distribution $f(a)$ and extinction efficiency as follows:

$$K_{\text{ext}} = N \int_0^{\infty} Q_{\text{ext}}(x, \lambda) \pi a^2 f(a) da \quad (7-15)$$

where N is the particle concentration and $x = 2\pi a/\lambda$. Q_{ext} is a function of x , λ , and the refractive index of the atomized liquid. Drop number distribution $f(a)$ is found from Eq. (7-15) by direct numerical inversion using the Phillips-Twomey method [17, 20] (this method is described in great detail in [10]). The refractive index of the liquid sprayed is usually known.

In the instrument developed by Bayvel *et al.* (Fig 7-20) a xenon arc lamp is used as a light source. A monochromator is used to transmit the appropriate wavelength. The monochromator is under computer control via a stepping motor drive. A photodiode is used as a detector, and its response is measured for a sequence of wavelengths in the spectral range 360–800 nm in the absence of drops and in their presence. These responses are sufficient to calculate the values of the extinction coefficient K_{ext} according to (7-14). Control of the monochromator and all the calculations and processing of the experimental data are accomplished by a microprocessor. The microprocessor also calculates the set of values of $Q(x, \lambda)$ from the Mie theory for the given refractive index of the liquid atomized. This set of values of Q_{ext} is used when the particle size distribution is calculated from expression (7-15). The computer printout contains the number size distribution, volume size distribution, and cumulative undersize distribution with the desired increment in the size range 0.1–2 μm .

Drop size measurements using instruments based on inversion of light scattering or extinction data are absolute and do not require a calibration procedure. However, most of these instruments require assumptions that do not always comply with reality. Because of this and considering the possible changes in the performance of the optical and electronic components, it is advisable to check these instruments periodically against some standard materials. The following methods of verifying or comparing the performance of drop sizing instruments are used: certified reference materials (glass beads provided by the U.S. National Bureau of Standards, quartz materials supplied by the EEC

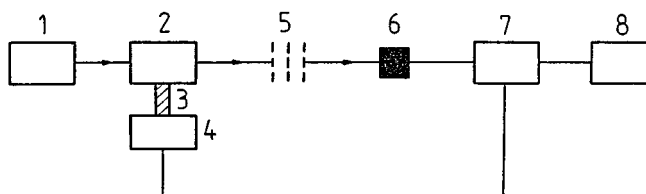


Figure 7-20 Schematic diagram of the instrument for drop size measurement in the region 0.1–2 μm . 1, Xenon arc lamp; 2, monochromator; 3, shaft; 4, stepping motor; 5, drop cloud; 6, photodiode; 7, microcomputer; 8, printer.

Bureau of References, and polystyrene microspheres, dispersed in a liquid cell), standard spray nozzles carefully maintained and run under standardized conditions, and droplet generators designed to produce nominally monodisperse aerosols. Unfortunately, all of these approaches have substantial limitations, particularly with respect to stability and reproducibility during interlaboratory comparisons over extended time periods. In order to circumvent these difficulties, Hirleman [45, 48] developed a synthetic particle size distribution (reticules) composed of two-dimensional arrays of particle images on a glass substrate. The particles on the diffraction reticule are actually opaque circular disks of chrome thin film photoetched on the glass. These disks (simulated drops) are randomly positioned over an 8-mm-diameter sample area. Typically 23 discrete diameters with one to several thousand replications of each size approximate a specified particle size distribution.

The particle size distribution on the reticule is inherently stable and can be independently characterized with very high accuracy. There is an acceptable limit for discrepancies between the results produced by a particle sizing instrument and the known size distribution of the reticule. Malvern Instruments offer reticules of the type described as a standard option to be used for verification of the performance of Malvern drop sizers. It must be understood that a check using a certified material or a reticule cannot provide a calibration of an instrument, since there is no component that can be altered to correct the output if the wrong answer is obtained. An incorrect answer indicates a fundamental misalignment, for which the only solution is to discover and correct the offending component.

Single-particle (drop) counters, both imaging and nonimaging, are in need of actual calibration. The earlier calibration techniques include glass or polystyrene microspheres, particles deposited on oil-coated glass slides, and quasi-monodisperse droplet streams produced by mechanical breaking of jets or sheets of liquid. Hovenac *et al.* [53] used particle images of chrome thin film photoetched on a glass substrate with diameters ranging from 80 to 455 μm for calibration of single-particle counters.

7-5.4 Laser Doppler Anemometry

When radiation of frequency ν strikes a drop traveling with velocity \mathbf{u} the scattered radiation suffers a frequency shift (Fig. 7-21). The new frequency ν_1 is a function of the angles α and β , given by

$$\nu_1 = \nu \left[1 - \frac{2u}{C} \sin \frac{\beta}{2} \sin \left(\theta - \frac{\beta}{2} \right) \right]$$

If $\theta = \pi/2$, then

$$\nu_1 = \nu \left[1 - \frac{u}{C} \sin \beta \right]$$

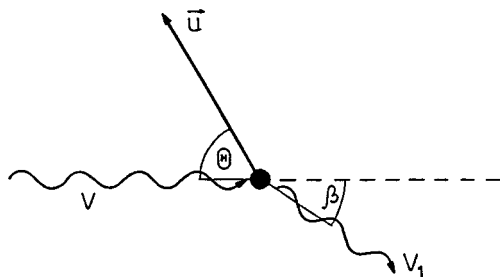


Figure 7-21 Interaction between radiation of frequency ν and a drop traveling with velocity \mathbf{u} .

In order to measure the small change in frequency (the Doppler shift), the scattered light is mixed with unscattered radiation giving a beat frequency ν_b

$$\nu_b = |\nu_1 - \nu| = \frac{u}{C} \sin \beta$$

It can be seen that the accuracy with which velocity can be determined depends on the precision to which β is known. The problem of determining the angle can be overcome by using two crossed beams of equal frequency. This device for measuring particle velocities is called a fringe anemometer and is illustrated in Fig. 7-22. Two laser beams cross at an angle 2γ , producing an interference pattern with fringe spacing

$$\lambda_f = \frac{\lambda}{2 \sin \gamma}$$

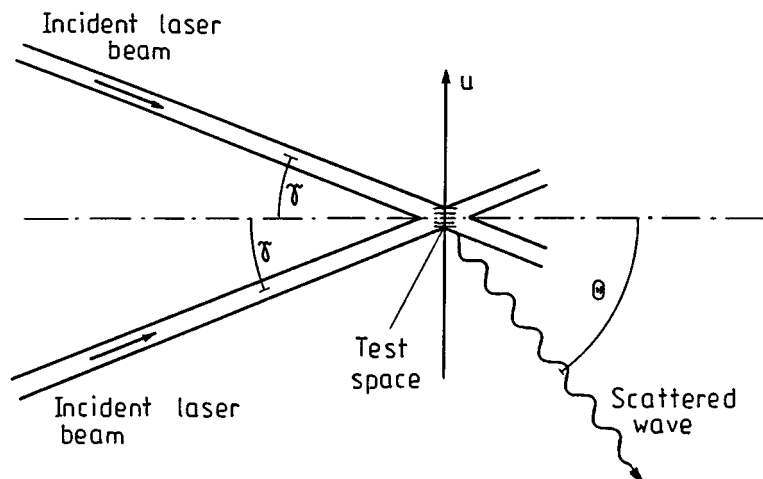


Figure 7-22 Principle of fringe anemometer.

Particles crossing this pattern produce a frequency

$$\nu_b = \frac{2u \sin \gamma}{\lambda} = \frac{u}{\lambda_f}$$

which is exactly given by the time it takes the particles to traverse one fringe.

The scattered intensity depends on the drop size, and a number of authors have explored the use of fringe anemometers to obtain this. The general form of the scattered signal may be written

$$I_{\text{sca}} = A + B \cos 2\bar{u}\nu_b t$$

It is possible to measure either the time-averaged scattered intensity (A) of the signal or the signal visibility, the latter being defined by

$$V = \frac{I_{\text{sca},\max} - I_{\text{sca},\min}}{I_{\text{sca},\max} + I_{\text{sca},\min}}$$

For the above form this is

$$V = \frac{B}{A}$$

The visibility has the advantage of being a relative value. It can be shown that for large spherical particles the visibility in the extinction should have the form

$$V = \frac{2J_1(K_f a)}{K_f a}$$

where $K_f = 2\pi/\lambda_f$.

Farmer [114, 115], Fristrom *et al.* [119], Jones [116], Hong and Jones [117, 118, 120], and others have explored this method. They developed a computer program that integrates the scattered intensity over the angular field of view of the detector. The calculated visibility was compared with experimental signals from single drops, and a size distribution built up.

Use of a fringe anemometer as a means of sizing drops has the advantages that it measures the size distribution directly, is insensitive to refractive index, is simple to operate, and is capable of automation. The nature of the signal makes it easy to distinguish from noise. Its limitations include the fact that some foreknowledge of the drop size is needed to select the correct fringe spacing. It may be possible to overcome this by using a variable fringe spacing beginning with λ_f such that all visibilities are unity and then slowly decreasing λ_f until a sensible distribution is obtained. A second disadvantage is that only one drop at a time must be present in the test space, which limits the concentration to 10^9 m^{-3} . Reduction in the dimensions of the test space to 0.1 mm enables a maximum concentration of 10^{12} m^{-3} to be examined. Yule *et al.* [107] measured mean scattered intensity for drop diameters larger than the fringe spacing. They claimed a linear relationship with size over a wide range.

This method was refined later [121]. The improvements included the use of a specially tailored “top hat” light distribution to provide unambiguous particle size-signal amplitude, the use of backscattered light collection, and the use of Mie theory to complete the relationships between signal amplitude and particle diameter to the backscattered mode. This technique was used to investigate twin-fluid atomized kerosene sprays. The data obtained show the variation of spray structure with atomizer input parameters, the preferential vaporization of smaller droplets, and the differing trajectories of the large and small droplets. This method has the disadvantages of needing extremely careful alignment and beam quality control, it needs relatively frequent calibration, and is subject to errors produced by beam and scattered light alternation.

The phase Doppler method developed by Bachalo [5–9, 122] has the potential for fulfilling most of the drop size and velocity measurement needs for two-phase flow research. Bachalo’s analysis revealed that the relative phase shift of the light scattered by the mechanism of reflection or refraction is proportional to the drop size. Off-axis collection of the refracted component of the scattered light represents a significant advantage of this method. The optical system proposed by Bachalo is shown in Fig. 7-23. Three detectors are located at selected spacing behind a single receiver aperture. Droplets passing through the intersection of the two laser beams scatter light, which forms an interference fringe pattern inversely proportional to the droplet diameter. Dynamic measurements of the spatial frequency of the interference fringe pattern are achieved using pairs of detectors placed at appropriate locations and separations. This approach has the following advantages: measurements are relatively unaffected by random beam attenuations, the instrument response is linear over the entire working range, and the instrument has a potentially large size dynamic range. The method developed by Bachalo has been implemented in a commercially available instrument called Phase/Doppler Particle Analyzer [76]. It consists of

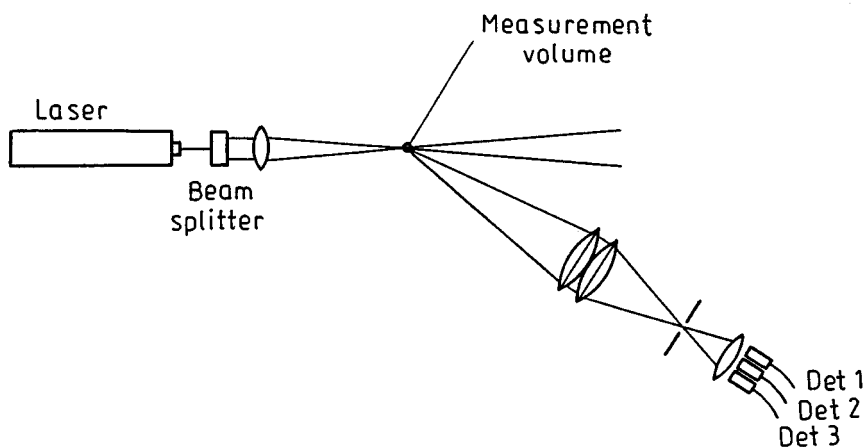


Figure 7-23 Optical diagram of phase Doppler particle analyzer.

a 10-mW He-Ne laser, beam expander, and beamsplitter. The receiving lenses are located at 30° to the direction of the laser beam. Signals from three photodetectors are transferred to a signal processor. Histograms of drop size and velocity distributions are displayed in real time. At the completion of the data acquisition, various mean sizes and velocities are calculated. The drop size range of the instrument is 0.5–3000 μm provided the drops remain spherical. The range of drop velocities measured is 1–200 m s^{-1} . Data acquisition and transfer to computer memory require 20 μs per drop. The accuracy of the instrument is 5% for size measurement and 1% for velocity measurement. Maximum particle concentration is 10^{12} m^{-3} .

Another instrument for simultaneous measurements of drop size, concentration, and velocity based on laser Doppler anemometry was developed by Dantec Electronik and is called the Particle Dynamics Analyzer [75, 122, 123]. As it was shown in [122, 123, 125, 126] that under appropriate optical conditions the signals from two detectors looking at the same drop but located at different scattering angles have a phase difference that is related to particle size. By placing the detectors at a scattering angle near 90°, the phase shift becomes less sensitive to refractive index variations and linearly dependent on particle diameter. Using three detectors placed at appropriate angles, the instrument can be operated over a very wide size range. Use of a fourth detector makes it possible to determine whether the drop is not spherical. Thus the method can discriminate between spherical and nonspherical drops. Signal processing is based on software analysis of digitized Doppler bursts. Size range of the instrument is 5 μm to 10 mm, maximum measured velocity is 200 m s^{-1} , maximum concentration is 1000 drops/ mm^3 , measuring volume is $0.5 \times 0.3 \times 0.3 \text{ mm}$, and measuring distance is up to 600 mm. The laser used is either a 25-mW He-Ne or a 2-W argon-ion laser. The instruments described have been used successfully in many practical situations.

Several other methods for simultaneous measurement of drop size and velocity should be mentioned. Hess and collaborators [42, 43, 104] developed several instruments for simultaneous measurements of drop size and velocity in a spray. The instruments are commercially available through Spectron Development Laboratories. In one instrument the method called IMAX (intensity maximum) is used. This method of drop size determination is based on measurement of the absolute intensity of the light scattered by individual drops crossing an illuminated probe volume. The velocity is obtained from Doppler signal using the standard laser Doppler velocimeter approach. The difficulty of defining the test space is overcome by having two small beams of one wavelength cross within a wide beam of another wavelength. Thus an interferometric pattern of fringes is formed in the crossover, defining a region of almost uniform intensity within the large beam. The IMAX technique, using a probe volume and known illumination to avoid ambiguity of particle position, can be used to measure the intensity from a uniform-intensity region and obtain velocity from the fringe system, provides a self-calibrating system, and is characterized by a large dynamic size range.

Yeoman and collaborators [41, 86, 106] developed a two-color laser-based instrument for drop size, velocity, and concentration measurement. They used a combination of the pedestal and visibility methods, which allows extension of this combined method to a size range of drops in which one method on its own would give ambiguous results. In particular, a problem with the Laser Doppler Velocimetry (LDV) methods for drop size measurements based on scattered visibility is that the fringe contrast is sufficiently high only in the center of the crossover volume. This volume has to be defined, and the authors use a second beam of a different color for this purpose.

7-5.5 Nonlinear Light Scattering

One of the most promising new techniques for ultrahigh resolution sizing of individual liquid droplets is resonance light scattering [34, 57, 58, 62, 63]. This technique is used to make measurements of droplet size with resolution 10 ppm. This is at least two orders of magnitude better than that obtainable with conventional light scattering technique based on Fraunhofer diffraction or Mie theory. The first experimental observation of resonance light scattering from individual liquid droplets was reported by Aszkin and Dziedzić [3]. Their study showed the existence of sharp resonances in the radiation pressure cross section of silicone oil and index-matching oil droplets ranging in diameter from 4 to 30 μm . The feedback apparatus keeps the drops locked at a fixed height. Since the drop diameter is constant, the wavelengths at which resonances occur give the absolute drop size.

The authors of [3] were able to distinguish diameter differences of 30 ppm between two droplets. Lettieri *et al.* [62, 63] measured the size of evaporating and growing droplets with resolution 300 ppm (about 3 nm). Szymanski *et al.* [90] measured the mean drop size of a narrow distribution (width 0.6–2.4%) aerosol of growing water droplets.

Nonlinear optical emission, e.g., lasing and stimulated Raman scattering, is used to provide a nearly instantaneous in-site, nonintrusive technique for obtaining morphological and chemical information on a single droplet in a gas flow. For example, Eickmans *et al.* [34] used stimulated Raman scattering for size measurement of supermicronic water droplets containing different anions (e.g., NO_3^- , SO_4^{2-} , and PO_4^{3-}) as well as for obtaining information on molarity of KNO_3 , etc.

Knight *et al.* [57], Bayvel *et al.* [58] used the morphology-dependent resonances observed from lasing supermicronic droplets produced by the Berglund-Liu generator. In order to measure the drop size distribution a vertically flowing stream of droplets was produced by a commercially available TSI generator (nominal size from 15 to 45 μm). Single droplets in the stream were illuminated with the focused beam of a pulsed single-longitudinal-mode, Q-switched Nd:YAG laser (Fig. 7-24). The frequency-doubled green beam used had a wavelength of 532 nm, a pulse length of 15 ns, and input power of about 1 GW cm^{-2} . Droplets of ethanol doped with the organic fluorescent laser dye rhodamine were used.

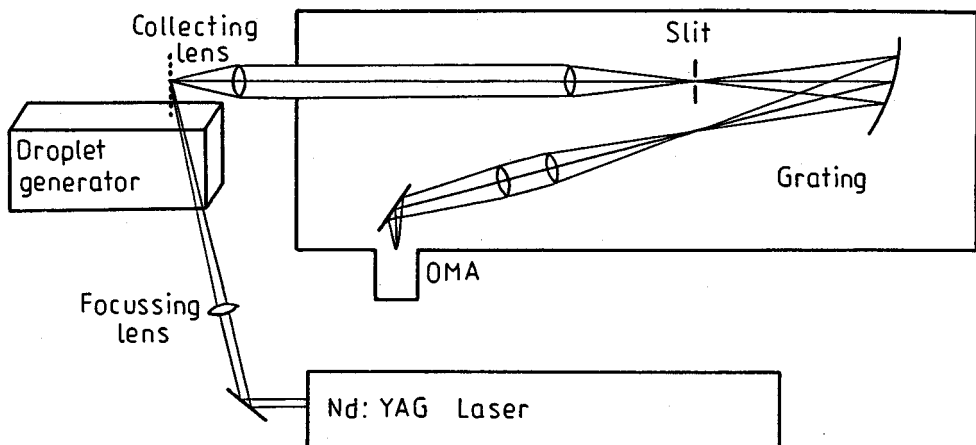


Figure 7-24 Experimental arrangement for drop size measurement using resonance light scattering.

The fluorescent radiation was at a longer wavelength than the excitation beam. Dye concentrations used were 80–200 mg/L. Scattered radiation was collected by a lens at right angles to both the incident beam and the droplet stream and imaged onto the spectrometer and optical multichannel analyzer. The repetition rate of the pulsed laser was set to 1 Hz and one in every 35,000 to 50,000 droplets produced by the generator was sampled. Absolute size of individual droplets was determined from the observed spectral peaks. In this way the drop size is measured with high speed and accuracy.

7-6 ANALYSIS OF DROP SIZE DISTRIBUTION DATA TO OBTAIN THE “BEST” FIT TO STANDARD DISTRIBUTIONS AND DISTRIBUTION PARAMETERS

Size distribution data can be fitted to several standard distribution functions numerically [127] or graphically [128, 129]. Determined parameters are, for example, an average size and a measure of spread of sizes expressed as a variance. Conventionally, graphical methods are favored in which the distribution function is expressed as a straight line by using an appropriate abscissa and ordinate and the parameters are deduced from the slope and the position of the straight line. This method has been referred to as “the craze of straight line plotting” [128] because it is assumed that the line selected represents the “best fit” to the data.

Regression analysis of such straight lines related to distribution functions and analysis of the resulting confidence limits from which the most accurate or best mean (i.e., the one with the smallest variance) can be obtained was carried out by Bayvel [13].

7-6.1 Rosin-Rammler Volume (or Mass) Distribution

This distribution is given by

$$G(x) = 1 - \exp\left(-\frac{x}{\bar{x}}\right)^n \quad (7-16)$$

where n is a distribution parameter and \bar{x} is the Rosin-Rammler mean. Equation (7-16) is rearranged to

$$\log \ln \frac{1}{1 - G(x)} = n \log x - n \log \bar{x} \quad (7-17)$$

or, with $X = \log x$, $Y = \log \ln\{1/[1 - G(x)]\}$:

$$Y = b_1 X + a_1 \quad (7-18)$$

where $b = n$ and $a_1 = -n \log \bar{x}$, so that

$$\bar{x} = 10^{-a_1/b_1} \quad (7-19)$$

(see [13] for derivation).

The variances of the intercept a_1 of Eq. 7.18, $\text{var}(a_1)$, and the slope b_1 , $\text{var}(b_1)$, are obtained from straight line regression analysis. The variance of the mean \bar{x} (see [13] for derivation) comes to

$$\text{var}(\bar{x}) = \frac{5.3}{b_1^2} 10^{-2a_1/b_1} \left[\text{var}(a_1) + \frac{a_1^2}{b_1^2} \text{var}(b_1) \right] \quad (7-20)$$

Thus, given a distribution function $G(x)$, as in Eq. (7-16), the parameters a_1 , b_1 and their variances are obtained from linear regression analysis of Eq. (7-18) and the Rosin-Rammler mean and its variance are obtained from Eqs. (7-19) and (7-20), respectively.

7-6.2 Log-normal Distribution

Number distribution

$$F(x) = \frac{1}{\sigma_g \sqrt{2\pi}} \int_{-\infty}^{\ln x} \exp\left[-\frac{(\ln x - \ln \bar{x}_{GM})^2}{2\sigma_g^2}\right] d(\ln x) \quad (7-21)$$

where σ_g is the geometric standard deviation and \bar{x}_{GM} is the geometric mean size. The relevant straight line (see [13] for derivation) is

$$Y_2 = b_2 X_2 + a_2$$

where $X_2 = \ln x$ and $Y_2 = u$ (see below). \bar{x}_{GM} is obtained from the line at $F(x) = 0.5$ on the probability scale, and σ_g is obtained from the slope of the line, $\sigma_g = 1/b_2$. In the statistical analysis, which is developed in [13], the two

parameters a_2 and b_2 are obtained by linear regression of u against $\log x$:

$$u = \frac{\ln x - \ln \bar{x}_{GM}}{\sigma_g} = b_2 x_2 + a_2 \quad (7-22)$$

From the intercept a and slope b it follows (see [13]) that

$$\bar{x}_{GM} = \exp\left(-\frac{a_2}{b_2}\right) \quad (7-23)$$

$$\text{var}(\bar{x}_{GM}) = \frac{x_{GM}^2}{b_2^2} \left[\text{var}(a_2) + \frac{a_2^2}{b_2^2} \text{var}(b_2) \right] \quad (7-24)$$

Mass (or volume) distribution

$$G(x) = \frac{1}{\sigma'_g \sqrt{2\pi}} \int_{-\infty}^{\ln x} \exp - \left[\frac{(\ln x - \ln \bar{x}_{MM})^2}{2\sigma'^2_g} \right] \quad (7-25)$$

The relevant straight line (see [13]) is

$$Y_3 = b_3 X_3 + a_3$$

where

$$Y_3 = u' = \frac{\ln x - \ln \bar{x}_{MM}}{\sigma'_g}$$

and

$$X_3 = -\ln x$$

The mass median diameter \bar{x}_{MM} is obtained at $G(x) = 0.5$ on the probability scale or analytically (see [13])

$$\ln \bar{x}_{MM} = -\frac{a_3}{b_3}$$

or

$$\begin{aligned} \bar{x}_{MM} &= \exp\left(-\frac{a_3}{b_3}\right) \\ \sigma'_g &= \frac{1}{b_3} \end{aligned} \quad (7-26)$$

and

$$\text{var}(\bar{x}_{MM}) = \frac{x_{MM}^2}{b_3^2} \left[\text{var}(a_3) + \frac{a_3^2}{b_3^2} \text{var}(b_3) \right] \quad (7-27)$$

Because of the close relations between the number and mass distributions, there is a simple algebraic relation between \bar{x}_{mm} and \bar{x}_{GM} and their respective variances as developed in [13].

7-6.3 Root-Normal Mass (or Volume) Distribution

$$G(x) = \frac{1}{\sigma_g'' \sqrt{2\pi}} \int_{-\infty}^{\sqrt{x}} \exp - \frac{(\sqrt{x} - \sqrt{\bar{x}_{RM}})^2}{2\sigma_g''^2} d(\sqrt{x}) \quad (7-28)$$

The relevant straight line (see [13] for derivation) is

$$Y_4 = b_4 X_4 + a_4$$

$$Y_4 = u'' = \frac{\sqrt{x} - \sqrt{\bar{x}_{RM}}}{\sigma_g''} \quad \text{and} \quad X_4 = \sqrt{x}$$

The plotting procedure is followed as before where Y_4 is $G(x)$, plotted on the probability scale, against $X_4 = \sqrt{x}$, obtaining the mean \bar{x}_{RM} at $G(x) = 0.5$ and σ_g'' from the slope. Analytically,

$$a_4 = -b_4 \sqrt{\bar{x}_{RM}} \quad \text{and} \quad b_4 = \frac{1}{\sigma_g''}$$

$$\bar{x}_{RM} = \frac{a_4^2}{b_4^2} \quad (7-29)$$

Regression analysis (see [13]) leads to

$$\text{var}(\bar{x}_{RM}) = \frac{4a_4^2}{b_4^2} \left[\text{var}(a_4) + \frac{a_4^2}{b_4^2} \text{var}(b_4) \right] \quad (7-30)$$

7-6.4 Nukiyama-Tanasawa Number Distribution

$$f(x) = Cx^2 \exp(-px^\delta) \quad (7-31)$$

with C and p as constants. The relevant straight line is

$$Y_5 = b_5 X_5 + a_5$$

where

$$Y_5 = \ln \frac{f(x)}{x^2}$$

The analysis, shown in [13], gives for the constants in terms of slope and intercept $a_5 = \ln C$ and $b_5 = -p$. The mean of this distribution is obtained in the form of gamma functions [127]. For $\delta = 1/2$, which is applicable to sprays [128], the mean mass size $\bar{x}_{3,0}$ is given by

$$\bar{x}_{3,0} = 69.3b_5^{-2} \quad (7-32)$$

and its variance is given by

$$\text{var}(\bar{x}_{3,0}) = \frac{19,210}{b_5^6} \text{var}(b_5) \quad (7-33)$$

7-6.5 Upper Limit Volume (or Mass) Distribution

$$G(x) = \frac{1}{\sigma_g''' \sqrt{2\pi}} \int_{-\infty}^{\ln x} \exp - \frac{[\ln(Cx) - \ln(x_{\max} - x)]^2}{2\sigma_g'''^2} \quad (7-34)$$

where the upper limit x_{\max} is specified and C is a constant. The relevant straight line equation is

$$Y_6 = b_6 X_6 + a_6$$

where

$$Y_6 = u''' = \frac{\ln(Cx) - \ln(x_{\max} - x)}{\sigma_g'''}$$

and

$$X_6 = \ln x - \ln(x_{\max} - x)$$

The mean \bar{x}'_{GM} is obtained from the following equation (see [13]):

$$\bar{x}'_{GM} = \frac{x_{\max}}{1 + \exp(a_6/b_6)} \quad (7-35)$$

and σ_g''' is obtained from the slope:

$$\sigma_g''' = \frac{1}{b_6}$$

From the error calculation in [13]:

$$\text{var}(\bar{x}'_{GM}) = \frac{x_{\max}^2 \exp(2a_6/b_6)}{[1 + \exp(a_6/b_6)]^4} \left[\frac{1}{b_6^2} \text{var}(a_6) + \frac{a_6^2}{b_6^2} \text{var}(b_6) \right] \quad (7-36)$$

7-6.6 Example Analysis of Drop Size Distribution of a Spray

The spray originated from a vibratory atomizer of ultrasonic type. The drop size distribution was measured by using a light scattering method and instrument as described in [11, 14]. The volume (mass) size distribution of the spray is shown in Fig. 7-25. The data were processed using appropriate computer programs solving Eqns. (7-19), (7-20), (7-23), (7-24), (7-26), (7-27), (7-29), (7-30), (7-32), (7-33), (7-35), (7-36). Distribution patterns are presented in Figs. 7-26 to 7-30 for the five standard distributions described earlier. The mean values of the distributions and their variances are found and given below with a degree of freedom of 22:

1. Rosin-Rammler

$$\bar{x} = 15.7 \mu\text{m}; n = 3; \text{var}(\bar{x}) = 1.2 \mu\text{m}^2$$

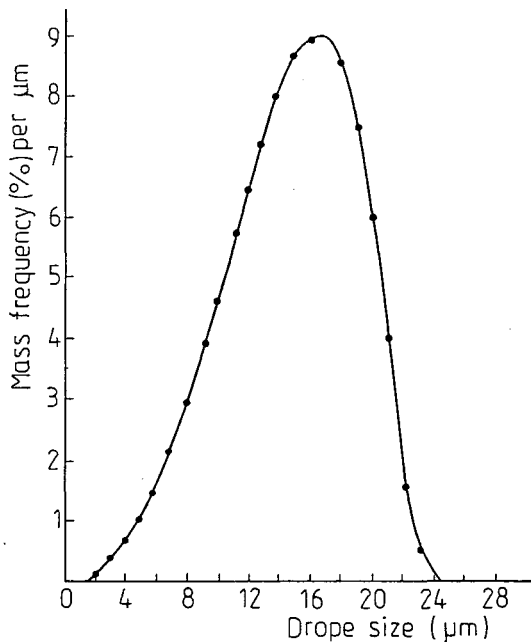


Figure 7-25 Drop size distribution of a spray.

2. Log-normal number

$$\bar{x}_{\text{GM}} = 12.8 \mu\text{m}; \sigma'_g = 0.5 \mu\text{m}; \text{var}(\bar{x}_{\text{GM}}) = 3.5 \mu\text{m}^2$$

3. Root-normal

$$\bar{x}_{\text{RM}} = 14.8 \mu\text{m}; \sigma''_g = 0.7 \mu\text{m}; \text{var}(\bar{x}_{\text{RM}}) = 2.8 \mu\text{m}^2$$

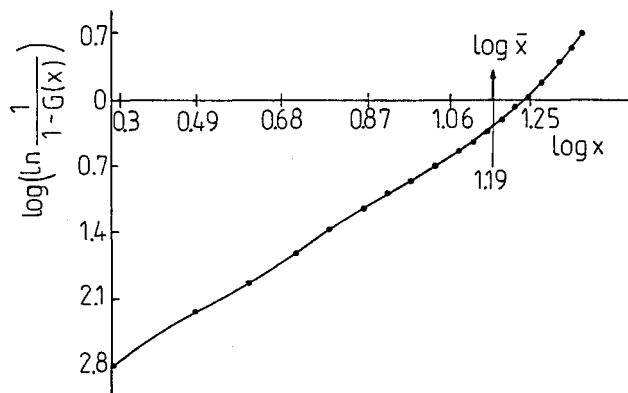


Figure 7-26 Rosin-Rammler distribution.

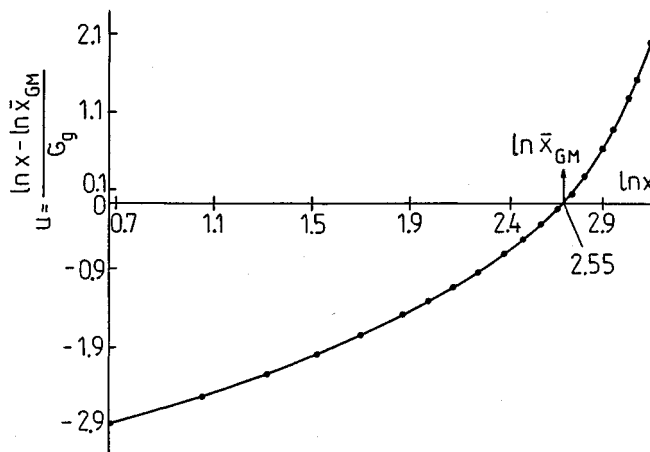


Figure 7-27 Log-normal number distribution.

4. Nukiyama-Tanasawa

$$\bar{x}_{3,0} = 11.2 \text{ } \mu\text{m}; p = 2.5 \text{ } \mu\text{m}^{-1}; C = 1.1; \text{var}(\bar{x}_{3,0}) = 0.6 \text{ } \mu\text{m}^2$$

5. Upper limit

$$x'_{GM} = 14.1 \text{ } \mu\text{m}; \sigma''' = 0.9 \text{ } \mu\text{m}; x_{max} = 22.8 \text{ } \mu\text{m}; C = 1.5; \text{var}(\bar{x}'_{GM}) = 0.02 \text{ } \mu\text{m}^2$$

The upper limit distribution provides the most reliable or best fit, and the log-normal number distribution provides the worst because the variance of the

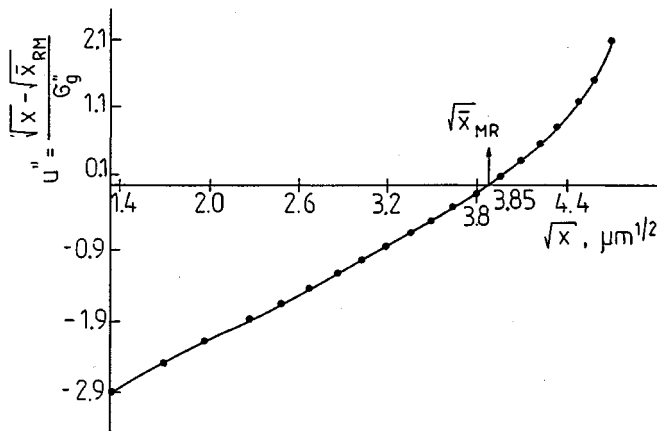


Figure 7-28 Root-normal distribution.

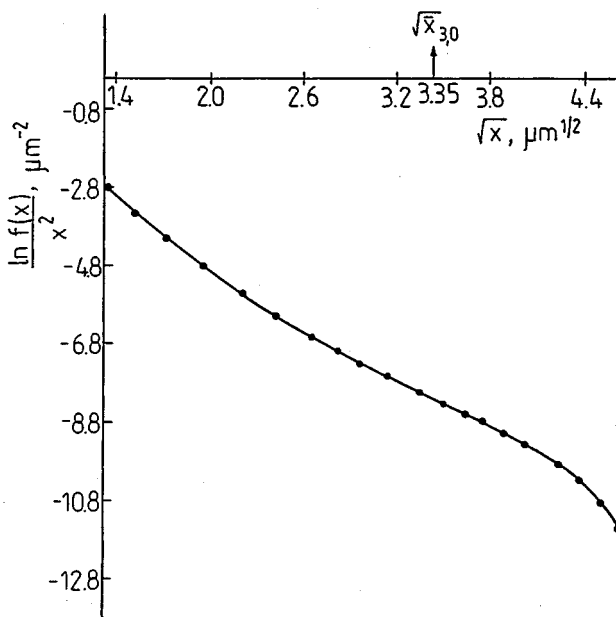


Figure 7-29 Nukiyama-Tanasawa distribution.

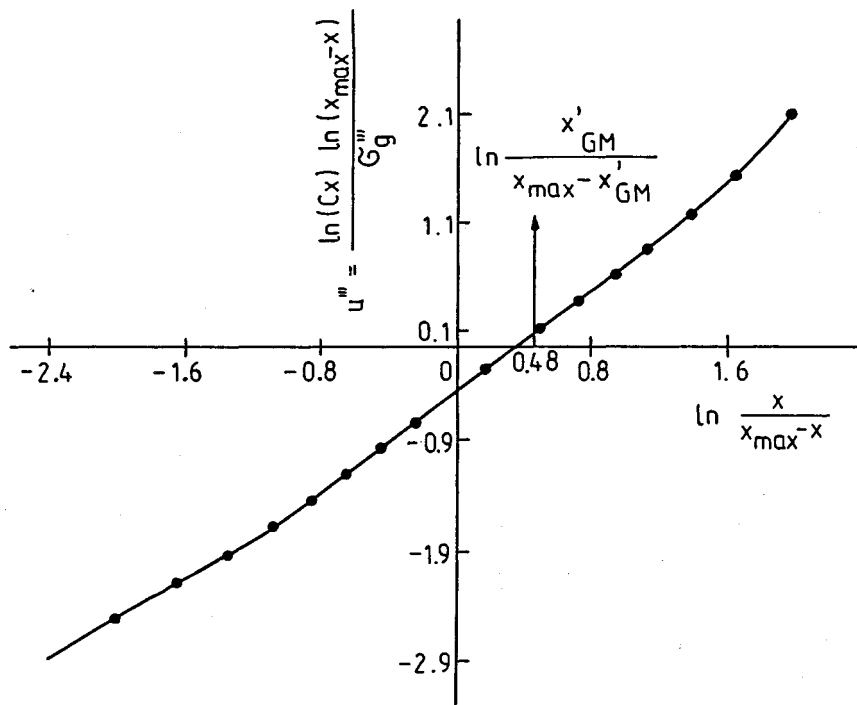


Figure 7-30 Upper-limit distribution.

mean is smallest in the case of the former distribution and greatest in the case of the latter. The nonlinearity of the lines in Figs. 7-26 to 7-30 demonstrates that application of the graphical method leads to large errors except in the case of the Rosin-Rammler distribution, which, however, does not provide the best mean.

REFERENCES

1. Aihara, T., Shimoyama, T., Hongoh, M., Fujinawa, K. Instrumentation and error sources for the measurement of the local drop-size distribution by an immersion-sampling cell. *Proceedings of the Third International Conference on Liquid Atomisation*, London, Vol. 2, pp. VC/5/1-11, 1985.
2. Arai, M., Kishi, T., Hiroyasu, H. A laser diagnostic technique for Sauter mean diameter of fuel oil sprays. *Proceedings of the Second International Conference on Liquid Atomisation*, Madison, Wisconsin, pp. 309-316, June 1982.
3. Aszkin, A., Dziedzić, J. M. *Phys. Rev. Lett.*, Vol. 38, pp. 1351-1354, 1977.
4. Azzopardi, B. J. Measurement of drop sizes. *Int. J. Heat Mass Transfer*, Vol. 22, pp. 1245-1279, 1979.
5. Bachalo, W. D., Hauser, M. J. Phase/Doppler spray analyser for simultaneous measurement of drop size and velocity distributions. *Opt. Eng.*, Vol. 23, pp. 583-590, 1984.
6. Bachalo, W. D. Droplet analysis techniques: their selection and applications. In *Liquid Particle Size Measurement Techniques* (J. M. Tishkoff, R. D. Ingebo, and J. B. Kennedy, eds.), pp. 22-34. ASTM STP 848, American Society for Testing and Materials.
7. Bachalo, W. D., Hauser, M. J. Spray drop size and velocity measurements using the phase/Doppler particle analyzer. *Proceedings of the Third International Conference on Liquid Atomisation*, London, Vol. 2, pp. VC/2/1-12, 1985.
8. Bachalo, W. D., Houser, M. I., Smith, J. N. Behaviour of sprays produced by pressure atomisers as measured using a phase/Doppler instrument. *Atomisation Spray Technol.* Vol. 3, pp. 53-72, 1987.
9. Bachalo, W. D. The phase Doppler method: analysis and application. In *Optical Particle Sizing* (G. Gousbet and G. Grehan, eds.), pp. 283-299. Plenum Publishing, New York, 1988.
10. Bayvel, L. P., Jones, A. R. *Electromagnetic Scattering and its Applications*. Elsevier Applied Science Publishers, London, 1981.
11. Bayvel, L. P., Eisenklam, P., Jones, A. R. A light scattering instrument for measuring drop sizes in the range of 0.1 to 1,000 μm . *Proceedings of the Second International Conference on Liquid Atomisation and Spray Systems*, Madison, Wisconsin, pp. 329-334, June 1982.
12. Bayvel, L. P. Direct inversion methods for particle size distribution measurement from light scattering. *Anal. Proc. R. Soc. Chem.*, Vol. 21, pp. 281-283, 1984.
13. Bayvel, L. P. An analysis of drop size distribution data to obtain the "best" fit to standard distribution and distribution parameters. *Atomisation Spray Technol.*, Vol. 1, pp. 3-20, 1985.
14. Bayvel, L. P., Symons, M., Wood, R. Optical instrument for monitoring the drop size of sprays. *Proceedings of the Third International Conference on Liquid Atomisation and Spray Systems*, London, Vol. 2, pp. P/1/1-4, 1985.
15. Bayvel, L. P., Symons, M., Wood, R. Optical instrument for monitoring the particle size distribution. *Proceedings of the First World Congress on Particle Technology*, Nürnberg, Part 1, pp. 155-164, April 1986.
16. Bayvel, L. P. New developments in particle and drop size measurement and analysis. *Atomisation Spray Technol.*, Vol. 2, pp. 83-88, 1986.
17. Bayvel, L. P., Eisenklam, P., Symons, M., Wood, R. An instrument for particle size distribution measurement in the submicronic size range. *Atomisation Spray Technol.* Vol. 3, pp. 135-143, 1987.

18. Bayvel, L. P., Knight, J., Robertson, G. Alternative model independent inversion programme for Malvern particle sizer. *Particle Characterisation*, Vol. 4, pp. 49–53, 1987.
19. Bayvel, L. P., Knight, J. C., Robertson, G. N. Application of the Shifrin inversion to the Malvern particle sizing. In *Optical Particle Sizing* (G. Gousbet and G. Grehan, eds.), Plenum Publishing, New York, pp. 311–320, 1988.
20. Bayvel, L. P., Eisenklam, P., Symons, M., Wood, R. Particle size measurement in the submicronic size range of light extinction. In *Particle Size Analysis* (P. J. Lloyd, ed.), Wiley, Chichester, pp. 303–309, 1988.
21. Beretta, F., Cavalieri, A., D'Alessio, A. *Combust. Flame*, Vol. 49, p. 183, 1983.
22. Beretta, F., Cavalieri, A., D'Alessio, A. *Combust. Sci. Technol.*, Vol. 36, p. 19, 1984.
23. Beretta, F., Cavalieri, A., D'Alessio, A. 20th Symposium On Combustion, Ann Arbor, Michigan, 1984.
24. Beretta, F., Cavaliere, A., D'Alessio, A., Ragucci, R. Ensemble laser light scattering technique for the analysis of atomisation of coal-water slurry. *Proceedings of the Third International Conference on Liquid Atomisation*. London, Vol. 2. IVA/5/1–11, 1985.
25. Borodin, V. A., Dityakin, Yu. F., Klyachko, L. A., Yagodkin, V. I. *Raspilivanie Zhidkostei. (Liquid Atomization)* "Mashinostroenie," Moscow, 1967 (in Russian).
26. Brault, F., Lourme, D. Experimental characterisation of the spray formed by two impinging jets in liquid rocket injector. *Proceedings of the Third International Conference on Liquid Atomisation*, London, Vol. 1, pp. 11C/4/1–13, 1985.
27. Chehroudi B., Lombardi, P., Felton, P. G., Bracco, F. V. Spray photographs, poppet lift, and injection pressure of an oscillating poppet injector. *Trans. ASME J. Fluids Eng.*, Vol. 109, p. 289, September 1987.
28. Chella, G., Tognetti, L., Zanelli, S. *Atomisation Spray Technol.*, Vol. 2, pp. 187–200, 1986.
29. Chigier, N. Group combustion models and laser diagnostic methods in sprays. *Combust. Flame*, Vol. 51, pp. 127–139, 1983.
30. Chigier, N., Stewart, G. Particle sizing and spray analysis. *Opt. Eng.*, Vol. 23, pp. 554–556, 1984.
31. Chigier, N. Comparative measurements using different particle size instruments. In *Liquid Particle Size Measurement Techniques* (J. M. Tishkoff, et al., eds.), pp. 153–187, ASTM STP 848, 1984.
32. Dodge, L. G. Change of calibration of diffraction based particle sizers in dense sprays. *Opt. Eng.*, Vol. 23, pp. 626–630, 1984.
33. Dodge, L. G. Calibration of Malvern particle sizer. *Appl. Opt.*, Vol. 23, pp. 2415–2419, 1984.
34. Eickmans, J., Qian, S.-X., Chang, R. K. Detection of water droplet size and anion species by non-linear optical scattering *Proceedings of the First World Congress on Particle Technology*, Nürnberg, pp. 125–139, April 1986.
35. El-Emam, S. H. Experimental and theoretical study on liquid atomisation into a gas stream. *Proc. ICCLASS-85*, London, LP/VIIC/3/3–13, 1985.
36. Elkotb, M. M., Rafat, N. M., Hanna, M. A. The influence of swirl atomizer geometry on the atomization performance. *Proc. ICCLASS-78*, Tokyo, 5-1, 109–115, 1978.
37. Ewan, B. C. R., Swithenbank, J., Sorusbay, C. Measurement of transient spray size distribution. *Opt. Eng.*, Vol. 23, pp. 620–625, 1984.
38. Felton, P. G. In-stream measurement of particle size distribution. International Symposium on In-stream Measurements of Particle Solid Properties, Bergen, August 1978.
39. Felton, P. G., Hamidi, A. A. Aigal, A. K. Measurement of drop size distribution in dense sprays by laser diffraction. *Proceedings of the Third International Conference on Liquid Atomisation*, London, Vol. 2, pp. IVA/4/1–1, 1985.
40. Hamidi, A. A., Swithenbank, J. In *Optical Particle Sizing* (G. Gousbet and G. Grehan, eds.), Plenum Publishing, New York, pp. 321–333, 1988.
41. Hemsley, D. J., Yeoman, M. L., Bates, C. J., Maddad, O. The use of calibration techniques for the development and application of optical particle sizing instruments. In *Optical Particle Sizing* (G. Gousbet and G. Grehan, eds.), Plenum Publishing, New York, pp. 585–601, 1988.
42. Hess, C. F., Espinosa, V. E. *Opt. Eng.* Vol. 23, pp. 604–609, 1984.
43. Hess, C. F., Li, F. An instrument to measure the size, velocity, and concentration of particles in

- a flow. In *Optical Particle Sizing* (G. Gousbet and G. Grehan, eds.), Plenum Publishing, New York, pp. 271–281, 1988.
44. Hirleman, E. D. Non-intrusive laser particle diagnostics. *AIAA paper*, No. 83-1514, 1983.
 45. Hirleman, E. D. On-line calibration technique for laser diffraction droplet sizing instruments. *ASME paper* 83-GT-232, 1983.
 46. Hirleman, E. D. Particle sizing by optical non-imaging techniques. In *Liquid Particle Size Measurement Techniques* (J. M. Tishkoff, ed.), pp. 35–60, ASTM STP 848, 1984.
 47. Hirleman, E. D., Oechsle, V., Chigier, N. A. Response characteristics of laser diffraction particle size analyzers: optical sample volume extent and lens effect. *Opt. Eng.*, Vol. 23, pp. 610–619, 1984.
 48. Hirleman, E. D., Dodge, L. G. Performance comparison of Malvern Instruments laser diffraction drop size analyzers. *Proceedings of the Third International Conference on Liquid Atomisation*, London, pp IVA/3/1–14, 1985.
 49. Hiroyasu, H., Kadota T., Arai, M. Supplementary comments: fuel spray characterization in diesel engines. *Proceedings of the Symposium on Combustion Modeling in Reciprocating Engines*. Plenum Publishing, New York, 1980.
 50. Hiroyasu, H., Shimizu, M., Arai, N. The breakup of high speed jet in a high pressure gaseous atmosphere. *Proc. ICCLASS-82*, Madison, Wisconsin, 2-5, 69–74, 1982.
 51. Holve, D. J., Annen, K. D. Optical particle counting, sizing and velocimetry using intensity deconvolution. *Opt. Eng.*, Vol. 23, pp. 591–603, 1984.
 52. Hotham, G. A. A laser video imaging device for spray characterisation and particle size measurement. Second ASTK Symposium on Liquid Particle Size Measurement Techniques, Atlanta, Georgia, November 1988.
 53. Hovenac, E., Hirleman, E. D., Ide, R. F. Calibration and sample volume characterisation of the PMS optical array probe. Presented at the Third International Conference on Liquid Atomisation and Spray Systems, London, 1985.
 54. Jones, A. R. CEGB Marchwood, Report No. R/M/N 920, 1976.
 55. Jones, A. R., et al. CEGB Marchwood, Report No. R/M/N 936, 1977.
 56. Jones, A. R., Sargeant, M. CEGB Marchwood, Report No. R/M/N 1049, 1979.
 57. Knight, J., Driver, S., Robertson, G., Bayvel, L. P. Measurement of the dispersion of droplets produced by the Bergland-Liu droplet generator by study of the morphology dependent resonances. Second ASTM Symposium on Liquid Particle Size Measurement Techniques, Atlanta, Georgia, November 1988.
 58. Bayvel, L. P., Driver, S., Knight, J., Robertson, G. Morphology dependent resonance measurement of Bergland-Liu generator droplet dispersion. In *Liquid Particle Size Measurement Techniques* (E. D. Hirleman, W. Bachalo, and P. Felton, eds.), Vol. 2, pp. 19–29. STP 1083, American Society for Testing and Materials, Philadelphia, 1990.
 59. Knollenberg, R. G. NBS Special Publication 412, 1974.
 60. Kouzelis, D., Candel, S. M., Esposito, E., Zikikout, S. Particle sizing by laser light diffraction. In *Optical Particle Sizing* (G. Gousbet and G. Grehan, eds.), pp. 335–349, Plenum Publishing, New York, 1988.
 61. Kurabayashi, T., Karasawa, T., Hayno, K. Liquid Nitrogen freezing method for measuring spray droplet sizes. *Proc. ICCLASS-78*, Tokyo, 12-1, 285–292, 1978.
 62. Lettieri, T. R., Jenkins, W. D., Swyt, D. A. *Appl. Opt.*, Vol. 20, pp. 2799–2805, 1981.
 63. Lettieri, T. R., Jenkins, W. D. A review of ultrahigh resolution sizing of single droplets by resonance light scattering. In *Liquid Particle Size Measurement Techniques* (J. M. Tishkoff, et al., eds.), pp. 98–110, ASTM STP 848, 1984.
 64. Lyshevskii, A. S. *Protsess rasplivaniya topliva dizel'nymi forsunkami* (Process of fuel atomization in diesel nozzles). Mashgiz, Moscow, 1963 (in Russian).
 65. Malloggi, S., Tognotti, L., Zanelli, S. An experimental study on the mechanism of jet breakup. *Proceedings of the Two Day Meeting on Sprays and Their Applications*, Milan, Italy, 1986.
 66. Malvern Instruments Ltd., Malvern, Worcestershire, England.
 67. Malyak, P. M., Thompson, B. J. Particle displacement and velocity measurement using holography. *Opt. Eng.*, Vol. 23, pp. 567–576, 1984.

68. Matsumoto, S., Crosby, E. J. Flow characteristics of impact jet nozzles. *Atomisation Spray Technol.*, Vol. 3, No. 2, pp. 77–78, 1987.
69. Matsumoto, S., Takashima, Y. Flow behaviour of a Newtonian liquid on a spinning disk. *Proc. ICLASS-85*, London, VI B/4/1–8, 1985.
70. McVey, J. B., Kennedy, J. B., Owen, F. K. Diagnostic techniques for measurements in burning sprays. Presented at the meeting of West St. Sect., Combustion Institute, October 1976.
71. Meyer, P., Chigier, N. Characterisation of the atomisation process in coal water slurry sprays. *Proceedings of the Third International Conference on Liquid Atomisation and Spray Systems*, London, Vol. 2, pp. IVB(C)/1/1–23, 1985..
72. Meyer, P., Chigier, N. Drop size measurements using a Malvern 2200 particle sizer. *Atomisation Spray Technol.*, Vol. 2, pp. 26–285, 1986.
73. Non-intrusive particle counter-sizer-velocimeter. Instec Co., Danville, California.
74. Orzechowski Z. *Rozpylanie cieczy* (Liquid Atomization) WNT, Warsaw, 1976 (in Polish).
75. Particle Dynamics Analyzer, Dantec, Electronik, Skovlunde, Denmark.
76. Phase/Doppler Particle Analyzer, Aerometrics, Mountain View, California.
77. Rao, K. V. L. Liquid nitrogen cooled sampling probe for the measurement of spray drop size distribution in moving liquid-air sprays. *Proc. ICLASS-78*, Tokyo, 12-2, 293–300, 1978.
78. Rizk, N. K., Lefebvre, A. H. Measurement of drop-size distribution by a light scattering technique. In *Liquid Particle Size Measurement Techniques*, (J. M. Tishkoff, et al, eds.), pp. 61–71. ASTM, STP 848, 1984.
79. Ruiz, F., Chigier, N. The mechanics of high speed atomization. *Proc. ICLASS-85*, London, VI B/3/1–15, 1985.
80. Sakai, T., Sadakata, M., Saito, M. Mean diameters and drop size distribution of suspension sprays. *Atomisation Spray Technol.*, Vol. 1, No. 2, pp. 147–164, 1985.
81. Simmons, H. C. Lapera, D. J. Parker-Hannifin Corporation, Cleveland, Ohio, ASME Gas Turbine Conference, 1969.
82. Simmons, H. C. U.S.A. Patent 3609043, 1971.
83. Simmons, H. C. *Trans. ASME J. Eng. Power*, Vol. 99, p.309, 1977; Vol. 102, p. 646, 1980; Vol. 103, p.118, 1981.
84. Simmons, H. C. Investigating the commercial instrument market. In *Liquid Particle Size Measurement Techniques* (J. M. Tishkoff, et al., eds.), pp. 22–23, ASTM STP 848, 1984.
85. Skifstad, J. G. An automated imaging-type spray analysis system for local spray properties. *Proceedings of the Second International Conference on Liquid Atomisation and Spray Systems*, Madison Wisconsin, pp. 317–328, June 1982.
86. Smith, N. P., Norris, J. O., Yomen, M. L. Wright, C. J. Measurement of the size and velocity of liquid metal droplets during atomisation. *Proceedings of the Third International Conference on Liquid Atomisation and Spray Systems*, London, Vol. 2, pp. IVB (C) 11/1–9, 1985.
87. Spray Droplet Technology, Delavan Corporation, West Des Moines, Iowa, 1982.
88. Stanton, A. C., Caulfield, H. J., Stewart, G. W. *Opt. Eng.*, Vol. 23, pp. 577–582, 1984.
89. Swindenbank, J., Beer, J. M., Taylor, D. S., Abbot, D., McCreathe, G. C. A laser diagnostic technique for the measurement of droplet and particle size distribution. *Prog. Astron. Aeron.*, Vol. 53, pp. 422–451, 1977.
90. Szymanski, W., Pohl, F., Wagner, P. *J. Colloid Interface Sci.*, Vol. 85, pp. 289–301, 1982.
91. Takehira, A., Kawashima, T., Morita, S. Spray characteristics of the atomizer using a high speed gas flow. *Proc. ICLASS-78*, Tokyo, 10-3, 251–258, 1978.
92. Tanno, S., Miura, T., Ohtani, S. Development of a crossflow type pneumatic nozzle. *Atomisation Spray Technol.*, Vol. 2, No. 1, pp. 17–34, 1986.
93. Tate, R. W. Some problems associated with the accurate representation of droplet size distributions. *Proceedings of the Second International Conference on Liquid Atomisation and Spray Systems*, Madison, Wisconsin, pp. 341–351, June 1982.
94. Tate, R. W. Droplet size distribution data for internal-mixing pneumatic atomizers. *Proceedings of the Third International Conference on Liquid Atomisation*, London, Vol. 1, pp. 11c/1/1–13, 1985.

95. Thompson, B. J. *J. Phys. E*, Vol. 7, pp. 781–788, 1984.
96. Thompson, B. J. Droplet characteristics with conventional and holographic imaging techniques. In *Liquid Particle Size Measurement Techniques* (J. M. Tishkoff, ed.), pp. 111–122, ASTM STP 848, 1984.
97. Tishkoff, J. M. Measurement of particle size and velocity in a fuel spray. *Proceedings of the Second International Conference on Liquid Atomisation and Spray Systems*, Madison, Wisconsin, pp. 245–252, June 1982.
98. Tishkoff, J. M. Spray characterisation: practices and requirements. *Opt. Eng.*, Vol. 3, pp. 557–560, 1984.
99. Tokuoka, N., Nagaosa, S., Hora, S., Sato, G. T. Study on the disintegration of a liquid film by air impingement. *Atomisation Spray Technol.*, Vol. 1, No. 2, pp. 103–123, 1985.
100. Watson, D. J. Pulse spray analysis using the Malvern particle sizer. Malvern Instruments, MAR100, 1982.
101. Watson, D. J. Laser diffraction measurement transient spray conditions. *Proceedings of the Third International Conference on Liquid Atomisation and Spray Systems*, London, Vol. 2, pp. VC/4/1–15, 1985.
102. Webster, J. M. CEGB Marchwood, Report No. RD/M/R 132, 1971.
103. Weiss, B. A., Derov, P., De Biase, D., Simmons, H. C. Fluid particle sizing using a fully automated optical imaging system. *Opt. Eng.*, Vol. 23, pp. 561–566, 1984.
104. Wuerer, J. E., Deding, R. G., Poon, C. C., Hess, C. F. Application of nonintrusive optical methods to physical measurements in combustion, 20th AJAA meeting, paper 82-02-36, 1982.
105. Yates, W. E., Cowden, R. E., Akesson, N. T. Procedure for determining in situ measurements of particle size distribution produced by agricultural aircraft. *Proceedings of the Second International Conference on Liquid Atomisation and Spray Technology*, Madison, Wisconsin, pp. 335–339, June 1982.
106. Yeoman, M. L., Hemsley, D. J., Hadded, O., Bates, C. J. A single particle optical combining instrument for on line simultaneous measurement of drop size, velocity, and concentration in sprays and spray systems. *Proceedings of the Third International Conference on Liquid Atomisation*, London, Vol. 2, pp. VC/1/1–13, 1985.
107. Yule, A. J., Chigier, N. A., Atakan, S., Ungut, A. J. *Energy*, pp. 220–228, 1977.
108. Yule, A. J., Chigier, N. A., Cox, N. W. Measurement of particle size in sprays by the automated analysis of spark photographs. In *Particle Size Analysis* (M. J. Groves, ed.), pp. 61–73, Heyden, London, 1978.
109. Yule, A. J., Ahseng, C., Felton, P. G., Ungut, A., Chigier, N. A. Laser tomographic investigation of liquid fuel sprays. *18th International Symposium on Combustion*, pp. 1981–10, 1981.
110. Yule, A. J., et al. *Combust. Flame*, Vol. 44, pp. 71–84, 1982.
111. Yule, A. J., Mo, S.-L., Tham, S. Y., Aval, S. M. Diesel spray structure. *Proceedings of the Third International Conference on Liquid Atomisation and Spray Systems*, London, Vol. 1, pp. 11B/2/1–15, 1985.
112. Zhu, H. M., Sun, T. Y., Chigier, N. Tomographical transformation of Malvern spray measurements. *Atomisation Spray Technol.*, Vol. 3, pp. 89–105, 1987.
113. Particle Sizer Series HC, Polytec GmGH, Waldbronn-KA.
114. Farmer, W. M. *Appl. Opt.*, Vol. 11, pp. 2603–2612, 1972.
115. Farmer, W. M. *Appl. Opt.*, Vol. 13, pp. 610–622, 1974.
116. Jones, A. R., *J. Phys. D*, Vol. 7, pp. 1369–1370, 1974.
117. Hong, N. S., Jones, A. R. *J. Phys. D*, Vol. 9, pp. 1839–1848, 1976.
118. Hong, N. S., Jones, A. R. *Appl. Opt.*, Vol. 15, pp. 2951–2953, 1976.
119. Fristrom, R. M., Jones, A. R., Schwar, M. J. R., Weinberg, F. J. *Proceedings of the 7th Faraday Symposium*, pp. 183–197, Chemical Society, London, 1977.
120. Hong, N. S., Jones, A. R. *J. Phys. D*, Vol. 11, pp. 1963–1967, 1978.
121. Ereaut, P. R., Ungut, A., Yule, A. J., Chigier, N. Measurement of drop size and velocity in vaporizing sprays. *Proceedings of the Second International Conference on Liquid Atomisation*, Madison, Wisconsin, pp. 262–266, 1982.

122. Young, B. W., Bachalo, W. D., The direct comparison of three "on-flight" droplet sizing techniques for pesticide spray research. In *Optical Particle Sizing* (G. Gousbet and G. Grehan, eds.). Plenum Publishing, New York, London, pp. 483-497, 1988.
123. Saffman, M., Buchhave, P., Tanger, H. Simultaneous measurement of size, concentration and velocity of spherical particles by a laser Doppler method. *Proceedings of the Second International Symposium on Application of Laser Anemometry to Fluid Mechanics*, Lisbon, 1984.
124. Bayvel, L. P. Methods and instruments for ensembling particle sizing by light scattering. *South African Journal of Science*, Vol. 82, pp. 14-18, 1986.
125. Saffman, M. Automatic calibration of LDA measurement volume size. *Appl. Opt.*, Vol. 26, pp. 2592-2597, 1987.
126. Saffman, M. Spray characterization and volume flux measurement with a phase-Doppler particle dynamics analyzer. Second ASTM Symposium on Liquid Particle Size Measurement Techniques, Atlanta, Georgia, November 1988.
127. Mugele, R. A., Evans, H. D. *Ind. Eng. Chem.*, Vol. 43, p. 1317, 1951.
128. Fraser, R. P., Eisenklam, P. *Trans. Inst. Chem. Eng.*, Vol. 34, p. 294, 1956.
129. Matsumoto, S., Takashima, Y. *Bull. Tokyo Inst. Technol.*, Vol. 96, p. 95, 1970.
130. Pesticide Spray Droplet Analysis, Analytical Measuring Systems, Cambridge.
131. Last, A. J., Parkin, C. S. The measurement of spray deposits on natural surfaces by image analysis. *Aspects Appl. Biol.*, Vol. 14, pp. 85-96, 1987.
132. Pover, P. S. Studies of pesticide deposition of leaf surfaces by image analysis. *Lab. Pract.*, Vol. 37, p. 72, 1988.
133. Karasawa, T., Kurabayashi, T. Coalescence of droplets and failure of droplets to impact the sampler in the immersion sampling technique. *Proc. ICLASS-82*, Madison, Wisconsin, 11-1, pp. 285-291, 1982.
134. Wicks, M., Dukler, A. E. Proceedings of ASME Heat Transfer Conference, Vol. V, p. 39, Chicago, 1966.

AUTHOR INDEX

- Abbot, P., 448
Abou-Ellail, M. M., 158
Abramovich, G. N., 258
Adachi, K., 119
Adamovich, K., 35, 235, 301, 381
Ahseng, C., 449
Aigal, A. K., 446
Aigner, M., 235
Aihara, T., 445
Akesson, N. B., 121, 449
Akhrameev, V. I., 383
Anderson, B. J., 36
Andreussi, P., 35, 235
Antkowiak, W., 35, 381
Annen, K. D., 424
Arai, M., 158, 382, 383, 445, 447
Araki, K., 119
Arkhipov, V. A., 119
Astakhov, I. V., 301
Aszkin, A., 436
Atakan, S., 449
Aval, S. M., 158, 383, 449
Azzopardi, B. J., 407, 445

Bachalo, W. D., 407, 416, 434, 445
Bailey, A. G., 205, 235
Balachandran, W., 235

Barrere, M., 381
Basargin, B. N., 120
Bates, C. J., 446
Bayvel, L. P., 416, 428, 429, 430, 436, 437,
 445, 446
Bazarov, V. G., viii, 119
Bednarek, K., 35, 119
Beer, J. M., 448
Belcher, D. W., 235, 301, 382
Beloshkurskaya, O. N., 119
Beretta, T., 424, 446
Berevin, S. R., 119
Berger, H. L., 35
Biasi, L., 36
Bode, L. E., 120
Borisov, A. A., 119
Borodin, V. A., viii, 39, 71, 119, 301, 381
Braceo, F. V., 446
Brauer, H., 120, 381
Brault, F., 446
Brykowski, L., 235, 381
Brzustowski, T. A., 158
Buchhave, P., 449
Bukhman, S. V., 71
Burns, P. A., 36
Bushlanov, V. P., 119

- Candel, S. M., 447
 Caulfield H. J., 448
 Cavalieri, A., 446
 Chang, R. K., 446
 Chao, K. K., 35
 Chaudhary, K. C., 39
 Chechroudi, B., 446
 Chella, G., 47, 446
 Chiba, C., 235
 Chigier, N., viii, 36, 235, 302, 407, 416,
 446–449
 Child, C. A., 35
 Chin, J. S., viii, 158
 Chufarovskii, A. I., 120
 Clarke, S. W., 36
 Clay, M. M., 36
 Courshee, R. J., 35
 Cowden, R. E., 121
 Cox, N. W., 449
 Crosby, E. J., viii, 235, 301, 382, 447
- D'Alessio, A., 446
 Davies, C. R., 447
 De Biase, D., 449
 Deding, R. G., 449
 De Michele, G., 36, 235
 Derov, P., 449
 Deysson, J. Y., 235
 Deuham, R. O., 447
 De Veubeke, B. F., 381
 Dityakin, Yu. F., viii, 38, 119, 235, 301
 Dodge, L. G., 416, 446
 Dombrowski, N., viii
 Doyle, B. W., 235
 Driver, S., 447
 Dukler, A. E., 415
 Dunsckii, V. F., 120
- Eikmans, J., 436, 446
 Eisenklam, P., viii, 36, 71, 120, 445, 446,
 450
 El-Emam, S. H., 120, 446
 Elkotb, M. M., viii, 158, 381, 446
 Ereaut, P. R., 449
 Espinosa, V. E., 446
 Esposito, E., 447
 Evans, H. D., 158
 Ewan, B. S. R., 121
- Farmer, W. M., 433
 Fedder, I. E., 36
- Felton, P. G., 416, 446
 Filyand, L. V., 120
 Fraser, R. P., viii, 450
 Fristrom, R. M., 433
 Fujimoto, H., 382
- Galustov, V. S., viii, 36, 120, 158, 236,
 301
 Gel'fand, B. E., 119
 Gel'perin, N. I., 120
 Giffen, E., viii, 36, 120
 Goering, C. E., 120
 Gonor, A. L., 120
 Graziadio, M., 35, 36
 Grens, E. A., 35
 Gubin, S. A., 120
 Gupta, J. P., 235, 382
- Haddad, O., 446
 Hamidi, A. A., 446
 Hanna, M. A., 381, 446
 Hathaway, D., 36
 Hauser, M. J., 445
 Hay, N., 36
 Hayakawa, Y., 235
 Heim, A., 35, 381
 Hemsley, D. J., 36, 446
 Herring, W. H., 380
 Hess, C. F., 416, 435, 449
 Hinze, J. O., 293, 375
 Hirleman, E. D., 407, 416, 431, 447
 Hiroyasu, H., 158, 382, 383, 445
 Holve, D. J., 416, 424, 447
 Hong, N. S., 433
 Hongo, M., 445
 Honoki, H., 121, 236
 Hora, S., 383
 Hoshino, N., 121
 Hotham, G. A., 419, 447
 Hovenac, E., 431
 Hurley, J. F., 235
- Iciek, J., 120, 382
 Ide, R. F., 447
 Inamura, T., 235, 382
 Ingebo, R. D., viii, 382
 Ishikawa, M., 382
- Jameson, G. J., 121
 Jasyja, A. K., 236, 382

- Jenkins, W. D., 447
 Jones, A. R., 416, 417, 421, 433, 445, 447, 449
 Juen Man Chuen, 39
- Kadota, T., 158
 Kamiya, T., 301
 Kanabe, T., 382
 Karasawa, T., 120
 Karian, J., 235
 Kasperski, K., 36
 Kawashima, T., 236, 383
 Kawase, W., 120
 Kayano, A., 301
 Keller, V. W., 36
 Kelly, A. J., viii, 205, 235
 Kemblowsky, Z., 36
 Kennedy, J. B., 448
 Kiriyama, S., 119
 Kishi, T., 445
 Kito, M., 382
 Klyachko, L. A., viii, 38, 119, 236, 301
 Knight, J., 436, 446, 447
 Knollenberg, R. G., 416, 446
 Kogarko, S. M., 120
 Kossov, O. M., 119
 Kouzelis, D., 429, 446
 Kudryavtsev, A. V., 302
 Kulagin, L. V., viii, 301
 Kumazawa, T., 235
 Kuntsev, G. M., 302
 Kurabayashi, T., viii, 120
 Kutovoi, V. A., 36, 382
- Lafrance, P., 39
 Lala, G. G., 36
 Lapera, D. J., 419
 Last, A. J., 450
 Law, S. E., 227
 Lee, S. Y., 382
 Lefebvre, A. H., viii, 158, 301, 302, 416,
 448
 Lettieri, T. R., 436
 Li, F., 446
 Lipatov, A. S., 121
 Liu, B. Y. H., 121
 Lombardi, P., 446
 Loparev, V. P., 120
 Lourme, D., 446
 Lyshevskii, A. S., viii, 120, 140, 158, 301
- McCreath, C. C., 448
 McVey, J. B., 448
 Mahoney, T. J., 120
 Makarov, V. V., 301
 Malloggi, S., 120, 447
 Malyak, P. M., 447
 Mao, C.-P., 302
 Marshall, W. R., 380
 Masters, K., viii, 36, 120, 235, 301
 Masuda, A., 119
 Matsui, H., 120
 Matsumoto, S., viii, 120, 158, 301, 374,
 450
 Melaniuk, M., 36
 Melenchuk, A. I., 235
 Melodiev, E. A., 301
 Meyer, M. B., 36
 Meyer, P. L., 36, 235
 Milborn, H., 293, 375
 Milkin, A. C., 120
 Miyasaka, Y., 383
 Mo, S.-L., 158, 383
 Mochida, T., 235
 Mohan, R., 235, 382
 Morelli, F., 35, 36, 235
 Moren, F., 36
 Morita, S., 236, 383
 Mugele, R. A., 158, 450
 Mullinger, P. J., 235
 Murakami, T., 382
 Muraszew, A., viii, 36, 120
- Nagai, N., viii, 235, 382
 Nagaosa, S., 120, 383
 Nakayama, M., 382
 Narasimhan, M. V., 158, 301
 Narayanaswamy, K., 158, 301
 Natanzon, M. S., 119
 Newman, S. P., 36
 Neubauer, L., 205
 Nieuwkamp, W. C., 301
 Nikitin, N. V., 120
 Norris, J. O. W., 36, 448
 Novikov, A. A., 120, 235
 Novvegut, B., 205
 Nukiyama, S., viii, 357
- Oda, M., 235
 Oechsle, V., 447

- Ohono, T., 382
 Ohtani, S., 36, 236, 383
 Okazaki, H., 235
 Okhotskii, V. B., 120
 Ono, Y., 235
 Orzechowski, Z., viii, 35, 36, 120, 158, 236, 301
- Parkin, C. S., 450
 Patel, S. L., 236
 Pazhi, D. G., viii, 121, 158, 236, 301
 Pellow, P. G. D., 36
 Petela, R., 36, 121
 Picot, J. J. C., 236
 Pikering, S. J., 36
 Pohl, F., 448
 Polenov, A. N., 119
 Poon, C. C., 449
 Pover, P. S., 450
 Prasad, K. S. L., 382
 Pui, D. Y. H., 121
- Qian, S.-X., 446
- Radganadha Babu, K., 301
 Rafat, M. M., 158, 381, 446
 Ragucci, R., 446
 Rao, K. V. L., 448
 Raushenbakh, B. V., viii
 Rayleigh, J. S. W., 38, 42
 Redecopp, L. G., 39
 Rizk, N. K., viii, 301, 302, 448
 Robertson, D. G. C., 236
 Robertson, G. N., 446, 447
 Rowinski, R., 121
 Roylance, T. F., 36
 Ruiz, F., 448
 Rusakov, V. V., 119
 Rutland, D. F., 121
- Saffman, M., 449, 450
 Sadakato, M., 39, 382, 448
 Saito, M., 121, 382, 448
 Sakai, T., 120, 382, 448
 Sankaran Kutty, P., 158, 382
 Sargeant, M., 236, 417
 Sato, G. T., viii, 120, 121, 236, 382
 Sato, H., 39, 121
 Schwar, M. J. R., 449
 Shaw, S. G., 236, 382
 See, J. B., 36
- Sellens, R. W., 158
 Semichastryi, N. N., 383
 Senuma, S., 121
 Shamanaev, V. S., 301
 Shiga, S., 120
 Shimizu, M., 382, 447
 Shimoyama, T., 445
 Shummer, P., 121
 Shiotsuka, T., 120
 Simmons, H. C., viii, 383, 416, 419, 448
 Sinitsyn, B. D., 301
 Skifstad, J. G., 419, 448
 Smith, D. B., 120
 Smith, J. N., 445
 Smith, N. P., 36, 448
 Sorusbay, C., 446
 Spalding, D. B., 121
 Sterling, A. M., 120
 Stewart, G. W., 446
 Stubbs, M. E., 39
 Sun, T. Y., 449
 Swithenbank, J., viii, 121, 416, 446
 Swithenbank, J. R., 121
 Symons, M., 445, 446
 Szydlo, Z., 36, 121
- Tabata, M., 383
 Takahashi, T., 120
 Takashima, Y., viii, 120, 158, 374, 450
 Takehira, A., 236, 383
 Tanabe, H., 382
 Tanasawa, Y., viii, 149, 236, 357, 383
 Tanger H., 449
 Tankin, R. S., 382
 Tanno, S., 36, 236, 383
 Tate, R. W., 383, 416, 424, 448
 Taylor, D. S., 121, 448
 Tebel, K. H., 121
 Tek, M., 39
 Tesimo, T., 149
 Tham, S. Y., 158, 383
 Thomas, G. H., 36
 Thompson, B. J., 416, 420, 447
 Timofeev, E. I., 119
 Tishkoff, J. M., 383, 416, 449
 Tognotti, L., 35, 36, 120, 236, 446
 Tokuoka, N., 120, 121, 236, 383
 Troshkin, O. A., 236, 302, 383
 Tsyganov, S. A., 119
 Tul'skii, V. F., 36
 Tumanovskii, A. G., 36

- Umehara, O. A., 383
Unal, A., 236
Ungut, A., 449
- Valev, R. S., 302
Vandenkerkhove, J., 381
Van Vliet, M. W., 236
Vasenin, I. M., 119
Vijayraghvan, K., 235, 382
Volynskii, M. S., viii, 121
Voronin, V. V., viii, 121
- Wagner, P. P., 448
Walzel, P., 302
Wang, D. P., 39
Wang, G., 39, 382
Warych, J., 36
Watson, D. J., 416, 449
Weber, C., 38, 42
Webster, J. M., 420
Weinberg, F. J., 449
Wicks, M., 415
Wilk, R., 36, 120
- Williams, M. C., 35
Witting, S., 235, 381
Wood, R., 445, 446
Wright, C. J., 448
Wuerer, J. E., 449
- Yagi, M., 121, 236
Yagodkin, V. I., viii, 38, 119, 235, 302
Yates, W. E., 121, 420
Yeoman, M. L., 36, 416, 436
York, J. L., 39
Yoshioko, N., 119
Young, B. W., 449
Yule, A. J., viii, 158, 383, 416–418, 427,
 433, 449
- Zablocki, M., 36
Zaindel, A., 36, 121, 383
Zanelli, S., viii, 120, 446
Zhu, H. M., 427, 449
Zikikout, S., 447
Zolotova, N. V., 120
Zvezdin, Yu. G., 120



Taylor & Francis
Taylor & Francis Group
<http://taylorandfrancis.com>

SUBJECT INDEX

- Acoustic atomizers, 221–224
Acoustic vibrations, 114
Aerial spraying, 109, 142
Aerodynamic forces, 41, 43, 44, 68–70, 91–95, 154
Aerosols, 17, 109, 119
Afterinjection, 171, 390
Agriculture, 15–16, 84–86, 129–133, 144, 165
Air conditioning, 21, 136, 139, 144
Air pollution, 19–22
Air pumping effect, 217
Air vortex, 108
Air-assisted atomizers, 194–195, 210–212
Airy formula, 425
Allen equation, 89
Analysis of drop size distribution data, 437–445
Angular atomizers, 174
Asymmetric waves, 41, 43, 54
Asymmetry, of atomizer, 340
Atomization quality, 143–144, 282, 317, 368
Atomization theory, 37–121
(*See also* Atomizers)
Atomizers:
 characteristics of, 128, 181
 classification of, 1–7
 design of, 159–236, 237–302
efficiency of, 7, 258, 275, 430
energy sources, 1–7
 internal operations, 200–201
Attemperation, 9, 24
Axial atomizers, 175
Axisymmetric waves, 38, 41
Berglund-Liu generator, 436
“Best” fit to standard distributions, 437–445
Bernoulli equation, 123, 239, 242, 252, 274
Blast atomizers, 163–165
Bleeding, of atomizers, 173
Boilers, 160, 200
 attemperation, 9, 24
 burners, 8–10, 85, 385
 cleaning of, 52
 firing up, 350
Bond number, 77
Bosch nozzle, 250–251
Bowl atomizers, 213
Burst disintegration, 72
Capillary structure, 44
Capillary wave hypothesis, 222
Cascade atomizers, 164–166
Cavitation, 39, 222

Charged probe method, 415
 Claviform disintegration, 75
 Clogging, 164, 175, 233, 235
 Clustered nozzles, 133
 Coagulation, 84
 Coalescence, 81, 82
 Coal-oil mixtures, 23, 368
 Coal-water mixtures, 24, 201, 207, 348
 Combustion chamber, 108, 135
 Combustion, of fuels, 8–10, 85, 125, 144
 Compact zone, 43
 Conical deflector, 242
 Contact probe method, 407, 415
 Contamination, 340
 Continuous atomizers, 123–124, 160, 386,
 395–396
 Continuous nozzles, 171
 Contraction, 238, 264, 305
 Cooling, 13
 Countercurrent regime, 108, 207
 Cross-flow atomizers, 199, 284–287, 355, 360,
 365
 Cross swirlers, 192
 Cup atomizers, 213, 294–296, 376

Deflect atomizers, 163
 Degree, of atomization, 144
 Density, of atomization, 32, 138
 Design, of atomizers (*see specific types*)
 Diesel engines, 13, 23, 101–109, 231, 307, 385
 Diffusion models, 86
 Dimensional analysis, 40, 50, 63–69, 643
 Direct feeding, 208
 Direct injection, 166
 Discharge coefficient, 124, 238, 258, 279, 323,
 325
 Discharge orifice, 310
 Discharge velocity, critical, 68
 Disintegration, 37–40, 69–81, 93, 153
 Disk atomizers, 209–210, 215, 289–292, 374
 Divided chambers, 166
 Drag forces, 70, 153–154
 disintegration and, 91–93
 Reynolds number and, 87
 Weber number and, 92
 Droplets:
 ablation process, 357
 ballistics of, 84–102
 buoyancy of, 86
 circulation inside, 91
 collision of, 81–83, 162
 dimensions of, 62, 405–410, 416
 disintegration of, 37–40, 69–81, 153

drag forces, 90–94, 96–97
 drifting, 74
 evaporation method, 414
 fall of, 85–90
 fall velocity curve, 90
 formation of, 368
 freezing method, 412
 gas jets, 94
 jets of, 101–109, 133, 136
 kinds of, 71
 laminar motion, 99
 linking of, 69
 maximum diameter, 70
 mean diameters, 37, 40
 mists, 119
 number distribution, 148
 radial penetration, 297
 satellite drops, 110–112
 separation of, 119
 sizing methods, 405–410, 416
 surface tension, 153
 trajectories of, 108
 transient motion, 40, 99
 turbulent motion, 99, 101–102
 uniform, 109
 volume distribution, 149
 wall collisions, 40
 Drop size distribution functions, 143–158,
 437–445
 Dual-range atomizers, 179
 Duplex atomizers, 173, 178–185, 267–270, 331,
 337
 Dynamic generator, 225

Efficiency values, 7, 258, 275, 430
 Electrostatic atomizers, 226–227
 Emulsion component production, 226
 Engel equation, 78
 Ensemble analyzing instruments, 424–426
 Entrainment regime, 101
 Environmental protection, 19
 Erosion, 141, 233
 Evaporation, 39
 Excess liquid coefficient, 185
 External operation, 202

Fan atomizers, 164–165, 243
 Filling efficiency, 272, 275, 342
 Films, 240, 290–300, 344, 400–401
 Filtration, 101, 233
 Firefighting, 52

- Fire protection, 21, 165
 Flare, angle of, 376
 Flat disk atomizers, 210
 Flat seat nozzle, 170
 Flow number, 125
 Flow rate, 123–132, 387
 Food industry, 22
 Forest industry, 15–16
 Fraunhofer diffraction, 425, 427
 Free turbulence, 312
 Free vortex equation, 135
 Fringe anemometer, 432, 433
 Froude number, 258
 Frozen drop techniques, 407
 Fuel additives, 24
 Fuel charge, 125
 Fuel combustion, 8–10, 85, 125, 144
 Fuel densities, 25
 Fuel injection, 244, 250–251, 307
 Fuel pump, 245
 Full cone jet, 189
 Fumes, 207
- Gas action, 197
 Gas-assist atomizers, 4
 Gas-liquid impingement, 362
 Gas nitriding, 231
 Gas pressure drop, 196–197
 Gas scrubbing, 19
 Gas turbines, 14, 135, 173, 204, 218, 265, 348, 365
 General loss coefficient, 279
 Geometric constant, 172, 187, 272, 342
 Granulation, 19
 Gravitational classification, 407, 414
 Group atomizers, 142, 161
- Hartmann generator, 222
 Health protection, 21–22
 Herring-Marshall equation, 297, 380
 High-speed photography, 43
 Hinze-Milborn relation, 293, 375
 Holographic methods, 321, 420
 Humidifiers, 21, 144, 178, 210, 234
 Hybrid atomizer, 210
 Hydrocarbon fuels, 23, 66, 228
 Hydrodynamic thrust method, 393
- Ideal liquid theory, 252, 273
 Imaging techniques, 416
 IMAX technique, 435
- Immersion drop sampling method, 409–410
 Impact atomizer, 240–242, 321
 Impeller atomizer, 215
 Impingement, 162, 192, 239, 322–328
 Indicator method, 392–393
 Indirect injection, 166
 Inhalation therapy, 109
 Injection, 171
 afterinjection, 390
 angular frequency and, 127
 characteristic of, 127, 244, 391
 constant pressure and, 394
 constant volume and, 394
 nonrepeatability, 389
 pulsing and, 26
 Instability, 38
 Interface, liquid-gas, 194
 Intermittent atomizers, 3, 125–128, 165, 231–232, 306, 385–396
 Internal gas action, 359
 Internal mix atomizer, 200
 Inversion technique, 426, 429
- Jet atomizers, 1–3, 141
 circular orifice, 237
 continuous operation, 160–171, 237–244
 design of, 237–252
 diesel engines and, 101
 discontinuous operation, 165–167
 drop jet motion, 101–109
 experimental data, 303–322
 horizontal discharge in, 97–99
 intermittent operation, 244–252
 jet swirl atomizers, 189–194, 273–280
 liquid density and, 140
 spray angle, 133
(See also Jets)
- Jet engines, 14, 23
- Jets:
- basic equation for, 49
 - collision of, 56, 57, 162
 - compact, 51–52
 - contraction, 239, 328
 - density of, 138, 340
 - disintegration of, 37–40
 - free turbulent jet, 102
 - impinging, 162, 239
 - interfaces and, 45
 - mixing of, 193–194
 - stability, 41–55
 - turbulent, 54
- (See also Jet atomizers)*

- Körting atomizer, 177
- Laminar flow, 38, 53, 90
- Laplace number, 50, 53, 66, 74, 77, 251, 308, 345
- Laser Doppler anemometry, 431–437
- Law atomizer, 227
- Ligament formation, 292, 368, 373
- Limiting discharge velocity, 68
- Limiting state, of spray, 371
- Liquid distribution, 138–142, 315–317, 372
- Liquid films, 240, 294–296, 300, 344, 400
- Liquid fuels, 22
- Liquid sheets (*see* Sheets)
- Log-normal distribution, 151, 438–439
- Lorentz-Mie theory, 424
- Loss coefficient, 279
- Lubrication, 10–11
- Macrostructure, of atomized liquid, 354–357
diesel engines and, 307–322
liquid distribution, 138–142
measurements of, 396–404
swirling and, 334–337
(*See also* Spray angle; specific parameters)
- Magnetostrictive vibrator, 225, 226
- Malvern particle sizer, 425, 427–428
- Mean Sauter diameter, 141, 151–155, 206, 318, 346
- Microphotography, 416
- Microstructure, of liquid:
disintegration and, 357–368
quality of, 143–145, 156–158, 317–322
theory of, 344–350, 373–375
Weber number and, 360–365
(*See also* Droplets; specific parameters)
- Mie theory, 430
- Misting, 119–120
- Mixing effects, 102, 182, 193, 359
- Monodisperse atomizer, 109
- Multijet atomizers, 197
- Multiorifice atomizer, 128, 129, 168, 248
- Multiple spray nozzles, 178
- Multistage atomizers, 197
- Navier–Stokes equation, 40, 45, 89, 252, 289
- Newtonian liquids, 28, 39
- NIRO atomizer, 216
- Nonhomogeneous liquids, 28
- Nonintrusive imaging, 416
- Nonlinear scattering, 436–437
- Non-Newtonian liquids, 24–25, 30
- Nonuniformity, 141–143
- Nozzles, 167
assembly flaws, 340
contamination of, 141
design of, 104
flat seat, 170
grooves in, 343
injection characteristic, 126
types of, 168
wave effects inside, 359
Y-jet, 200
(*See also* specific types)
- Nukiyama-Tanasawa distribution, 151, 440–441, 444
- Nukiyama-Tanasawa equation, 357
- Ohnesorge number, 42, 67
- Oil mist, 10–11, 119
- Oil-water slurries, 9, 207
- Optical drop sizing, 416, 420
- Paint spraying, 226
- Parachute-type disintegration, 72, 74
- Parallel flow atomizers, 197–199, 280–284, 350–357
- Particle-counter-sizer velocimeter, 424
- Perforated atomizer, 56, 219, 297, 381
- Pesticides, 15, 24, 84
- Pharmaceuticals, 85
- Phillips-Twomey method, 430
- Piezoelectric transducer, 226
- Piston engines, 13, 171
- Plain-jet atomizer, 205
- Plant spraying, 136, 228
- Pneumatic (twin-fluid) atomizers 194
(*See also* specific designs)
- Polarized components method, 424
- Pollution, 19–22
- Porous atomizers, 220
- Power engineering, 8–10
- Precombustion chambers, 308
- Prefilming atomizer, 205
- Pressure atomizers (*see* specific types)
- Principle of maximum flow, 257–258
- Quality control, 385–387
- Quality, of atomization, 143–145, 156–158, 282, 317–322
- Radial channel atomizers, 217
- Radial liquid distribution, 139, 357

- Rayleigh-Lamb-Taylor instability, 77
 Rayleigh theory, 38, 44
 Reaction atomizers, 218–219
 Recirculation atomizer, 188
 Resistant crisis, 89
 Reynolds number, 42, 66, 87–89, 95, 124, 263
 Rheological models, 28
 Ricardo-Pintaux nozzle, 169
 Rocket engines, 14, 23, 161, 162, 365
 Rosin-Rammler equation, 141, 148, 151, 155, 317, 380, 438, 443
 Rotary atomizers, 6, 39, 100, 110, 123, 208–220, 289–301, 368–383, 396
 Rotary method, 391
 Rotating generator, 225
 RSF factor, 158
- Satellite drops, 110
 Sauter mean diameter, 151–155, 206, 251, 318, 346
 Scattered light method, 347
 Scattering methods, 347, 425
 Screen analysis, 414
 Scrubbers, 139, 178
 Secondary feeding, 348
 Sedimentation, 407, 414–415
 Segner atomizer, 218
 Shearing, 48, 72, 77, 164, 194
 Sheet formation, 37–40, 55–63, 368, 373
 Shifrin theory, 428–429
 Simplex atomizers, 174, 322, 326, 335
 Single-drop counters, 423–424
 Single-jet atomizers, 197
 Single-orifice nozzles, 168
 Slide sampling method, 407
 Small disturbances method, 38, 44
 Solid-liquid fuels, 23
 Spark-ignition engines, 14
 Spill-return atomizers, 173, 185–188, 270–272, 332, 339, 348
 Spray angle, 132–136, 258–259, 308, 335, 370–371, 396–399
 Spray coating, 12
 Spray drying, 18, 85, 108, 213, 380, 385
 Spray painting, 136
 Spray penetration, 136, 311–314, 371, 399–403
 Spray quality, 156
 Stability conditions, 45, 60, 258, 363
 Stagnation zones, 88, 135
 Static generator, 224
 Steam attemperation, 9, 139, 204
 Stroboscope method, 393
 Stroke measurement, 391
- Substitute liquid method, 413–414
 Surface coating, 143
 Surface tension, 30–34, 47, 58, 153, 319
 Swirl atomizers, 1, 4, 232, 346
 advantages of, 172–189
 countercurrent swirl, 367
 density distribution, 139
 design of, 252–273, 285–287
 drop in, 56, 97, 106
 experimental method, 322
 inserts for, 191, 275
 radial liquid distribution, 141
 spray angles, 134–135
 spray quality, 157
 swirl chambers, 166, 308, 329
 uses of, 204–207
 vanes, 192
- Tester systems, 387–389
 Theory of turbulent jets, 283
 Three-orifice atomizer, 185
 Throttling, 170, 286, 353
 Through-flow atomizer, 176, 177
 Trajectory models, 86
 Transverse distribution, 404
 Turbulence, 90
 atomizers and, 193
 boundary layer, 273
 jet model, 54, 102
 k-e model of, 102
 range of, 90
 theory of, 283
- Twin-fluid atomizers
 (*See* Pneumatic atomizers)
- Two-chamber atomizer, 181, 331
 Two-manifold atomizers, 179
 Two-nozzle atomizers, 270
 Two-orifice atomizers, 182–185, 348
 Two-sided atomizers, 197
- Ultrasonic atomizers, 225–226
 Uniform drops, 109–119
- Vaned atomizers, 216, 296–297, 380
 Variable-geometry atomizers, 188–189, 272
 Velocity coefficient, 325
 Velocity loss coefficient, 238
 Venturi tube, 396
 Vibrating capillary method, 116

Viscosity:

- atomization and, 27–32, 38, 42
 - barrier, 323
 - discharge coefficient, 325
 - effects, 104, 261–264
 - Laplace number and, 66
 - Newtonian liquids, 28
 - Sauter diameter and, 318
 - spray angle and, 337
 - theory of, 208, 213, 261, 278–279
 - Weber number and, 77
- Volume mean diameter, 153

Water cooling, 9

Water hardness, 234

Water-in-oil emulsions, 23

Water treatment, 10, 22

Weber equation, 52

- Weber number, 50, 251
 - alternate form of, 66, 68
 - amplitude growth and, 61–62
 - collision and, 83
 - critical, 40, 74
 - disintegration and, 71, 154
 - disturbance and, 357
 - drag coefficient and, 92
 - drop diameter and, 62
 - expansion wave and, 77
 - film thickness and, 345
 - viscosity and, 77
- Wheel atomizers, 296–300
- Wigg correlation, 361
- Wire mesh drums, 220
- Wright principle, 119
- Y type atomizers, 200, 351, 360